SOVIET PHYSICS

JETP

A translation of the Zhurnal Éksperimental'noĭ i Teoreticheskoĭ Fiziki

Vol. 14, No. 5, pp. 951-1208 (Russ. orig. Vol. 41, No. 5, pp. 1337-1696, Nov., 1961) May, 1962

COMPARATIVE MEASUREMENTS OF THE SHAPE OF Au^{198} *AND* Zn^{69} *BETA SPECTRA*

N. A. BURGOV, A. V. DAVYDOV, and G. R. KARTASHOV

Submitted to JETP editor June 28, 1961

J. Exptl. Theoret. Phys. (U.S.S.R.) 41, 1337-1339 (November, 1961)

The β spectra of Au^{198} and Zn^{69} were measured under identical conditions using an iron-free toroidal β spectrometer; the β spectrum of Zn^{69} is known to have a Fermi shape. A difference between the β spectra was observed at low energies (100—300 kev) which at 100 kev reached (6.5 ± 0.5)% on the Fermi plot, a lack of electrons being discovered in the Au^{198} spectrum in this region. It is interesting to note that some time ago a deviation from v/c in the longitudinal polarization of Au^{198} β electrons was observed at the same energies.

IT has been observed[1] when measuring the longitudinal polarization of Au^{198} β electrons that the magnitude of this polarization differs considerably from v/c at low energies. Geshkenbeĭn and Rudik have shown[2] that such a difference should be accompanied by a deviation of the β spectrum from the Fermi shape in this energy region. We performed an experiment aimed at detecting such deviations in the β spectrum of Au^{198}.

Distortions in the shape of the β spectrum may arise in measurements made with ordinary spectrometers, especially at low electron energies. The causes of this distortion may be divided into two groups. The first group has to do with the composition of the source. The scattering and slowing down of electrons in the source increase the number of low-energy electrons in the spectrum. Back scattering of electrons from the source backing can produce a similar effect.

The second group of causes is associated with the scattering of electrons inside the spectrometer and with the passage of electrons through the counter entrance window. If the measured β-spectrum shape is found to remain unchanged when thin sources of varying thickness (thinner than 100 $\mu g/cm^2$) are used, it may be supposed that the distortions in shape are due only to the second group of causes.

When comparative measurements are made of spectra with identical end-point energies, the difference observed in spectrum shape can be expected to reflect true differences in these spectra (in spite of the deviation of both spectra from the Fermi shape).

For this reason it was decided to compare under strictly identical conditions the β spectrum of Au^{198} with a spectrum of known Fermi shape. The β spectrum of Zn^{69} is especially suitable for such a comparison. When Zn^{68} is irradiated with neutrons, Zn^{69} is formed both in the ground state, from which β decay proceeds to the ground state of Zn^{69} (half-life 51 minutes), and in the isomer state, from which a γ transition to the ground state of Zn^{69} (half-life 14 hours) is followed by a 51-minute β decay.[3] The end-point energy of the Zn^{69} electrons is 914 kev, which is comparatively close to the maximum energy of the Au^{198} β spectrum (960 kev). A less essential but advantageous circumstance is the proximity of the energies of the γ rays emitted by both sources (411.8 kev for Au^{198} and 436 kev in the case of Zn^{69}). The β spectrum of Zn^{69} has

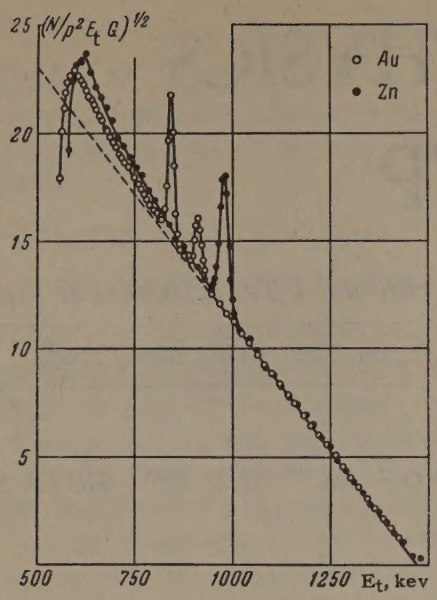

Fermi plot for Au^{198} and Zn^{69}. p and E_t are the momentum and total energy of the β electron, G is a modified Fermi function, and N is the number of counts per unit time.

log ft = 4.4,[3] indicating that this spectrum should have an allowed shape. This has been confirmed by earlier experiments, at least up to 200 kev.[4] Data on the longitudinal polarization of Zn^{69} β electrons are, unfortunately, lacking.

The measurements were made with a large iron-free β spectrometer.[5] The sources were prepared by evaporating one drop of the corresponding nitrate solution on a layer of insulin coating a 0.6-mg/cm^2 aluminum backing. This procedure is known to lead to considerable improvement in source homogeneity. The sources were 25 mm in diameter.

The β spectrum of the gold was measured using sources 25, 50, and 100 μg/cm^2 thick. Within an experimental error of $\sim 1\%$, the spectra obtained from the various sources were identical in shape for electron energies greater than 80 kev. The zinc β-spectrum measurements were performed with 50- and 100-μg/cm^2 sources; with the same accuracy, no marked differences in β-spectrum shape were observed.

Sources from 50 to 60 μg/cm^2 thick were employed for the principal measurements. Ten series of such measurements were made with Au^{198} and Zn^{69}, fresh sources being prepared each time. The good reproducibility of the results thus attained is evidence of the absence of significant inhomogeneities in the sources. An end-window Geiger counter with a 1.6-mg/cm^2 mica window served as electron detector. The β spectra were compared by superposing the straight-line sections of the Fermi plots. The Zn^{69} and Au^{198} spectra superposed in this way are shown in the figure (the scales of the coordinate axes for the Zn^{69} spectrum are changed). The divergence between the plots in the low-energy region, which becomes as large as $(6.5 \pm 0.5)\%$, is distinctly visible; there is a lack of low-energy electrons in the Au^{198} spectrum. The Au^{199} β spectrum is estimated to contribute several hundredths of a percent. The deviation of the zinc Fermi plot from a straight line at low energies is due to the scattering of electrons inside the spectrometer, in particular on the current-conducting wires of the magnet coil. It was this circumstance which compelled us to employ a comparative method. Our result shows that the surplus of low-energy electrons discovered by Steffen[6] in the Au^{198} β spectrum is not connected with the increase in the β-spectrum shape factor in this region.

The authors express deep gratitude to O. N. Vasil'eva for mathematical treatment of the experimental results, and also to V. G. Alpatov and Yu. I. Nekrasov for participating in the measurements.

[1] Alikhanov, Eliseev, and Lyubimov, JETP 39, 587 (1960), Soviet Phys. JETP 12, 414 (1961). Vishnevskii, Grigor'ev, Ergakov, Nikitin, Pushkin, and Trebukhovskii, Sb. Yadernye reaktsii pri malykh i srednikh energiyakh (Collection: Nuclear Reactions at Low and Medium Energies), AN SSSR, 1958, p. 336.

[2] B. V. Geshkenbeĭn and A. P. Rudik, JETP 38, 1894 (1960), Soviet Phys. JETP 11, 1361 (1960).

[3] B. S. Dzhelepov and L. K. Peker, Skhemy raspada radioaktivnykh yader (Decay Schemes of Radioactive Nuclei), AN SSSR, 1958, p. 161.

[4] R. B. Duffield and L. M. Langer, Phys. Rev. 89, 854 (1953).

[5] Burgov, Davydov, and Kartashov, Report at the Tenth Conference on Nuclear Spectroscopy in Moscow, January 1960; Nucl. Instr. 12, 316 (1961).

[6] R. M. Steffen, Proc. of the Rehovoth Conference on Nuclear Structure, September 1957, New York, 1958, p. 419.

Translated by Mrs. J. D. Ullman
231

INJECTION OF A PLASMA FROM A POWERFUL PULSED DISCHARGE INTO VACUUM

Yu. D. KLEBANOV and V. I. SINITSYN

Submitted to JETP editor March 21, 1961

J. Exptl. Theoret. Phys. (U.S.S.R.) 41, 1340-1346 (November, 1961)

Experiments are described in which plasma is ejected from a powerful pulsed discharge in hydrogen. The plasma parameters are investigated under various conditions of operation of the injector by photographic, photoelectric, and thermal probe methods. A plasma formation containing a total of the order of 10^{16} charged particles is shown to move in vacuum with a velocity $\sim 10^7$ cm/sec. The injection time is 2—5 μsec.

1. INTRODUCTION

THE interaction between a plasma and a magnetic field as well as the injection and confinement of a plasma in magnetic traps has been the subject of many investigations.[1-6] The behavior of a plasma inside a trap is determined in many respects by the properties of the plasma injector. The main parameters of a moving plasma, such as its velocity, temperature, and density, must be determined experimentally. It is equally important to choose an injector that ensures control of these parameters within certain limits. The electrodynamic coaxial accelerators described in the literature[7,8] can generate within several microseconds, under normal conditions, up to 1 cm^3 of hydrogen plasma moving in vacuum at velocities $5 \times 10^6 - 1.5 \times 10^7$ cm/sec.

The temperature of the particles forming an accelerated plasma layer apparently does not differ greatly from the temperature of the plasma produced during the earlier stages of development of a high-power pulsed discharge in cylindrical chambers.[9] It is impossible to increase appreciably the conductivity of the plasma in such a system ($\sigma \sim 10^{13}$ cgs esu).

Certain interest is attached to experiments on the production of a cumulative jet by contracting a conical plasma sheath.[10,11] When the jet moves in hydrogen at a gas pressure 0.2 mm Hg, the glow propagates at about 1×10^7 cm/sec.[11] However, it is difficult to estimate the properties of the plasma emerging from such a system into vacuum without special experiments.

Vasil'ev et al[12] demonstrated the possibility of obtaining a long lived (up to 40 μsec) dynamically stable current pinch. The plasma jets thus formed moved in hydrogen at a pressure 0.1 mm Hg with a velocity $\sim 5 \times 10^6$ cm/sec. Such a system can obviously be used as a plasma injector, although, just as in the preceding case, no data are given on the parameters of the "fountain pinch" propagating in the free space.

Plasma sources based on a different principle[13-15] have ejected plasmoids with velocity $\sim 1 \times 10^7$ cm/sec. The plasma itself, however, was of indefinite composition and, as a rule, of low temperature and density.

In the study of the interaction between a magnetic field and a high-conductivity plasma, such constructions are apparently of little use. In this case the systems of interest are those producing streams of pre-heated plasma.

It is known that during the instant of maximum contraction of the current pinch in a powerful pulsed discharge a certain amount of hot plasma with parameters $n = 10^{17}$ cm^{-3} and $T_i = 100$ ev[16] is produced on the chamber axis. This suggests the attractive idea of extracting such a plasma from the discharge zone into the vacuum. The present paper is devoted to an experimental investigation of such ejection.

If the plasma current pinch is strongly overcompressed, say with a diaphragm, then the self-magnetic forces of the current will produce an excess pressure at the pinch contraction. The pressure drop along the axis will tend to become equalized by the macroscopic plasma flow.[17,18] Filippov et al[19] have noted in an investigation of a pulsed hydrogen discharge in a chamber with conducting walls that the contraction of the discharge towards the axis is not uniform over the entire height of the chamber, and begins at one of the electrodes. In this case a natural neck is formed, as it were, in the discharge channel, which should lead to the formation of an axial plasma stream. On the other hand, owing to the conical character of the compression, a certain amount of plasma can be captured in the axial cumulative jet. Experimental apparatus was

therefore designed to verify these premises and to measure the parameters of the plasma ejected into vacuum. The experiments were carried out with two models of the apparatus, small and large.

2. EXPERIMENTS WITH THE SMALL MODEL

The character of discharge formation in a chamber with conducting walls and the effect of ejecting of the plasma from the discharge were investigated by optical means, using the small apparatus. Figure 1 shows the construction of the apparatus and the shapes of its various elements. The discharge chamber was made of a copper cylinder 1, on one end of which electrode 2 was mounted on a porcelain insulator. The second electrode comprised the lateral surface and the second end of the chamber. The process inside the chamber could be viewed through small holes in the side walls of the cylinder. Symmetrical placement of the holes prevented distortion in the formation of the discharge. The plasma was ejected through a 40 mm diameter hole 3 in the end of the chamber. To observe the ejection in the backward direction, a corresponding hole was drilled in the second electrode. In either case, the plasma stream detached from the discharge zone propagated further in glass chamber 4, the pressure in which was determined by the initial pressure in the discharge volume. The experiments were carried out in hydrogen at initial pressures ranging from 0.1 to 1.0 mm Hg.

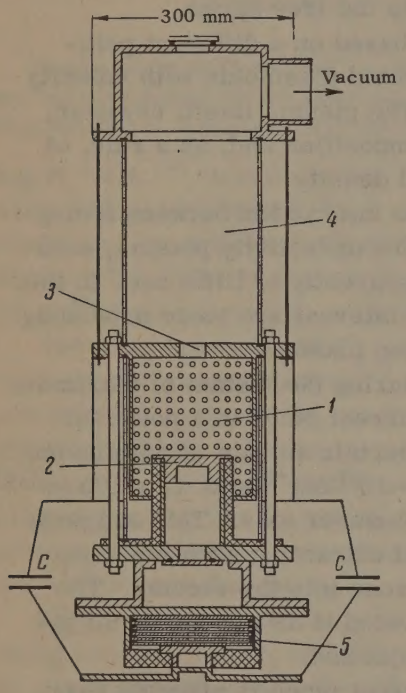

FIG. 1. Small model (explanation in text).

The discharge circuit was a 40 μf capacitor bank charged to 20—30 kv, with maximum discharge current 400 kiloamp. Switching was by means of vacuum discharge gap 5.

Motion pictures of the discharge taken with an SFR high-speed camera confirmed the predicted assumptions concerning the plasma ejection. Figures 2 and 3 show by way of an example certain frames taken at intervals $\tau = 0.5$ μsec apart at different initial hydrogen pressures and at different capacitor-bank polarities (the outlines of the photographed object are shown for clarity on the left of the illustrations).

The experiments made with the small model lead to the following picture of the process: the discharge contracts towards the chamber axis unevenly both in time and in space. The bright central rod formed at the electrodes increases along the axis with a velocity close to 1×10^7 cm/sec. The diameter of the rod does not exceed 1.5—2 cm. After passing through the opening in the bottom of the chamber, the plasma jet con-

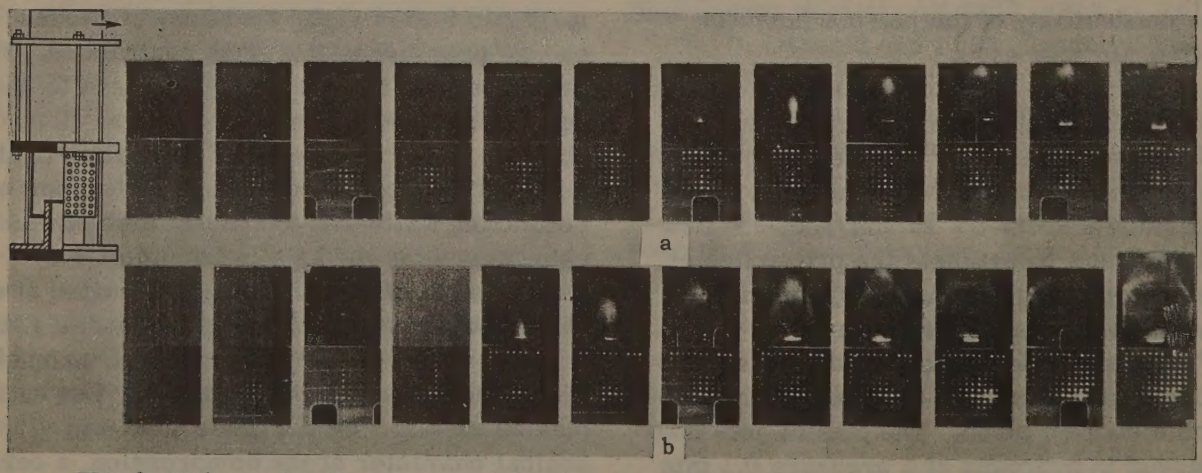

FIG. 2. High-speed motion pictures of plasma ejection from a discharge chamber with U = 30 kv, P_0 = 0.1 mm Hg: a—on positive electrode, b—on negative electrode.

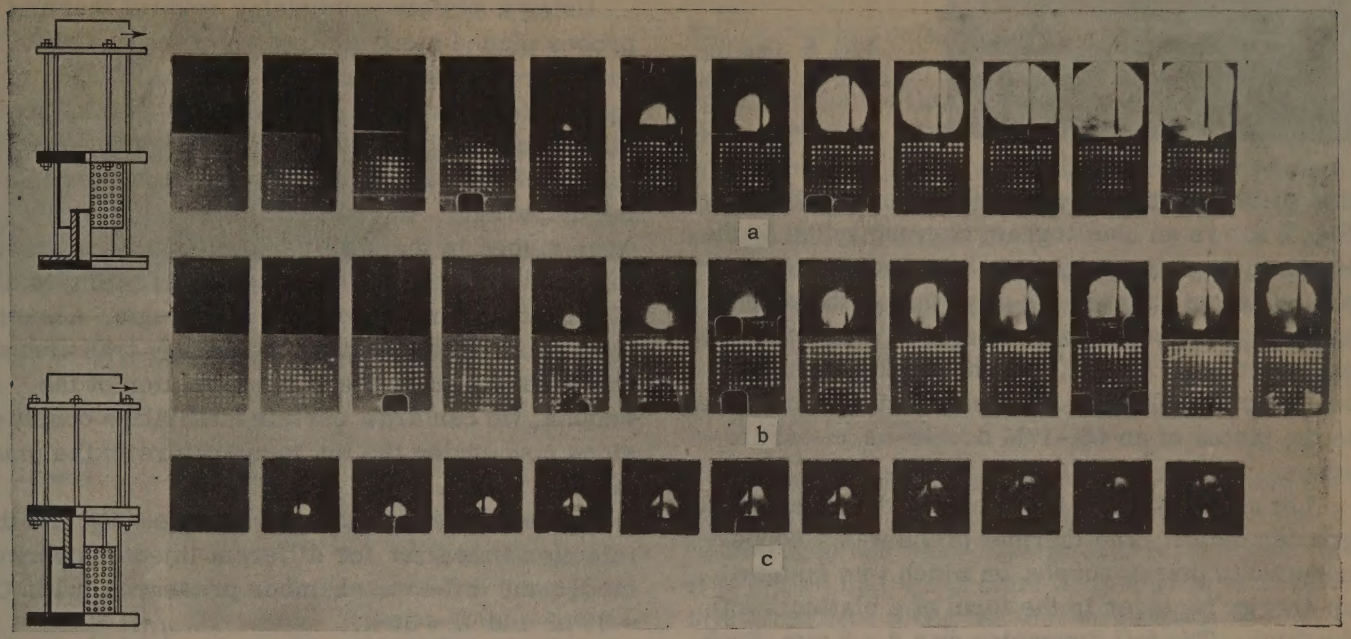

FIG. 3. Motion pictures of plasma ejection (U = 30 kv and P_0 = 1 mm Hg): a – on negative electrode, b – on positive electrode, c – ejection towards the electrode (V = 30 kv, P_0 = 0.1 mm Hg)

tinues to move outside the discharge zone. Plasma is also ejected in the opposite direction.

We recall that the plasma jet propagates in hydrogen at a pressure equal to the initial pressure in the discharge chamber, i.e., at P = 0.1—1.0 mm Hg. Calculation shows that the characteristic time for charge exchange with molecular hydrogen under similar conditions is $\sim 10^{-7}$ sec. Since the ejection time was several microseconds, much of the moving plasma was under these conditions the product of interaction between the primary plasma and the residual gas. These difficulties were overcome to some extent in the investigations made with the second, large experimental model.

3. EXPERIMENTS WITH THE LARGE MODEL

A diagram of the apparatus is shown in Fig. 4. Unlike the small model, the discharge chamber was separated from the observation chamber by two diaphragms with holes 5 and 10 mm in diameter. The space between the two diaphragms was evacuated with a BNM-1500 booster pump. The vacuum chamber was pumped out with a VNM-2000 diffusion pump. The differential pumping produced in the observation chamber a vacuum sufficient to make the charge exchange negligible. The pressure drop in both chambers was 1:2000 and remained approximately constant as the pressure in the discharge chamber was varied from 0.1 to 1.0 mm Hg. The distance from the diaphragm to the point of observation was too large to be covered by contamination from the diaphragm edges during the lifetime of the plasma jet.

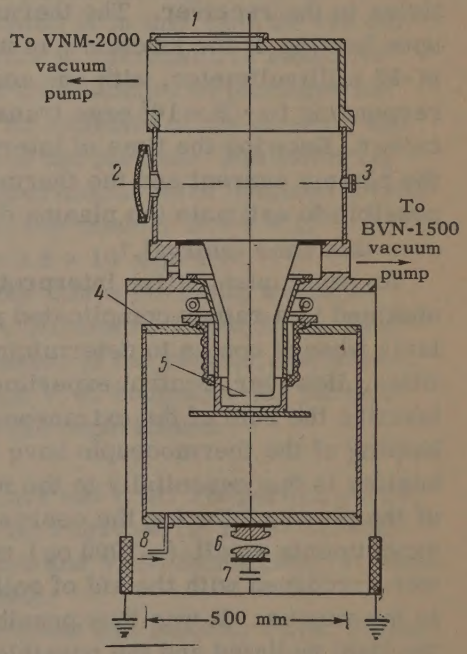

FIG. 4. Large model: 1, 2, 3 – viewing windows, 4 – discharge chamber, 5 – diaphragms, 6 – discharge gap, 7 – capacitor bank, C = 80μf, 8 – gas inlet

The rating of the discharge bank was C = 80 μf, and the charging voltage was 30—40 kv. The current at the maximum was about 500 kiloamp at an initial build-up rate of about 1×10^{11} amp/sec.

Attempts to use photographic methods failed because of the low brightness of the plasma moving in the vacuum. Only a photoelectric procedure in conjunction with thermal sounding made it possible to determine the dimensions of the plasmoid, the density of the charged particles in it, and its translational velocity.

The determination of the velocity by measuring the shift of the maxima of like pulses needs no special explanation. To illustrate the determina-

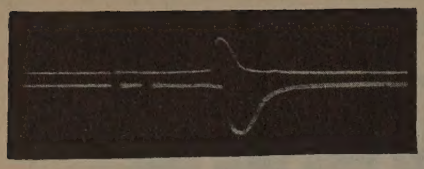

FIG. 5. Oscillogram of H_β line glow.

tion of the plasma velocity from the transit time, Fig. 5 shows an oscillogram corresponding to the H_β line, registered by two photoelectric receivers placed 15 cm apart in the direction of the plasma motion. Each receiver consisted of a UM-2 monochromator and an FÉU-12 photomultiplier, the collector signal of which was amplified and applied to the plates of an OK-17M double-beam oscilloscope.

Let us discuss the thermal sounding method in greater detail. The thermal probe was a copper-constantan thermocouple, on which was fastened an energy receiver in the form of a platinum foil 6 μ thick. The foil dimension was 8 × 8 mm. Such a probe, when placed in a particle current, registers the total energy transferred from these particles to the receiver. The thermal emf produced upon heating of the junction was measured with an M-95 millivoltmeter, with one scale division corresponding to $\sim 3 \times 10^2$ ergs transferred to the receiver. Knowing the time of interaction between the plasma current and the thermal probe, it is possible to estimate the plasma density averaged over this time interval.

An exact quantitative interpretation of the data obtained is a rather complicated matter, particularly when it comes to determining absolute quantities. However, control experiments set up to determine the role of the extraneous factors in the heating of the thermocouple have shown that this heating is due essentially to the moving protons of the plasma. During the course of the control experiments small ($\sim$ 1000 oe) magnetic fields were produced with the aid of coils placed directly in the vacuum. It was thus possible to show that the light radiated and the possible flow of neutral particles make a negligibly small contribution to the observed effect. In the data reduction it was assumed that the plasma particles give up all their energy as they collide with the surface of the heat receiver.

Using a system comprising several thermal probes placed along the radius of the chamber, data were obtained on the radial distribution of the particle current. The system was displaced along the chamber axis, and the distribution pattern could be studied at different distances from the diaphragm. In addition, three thermal probes were placed in the chamber, oriented to measure the axial, radial, and azimuthal energy fluxes at different distances from the diaphragm. Assuming that in the latter case the energy transferred was determined by the thermal motion of the plasma, we can draw certain qualitative conclusions concerning the ion temperature in the plasmoids.

Table I lists the plasma velocities V_z and the injection times $\Delta\tau$ for different injector operating modes and different chamber pressures, with C = 80 μf and U = 35 kv.

It should be noted that the modes of greatest interest are those in which the injection is in pulses ranging from 1.5 to 5 μsec (C = 80 μf, U = 16 kv, P_0 = 0.2 mm Hg). An illustration is Fig. 6, where the light pulse registered by a collimated photoelectric receiver is phased with the discharge current. In other cases, particularly at large capacitor-bank voltages and considerable initial pressures (up to 1 mm Hg), the light pulse is strongly stretched out (see Fig. 7, for which C = 80 μf, U = 35 kv, P_0 = 1 mm Hg). This apparently points to repeated additional discharges inside the chamber, leading to additional ejection of the plasma through the diaphragms. The photoelectric and thermal-sounding research methods do not yield in this case any definite conclusions concerning the translational velocity and density of the charged particles.

Figure 8 (P_0 = 1 mm Hg) shows the characteristic curve of radial distribution of a plasma current inside a vacuum chamber, from which we can

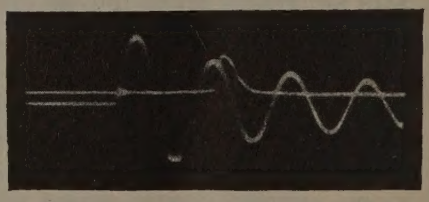

FIG. 6. Oscillogram of light pulse from plasma moving in a vacuum, phased with the current in the discharge chamber.

Table I

Injection direction	towards electrode						away from electrode		
Polarity of electrode	−			+			−		
P_0, mm Hg	0.1	0.2	0.5	0.1	0.2	0.5	0.1	0.2	0.5
$V_z \cdot 10^{-7}$, cm/sec	2.2	2.2	1.4	2.5	2.8	—	0.8	0.6	0.5
$\Delta\tau$, μsec	1.4	1.5	2.2	1.6	1.1	—	5	5	4

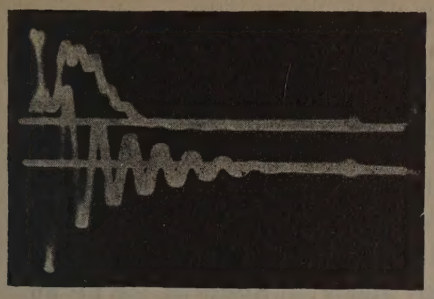

FIG. 7. Oscillogram of stretched-out light pulse.

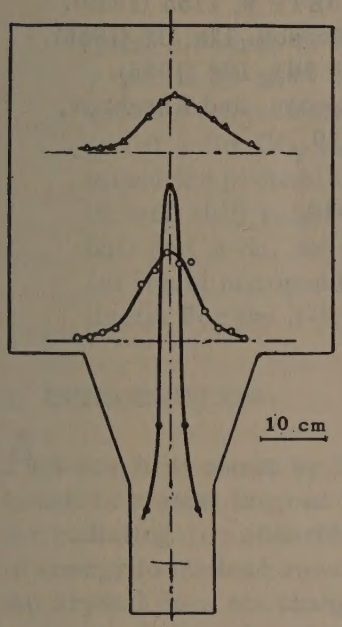

FIG. 8. Distribution of the density of a plasma moving in vacuum, at different distances from the diaphragm (the lower distribution curve is drawn to a scale 1:2).

estimate the localization of the plasma in free space. We give the values of the charged-particle density n, obtained by thermal-sounding measurement with heat receivers placed at different distances from the diaphragm:

Distance from upper diaphragm, cm:	6	35	54
Density of charged particles $n \times 10^{-13}$, cm^{-3}:	38	5,0	4.0
Total number of charged particles, $N \times 10^{-16}$:	3,8	4.0	3,8

A characteristic feature is that the total number of particles N, measured at different distances from the diaphragm, remains constant, within the measurement accuracy limit, thus showing that few particles are lost by the plasmoid as it moves along the chamber axis. Data on the number of protons injected into the vacuum in each discharge under different initial conditions and on the density of the charged particles, obtained under these conditions in the central section of the chamber, are summarized in Table II.

A rough estimate of the ion temperature of the plasmoid, based on experiments with differently oriented heat receivers, yields $T_i = 5 \times 10^5$ deg K.

4. CONCLUSIONS

1. The effect of injection of a certain amount of plasma into vacuum from a pulsed discharge in hydrogen has been experimentally demonstrated. It is shown that the plasma is ejected in two opposite directions along the discharge axis.

2. Operating conditions have been determined, under which the system can inject plasma in the form of individual pulses lasting 2—5 μsec. The length of the plasmoid is in this case 30—40 cm.

3. Photoelectric and calorimetric measurements yielded the total number of particles injected per pulse, an estimate of the density, and the axial velocity of the plasma. The following values in these experiments were obtained for the parameters in various modes: $N = 8 \times 10^{16}$, $n = 6 \times 10^{13}$ cm^{-3}, $V_z = 2.8 \times 10^7$ cm/sec.

The authors take this opportunity to thank Academician L. A. Artsimovich and S. Yu. Luk'yanov for a discussion of the results, and also to M. A. Savenkov and V. S. Shumanov for participating in some of the experiments.

[1] S. Yu. Luk'yanov and I. M. Podgornyi, JETP 37, 27 (1959), Soviet Phys. JETP 10, 18 (1960).

[2] I. M. Podgornyi and V. N. Sumarokov, J. Nucl. Energy 1, 236 (1960).

[3] Coensgen, Sherman and Nexsen, Phys. Fluids 3, 765 (1960).

Table II

Injection direction	from electrode		towards electrode			
Polarity of electrode	−	−	−	−	+	+
Electric parameters	C=16 μf U=36 kv	C=80 μf U=16 kv	C=80 μf, U=36 kv			
P_0, mm Hg	0.2	0.2	0.2	1.0	0.2	1.0
Total number of particles injected per pulse	$4 \cdot 10^{16}$	$8 \cdot 10^{16}$	$4 \cdot 10^{14}$	$4 \cdot 10^{16}$	$8 \cdot 10^{14}$	$2 \cdot 10^{16}$
Plasma density 35 cm away from the diaphragm	$1 \cdot 10^{13}$	$3 \cdot 10^{13}$	$1 \cdot 10^{12}$	$5 \cdot 10^{13}$	$2 \cdot 10^{12}$	$6 \cdot 10^{13}$

[4] F. R. Scott and R. F. Wenzel, Phys. Rev. **119**, 1187 (1960).

[5] Finkelstein, Sowyer, and Stratton, Phys. Fluids **1**, 188 (1958).

[6] J. Tuck, Phys. Rev. Lett. **3**, 313 (1959).

[7] J. Marshall, Second Geneva Conference, Paper No. 355.

[8] J. Marshall, Phys. Fluids **3**, 134 (1960).

[9] Andrianov, Bazilevskaya, and Prokhorov, Coll. Fizika plazmy i problema upravlyaemykh termoyadernykh reaktsii (Plasma Physics and the Problem of Controllable Thermonuclear Reactions), vol. 2, AN SSSR, 1958, p. 185.

[10] V. Josephson, J. Appl. Phys. **29**, 31 (1958).

[11] Borzunov, Orlinskii, and Osovets, JETP **36**, 717 (1959), Soviet Phys. JETP **9**, 502 (1959).

[12] Vasil'ev, Komel'kov, Skvortsov, and Tserevitinov, ZhTF **30**, 756 (1960), Soviet Phys.-Tech. Phys. **5**, 709 (1961).

[13] W. H. Bostik, Phys. Rev. **104**, 292 (1956).

[14] R. Post, Second Geneva Conference, 1958, paper No. 377.

[15] Sinel'nikov, Safronov, Guzhovskii, and Yaremenko, Report, Phys.-Tech. Inst. Acad. Sci. Ukr. S.S.R., Khar'kov, 1960, pp. 158 and 183.

[16] S. Yu. Luk'yanov and V. I. Sinitsyn, JETP **36**, 1621 (1959), Soviet Phys. JETP **9**, 1155 (1959).

[17] H. Maecker, Z. Naturforsch. **11a**, 32 (1956).

[18] H. Maecker, Z. Physik **141**, 198 (1955).

[19] Petrov, Filippov, Filippova, and Khrabrov, op. cit. ref. 9, vol. 4, p. 170.

Translated by J. G. Adashko
232

RESONANCE ABSORPTION OF 23.8-kev GAMMA QUANTA BY Sn^{119} *NUCLEI IN CRYSTALS*

N. N. DELYAGIN, V. S. SHPINEL', and V. A. BRYUKHANOV

Nuclear Physics Institute, Moscow State University

Submitted to JETP editor April 27, 1961

J. Exptl. Theoret. Phys. (U.S.S.R.) 41, 1347-1358 (November, 1961)

Using a source of Sn^{119m} in SnO_2, we have studied the resonance absorption of 23.8-kev γ quanta by Sn^{119} nuclei in crystals of SnO_2, SnO, β-Sn and $SnNb_3$. Resonance absorption spectra were obtained for different absorber thicknesses at liquid nitrogen temperature, and at solid CO_2 termperature for the β-Sn crystal. For each of the crystals we determined the probability of absorption without energy loss to recoil, and the magnitude of the isomer shift relative to the energy of the γ transition in the SnO_2 crystal. For crystals of SnO and β-Sn, we observed quadrupole splittings of the absorption line, which were equal (at liquid nitrogen temperature) to $(12.5 \pm 1.5) \times 10^{-8}$ and $(11.0 \pm 1.5) \times 10^{-8}$ ev, respectively. For the β-Sn crystal, the quadrupole splitting has a strong temperature dependence.

1. INTRODUCTION

As was first shown by Mössbauer,[1] nuclei contained in crystal lattices have a certain probability for radiating (or absorbing) γ quanta without loss of energy to nuclear recoil. The quantum state of the crystal does not change and the recoil momentum is transferred to the crystal as a whole; since the mass of the crystal can be regarded as infinitely large, there is no loss of energy of the quantum as a result of the recoil. The probability for such a process, calculated in the Debye approximation using Lamb's theory,[2] coincides with the Debye-Waller factor which appears in coherent x-ray scattering. This probability increases with decreasing recoil energy of the free atom $R = E_0^2/2Mc^2$ (where E_0 is the energy of the γ transition and M is the mass of the atom), with decreasing temperature of the crystal and increase of its Debye temperature. Thus we may expect a sizable probability of the Mössbauer effect for low energy γ transitions ($E_0 \leq 100$ kev); in addition in most cases it is necessary to resort to cooling the source and absorber.

The experimental data which have been obtained and the theoretical computations, which have been made by Kagan,[3] show that the Debye temperature is generally not the determining factor of the probability for this process, except possibly for the case of monatomic crystals. The probability for recoilless emission or absorption of γ quanta depends essentially on the specific form of the vibrational spectrum of the crystal lattice. The fundamental theory of the Mössbauer effect and the relation of its probability to crystal properties is treated in the papers of Visscher,[4] Lipkin,[5] and Shapiro.[6]

The presence in the emission and absorption spectra of lines having natural width and not subject to any Doppler broadening or shift due to recoil provides favorable conditions for observing the resonance absorption of γ quanta in crystals. By giving the source a velocity v relative to the absorber, we can artificially produce a Doppler shift of the absorption line by an amount $\Delta E = E_0 v/c$. By observing the resulting change in the effective cross section for the resonance absorption, we can investigate various effects associated with very small changes in the energy of the γ transition. The required velocities are equal to a few millimeters or centimeters per second. Experiments carried out recently using the Mössbauer effect are discussed in the published summaries.[7]

In the present work, we investigate the spectra of resonance absorption of 23.8-kev γ quanta by Sn^{119} nuclei contained in the crystal lattices of various tin compounds. Some preliminary results of these experiments have been published previously.[8,9]

2. CALCULATION OF MAGNITUDE OF RESONANCE ABSORPTION

In studying the dependence of the resonance absorption on the relative velocity v of source and absorber, the quantity which is measured experimentally is

$$\varepsilon(v) = [N(\infty) - N(v)]/N(\infty), \quad (1)$$

where N(v) is the counting rate for γ quanta transmitted through the absorber when the velocity is v; $N(\infty)$ is the counting rate at high velocity, where the resonance absorption is absent. In the future, for brevity, we shall call the quantity $\epsilon(v)$ the magnitude of the effect. It is not hard to show that the expression (1) for the magnitude of the effect can be written in the form

$$\varepsilon(v) = \varkappa f\left(1 - \int_0^\infty e^{-\sigma(E)n} W_e(E)\,dE\right), \quad (2)$$

where $\sigma(E)$ is the effective cross section for resonance absorption of γ quanta of energy E, $W_e(E)$ is the distribution function for the emission spectrum, n is the number of atoms of the particular isotope per cm^2 of the absorber, f is the probability of recoilless radiation of the γ quanta, κ is a parameter which determines the relative contribution of the particular γ quanta to the total counting rate. The parameter κ takes account of the presence of background, i.e., the recording by the counter of γ radiation whose resonance absorption is not under investigation.

The effective cross section is given by the formula

$$\sigma(E) = \frac{\Gamma^2}{4}\sigma_0 \frac{f'}{(E - E_0)^2 + \Gamma^2/4}, \quad (3)$$

where Γ is the total width of the level, f' is the probability of recoilless absorption of the γ quanta, and

$$\sigma_0 = \frac{2I_1 + 1}{2I_0 + 1}\frac{\lambda^2}{2\pi}\frac{\Gamma_\gamma}{\Gamma}.$$

(Here I_0 and I_1 are the spins of the ground and excited states, λ is the wave length of the γ radiation, Γ_γ is the radiative width; for the first excited state, $\Gamma_\gamma/\Gamma = 1/(1 + \alpha)$ where α is the total internal conversion coefficient.)

In the following we shall, for simplicity, consider the case where the source and absorber are chemically identical and are at the same temperature i.e., the case where there is an exact overlap of the emission and absorption lines for v = 0. This does not cause any loss of generality, since the presence of a constant line shift δ can be taken into account by simply changing the velocity v to $v + \delta$.

If the source does not contain the nuclei whose resonance absorption is being studied (or if the source is sufficiently thin) the emission spectrum has the form

$$W_e(E) = \frac{\Gamma}{2\pi}\frac{1}{(E + E_0 v/c - E_0)^2 + \Gamma^2/4}, \quad (4)$$

and the magnitude of the effect can be written in the following form:

$$\varepsilon(v) = \varkappa f\left(1 - \frac{1}{\pi}\int_{-\infty}^{+\infty}\frac{\exp[-C/(1 + x^2)]}{1 + (x + y)^2}dx\right),$$

$$x = \frac{E - E_0}{\Gamma/2}, \quad y = \frac{E_0 v/c}{\Gamma/2}, \quad C = \sigma_0 f' n. \quad (5)$$

The integral in (5) can in general be computed only by numerical integration. An exception is the case of v = 0, where the expression (5) can be brought to the form (cf., for example, [10]):

$$\varepsilon(0) = \varkappa f[1 - I_0(C/2)e^{-C/2}], \quad (6)$$

where $I_0(x) = J_0(ix)$ is the Bessel function of zero order and imaginary argument.

Expression (6) can be used to determine the value of f', if we determine experimentally the dependence of the magnitude of the effect on absorber thickness. Formula (6) contains two unknown parameters (f' and κf), so it is convenient to make a comparison with experiment of the ratio $\epsilon(0, n)/\epsilon(0, n_0)$, where n_0 is some fixed value of n.

Formula (5) enables us to compute the shape of the experimentally measured absorption spectrum. In particular we can find the width of the line in the resonance absorption spectrum as a function of the absorber thickness. For sufficiently thin absorbers ($C \ll 1$) the line width at half maximum is equal to 2Γ; with increasing absorber thickness the line width increases because of the effect of saturation. The natural width of the level can be found by extrapolating to zero thickness or by making corrections to the observed width in accordance with formula (5); in the latter case a prior determination of f' is required.

If the source contains nuclei of the isotope whose resonance absorption is being investigated, formulas (5) and (6) are not exact, since the emission spectrum will be distorted because of self-absorption and cannot be represented by formula (4). It is easy to show that in this case the distribution function for the emission spectrum will have the form (for v = 0):

$$W_e(E) = \text{const}\cdot\frac{1 - \exp\left[-\left(\frac{\mu d_0 + C + \mu d_0 x^2}{1 + x^2}\right)\right]}{\mu d_0 + C + \mu d_0 x^2}, \quad (7)$$

where $C = \sigma_0 f' n$, d_0 is the source thickness and μ is the coefficient of nonresonant absorption. We note that the function (7) practically coincides with expression (4) when v = 0, if we simply replace the natural width Γ by a width Γ_{eff}, which is larger than Γ. So for practical computations

formula (7) can be written in the form

$$W_e(E) = b\frac{\Gamma}{2\pi}\frac{1}{b^2(E-E_0)^2+\Gamma^2/4}, \qquad (8)$$

where $b = \Gamma/\Gamma_{eff}$. The parameter b can be calculated for different values of f′ by using formula (7).

If the nucleus has electric or magnetic moments (in its ground or excited states), then as a result of interaction with external or crystalline fields the emitted line, the absorption line or both may be split into a number of components. In this case the results obtained above cannot be used directly since every splitting causes a change in the form of the functions $\sigma(E)$ and $W_e(E)$.

The simplest case is that in which the emission line is split into a number of components with relative intensities J_i ($\Sigma J_i = 1$), while the absorption line is unsplit. From formula (2) it immediately follows that in this case the magnitude of the effect can be represented as a sum of terms like (2), each of which enters with weight J_i. The presence of a shift between the i-th component of the emission line and the absorption line must be taken into account by an appropriate choice of the form of the function $W_e(E)$. It is easy to see that for the case of such a splitting the magnitude of the effect can be written in the form

$$\varepsilon(v) = \sum_i J_i \varepsilon(\delta_i), \qquad (9)$$

where δ_i is the shift between the i-th component of the emission spectrum and the absorption line, for a given relative velocity of source and absorber.

The computation is more difficult for the case where the absorption line is split. Then the function $\sigma(E)$ splits into a sum of terms: $\sigma(E) = \Sigma_i J_i \sigma(E + \delta_i)$, where J_i is the relative intensity of the i-th component in the absorption spectrum, and δ_i is the shift between the emission line and the i-th component of the absorption line. Since the function $\sigma(E)$ is in the exponent of the formula (2), in this case the expression for the magnitude of the effect cannot be written as a sum of terms, as we did above. The computation of the quantity $\epsilon(v)$ can be done only by numerical integration.

Let us consider in more detail the case of quadrupole splitting of the absorption line for the case of Sn^{119}. The interaction of the nuclear quadrupole moment with the electric field gradient $q_{ij} = \partial^2 V/\partial x_i \partial x_j$ is described by the Hamiltonian

$$\mathcal{H} = \frac{eQ}{2I(2I-1)}\sum_{i,j} q_{ij} I_i I_j,$$

where Q is the nuclear quadrupole moment and I is the nuclear spin operator. As a result of such an interaction, the excited state of the Sn^{119} nucleus (which has spin $3/2$) splits into two sublevels, which are degenerate in the sign of the spin projection; their separation is

$$\Delta = \tfrac{1}{2} e^2 Q q_{zz}\left(1 + \tfrac{1}{3}\eta^2\right)^{1/2}, \qquad (10)$$

where the asymmetry parameter $\eta = (q_{xx} - q_{yy})/q_{zz}$.

The ground state of Sn^{119} (with spin $1/2$) is not split by quadrupole interaction. Consequently the absorption spectrum should consist of two lines, of equal intensity, whose separation is given by formula (10). Let us find the expression for the magnitude of the effect for the case where, at a given velocity v_0, the unsplit emission line exactly overlaps one of the two components of the absorption line. Using formulas (2) and (5) one can easily show that in this case the magnitude of the effect is

$$\varepsilon(v_0) = \varkappa f\left(1 - \frac{1}{\pi}\int_{-\infty}^{+\infty} \frac{\exp\left\{-\frac{C}{2}\left(\frac{1}{1+x^2} + \frac{1}{1+(x+y)^2}\right)\right\}}{1+x^2}\,dx\right), \qquad (11)$$

where x has the same meaning as in (5), and $y = \Delta(\Gamma/2)^{-1}$. The integral in (11) was calculated by numerical integration for different values of the parameters C and Δ. The results were used for determining the values of f′ for cases of quadrupole splitting of the absorption line.

3. DESCRIPTION OF THE EXPERIMENT

Measurements of the dependence of the resonance absorption effect on the relative velocity of source and absorber (the resonance absorption spectrum) were made with an apparatus whose principle of operation was described briefly earlier.[8] An overall view of the arrangement (omitting the electronics) is shown in Fig. 1. The absorber 9 moved relative to the fixed source 5, where the absorber velocity changed linearly with time between given limits (from $-v_0$ to $+v_0$, where v_0 is the maximum velocity). The absorber velocity was produced by rotation of the cam 2, whose profile was cut to correspond to a linear variation of velocity. The rate of rotation of the cam (and consequently the limits of variation of the absorber velocity) could be changed by a system of gears and pulleys. The cam set in motion a rod to which the frame-holder 4 of the absorber was attached.

The source was at room temperature in all the measurements. In many of the measurements the absorbers were cooled with liquid nitrogen or dry ice; in these cases the absorbers were placed in a

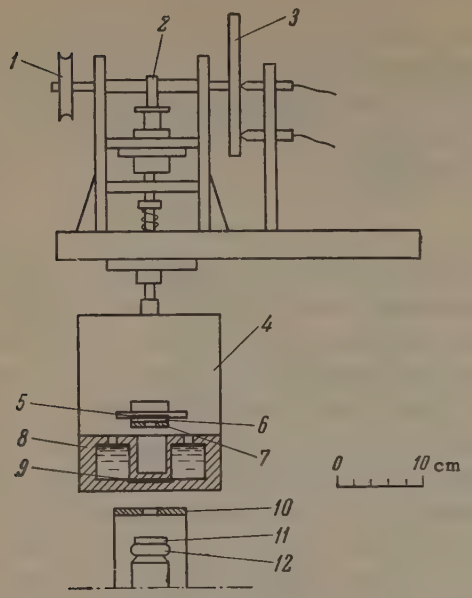

FIG. 1. Schematic diagram of apparatus for measuring reasonance absorption spectra: 1 – pulley, 2 – cam, 3 – contact disc for amplitude modulation circuit, 4 – absorber holder, 5 – source, 6 – palladium filter, 7 – lead collimator, 8 – low-temperature styrofoam vessel, 9 – absorber, 10 – lead collimator, 11 – NaI(Tl) crystal, 12 – photomultiplier.

low-temperature vessel 8 of styrofoam. The construction of the container was such that a γ quantum on its path to the counter encountered no liquid nitrogen but only styrofoam, which absorbs the 24 kev γ quanta weakly. The x rays of tin are practically completely absorbed by the 0.6 mm thick characteristic filter 6 of palladium.

Gamma quanta passing through the absorber were recorded by a NaI(Tl) crystal 1.5 mm thick and a FÉU-11 photomultiplier. The amplified pulses entered a single-channel pulse analyzer, whose window was set on the 24 kev photopeak. Separate recording of counts of γ quanta for different absorber velocities was accomplished by linear (in time) amplitude modulation of the pulses. The pulses from the output of the single-channel analyzer entered a gating circuit at whose other input a modulating voltage was applied which increased linearly in time in synchronism with the change in velocity of the absorber. The amplitude-modulated pulses entered a 100-channel AI-100 pulse analyzer. The period of variation of the modulation voltage was exactly equal to the period of rotation of the cam; thus there was a one-to-one correspondence between absorber velocity and amplitude of the output pulse, which enabled us to measure the whole absorption spectrum simultaneously, i.e., the dependence of the resonance absorption effect on velocity over the whole selected range of velocities. In the present work measurements were made for three different values of the maximum velocity: 2.5, 5, and 6.5 mm/sec.

A source in the form of SnO_2 was prepared from metallic tin, enriched to 92% of Sn^{118} and then irradiated with thermal neutrons in a reactor.

The powder of irradiated tin was then oxidized by heating to form SnO_2; at the beginning the SnO_2 is formed mainly in an amorphous state. After a long period of baking (ten days) at a temperature $\sim 700°$ C a transformation of the SnO_2 to the metallic state occurs. The source thickness was 6 mg/cm^2.

As was already mentioned earlier, for the SnO_2 crystal the probability of recoilless emission of γ quanta is already reasonably large at room temperature. There is no quadrupole splitting of the emission line for the SnO_2 crystal. Thus the source of Sn^{119m} in the form of tin dioxide is convenient for the investigation of the resonance absorption of 23.8-kev γ quanta by Sn^{119} and has definite advantages over, for example, the source of white metallic tin previously used by us.[8,9]

Absorbers of white metallic tin were prepared by rolling tin foil or by depositing tin on an organic backing in vacuum. Absorbers of SnO_2, SnO and $SnNb_3$ were prepared by precipitating powders on a thin aluminum foil.

4. RESULTS OF EXPERIMENT

In all the measurements, the $Sn^{119m}O_2$ source was at room temperature, while the absorbers were either at room temperature or at liquid nitrogen temperature or (for the white tin absorbers) at dry ice temperature.

SnO_2. The measurements of the resonance absorption spectrum for a SnO_2 polycrystal were done with absorbers of seven different thicknesses in the range from 4.2 to 37 mg/cm^2. In Fig. 2 we show one of these spectra, for an absorber thickness of 9.4 mg/cm^2 at room temperature. For each of the measured spectra we determined the

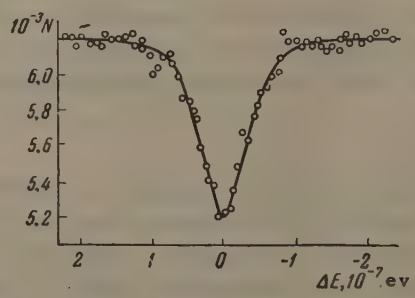

FIG. 2. Resonance absorption spectrum for an SnO_2 absorber. The abscissa is $\Delta E = E_0 v/c$ (where $E_0 = 23.8$ kev and v is the absorber velocity). Positive values of ΔE correspond to motion of the absorber toward the source. The ordinates give the number of quanta passing through the absorber, which is proportional to the number N of quanta recorded.

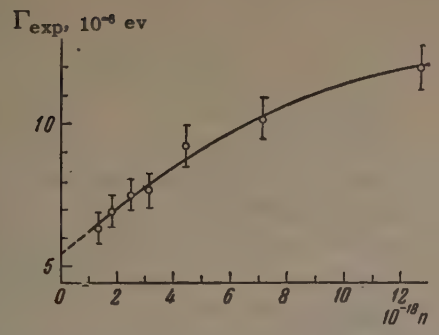

FIG. 3. Dependence of width of absorption line Γ_{exp} on absorber thickness. The abscissa gives the number of atoms containing the Sn^{119} isotope per cm^2 of absorber.

width of the absorption at half height Γ_{exp} and the maximum value of the resonance absorption effect $\epsilon(0)$.

The dependence of the line width of the absorption spectrum on absorber thickness is shown in Fig. 3. Extrapolation to zero absorber thickness gives the value $(5.5 \pm 0.5) \times 10^{-8}$ ev. This is equal to the sum of the natural width Γ and the width of the line in the emission spectrum. A computation shows that for the source which we used (containing 2.3% of Sn^{119}) the broadening of the line in the emission spectrum is only 12%. Thus we get for the natural width of the 23.8 kev excited state of Sn^{119} the value

$$\Gamma = (2{,}60 \pm 0{,}25) \cdot 10^{-8} \text{ ev},$$

which is in good agreement with the value found earlier by a delayed coincidence method.[11]

The probability for recoilless absorption of the γ quanta, f', was determined for the SnO_2 crystal from the dependence of $\epsilon(0)$ on absorber thickness. From formula (6), for different values of f' we can calculate the dependence on n of the ratio $\epsilon(0,n)/\epsilon(0,n_0)$. To improve the accuracy and reliability of the results, we took for n_0 in turn the thicknesses of all the seven absorbers which we used. In Fig. 4, the dependence is shown for $n_0 = 1.45 \times 10^{18}$ (4.2 mg/cm^2).

The average value of f' for the SnO_2 crystal at room temperature was found to be 0.7 ± 0.1. With the absorber cooled to liquid nitrogen temperature, the value of f' is close to unity. Knowing the value of f' enables us to determine the parameter κf [cf. formula (6)] for the source. It was equal to 0.25 ± 0.02. The parameter κf was much less than unity, mainly because the source radiation contained x rays of indium produced from decay of the long-lived isotope Sn^{113}. Since this parameter is practically independent of the form of the absorber, this value can now be used for determining f' for the other crystals.

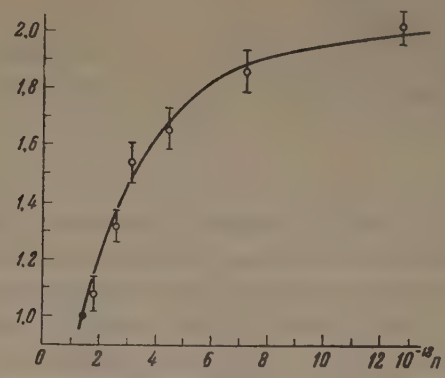

FIG. 4. Dependence of maximum value of resonance absorption effect $\epsilon(0)$ on thickness of SnO_2 absorber. The abscissa is the number of atoms containing the Sn^{119} isotope per cm^2 of absorber. The ordinate is $\epsilon(0,n)/\epsilon(0,n_0)$, where $n_0 = 1.45 \times 10^{18}$. The solid curve was calculated theoretically for $f' = 0.7$.

SnO. Resonance absorption spectra for a SnO polycrystal were measured with absorbers of various thicknesses in the range from 4.8 to 27 mg/cm^2, at liquid nitrogen temperature and at room temperature. Two of these spectra are shown in Fig. 5. Both spectra have a doublet structure, corresponding to a splitting of the absorption line in the SnO crystal into two components. Such a splitting can be interpreted as the result of the interaction of the quadrupole moment of the Sn^{119} nucleus in its excited state with the electric field gradient in the SnO crystal. The center of the absorption line is shifted toward positive energies relative to the emission line.

It is apparent that changes of temperature have little effect on the appearance of the absorption spectrum (in contrast to the case of white tin, which will be considered later). The value of the shift of the absorption line in the SnO crystal relative to the energy of the emission line in an SnO_2

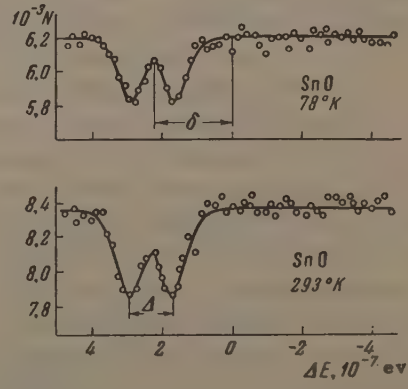

FIG. 5. Absorption spectrum for SnO crystal. The upper figure is for a 4.8 mg/cm^2 absorber at liquid nitrogen temperature. The lower is for a 15 mg/cm^2 absorber at room temperature.

crystal is equal to $+(22 \pm 2) \times 10^{-8}$ at 78°K and $(21.5 \pm 1.5) \times 10^{-8}$ ev at 293°K. The values of the quadrupole splitting Δ are equal to $(12.5 \pm 1.5) \times 10^{-8}$ ev at 78°K and $(11.0 \pm 1.5) \times 10^{-8}$ ev at 293°K.

The probability f′ for recoilless absorption of γ quanta by the SnO crystal was determined from the dependence of the magnitude of the effect on absorber thickness. The experimental values of the effect were compared with those computed for different values of f′ according to formula (11). We found a value of 0.47 ± 0.07 at liquid nitrogen temperature and 0.15 ± 0.05 at room temperature.

β-Sn. The resonance absorption of 23.8 kev γ quanta by Sn^{119} nuclei in a polycrystal of white tin (β-Sn) was first observed in the work of Lyubimov and Alikhanov[12] and of Barloutaud et al.[13] In our previous work,[8,9] in which we used a source of Sn^{119m} in the form of a β-Sn polycrystal, we showed that at liquid nitrogen temperature the absorption line (or the emission line) in a β-Sn crystal is split by the quadrupole interaction into two components whose separation Δ is equal to $(11.0 \pm 1.5) \times 10^{-8}$ ev.

The observation of the quadrupole splitting with source and absorber in the form of polycrystals of β-Sn presents considerable difficulties. The structure of the absorption spectrum is well resolved only if one uses a source and absorber which are thin (in the Sn^{119} isotope). If this is not the case, the broadening of the emission line in the source because of self-absorption and of the absorption line because of saturation prevents a satisfactory separation of the side maxima from the central absorption maximum, which has an amplitude twice that of the side maxima.

The effect of absorber thickness on the shape of the absorption spectrum for this case is graphically illustrated by Fig. 6, in which are shown absorption spectra in a β-Sn crystal at liquid nitrogen temperature, obtained with a source of white metallic tin, which was also at liquid nitrogen temperature. Despite the fact that the source was very thin (9 mg/cm², content of Sn^{119} isotope equal to 2.3%), for an absorber thickness of 31.3 mg/cm² the side maxima are poorly resolved from the central one. The considerable broadening of the line may explain the result of Picou et al.,[14] who used relatively thick sources and absorbers and did not observe any quadrupole splitting in β-Sn at liquid nitrogen temperatures.

The use of an Sn^{119m} source in a polycrystal of SnO_2, in which there is no quadrupole splitting of the line, considerably simplifies the problem of investigating the hyperfine structure of the absorption line in the β-Sn crystal, though even in this case the source and absorber must be sufficiently thin.

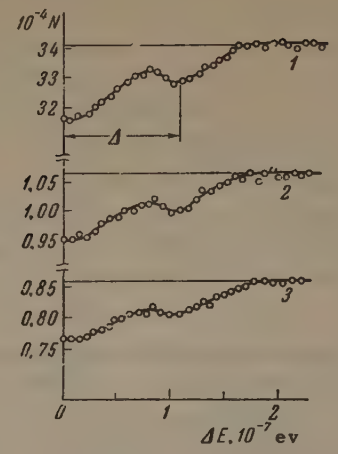

FIG. 6. Resonance absorption spectrum for a β-Sn crystal, obtained with a source of Sn^{119m} in the form of white metallic tin. The absorber thicknesses were: 1 – 5 mg/cm², 2 – 14.4 mg/cm², 3 – 31.3 mg/cm². The spectra are symmetric about zero velocity, so the figure shows only the half of the spectrum for positive velocities.

The measurements of the resonance absorption spectrum for a β-Sn polycrystal were done with absorbers of varying thickness in the range from 5 to 50 mg/cm² of natural tin, at liquid nitrogen temperature, dry ice temperature and room temperature. The main results of these measurements were discussed in our previous paper,[15] where we gave the resonance absorption spectra. It was shown that the quadrupole splitting Δ in the β-Sn crystal depends strongly on temperature. We found the following values for Δ: $(11.1 \pm 1.5) \times 10^{-8}$ ev at liquid nitrogen temperature, $(8.0 \pm 1.6) \times 10^{-8}$ ev at dry-ice temperature and $(4.6 \pm 1.5) \times 10^{-8}$ ev at room temperature.

Thus, with increasing temperature the value of the quadrupole interaction decreases, and at room temperature the splitting Δ does not exceed the line width in the absorption spectrum (5×10^{-8} ev) even for a thin source and absorber. In this case one can only judge the quadrupole interaction from the considerable broadening of the line in the absorption spectrum. This fact may explain the results of Boyle et al.,[16] who observed no splitting of the line from β-Sn with the absorber at room temperature. In their work they used a thick source for which the width of the emission line was twice the natural width; under such conditions of measurement, the quadrupole splitting of the line could not be seen.

The probability of recoilless absorption of γ quanta, f′, was determined for the β-Sn crystal by the method discussed above for the case of the

SnO crystal. For f′ at liquid nitrogen temperature we obtained the value 0.4 ± 0.1, which is in good agreement with the value of 0.36, found by Picou et al.[14] The determination of f′ at room temperature for the case of β-Sn is difficult, because at this temperature the hyperfine structure components are not resolved and the magnitude of the quadrupole interaction is not determined sufficiently accurately. From an analysis of the line shape in the absorption spectrum and of the dependence of the magnitude of the effect on absorber thickness, we found for f′ at room temperature a value of the order of 0.1. Picou et al.[14] found a value 0.04 ± 0.01 for f′ at room temperature, but they did not take into account the change in the quadrupole splitting of the absorption line with temperature.

$SnNb_3$. We have shown previously[8] that there is no quadrupole splitting of the absorption line in the $SnNb_3$ crystal and that at liquid nitrogen temperature the energy of the γ transition in the $SnNb_3$ crystal is close to the energy in a crystal of white tin. Resonance absorption spectra obtained with the absorber temperature equal to that of liquid nitrogen and room temperature, respectively, are shown in Fig. 7. A striking feature is the considerable reduction in the energy of the γ transition with increasing temperature of the crystal. The shift in energy of the γ transition in the $SnNb_3$ crystal is equal to $+(15 \pm 2) \times 10^{-8}$ ev at liquid nitrogen temperature and $+(11 \pm 2) \times 10^{-8}$ ev at room temperature. The values of f′ were determined from the dependence of the magnitude of the effect on absorber thickness, and were equal to 0.3 ± 0.1 at liquid nitrogen temperature and 0.06 ± 0.02 at room temperature.

5. DISCUSSION OF RESULTS

The results of our measurements of the resonance absorption spectra of the 23.8 kev γ quanta

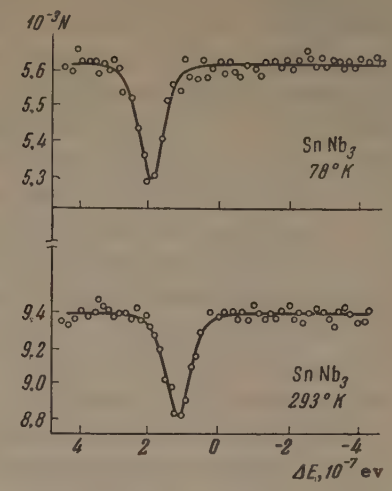

FIG. 7. Absorption spectra of $SnNb_3$ crystal. Upper figure – 26 mg/cm² absorber at liquid nitrogen temperature; lower figure – 62 mg/cm² absorber at room temperature.

by Sn^{119} nuclei in crystals of SnO_2, SnO, β-Sn and $SnNb_3$ are given in the table.

The values found for the probability of absorption of γ quanta without loss of energy to recoil vary over quite a wide range for the various crystals. It is not possible at present to make a detailed comparison of the experimentally determined values of f′ with the theoretical computations, since such computations can be carried out only if one knows the phonon spectrum of a real crystal. Computations on the Debye approximation are certainly only a rough approximation; the Debye temperature cannot in general serve as a parameter to determine the probability of the Mössbauer effect.[3] For example, on the Debye approximation one cannot explain the low value of f′ for the $SnNb_3$ crystal and the extremely high value for the SnO_2 crystal.

Such an approximation might be reasonable for the monatomic β-Sn crystal; but the known values of the Debye temperature of tin, as found from specific heat measurements, give considerably

Quantity*		SnO_2	SnO	β-Sn	$SnNb_3$
f′	78°K	~1	0,47±0,07	0,4±0,1	0,3 ±0,1
	293°K	0,7±0,1	0,15±0,05	~0,1	0,06±0,02
$\delta, 10^{-8}$ ev	78°K	⩽2	22±2	20,0±1,5	15±2
	293°K	0,0	21,5 ±1,5	19,5±1,0	11±1
$\Delta, 10^{-8}$ ev	78°K	0	12,5 ±1,5	11,0±1,5	0
	194°K	—	—	8,0±1,6	—
	293°K	0	11,0 ±1,5	4,6±1,5	0

*f′ is the probability of recoilless absorption of γ quanta, δ is the shift of the γ transition energy relative to the transition energy in the SnO_2 crystal, Δ is the quadrupole splitting. For the SnO and β-Sn crystals, δ was determined from the position of the "center of gravity" of the split line.

greater values of f' than the experimental value. Mitrofanov and Shpinel'[17] measured the temperature dependence of the resonance absorption effect for the β-Sn crystal; the dependence is not in agreement with that computed theoretically on the Debye approximation. Agreement could be obtained if one assumed that the Debye temperature of the β-Sn crystal changes from 180° at liquid nitrogen temperature to 165° at temperatures above 200° K. But these values of the Debye temperature lead to values of f' which are far greater than the value of f' found in the present work. Furthermore, the relative change in the magnitude of the effect with temperature which they found is in agreement with the change in the value of f' found in the present work.

The lattices of the β-Sn and SnO crystals are tetragonal, and in both crystals the tin atoms do not have spherically symmetric surroundings. In such lattices we may expect considerable electric field gradients at the tin nuclei, and this is confirmed by the observed quadrupole splitting in these crystals. The $SnNb_3$ crystal has a lattice like that of β-tungsten, which is very close to cubic; in such a lattice one should not find any sizable quadrupole splitting. The SnO_2 lattice is not cubic, but in this lattice the surroundings of the tin atom should be much more symmetric than they are in β-Sn and SnO, which is probably the reason for the absence of a quadrupole splitting in the SnO_2 crystal. Unfortunately it is not possible at present to make a sufficiently exact calculation of the electric field gradients in the β-Sn and SnO crystals and thus to determine the quadrupole moment of the Sn^{119} nucleus in the excited state.

The observed changes in energy of the γ transition for the different crystals (the values of δ in the table) can be explained very naturally as the result of the interaction of the nucleus with the outer electrons (mainly with s-electrons), which is different for the ground and excited states of the nucleus and changes according to the chemical surroundings of the tin atom in the crystal (the isomer shift).[9,18,19] The value of the shift should be proportional to the product $\Delta\langle R^2\rangle \cdot \Delta\rho_e(0)$, where $\Delta\langle R^2\rangle$ is the change in the square of the effective radius of the nucleus when we go from the ground state to the excited state and $\Delta\rho_e(0)$ is the change in the electron density in the neighborhood of the nucleus when we change the chemical environment of the tin atom in the crystal. The theoretical calculation of the interaction of the nucleus and the electrons requires a knowledge of the electron wave functions for atoms in crystals; such calculations would enable us to get additional information concerning the charge distribution in the nucleus and its change when the nucleus is brought to the excited state.

The influence of the temperature on the hyperfine structure of the γ radiation and on the energy of the γ transition is an extremely interesting effect. When the crystal temperature changes there is a change in the amplitude of thermal vibration and a change in the interatomic spacings; as a consequence we may expect a change in the electric field gradient at the nucleus and a change in the interaction of the nucleus with the outer electrons in the crystal. Other factors, such as pressure, can also have an analogous effect. Such effects can be calculated in principle (cf., for example,[20]). A comparison of the theoretical computations with experimental data would also be very interesting for this case.

The authors thank N. E. Alekseevskii for useful discussions.

[1] R. L. Mössbauer, Z. Physik **151**, 124 (1958).

[2] W. E. Lamb, Phys. Rev. **55**, 190 (1939).

[3] Yu. M. Kagan, Reports of the All-Union Conference on Nuclear Spectroscopy, Riga, 1961.

[4] W. Visscher, Ann. Phys. **9**, 194 (1960).

[5] H. J. Lipkin, Ann. Phys. **9**, 332 (1960).

[6] F. L. Shapiro, UFN **72**, 685 (1960), Soviet Phys.-Uspekhi **3**, 881 (1961).

[7] E. Cotton, J. phys. radium **21**, 265 (1960). G. N. Belozerskii and Yu. A. Nemilov, UFN **72**, 433 (1960), Soviet Phys.-Uspekhi **3**, 883 (1961). R. L. Mössbauer, UFN **72**, 657 (1960), Soviet Phys.-Uspekhi **3**, 866 (1961). R. V. Pound, UFN **72**, 673 (1960), Soviet Phys.-Uspekhi **3**, 875 (1961). F. L. Shapiro, UFN **72**, 685 (1960), Soviet Phys.-Uspekhi **3**, 881 (1961).

[8] Delyagin, Shpinel', Bryukhanov, and Zvenglinskii, JETP **39**, 220 (1960), Soviet Phys. JETP **12**, 159 (1961).

[9] Bryukhanov, Delyagin, Zvenglinskii, and Shpinel', JETP **40**, 713 (1961), Soviet Phys. JETP **13**, 499 (1961).

[10] R. L. Mössbauer and W. H. Wiedemann, Z. Physik **159**, 33 (1960).

[11] Olsen, Mann, and Lindner, Phys. Rev. **106**, 985 (1957).

[12] V. A. Lyubimov and A. I. Alikhanov, Izv. AN SSSR, ser. fiz. **24**, 1076 (1960), Columbia Tech. Translation, p. 1084.

[13] Barloutaud, Cotton, Picou, and Quidort, Compt. rend. **250**, 319 (1960).

[14] Picou, Quidort, Barloutaud, and Cotton, preprint, 1960 (cf. also E. Cotton, J. phys. radium **21**, 265 (1960)).

[15] Shpinel', Bryukhanov, and Delyagin, JETP **40**, 1525 (1961), Soviet Phys. JETP **13**, 1068 (1961).

[16] Boyle, Bunbury, and Edwards, preprint, 1960.

[17] K. P. Mitrofanov and V. S. Shpinel', JETP **40**, 983 (1961), Soviet Phys. JETP **13**, 686 (1961).

[18] O. C. Kistner and A. W. Sunyar, Phys. Rev. Letters **4**, 412 (1960).

[19] DeBenedetti, Lang, and Ingalls, Phys. Rev. Letters **6**, 601 (1961).

[20] Kushida, Benedek, and Bloembergen, Phys. Rev. **104**, 1364 (1956).

Translated by M. Hamermesh
233

CATHODE SPUTTERING OF SINGLE-CRYSTAL BALLS

V. E. YURASOVA and I. G. SIROTENKO

Moscow State University

Submitted to JETP editor April 27, 1961

J. Exptl. Theoret. Phys. (U.S.S.R.) 41, 1359-1364 (November, 1961)

Single-crystal balls of copper, tungsten, chromium, iron, cobalt, and germanium and of indium-antimony alloy were bombarded with 1—10 kev krypton ions. The sputtered material was deposited on a spherical or a cylindrical surface, and the emission directions of sputtered particles were determined. Substances with diamond-type and face-centered cubic lattices were sputtered predominantly in the [110] and [100] directions, whereas for metals with body-centered cubic lattices the [111] and [100] directions were predominant. The deposited patches were more clearly defined than when plane single crystals are sputtered. Photometric measurements indicated that the density decreased from the center to the edge of a patch more rapidly than by a cosine law. The dependence of cathode sputtering anisotropy on crystal structure, atomic number, temperature, and sputtering coefficient is discussed.

INTRODUCTION

WHEN metal single crystals are bombarded with ions, sputtered material is concentrated on the collector in separate well-defined spots.[1] At ion energy close to threshold the spots are formed by atoms ejected only in close-packed crystallographic directions. With increasing ion energy the target material also begins to be sputtered in other directions.[2] For example, when the (111) plane of a face-centered lattice is sputtered the deposition pattern consists of six spots instead of the three spots observed at low energies. The three new spots are assigned by different authors to different directions: by Henschke[3] to the [112] direction, by Koedam and Hoogendoorn[4] to [114], and by the authors of [2] to [100].

The disagreement between the interpretations evidently results from the fact that the angles between the directions corresponding to different spots were not determined very accurately. The arrangement and shapes of the patches are affected by the position of the sample with respect to the collector, by the angle that the dominant sputtering direction makes with the ion beam (α_1) and with the sputtered plane (α_2), and also by effects arising when a small area to be sputtered is delimited by Aquadag or a mica diaphragm.

Some of the foregoing difficulties disappear when spherical single crystals are used and the sputtered material is deposited on a spherical collector. In this case all directions (whether close-packed or not) of particle ejection are equivalent with respect to the ion beam direction and the orientation of the target surface. The use of a spherical sample makes it unnecessary to limit the target area with a diaphragm. Also, it becomes possible to detect and index easily a considerably larger number of spots corresponding to definite crystallographic directions than for a plane target.

EXPERIMENTAL PROCEDURE

The cathode sputtering of single-crystal balls of copper, tungsten, chromium, iron, cobalt, and germanium and of an indium-antimony alloy was performed in a low-pressure plasma of high density (at a krypton pressure of $\sim 5 \times 10^{-3}$ mm Hg), with a current of 1—2 amp between the anode and cathode. Spherical samples with 3—6 mm diameters were mounted in the tube through a ground-glass joint and were surrounded by a spherical glass bulb with diameter from 18 to 35 mm. Samples introduced into the plasma in the manner of a Langmuir probe were maintained at a high negative voltage of from 1 to 10 kv. The current density to the sample was usually 5—7 ma/cm^2, and in some experiments reached 13—15 ma/cm^2. The sputtering time varied from a few minutes to two hours. Krypton ions always struck the target perpendicularly, since the thickness of the Langmuir sheath around the sample was less than the mean free path of bombarding ions.

Deposited spots were indexed according to their relative arrangement (pattern symmetry) and angles. For a known radius of the glass bulb the angles were determined from the separation of spots on the spherical surface of the bulb. Since spots on the spherical bulb could not be scanned photometrically, in some instances the glass spheres were replaced with mica cylinders, on which undistorted spots were deposited around the equator of the single-crystal ball. The mica was then unrolled and the spots were scanned photometrically.

Cathode sputtering as a function of temperature was studied as the balls were heated by the ion bombardment. The temperature of a ball was measured by comparing its glow with that of an adjacent tungsten filament 0.1 mm thick. The filament temperature was known from a calibration table as a function of current.

RESULTS

1. Sputtering of face-centered cubic single-crystal balls of Cu and β-Co. After a copper ball of 4-mm diameter had been sputtered for 15 minutes the glass collector of 35-mm diameter revealed well-defined equally spaced spots (Fig. 1a). The angles between all nearest directions of deposition were 60°, i.e., all spots represented sputtering in the [110] direction. When the sputtering period is a few times longer an additional series of spots is observed; these are considerably less defined and broader than those in the [110] direction. The directions of the new spots are 45° from the [110] direction; they therefore represent sputtering in the [100] direction (Fig. 1b). The spots in the [112] or [114] directions that are mentioned in [3] and [4] were not observed in the sputtering of a copper ball.

A similar pattern consisting of spots in the [110] direction was obtained by sputtering a face-centered β-Co single crystal, although the individual spots were considerably less well defined than in the case of Cu.

In the experiments with a copper ball it was noticed that patch size decreases as the collector approaches the ball, and that the patches can even become smaller than the diameter of the ball. Figure 2 shows spots on an unrolled cylindrical collector which had been positioned eccentrically with respect to the ball. The smallest spots, which were obtained at a distance of 6 mm from the Cu ball, had one-half the diameter of the latter. Somewhat larger spots were produced at 11 mm separation.

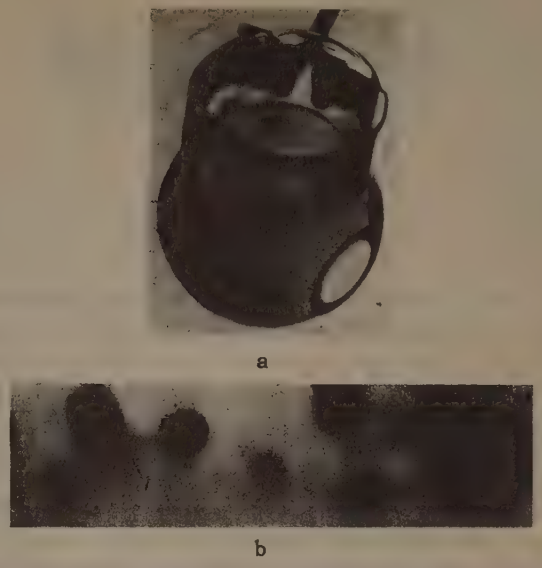

a

b

FIG. 1. a – spots formed on a spherical collector by sputtering a single-crystal copper ball; b – spots of sputtered copper on an unrolled cylindrical collector. Spot 1 corresponds to the [100] direction; the other spots correspond to [110].

The production of spots with diameters smaller than that of the target sphere evidently resulted from the fact that at incident ion energies greater than 1 kev perpendicular ejection from the surface is favored, all other conditions being equal, over oblique ejection. Therefore sputtering in a given crystallographic direction originates most efficiently on a small region of the spherical surface from which particles are ejected close to the normal.

Photometric scanning showed that on spots in the [110] direction, which were very much more clearly defined than when a plane was sputtered, the deposit density decreases from the center to the periphery considerably more rapidly than by a cosine law. The density distribution in the [100] direction is close to a cosine law.

2. Sputtering of body-centered cubic single-crystal balls of Fe, Cr, and W. Ion bombardment of Fe, Cr, and W balls resulted in identical patterns on a spherical collector. Each pattern consisted of two series of spots: a) small but very well defined spots separated by angles of 70° (the [111] direction), and b) larger and somewhat dif-

FIG. 2. Deposition pattern on an unrolled cylindrical collector that had been positioned eccentrically with respect to the copper ball.

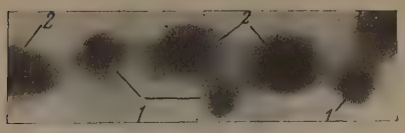

FIG. 3. Spots formed on a cylindrical collector by sputtering a single-crystal tungsten ball. Spot 1 corresponds to the [111] direction; spot 2 corresponds to [100].

fuse spots separated by 90° (the [100] direction). This difference between spots in the [111] and [100] directions appears in Fig. 3 and in the photometric curves 1 and 2 of Fig. 4. The most clearly defined pattern was obtained for W, and the least well defined for Fe.

Tungsten was sputtered at different temperatures. At 1300° C the spots were more sharply defined than when the target was heated to only 200 —300° by ion bombardment (curves 2 and 3 in Fig. 4). At higher temperatures two processes occur. First, various impurities are removed from the surface, thus enhancing the sharpness of the pattern; secondly, atomic oscillations around their equilibrium positions are intensified, thus impairing the sharpness of the pattern. At ~1300° the first process probably prevails in W.

3. Sputtering of single-crystal balls of Ge and InSb (diamond-type lattice). Wehner[1] has shown that when plane faces of a Ge single crystal are sputtered particles are ejected predominantly in the [111] direction. When we sputtered Ge balls, using a spherical collector, we observed spots in the [110] and [100] directions.

The same result was obtained when an indium-antimony alloy was sputtered (Fig. 5a), although spots in the [110] and [100] directions were more sharply defined than in the case of Ge sputtering.

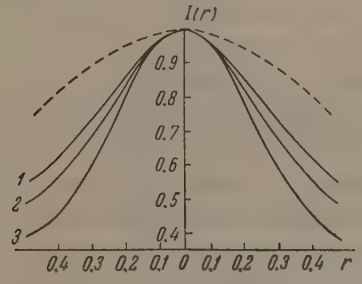

FIG. 4. Photometric density curves of separate spots produced by sputtering a single-crystal tungsten ball. Dashed curve — cosine law. Experimental curves for spots at 200°: 1 — in the [100] direction; 2 — in the [111] direction. At 1300°: 3 — in the [111] direction. The ordinate I(r) is proportional to the density at points of the collector, in relative units.[2] The abscissa is r = x/d, where x is the distance from the center of the spot to the given point in the scanning direction, and d is the distance between the target and collector. The same notation is used in Fig. 5b.

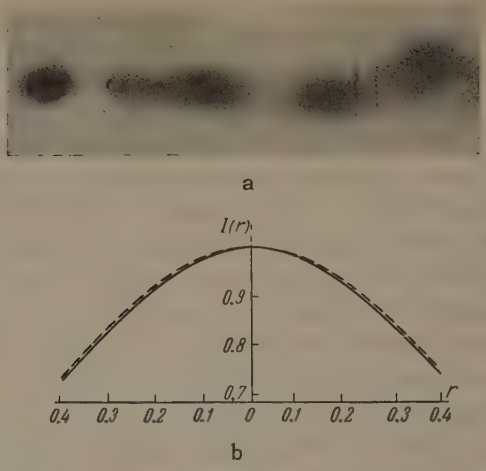

FIG. 5. a — spots in the [110] direction on a cylindrical collector, obtained by sputtering InSb; b — result obtained by photometric scanning of Fig. 5 a. The dashed curve represents a cosine law.

The pattern obtained from a diamond-type lattice is considerably less well defined than from body-centered and face-centered lattices. This could result from the fact that the lattice constant, and therefore the separation of neighboring atoms, in the predominant sputtering directions from the diamond-type lattices of Ge and InSb is considerably larger than in the case of the other metals. The density distribution of the deposit in the [110] direction for InSb is well fitted by a cosine law (Fig. 5b).

DISCUSSION OF RESULTS

The predominant crystallographic directions of single-crystal sputtering and a number of other characteristics are best accounted for by the focusing effect[5,6] arising in some instances of collisions between heavy particles (atoms or ions) in solid matter.

When a solid is irradiated with a stream of heavy particles (specifically, in ion bombardment) atoms of the target are displaced. The moving particles bring about displacements mainly through elastic collisions. Over a broad energy range of incident particles (up to several times ten kev for heavy atoms) the interaction between the incident particles and target atoms (and also the interaction between displaced and fixed atoms) can be calculated quite accurately using the model of elastic solid spheres.

The effective diameter r_0 of a solid sphere depends on the incident-particle energy E, and is determined from the expression for the potential V(r) describing the field due to the charges of the nuclei and electron shells of the interacting atoms. In the first approximation r_0 is deter-

mined from $V(r_0) = E/2$.[5] It is difficult to obtain an exact expression for $V(r)$. Bohr's analysis[7] gives

$$V(r) = \frac{z_1 z_2 \cdot e^2}{r} e^{-r/a}, \qquad (1)$$

where z_1 and z_2 are the charges of the moving and fixed nuclei, a is the screening constant, and r is the distance between the centers of the moving and the fixed particle. For the special case of copper bombardment Huntington[8] found that a good approximation of the potential is given by

$$V(r) = 0.038 \exp[-17.2(r-d)/d]\,\text{ev}, \qquad (2)$$

where d is the distance to the nearest neighboring atom which is in its equilibrium position.*

The equation $V(r_0) = E/2$ thus determines the effective diameter of a solid atomic sphere of copper for different ion energies. The results for some small values of E are given in the table, where d is taken to be the smallest distance between copper atoms in the [110] direction (2.55×10^{-8} cm).

E, ev	r_0, Å	d/r_0
11.6	2.23	1.41
50	1.57	1.80
100	1.51	1.69
400	1.28	1.99

Silsbee's analysis[5] shows that in some instances where r_0 is close to d and where d is small (i.e., where d/r_0 exceeds unity by an insignificant amount), the moving particle transfers its momentum to the fixed atom in such a way that displacement occurs mainly along close-packed rows of the crystal lattice (the focusing effect). Silsbee's focusing condition is

$$1 < d/2 < 2 \qquad (3)$$

and is satisfied for copper atoms in the [110] direction when E is small. When (3) is fulfilled in the [110] direction for copper atoms, focusing in the [100] direction is impossible, according to Silsbee's theory, because a particle displaced in the latter direction must collide with an atom in a [110] row before it reaches an atom in the [100] row.

A more rigorous analysis, however, can also account for the experimentally observed focusing in the [100] direction. It has recently been shown[9,10] that when interactions between neighboring atoms are taken into account focusing is also possible (although less efficient) in directions other than those of close packing.

For body-centered crystals (3) ean also be fulfilled in the [100] direction, although not so well as in the close-packed [111] direction. Sputtering in the second most closely packed direction [100] is therefore probably more efficient for body-centered crystals than for face-centered crystals, as we have observed experimentally. The emission in the [110] and [100] directions from the diamond-type lattices of Ge and InSb is not accounted for by the focusing effect. Equation (3) is not fulfilled for either of these directions; otherwise the spheres of two neighboring atoms separated by the distance $a\sqrt{3/4}$ in the [111] direction would overlap. In this case, to account for focusing in the [110] and [100] directions we must use the more rigorous analysis of Vineyard et al.[10]

As already mentioned, the focusing effect is possible only at low energies of the moving particles. However, preferentially directed ejection from sputtered single crystals is also observed at high incident-ion energies of the order of several times ten kev.[2] Yet even at high primary energies most displacements of atoms from crystal sites are produced by slow particles, very many more of which are present in matter than fast particles.

Therefore even in the case of sputtering by fast ions directed ejection can result from the focusing effect.

Equation (1) shows that the effective radius r_0 of a solid sphere depends in general not only on E but also on the nuclear charges z_1 and z_2 of both the moving and fixed particles, respectively. r_0 increases with z_1 and z_2, so that the focusing condition should be satisfied best by substances with large values of z_2. This agrees with the experimental results for W and Cr sputtering. These two metals have approximately identical values of the sputtering coefficient N, but the lattice constant of W is larger than that of Cr. Nevertheless, the spot pattern for W is more clearly defined than for Cr. This can possibly be associated with the fact that the radius r_0 for W, all other conditions being equal, is considerably larger than for Cr (since $z_W > z_{Cr}$). A similar explanation is perhaps possible for the fact that InSb produces a clearer pattern than Ge, although in this case the results are also affected by the circumstance that N is larger for InSb than for Ge.

It appears from the experimental results that some relation exists between the magnitude of

*A potential similar to (2) can also be obtained for copper from (1), subject to the condition that r is close to d/2.[6]

the sputtering coefficient and the distinctness of spots for different substances. For example, Cr and Fe have identical lattice structures and very close values of both the lattice constant a and nuclear charge z_2. Yet $N_{Cr} > N_{Fe}$, and this can possibly account for the fact that the spot pattern is more clearly defined for Cr than for Fe. The same conclusion can be reached by comparing the sputtering patterns for face-centered cubic crystals (Cu and β-Co), which have close values of a and z_2. In this case $N_{Cu} > N_{Co}$ and therefore the spots are more clearly defined for Cu than for β-Co. For large values of N and at high ion current densities the surface layers of the target are removed more rapidly. This can possibly result in clearer sputtering patterns.

CONCLUSIONS

When face-centered metal lattices are sputtered by krypton ions having energies up to 10 kev, particles are ejected mainly in the close-packed [110] direction, and only to a very small extent in the [100] direction. For metals with body-centered lattices the [111] and [100] directions are predominant, and for diamond-type crystals the predominant directions are [110] and [100].

The patterns of sputtered deposits are most clearly defined for face-centered lattices and are least clear for diamond-type crystals. For the latter the density distribution in individual spots nearly obeys a cosine law, whereas for the former lattices the density decreases much more rapidly with increasing distance from the center of a spot.

When sputtered patterns are compared, a greater relative sharpness is found to accompany a larger sputtering coefficient, a larger atomic number, or a smaller lattice constant of the target (other conditions being identical). The definition is also improved by a temperature rise, within certain limits.

Many results can be accounted for by a focusing effect (according to Silsbee), which should occur under certain conditions if the interaction between moving and stationary atoms is regarded as a two-body collision of elastic solid spheres.

In conclusion the authors wish to thank Professor G. V. Spivak for a valuable discussion, and V. M. Bukhanov for experimental assistance.

[1] G. K. Wehner, Phys. Rev. 102, 690 (1956).
[2] Yurasova, Pleshivtsev, and Orfanov, JETP 37, 966 (1959), Soviet Phys. JETP 10, 689 (1960).
[3] E. B. Henschke, J. Appl. Phys. 28, 411 (1957).
[4] M. Koedam and A. Hoogendoorn, Physica 26, 351 (1960).
[5] R. H. Silsbee, J. Appl. Phys. 28, 1246 (1957).
[6] G. Leibfried, J. Appl. Phys. 30, 1388 (1959).
[7] N. Bohr, Kgl. Danske Videnskab. Selskab, Mat.-fys. Medd. 18, No. 8 (1948).
[8] H. B. Huntington, Phys. Rev. 91, 1092 (1953).
[9] Gibson, Goland, Milgram, and Vineyard, Phys. Rev. 120, 1229 (1960).
[10] Vineyard, Gibson, Goland, and Milgram, Bull. Am. Phys. Soc. 5, 26 (1960).

Translated by I. Emin
234

PRODUCTION OF N^{17} NUCLEI BY BOMBARDMENT OF SOME ELEMENTS WITH HEAVY IONS

G. N. FLEROV, V. V. VOLKOV, L. POMORSKI,* and J. TYS†

Joint Institute for Nuclear Research

Submitted to JETP editor May 9, 1961, resubmitted August 9, 1961

J. Exptl. Theoret. Phys. (U.S.S.R.) 41, 1365-1369 (November, 1961)

A new method of investigating the transfer reactions by detecting the delayed neutron activity is proposed. Li, C, Al, and Cu targets were bombarded with N^{15}, O^{16}, and Ne^{22} ions using the accelerator of the Joint Institute for Nuclear Research in Dubna. Production of N^{17} nuclei was observed in all cases. The cross sections for the production of N^{17} by bombarding the above-mentioned targets with 95 Mev N^{15} ions were measured, as well as the yield of N^{17} from thick C, Al, and Cu targets irradiated with O^{16} and Ne^{22} ions.

AMONG the many types of reactions involving heavy ions, those occuring in the peripheral collisions of the incident nuclei with those of the target are of special interest. A direct transfer of a single nucleon or even of a whole group of nucleons from one nucleus to the other, without passing through the stage of the compound nucleus, may occur in such collisions. Such reactions have lately been called transfer reactions. Since such processes occur on the surface of the nuclei, we can expect their study to reveal the state of the peripheral nucleons.

The capture of neutrons, protons, and α particles has been observed in a number of experiments.[1-13] The capture of two neutrons was observed in[14], and possibly in[15], and the transfer of larger fragments in[16].

The detection of β-active reaction products is usually employed in the study of transfer reactions. In the present experiment an attempt has been made to study transfer reactions by another experimental method.

1. PRINCIPLE OF THE METHOD

One of the possible transfer reaction products of the irradiation of nuclei by beams of various heavy ions is N^{17}, which emits delayed neutrons with a half-life of 4.15 sec.[17,18] This neutron activity, unique among all nonfissionable nuclei, enables us to overcome the problem of background radioactivity from other reaction products, which is especially important in the study of the reactions having a small cross section.

Other neutron-active nuclei can also be produced in the reactions, such as Li^9 ($T_{1/2}$ = 0.16 sec)[17] and C^{16} ($T_{1/2}$ = 0.74 sec).[19] However, in view of the marked difference in the half-lives, the identification is not difficult. Moreover, the proposed method enables us to find new nuclei emitting delayed neutrons.

The method was first proposed for studying the two-neutron capture by the N^{15} nucleus:

$$A_Z + N^{15} = (A-2)_Z + N^{17}.$$

However, from the experiment carried out, it is clear that the method can be successfully applied to the study of other transfer reactions as well.

2. APPARATUS AND PROCEDURE

The experiments were carried out using the internal beam of the heavy-ion cyclotron of the Joint Institute for Nuclear Research. Proportional BF_3 counters were used to detect the neutrons from the N^{17} nuclei. The counters were placed in a 140×250×340 mm lucite moderator (Fig. 1) with a hollow central part containing the target. The assembly was placed in a copper casing cooled by water. The casing also contained an emitter follower. A graphite beam collimator was placed before the casing, which helped to guide the beam to the casing. (The collimator is omitted in the figures.) Eight proportional counters 2 cm in diameter and 25 cm long were placed in two groups in the upper and lower parts of the assembly. Since all counters had practically identical characteristics, their cathodes were connected together and were supplied with the same high voltage.

*Center for Nuclear Studies, Krakow, Poland.
†Institute for Nuclear Research, Warsaw, Poland.

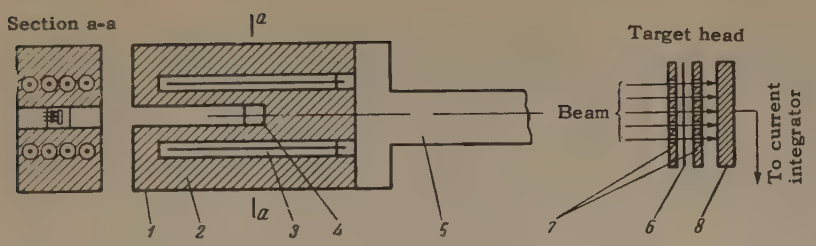

FIG. 1. General view of the detector: 1 – copper casing, 2 – lucite moderator, 3 – BF_3 counters, 4 – target head, 5 – probe support, 6 – aluminum foil, 7 – collimator grid, 8 – target current collector.

A block diagram of the apparatus is shown in Fig. 2. The pulse produced in any of the counters was fed to the emitter follower and transmitted to a linear amplifier and amplitude discriminator and to a 13-channel time analyzer. A scaler was connected in parallel to the analyzer. It was found by trial and error that the most satisfactory counter operation was at 3000 v, with an amplifier gain equal to 400 and a discriminator level of 25 v. Under these conditions, the efficiency of the detector amounted to 0.5% for the polonium-beryllium source in the position of the target. The background, in the presence of 2 mC of Co^{60}, amounted to 2 pulses per minute.

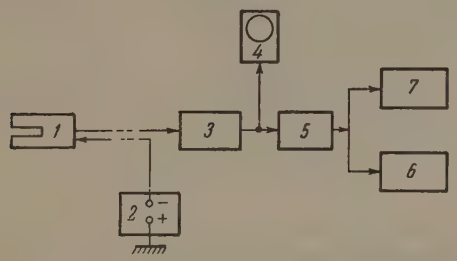

FIG. 2. Block diagram of the apparatus: 1 – neutron detector, 2 – high-voltage supply, 3 – linear amplifier, 4 – oscilloscope, 5 – amplitude discriminator, 6 – time analyzer, 7 – scaler.

Since the proportional neutron counters had to operate in the magnetic field of the cyclotron, a preliminary experiment was carried out to determine the influence of the magnetic field on their counting rate. It was found that a magnetic field perpendicular to the counter axis does not change its counting properties.

In order to test the method, thick targets of Li_2CO_3, aluminum, copper, and graphite were irradiated by $N^{15(3+)}$ ions and $O^{16(3+)}$ ions. The graphite was also irradiated by $Ne^{22(4+)}$ ions. The shape of the target is shown in Fig. 1.

In the irradiation of the aluminum and copper, all parts of the target head exposed to the beam were made of one material. In the irradiation of graphite with Li_2CO_3, a 15 μ aluminum foil was used to stop singly charged ions. In the two latter cases, the contribution from the "impurity" elements was estimated from the data obtained with aluminum and copper.

The beam intensity, measured using a current integrator, varied from 0.05 μa to 1 μa. The energy of the bombarding ions was determined from the beam radius. Pulsed operation of the cyclotron was employed in the measurements. Since the half-life of N^{17} is 4.15 sec, the target was irradiated for 30 sec. The high-frequency voltage on the dee was then switched off, and the neutron activity was counted for 30 sec.

At the moment the beam was switched off, the counter voltage was automatically switched on, and the time analyzer and scaler began counting. The counter voltage was removed when the beam was switched on.

For each value of ion energy, 4—5 irradiation cycles were carried out. Since the vertical distribution of the ion beam varied with the radius

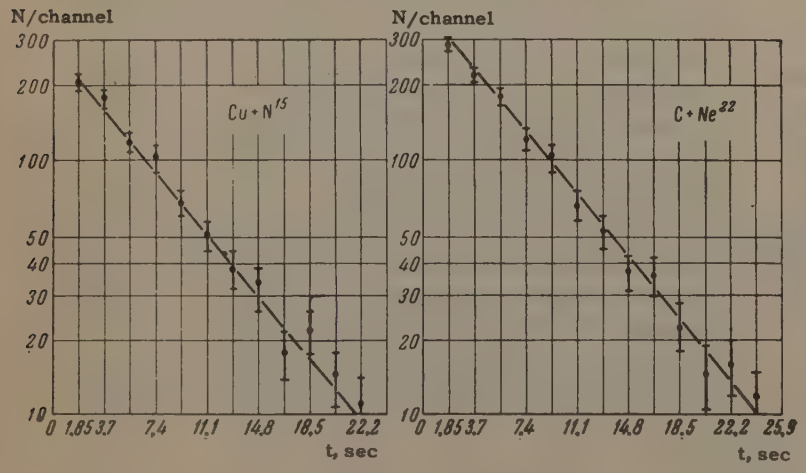

FIG. 3. Typical curves of neutron activity decay for the Cu + N^{15} and C + Ne^{22} reactions.

Table I. Effective cross section for the $N^{15} \rightarrow N^{17}$ reaction for 95 Mev energy of N^{15} ions, and the value of Q* for these reactions

Target	σ, mb	Q, Mev	Target	σ, mb	Q, Mev
Li_2CO_3	4	— 4.40**	Al	0.1	—16.05
Cu	1	−10.85*** / — 9.36	C	0.01	—23.69

*The Q values were calculated from the isotope masses using the Wapstra tables.[21]

**Q was calculated for Li^7, and the contribution of C and O was neglected.

***Q values for Cu^{63} and Cu^{65} respectively.

(influence of the magnetic focusing of the cyclotron), a graphite beam collimator was placed before the experimental assembly 24 cm ahead of the target (Fig. 1). The background measurements carried out showed that the yield from the graphite collimator amounted to not more than 10% of the effect when the whole beam fell only on the upper or lower part of the collimator. During irradiation, only a small part of the beam fell on the collimator, so that the background from the collimator could be neglected.

3. RESULTS OF THE MEASUREMENTS

A. Irradiation with N^{15} ions. In order to observe the two neutron-capture reactions, Li, C, Al, and Cu were irradiated. Lithium (natural isotope mixture) was used in the form of Li_2CO_3; the carbon target was made of pure graphite. In all cases, the onset of neutron activity was observed, which decreased with a half-life of 4 sec. A typical picture of the decay is shown in Fig. 3. The effective reaction cross section was calculated from the yield from a thick target (see Table I). The range of N^{15} necessary for this calculation was computed using formulas given by Northcliffe.[20]

Table II. Yield of N^{17} nuclei per bombarding particle in the irradiation of C, Al, and Cu targets by O^{16} ions of 95 Mev and Ne^{22} ions of 184 Mev

Target	Bombarding ion	
	O^{16}	Ne^{22}
C	$1 \cdot 10^{-10}$	$2 \cdot 10^{-8}$
Al	$5 \cdot 10^{-10}$	—
Cu	$6 \cdot 10^{-9}$	—

B. Irradiation with O^{16} and Ne^{22} ions. The onset of neutron activity with a 4-sec half-life was also observed upon irradiation of the above-mentioned targets with O^{16} ions and of a graphite target with Ne^{22} ions. The yields of these reactions are shown in Table II. It can be assumed that the N^{17} nucleus, in these cases, is produced as a result of reactions in which the O^{16} nucleus transfers a proton to the target nucleus and captures neutrons from it. The Ne^{22} nucleus transfers a proton and an α particle. The possibility cannot be excluded that N^{17} is produced on light nuclei as one of the decay fragments of a strongly excited compound nucleus.

To obtain a final answer to this question, additional and more detailed experiments are necessary. However, apart from the final solution of this problem, the results obtained show that the neutron activity of N^{17} can successfully be used for the study of a wide range of transfer reactions.

In conclusion, the authors consider it their pleasant duty to thank all members of the cyclotron team who ensured a trouble-free operation of the machine, and especially to Iu. Ts. Oganesyan, Yu. V. Lobanov, A. S. Pasyuk, B. N. Markov, I. A. Shelaev, and V. A. Shchegolev. We would also like to thank A. F. Linev and L. Kumpf for the design and construction of the time analyzer, and A. N. Filipson for testing the vacuum probe.

[1] K. F. Chacket and J. H. Fremlin, Phil. Mag. 45, 735 (1954).

[2] K. F. Chacket and J. H. Fremlin, Phil. Mag. 46, 1 (1955).

[3] A. Zucker and H. L. Reynolds, Phys. Rev. 94, 748 (1954).

[4] H. L. Reynolds and A. Zucker, Phys. Rev. 101, 166 (1956).

[5] Reynolds, Scott, and Zucker, Phys. Rev. 102, 237 (1956).

[6] Webb, Reynolds, and Zucker, Phys. Rev. **102**, 749 (1956).
[7] Halbert, Handley, Pinajian, Webb, and Zucker, Phys. Rev. **106**, 251 (1957).
[8] Volkov, Pasyuk, and Flerov, JETP **33**, 595 (1957), Soviet Phys. JETP **6**, 459 (1958).
[9] R. Kaufmann and R. Wolfgang, Phys. Rev. Letters **3**, 232 (1959); Phys. Rev. **121**, 198 (1961).
[10] M. L. Halbert and A. Zucker, Phys. Rev. **108**, 336 (1957).
[11] C. E. Anderson and W. J. Knox, Phys. Rev. Letters **3**, 557 (1959).
[12] McIntyre, Watts, and Jobes, Phys. Rev. **119**, 1331 (1960).
[13] Kenneth S. Toth, Phys. Rev. **121**, 1190 (1961).
[14] Karnaukhov, Ter-Akop'yan, and Khalizev, JETP **36**, 748 (1959), Soviet Phys. JETP **9**, 525 (1959).
[15] Alkhazov, Gangrskii, and Lemberg, JETP **33**, 1160 (1957), Soviet Phys. JETP **6**, 892 (1958).
[16] R. Kaufmann and R. Wolfgang, Phys. Rev. **121**, 192 (1961).
[17] Strominger, Hollander, and Seaborg, Revs. Modern Phys. **30**, 606 (1958).
[18] L. W. Alvarez, Phys. Rev. **75**, 1127 (1949).
[19] Hinds, Middleton, Litherland, and Pullen, Phys. Rev. Letters **6**, 113 (1961).
[20] L. C. Northcliffe, Phys. Rev. **120**, 1744 (1960).
[21] A. H. Wapstra, Physica **21**, 367 (1955).

Translated by H. Kasha
235

MAGNETIC RESONANCE OF F^{19} NUCLEI IN THE FERROELECTRIC SUBSTANCE $(NH_4)_2BeF_4$

G. M. MIKHAĬLOV, A. G. LUNDIN, and S. P. GABUDA

Physics Institute, Siberian Branch, Academy of Sciences, U.S.S.R.

Submitted to JETP editor May 16, 1961

J. Exptl. Theoret. Phys. (U.S.S.R.) 41, 1370-1374 (November, 1961)

A polycrystalline sample of ammonium fluoroberyllate was investigated from −183° C up to room temperature and a single crystal of $(NH_4)_2BeF_4$ was investigated at room temperature by means of magnetic resonance of F^{19} nuclei. Reorientation of $(BeF_4)^{2-}$ ions has been established above the ferroelectric Curie point at −97° C. Reorientation of $(BeF_4)^{2-}$ ions is shown to occur about an axis fixed with respect to the crystal structure and coincident with the c axis of the crystal. The height of the potential barrier for the reorientation of the BeF_4 group is 9.5 ± 0.4 kcal/mole.

THE method of nuclear magnetic resonance (n.m.r.) is a comparatively simple and convenient method for studying the position and the degree of mobility of nuclei in crystals. We have used the n.m.r. method to study a number of ferroelectrics [1-3] and in some cases we have established the existence of a correlation between the ferroelectric properties and the change in the degree of mobility of certain groups occurring in the structure of these ferroelectric substances.

In the present work we have used the method of magnetic resonance of F^{19} nuclei to investigate samples of ammonium fluoroberyllate $(NH_4)_2BeF_4$, the ferroelectric properties of which below −97° C have been discovered by Pepinsky and Yona. [4] We have studied the temperature dependence of the second moment of the n.m.r. absorption line in the temperature range from −183° C up to room temperature. This dependence is shown in Fig. 1. The second moment of the n.m.r. absorption line is determined by the crystal structure and can be calculated by means of Van Vleck's formula. [5] In the case of ammonium fluoroberyllate the second moment can be written in the form of the following sum:

$$S_2 = S_2^{F-F} + S_2^{F-F'} + S_2^{F-Be} + S_2^{F-H}. \quad (1)$$

Here the first term on the right represents the contribution to the second moment of the dipole-dipole interaction between the F^{19} nuclei in a BeF_4 group, the second term represents the contribution due to the interaction between the F nuclei of neighboring BeF_4 groups, the third term represents the contribution of the Be^9 nuclei, and the fourth term represents the contribution of the protons of the NH_4 groups.

In the case of a polycrystalline sample these terms depend on the distances between the nuclei and their direct calculation by means of Van Vleck's formula gives for a fixed position of the nuclei

$$S_2^{F-F} = 316{,}3 \cdot 10^{-48} \sum_i r_i^{-6}, \quad (2)$$

$$S_2^{F-Be} = 15.6 \cdot 10^{-48} \sum_j r_j^{-6}, \quad (3)$$

$$S_2^{F-H} = 155.0 \cdot 10^{-48} \sum_k r_k^{-6}, \quad (4)$$

where the subscripts i, j, k refer respectively to the distances from a given F nucleus to other fluorine nuclei belonging to the same BeF_4 group and to neighboring groups, from a given F nucleus to the beryllium nuclei, and from the F nucleus to the protons.

For the numerical evaluation of the second moment it was assumed that the BeF_4 group can be represented by a regular tetrahedron with the Be atom at the center, and that the F—F and the F—Be distance (cf. reference [6]) are respectively equal to 2.63 and 1.61 A. Since the complete structure of ammonium fluoroberyllate is as yet unknown, the calculation of the second and of the fourth terms in the sum S_2 presents certain difficulties. However, it is known that in general terms the structure of $(NH_4)_2BeF_4$ is close to the structure of the $(NH_4)_2SO_4$ crystal. Until very recently these structures were even considered to be isomorphic, but Pepinsky et al. [7] have shown

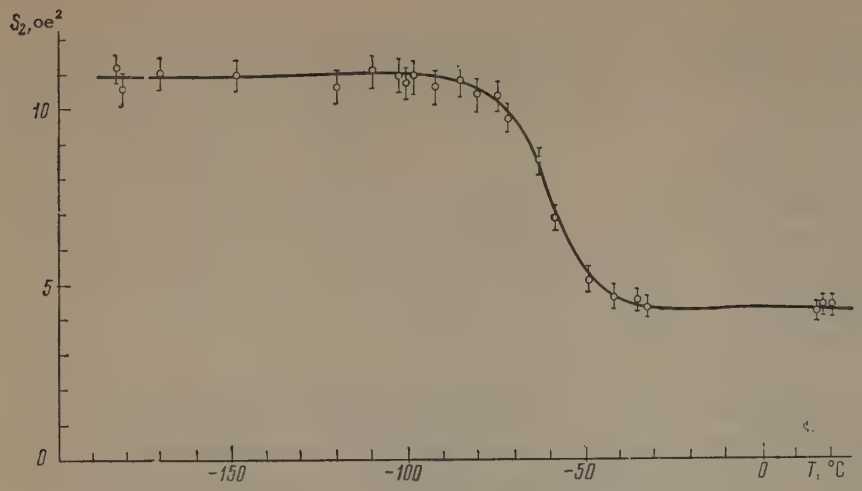

FIG. 1. Temperature dependence of the second moment of the magnetic resonance absorption line due to F^{19} nuclei in $(NH_4)_2BeF_4$.

that small differences between these structures exist even at room temperature. In carrying out the calculation it was assumed that the BeF_4 and NH_4 groups in ammonium fluoroberyllate are situated similarly to the SO_4 and NH_4 groups in the structure of $(NH_4)_2SO_4$. For this reason the calculation can be regarded only as a first approximation, particularly at low temperatures.

With respect to the NH_4 groups it was assumed that they undergo spherically isotropic reorientation within the whole range of temperatures studied. This follows from the experimental data of Blinc and Levstek[8] who drew this conclusion on the basis of studying $(NH_4)_2BeF_4$ by proton n.m.r. We have also observed proton resonance in $(NH_4)_2BeF_4$ at room temperature: the results obtained confirm the conclusion with respect to the isotropic reorientation of the NH_4 groups.

The results of the calculation are shown in the table. The calculations have been carried out for two cases. In the first case it was assumed that the BeF_4 groups are stationary—"rigidly" fixed in the structure, in the second case it was assumed that they undergo reorientation about axes fixed in the structure and coincident with the third order axes of the BeF_4 groups themselves. As can be seen from the table, the results of the calculation in the first case agree with the experimental values of the second moment in the range from −183° C to −100° C, and in the second case agree with the value of S_2 measured in the range from −20° C to +20° C. Therefore, the variation in the second moment within the range from −100° C to −20° C is a consequence of the usual rotational transition associated with a reorientation of the BeF_4 groups about fixed axes.

In order to answer the question as to the direction in the elementary crystal cell about which the BeF_4 groups undergo reorientation additional experiments were carried out on a single crystal sample of ammonium fluoroberyllate at room temperature. The sample was a crystal of 10×6×1.5 mm with well defined faces; the crystal axes were denoted by a, b, c, and their directions coincided with the directions of the axes of the elementary cell whose parameters are equal to a = 5.89 A, b = 10.39 A and c = 7.49 A.

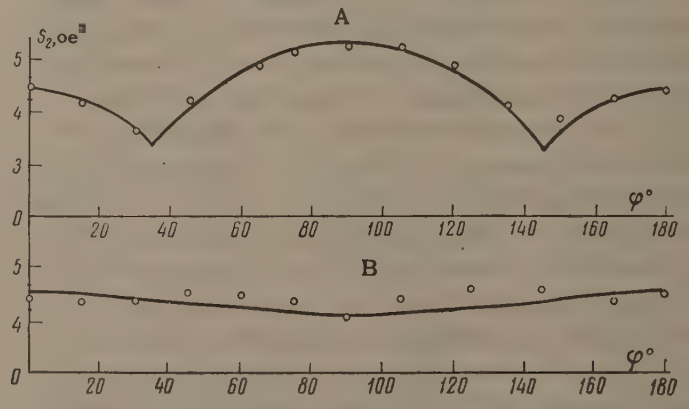

FIG. 2. Dependence of the second moment on the orientation of the single crystal of $(NH_4)_2BeF_4$ at t = 20°C: A – for a rotation about the a axis; B – for a rotation about the c axis. The angle φ is measured from the b direction.

BeF_4 groups	S_2^{F-F}	S_2^{F-Be}	$S_2^{F-F'}$	S_2^{F-H}	S_2	Experimental values of S_2	T, ° C
Stationary	2.835	0.90	0.10	6.25	10.1	11.0±0.5	to −183 from −100
Undergoing reorientation	0.71	0.25	0.03	3.10	4.1	4.2±0.2	to −20 from +20

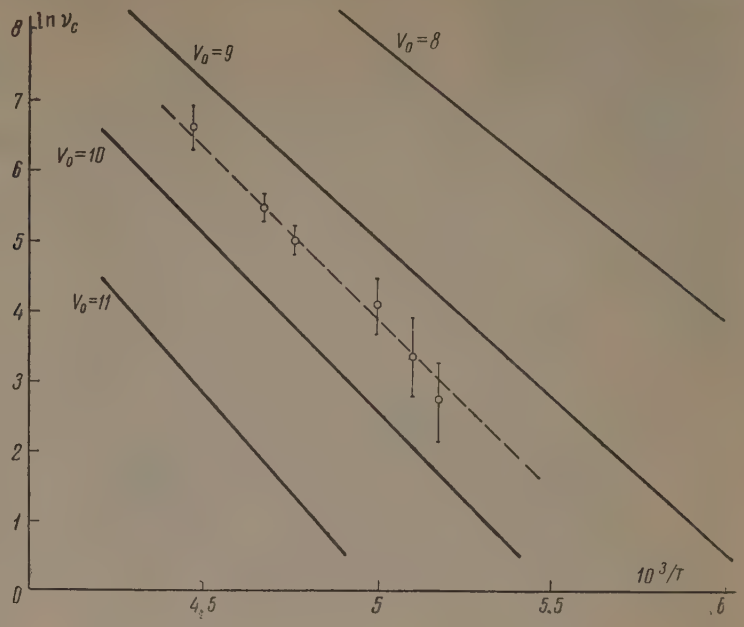

FIG. 3. Temperature dependence of the correlation frequency for the reorientation of the BeF_4 group in ammonium fluoreberyllate (the value of V_0 is given in kcal/mole).

We have studied the dependence of the second moment of the n.m.r. absorption line on the orientation of the crystal in a magnetic field as the crystal was rotated about the a and c axes. The results of this experiment are shown in Fig. 2. The solid lines on the same diagram represent the results of a numerical calculation of the angular dependence of the second moment on the assumption that all the BeF_4 undergo reorientation about the c axis. In this calculation we have used Van Vleck's formula for a single crystal; in order to take into account the reorientation of the BeF_4 groups we have averaged over all the motions occurring. The method of evaluating such an average in the general case is given by Andrew and Eades.[9]

The absence of any appreciable angular dependence of the second moment as the crystal is rotated about the c axis is explained by the fact that the BeF_4 groups themselves undergo reorientation about this axis. The small angular dependence which appears in the calculated curve is explained by the contribution to the second moment of the neighboring BeF_4 and NH_4 groups.

Thus, the experimental results shown above give evidence for the existence of reorientation ("hindered rotation") of the BeF_4 groups in the $(NH_4)_2BeF_4$ crystal about the c axis at temperatures above −100° C. The temperature dependence of the second moment enables us to determine the height of the potential barrier hindering the rotation of these groups. As Gutowsky and Pake[10] have shown, the temperature dependence of the second moment is given by the expression

$$S_2(T) = S_2^{rig} + (S_2^{rot} - S_2^{rig}) \cdot \tfrac{1}{2}\pi \tan^{-1}(\gamma\sqrt{S_2(T)}/2\pi\nu_c), \quad (5)$$

where S_2^{rig}, S_2^{rot} and $S_2(T)$ are respectively the second moments at low temperatures (when there is no reorientation), at high temperatures (above the rotational transition) and at the given temperature; ν_c is the correlation frequency for reorientation, which can be represented in the form[11,3]

$$\nu_c = \frac{1}{2\pi}\left(\frac{2V_0}{J}\right)^{1/2}\exp\left(-\frac{V_0}{kT}\right), \quad (6)$$

where k is the Boltzmann constant, T is the absolute temperature, V_0 is the height of the potential barrier for reorientation, J is the moment of inertia equal to 219.1×10^{-40} g-cm^2 for the rotation of the regular BeF_4 tetrahedron about its threefold axis. This formula is valid for the case of the so-called classical reorientation when the tunnel effect can be neglected. As Das[11] has shown, the tunnel effect can always be neglected when the nuclei undergoing reorientation are heavier than protons. Thus, the use of formula (6) in our case is completely justified.

Figure 3 shows the dependence of the correlation frequency on the temperature for different values of V_0; it also shows the experimental values of ν_c calculated by means of formula (5). The experimental values agree well with the calculated ones for $V_0 = 9.5 \pm 0.4$ kcal/mole, and this once again confirms the classical mechanism for the reorientation of the BeF_4 groups.

The correlation between the beginning of the decrease in S_2 at a temperature of −100° C and the Curie point of ammonium fluoroberyllate is noteworthy. At the present time it is difficult to say whether this correlation indicates some deeper relation between the decrease in the mobility of the BeF_4 groups at temperatures below −100° C

and the existence of spontaneous electric polarization in $(NH_4)_2BeF_4$ at these temperatures. It is also possible to assume that the appearance of spontaneous polarization is accompanied by a change in the relative position of the structural elements of the lattice, and also by deformations of the structure elements themselves. The latter possibility, apparently, agrees with the deformation of the electronic shells of the $[NH_4]^+$ and $[BeF_4]^{2-}$ ions found by Blinc [8] in the course of his investigation of the infrared spectra of ammonium fluoroberyllate below the Curie point. The appearance of spontaneous polarization in this crystal can, thus, be related to the combined effect of these factors. As regards the mechanism responsible for the appearance of polarization as a result of the ordering of the rotational transitions of the NH_4 groups proposed by Matthias and Remeika, [12] in the light of the proton magnetic resonance data [8] we can be dealing only with the ordering of the positions or of the polarization of the ammonium ions themselves, since the nature of the reorientation of these ions does not change as a result of passage through the Curie point.

The authors are grateful to V. A. Koptsik for his having kindly supplied us with the ammonium fluoroberyllate crystals, and to K. S. Aleksandrov for his interest in the work and useful comments.

[1] Lundin, Aleksandrov, Mikhaĭlov, and Gabuda, Izv. AN SSSR Ser. Fiz. **24**, 1195 (1960), Columbia Tech. Transl. p. 1278.

[2] Lundin, Mikhaĭlov, and Gabuda, DAN SSSR **136**, 864 (1961).

[3] Lundin, Mikhaĭlov, and Gabuda, ZhTF **31**, 1282 (1961), Soviet Phys.-Tech. Physics, in press.

[4] R. Pepinsky and F. Yona, Phys. Rev. **105**, 344 (1957).

[5] J. H. Van Vleck, Phys. Rev. **74**, 1168 (1948).

[6] R. Hultgren, Z. Krist. **88**, 233 (1938).

[7] Okaya, Vedam, and Pepinsky, Acta Cryst. **11**, 307 (1958).

[8] R. Blinc and I. Levstek, J. Phys. Chem. Solids **12**, 295 (1960).

[9] E. R. Andrew and R. G. Eades, Proc. Roy. Soc. (London) **216A**, 398 (1953).

[10] H. E. Gutowsky and G. E. Pake, J. Chem. Phys. **18**, 162 (1950).

[11] T. P. Das, J. Chem. Phys. **27**, 673 (1957).

[12] B. Matthias and D. Remeika, Collection of articles "Fizika dielektrikov" (The Physics of Dielectrics), Gostekhizdat, 1960, p. 305.

Translated by G. Volkoff
236

ON THE DETERMINATION OF THE VALUES $\omega_H\tau$ AND THE EFFECTIVE COLLISION FREQUENCIES OF PLASMA ELECTRONS AND IONS IN A MAGNETIC FIELD

É. I. URAZAKOV and V. L. GRANOVSKII

Moscow State University

Submitted to JETP editor May 16, 1961

J. Exptl. Theoret. Phys. (U.S.S.R.) 41, 1375-1377 (November, 1961)

The values of $\omega_H\tau$ for ions and electrons of a plasma column in a longitudinal magnetic field can be determined with aid of two plane probes (single and double), by measuring the radial and azimuthal diffusion currents with them. The values thus obtained can be used to determine the mean collision frequencies of electrons and ions. Examples of such measurements in argon are presented for various gas pressures. The values thus derived are compared with the calculated values.

A longitudinal homogeneous magnetic field applied to a low pressure cylindrical plasma (positive column) produces in the plasma a transverse drift ("Hall" diffusion) of the electrons and ions in the azimuthal direction, perpendicular both to the direction of the concentration gradient ($\nabla n \parallel r$), and to the magnetic field ($H \parallel Oz$).[1] The diffusion of the electrons and ions towards the walls in a tube with non-conducting walls is ambipolar, with total velocity $v_r = -D_a \nabla n/n$. To the contrary, the azimuthal drift takes place with velocities $v_{p\varphi} = -\omega_{Hp}\tau_p v_r$ and $v_{e\varphi} = \omega_{He}\tau_e v_r$, which differ from each other in direction and in magnitude. One of the results of this drift is the rotational magnetomechanic effect of the plasma.[2]

This azimuthal diffusion can be used to determine the influence of the magnetic field on the plasma electrons and ions, and also the mean collision frequencies of both ($\nu_e = \tau_e^{-1}$, $\nu_p = \tau_p^{-1}$). For this purpose it is sufficient to measure the densities of the electron and ion currents towards the walls (j_{er} and j_{pr}) and in the azimuthal direction ($j_{e\varphi}$ and $j_{p\varphi}$) in the same place (say at the wall). Since

$$j_{pr} = -j_{er} = e_0 n v_r, \quad j_{e\varphi} = -e_0 n v_{e\varphi}, \quad j_{p\varphi} = e_0 n v_{p\varphi},$$

we have

$$j_{p\varphi}/j_{pr} = v_{p\varphi}/v_r = \omega_{Hp}\tau_p, \quad j_{e\varphi}/j_{er} = v_{e\varphi}/v_r = \omega_{He}\tau_e.$$

We made measurements of this kind in inert gases with the aid of two probes. One probe was flat, and perpendicular to the radius of the tube, and is used to measure j_r. The second was a flat double probe, made of two metallic square plates separated by a thin glass plate, the ends sealed in glass (Fig. 1), and placed parallel to the z, r plane at the same distance from the axis as the first probe. This probe measured the φ-component of the particle current on both sides of the probe. By applying to these probes suitable potentials relative to the comparison electrode, we determined the electronic and ionic currents in the radial and azimuthal directions; from these currents we calculated the mean collision frequencies ν_e and ν_p of the plasma electrons and ions in the magnetic field.* The values of ν_e and ν_p thus obtained were compared with the calculations based on the effective cross sections of the gas molecules relative to the electrons and ions and

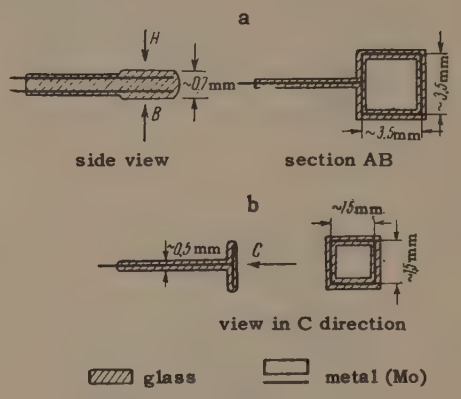

FIG. 1. Diagrams of probes: a) dual b) single.

*At small values of $\omega_H\tau$ (high pressures, weak magnetic fields), an error can creep into the determination of the azimuthal drift current j_ϕ if the probe is not accurately set relative to the (z, r) plane. The relative error in j_ϕ may be of the order of unity if the probe is tilted relative to the radius r by an angle $\alpha \sim \omega_H\tau$. However, in repeated installations of the probe this error becomes random and not systematic, and is thus averaged in the repeated measurements.

p, μ Hg	j, ma/cm²			$\omega_{He}\tau_e$	$\omega_{Hp}\tau_p$	$10^{-6}\nu_p$, sec^{-1}		$10^{-6}\nu_e$, sec^{-1}	
	j_r	$j_{e\varphi}$	$j_{p\varphi}$			measurement	calculation	measurement	calculation
5	0,6	70.2	0.45	117	0.75	0,13	0.15	0.6	~0.1
50	0,61	11.8	0,05	19,5	0,075	1,3	1,5	3.6	~1
500	0,62	3,1	0.006	5	0.0091	11	15	14	~10

on the mean energy of these particles.[3-5] The measurements were made in an argon-filled tube 37 mm in diameter, at H = 400 oe and a discharge current of 0.5 amp. The azimuthal and radial currents were measured with the corresponding probes many times. Example: at a pressure of 50 μ Hg, the values obtained were $I_{e\varphi}$ = 1.2, 1.1, 1.0, 1.3, 1.2, 1.2, 1.1, 1.2, and 1.3 ma, with an average of 1.18 ma. The area of the probe used to measure the azimuthal current was S ≈ 10 mm², so that the average of j_e was 11.8 ma/cm². The average measurement error does not exceed 10 percent.

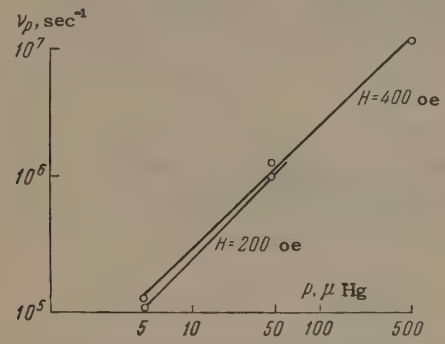

FIG. 2. Dependence of the mean frequency of ion collision on the pressure.

The ion and electron current densities (identified by the subscripts p and e, respectively) obtained in this fashion are listed in the table together with the values of $\omega_H\tau$ calculated for both particles. The results pertain to argon at H = 400 oe, I_z = 500 ma, and tube diameter 37 mm. The dependence of the experimentally obtained values of ν_p on the gas pressure in the plasma is shown in Fig. 2 for two magnetic fields.

These results show that: a) in a field H = 400 oe the influence of the magnetic field on the electron (the value of $\omega_H\tau$) remains appreciable up to p ≤ 10^3 μ Hg; in ions it is small even when p ≈ 5 μ Hg; b) the ion collision frequency ν_p is proportional to the pressure p, and consequently the mean ion velocity does not change noticeably.

[1] S. Chapman and T. G. Cowling, The Mathematical Theory of Non-uniform Gases, Cambridge Univ. Press, 1939, Ch. 18.

[2] V. L. Granovskii and É. I. Urazakov, JETP 38, 1354 (1960), Soviet Phys. JETP 11, 974 (1960).

[3] V. L. Granovskii, Elektricheskii tok v gaze (Electric Currents in Gases), Gostekhizdat 1952, Sec. 2, Ch. 4.

[4] S. C. Brown, Basic Data of Plasma Physics, Wiley, N.Y., 1959.

[5] A. von Engel, Ionized Gases, Clarendon Press, Oxford, 1955.

Translated by J. G. Adashko
237

FORMATION OF A CURRENT CHANNEL IN A GAS DISCHARGE IN A WEAK MAGNETIC FIELD

A. P. BABICHEV, A. I. KARCHEVSKII, Yu. A. MUROMKIN, and V. V. SOKOL'SKII

Submitted to JETP editor May 17, 1961

J. Exptl. Theoret. Phys. (U.S.S.R.) 41, 1378-1381 (November, 1961)

The configuration of a strong-current toroidal discharge in a weak magnetic field is experimentally investigated for a magnetic flux uniform over the liner cross section, and for both constant and variable longitudinal field on the discharge periphery. It is shown that the experimentally observed formation of a current channel outwardly reminiscent of the pinch effect can be described, for both constant and variable external magnetic fields, by a stationary force-free discharge model.

In order to study certain features of a strong-current discharge, we have carried out experiments with a toroidal chamber having a thick-wall aluminum case with diameters 750 and 250 mm. Inside the case was mounted a discharge chamber (liner) 160 mm in diameter. In one series of experiments the liner was assembled of 16 aluminum sections (wall thickness 4 mm), insulated from each other with teflon gaskets; in the second series, an analogous sectionalized liner was made of nonmagnetic steel 0.1 mm thick. The steel liner was placed in a supplementary coil to introduce a variable longitudinal magnetic field into the plasma. The discharge current and voltage were measured. The distribution of the magnetic fields in the discharge was determined with magnetic probes.

In experiments with the aluminum liner, the amplitude of the discharge current reached 50 kiloamp at an initial loop voltage 1.1 kv, duration of first half wave 600 μsec, initial magnetic field up to 1000 oe, and hydrogen pressure $10^{-2} - 10^{-3}$ mm Hg. The conductivity of the plasma, calculated at the current maximum, was 6×10^{14} cgs esu on the chamber axis.

When the steel liner was used and the supplementary coil turned on, the amplitude of the discharge current reached 35 kiloamp and the conductivity did not exceed 8×10^{13} cgs esu, other conditions being equal. An appreciable change took place in the configuration of the magnetic field in the discharge region: in the first case the distribution of the azimuthal component of the magnetic field indicates that a current channel, "detached" from the walls, was formed; in the second case the current has practically constant density over the entire section of the liner (Fig. 1). It must be noted that in both cases the configuration

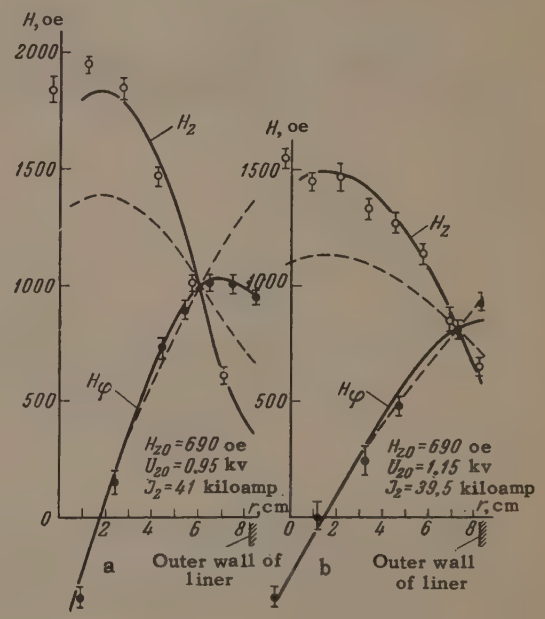

FIG. 1. Distribution of the longitudinal (H_z) and azimuthal (H_ϕ) components of the magnetic field in the discharge: a – thick-wall aluminum liner; b – thin-wall liner made of nonmagnetic steel. Solid curves – force-free model, dashed – paramagnetic model.

of the discharge is completely determined by the initial magnetic field and by the current flowing in the plasma at the given instant of time, regardless of the discharge phase at which this current is reached.

For a further study of the character of the discharge, alternating current was passed through the supplementary winding at approximately four times the fundamental frequency of the process. (The influence of an alternating magnetic field on the discharge configuration was investigated by Ivanov and Kirillov.[1]) The amplitude, sign, and instant of application of the supplementary field

could be varied. In some experiments the field was introduced simultaneously with the start of the discharge, and its first half wave amplified the initial field. Up to the time t_1 (Fig. 2) the longitudinal field on the edge changes in phase with the field in the central region of the discharge, but beyond this instant the field in the central region remains constant, or even decreases somewhat, whereas the field on the edge decreases with the current in the exciting coil. Within 2—4 μsec after t_2 the longitudinal field inside the plasma reverses direction. The value of the field before the instant t_2 is proportional to the discharge current.

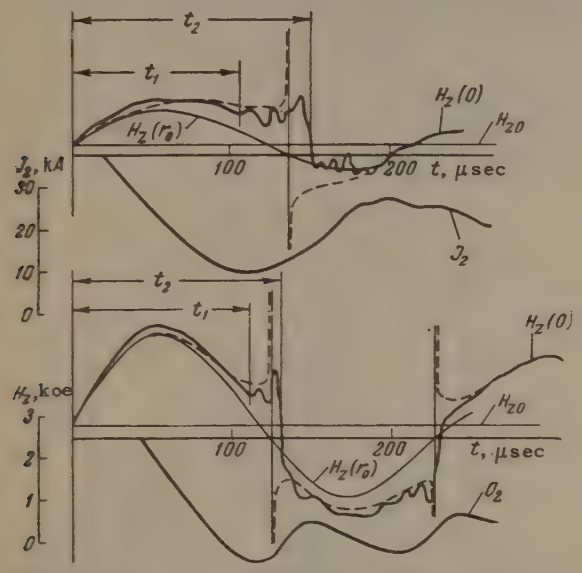

FIG. 2. Oscillograms of discharge current J_z and longitudinal magnetic field $H_z(0)$ at the center of the chamber upon application of an alternating magnetic field (r_0 – radius of liner). The dashed curve is calculated in force-free model.

From an examination of all the oscillograms obtained it follows that t_1 practically coincides with the time when the longitudinal component of the magnetic field on the edge of the liner becomes equal to the azimuthal component, and t_2 coincides with the instant when the external longitudinal field passes through zero.

Measurements of the azimuthal component of the field show that a current channel exists in the discharge between the instant t_1 and t_2, with a radius that decreases gradually to about half the initial radius at the instant t_2. A comparison of the results of different experiments shows that in this case, too, the configuration of the discharge is determined by the external magnetic field on the edge of the liner and by the discharge current flowing at the given instant of time, and is practically independent of the rate of change of the external field. The quantities also determine the times t_1 and t_2. Accordingly, for a given discharge current, the time $t_2 - t_1$ was found to be, inversely proportional to the rate of decrease of the external magnetic field.

The low conductivity of the plasma in the experiments described should cause the diffusion time of the magnetic field in the gas-discharge column to be much less than the periods of variation of the external fields, and in the first approximation there should be no "frozen-in" magnetic field in the plasma. Yet a pronounced formation of a current channel is observed, along with an increase in the longitudinal magnetic field in the central region of the discharge (only outwardly reminiscent of the "pinch"). These phenomena can be reconciled with the stationary discharge theory [2] by imposing as an additional requirement the vanishing of the current density perpendicular to the magnetic field. This leads to the force-free discharge model, which is natural for a low-temperature plasma.

The discharge configuration calculated by this theory agrees with experiment (Fig. 1). The different behavior of the discharges in aluminum and steel liners is explained by the fact that in the former case the magnetic flux is constant over the cross section of the liner during the discharge, while in the latter the magnetic field intensity is maintained practically constant on the edge of the liner. An account of this difference permits a correct interpretation of both cases.

The jump-like change in the longitudinal field inside the plasma also has a natural explanation. The direction of the current helix in the discharge is determined by the sign of the external longitudinal magnetic field. At the instant when this field passes through zero, the helix direction should reverse and cause a corresponding jump-like change in the magnetic field. It is seen from the oscillograms that the change in the sign of the longitudinal field in the plasma actually occurs somewhat later than the passage of the field on the periphery of the discharge through zero. It would be incorrect to attribute this phenomenon entirely to the finite diffusion time of the magnetic field in the plasma, since the delay in the reversal of the sign of the field at the center of the plasma relative to the periphery (Fig. 2) depends on the rate of change of the external magnetic field, although the plasma conductivity is the same in these experiments. We propose that this phenomenon is connected both with the insignificant frozen-in magnetic field in the plasma and with the toroidal

geometry of the discharge and the existence of magnetic-field inhomogeneities.

The absence of a perpendicular current-density component can be explained by using the mechanism of convective instability (B. B. Kadomtsev, private communication).

In other installations of similar type[3-6] the conductivity and the ratio of the characteristic geometrical dimensions to the duration of the process differ somewhat from those given above. This raises the hope that the stationary force-free model can be employed to explain a large number of experimental facts. This model was successfully used by Lees and Rusbridge[7] to calculate the distribution of the magnetic fields in the "Zeta".

The authors are grateful to I. K. Kikoin, B. B. Kadomtsev, and V. D. Shafranov for useful discussions of this work.

[1] D. P. Ivanov and V. D. Kirillov, DAN SSSR 133, 793 (1961), Soviet Phys.-Doklady 3, 820 (1961).

[2] S. I. Braginskii and V. D. Shafranov, Collection: Fizika Plazmy (Plasma Physics) 3, AN SSSR, 1958, p. 26.

[3] Butt, Carruthers, Mitchell, Pease, Thoneman, Bird, Blears, and Hartill, 1958 Geneva Conference, paper No. 1519.

[4] Bezbatchenko, Golovin, Ivanov, Kirillov, and Yavlinskii, Atomnaya energiya (Atomic Energy) 5, 26 (1956).

[5] Allibone, Chick, Thomson, and Ware, 1958 Geneva Conference, paper No. 3.

[6] Afrosimov, Glukhikh, Golakt, Zaidel', Komar, Konstantinov, Malyshev, Malyshev, Monoszek, Stolov, and Fedorenko, ZhTF 30, 1381 (1960), Soviet Phys. Tech. Phys. 5, 1311 (1961).

[7] D. J. Lees and M. G. Rusbridge, Conference Report, Uppsala, IVA, p. 955, 1959.

Translated by J. G. Adashko
238

IRREGULAR CONDITIONS OF OBLIQUE COLLISION OF SHOCK WAVES IN SOLID BODIES

L. V. AL'TSHULER, S. B. KORMER, A. A. BAKANOVA, A. P. PETRUNIN, A. I. FUNTIKOV, and A. A. GUBKIN

Submitted to JETP editor May 18, 1961

J. Exptl. Theoret. Phys. (U.S.S.R.) 41, 1382-1393 (November, 1961)

A method for producing and recording irregular modes of shock-wave collisions in solids is described. The parameters of three-shock configurations due to the collision of 300—400 thousand atm and 1.0—1.8 million atm shock waves are presented for four metals. In the first series of experiments a six- to eightfold pressure increase was observed at angles close to the critical angles of appearance of the leading waves. For waves of greater amplitude the pressure increased to 4 million atm for aluminum and to 7 million atm for steel, copper, and lead in the collision region when the waves cross at right angles.

The results obtained are analyzed by the method of shock-wave polar curves. It is shown that the model with a single tangential discontinuity cannot describe irregular modes of oblique collision of "weak" shock waves in metals. A method is described for determining the pressure and density behind the reflected wave front from the parameters of the three-shock configurations. As an example, the pressures and densities are calculated for the collision of strong shock waves in aluminum. Consecutive compression by the incident and reflected waves increased the density of aluminum by 2.26 times, i.e., to 6.12 g/cm^3.

INTRODUCTION

THE transition from regular to irregular reflection is connected with the appearance of a leading wave moving away from the reflecting wall; this wave forms together with the incident and reflected waves a characteristic three-shock configuration (Fig. 1). Irregular reflections of air shock waves were discovered in 1869 by E. Mach. They were subsequently the subject of numerous experimental researches, described in sufficient detail in the review by Bleakney and Taub.[1]

The theory of a three-shock configuration in a perfect gas has been treated by Landau and Lifshitz[2] and by Courant and Friedrichs.[3] The simplest and most probable flow is usually assumed to have a single tangential discontinuity between the region of single compression (behind the front of the leading wave) and the region of the two-stage (or double) compression of the reflected wave. Nonlinear reflections of weak shock waves in air were recently calculated by Ryzhov and Khristyanovich.[4] The flow modes are characterized in this case by large pressure gradients both along the normal to the discontinuity surface and along the front of the leading wave.

The conditions under which three-shock configuration occurs in certain condensed substances were examined by Zel'dovich and Gandel'man in 1947. At approximately the same time the leading

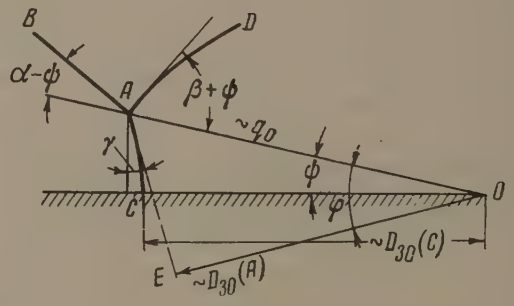

FIG. 1. Diagram of three-shock configuration: AB—incident wave, AD—reflected wave, AC—frontal wave, OA—trajectory of the branching point, OC—mass of frontal wave, proportional to $D_{30}(C)$, OE—segment proportional to $D_{30}(A)$.

wave in solids was observed experimentally by Feoktistova,[5] who recorded with a high-speed photochronograph pictures of collisions between shock waves in a solid explosive and in aluminum.

We report in this article the results of experimental studies of irregular modes in solids, undertaken by the authors to determine their equations of state. An oblique collision between shock waves results in regions of extra high pressures, several times greater than the pressures of the incoming incident shock waves prior to collision.

Compressibility is of greatest interest in the regions of two-stage compression behind the fronts of reflected waves. The successive application of the pressures of the incoming and reflected waves

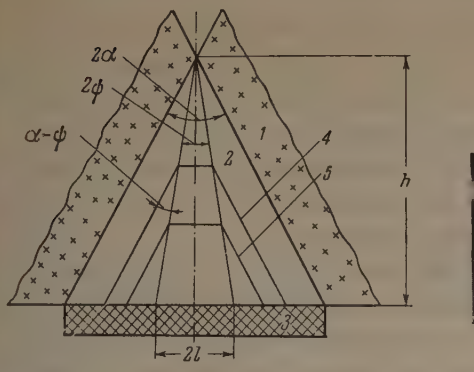

a

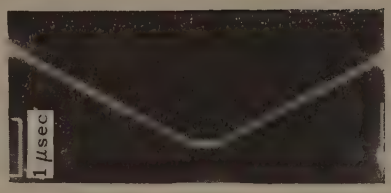

b

FIG. 2. a – diagram of the first series of experiments. 1 – charge of explosive, 2 – prismatic specimen with vertex angle 2α, 3 – Plexiglas plate, 4, 5 – fronts of three-shock configurations at different instants of time, h – height of specimen, $2l$ – width of leading wave at the instant of emergence to the surface of the Plexiglas; b – photochronogram of three-shock configuration.

results in a smaller increase in the entropy than a single shock transition. The states obtained on the pressure-density diagram in the region of two-fold compression lie therefore below the Hugoniot adiabat and approach essentially the compression curve for absolute zero temperature.

In the first section of this article we describe methods for obtaining and registering three-shock configurations and report the experimental results. We then use several metals of known equations of state as examples to analyze the conditions under which the regular modes set in and the character of the resultant flow. The concluding section considers a method for investigating compressibility by registering the parameters of the irregular reflection.

1. INVESTIGATION PROCEDURE AND EXPERIMENTAL RESULTS

The direct purpose of the experiment was to register the dimensions and the form of the leading wave at a certain fixed distance h from the point of its initiation. The specimens used for the investigation of oblique collision modes were made in the form of isosceles triangular prisms (Fig. 2a). In the first series of experiments plane detonation waves were applied to the side faces of the prisms in synchronism, and produced in the specimens shock waves with amplitudes on the order of several hundred thousand atmospheres. The fronts of the shock waves, parallel to the faces of the specimen, collided at an angle 2α. The angle α ranged from 30 to 60°.

In the second series of experiments pressures on the order of 1 or 2 million atmospheres were obtained by shock in aluminum plates accelerated by the explosion products (Fig. 3a). In this case the investigated specimen with a right-angle vertex was covered with steel plates and was placed in bulky lead blocks with two conical openings. Aluminum pistons were inserted in the openings

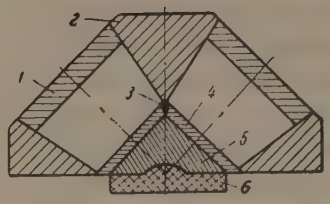

a

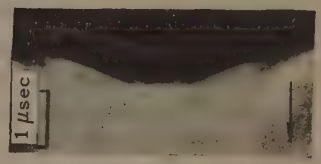

b

FIG. 3. a – Setup of second series of experiments. 1 – aluminum pistons, 2 – lead blocks, 3 – lead wedge, 4 – steel plates, 5 – specimens, 6 – arched Plexiglas receiver; b – photochronogram obtained with this setup.

of the block from the outside. The explosion products moved the pistons at high speed along the openings, causing them to strike the faces of the specimen in synchronism. The pistons overtook the shock waves in the lead block. A narrow lead wedge inserted between the steel plates guaranteed initiation of the three-shock configuration on the upper edge of the prism.

The specimen heights h were 20—40 mm in Fig. 2, and 8—14 mm in Fig. 3. The bases of the specimens were covered with transparent Plexiglas plates.

The collision inside the specimens (Fig. 2a) gave rise to a self-similar propagating configuration with a leading wave located inside a dihedral angle 2ψ. As the incident waves moved on, the line of intersection between the shock fronts and the surface of the Plexiglas shifted gradually from the edges of the specimen to the center of its base. The shift in the front of the wave was accompanied by bright but very brief glow of the air in the gap between the Plexiglas plate and the specimen. The cessation of the glow was due to the dispersion of the Plexiglas by the shock wave. When the leading wave emerged to the lower surface of the specimen, the entire portion of surface ($2l$ wide) occupied by the wave (Fig. 2a) began to glow simultaneously. The consecutive crossings of the transparent plate surface by the waves were

recorded with a high-speed photochronograph through a slit perpendicular to the plane of wave collision. A typical photochronogram is shown in Fig. 2b. The inclined lines of the picture characterize the speed with which the incident wave glides along the base of the specimen, while the tie represents the width of the leading wave at the instant of its emergence to the base of the specimen.

If the gliding speed of the incident waves along the base of the prism is less than the speed of propagation of the shock wave in the Plexiglas, the leading wave may be partially or completely "covered" by the advance waves propagating in the Plexiglas. To avoid this phenomenon, specimens with cylindrical slots in the bases were used (Fig. 3a). When the slot has a cylindrical form, the leading and incident waves emerge to the surface of the convex Plexiglas receiver almost simultaneously. The photochronogram obtained under these conditions is shown in Fig. 3b.

With increasing collision angle α, the dimension of the leading wave increases. Its curvature then becomes noticeable (see the diagram, Fig. 1). The bending is particularly pronounced at large sweep velocities, on the order of several tens of kilometers per second, obtained with the aid of an electron-optical converter. The photochronogram in Fig. 4 of the collision of waves in the aluminum specimen shows quite clearly the bending of the frontal wave. The collision angle 2α was 110° with $\psi = 6°$.

FIG. 4. Photochronogram of three-shock configuration in aluminum, obtained with an electron-optical converter. $P_1 = 0.33 \times 10^{12}$ bar, $\alpha = 55°20'$, $\psi = 6°$, h = 86.9 mm.

In experiments with colliding waves of large amplitude, the bending of the leading wave was registered by placing on the base of the specimen, along a line perpendicular to its axis, a series of contacts shorted by the leading wave as it emerged to the lower surface of the specimen. The successive shorting of the contacts was registered on a high-speed oscilloscope. In estimating the shape of the leading wave and the degree of its bending, the curvature was assumed constant. A quantitative measure of the bending was either the angle γ or $\varphi = \psi + \gamma$ (Fig. 1).

The parameters of the incident shock waves prior to collision were determined in individual experiments by measuring their velocity D_{10} in a direction perpendicular to the side faces of the specimen. The remaining characteristics of the incident waves were determined from the equations of the dynamic adiabats.

Records of the collision process yielded the width $2l$ of the frontal wave and the time difference Δt between the emergences of its edges and of its center from the base of the specimen. Subsequent reduction of the experimental data yielded the angle

$$\psi = \text{arc tg}\,(l/h), \tag{1}*$$

which the outgoing symmetrical frontal wave makes with the symmetry plane, and the bend angle of the leading wave

$$\gamma = \text{arc tg}\,\frac{2\Delta t D_{10}\cos\psi}{l\sin(\alpha-\psi)}. \tag{2}$$

From these quantities we calculated the velocity of the branching point

$$q_0 = D_{10}/\sin(\alpha-\psi), \tag{3}$$

the velocity and pressure of the leading wave near the branching point

$$D_{30}(A) = q_0\cos(\psi+\gamma) = q_0\cos\varphi, \tag{4}$$

$$P_{30}(A) = \rho_0 D_{30}(A)\,\Delta U_{30}(A), \tag{4a}$$

and the velocity and pressure of the leading wave in the symmetry plane

$$D_{30}(C) = q_0\,[\cos\psi - \sin\psi\,\text{tg}\,(\gamma/2)], \tag{5}\dagger$$

$$P_{30}(C) = \rho_0 D_{30}(C)\,\Delta U_{30}(C). \tag{5a}$$

The discontinuities in the mass velocities $\Delta U_{30}(A)$ and $\Delta U_{30}(C)$ on the front of the leading waves were calculated from the velocities $D_{30}(A)$ and $D_{30}(C)$ by using the equations of the dynamic adiabats. In all the calculations we used the previously determined dynamic single-compression adiabats and the equations of state for lead and copper,[6], iron,[7] and aluminum[6,9].

The parameters of the incoming wave are shown in Table I. The results obtained in the first series of the experiments are plotted as ψ-α and P-α diagrams in Figs. 5a, b, and 6.

The coordinates of Figs. 5a and b are the angle variables ψ and α. Each point is the average of several experiments. All the experiments pertaining to a single material exhibit a rather wide dispersion band. With decreasing α, the slope of the ψ-α curves decreases. This, as well as the dis-

*arctg = $\tan^{-1}$

†tg = tan.

Table I

Metal	First series				Second series			
	D_{10}, km/sec	ΔU_{10}, km/sec	P_1, 10^{12} bar	σ_1	D_{10}, km/sec	ΔU_{10}, km/sec	P_1, 10^{12} bar	σ_1
Aluminum	7.48	1.61	0.33	1.27	10.22	3.58	0.99	1.54
Copper	5.15	0.81	0.37	1.19	7.82	2.57	1.79	1.49
Lead	3.33	0.86	0.32	1.33	5.92	2.61	1.75	1.79
Iron	5.38	1.0	0.42	1.23	8.21	2.66	1.71	1.48

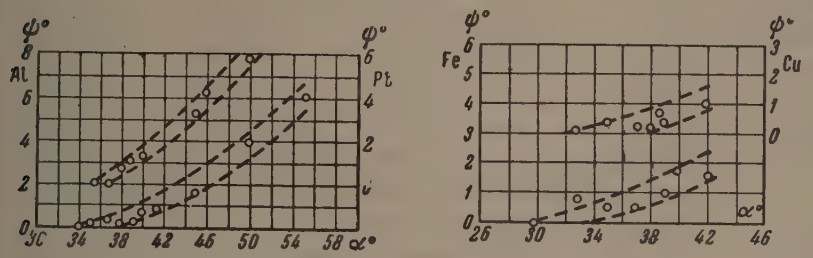

FIG. 5. a – ψ-α diagram of aluminum and lead; b – ψ-α diagram for copper and iron.

persion of the experimental data, does not enable us to determine the accurate values of the critical angles at which irregular modes set in. For aluminum and lead, α_{cr} lies between 34° and 38° and between 35 and 37°; the ranges are 32° to 37° 30′ for copper and 30° to 34° for iron.

More detailed data, obtained with aluminum, are found in Table II and in Fig. 6. The left part of Fig. 6 shows the calculated pressures P_2 due to regular reflection. Of the two possible modes, the one with the lower pressures, described by the segment OK, is always realized. There are no solutions for regular reflections at angles $\alpha \geq \alpha''_{cr}$.

The right part of Fig. 6 shows the experimental pressures $P_{30}(C)$ on the symmetry axis, calculated from the data of Table II. When these data were calculated from Eq. (5), the term containing γ was disregarded. When $\alpha - \psi \leq 50°$, the pressure is not overestimated by more than 1 or 2 percent. The bending of the leading wave affects more the pressures near the branching point, calculated by Eq. (4). The resultant values of $P_{30}(A)$ for $\alpha - \psi = 47° 20'$ and $\alpha - \psi = 49° 20'$ are marked in Fig. 6 by points which deviate from the curve $P_{30}(C)$ by 6–8%.

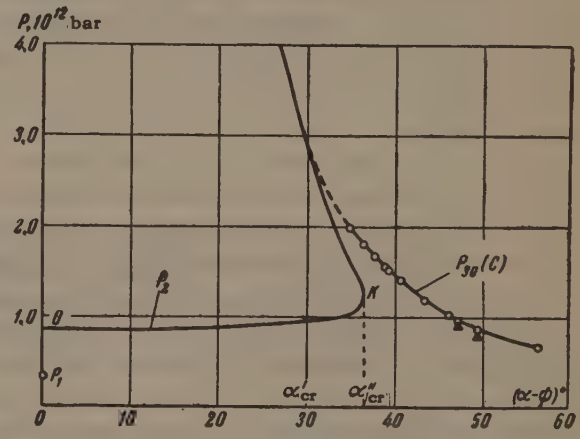

FIG. 6. Pressure of regular and irregular reflections in aluminum. $P_1 = 0.33 \times 10^{12}$ bar.

When $\alpha = 0$, P_2 is a head-on collision pressure which is some 2.5 times greater than the pressure of the incident wave P_1. The pressure of the leading wave is much higher at collision angles close to the critical angles at which three-shock configuration occurs. Thus, when $\alpha - \psi = 35°$ we have $P_{30}(C) = 2 \times 10^{12}$ bar, which is six times the initial pressure of the colliding waves.

An interesting feature is the appearance of the leading waves at angles $\alpha < \alpha''_{cr}$ in the region

Table II

α	ψ	$P_{30}(C)$, 10^{12} bar	α	ψ	$P_{30}(C)$, 10^{12} bar
34°	0°	—	41°40′	50′	1.41
35°	10′	1.98	45°	1°30′	1.19
36°50′	20′	1.80	50°	3°50′	1.02
37°50′	10′	1.67	55°20′	6°	0.86
39°10′	15′	1.56	65°	8°30′	0.66
40°	40′	1.52			

where regular reflection is still possible. With increasing collision angle the pressures of the leading wave decrease rapidly. Obviously, at gliding-wave angles, i.e., at $\alpha = 90°$, we get $P_{30} = P_1$.

The results of the second series of experiments are listed in Table II. For each metal, the table indicates the pressures of the incident waves, the angles α, ψ, and γ, the propagation velocities of the leading waves near the branch point and on the symmetry plane, and the pressures corresponding to these velocities. The table shows that the wave collision increases the pressure to 4—7 million atmospheres. The angles ψ are accurate to $\pm 30'$. The accuracy in γ is much less.

2. ANALYSIS OF THREE-SHOCK CONFIGURATIONS

In the present section we analyze irregular reflections in copper, aluminum, lead, and iron. We carry out the analysis, following [3], by the method of shock polars in a coordinate system fixed to the branching point A.

In the $U_x - U_y$ diagram (Fig. 7), OO′ is the trace of the symmetry plane of the two colliding waves. The plane OO′ can be treated also as the boundary surface of an absolutely rigid partition. The trajectory OA of the branching point makes an angle ψ with this surface, and this angle determines the angular aperture of the sector in which the leading wave propagates. In the general case the front of the leading wave is not perpendicular to the surface of the partition, deviating from it by a certain skew angle γ. The half space above the partition is subdivided by the discontinuity surfaces into four regions: rest region — 0, single-shock compression by the incoming shock wave — 1, successive twofold compression by the incoming and reflected waves — 2, single compression by the leading wave — 3.

In the simplest possible flow scheme, regions 2 and 3 are separated from each other by a single surface of tangential discontinuity AT. On both sides of the discontinuity the streams are parallel and the pressures are equal. The fronts of the incoming, reflected, and leading waves make angles $\alpha - \psi$, $\beta + \psi$, and $90° - \varphi$ with the direction OA of propagation of the branching point; $\varphi = \psi + \gamma$.

The vectors ΔU_{10}, ΔU_{21}, and ΔU_{30} in Fig. 7 denote mass-velocity discontinuities on the fronts of the same waves. The stream velocities in region 0, 1, 2, and 3 are given respectively by the vectors $\mathbf{q}_0$, $\mathbf{q}_1 = \mathbf{q}_0 + \Delta\mathbf{U}_{10}$, $\mathbf{q}_2 = \mathbf{q}_1 + \Delta\mathbf{U}_{21}$, and $\mathbf{q}_3 = \mathbf{q}_0 + \Delta\mathbf{U}_{30}$ ($\mathbf{q}_3$ is not designated in Fig. 7).

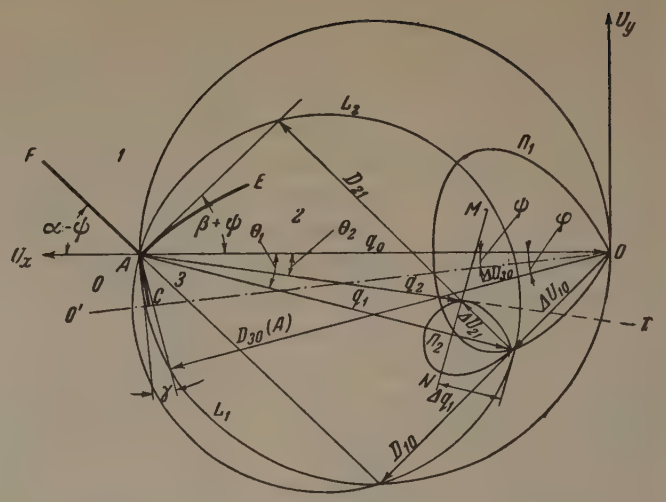

FIG. 7. U_x-U_y diagram of irregular reflection.

The angle between $\mathbf{q}_0$ and $\mathbf{q}_1$ is θ_1, while the angles that $\mathbf{q}_0$ makes with $\mathbf{q}_2$ and $\mathbf{q}_3$ are designated θ_2 and θ_3 and are equal to each other. The vectors $\mathbf{D}_{10}$ and $\mathbf{D}_{30}(A)$ are collinear with $\Delta\mathbf{U}_{10}$ and $\Delta\mathbf{U}_{30}$ respectively and are projections of the vector $\mathbf{q}_0$ on the normals to the fronts of the incident and leading waves. The vector $\mathbf{D}_{21}$ is an analogous projection of the vector $\mathbf{q}_1$ on the normal to the front of the reflected wave.

Assuming the parameters of the incoming wave, and the vectors $\mathbf{q}_0$ and $\mathbf{q}_1$ (and consequently the angles $\alpha - \psi$ and θ_1) known, we determine the possible states of regions 3 and 2, corresponding to different positions of the discontinuity surfaces of the leading wave and the reflected wave. As the angle φ is varied, the end of the vector $\mathbf{D}_{30}$ traces a circular segment L_1 with $\mathbf{q}_0$ as diameter. At the same time the end of the vector $\Delta\mathbf{U}_{30}$, which is collinear with $\mathbf{D}_{30}$, traces the shock polar Π_1. Analogously, as the position of the front AE changes, the end of the vector $\Delta\mathbf{U}_{21}$ traces the polar Π_2 which is symmetrical relative to the vector $\mathbf{q}_1$.

The form of the polars is determined by the equations $\Delta U_{30} = f(D_{30})$ and $\Delta U_{21} = f(D_{21})$ of the single and twofold compression adiabats. To each direction of the vector $\Delta\mathbf{U}_{30}$ corresponds its own angle θ_3 and its pressure $P_{30} = \rho_0 D_{30} \Delta U_{30}$. The analogous quantities for the reflected waves are the angle θ_2 and the pressure $P_2 = P_1 + \rho_1 D_{12} \Delta U_{12}$. Plotted in P and θ coordinates, the relationships between P_3, θ_3 and P_2, θ_2 are represented by the curves Π_1 and Π_2, which are also called shock polars.

By way of an example, Fig. 8a shows the polars of air. When $\theta = 0$ the polar Π_1 crosses the ordinate axis. The maximum pressures at its vertex correspond to shock-wave propagation veloci-

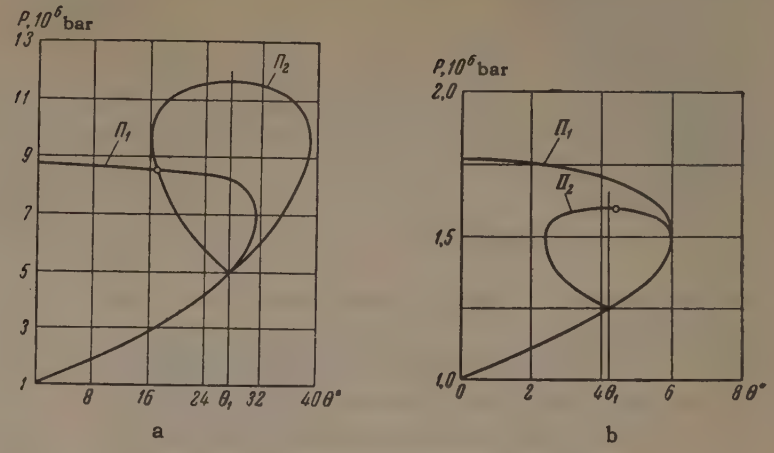

FIG. 8. a – P-θ diagram of oblique collision of "strong" shock waves in air, b – P-θ diagram of oblique collision of "weak" shock waves in air, o – state behind the front of the reflected wave.

ties $D_{30} = q_0$. When the stream deflection angle is $\theta = \theta_1$, the polar Π_1 passes through the incident-wave state. The vertical $\theta = \theta_1$ is the symmetry axis of the polar Π_2 of the reflected wave. Flow with one tangential discontinuity is characterized on the P-θ diagram by the intersection of the polars. Such an intersection, however, does not always take place. In particular, it does not occur, as shown in Fig. 8b, for collisions between "weak" shock waves in air.

Let us turn now to the region of critical angles where the reflection mode turns from regular to irregular. At a certain angle α'_{cr} the polars on the P-θ diagram of Fig. 9a intersect on the ordinate axis. Starting with this instant, irregular reflection can exist for angles $\alpha > \alpha'_{cr}$. Another characteristic angle is $\alpha''_{cr} > \alpha'_{cr}$, at which the polar Π_2 is tangent to the ordinate axes of the P-θ diagram of Fig. 9 and to the symmetry plane on the $U_x - U_y$ diagram of Fig. 7. When $\alpha > \alpha''_{cr}$ the regular mode has no solutions. In the angle interval $\alpha''_{cr} > \alpha > \alpha'_{cr}$ both regular and irregular reflections are possible.

Figure 10 shows the calculated dependence of the critical angles α''_{cr} on the pressures for aluminum, iron, copper, and lead. As $P \to 0$, $\alpha''_{cr} \to 90°$. When $P > 50 \times 10^{10}$ bar, the critical angles assume stable values in the range 32°—38°. A comparison of the calculated and experimental values (Fig. 5) shows that in aluminum, copper, and possibly also iron the three-shock configuration occurs when $\alpha < \alpha''_{cr}$. In aluminum and copper the difference is 2—3°. At the same time, the experimental value is $\alpha_{cr} > \alpha'_{cr}$ (see Fig. 6). A possible reason for the occurrence of the leading wave is the transition of the branching point to subsonic motion, at which $c_2 + q_2 > q_0$. For lead the experimental value is $\alpha_{cr} > \alpha''_{cr}$. We attribute this fact to the known experimental error in the determination of the leading wave in the lead specimens, the reason for which was explained in the preceding section.

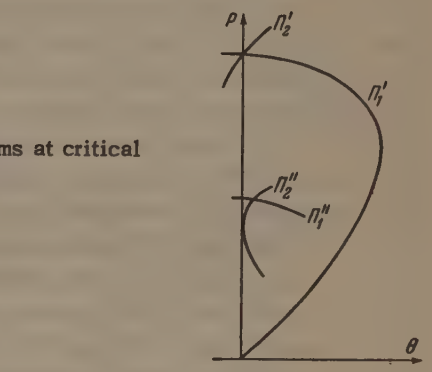

FIG. 9. P-θ diagrams at critical collision angles.

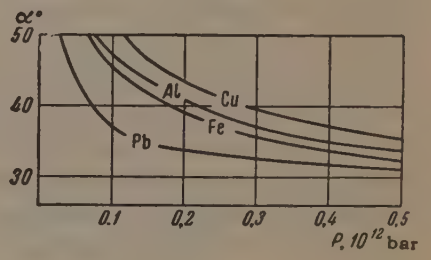

FIG. 10. Dependence of the critical angles α'' of aluminum, copper, lead, and iron on the pressure of the colliding waves.

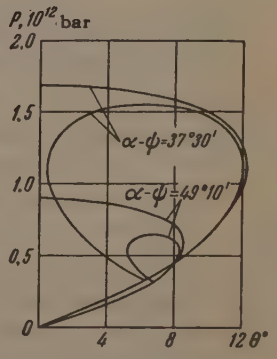

FIG. 11. P-θ diagram of oblique collision of shock waves in aluminum, $P_1 = 0.33 \times 10^{12}$ bar.

Figure 11 shows the relative positions of the polars of aluminum for the first series of experiments at $\alpha - \psi = 37°30'$ and $\alpha - \psi = 49°10'$. A similar picture occurs for copper (Fig. 12) at $\alpha - \psi = 37°30'$ and $\alpha - \psi = 44°$, and also for lead and iron. For all four metals, the polars Π_2 are situated inside the polars Π_1 and do not cross the latter. The right-hand branches of the polars Π_1 and Π_2 are quite close to each other. These features are equally typical of the P-θ diagrams for

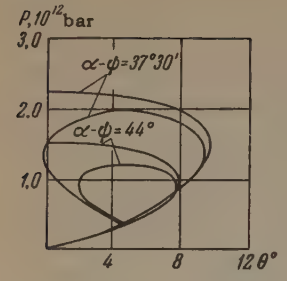

FIG. 12. P-θ diagram of oblique collision of shock waves in copper. $P_1 = 0.37 \times 10^{12}$ bar.

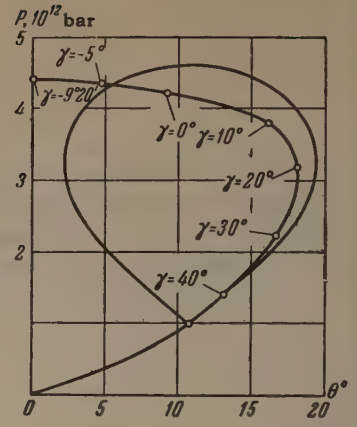

FIG. 13. P–θ diagram of oblique collision of shock waves in aluminum. $\alpha-\psi = 35°40'$; $\psi = 9°20'$; $P_1 = 0.99 \times 10^{12}$ bar.

the collisions of "weak" shock waves in air (see Fig. 8a).

Optical registration of three-shock modes in air yields, in addition to the angles $\alpha - \psi$, also information on the reflection angle β. The values of α, ψ, and β for air are given by Bleakney and Taub [1] for both "weak" and "strong" shock waves. Using these values, we have calculated the state parameters behind the front of the reflected wave. For "strong" shock waves, in accordance with the simplest scheme of three-shock flow, the coordinates of the reflection region are determined (Fig. 8) by the point of intersection of the polars. For weak shock waves, this scheme might be realized for states situated on the right branches of the Π_2 polars, which merge with the right branches of the Π_1 polars. Actually, however, in collisions between weak shock waves in air (Fig. 8a) the coordinates P and θ of region 2 correspond to the upper portion of the polar Π_2, which is a considerable distance from Π_1. The modes occurring in this case can of course not be described by a flow with a single tangential discontinuity. This deduction applies to collisions of weak waves in air equally well as to the collisions of weak waves in metals.

The condition for the existence of flow with one tangential discontinuity is thus that the polars intersect to the left of the vertical $\theta = \theta_1$. The presence or absence of these intersections depends obviously on the relative dimensions of the polars. Their relative magnitudes are determined in turn by the relative locations of the single and twofold compression adiabats on the P-ρ or P-v diagrams. The polars intersect if the adiabats of the second shock are more gently sloping and lie appreciably below the adiabat of the single compression.

Similar adiabats are observed for shock waves of large amplitude, when the thermal pressures in the shock compression begin to play an appreciable role. Calculations show that in the second series of experiments crossings of polars at a collision angle $2\alpha = 90°$ occur for aluminum but still not for iron, copper, or lead. The P-θ diagram calculated from the equation of state [9] is shown in Fig. 13. The numbers on the polar Π_1 denote the bend angles of the leading wave for different points of the polar Π_1.

3. DETERMINATION OF THE PARAMETERS OF THE REGION OF TWOFOLD COMPRESSION BEHIND THE REFLECTED WAVE

The experimentally observed characteristics of the irregular modes can be used to study the compressibility at rather high colliding-wave pressures. For flow conditions corresponding to the model with a single tangential discontinuity, the parameters of the region of twofold compression behind the front of the reflected wave are determined from the experimental values of $\alpha - \psi$ and $\varphi = \gamma + \psi$. We must also know the parameters of the incident shock wave and the single compression adiabat at the collision pressures given by the relation $\Delta U_{30} = f(D_{30})$.

Knowing the foregoing quantities, we can successively determine the vector $\mathbf{q}_0$, the direction and magnitude of the vectors $\mathbf{D}_{30}$ and $\Delta\mathbf{U}_{30}(\mathbf{D}_{30})$, the direction of the tangential discontinuity AT along the vector $\mathbf{q}_3 = \mathbf{q}_0 + \Delta\mathbf{U}_{30}$, and the pressure on the front of the leading wave

$$P_{30} = \rho_0 D_{30} \Delta U_{30}, \tag{6}$$

which is equal to the pressure in region 2. An independent expression for the latter is the equation

$$P_2 = P_1 + \rho_1 D_{21} \Delta U_{21} \tag{7}$$

which represents the conservation of the momentum as $\mathbf{q}_1$ crosses the front of the reflected wave.

The conditions that P_2 and P_3 be equal, as can be readily shown, are fulfilled for all vectors $\Delta\mathbf{U}_{21}$ that terminate on the chord MN (Fig. 7) perpendicular to the vector $\mathbf{q}_1$ and located at a distance

$$\Delta q_1 = (P_3 - P_1) / \rho_1 q_1 \tag{8}$$

away from its right end.

From the condition that $\mathbf{q}_2$ must be parallel to $\mathbf{q}_3$ it follows that the vector $\Delta\mathbf{U}_{21}$ also terminates

Table III

Metal	P_1, 10^{12} bar	α	ψ	τ	$D_{20}(A)$, km/sec	$D_{20}(C)$, km/sec	$P_{20}(A)$, 10^{12} bar	$P_{20}(C)$, 10^{12} bar
Aluminum	0,97	45°	9°20′	0	17,36	17,36	4,25	4,25
Copper	1,79	45°	10°	14°	12,39	13,07	6,28	7,21
Lead	1,75	45°40′	8°30′	—	—	—	—	—
Iron	1,71	45°40′	8°50′	8°	13,10	13,38	6,08	6,42

on the tangential discontinuity line AT. The intersection between the chord MN and the tangential discontinuity determines the directions and magnitudes of the vectors ΔU_{21} and D_{21}, and consequently the density

$$\rho_2 = \rho_1 D_{21} / (D_{21} - \Delta U_{21})$$

behind the front of the reflected waves, acquired by the investigated substance after successive application of the pressures P_1 and $P_2 = P_3$.

The method developed here is not universal. The possibility and usefulness of its application call for a preliminary analysis, based on the use of the approximate equations of state of the investigated substances. As follows from the data given in the preceding section, the procedure for measuring the twofold compressibility under conditions of oblique collision between strong shock waves can be used, in particular, to investigate the equation of state of aluminum. The parameters of the collision region were calculated for this metal using the above method and the data of Tables I and III.

The results of the investigation of the twofold compressibility of aluminum are shown on the P-δ (pressure vs. relative compression) diagram in Fig. 14. The diagram shows the single compression adiabat P_{G1} with its experimentally determined [6] and extrapolated [9] isotherm P_x for 0° K and the adiabat P_{G2} of the second shock. The line OA represents (in P-δ coordinates) the possible points of intersections of the polars for different angles γ (see Fig. 13). Modes with a single tangential discontinuity cannot be realized for twofold compression adiabats located to the left of OA (more accurately, to the left of the point on this line with $\gamma = 3°$). The resultant experimental point of twofold compression of aluminum is marked by a cross in the figure. It is located somewhat above the calculated adiabat P_{G2}. The compression curve at absolute zero should be raised by approximately the same amount.

Figure 14 shows that the collision causes the pressure behind the front of the reflected wave to rise to 4.25×10^{12} bar, i.e., approximately 4 times,

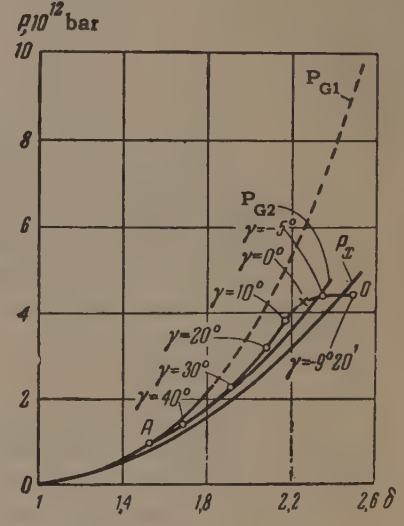

FIG. 14. Curves showing the compressibility of aluminum: P_{G1} – dynamic adiabat of single compression; P_{G2} – calculated adiabat of two-fold compression, P_x – calculated isotherm at 0°K, x – experimental point of twofold compression, OA – trajectory of the points of intersection of the polars.

while the increase in density is 1.5-fold. Relative to the normal state of aluminum, its density increases 2.26 times to 6.2 g/cm^3.

A study of oblique collisions of shock waves was started by the authors some 10 years ago. In the first series of researches, the most active part in the laborious and complicated experiment was played by M. P. Speranskaya, the late N. S. Tenigin, A. N. Kolesnikova, M. S. Shvetsov, and L. N. Gorelova. Some of the results on aluminum and lead were obtained by M. V. Sinitsyn. Many valuable hints were made by Ya. B. Zel'dovich and S. A. Khristianovich. The authors are deeply grateful to all these persons.

[1] W. Bleakney and A. H. Taub, Revs. Modern Phys. 21, 584 (1949).

[2] L. D. Landau and E. M. Lifshitz, Mekhanika sploshnykh sred (Mechanics of Continuous Media), Gostekhizdat, 1954.

[3] R. Courant and K. O. Friedrichs, Supersonic Flow and Shock Waves, Interscience, N.Y., 1948.

[4] O. S. Ryzhov and C. A. Khristianovich, PMM (Applied Mechanics and Mathematics) 22, 586 (1958).

[5] E. A. Feoktistova, DAN SSSR 136, 1325 (1961), Soviet Phys.-Doklady 6, 162 (1961).

[6] Al'tshuler, Kormer, Bakanova, and Trunin, JETP 38, 790 (1960), Soviet Phys. JETP 11, 573 (1960).

[7] Al'tshuler, Krupnikov, Ledenev, Zhuchikhin, and Brazhnik, JETP 34, 874 (1958), Soviet Phys. JETP 7, 606 (1958).

[8] V. N. Zharkov and V. A. Kalinin, DAN SSSR 135, 811 (1960), Soviet Phys. Doklady 5, 1253 (1961).

[9] Kormer, Urlin, and Popova, FTT 3, 2131 (1961), Soviet Phys.-Solid State 3, 1547 (1962).

Translated by J. G. Adashko
239

ELASTIC SCATTERING OF 2.8- *AND* 6.9 *Bev/c* π^- *MESONS ON CARBON*

B. P. BANNIK, A. M. GAL'PER, V. G. GRISHIN, L. P. KOTENKO, L. A. KUZIN, E. P. KUZNETSOV, G. I. MERZON, M. I. PODGORETSKII, and L. V. SIL'VESTROV

Joint Institute for Nuclear Research; P. N. Lebedev Physics Institute, Academy of Sciences, U.S.S.R.

Submitted to JETP editor May 18, 1961

J. Exptl. Theoret. Phys. (U.S.S.R.) 41, 1394-1401 (November, 1961)

Elastic scattering of π^- mesons with momenta of 2.8 and 6.8 Bev/c on carbon nuclei was studied. The differential cross sections obtained are analyzed with the aid of the optical model. It is shown that the characteristics for elastic scattering of π^- mesons on carbon depend only on the momentum transfer in the energy range under investigation. The cross section for scattering of π^- mesons by neutrons into the back hemisphere in the laboratory system is also estimated: $\sigma_{\pi n}(\geq 90°) \lesssim 0.4$ mb (2.8 Bev/c) and $\sigma_{\pi n}(\geq 90°) \lesssim 0.1$ mb (6.8 Mev/c).

INTRODUCTION

THE aim of the present experiment was to measure the total and differential cross sections for elastic scattering of negative pions on carbon nuclei. The obtained data make possible, with the aid of the optical model, the determination of the magnitude and sign of the spin-independent real part of the pion-nucleon scattering amplitude,[1,2] which result from interference between Coulomb and nuclear scattering. These data yield information on the energy dependence of the elastic scattering differential cross section for the same momentum transfer.

1. EXPERIMENTAL METHOD

A. Measurements of 2.8-Bev/c π^- meson scattering. The scattering of π^- mesons of momentum 2.8 ± 0.15 Bev/c[3] was measured with a $37 \times 10 \times 10$ cm propane bubble chamber without a magnetic field. We selected for measurement tracks of relativistic particles entering the chamber at angles not greater than 2° relative to its horizontal axis (projected angle on the plane of observation) and lying in the effective region of the chamber of length 28.4 cm (60 mm on the film), where the distortion of the tracks is a minimum and approximately uniform in magnitude.

In order to speed up the selection of cases of scattering we measured under high magnification the deviation of the track from a straight line traced on a transparent rule which was aligned with the points of intersection of the track with the boundaries of the effective region. This method made it possible to select, with practically no loss, cases of scattering by an angle $\varphi \geq 1°$.* The use of the rule speeded up the selection of cases of scattering approximately ten-fold, and also decreased the number of stars lost in an ordinary scanning. Cases of scattering selected with the rule were measured twice on an MBI-9 microscope under a magnification of 3.5×15. The measurements were made with a 10-mm cell, which reduced to a minimum the error of the angle measurement due to multiple Coulomb scattering and dispersion of the track bubbles ($\sim 0.06°$). A reliable method of separating true scatters from cases of spurious scattering is to localize the scattering point. For all selected cases of scattering by an angle $\varphi \geq 1°$ the scattering point was determined visually within the limits of 1 mm in the chamber. The scattering points were uniformly distributed over the chamber length. A comparison of the number of cases of scattering on different sides (67 and 54) indicates that the selection of cases was independent of the sign of the scattering angle.

We examined a total of $\sim 1.49 \times 10^5$ cm of π^--tracks and selected more than 800 cases. After the microscope measurements, there remained 121 cases of scattering by angles from 1° to 10°

*By the angle φ we understand the projection of the space scattering angle ϑ on the plane of observation. In the present experiment we measured the projections of the scattering angles on the plane of the photograph, which provided considerably better accuracy than measurements of the space angles.

and 30 cases of scattering by angles greater than 10°.

B. Measurements of 6.8-Bev/c π^--meson scattering. We measured the elastic scattering of π^- mesons on carbon nuclei with the aid of a 24-liter propane bubble chamber placed in a magnetic field of 13 700 oe.* The π^- mesons entered the chamber with a momentum of 6.8 ± 0.6 Bev/c. The μ^--meson contamination was (5 ± 2)%. The details of the experimental arrangement have been described by Wang et al. [4]

For the measurements we chose an effective chamber region 42 cm long, where the distortion of the tracks was a minimum and approximately constant. We selected relativistic particle tracks passing through this region with an angle no greater than ±0.6° relative to the beam axis. The scanning for cases of scattering and the measurements were performed on an MBI-9 microscope under a magnification of 6.3×15. The cell length on the film was 6 mm. After all tracks were measured once, the cases with scattering angles $\varphi \geq 0.33°$ were measured again with the cell shifted. This permitted a more accurate localization of the scattering point and increased the accuracy of the angle measurements from 0.15 to 0.09°. The scanning for cases of scattering with a reprojector showed that, for angles $\geq 0.5°$, more than 80% of the cases had a point of deflection in the region where, according to the microscope measurements, the point of scattering should have occurred. It was also shown that there was no correlation between cases of scattering and scattering on neighboring tracks. The points of scattering were uniformly distributed over the effective length of the chamber. A comparison of the number of cases of scattering on different sides (142 and 159) indicated that the selection of cases was independent of the sign of the scattering angle.

As a result of the measurement of 3.25×10^5 cm of π^--meson tracks, we found 301 cases of scattering by angles $\varphi \geq 0.33°$ (among them, 218 cases of scattering by angles $\varphi \geq 0.5°$).

2. CORRECTIONS TO THE EXPERIMENTAL DISTRIBUTIONS

We have to introduce corrections to the experimental material to take into account the character of the measurement procedure and the contribution of interactions whose nature is different from π^--meson scattering on carbon nuclei (see Table I).

The correction for one-prong stars associated with multiple production of π^0 mesons was taken into account by the extrapolation of the one-prong star distribution from the large angle region to the small angles. The extrapolation was based on the angular distribution of the products of multiprong stars, since measurements made on 2.8-Bev/c π^- mesons (see Table II) showed that the angular distribution of relativistic charged particles depended weakly on the number of particles in the star. A similar result was obtained for 6.8-Bev/c π^- mesons. Estimates of the one-prong star contribution based on the number of γ quanta from the decay of π^0 mesons produced in one-prong stars (by 6.8 Bev/c π^- mesons) confirmed the correctness of this procedure.

The most important correction is associated with the contribution from elastic scattering on quasi-free neutrons of the nucleus. In a number of reports [5,6] it has been shown that the angular dependence of the elastic and quasi-elastic scattering cross sections practically coincide. Since we cannot determine the effective number of quasi-free neutrons with sufficient accuracy, the correction was made by recalculating the background remaining after the introduction of other corrections for the small-angle region. Here we based ourselves on the differential cross sections of π^-p scattering measured at the same π^--meson energies. [4] This correction actually also takes into account the contribution from π^--meson inelastic scattering processes involving the excitation of the carbon nucleus, since the dependence of the excitation cross section [7] and the quasi-elastic scattering cross section on the momentum transfer do not differ from one another by more than a factor of 1.5. It should be noted that the correction used for quasi-elastic scattering corresponds to approximately one quasi-free neutron per carbon nucleus, which is in agreement with the estimate made by Birger et al. [8]

Another method of correction (for example, by linear extrapolation of the background from the large-angle regions) changes the final result very little.

3. CROSS SECTION FOR THE INELASTIC INTERACTION OF π^- MESONS ON CARBON

The available material made it possible to determine the inelastic scattering cross section of 6.8-Bev/c π^- mesons on carbon

$$\sigma_{in}(\pi^-, C) = 197 \pm 7 \text{ mb}.$$

*The authors are indebted to the bubble chamber group of the High Energy Laboratory of the Joint Institute for Nuclear Research under the direction of Professor Wang Kang-ch'ang for providing the chamber photographs.

Table I. Corrections to the experimental distribution of cases of scattering and differential cross section for elastic scattering of π^- mesons on carbon*

Angular interval $\Delta\varphi$, deg	Number of one-prong stars	Corrections to experimental distribution						Total correction in given angular interval	Number of cases of elastic scattering of π^- mesons on C	Differential cross section of elastic scattering of π^- mesons on C, mb/rad
		Overlapping of intervals	Geometrical corrections	Coulomb scattering of μ^- mesons	Elastic and quasi-elastic π^-p scattering	Inelastic one-prong stars	Quasi-elastic π^-n scattering and scattering with excitation of nucleus			
1	2	3	4	5	6	7	8	9	10	11
2.8 Bev/c π^- mesons										
0.6—1	56									
1—1.4	28	—1.2	—	—0.5	—1	—0.5	—1.5	—4.7	23.3	1380 ± 330
1.4—1.8	14	—0.7	—	—0.2	—0.7	—0.5	—1.5	—3.6	10.4	620 ± 240
1.8—2.2	21	—0.9	—1.8	—	—0.3	—0.5	—1.5	—5	16	950 ± 300
2.2—2.6	14	—0.6	—1.2	—	—0.2	—0.5	—1.5	—4	10	600 ± 250
2.6—3.0	11	—0.4	—0.9	—	—0.2	—0.5	—1.5	—3.5	7.5	450 ± 210
3.0—3.4	10	—0.4	—0.8	—	—0.2	—0.5	—1.7	—3.6	6.4	380 ± 210
3.4—3.8	3	—	—0.2	—	—	—0.4	—1.8	—2.4	0.6	36^{+120}_{-36}
3.8—4.2	2	—	—0.2	—	—	—0.4	—1.4	—2	0	0 ± 120
4.2—4.6	3	—	—0.3	—	—	—0.4	—1.5	—2.2	0.8	48^{+180}_{-48}
4.6—5	1	—	—0.1	—	—	—	—0.9	—1	0	0 ± 80
1—5	107	—4.2	—5.5	—0.7	—2.6	—4.2	—14.8	—32	75	31.1 ± 5.1**
5—10	14	—	—1.2	—	—	—4.7	—8.1	—14	0	0
10—180	30	—	—2.6	—	—	—27.0	—0.4	—30	0	0
1—180	151	—4.2	—9.3	—0.7	—2.6	—35.9	—23.3	—76	75	31.1 ± 5.1**
6.8 Bev/c π^- mesons										
0.33—0.5	59	—								
0.5—0.7	62	+1.5	—	—	—1.7	—1.2	—1.7	—3.1	58.9	2940 ± 400
0.7—0.9	46	—0.2	—	—	—1.5	—0.9	—1.9	—4.5	41.5	2080 ± 360
0.9—1.1	26	—0.2	—	—	—1.0	—0.5	—2.0	—3.7	22.3	1120 ± 270
1.1—1.3	15	—0.2	—	—	—	—0.3	—1.6	—2.1	12.9	640 ± 210
1.3—1.5	10	—0.2	—	—	—	—0.2	—1.6	—2	8	400 ± 170
1.5—1.7	10	—	—	—	—	—0.2	—1.5	—1.7	8.3	410 ± 170
1.7—1.9	2	—	—	—	—	—	—1.4	1.4	0.6	30^{+180}_{-30}
0.5—1.9	171	+0.7	—	—	—4.2	—3.3	—11.7	—18.5	152.5	26.5 ± 2.4**
1.9—5	31	—	—	—	—	—6.8	—24.2	—31	0	—
5—180	40	—	—	—	—	—4.0	—	—40	0	—
0.5—180	242	+0.7	—	—	—4.2	—50.1	—35.9	—89.5	152.5	26.5 ± 2.4**

*Errors in the cross sections are statistical.

**Cross sections in millibarns.

Table II. Angular distribution of fast secondary prongs produced in propane by 2.8 Bev/c π^- mesons

Prong multiplicity		Percentage of cases in angular interval			Number of cases in angular interval 0—180°
black and gray	relativistic	0—5°	5—10°	10—180°	
0	2	17.0	14.7	68.5	401
1	2	11.1	13.5	75.5	126
2, 3, 4	2	14.5	10.0	75.5	200
0	3, 4	14.6	12.6	73.0	302
1, 2, 3, 4	3, 4, 5, 6	12.6	11.8	75.5	508
All stars:		14.2	12.6	73.2	1537

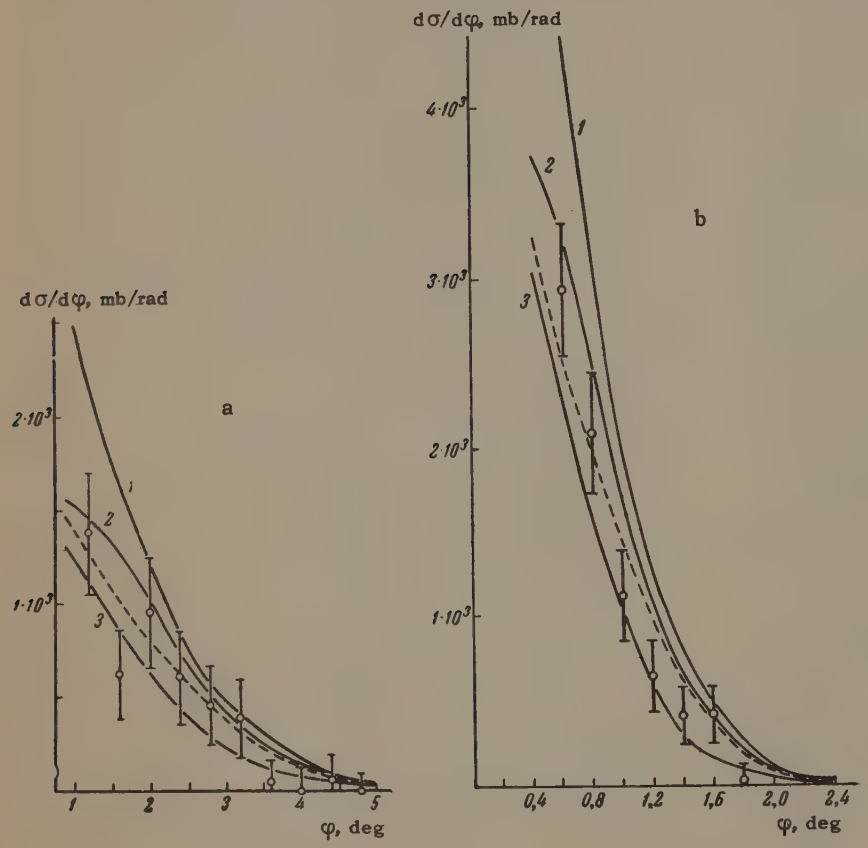

FIG. 1. Elastic scattering differential cross sections: a – for $p_\pi = 2.8$ Bev/c, b – for $p_\pi = 6.8$ Bev/c.

We used here the total cross section of the π^-p interaction $\sigma_t = 28$ mb.[9] The total π^--meson interaction cross section with a bound nucleon of the nucleus obtained from $\sigma_{in}(\pi^-, C)$ with the optical model, was 28.5 ± 1.5 mb, i.e., the same as the interaction cross section on a free nucleon.

This result was used to determine the μ^--meson contamination in the 2.8-Bev/c beam. Here we used the pion-nucleon total cross section σ_t = 30 ± 1.5 mb.[9] The calculation showed that the cross section for the inelastic scattering of π^- mesons on carbon at this energy is 202 ± 5.6 mb. Knowing the total number of events in the chamber, we thus found that the μ^--meson contamination in the 2.8-Bev/c beam was (27 ± 4)%.

4. DISCUSSION OF RESULTS

Figures 1a and 1b show the experimental differential cross section for the scattering of 2.8—6.8-Bev/c π^- mesons in the projection on the plane of observation.* Curves 1—3 are calculated from the optical model of the nucleus, under the assumption that the real parts of the pion-nucleon forward scattering amplitude are†

*It was shown that the difference between the central and orthogonal projection is negligible under our conditions.

†The values $\mathrm{Re}\, f_{\pi N}(0) = 3.39 \times 10^{-13}$ cm ($p_\pi = 2.8$ Bev/c) and $\mathrm{Re}\, f_{\pi N}(0) = 6.9 \times 10^{-13}$ cm ($p_\pi = 6.8$ Bev/c) correspond to the effective potential ~ 30 Mev.

$+3.39\cdot10^{-13}$ cm, $-3.39\cdot10^{-13}$ cm, 0 for $p_\pi = 2.8$ Bev/c;
$+6.9\cdot10^{-13}$ cm, $-6.9\cdot10^{-13}$ cm, 0 for $p_\pi = 6.8$ Bev/c.

According to the optical theorem, the imaginary part of the pion-nucleon scattering amplitude is

$$\operatorname{Im} f_{\pi N}(0) = \frac{k\sigma_t}{4\pi} = \begin{cases} 3{,}39\cdot10^{-13} \text{ cm for } p_\pi = 2{,}8 \text{ Bev/c}; \\ 7.96\cdot10^{-13} \text{ cm for } p_\pi = 6.8 \text{ Bev/c}. \end{cases}$$

In the calculations we took into account the anisotropy in pion-nucleon scattering at these energies [10,4] (in Figs. 1a and 1b the dotted lines represent the results of the calculations with $\operatorname{Re} f_{\pi n}(0) = 0$ with no allowance for this effect).

The experimental and calculated values of the elastic scattering total cross section are shown in Table III. On the basis of these data we can limit the possible values of the real part of the scattering amplitude to

$$+3.39\cdot10^{-13} \text{ cm} > \operatorname{Re} f_{\pi N}(0) \geqslant -3{,}39\cdot10^{-13} \text{ cm} \quad (p_\pi = 2{,}8 \text{ Bev/c}),$$

$$+6.9\cdot10^{-13} \text{ cm} > \operatorname{Re} f_{\pi N}(0) \geqslant -6{,}9\cdot10^{-13} \text{ cm} \quad (p_\pi = 6.8 \text{ Bev/c}).$$

(The values are considered to be in disagreement if the experimental values differ from the theoretical values by more than two standard deviations. The corresponding values of the effective potential of the interaction lie in the limits

$$-30 \text{ Mev} < V_{\text{eff}} \leqslant 30 \text{ Mev} \ (p_\pi = 2{,}8 \text{ Bev/c});$$
$$-30 \text{ Mev} < V_{\text{eff}} \leqslant 30 \text{ Mev} \ (p_\pi = 6{,}8 \text{ Bev/c}).$$

As is known, a small real part for the pion-nucleon scattering amplitude was also obtained with the aid of the dispersion relations,[11,12] which predict the following values of the real part of the πN scattering amplitude $\operatorname{Re} f_{\pi N}(0) = \frac{1}{2}[\operatorname{Re} f_{\pi^- p}(0) + \operatorname{Re} f_{\pi^+ p}(0)]$:

$$\operatorname{Re} f_{\pi N}(0) = \begin{cases} -0.49\cdot10^{-13};\ -0.36\cdot10^{-13} \text{ cm} & (2.8 \text{ Bev/c}); \\ -0{,}33\cdot10^{-13} \text{ cm} & (6.8 \text{ Bev/c}). \end{cases}$$

The data obtained in the present experiment are not sufficiently accurate for a quantitative comparison with conclusions drawn on the basis of the dispersion relations, but are in agreement with them within the limits of error.

The agreement of the differential cross sections $d\sigma/dq$, where q is the projection of the momentum transfer on the plane of observation (Fig. 2) indicates that, within the limits of error, the elastic scattering in the investigated energy interval is determined only by the momentum transfer. From the point of view of the optical model this means that the optical parameters of the πN interaction in this region do not change with energy. Our data allow us to make this conclusion for momentum transfer from 60 to 200 Mev/c. The available data on the $\pi^- p$ scattering lead to the same result in the momentum transfer region ≥ 200 Mev/c (see, for example, [4]).

5. ESTIMATE OF THE $\pi^- n$ SCATTERING CROSS SECTION IN THE BACK HEMISPHERE

Among the one-prong stars found by us we did not observe any cases in which a π^- meson, after interaction, was emitted in the back hemisphere in the laboratory system (l.s.). Hence, as an estimate of the upper limit of the scattering cross section of 2.8- and 6.8-Bev/c π^- mesons on neutrons in the back hemisphere, we obtain $\sigma_{\pi^- n}(\geq 90°) \lesssim 0.4$ mb and $\sigma_{\pi^- n}(\gtrsim 90°) \lesssim 0.1$ mb. (We assumed that the number of quasi-free neutrons in the carbon nucleus is not less than one.[5,8])

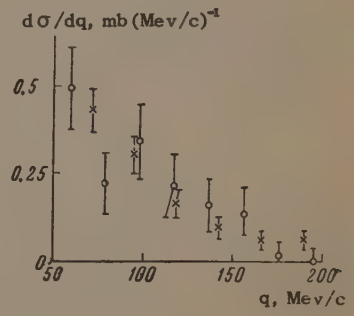

FIG. 2. Differential cross sections for π mesons with a momentum of: o – $p_\pi = 2.8$ Bev/c, x – $p_\pi = 6.8$ Bev/c.

Table III. Comparison and experimental theoretical cross sections for the elastic scattering of π^- mesons on carbon

p_{π^-}, Bev/c	$\Delta\varphi$, deg	Experimental cross section, mb	Calculation with optical model*			
			$\alpha=0{,}9$ $V_{\text{eff}} \approx -30$ Mev	$\alpha=0.5$ $V_{\text{eff}} \approx -15$ Mev	$\alpha=0$ $V_{\text{eff}} = 0$	$\alpha=-0{,}9$ $V_{\text{eff}} \approx 30$ Mev
2.8	1–5	31.1±5,1	51.2	36.5	25,3	40
6,8	0.5–1,9	26,5±2,4	43	30.4	21.3	34

* $\alpha = \operatorname{Re} f_{\pi N}(0)/\operatorname{Im} f_{\pi N}(0)$.

Pomeranchuk has drawn attention to the existence of the diagram in Fig. 3, which can lead to an increase in the π^+p and π^-n scattering cross sections in the back hemisphere (in the l.s.) at high energies to ~ 1 mb. The estimate of Bayukov et al.[13] and the results of the present experiment indicate that the contribution of this diagram is evidently offset by other diagrams.

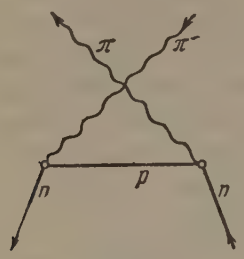

FIG. 3

The authors thank Professor A. I. Alikhanyan for discussions, Wang Ts'u-tseng, I. M. Gramenitskii, E. N. Kladnitskaya, V. B. Lyubimov, Nguyen Dinh Tu, and M. I. Solov'ev for discussions and aid in the work, A. M. Sosul'nikovaya, M. A. Balashova, O. V. Kol'ga, M. I. Filippova, and V. D. Shapkova for taking part in the measurements and reduction of the experimental data, and A. A. Bednyakov for aid during the work with the accelerator. The authors are indebted to the proton synchrotron crew for making the experiment possible. One of us (E. Kuznetsov) thanks D. Yu. Bayukov, G. A. Leksin, and Ya. Ya. Shalamov for helpful discussions.

[1] H. Bethe, Ann. Phys. **3**, 190 (1958).

[2] B. P. Bannik and V. G. Grishin, JETP **39**, 94 (1960), Soviet Phys. JETP **12**, 69 (1961).

[3] Viryasov, Vovenko, Vorob'ev, Kirillov, Kim, Kulakov, Lyubimov, Matulenko, Savin, Smirnov, Strunov, and Chuvilo, JETP **38**, 445 (1960), Soviet Phys. JETP **11**, 327 (1960).

[4] Wang, Wang, Ding, Ivanov, Katyshev, Kladnitskaya, Kulyukina, Nguyen, Nikitin, Otwinowski, Solov'ev, Sosnowski, and Shafranova, JETP **38**, 426 (1960), Soviet Phys. JETP **11**, 313 (1960).

[5] Ballam, Hang, Scandrett, and Walker, Nuovo cimento **14**, 240 (1959).

[6] V. A. Nikitin and E. N. Tsyganov, JETP **40**, 1027 (1961), Soviet Phys. JETP **13**, 722 (1961).

[7] H. Tyrén and A. J. Maris, Nuclear Phys. **4**, 637 (1957).

[8] Birger, Wang, Wang, Ding, Katyshev, Kladnitskaya, Kopylova, Lyubimov, Nguyen, Nikitin, Podgoretskii, Smorodin, Solov'ev, and Trka, JETP **41**, 1461 (1961), this issue, p. 1043.

[9] V. S. Barashenkov, UFN **72**, 53 (1960), Soviet Phys.-Uspekhi **3**, 689 (1961).

[10] V. G. Grishin and M. I. Podgoretskii, JETP **36**, 1593 (1959), Soviet Phys. JETP **9**, 1132 (1959); Joint Institute for Nuclear Research, Preprint No. R-289.

[11] J. W. Cronin, Phys. Rev. **118**, 824 (1960).

[12] V. S. Barashenkov and Hsien Ting-Ch'ang, DAN SSSR **134**, 65 (1960), Soviet Phys.-Doklady **5**, 993 (1961).

[13] Bayukov, Leksin, Suchkov, Shabanov, and Shalamov, Institute of Theoretical and Experimental Phys., Preprint No. 61-6, 1961.

Translated by E. Marquit
240

INVESTIGATION OF HIGH-ENERGY MUONS IN EXTENSIVE AIR SHOWERS

B. A. KHRENOV

Nuclear Physics Institute, Moscow State University

Submitted to JETP editor May 20, 1961

J. Exptl. Theoret. Phys. (U.S.S.R.) 41, 1402-1411 (November, 1961)

Results of an experimental study of the following average characteristics of the μ-meson flux in extensive air showers at sea level are presented: the lateral distribution, the dependence of the μ-meson flux on shower-size, the energy spectrum in the 5—10 Bev range, and the μ-meson density spectrum.

A study of the high-energy μ-meson flux in extensive air showers (EAS) was carried out from 1958 to 1960 using the Moscow State University array for the comprehensive study of EAS. Results were obtained concerning the irregularities in the lateral distribution of the μ mesons and the fluctuations in the μ-meson flux in individual showers.[1-3] Using the same array, we have obtained detailed data concerning the following average characteristics of the μ-meson flux in EAS: the lateral distribution of the μ mesons, the dependence of the μ-meson flux on the shower size, the energy spectrum of μ mesons in the 5—10 Bev range, and the density spectrum of μ mesons. The large array has enabled us to carry out a more thorough study of the above characteristics of μ mesons than had been possible in a number of earlier experiments.[4,5]

METHOD AND EXPERIMENTAL SETUP

The study of average characteristics of μ mesons in EAS requires the measurement of three quantities: the μ-meson density, the total number of particles N in the shower, and the distance R from the shower axis to the μ-meson detector. In addition, the density of μ mesons with various energies can be measured, so that data on the energy spectrum of μ mesons can also be obtained.

The array which was used to measure these quantities was situated partly on the surface of the earth (that part of the array which served to determine the shower size and axis location), and partly underground (μ-meson detectors) at the depths of 20 and 40 m water equivalent. The minimum μ-meson energy necessary for penetrating to these depths amounted to 5 and 10 Bev respectively. Both underground laboratories were situated on one vertical line, below the center of the array detecting the EAS on the surface of the earth.

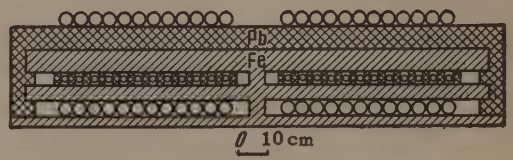

FIG. 1. μ-meson detector.

The underground laboratories have been described in detail in[1].

The array for the detection of EAS consists of a large number of hodoscoped Geiger-Müller counters placed in groups at points forming the geometric array described in detail in[2]. The method of shower-size determination and axis location using such an array has already been described.[6,7]

Hodoscoped Geiger-Müller counters shielded by lead and iron served as the μ-meson detectors in the underground laboratories. At the depth of 20 m w.e., we used the detector described in[2]. At the depth of 40 m w.e., the same detector was used from 1958 to 1959, while, in 1960, the detector shown in Fig. 1 was substituted. The hodoscope used has been described by Korablev.[8]

The study of the μ-meson flux density at different distrances from the shower axis and in showers of different size made it necessary to trigger the array by different selection systems. Table I presents general data on the triggering systems of the array that were used in different variants of the experiment. The results obtained using systems 2 and 3 have been published earlier.[3]

RESULTS

For showers selected by means of triggering systems 1 and 2, the shower size and the axis location on the surface of the earth were determined for each shower. The detected showers were divided into the following groups with respect to

Table I.

System	Distance from the triggering system to the array center, m	Range of distances R, m	Range of N	Method of shower selection
1	0	> 20	10^5–$5 \cdot 10^7$	According to electron density. Sixfold coincidences, $\sigma = 0.132$ m²
2	25	22–27	10^4–$6 \cdot 10^5$	According to electron density. Sixfold coincidences, $\sigma = 0.132$ m²
3	100	70–130	$5 \cdot 10^4$–10^6	According to high-energy electrons. Core selector + double coincidence, $\sigma = 0.264$ m²
4	250	200–300	$2 \cdot 10^5$–10^7	According to electron density. Sixfold coincidence system, $\sigma = 330$ cm²
5	0	< 25	10^4–10^5	Single μ meson with energy > 10 Bev on an area of 4.75 m² + twofold coincidence in laboratory I[1], $\sigma = 0.264$ m².

shower size N and the distance R from the intersection of the shower axis with the surface of the earth to the vertical passing through the μ meson detectors.

ΔN:	10^4—10^5	10^5—$6 \cdot 10^5$	$2 \cdot 10^5$—$1 \cdot 10^6$	$1 \cdot 10^6$—$2 \cdot 10^6$	$2 \cdot 10^6$—$4 \cdot 10^6$	$4 \cdot 10^6$—10^7	$>10^7$
ΔR, m:	22—27	22—27	20—40	20—40	20—40	20—40	20—40
				60—100	60—100	60—100	60—100
						100—160	100—160

The μ-meson density for each shower group was determined according to the formula

$$\rho = \sum_{i=1}^{n} m_i / ns, \qquad (1)$$

where m_i is the number of discharged counters in the lower (or middle) counter tray of the detector in Fig. 1 in the i-th shower, n is the number of showers in the group, and s the total area of the counter of the lower (or middle) detector tray. Eq. (1) is correct if $m_i \ll M$ (where M is the total number of counters of the lower or middle detector tray) a condition which was always satisfied during the experiments. The contribution of the electron-photon component in equilibrium with the μ-meson flux to the number of discharged counters was not greater than 10% for the counters of the lower tray, and 1% for the counters of the middle tray.

The statistical errors $\Delta\rho$ in the μ meson flux density were calculated for $m_i = 0, 1$ according to the formula

$$\Delta\rho = \sqrt{\Sigma m_i}/ns, \qquad (2)$$

and for larger values of m_i according to the formula

$$\Delta\rho = \sqrt{D(\rho)/n}, \qquad (3)$$

where $D(\rho)$ is the dispersion of the distribution $Q(\rho', \rho)$ of the values ρ' with respect to ρ. The distribution $Q(\rho', \rho)$ has been studied in[2]. Using this distribution, and from the following

$$D(\rho) = \sum_j (\rho'_j - \rho)^2 Q(\rho'_j, \rho) \qquad (4)$$

we find $D(\rho) = 1.2\rho^2$. Hence,

$$\Delta\rho = 1.1 \sum_{i=1}^{n} m_i / n^{1.5} s. \qquad (3')$$

The μ-meson flux density given by Eq. (1) was referred to the mean arithmetic value of $\bar{N}$ and $\bar{R}$ of the corresponding shower group. To identical intervals ΔN and ΔR correspond average values of $\bar{N}$ and $\bar{R}$ differing by not more than 20%.

The densities of μ mesons with energy $E \geq 5$ and $E \geq 10$ Bev obtained for the two distance ranges ΔR from 20—40 m ($\bar{R} = 25$ m) and from

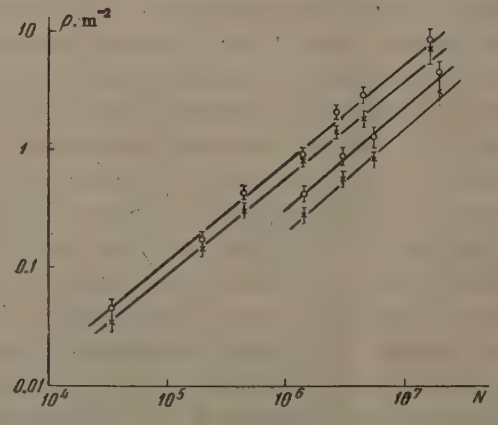

FIG. 2. Dependence of the μ-meson flux density on the total number of particles in the shower for a given distance from the shower axis: o – for $E \geq 5$ Bev, × – for $E > 10$ Bev.

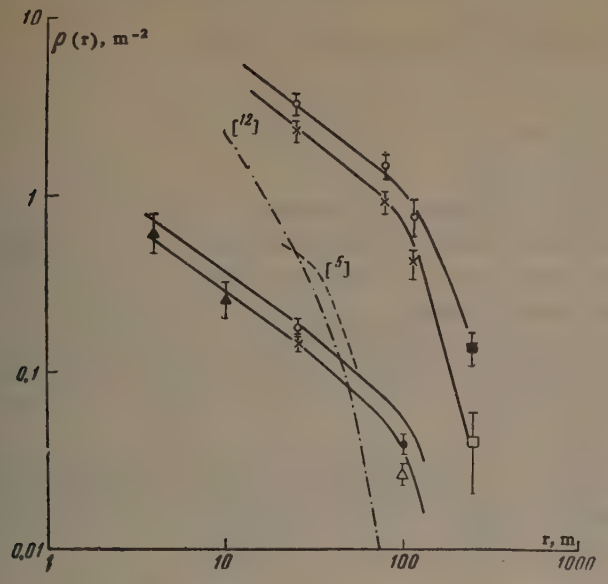

FIG. 3. Lateral distribution of μ mesons in EAS with 2×10^5 particles and 6×10^6 particles. ○, ●, ■ – density of μ mesons with $E \geqslant 5$ Bev, ×, △, □ – density of μ mesons with $E \geqslant 10$ Bev obtained with the triggering systems 1, 3, and 4 respectively, ▲ – density of μ mesons with $E \geqslant 10$ Bev obtained for showers with known zenith angle.

60—100 m ($\bar{R}$ = 80 m) and for different shower sizes are shown in Fig. 2. If we take the function $\rho(N)$ for each distance R as $\rho(N) \sim N^{\alpha}$, then we can obtain the value of α for different E and $\bar{R}$ from Fig. 2 by the least-squares method. Within the limits of experimental error, the values of α were found to be the same for $E \geq 5$ and $E \geq 10$ Bev, and for $\bar{R}$ = 25 and 80 m and equal to $\alpha = 0.85 \pm 0.10$.*

From the mean values of ρ for $E \geq 5$ Bev and $E \geq 10$ Bev, corresponding to the straight lines in Fig. 2, we can obtain the exponent γ on the integral μ-meson spectrum in the 5—10 Bev range: $\gamma = 0.5 \pm 0.1$ for $\bar{R}$ = 25 m, and $\gamma = 0.67 \pm 15$ for $\bar{R}$ = 80 m.

The independence of α from the distance $\bar{R}$ in the range $\Delta\bar{R}$ = 25—80 m indicates that the lateral distribution of the μ-meson flux in that same range is independent of the shower size. From Fig. 2 we can obtain data on the function $\rho(\bar{R})$. The lateral distribution function of μ mesons may, however, be different from the function $\rho(\bar{R})$. In fact, the spectrum $\Phi(r, R)$ of possible distances r from the μ-meson detector to the shower axis corresponds to a given distance R on the surface of the earth. The distance r is different for different angles θ and φ of the shower axis. The μ-meson density detected in the experiment was

$$\rho(R) = \int \Phi(r, R)\, f(r)\, dr = \bar{f}(R), \qquad (5)$$

where f(r) is the μ-meson lateral distribution function.

It can be shown that, for a zenith-angle distribution of the type $I_0 \cos^8\theta \, d\cos\theta$ and for $f(r) \sim r^{-n}$ where $n \leq 1$, the values of $\bar{f}(R)$ do not differ from the values of f(R) by more than 10% for R > H, where H is the depth of the μ-meson detector. For an experimental distribution of $\rho(\bar{R})$ represented by the formula $\rho(\bar{R}) \sim \bar{R}^{-n}$, we obtain from Fig. 2 $n \lesssim 1$, where $\Delta\bar{R}$ = 25—80 m. We can, therefore, assume with an accuracy of 10% that the distribution $\rho(\bar{R})$ for R > 25 m is the true lateral distribution of the μ mesons. In order to obtain complete data on the lateral distribution function of the μ mesons, measurements of the μ-meson density were carried out at distances r < 25 m and r > 100 m.

For a small number of showers, the zenith angle of the shower axis was found in [3] from the data of the diffusion chamber placed at the surface of the earth, and the density of μ mesons with energies $E \geq 10$ Bev were obtained at distances $\bar{r}$ = 4 and 10 m. These data are shown in Fig. 3 for showers with $N = 2 \times 10^5$.

On the periphery of the shower, the μ-meson density with $E \geq 5$ Bev and $E \geq 10$ Bev was obtained by means of triggering systems 3 and 4. The triggering system 3 enabled us to study μ-meson densities at distances $\bar{r}$ = 100 m in showers with $N = 2 \times 10^5$, the results being shown in Fig. 3. (The reduction of the data obtained with the triggering system 3 has been described in [3].)

The triggering system 4 enabled us to study the μ-meson density at a distance $\bar{r}$ = 250 m in showers with $\bar{N} = 6 \times 10^6$. In selecting the showers using the triggering system 4, it was necessary that the density ρ_e of all charged particles on the surface of the earth above the μ-meson detectors be within the range 1—5 m^{-2}, (which meant that 9 to 45 counters out of 264 with an area σ = 330 cm^2 were discharged). The number of particles N and the distance r was not determined for individual showers. For the showers selected by the triggering system 4, the mean number of particles in a shower $\bar{N}$ and the mean distance $\bar{r}$ were calculated using the formulae

$$\bar{N} = \iint N W(N, r)\, \rho(N, r)\, dN\, dr,$$
$$\bar{r} = \iint r W(N, r)\, \rho(N, r)\, dN\, dr, \qquad (6)$$

where W(N, r) is the detection probability of a shower such that $1 \leq \rho_e \leq 5$ m^{-2} for the triggering system 4, and $\rho(N, r)$ is the density of the μ

*The value of $\alpha = 0.6 \pm 0.1$ given in [3] is less reliable, since it was obtained from two points only.

mesons in a shower of size N at a distance r from the shower axis. The probability W(N, r) could be calculated knowing the lateral distribution functions of all charged particles in the shower.[9] It was assumed that $\rho(N, r) = kN^{0.85}r^{-n}$.

The mean values of $\overline{N}$ and $\overline{r}$ were calculated for various values of n (n = 1, 2, 3). The calculation showed that the mean values of $\overline{N}$ and $\overline{r}$ vary little as n varies from 1 to 3, and, in particular, r agrees to an accuracy of 15% with the distance from the triggering system 4 to the μ-meson detectors equal to 250 m. The calculation of the contribution of showers with different N and r to the number of detected μ mesons showed that showers with N from 2×10^6 to 10×10^6 and with r from 200 to 300 m contribute 70%. The density of the μ mesons with energy $E \geq 5$ Bev and ≥ 10 Bev for $\overline{N} = 6 \times 10^6$ and $\overline{r} = 250$ m is shown in Fig. 3.

We have thus obtained the lateral distribution of the μ mesons with energy $E \geq 5$ and ≥ 10 Bev at distances from 4 to 250 m, as shown in Fig. 3. This lateral distribution can well be described by the function

$$\rho(N, r) = kN^{\alpha}r^{-n}\exp(-r^2/r_0^2), \qquad (7)$$

where $n = 0.7 \pm 0.1$, $\alpha = 0.85 \pm 0.1$, and

$$k = 5.8 \cdot 10^{-5}, \quad r_0 = 195 \pm 15 \text{ for } E \geqslant 5 \text{ Bev},$$
$$k = 4.1 \cdot 10^{-5}, \quad r_0 = 155 \pm 15 \text{ for } E \geqslant 10 \text{ Bev}.$$

The distributions (7) for $N = 2 \times 10^5$ and $N = 6 \times 10^6$ are shown in Fig. 3 by solid lines.

Using distribution (7), we shall calculate the total flux of μ mesons with energies $E \geq 5$ and ≥ 10 Bev in EAS. We have

$$N_{\mu} = \int_0^{\infty} kN^{\alpha}r^{-n}\exp(-r^2/r_0^2)\,2\pi r dr$$
$$= \pi k r_0^{2-n}\Gamma(1 - n/2)\,N^{\alpha}. \qquad (8)$$

For $E \geq 5$ Bev we find $N_{\mu} = 0.24\,N^{0.85}$ and for $E \geq 10$ Bev we have $N_{\mu} = 0.13\,N^{0.85}$.

The calculated total number of μ mesons* shows that the exponent γ of the integral μ-meson energy spectrum over the whole shower is equal to 1 in the 5—10 Bev energy range.

We have studied the spectrum of EAS accompanied by m μ mesons traversing a detector with a given area s. This spectrum is related to the μ-meson density spectrum $I(\rho)d\rho = B\rho^{-\kappa'-1}d\rho$ in the following way:

$$I(m, s) = \int_{\rho_m}^{\infty} B\rho^{-\kappa'-1}(\rho s)^m e^{(-\rho s)}d\rho/m!$$
$$= Bs^{\kappa'}\int_{\rho_m s}^{\infty} x^{m-\kappa'-1}e^{-x}dx/m!. \qquad (9)$$

For μ mesons with energy $E \geq 10$ Bev, the spectrum I(m, s) was obtained with the triggering systems 1 and 5. The experimental values of I(m) for detector areas s equal to 3.15 and 6.3 m^2 respectively are shown in Fig. 4. In the figure, the m-1 scale is logarithmic to facilitate comparison with Eq. (11).

For $s = 6.3$ m^2 and $m > 7$, the spectra I(m) obtained with triggering systems 1 and 5 coincide. For the same value of s but for $m < 7$, the spectra are different. The spectrum $I(m < 7)$ ob-

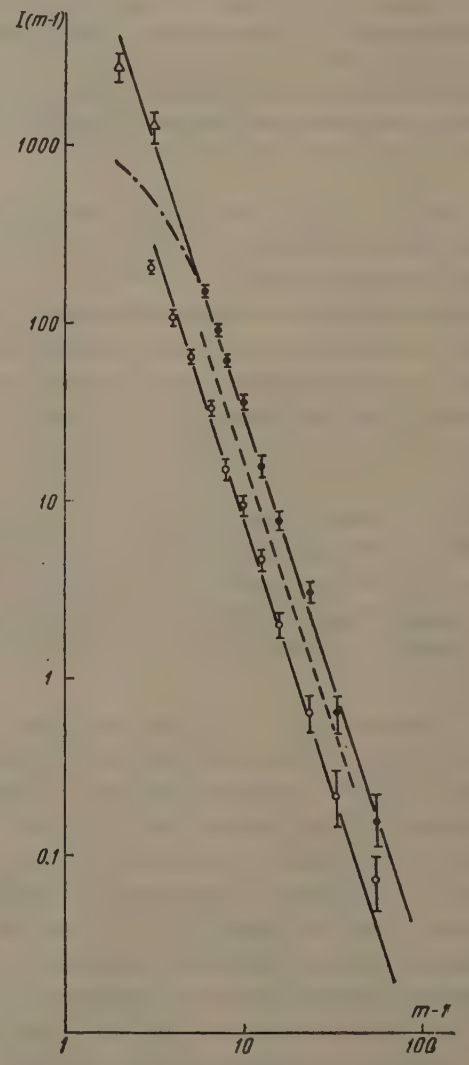

FIG. 4. Spectra I(m, s) for different E and s: o — $E \geqslant 10$ Bev, $s = 3.15$ m^2, triggering system 1; • — $E \geqslant 10$ Bev, $s = 6.3$ m^2, triggering system 1; △ — $E \geqslant 10$ Bev, $s = 6.3$ m^2, triggering system 5; dots — $E \geqslant 5$ Bev, $s = 3.15$ m^2; dot-dash — $E \geqslant 10$ Bev, $s = 6.3$ m^2, triggering system 1. The y axis represents the number of events in 1000 hours.

*The distributions $k_1 \exp(-r/r_1)$ or $k_2 r^{-n}\exp(-r/r_2)$, for which $k_{1,2}$ and $r_{1,2}$ were so chosen as to approximate the experimental lateral distribution in the range $r > 80$ m, give a result differing from Eq. (8) by not more than 10–15%.

Table II.

m	$I(\geq m)$, $s = 6.3$ m²	$I(\geq m)$, $s = 3.15$ m²	$\varkappa'$	m	$I(\geq m)$, $s = 6.3$ m²	$I(\geq m)$, $s = 3.15$ m²	$\varkappa'$
7	539	146	1.9±0.18	15	80	21	1.93±0.48
8	390	107	1.86±0.2	20	40	12	—
9	297	77	1.95±0.25	30	11	5	—
10	238	60	2.0±0.3	40	6	3	—
13	116	30	2.0±0.4	50	3	1	—

tained with system 1 is shown in Fig. 4 by the dashed line. The values of $I(m < 7)$ obtained with system 5 are shown in Fig. 4 by triangles.

The dependence of the selection system on the spectrum $I(m)$ can be described qualitatively by introducing the minimum μ-meson density ρ_m which will still be detected by the triggering system. The triggering systems 1 and 5 have different ρ_m. However, for $m > 7$ ($s = 6.3$ m²), both triggering systems give identical results. This means that the contribution of densities $\rho \sim \rho_m$ to the number of events with $m > 7$ is not important. In such a case, we can set $\rho_m = 0$. Equation (9) then simplifies to

$$I(m, s) = Bs^{\varkappa'}(m - \varkappa' - 1)!/m!,$$

$$\varkappa' = \log [I_1(m, s_1)/I_2(m, s_2)]/\log (s_1/s_2). \qquad (10)$$

Table II presents the integral spectra $I(>m)$ for μ mesons with $E \geq 10$ Bev and for two values of s, obtained during 1000 hours of operation. In the same table, the values of κ' calculated according to Eq. (10) are given. The mean value of κ' for the range $7 \leq m \leq 15$ is $\kappa' = 1.95 \pm 0.1$. Assuming $\kappa' = 2$, we obtain from Eq. (10)

$$I(m, s) \approx Bs^2 (m - 1)^{-3}. \qquad (11)$$

The straight lines of Fig. 4, with exponent equal to 3, are in good agreement with the experimental spectrum in the range $3 \leq m \leq 50$ for $s = 6.3$ m².

The shape of the spectrum $I(m)$ for μ mesons with energy $E \geq 5$ Bev coincides, within the limits of error, with the spectrum $I(m)$ for $E \geq 10$ Bev. In Fig. 4, the spectrum $I(m)$ for $s = 3.15$ m², $E \geq 5$ Bev is denoted by a dashed line. Thus, the exponent of the density spectrum of μ mesons with energy $E \geq 10$ Bev and $E \geq 5$ Bev has the value $\kappa' = 1.95 \pm 0.1 \approx 2$. The coefficient B is $B_1 = 0.8$ hour^{-1}m^{-4} for $E \geq 10$ Bev and $B_2 = 1.3$ hour^{-1} m^{-4} for $E \geq 5$ Bev.

The value of κ' obtained in studying the spectrum $I(m)$ is simply related to the exponent κ of the size spectrum of showers and to the exponent α in Eq. (7). If the size spectrum is $F(N)dN = AN^{-\kappa-1}dN$, and the μ-meson density is connected with r and N by Eq. (7), then the μ-meson density spectrum is

$$I(\rho)\, d\rho = B\rho^{-\varkappa/\alpha-1} d\rho,$$

$$B = A\alpha^{-1}k^{\varkappa/\alpha} 2\pi \int_0^\infty r\, [r^n \exp(r^2/r_0^2)]^{-\varkappa/\alpha} dr. \qquad (12)$$

The experimentally obtained value $\kappa' = \kappa/\alpha$ is in good agreement with the value $\alpha = 0.85$ for $\kappa = 1.65$.

The factor A can be determined for $\kappa = 1.65$ from the intensity of EAS of a given size given in [10]. We find $A = 1.25 \times 10^6$ hour^{-1} m^{-2}. Substituting the values n, α, and k from (7) into Eq. (12), we find $B_1 = 0.72$ hour^{-1} m^{-4}, which agrees with the experimental value of B_1.

DISCUSSION OF RESULTS

We compare the results obtained with the data of Andronikashvili and Bibilashvili [5] and Fukui et al [11] on the μ-meson flux with energy 5—10 Bev in EAS at sea level. Data of the Tokyo group on the lateral distribution of μ mesons with $E \geq 5$ Bev at distances $r < 100$ m from the shower axis are in good agreement with the data of the present experiment, both with respect to the absolute number of the μ mesons and with respect to the shape of the lateral distribution.

The results of Andronikashvili and Bibilashvili contradict the present data. In Fig. 3, the lateral distribution of μ mesons from [5] is shown by a dashed line. Analytically, this distribution can be written in the form

$$\rho(r) = 0.6 \exp(-r^2/r_0^2), \qquad r_0 = 41.7 \text{ m}.$$

As can be seen from Fig. 3, this distribution is much narrower than the lateral distribution obtained in the present experiment. The difference in the energy of the μ mesons investigated (corresponding to a depth of observation of 65 and 40 m w.e.) cannot explain the discrepancy. It is possible that the results of [5] are due to an inaccurate determination of the shower size at different distances from the shower axis because of the small size of the array used at sea level for detecting the EAS.

We shall, moreover, discuss which factor should play the main role in producing the observed

difference in the lateral distribution of high-energy μ mesons. Khristiansen[12] has calculated the lateral distribution of μ mesons with energy $E \geq 1.5 \times 10^{10}$ ev due to multiple scattering of particles in the atmosphere and their deflection in the earth's magnetic field. This distribution is shown in Fig. 3 by the dot-dash line. As can be seen from Fig. 3, the Coulomb scattering and the deflections in the earth's magnetic field cannot play a determining role in producing the discrepancy. A more probable main reason for the observed difference is the angular spread of π mesons in the nuclear interactions.

Let us estimate what transverse momentum must be gained by the π mesons in the nuclear interactions in order to explain the effect. For this we use the following approximate relation between the effective height h of π-meson production, the radius r of the μ-meson shower, the momentum p of the detected μ mesons, and the effective value of the transverse momentum $p_\perp$:

$$p_\perp = rp/h. \quad (13)$$

We assume that the height h can vary from 5 to 10 km. Then, substituting the values of r and p from (7) into (13), we find $p_\perp = 1-2 \times 10^8$ ev/c. It is interesting to note that the lateral distribution of μ mesons with energy $E \geq 6 \times 10^{11}$ ev obtained by Barrett et al,[13] characterized by a radius r = 10 m, leads to the value $p_\perp \approx 6 \times 10^8$ ev/c.

The mean energy of nuclear interactions in which μ mesons of $E \sim 10^{12}$ ev are produced is about 100 times higher than the energy of interactions producing μ mesons with $E \sim 10^{10}$ ev. Thus, the experimental data on the lateral distribution of μ mesons of different energies show that the mean transverse momentum gained by the π mesons increases with increasing energy of the nuclear interaction. This experimental prediction is in good agreement with the predictions of the hydrodynamical theory of the interaction of ultra-high-energy particles.[14]

Comparison of the data of the present experiment with those of Barrett et al.[13] also enables us to find a more exact energy spectrum of μ mesons in EAS. The spectrum of events involving μ mesons with energy $E \geq 6 \times 10^2$ Bev was found to be of the form $bN_\mu^{-3.4} dN_\mu$. Assuming that the relation between the number of μ mesons N_μ and the total number of particles in the shower N is $N_\mu \sim kN^\alpha$, we can relate the spectrum of events with a given size with the spectrum of events with a given number of μ mesons, and obtain the values of k and α (see the article of Greisen in[15]). However, it has been shown[2,11] that the relation between N_μ and N is correct only on the average, and that the number of μ mesons in showers with a given N fluctuates. If these fluctuations are taken into account in estimating N_μ, the number of μ mesons in EAS with given N decreases. Therefore, the estimate of the number of μ mesons with $E \geq 6 \times 10^2$ Bev given in[15] (60 μ mesons per shower with $N = 10^6$) should be regarded as the upper limit for N_μ. Using the number of μ mesons with energy $E \geq 10$ Bev found in present experiment, and the estimate of the number of μ mesons with energy $E \geq 6 \times 10^2$ Bev from[15], we find that the exponent of the integral energy spectrum of μ mesons in the range of E = 10—600 Bev should be $\gamma \geq 1.4$.

Assuming the spectrum of μ mesons to be of the form

$$f_\mu(E)\,dE = \begin{cases} k_1 E^{-2} dE & \text{for } E = 5 \div 10 \text{ Bev} \\ k_2 E^{-2.4} dE & \text{for } E \geqslant 10 \text{ Bev} \end{cases},$$

we obtain an energy of the μ mesons with $E \geq 5$ Bev equal to 7.2×10^{14} ev in a shower with $N = 10^6$. The energy of the particle producing a shower with $N = 10^6$ amounts to $E = 10^{16}$ ev, according to the usual estimate. Consequently, the energy of the μ-meson flux with $E \geq 5$ Bev amounts to ~7% of the primary particle energy.*

In conclusion, the author would like to thank Prof. S. N. Vernov and G. B. Khristiansen for constant attention and interest in the work and for discussing the results. The author expresses his gratitude to A. U. Fomin, who carried out a number of calculations, to N. I. Kvitek, M. Muminov, M. Zhadin, K. I. Solov'ev, V. I. Putintsev, V. K. Sokolov, E. V. Shein, G. Dyagtyareva, N. Proshina, and I. Massal'skaya, who took part in the measurements and the analysis of the results.

[1] Vernov, Khrenov, and Khristiansen, JETP **37**, 1252 (1959), Soviet Phys. JETP **10**, 891 (1960).

[2] Vernov, Solov'eva, Khrenov, and Khristiansen, JETP **41**, 340 (1961), Soviet Phys. JETP **14**, 246 (1962).

[3] Vernov, Tulupov, Khrenov, and Khristiansen, Proc. Cosmic Ray Conf. IUPAP, Moscow, 1959, Vol. II, p. 169.

[4] George, MacAnnuf, and Sturgess, Proc. Phys. Soc. **66A**, 345 (1953).

*It should be noted that the energy of the μ meson flux detected in the present experiment with E in the 5–10 Bev range amounts to 1.5×10^{14} ev for $N = 10^6$, which is roughly equal to the energy of the electron-photon component in EAS at sea level.

[5] E. L. Andronikashvili and M. R. Bibilashvili, JETP **32**, 403 (1957), Soviet Phys. JETP **5**, 341 (1957).

[6] G. V. Kulikov and G. B. Khristiansen, JETP **35**, 635 (1958), Soviet Phys. JETP **8**, 441 (1959).

[7] G. V. Bogoslovskii and B. A. Khrenov, PTÉ (Instruments and Exptl. Techniques) No. 4, 37 (1959).

[8] L. N. Korablev, ibid. No. 2, 56 (1956).

[9] Abrosimov, Goryunov, Dmitriev, Solov'eva, Khrenov, and Khristiansen, JETP **34**, 1077 (1958), Soviet Phys. JETP **7**, 746 (1958).

[10] Kulikov, Nesterova, Nikol'skii, Solov'eva, Khristiansen, and Chudakov, Proc. Cosmic Ray Conf. IUPAP, Moscow 1959, vol. II.

[11] Fukui, Hasegawa, Matano, Miura, Oda, Ogita, Suga, Tanahashi, and Tanaka, Proc. Cosmic Ray Conf. IUPAP, Moscow, 1959, vol. II.

[12] G. B. Khristiansen, JETP **34**, 956 (1958), Soviet Phys. JETP **7**, 661 (1958).

[13] Barrett, Bollinger, Cocconi, Eisenberg, and Greisen, Revs. Modern Phys. **24**, 133 (1952).

[14] G. A. Milekhin, JETP **36**, 1185 (1958), Soviet Phys. JETP **9**, 843 (1959).

[15] K. Greisen, Progress in Cosmic Ray Physics **3**, North-Holland Publishing Co., Amsterdam, 1956.

Translated by H. Kasha
241

THE INFLUENCE OF ANTIMONY IMPURITIES ON THE DE HAAS-VAN ALPHEN EFFECT IN BISMUTH

N. B. BRANDT and V. V. SHCHEKOCHIKHINA

Moscow State University

Submitted to JETP editor May 23, 1961

J. Exptl. Theoret. Phys. (U.S.S.R.) 41, 1412-1420 (November, 1961)

The de Haas-van Alphen effect has been studied in Bi-Sb alloys with Sb concentration of 0—1 wt. % over a temperature range 1.6—4.2°K, for various orientations of the magnetic field relative to the crystallographic axes of the specimens. It was established that the shape of the Fermi surface and the electron effective-mass tensor do not change in first approximation with increasing Sb concentration, and the surface itself contracts toward its center, preserving its shape. At 1 wt. % Sb, the volume of every ellipsoid of the Fermi surface decreases to nearly one half. The limiting Fermi energy and the electron concentration decrease with increasing Sb concentration, changing by 24 and 38 %, respectively, for 0.8 wt. % Sb. The Sb impurity produces a nearly linear increase in the constant part of the magnetic susceptibility, amounting to 10—12 percent at one wt. % Sb. A comparison of the results with data on the influence of elastic deformations on the de Haas-van Alphen effect shows that changes in the energy spectrum of the Bi electrons can be fully explained by the change of the lattice parameters of Bi under the influences of the Sb impurities.

INTRODUCTION

In spite of the fact that a rather large number of researches[1-5] have been devoted to a study of the electrical and magnetic properties of Bi-Sb alloys, there have been no data to date which make possible a direct determination of the character of the change in the energy spectrum of Bi electrons with increasing Sb concentration.

The assumption has been made by Jones[6] that elements forming solid solutions with Bi should be regarded as donors or acceptors, depending on their position in the periodic system. This point of view has been emphasized in a number of researches.[7,8,2,3] In particular, it was shown in[8] that the Pb impurity, which is regarded as an acceptor, actually produces a decrease in concentration of conduction electrons in Bi, and that this process is not linear. The rate of change of the electron concentration increases with increase in Pb concentration and ~55 Pb atoms are required on average for a unit change in the electron concentration.

From Jones' viewpoint, impurities should not change the electron structure of the elements in the same group of the periodic system, as Bi. However, in the study of the effect of Sb impurities on the quantum oscillations of the magnetic susceptibility of Bi,[2] a decrease was observed in the lowest frequency of oscillations, to which the work mentioned was confined. Since the frequency of the oscillations is proportional to the area S_m of the extremal cross section of the Fermi surface in the plane perpendicular to the direction of the magnetic field H,[9] and the Fermi surface for Bi electrons consists of three strongly anisotropic ellipsoids, the result obtained shows a decrease in the area of the smallest of the three principal cross sections of the ellipsoids with increasing Sb concentration.* Moreover, in the study of the electrical properties of Bi-Sb alloys[6] a significant change has been discovered in the energy spectrum of the Bi electrons upon addition of Sb. Neither of these effects can be explained on the basis of the Jones model, since Bi and Sb are both located in the same (fifth) group of the periodic table.

X-ray studies of the structure of Bi-Sb alloys,[11,5] representing a series of solid solutions, demonstrate that the Sb produces a significant change in the parameters of the Bi lattice, even in the region of low Sb concentrations (Fig. 1).

*The ellipsoids are located in quasi-momentum space in such a way that the minor axes are parallel to the binary axes, while the major axes are inclined at an angle of $\zeta = 5.5°$ to a plane perpendicular to the trigonal axis. The ellipsoids transform into one another upon rotation through an angle of 120° about the trigonal axis.[10]

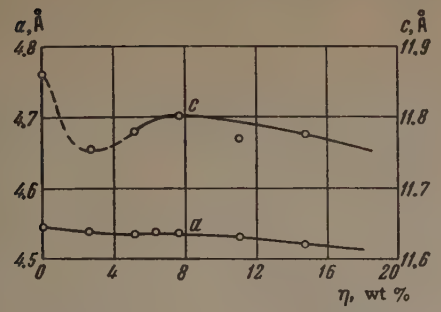

FIG. 1. Dependence of the lattice parameters of Bi, c (in the direction of the trigonal axis) and a (perpendicular to the trigonal axis), on the concentration of Sb.

Since hydrostatic compression also changes the band structure of Bi,[12-14] it can be assumed that the chief reason for the change in the energy spectrum of the Bi electrons upon addition of Sb is the decrease in the lattice parameters.

The present research was undertaken to obtain similar data on the character of the energy spectrum of the electrons in Bi-Sb alloys, as well as a comparison of the results with the data of[12-14].

METHODS OF MEASUREMENT; SPECIMENS

The anisotropy $\Delta\chi$ of the magnetic susceptibility of the samples was measured on a magnetic torsion balance with an automatic recording system.[15] The measurements were carried out in a homogeneous magnetic field up to 13 koe for temperatures 1.6—4.2°K in two modes; with continuous application of the magnetic field and recording the signal on the chart of an ÉPP-09 electronic potentiometer, and (as a control) with sudden application of the magnetic field and recording the output signal with a pointer galvanometer of the M-101 type. The temperature was determined from the vapor pressure of liquid helium.

Samples of cylindrical shape, with diameter ~3.8 and length 6—7 centimeters, were prepared from "Hilger" Bi (purity 99.998 %), purified by twenty vacuum recrystallizations, and from "Hilger" Sb. The method of preparation of the samples was similar to the method described earlier.[8] After preparation, the specimens were annealed in an atmosphere of gaseous helium at 260°C over a period of 40 days.

The crystallographic orientation of the specimens was determined by a goniometer with accuracy to within 0.2—0.3°.

To eliminate possible systematic error in the determination of the Sb concentration, two groups of samples were prepared with overlapping concentration values: 0; 0.1; 0.4; 0.6 and 0.3; 0.8; 1.0 wt. % Sb.

The correctness of the relative distribution of the impurities among the specimens is also confirmed by the monotonic increase in the residual electron resistance of the samples with increasing Sb concentration.

RESULTS OF MEASUREMENT

To obtain the most complete data on the character of the change in the Fermi surface for Bi electrons, measurements were carried out for a so-called "non-symmetric" orientation of the samples in the magnetic field: the trigonal axis is perpendicular, and the twofold axis is parallel, to the axis of suspension of the balance. For each specimen we plotted the dependence of the moment of forces N on the direction of the magnetic field H for different values of the angle x between the direction of the trigonal axis and the field. Measurements were obtained for the angles $x = 0, \pm 1, \pm 2, \pm 3, \pm 4, \pm 5, \pm 6, \pm 10, \pm 82, \pm 84°$ at 1.67°K, and $x = -25, -30, -35, \pm 40°$ at 3.37 and 1.685°K. Measurements were not made at other angles, since the N(H) curves observed for them are superpositions of adjacent frequencies with comparable amplitudes, which complicates their interpretation.

The dependence of the anisotropy of the magnetic susceptibility $\Delta\chi = N/H^2 \sin\psi \cos\psi$ on 1/H is shown in Fig. 2 for specimens of the original Bi and for Bi with 0.4 and 0.6 wt. % Sb (for $\psi = -35°$), and 0.8 and 1.0 wt. % Sb (for $\psi = -30°$), at 3.37 and 1.685°K. As is seen from the drawing, the amplitude of the oscillations ω falls off with increase in the Sb concentration. It should be noted that although the oscillations in the magnetic susceptibility continue at concentrations exceeding 1 wt. % Sb, analysis of the temperature dependence of the amplitude of these oscillations is exceedingly difficult, which forces us to limit ourselves to the concentration region 0 to 1 % Sb.

Curves are plotted in Fig. 3 for the angular dependence of the frequency of oscillations $E_0/\beta_i(\psi) \sim S_m(\psi)$ (see the formulas of Landau in[10]) for samples of the original Bi and Bi-Sb alloys with 0.8 and 1.0 wt. % Sb. It is seen from the drawing that the Sb impurities cause a decrease in the oscillation frequency for all values of ψ, and that the angle of rotation of the Fermi-surface ellipsoids around the twofold axes does not change within the limits of accuracy of the experiment ($\pm 0.3°$).

The values of the relative change of the oscillation frequency (and, consequently, of the quantity

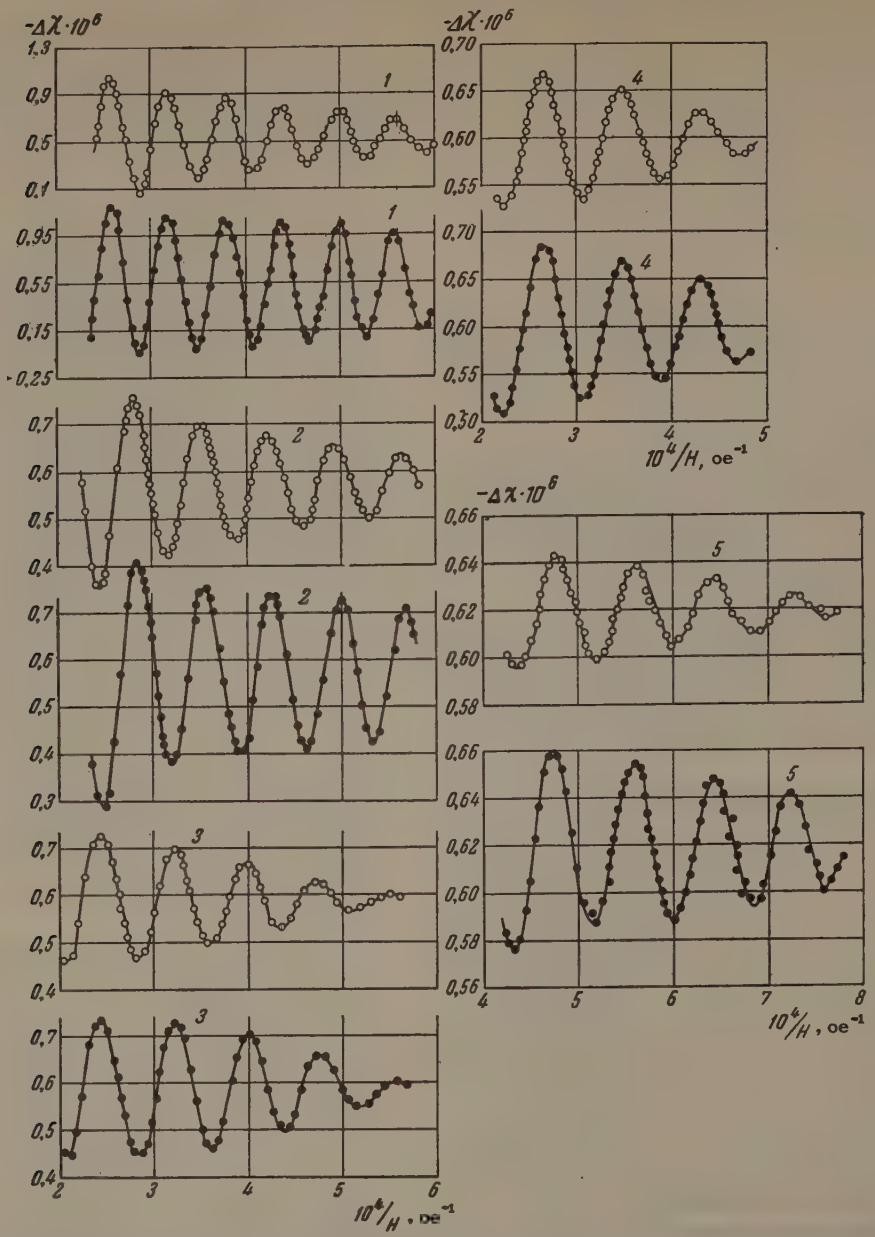

FIG. 2. Dependence of the anisotropy of the magnetic susceptibility for Bi-Sb alloys on the magnetic field intensity. Curves: 1 – original Bi, 2 – Bi with 0.4 % Sb and 3 – Bi with 0.6 % Sb (for $\psi = -35°$); 4 – Bi with 0.8 % Sb, and 5 – Bi with 1.0 % Sb (for $\psi = -30°$); white circles, T = 3.37°K, black circles, T = 1.685°K.

$\Delta S_m/S_m$) for different values of the angle ψ are shown in Fig. 4. The angle ψ = 82—84° corresponds to a change in the smallest principal cross section S_1 of the Fermi surface ellipsoids (which Shoenberg observed[2]). The change in the average principal cross section S_2 can easily be obtained by extrapolation of the curves of Fig. 4 from the region of negative values of ψ through the value ψ = 0 to 5.5°. It is thus evident that the minimum, average, and all intermediate cross sections of the Fermi surface are decreased by the same percentage, in first approximation. The small increase in the ratio $\Delta S_m/S_m$ as $\psi \to 0°$ for the sample with 0.3 % Sb (which, to be sure, was observed earlier[13]), is obviously connected with secondary reasons, and is not characteristic of the change in the Fermi surface of Bi upon change in the lattice parameters. Evidently certain divergences in the data for minimum S_1 and average S_2 of the principal cross sections also have the random character associated with possible inaccuracy of orientation of the specimens (especially for the specimen with 1.0 % Sb).

The dependence of the percentage change in S_m on the concentration of Sb impurity is given in Fig. 5. This dependence differs markedly from the linear in the region of small concentrations. The values of $\Delta S_1/S_1$ obtained by Shoenberg[2] for Bi-Sb alloys (0.67 and 0.9 % Sb) are in good agreement with the data given here.

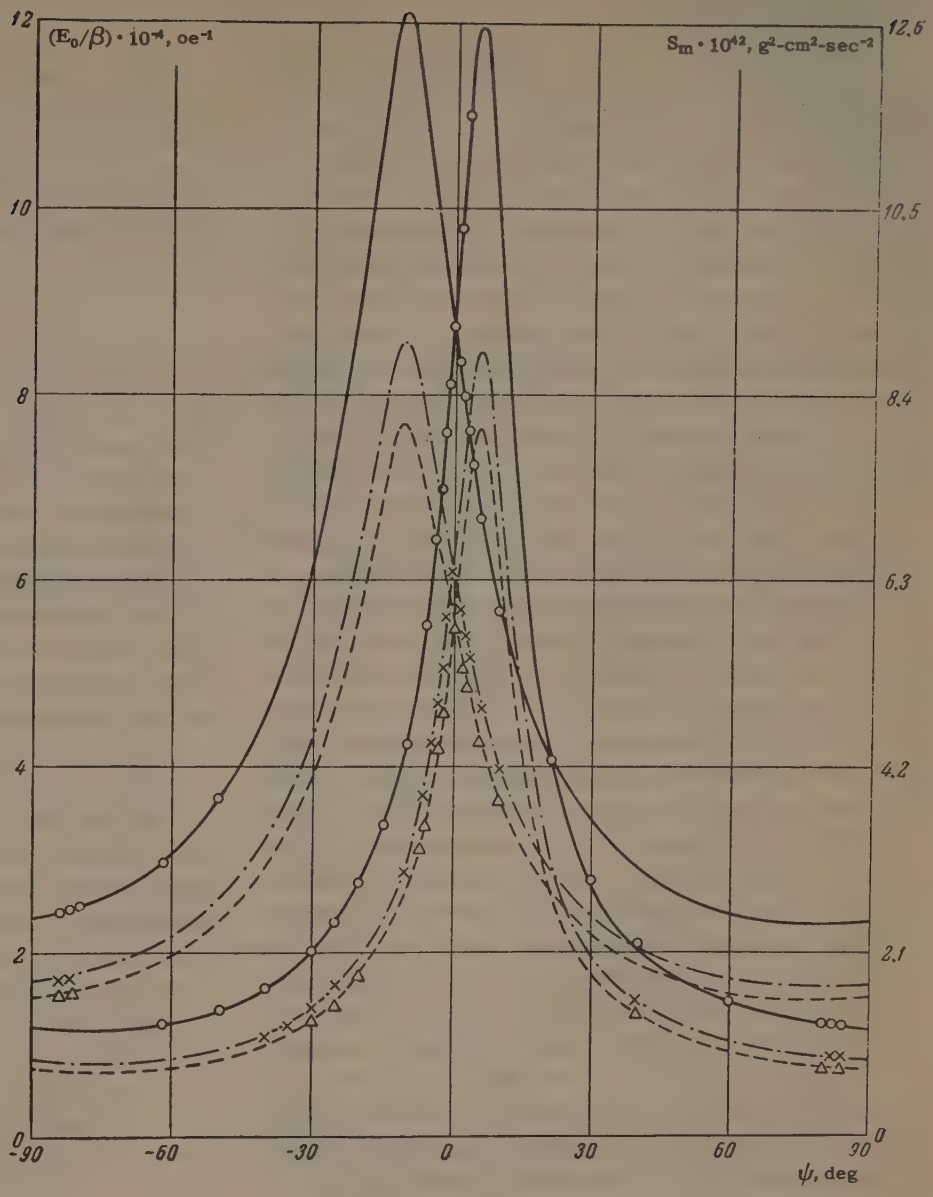

FIG. 3. Dependence of the oscillation frequency $E_0/\beta_i \sim S_m$ on the angle between the direction of the trigonal axis of the sample and the magnetic field (the two-fold axis is parallel to the suspension of the sample). o – original Bi (solid lines) × – Bi with 0.8 % Sb (dot-dash curve), Δ – Bi with 1 % Sb (dashed curve).

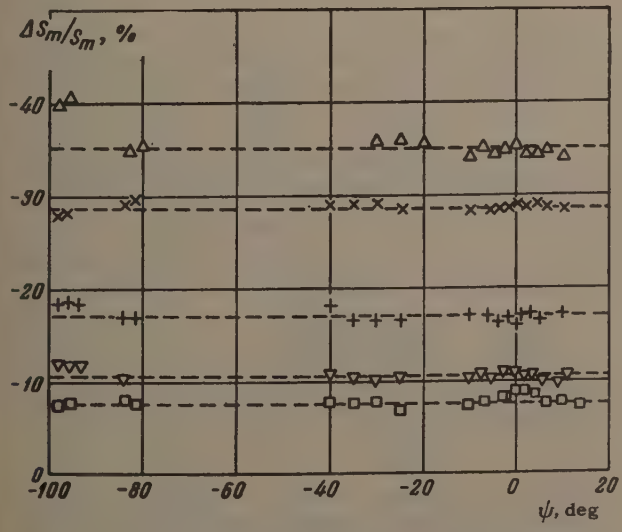

FIG. 4. Angular (ψ) dependence of the relative change in the area $\Delta S_m/S_m$ of the extremal cross sections of the Fermi surface; □ – Bi with 0.3 % Sb, ▽ – Bi with 0.4 % Sb, + – Bi with 0.6 % Sb, × – Bi with 0.8 % Sb, Δ – Bi with 1 % Sb.

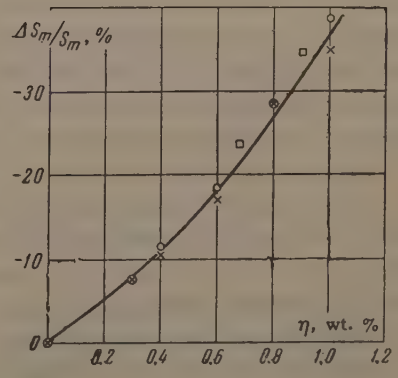

FIG. 5. Change in the area of the extremal cross sections of the Fermi surface with increase in the Sb concentration: o – for cross sections close to S_1, × – for cross sections close to S_2; □ – data of [2] for orientation of H perpendicular to the trigonal axis of the sample.

DISCUSSION OF RESULTS

1. Change in the shape of the Fermi surface for electrons. The anisotropy of the Fermi surface for electrons is determined on the basis of the anisotropies of the cross sections S_1 and S_2, which differ in area by a factor of about 10 (Fig. 3). The cross section S_3, according to Shoenberg's data,[10] exceeds S_2 by a factor of 3.2, while, from cyclotron resonance data,[10] the cross sections S_2 and S_3 are close to one another. It should be noted that the Shoenberg data on the cross section area S_3 are inaccurate, since the quantum oscillations of the magnetic susceptibility, which correspond to the cross section S_3 and cross sections close to it, have not been observed to date, because of their small amplitude, and the quantity S_3 was determined by an overextended extrapolation.

Taking it into account that the anisotropy of the cross sections S_2 and S_3 is not large in any case, while the cross sections S_1 and S_2 change under the action of the Sb impurity in the same percentage ratio, it is natural to assume that the cross section S_3 also changes in similar fashion. Thus, one can conclude that upon increase in the Sb concentration, the shape of the Fermi surface for the Bi electrons does not change, while the surface itself is drawn toward the central point, remaining similar to itself. At a concentration $\eta = 1$ wt. % Sb, the volume of each ellipsoid is reduced approximately by a factor of two. We note that the possibility of extrapolation of the dependence of $\Delta S_m/S_m$ on η (Fig. 5) in the region of large values of the Sb concentration depends on the mechanism of the effect of Sb on the energy spectrum of the Bi electrons. If this mechanism results in the change of the lattice parameters (Fig. 1), then, because of the lack of accurate data for the lattice parameters in the region of concentrations of less than ~3 % Sb, it is difficult to say in what manner the change of the volume of the ellipsoids will take place upon further increase in the Sb concentration, and whether the ellipsoids manage to reduce to points before the lattice parameter c reaches a minimum.

2. Change in the concentration of the electrons. On the basis of data on the change in the principal cross sections of the Fermi-surface ellipsoids brought about by changes in the Sb concentration, one can easily compute the change in the electron concentration (see[9]). The percent change in the electron concentration is shown in Fig. 6 (curve A).

3. Change in the limiting Fermi energy E_0 for electrons. The curves of the dependence of $\Delta\chi$ on H, taken at various temperatures, were used for the calculation of E_0 (Fig. 2). The value of $\beta(\psi)$ was determined from the increase in the ratio of the oscillation amplitudes, and E_0 was determined from the value of $E_0/\beta(\psi)$ known for each angle ψ. For each ψ, the oscillation amplitudes at different magnetic field intensities were compared and an average value was obtained from the data. The scheme of calculation, which is similar to that described earlier,[8] is illustrated in Table I, which applies to a Bi sample with 0.3 % Sb at $\psi = -30°$.

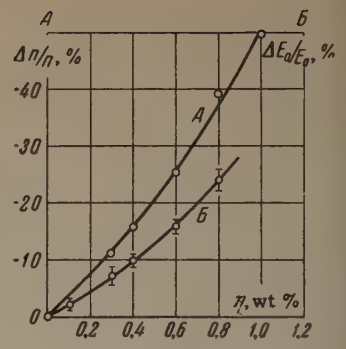

FIG. 6. Per cent change in the electron concentration n (curve A) and the limiting Fermi energy E_0 for Bi electrons (curve B) with increasing Sb concentration.

The values of E_0 computed for the specimens of Bi and Bi-Sb studied are shown in Table II for different values of the angle ψ. Data for a specimen with a 1% Sb content are not given, since the analysis of the temperature change of the amplitude becomes very difficult for such a concentra-

Table I

$(1/H)\cdot10^4$	ω, arbitrary units: 3,37°K	1,685° K	ω (1,685° K) / ω (3,37° K)	$\beta\cdot10^{18}$, ergs/oe
3,1	198	282	1,42	1,60
3,4	128	196	1,53	1,57
3,7	90	147	1,63	1,58
4,0	64	112	1,75	1,58
4,3	47	86	1,83	1,63
4,6	36	70	1,93	1,65
4,9	28	57	2,04	1,68
5,2	22	48	2,20	1,65
5,5	18	42	2,33	1,69
5,8	14,8	37	2,50	1,69
6,1	11	31	2,82	1,65
			β_{av}=1,63±0,04	

Table II

η, %	$E_0\cdot10^{14}$, ergs: ψ=−25°	−30°	−35°	−40°	$E_0\cdot10^{14}$, ergs
0,00	2,77	2,73	2,73	2,74	2,74±0,02
0,11	2,64	2,67	2,74		2,68±0,03
0,30	2,54	2,60	2,62	2,42	2,54±0,06
0,40	2,45	2,46	2,55	2,44	2,47±0,03
0,60	2,32		2,34	2,25	2,30±0,03
0,80	2,08	2,01	2,15	2,10	2,08±0,05

tion. The dependence on the Sb concentration of the percent change in the limiting Fermi energy is pictured in Fig. 6 (Curve B).

4. Change in the effective masses. As has been noted, all three principal cross sections of the ellipsoids S_1, S_2 and S_3 change in the same ratio upon increase in the concentration. It is easy to show that[8] in this case the change in the effective masses m_1, m_2 and m_3, in a system of coordinates connected with the principal axes of the Fermi-surface ellipsoids, is determined by the relation

$$\frac{\Delta m_1}{m_1} = \frac{\Delta m_2}{m_2} = \frac{\Delta m_3}{m_3} = \frac{\Delta S_m}{S_m} = \frac{\Delta E_0}{E_0}. \quad (1)$$

As is seen from Figs. 5 and 6, the curves for the dependence of $\Delta S_m/S_m$ and $\Delta E_0/E_0$ on η coincide with one another within the limits of accuracy. Therefore, it can be assumed that the effective masses for Bi do not change in the increase of Sb concentration from 0 to 1 per cent.

A similar conclusion can be obtained on the basis of Fig. 6. The dependences of $\Delta n/n$ and $\Delta E_0/E_0$ on the concentration η shown in Fig. 6 satisfy the relation $\Delta n/n = 3\Delta E_0/2E_0$, which is valid in the region of small changes of $\Delta E_0/E_0$ under the assumption that the effective mass of the electrons does not change upon increase in the Sb concentration.

5. Comparison of the results with experiments on the influence of elastic deformation on the de Haas-van Alphen effect in Bi. According to the data of Bridgman, the change in the lattice parameters in Bi, for unilateral compression (at room temperature), is given by the formula

$$-\Delta l/l_0 = \alpha \cdot 10^{-7} p, \quad (2)$$

where α are the coefficients of compressibility, equal, respectively, to 15.9 and 6.6 in directions parallel and perpendicular to the trigonal axis, and p is the pressure in kg/cm^2.

The maximum changes in the lattice parameters of Bi, brought about by Sb impurities in the region of small concentrations (for η = 2.5 % Sb) (Fig. 1) are: $-\Delta c/c$ = 0.9 %; $-\Delta a/a$ = 0.18 %. Since different pressures p (5700 and 2700 kg/cm^2) correspond to such changes in the parameters c and a [according to Eq. (2)], their change does not correspond to the conditions of hydrostatic compression. The effect of the change in the Bi lattice under the action of Sb can be represented as the result of hydrostatic (p) and a unilateral (σ) compression (along the c axis) of the specimen. Unfortunately, since the compressibility coefficients of Bi are not known at low temperatures, nor is there an accurate form of the dependence of the lattice parameter c for small Sb concentrations, we must limit ourselves to a rough comparison only, making use of the data at hand.

The changes in the parameters of the lattice under the action of impurities are associated with the values of p and σ by the relations

$$-(\Delta c/c) = 15.9 \cdot 10^{-7}(p + \sigma),$$
$$-(\Delta a/a) = 6.6 \cdot 10^{-7} p + 15.9 \cdot 10^{-7} j\sigma, \quad (3)$$

where j is Poisson's ratio, equal to −0.33 for Bi. For a concentration of 1 wt. % we have $-\Delta c/c \approx 0.6$ % and $-\Delta a/a \approx 0.12$ %. On the basis of Eq. (3), this change corresponds to a hydrostatic compression p ≈ 2400 kg/cm^2 and a unilateral compression with stress $\sigma \approx 1300$ kg/cm^2.

It is well known that a hydrostatic compression of ~1200 kg/cm^2 changes the relative area $\Delta S_m/S_m$ of the extremal cross sections of the Fermi surface for Bi by about −7 per cent,[12,13] while a unilateral compression with a stress σ = 350 kg/cm^2 causes a change of −6.5 %.[14] Extrapolation of these values to the region of high pressures gives (for p = 2400 kg/cm^2 and σ = 1300 kg/cm^2) changes in $\Delta S_m/S_m$ of ~14 and ~24 %, respectively. The general change of $\Delta S_m/S_m$ under the action of elastic deformations of the lattice, which is equivalent in magnitude to the deformations produced by an impurity of 1 wt. % Sb, amounts to about 38 % which is in excellent agreement with the experimental data given in Fig. 5.

It should be noted also that the data on the change of the constant part of the anisotropy of the magnetic susceptibility $\Delta\chi_0$ in Bi for hydrostatic compression, and for an increase in the Sb concentration, agree with one another within the limits of accuracy of the experiment. The Sb impurity produces an approximately linear increase in $\Delta\chi_0$ (see Fig. 2), amounting to 10—12 % for 1 wt % Sb. By considering this effect as the result of a change in the lattice parameters for Bi, one can expect hydrostatic compression to produce a small increase in $\Delta\chi_0$, not exceeding 2—3 % for a pressure of 1200 kg/cm^2. An effect of just this order was observed in a previous research.[13] Thus, one can assume that the change in the energy spectrum of the Bi electrons under the effect of the Sb impurities, in the region of small concentrations, is evidently connected in a fundamental way with changes that take place in this case in the parameters of the crystalline lattice of Bi.

In conclusion, we take this opportunity to thank A. I. Shal'nikov for his interest in the work and Yu. A. Bychkov for discussion of the results.

[1] A. W. Smith, Phys. Rev. **32**, 178 (1911).
[2] D. Shoenberg and M. Z. Uddin, Proc. Roy. Soc. (London) **A156**, 687 (1936).
[3] N. Thompson, Proc. Roy. Soc. (London) **A155**, 111 (1936), **A164**, 24 (1938).
[4] B. Abeles and S. Meiboom, Phys. Rev. **101**, 544 (1956).
[5] A. L. Jain, Phys. Rev. **114**, 1518 (1959).
[6] H. Jones, Proc. Roy. Soc. (London) **A147**, 396 (1934), **A155**, 635 (1936).
[7] Alekseevskii, Brandt, and Kostina, Doklady Akad. Nauk SSSR **105**, 45 (1955).
[8] N. B. Brandt and M. V. Razumeenko, JETP **39**, 276 (1960), Soviet Phys. JETP **12**, 198 (1961).
[9] I. M. Lifshitz and A. M. Kosevich, JETP **29**, 330 (1955), Soviet Phys. JETP **2**, 636 (1956), Doklady Akad. Nauk SSSR **96**, 963 (1954).
[10] D. Shoenberg, Phil. Trans. Roy. Soc. (London) **A245**, 1 (1952), Proc. Roy. Soc. (London) **A170**, 341 (1939).
[11] W. F. Ehret and M. B. Abramson, J. Am. Chem. Soc. **56**, 385 (1934).
[12] Verkin, Lazarev and Dmitrenko, JETP **31**, 538 (1956), Soviet Phys. JETP **4**, 432 (1958).
[13] H. B. Brandt and V. A. Venttsel', JETP **35**, 1083 (1958), Soviet Phys. JETP **8**, 757 (1959).
[14] N. B. Brandt and G. A. Ryabenko, JETP **37**, 389 (1959), Soviet Phys. JETP **10**, 278 (1960).
[15] N. B. Brandt and Ya. G. Ponomarev, PTÉ (Instrum and Exptl. Techniques) No. 6 (1961).
[16] Galt, Yager, Merrit and Cetlin, Phys. Rev. **114**, 1396 (1959).

Translated by R. T. Beyer
242

PHOTOPROTONS FROM Pr^{141}

V. G. SHEVCHENKO and B. A. YUR'EV

Institute of Nuclear Physics, Moscow State Unitersity

Submitted to JETP editor June 6, 1961

J. Exptl. Theoret. Phys. (U.S.S.R.) 41, 1421-1426 (November, 1961)

The angular and energy distributions and the yields of photoprotons from Pr^{141} are measured for maximum bremsstrahlung energies of 22.5 and 33.5 Mev. The results indicate that the maximum photoproton production cross section corresponds to γ quanta above 22 Mev and that the absorption of γ quanta in this energy region is chiefly of quadrupole character.

PROTON emission resulting from the dipole absorption of γ radiation is strongly inhibited by the high Coulomb barrier of heavy nuclei, so that the photodisintegration of these nuclei results mainly in neutron emission. It thus becomes possible to distinguish protons resulting from the quadrupole absorption of γ radiation. The cross section for the latter process must lie in a higher energy range, so that some of the emitted protons will have high energies.[1]

Several investigations of angular and energy distributions of photoprotons from heavy nuclei have been published.[2-5] In almost all instances bremsstrahlung having $E_{\gamma max} = 22-24$ Mev was used, whereas quadrupole resonance absorption evidently occurs at somewhat higher energy. Exceptions occurred in the photodisintegration of Pb and Bi for $E_{\gamma max} = 24$ Mev,[2,3] where strong asymmetry was observed favoring small angles. This effect apparently results from the fact that for heavy nuclei such as Pb and Bi, even at the given relatively low energies the total γ-ray abosrption cross section involves a considerable contribution from quadrupole transitions.

In the present work bremsstrahlung having $E_{\gamma max} = 22.5$ and 33.5 Mev was used to investigate the energy and angular distributions of protons from the photodisintegration of Pr^{141}.

EXPERIMENTAL PROCEDURE

Our bremsstrahlung source was the 35-Mev betatron of the Institute of Nuclear Physics at Moscow State University. The experimental arrangement is shown in Fig. 1. The γ-ray beam passed through a lead collimator 32 cm thick and a clearing magnet before impinging on the target in the vacuum chamber. The target was metallic praseodymium foil 31.1 mg/cm^2 thick placed at an angle of 30° to the γ-ray beam. The principal impurities in the target were not more than 1.5% of rare earth elements and not more than 0.1% of other elements.

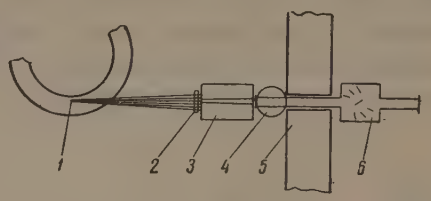

FIG. 1. Arrangement of apparatus: 1 – betatron target, 2 – thin-walled monitor chamber, 3 – collimator, 4 – clearing magnet, 5 – shielding wall, 6 – vacuum chamber in magnetic field.

Protons leaving the target were registered on photoplates with type T-3 NIKFI emulsion 400 μ thick disposed in the chamber at angles of 30, 45, 60, 75, 90, 120, 135, and 150° with respect to the γ-ray beam. Type T-3 plates were used to permit an increased radiation dose, since this emulsion is considerably less sensitive to the electron background than the type Ya-2 emulsion ordinarily used. In order to reduce the electron background of plates placed at acute angles, during irradiation

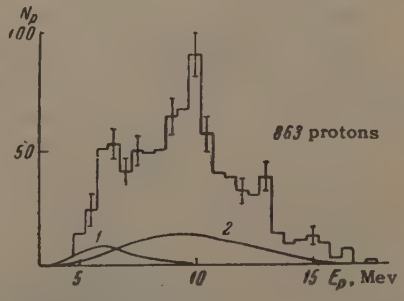

FIG. 2. Energy distribution of photoprotons from Pr^{141} produced by radiation having $E_{\gamma max} = 22.5$ Mev. The continuous curve 1 is the computed spectrum of evaporation protons; curve 2 is the computed spectrum of direct-photoeffect protons.

Table I. Parameters of type (1) curves approximating the angular distributions of photoprotons from Pr^{141}, and values of $\sigma_{E2}/\sigma_{E1+E2}$ derived from the $\sigma_{E2}/\sigma_{E1} = p^2/5$

$E_{\gamma max}$, Mev	Proton energy, Mev	a	b	p	$\sigma_{E2}/\sigma_{E1+E2}$, %
22.5	4.5—7.25	31	15.7	0.42	~3
	7.25—11.25	44	66	0.32	~2
	≥11.25	12	27.5	0.44	~4
33.5	4.5—7.25	71	23.4	1.4	~30
	7.25—11.25	153	57	2.2	~50
	≥11.25	50	71.4	1.8	~40

the vacuum chamber was placed in a ~600-oe magnetic field that deflected electrons emitted from the target to prevent their direct impingement on the emulsion. The permissible radiation dose thus became several times larger.

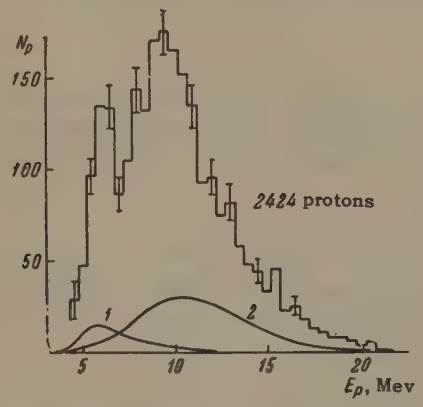

FIG. 3. Energy distribution of photoprotons from Pr^{141} produced by radiation having $E_{\gamma max}$ = 33.5 Mev. The notation is the same as in Fig. 2.

The position of the beam axis relative to the center of the chamber was determined by means of x-ray film and was monitored by comparing the effects on two plates positioned at 90° angles symmetrically with respect to the target center.

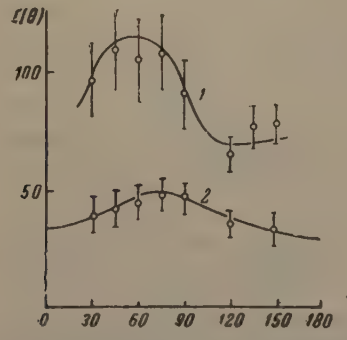

FIG. 4. Angular distribution of 4.5–7.25 Mev photoprotons (first group): 1 – for $E_{\gamma max}$ = 33.5 Mev; 2 – for $E_{\gamma max}$ = 22.5 Mev. The continuous approximating curves have the parameters given in Table I.

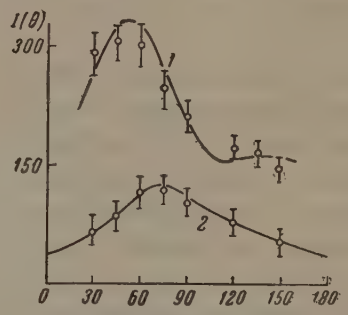

FIG. 5. Angular distribution of 7.25–11.25 Mev photoprotons (second group): 1 – for $E_{\gamma max}$ = 33.5 Mev; 2 – for $E_{\gamma max}$ = 22.5 Mev.

Absolute solid angles were determined graphically and by calculation. In scanning we selected tracks that started at the emulsion surface, corresponding to protons having energies ≥1.0 Mev and originating in the irradiated portion of the target. Proton energy was determined from the range-energy curve for Ilford C-2 emulsion, with a correction for the ~5% density difference between T-3 and C-2 emulsions. A correction was also introduced for energy loss in the target.

EXPERIMENTAL RESULTS

Figures 2 and 3 show the energy distributions of protons produced in the photodisintegration of

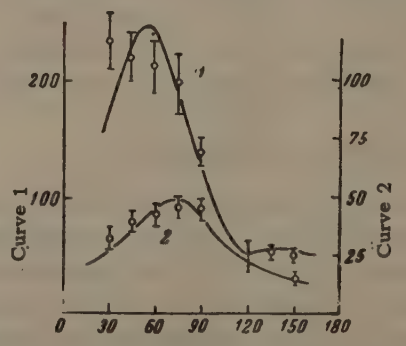

FIG. 6. Angular distribution of photoprotons of ≥11.25 Mev (third group): 1 – for $E_{\gamma max}$ = 33.5 Mev; 2 – for $E_{\gamma max}$ = 22.5 Mev.

Table II. Principal E1 and E2 proton transitions of Pr^{141}

Multipolarity	Transition	No. of nucleons in initial state	Proton energy, Mev*	γ-transition energy, Mev
E1	$2d_{5/2} \rightarrow 2f_{7/2}$	1	5— 7	11—13
	$2d_{5/2} \rightarrow 2f_{5/2}$	1	8—10	13—15
	$1g_{7/2} \rightarrow 1h_{9/2}$	8	7— 9	14—16
	$1g_{7/2} \rightarrow 2f_{7/2}$	8	5— 7	12—14
	$1g_{7/2} \rightarrow 2f_{5/2}$	8	8—10	15—17
	$1g_{9/2} \rightarrow 2f_{7/2}$	10	5— 7	17—19
	$2p_{1/2} \rightarrow 3d_{5/2}$	2	14—16	26—28
	$2p_{3/2} \rightarrow 3d_{5/2}$	4	13—15	26—28
E2	$1g_{9/2} \rightarrow 1i_{13/2}$	10	4— 6	16—18
	$1g_{7/2} \rightarrow 1i_{11/2}$	8	12—14	19—21
	$2d_{5/2} \rightarrow 2g_{9/2}$	1	10—12	16—18
	$2d_{5/2} \rightarrow 2g_{7/2}$	1	13—15	19—21
	$2d_{5/2} \rightarrow 4s_{1/2}$	1	14—16	20—22
	$2p_{1/2} \rightarrow 2f_{5/2}$	2	4— 6	16—18
	$2p_{3/2} \rightarrow 2f_{7/2}$	4	2— 4	15—17
	$2p_{3/2} \rightarrow 2f_{5/2}$	4	4— 6	17—19
	$1f_{5/2} \rightarrow 1h_{9/2}$	6	4— 6	20—22
	$1f_{7/2} \rightarrow 1h_{9/2}$	8	4— 6	22—24

*Proton and γ-ray energies in the case of E1 absorption have been increased by 4—5 Mev compared with single-particle calculations[5] in order to take account of residual interactions. This has not been done for E2 transitions, since the magnitudes of the residual interactions are unknown for highly excited states.

Pr^{141} by γ radiation with $E_{\gamma max}$ = 22.5 and 33.5 Mev. The graphs have taken into account the background, which was ~5% on the average, except at 30°, where the background was ~20%. The spectra included a small contribution from deuterons, tritons, and α particles, whose tracks were not identified. This contribution evidently did not exceed a few percent.

The energy spectra exhibit overall similarity. Both spectra have peaks at ~6 and ~10 Mev, which are more prominent in the case of $E_{\gamma max}$ = 33.5 Mev. The declining portions of the two spectra have approximately identical shapes.

Figures 4—6 show the angular distributions of different photoproton groups corresponding to the aforementioned peaks at 6 and 10 Mev and the declining portion of the spectrum.

The experimental values were fitted approximately by curves of the form

$$a + b \sin^2\theta (1 + p \cos\theta)^2. \quad (1)$$

The parameters of the approximating curves are given in Table I. The figures and the table show that the angular distributions of photoprotons for $E_{\gamma max}$ = 33.5 Mev have peaks at smaller angles than for $E_{\gamma max}$ = 22.5 Mev. The estimated yields are $\sim 8 \times 10^4$ and $\sim 1.3 \times 10^5$ protons/mole-roentgen for $E_{\gamma max}$ = 22.5 and 33.5 Mev, respectively. The yield increases markedly with $E_{\gamma max}$.

DISCUSSION OF RESULTS

A comparison of the photoproton yields from Pr^{141} for $E_{\gamma max}$ = 22.5 and 33.5 Mev shows that over 50% of the total proton yield for $E_{\gamma max}$ = 33.5 Mev (including ~40% of the first proton group, ~55% of the second group, and ~70% of the third group) is produced by γ radiation having $E_{\gamma max}$ > 22.5 Mev. This indicates that the maximum photoproduction cross section in Pr^{141} corresponds to γ radiation having energy > 22.5 Mev. A comparison of the experimental yields with calculations based on the evaporation model[4] and the direct photoeffect[4,6] shows that neither model can account for the results. The estimated photoproton yield based on the statistical model for Pr^{141} was smaller by a factor of 15 to 20 than the experimental value. The proton contribution from the direct photoeffect is somewhat larger, although[6] shows that our observed total yield is 4 to 5 times greater. As could be expected, a large fraction of the observed photoprotons result from direct resonance absorption of γ radiation.

Good agreement with experiment has recently been obtained in [7] by calculating the total γ-radiation absorption cross section on the shell model with mixed configurations. However, such calculations are possible practically only for doubly magic nuclei. Since this did not apply in our case, we calculated the energies of dipole proton transitions using single-particle levels computed for intermediate and heavy nuclei. [8]

These calculations did not take into account the residual interactions between nucleons, which we evaluated as follows. Since data are lacking for the $Pr^{141}(\gamma, p)$ cross section all comparisons between calculations and experiment were performed for the (γ, n) reaction. The center of dipole neutron transitions in the single-particle shell model was compared with the maximum $Pr^{141}(\gamma, n)$ cross section obtained experimentally. [9,10] The difference observed here gave 4—5 Mev for the residual interactions. Practically identical magnitudes were assumed for the residual interaction in Pr^{141} in the cases of both proton and neutron transitions, and the center of dipole proton transitions was found with this residual interaction taken into account. Table II gives the results for individual transitions. The center of dipole proton transitions is seen to correspond to 16—17 Mev γ rays and the maximum cross section, for γ rays having energy > 22.5 Mev, cannot be accounted for by direct resonance dipole transitions.

This is confirmed by the additional interesting result that very different angular distributions of photoprotons are obtained for $E_{\gamma\,max}$ = 22.5 and 33.5 Mev. The character of γ-ray absorption changes considerably when E_γ increases above 22 Mev. Considerable asymmetry is observed with respect to 90° and the angular distribution peak is shifted toward smaller angles. For E_γ < 22 Mev, on the other hand, the proton angular distribution is practically symmetrical with respect to 90°.

The approximation of angular distributions by curves plotted from Eq. (1) furnishes only a rough estimate of the quadrupole absorption contribution, which according to Table I would reach 50%. However, the results are in good agreement with the fact that the quadrupole transition center is in the region E_γ > 22 Mev, as can be seen by analyzing the E2 transition energies in Table II.

The energy spectra exhibit two peaks, for 6—7 and 9—10 Mev protons, respectively. For $E_{\gamma\,max}$ = 22.5 Mev these peaks are poorly resolved, while for $E_{\gamma\,max}$ = 33.5 Mev they are clearly defined at the same energies. It appears from Table I that the principal peak of the spectrum for $E_{\gamma\,max}$ = 22.5 Mev corresponds to the transitions $1g_{7/2} \rightarrow 1h_{9/2}$ and $1g_{7/2} \rightarrow 2f_{5/2}$, producing 8—10 Mev protons. The peak at 6—7 Mev can be associated with $1g_{9/2} \rightarrow 2f_{7/2}$ and $2d_{5/2} \rightarrow 2f_{7/2}$ transitions. In the spectrum for $E_{\gamma\,max}$ = 33.5 Mev these peaks are more pronounced, as already mentioned, and correspond to the enumerated dipole transitions as well as quadrupole transitions. The most intense of the latter, $1g_{7/2} \rightarrow 1i_{11/2}$ and $2d_{5/2} \rightarrow 2g_{9/2}$, produce 10—14 Mev protons, whereas 5—6 Mev protons result from $1g_{9/2} \rightarrow 1i_{13/2}$ and $1f_{5/2} \rightarrow 1h_{9/2}$ transitions and some others. It is not clear why the peaks for $E_{\gamma\,max}$ = 33.5 Mev are more pronounced. The analysis of the energy spectra is greatly hampered generally by the impossibility, in our case, of taking into account the effects resulting from the mixing of configurations.

Our results lead to the conclusion that the maximum photoproton production cross section of Pr^{141} corresponds to γ radiation in the energy region above 22 Mev, and that γ-ray absorption in this region is mainly of quadrupole character.

In conclusion the authors wish to thank V. V. Balashov and V. G. Neudachin for discussions of the results, S. Ovchinnikov for assistance in treating the results, and the betatron crew.

[1] Neudachin, Shevchenko, and Yudin, II Vsesoyuznaya konferentsiya po yadernym reaktsiyam pri malykh i srednikh energiyakh (Report at 2nd All-Union Conference on Nuclear Reactions at Low and Intermediate Energies), Moscow, 1960.

[2] M. E. Toms and W. E. Stephens, Phys. Rev. **92**, 362 (1953).

[3] M. E. Toms and W. E. Stephens, Phys. Rev. **98**, 626 (1955).

[4] W. K. Dawson, Can. J. Phys. **34**, 1480 (1956).

[5] E. D. Makhnovskii, JETP **38**, 95 (1960), Soviet Phys. JETP **11**, 70 (1960).

[6] E. D. Courant, Phys. Rev. **82**, 703 (1951).

[7] Balashov, Shevchenko, and Yudin, Nuclear Phys. **27**, 323 (1961).

[8] A. Schröder, Nuovo cimento **7**, 461 (1958).

[9] L. Katz and J. Chidley, in: Yadernye reaktsii pri malykh i srednikh energiyakh (Nuclear Reactions at Low and Intermediate Energies), Moscow, 1958, p. 371.

[10] J. H. Carver and W. Turchinetz, Proc. Phys. Soc. (London) **73**, 110 (1959).

Translated by I. Emin
243

KINETICS OF THE DESTRUCTION OF SUPERFLUIDITY IN HELIUM

V. P. PESHKOV and V. K. TKACHENKO

Institute for Physics Problems, Academy of Sciences U.S.S.R.

Submitted to JETP editor June 7, 1961

J. Exptl. Theoret. Phys. (U.S.S.R.) 41, 1427-1432 (November, 1961)

A study has been made of the kinetics of the destruction of superfluidity during heat transport along a helium-filled capillary 1.4 mm in diameter and 8 m long. For T = 1.34° K and superfluid component velocities exceeding the critical value by 1.04 — 1.6 times, turbulence fronts propagating at a constant velocity were observed, moving from the hot end to the cold at a rate of from 1 to 3.7 mm/sec, and from the cold end to the hot at from 0.1 to 2.5 mm/sec.

THE question of the nature of the destruction of superfluidity—of critical velocities—has remained up to now the least understood of all the properties of helium II. It has already been established by Kapitza [4] that critical velocities decrease as the dimensions of the passage increase, while Landau [2] has proposed a criterion for the destruction of superfluidity having the form $v_s > \epsilon/p$, where v_s is the superfluid component velocity, and ϵ is the energy and p the momentum of the excitation being created. The velocity must, however, according to this expression, be greater than the velocity of sound (~ 230 m/sec) for generation of a phonon, and greater than 70 m/sec for a roton, while the velocities observed for large capillaries are inversely proportional to their diameter and for d = 1.4 mm equal 0.11 cm/sec. The suggestion was first advanced by Onsager [3] that the cause of the destruction of superfluid motion lies in the generation of vortex structures. This viewpoint has since been confirmed and further developed. [4-7] The kinetics of the destruction of superfluidity have been investigated by Mendelssohn [8] who found a linear increase with time in the temperature difference between the ends of a long (1.5 m) capillary 1 mm in diameter with heat supplied to one end. He explained this as due to the movement of turbulence fronts, and observed velocities that were integral multiples of 4 cm/min. At the Institute for Physics Problems, V. Markov and Tkachenko have performed experiments to investigate the kinetics of the destruction of superfluidity, the results derived from which are presented in this paper.

The experiments were conducted in the apparatus represented in Fig. 1. A German-silver capillary 1 of 1.4 mm inside diameter and 800 cm long was located inside a vacuum jacket 2, 70 mm in diameter and 170 mm long. The capillary was attached by means of taut cotton threads to a framework 4 of glass rods. One end 5 of the capillary communicated with the helium bath. The other end was sealed off, and onto it was wound a heater (2580 Ω) of 50 μ diameter constantan. Twelve thermometers of 40 μ phosphor-bronze were also wound onto the capillary. One of these, R_1, was at a distance of 100 mm from the end of the capillary, another, R_{12}, 30 mm from the heater, and the remaining ten at approximately equal intervals between R_1 and R_{12}. The average resistance of the thermometers, at the tempera-

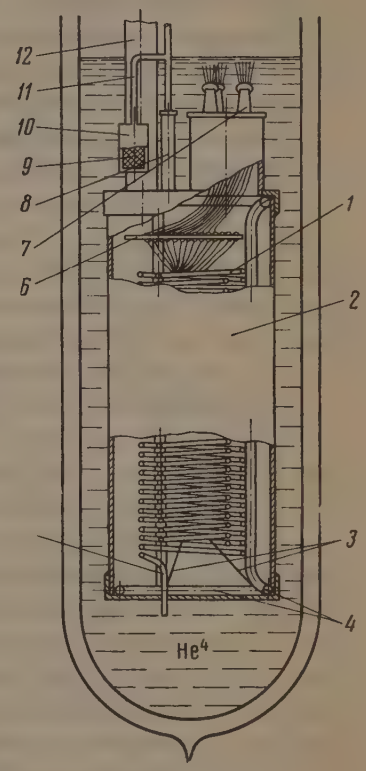

FIG. 1. Diagram of the apparatus (explanation in text).

tures of 1.3—1.4° K at which most of the runs were carried out, amounted to ~15—20 Ω. The thermometer leads were of 60 μ tinned constantan, soldered to a terminal strip 6. The leads were carried out of the vacuum jacket through a ferrochrome-glass seal 7. The vacuum jacket was evacuated at room temperature and then filled with 2 mm Hg of exchange gas (helium) through the tube 8. As the apparatus cooled to helium temperatures the exchange gas was gradually adsorbed by activated charcoal 9 placed in a bulb 10, via a tube 11 of 1.4 mm inside diameter and 100 mm long, and after a short while (~ 30 min) a hard vacuum was achieved within the jacket. By this time the capillary 1 had cooled to the temperature of the helium bath. The apparatus was supported from the Dewar cover by means of a tube 12.

Even with a capillary of this length (800 cm) the temperature difference between the ends was only $\sim 3 \times 10^{-3}$ deg for a thermal current near the critical value. The magnitude of the measuring current in the thermometers (0.2 ma) was limited by the power dissipated through them, which must be small (1—2%) as compared with the power liberated in the heater. The change in the voltage across the thermometers as the thermal current was applied was therefore only 15 mv or less. Since the thermal processes in the capillary require a long time to develop (up to 1 hour), it was necessary to maintain the temperature of the helium bath constant to 10^{-5} deg. The temperature stabilizer described by Vetchinkin [9] was employed for this purpose.

Measurements of the variation with time of the thermometer temperatures with a thermal current flowing in the capillary were performed automatically (see measuring circuit in Fig. 2). The voltage across each of two fixed thermometers (R_7 and R_{11} in the circuit diagram) in the absence of a thermal current was compensated with the aid of storage batteries and potential dividers. As the thermal current was turned on the voltage drop across the thermometers increased as a result of the rise in temperature, and the signals emerging from the compensating circuits were amplified by F 116/1 photoamplifiers and applied to the input of an ÉPP 09-M1 multi-channel automatic potentiometer. The voltage across any desired third thermometer, connected via the switch S, was compensated by a PMS-48 potentiometer and was also recorded by the ÉPP 09-M1. The amplifier gains were so chosen as to give equal deflections on the automatic potentiometer for equal temperature changes in the thermometers.

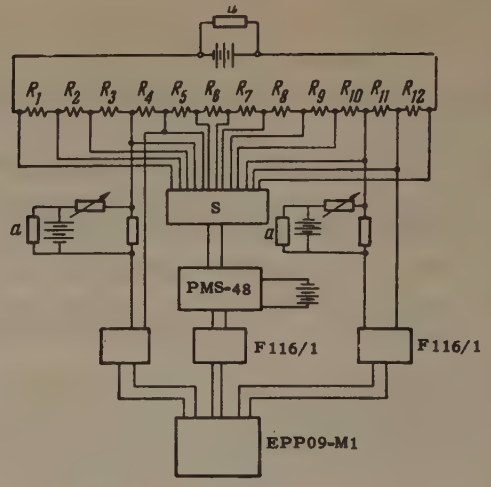

FIG. 2. Measuring circuit.

All four storage batteries in the circuit were maintained at the same temperature. A current of ~ 10 ma, adjusted with the aid of the resistances a to the same value as that in the potentiometer, flowed continuously in each of them. As a result, the possible variation with time in the emf's of the batteries was held to a minimum, and was identical for all four.

For a thermal current slightly exceeding the critical value, the way in which the thermal regime is established is found to depend strongly upon the previous history of the helium. When a supercritical heat transport regime had been set up in the capillary shortly (up to 10 min) prior to turning on the thermal current, the process usually occurred relatively rapidly, requiring no longer than 10 min. When, on the other hand, the helium had remained quiescent for some time—at least 20 min—then, as a rule, the establishment of the thermal regime occupied a prolonged interval—up to 1 hour. In this latter case, the process showed a number of characteristic features which made it possible to understand what was taking place.

In Fig. 3 is shown the variation with time of the thermometer readings for a typical slow proc-

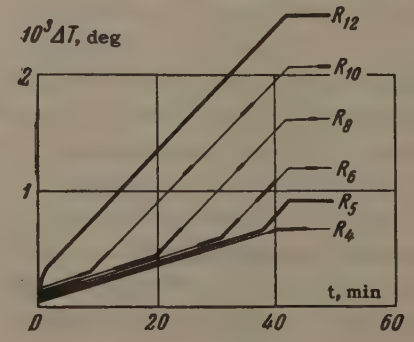

FIG. 3. Time dependence of thermometer temperatures for a thermal current in quiescent helium ($W = 4.4 \times 10^{-2}$ w/cm², T = 1.34°K).

ess of establishing the thermal regime ($T = 1.34°K$ and $W = 1.19 W_{cr}$). The readings of the hottest thermometer, R_{12}, and an intermediate one, R_5, were recorded continuously. The thermometers were numbered in order from the cold to the warm end of the capillary. The third input of the recorder was switched from one intermediate thermometer to another, as indicated by the heavy line segments in Fig. 3. The linearity of the rise in temperature with time over well-defined intervals, and the occurrence of quite sharp changes in the heating rate, are immediately evident. It can easily be seen that the breaks in the temperature vs time curves take place at the various thermometers in a definite sequence: R_{10}, R_8, R_6, R_5. This testifies to the fact that a turbulence front increasing the thermal resistance of the helium propagates at a constant velocity from the hot end of the capillary. The velocity of advance of the turbulence front, v_H, can be computed from the known times corresponding to the breaks in the curves for the various thermometers, and the positions of the thermometers along the capillary. In the case cited, $v_H = 2.2 \pm 0.1$ mm/sec. A similar pattern, it was found, is followed at the cold end: a turbulence front also advances from this end, with a propagation velocity $v_C = 1 \pm 0.03$ mm/sec.

The velocity of the fronts is shown as a function of thermal current density ($T = 1.34°K$) in Fig. 4. We found the critical thermal flux to be $3.7 \times 10^{-2} \pm 0.1 \times 10^{-2}$ w/cm^2, from measurements of the temperature gradient in the capillary. The corresponding velocities are $v_n = 1.85$ cm/sec and $v_s = 0.114$ cm/sec. It can easily be seen that for this current density the velocities v_H and v_C fall nearly to zero. We note that even for a thermal flux of 6×10^{-2} w/cm^2 —somewhat more than 1.5 times the critical value—turbulence is not generated within the capillary. The turbulence originates only at the ends of the capillary, from which it propagates at a well-defined velocity but does not completely fill the capillary. The temperature difference which develops almost at once between thermometers when the current is turned on, evident in the initial portions of the curves in Fig. 3, is associated with Poiseuille flow of the normal component of the helium. For still higher thermal currents the generation of turbulence within the capillary becomes possible, but is of a random character.

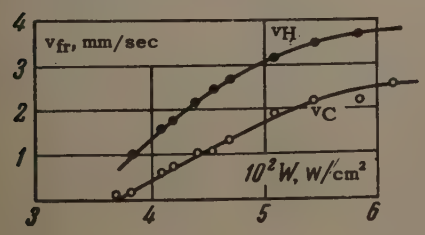

FIG. 4. Dependence of front velocity upon thermal current density ($T = 1.34°K$).

Turbulence within the capillary can develop even for only slightly supercritical fluxes if insufficient time has been allowed for the helium to become quiet. In Fig. 5 a run is recorded in which, in addition to the fronts advancing from the ends of the capillary, there was a source of turbulence within the capillary, in the vicinity of thermometer no. 8, from which turbulence fronts also moved outward. Figure 6 illustrates the pattern of propagation of the fronts. At each point in time t the portion of the capillary corresponding to the region showing steep temperature gradients in Fig. 6 was enveloped in turbulence. The break in the curve R_{11} at the point a corresponds to the passage through R_{11} of the front advancing from the hot end; the break b corresponds to the meeting between this front and the front advancing from R_8. At the point c the front proceeding from the center towards the cold end has passed through R_5, and at d it has encountered the front moving from the cold end, with which the process of es-

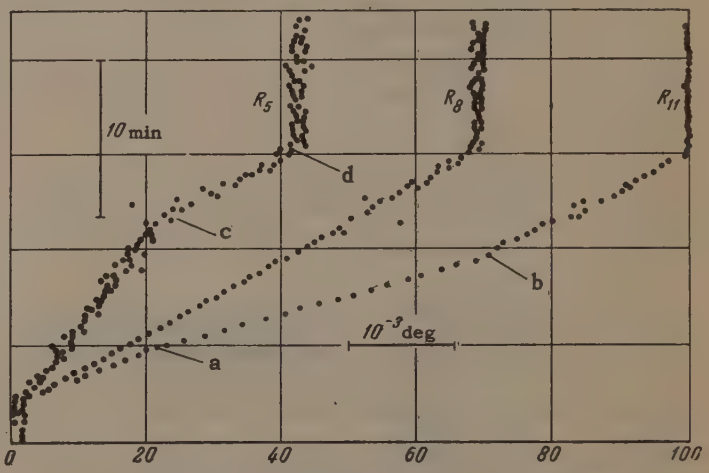

FIG. 5. Diagram of temperature readings as recorded by an EPP09-M1 for fronts propagating from ends and center of capillary.

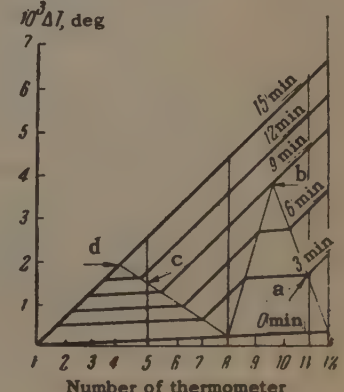

FIG. 6. Temperature distribution, relative to bath temperature, along the capillary. The spacing of the thermometers along the capillary is indicated on the x axis.

tablishing the thermal regime has come to an end. In other runs, central fronts arose at other points; for example, near R_6 or R_9.

The process of establishment of the thermal regime in quiescent helium in the case of a large thermal flux is represented in Fig. 7. The abundance of internal fronts makes it impossible to understand the process in detail.

The dependence of the temperature gradient upon the magnitude of the thermal flux is shown in Fig. 8. It is evident that the experimental data in the supercritical region are well represented by the formula

$$\operatorname{grad} T = (A\sigma_n/\rho_s^3 S^4 T^3)(W^3 - W_0^3),$$

where $W_0 = 2.25 \times 10^{-2} \pm 7\%$ w/cm^2, and $A = 32 \pm 5\%$ cm-sec/g. The value of the constant A agrees with the data of Vinen.[4]

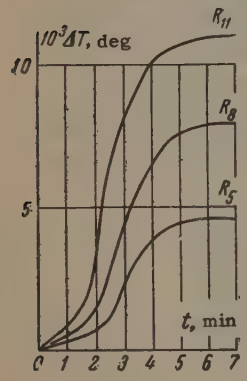

FIG. 7. Process of establishing regime for a large thermal flux (W = 7.05 w/cm^2, T = 1.34°K).

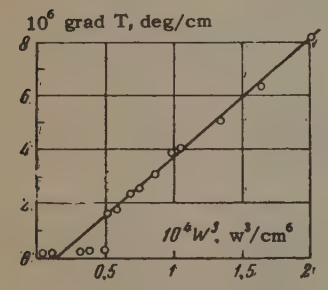

FIG. 8. Dependence of final temperature gradient in capillary upon thermal flux.

The experiments described above permit the following hypotheses to be advanced regarding the pattern of the destruction of superfluidity in broad capillaries. It has been established that even well beyond the critical condition (by 1.5 times) the development of sources of turbulence within the capillary is strongly opposed; if, however, such a source does appear, then turbulence fronts propagate from it in both directions. Since the force of interaction between the normal and superfluid components is proportional to $(v_s - v_n)^3$, the profile of v_s in the regime established will, as has already been pointed out[10,7] be closely parabolic, in order that the difference $v_n - v_s$ remain constant across the capillary. Hence at low temperatures, for which $v_n \gg v_s$, v_s will be in the same direction as v_n at the center of the capillary, and in the opposite direction near its periphery.

Thus the propagation of turbulence fronts may be represented in terms of the formation at some point of vortex rings, which, interacting with one another near the center of the capillary, slip past each other and move in the direction of the thermal current. Vortex rings having circulations of the same sign situated near the wall move in the opposite direction, also playing, as it were, a game of leap-frog. Vortices of large radius must accelerate their motion as they approach the wall, but in so doing they rapidly lose energy, decreasing their length—i.e., radius—and slowing their movement. This last circumstance leads to the situation that for conditions only slightly beyond criticality the velocity of turbulence front advancing from the cold to the hot end is much lower than the velocity of the front moving in the opposite direction. It is clear that this pattern is strongly distorted by the thermal motion, converting regular into chaotic turbulence; the general tendency, however, remains.

The authors take this opportunity to express their gratitude to P. L. Kapitza for his interest in and attention to this work.

[1] P. L. Kapitza, JETP **11**, 581 (1941).
[2] L. D. Landau, JETP **11**, 592 (1941).
[3] L. Onsager, Nuovo cimento **6**, Suppl. **2**, 249 (1949).
[4] W. F. Vinen, Proc. Roy. Soc. **A240**, 114, 128 (1957).
[5] R. P. Feynman, Progr. in Low Temp. Phys. **1**, 17 (1955).
[6] K. R. Atkins, Liquid Helium, Cambridge, 1959.
[7] V. P. Peshkov, JETP **40**, 379 (1961), Soviet Phys. JETP **13**, 259 (1961).
[8] K. Mendelssohn and W. A. Steele, Proc. Phys. Soc. **73**, 144 (1959).
[9] A. N. Vetchinkin, PTÉ (Instrum. and Exptl. Techniques) **1**, 192 (1961).
[10] C. J. Gorter and J. H. Mellinck, Physica **15**, 285 (1949).

Translated by S. D. Elliott
244

A $\beta\gamma$-CORRELATION INVESTIGATION OF THE Pr^{144} DECAY

V. M. LOBASHOV and V. A. NAZARENKO

Leningrad Physico-Technical Institute, Academy of Sciences, U.S.S.R.

Submitted to JETP editor June 9, 1961

J. Exptl. Theoret. Phys. (U.S.S.R.) 41, 1433-1437 (November, 1961)

The correlation between the β-electron and circular polarization of the γ-quantum in the allowed Pr^{144} decay transition was investigated. From the magnitude of the correlation we can assign to the ground state Pr^{144} spin a value of 1^-, instead of the previously accepted 0^-.

THE study of β transitions is one of the basic methods of establishing the characteristics of nuclear levels. Until recently, however, the basic information was obtained from forbidden transitions: the degree of their forbiddenness, the shape of the spectra, and the magnitude of the $\beta\gamma$ angular correlation. In a number of cases such investigations do not give unambiguous information, since the interpretation of the forbidden transitions is connected with estimates of the nuclear matrix elements by a very uncertain procedure.

The nonconservation of parity in the β decay results in a number of nonvanishing effects in the allowed transitions, the magnitude and sign of which have an appreciable dependence on the spins of the initial and final states. Then, in view of the reduction of the number of matrix elements to a maximum of two, the ambiguity in the interpretation of the results is removed.

In the present experiment, we investigated one of these effects, the correlation between the β-electron momentum and the circular polarization of the γ quantum in the Pr^{144} decay. The Pr^{144} decay has been investigated many times by various methods,[1-3] and the characteristics of the levels of the Nd^{144} daughter nucleus are well established. The adopted scheme is shown in Fig. 1.

Consideration of ft for the β transitions on the basis of the experimentally known spins and parities of the Nd^{144} levels determined from the $\gamma\gamma$ correlations allows one to assign the value 0^- or 1^- to the Pr^{144} ground state.

In[3-6] the shapes of the β-spectrum transitions and $\beta\gamma$ angular correlations in the Pr^{144} decay were carefully investigated. The shape of the spectrum for the 2.3-Mev transition proved to be very close to the unique first forbidden transition and the value of the coefficient A_2 of the $\beta\gamma$ angular correlation was almost a maximum. It was

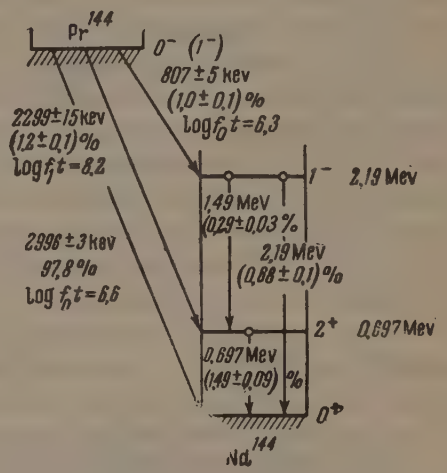

FIG. 1. Pr^{144} decay scheme. The value of the spin determined in our experiments is shown in parentheses. The relative intensities are taken from[5].

therefore concluded that the 2.3-Mev transition was a unique first forbidden transition and that the small difference in the correlation coefficient A_2 from the maximum value required for a unique transition is due to experimental errors. The ground state was therefore assigned a spin 0^-.

It should be noted that, on the basis of this value, a detailed analysis of the shape of the β spectrum of the transition between the ground states ($0^- \rightarrow 0^+$) was made to estimate the mixture of the pseudoscalar variant in the β interaction. In order to verify the conclusion regarding the ground-state spin, we investigated the allowed transition in the Pr^{144} decay, whose interpretation can be checked unambiguously.

We investigated the correlation between β electrons of the transition with an end-point energy of 807 kev and the circular polarization of the 2180-kev γ quanta. The experimental arrangement is shown in Fig. 2.

We detected the circular polarization by the

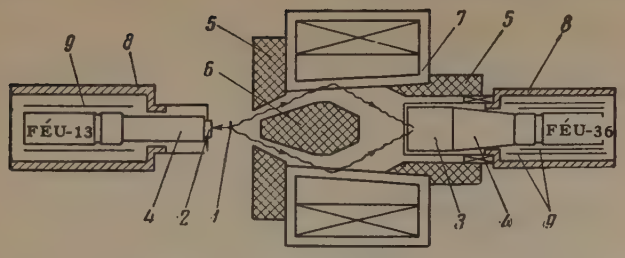

FIG. 2. Experimental arrangement: 1 – source, 2 – stilbene crystal, 3 – NaI(Tl) crystal, 4 – light guide, 5 – lead collimators, 6 – lead shield, 7 – γ-polarimeter magnet, 8 – Armco-iron housing, 9 – permalloy shields.

method of forward Compton scattering on magnetized iron, as in[7-9].

To fix the geometry, the beam of incident and scattered γ quanta passed through lead collimators. The scattering-magnet core was made of Armco iron. The measured flux density inside it was 22 000 gauss, which corresponds to saturation (21 000 gauss). The mean scattering angle was 45°. The scattered γ quanta were detected by a 70×70 mm NaI(Tl) crystal coupled to a light guide 100 mm long with an FÉU-13 photomultiplier. In order to decrease the influence of the magnetic field, the photomultiplier was enclosed in an Armco-iron housing 1 cm thick and a double permalloy shield. Moreover, a compensation winding was used. All this reduced the influence of the magnetic field to $\sim 0.08\%$ in amplitude.

The β electrons were detected by a stilbene crystal coupled to a light guide with an FÉU-36 photomultiplier. The photomultiplier was also shielded by 1 cm of Armco iron and 1 mm of permalloy.

The photomultiplier output was connected to a fast-slow coincidence circuit with a resolving time of $\tau = 5 \times 10^{-9}$ sec. The efficiency of the circuit was $\sim 95\%$. The transition had an intensity of 1% and was superimposed on a β spectrum with an end-point energy of 3 Mev. In order to provide a reasonable coincidence counting rate, we used a 10^6 sec^{-1} gate on the β channel. Of course, with such a gate the usual method of pulse amplitude selection in which the pulse from the FÉU dynode is fed directly to a slow differential discriminator cannot be used. We therefore used time preselection triggered by a pulse from the fast coincidence circuit.

The selection circuit was designed on the principle of an ordinary diode coincidence circuit and had a resolving time of 7×10^{-8} sec. Such a circuit passed linearly pulses 5×10^{-8} sec wide and 20 volts in amplitude with a pedestal of ~ 0.8 volts. The fast selecting pulse (7×10^{-8} sec) underwent preselection from the pulse of the differential discriminator connected in the β channel. After the selecting circuit, the pulse, which was passed linearly through the β channel, was fed to the slow differential discriminator and then to the counting circuit. With such an arrangement the superposition of pulses was reduced to a value no greater than 5%.

The limits of discrimination were set so that electrons of energy from 300 to 800 kev were selected.

To eliminate the effect of the gate on the operation of the FÉU, the three final dynodes of the FÉU were connected to a separate power supply.

In the measurements, the coincidence counting rate was 0.5 pulse/sec with a random coincidence background of 20%. In order to improve the stability, the temperature of the preamplifier was maintained constant by an automatic arrangement. The direction of magnetization was reversed automatically every 3.5 min.

The choice of the energy interval of the scattered γ quanta involved some special problems, since γ quanta of 2180 and 1480 kev with relative intensities 5.6 : 2.3 coincided with the 807-kev β transition. The spin decreases by one in the 2180-kev γ transition and increases by one in the 1480-kev transition. Therefore the circular polarization of these γ quanta was of opposite sign. Of course, the presence of the 1480-kev γ transition should decrease the correlation coefficient.

As a result of Compton scattering, the γ lines were greatly broadened, and one can therefore expect a certain overlapping of the 2180- and 1480-kev γ lines.

In order to estimate the contribution of the 1480-kev line we performed a special experiment. The β detector was replaced by a 70×50 mm NaI(Tl) crystal and we measured the spectrum of scattered γ quanta in coincidence with the 695-kev line. The coincidence and singles spectra of the scattered γ quanta are shown in Fig. 3. The chosen limits of discrimination in the γ channel are indicated by arrows. With this discrimination the contribution of the 1480-kev line was $\sim 5\%$. As a source we used, without a carrier, Ce^{144} whose daughter product is Pr^{144}. The source was prepared by the drop method on a terylene base $\sim 4\mu$ thick. Its density was about 100 μg/cm^2. The source activity was about 1 mC.

The results of the measurements were calculated, as usual, in the form

$$\Delta = 2(I_1 - I_2)/(I_1 + I_2), \qquad I_{1,2} = R_{\text{coinc}} / R_\gamma \theta_\beta.$$

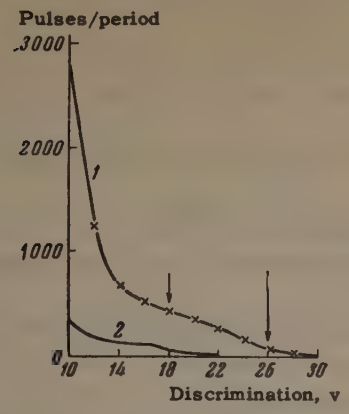

FIG. 3. Spectra of scattered γ quanta in coincidence with the 807-kev β spectrum (curve 1) and with the 695-kev γ line (curve 2). The scale on the ordinate axis corresponds to the same efficiency of the other coincidence channel (β or γ). The arrows indicate the limits of discrimination.

Here R_{coinc} is the coincidence counting rate, R_γ is the counting rate of the γ channel, θ_β is the correction for the influence of the magnetic field on the β channel, which, in this case, is 0.05%. The subscripts 1 and 2 refer to different directions of the γ-polarimeter magnetization. As a result of the measurements we obtain the value $\Delta = +(2.3 \pm 0.5)\%$ (the error represents the statistical standard deviation). From this we obtain the correlation coefficient with allowance for the random coincidence background, geometry, and mixture of the 1480-kev γ line:

$$A_1 = +0.43 \pm 0.09.$$

Since the electron energy was > 300 kev, the corrections for the source thickness were negligible. The scattering of the β electrons in air could also be neglected.

The correlation coefficient for the allowed transitions has been calculated by a number of authors.[10-11] The general form of the correlation, as is known, is

$$W(\theta) = 1 + A_1 \frac{v}{c} \cos\theta.$$

In the case of pure multipolarity of the γ quanta, we have for the A—V variant and conservation of combined parity

$$A_1 = \frac{j_1(j_1+1) - j_2(j_2+1) + I(I+1)}{2I(I+1)\sqrt{j_1(j_1+1)}} \times \left[\frac{2\lambda}{1+\lambda^2} + \frac{j_1(j_1+1) - j_0(j_0+1) + 2}{2\sqrt{j_1(j_1+1)}} \frac{1}{1+\lambda^2}\right]$$

$$\left(\lambda = -\frac{|C_V|M_F}{|C_A|M_{GT}}\right)$$

where j_0 and j_1 are the angular momenta of the initial and final states in the β transition, j_2 is the angular momentum of the final level of the γ transition, I is the multipolarity of the γ quanta, M_F, M_{GT} are the Fermi and Gamow-Teller matrix elements, C_A and C_V are the axial-vector and vector variants of the β interaction. Different combinations of the level spins and the correlation coefficients corresponding to them are shown in the table. It is seen that the first and third cases do not agree with the experimental value. In the second case, the value of A_1 depends on λ. This dependence is shown in Fig. 4. The shaded region indicates the limits of the experimental value of the correlation coefficient. Unfortunately, theoretical estimates of λ have not been made; however, the obtained value is not surprising, since in many jj transitions the Fermi matrix element proves to be small.

Case no.	Transition	$A_{theor.}$	$A_{exptl.}$
1	$0^- \xrightarrow{\beta} 1^- \xrightarrow{\gamma} 0^+$	+1,00	
2	$1^- \xrightarrow{\beta} 1^- \xrightarrow{\gamma} 0^+$	$+\frac{1}{2}\frac{2\sqrt{2}\lambda+1}{1+\lambda^2}$	+0,43±0,09
3	$2^- \xrightarrow{\beta} 1^- \xrightarrow{\gamma} 0^+$	—1/2	

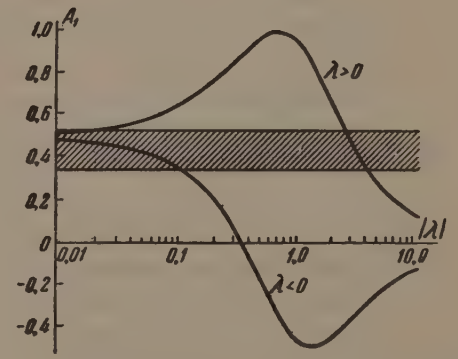

FIG. 4. Dependence of the value of the correlation coefficient on λ. The shaded region indicates the limits of the experimental value of the correlation coefficient.

Hence the obtained result indicates that the Pr^{144} ground state should be assigned a spin 1^-. The value 0^- adopted earlier cannot be reconciled with experiment.

It should be mentioned that Hickok et al[6] noted that, on the basis of the shell model, the ground state should be assigned a spin 1^-. Subsequent investigators,[3-5] however, did not consider this value to be in agreement with experiment and therefore concluded that there is a disagreement with the shell model which required special explanation.

It should also be noted that since the transition between the ground states is a $1^- \rightarrow 0^+$ transition, the earlier attempts to determine the mixture

of the pseudoscalar interaction from the shape of the spectrum are without justification.

From the above it can be concluded that the investigation of forbidden β transitions cannot, in a number of cases, give unambiguous information; therefore, wherever possible, the described method for the investigation of allowed transitions should be used in view of the simple interpretation of the results.

In conclusion the authors express their sincere gratitude to S. N. Oziraner for the preparation of the Ce^{144} source and also to V. V. Andryukevich, G. D. Chuklin, and V. B. Belyakov for taking part in the preparation of the equipment and measurements.

[1] R. L. Steffen, Phys. Rev. **95**, 614 (1954).
[2] D. Roberts, Phys. Rev. **91**, 497 (1953).
[3] Graham, Geiger, and Eastwood, Can. J. Phys. **36**, 1084 (1958).
[4] N. J. Freeman, Proc. Phys. Soc. (London) **73**, 600 (1959).
[5] F. T. Porter and P. P. Day, Phys. Rev. **114**, 1286 (1959).
[6] Hickok, McKinley, and Fultz, Phys. Rev. **109**, 113 (1958).
[7] H. Schopper, Phil. Mag. **2**, 710 (1957).
[8] F. Boehm and A. H. Wapstra, Phys. Rev. **106**, 1364 (1957).
[9] Lobashov, Nazarenko, and Rusinov, JETP **40**, 10 (1961), Soviet Phys. JETP **13**, 6 (1961).
[10] A. Z. Dolginov, JETP **35**, 178 (1958), Soviet Phys. JETP **8**, 123 (1959).
[11] Alder, Stech, and Winther, Phys. Rev. **107**, 728 (1957).

Translated by E. Marquit
245

IONIZATION IN THE COLLISIONS OF Ne^{n+} *WITH* Xe *ATOMS AND OF* Xe^{n+} *WITH* Ne *ATOMS* ($n = 0, 1, 2, 3, 4$)

I. P. FLAKS, G. N. OGURTSOV, and N. V. FEDORENKO

Leningrad Physico-Technical Institute

Submitted to JETP editor June 9, 1961

J. Exptl. Theoret. Phys. (U.S.S.R.) 41, 1438-1442 (November, 1961)

The total cross sections for the production of free electrons, i.e., the total ionization cross sections (σ_-) for single collisions between fast Ne^{n+} particles and Xe atoms and between fast Xe^{n+} particles and Ne atoms, have been measured. The fast ions had charges from 0 to 4 and were accelerated by a potential which varied from 3 to 30 kv. With increasing charge n of the fast particle, the cross section σ_- was found to increase for the Ne^{n+}—Xe pair and to decrease for the Xe^{n+}—Ne pair. An analysis of the elementary processes in which electrons are liberated from the shells of each of the colliding particles indicates that a behavior of this type could be expected. The increase of the cross section σ_- with the fast particle charge is due to the possibility of exothermal ionization processes involving capture. An opposite type of dependence occurs when the capture ionization is an endothermal process, so that the main contribution to the cross section σ_- is due to the "stripping" of the fast particle.

1. INTRODUCTION

ACCORDING to our views on collision ionization in the kev range of energies, the ionization cross sections for the collisions of particles with medium mass should be very small. Large cross sections in this energy range are due to a so-called "strong-interaction mechanism," which is connected with the perturbation of many electrons and with autoionization.[1,2] To investigate this mechanism, it is important to explain the variation of the ionization cross section with the relative velocity, the structure of the electron shells, and the charge of the fast ionizing particle. From general considerations, we should assume that, in the velocity range $v < e^2/\hbar$, the ionization cross section should increase with increasing velocity and with an increasing number of electrons in the shells of the colliding particles.[2]

As far as the influence of the charge is concerned, the investigations carried out by us in an earlier experiment[3] for singly, doubly, and triply charged ions of several inert gases showed that the charge dependence is weak and irregular. In order to explain more fully the influence of the charge of the ionizing atomic particles on the production of free electrons in the present experiment, we have measured the total ionization cross section σ_- for two groups of colliding particles strongly differing in the binding energy of the electrons in the shells of the ionizing particle and of the target atoms. In one case, the neutral atoms or ions of neon served as fast particles and the xenon atoms (the Ne^{n+}—Xe pairs) as the target, while in the second case the neon atoms were ionized by fast atoms or ions of xenon (the Xe^{n+}—Ne pairs).

The investigation was carried out using an experimental arrangement described earlier.[3-5] The determination of the total ionization cross section σ_- was based on the detection of the total number of electrons liberated from the shells of both colliding particles as a result of their decomposition or change of structure. As before,[3,4] the cross section σ_- was measured by the condenser

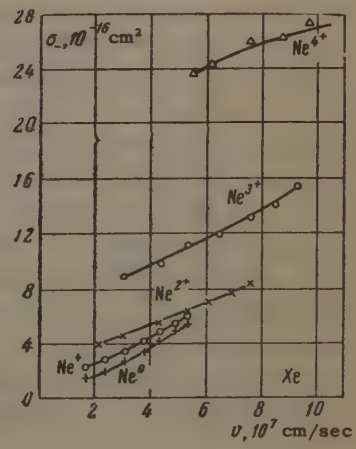

FIG. 1. Variation of the total ionization cross section σ_- of the Xe atoms with the velocity v of fast Ne^{n+} particles.

method for single collisions. The accelerating voltage varied from 3 to 30 kv. It was possible to obtain fast ion beams with a charge of 0 to 4. The multiply charged ions were identified by studying the isotopic composition, and also by analysis of the secondary spectrum produced in the capture of electrons by primary ions.[3] The total error in the determination of the cross section was not greater than 15%, for ions with charge n = 1, 2, 3, and 20% for fast neutral atoms and quadruply charged ions.

2. RESULTS OF THE MEASUREMENTS

Figure 1 shows the variation of the total ionization cross section σ_- with velocity v of fast ionizing particles Ne^0, Ne^+, Ne^{2+}, Ne^{3+}, Ne^{4+} in the passage through xenon. Fig. 2 shows the same for the fast particles Xe^0, Xe^+, Xe^{2+}, Xe^{3+}, Xe^{4+} in their passage through neon.

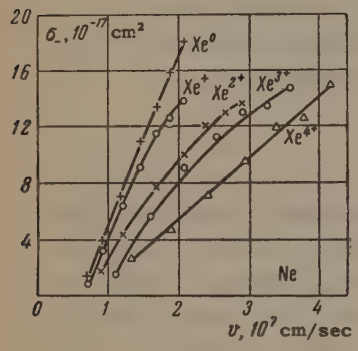

FIG. 2. Variation of the total ionization cross section σ_- of Ne atoms with the velocity v of Xe^{n+} particles.

The main experimental result of the work is that for the Ne^{n+}—Xe pairs the total ionization cross section increases with increasing charge of the fast Ne^{n+} particles, while for the Xe^{n+}—Ne pairs the cross section decreases for increasing charge of the fast Xe^{n+} particles. It can also be seen from Fig. 1 that for the Ne^{n+}—Xe pairs a sharp increase in the σ_- cross section occurs starting with n = 3. Thus, e.g., for v = 5.4 $\times 10^7$ cm/sec (particle energy T = 30 kev), the cross section σ_- equals 5.5×10^{-16} cm^2 for the Ne^0—Xe pairs, 6×10^{-16} cm^2 for Ne^+—Xe, 6.2×10^{-16} cm^2 for Ne^{2+}—Xe, 11.2×10^{-16} cm^2 for Ne^{3+}—Xe, and $\sim 24 \times 10^{-16}$ cm^2 for Ne^{4+}—Xe. The decrease of the σ_- cross section with increasing n for the Xe^{n+}—Ne pairs is smoother. For v = 2.1×10^7 cm/sec (T = 30 kev), the cross section σ_- equals 1.8×10^{-16} cm^2 for the Xe^0—Ne pairs, 1.4×10^{-16} cm^2 for Xe^+—Ne, 1×10^{-16} cm^2 for Xe^{2+}—Ne, 0.9×10^{-16} cm^2 for Xe^{3+}—Ne, and 0.6×10^{-16} cm^2 for Xe^{4+}—Ne. It can also be noted that, for the same velocity, the total ionization cross section σ_- is practically identical for the Ne^0—Xe and Xe^0—Ne pairs, and therefore these pairs are completely equivalent with respect to the production of free electrons.

All cross sections increase continuously with increasing velocity v. However, for the Ne^{n+}—Xe pairs, a slower rise of σ_- with velocity is observed than for the Xe^{n+}— Ne pairs, and the behavior of the curve $\sigma_-(v)$ depends little on the charge. For the Xe^{n+}—Ne pairs, the curvature of the curve $\sigma_-(v)$ increases with decreasing charge.

3. DISCUSSION OF RESULTS

In the collision of a fast particle I^0 with atoms of the gas A, the electrons are freed either as the result of pure ionization

$$I^0 + A \rightharpoonup I^0 + A^{k+} + ke, \tag{1}$$

as a result of stripping of the fast particle

$$I^0 + A \rightarrow I^{m+} + A + me, \tag{2}$$

or else through a combination of ionization and stripping

$$I^0 + A \rightarrow I^{m+} + A^{k+} + (m+k)e. \tag{3}$$

If the fast particle is an ion I^{n+}, then, in addition, we can have processes of capture ionization*

$$I^{n+} + A \rightarrow I^{m+} + A^{k+} + (m+k-n)e, \tag{4}$$

in which some of the electrons removed from the atomic shell are captured by the shell of the ion and some are freed.

The relative role of any process is determined primarily by the energy ε necessary for its occurrence. Thus, for instance, it is clear that for the Ne^{n+}—Xe pairs the ionization of the Xe atoms should predominate over the stripping of the fast Ne^{n+} particles, which calls for a much higher energy. The stripping can probably contribute appreciably to the total ionization cross section σ_- only for the Ne^0—Xe pair. For the Ne^+—Xe pair, the cross section $\sigma_-(Ne^+)$ is somewhat greater then the cross section $\sigma_-(Ne^0)$ (see Fig. 1), for in this case ε = 11.7 ev, and the following combined ionization and capture is possible

$$Ne^+ + Xe \rightarrow Ne^0 + Xe^{2+} + e. \tag{5}$$

Although the process (5) is endothermic, it needs less energy than the stripping process $Ne^0 \rightarrow Ne^+$.

The role of ionization with capture is evidently greater for highly ionized fast neon particles

*We consider only the atoms and ions of inert gases, and capture of the electron by fast atoms is therefore excluded.

where these processes become exothermic. For the Ne^{2+}—Xe pair, the energy $\varepsilon \approx -29$ ev liberated in a single-electron charge exchange

$$Ne^{2+} + Xe \rightarrow Ne^{+} + Xe^{+}, \quad (6)$$

is sufficient for the removal of a second electron from the Xe atom

$$Ne^{2+} + Xe \rightarrow Ne^{+} + Xe^{2+} + e \quad (\varepsilon = -7.75\,\text{ev}). \quad (7)$$

The liberated energy may be carried away by the free electron or used up for optical excitation.

For the Ne^{3+}—Xe pair in the single-electron and two-electron charge exchange

$$Ne^{3+} + Xe \rightarrow Ne^{2+} + Xe^{+} \quad (\varepsilon \approx -51\,\text{ev}), \quad (8)$$

$$Ne^{3+} + Xe \rightarrow Ne^{+} + Xe^{2+} \quad (\varepsilon \approx -71\,\text{ev}) \quad (9)$$

an energy $|\varepsilon| > 50$ ev is liberated, and for the Ne^{4+}—Xe pair, the charge exchange processes are even more exothermic:

$$Ne^{4+} + Xe \rightarrow Ne^{3+} + Xe^{+} \quad (\varepsilon \approx -85\,\text{ev}), \quad (10)$$

$$Ne^{4+} + Xe \rightarrow Ne^{2+} + Xe^{2+} \quad (\varepsilon \approx -127\,\text{ev}), \quad (11)$$

$$Ne^{4+} + Xe \rightarrow Ne^{+} + Xe^{3+} \quad (\varepsilon \approx -136\,\text{ev}) \quad (12)$$

and the energy liberated in these processes is sufficient for the removal of the next two electrons from the Xe atom, e.g.,

$$Ne^{4+} + Xe \rightarrow Ne^{3+} + Xe^{2+} + e \quad (\varepsilon \approx -64\,\text{ev}), \quad (13)$$

$$Ne^{4+} + Xe \rightarrow Ne^{3+} + Xe^{3+} + 2e \quad (\varepsilon \approx -32\,\text{ev}) \quad (14)$$

etc.*

It is clear that, at relatively large distances of approach of the nuclei in the case of multiply charged ions,[7] the liberation of electrons from the shells of colliding particles may not only be due to the kinetic energy of the relative motion (ionization mechanism discussed in[2]), but may also be a result of the excitation of the system due to the internal energy liberated in strongly exothermic charge-exchange processes. This explanation of the observed increase of the cross section σ_- with increasing charge is favored by the fact that the curves $\sigma_-(v)$ for the Ne^{2+}—Xe, Ne^{3+}—Xe, and Ne^{4+}—Xe pairs (see Fig. 1) are practically parallel, so that this ionization depends little on the relative velocity v. It is also interesting to note that the ionization due to the internal energy is similar to the field extraction of electrons from metals by ions of different charge as studied by us,[8] and may be regarded as a field ionization.

Whereas, the field ionization is the determining factor for the Ne^{n+}—Xe pairs when $n \geq 3$, for the opposite Xe^{n+}—Ne pair ionization of this type cannot occur even when $n \leq 5$. The charge exchange of Xe^{n+} ions in Ne is endothermic when $n \leq 3$, and when $n \leq 5$ the energy freed in exothermic charge-exchange processes is not sufficient to free the second electron from the Ne atom. For the Xe^{0}—Ne pair, the cross section σ_- is undoubtedly determined by the stripping of the fast atom of Xe^{0}, and the relative contribution of the pure ionization process of the Ne atoms is relatively small.

From indirect data* we can also establish that for the Xe^{+}—Ne pair the main role in the production of free electrons is also played by the stripping process, although the energy $\varepsilon = 21.2$ ev necessary for the stripping reaction

$$Xe^{+} + Ne \rightarrow Xe^{2+} + Ne + e, \quad (15)$$

is close to the ionization energy of neon ($\varepsilon = 21.56$ ev). Apparently, this is due to the excitation of a larger number of electrons in the outer shell of Xe than in Ne. The stripping with a higher degree of ionization of the fast Xe particles needs a relatively larger energy loss, and the total cross ionization σ_- therefore decreases with increasing charge. However, the fact that the σ_- cross section decreases continuously right up to the Xe^{4+}—Ne pair testifies to the considerable contribution of the stripping processes to the σ_- cross section also for the Xe^{2+}—Ne and Xe^{3+}—Ne pairs.

Thus, the results of the present experiment permit us to explain to a certain degree the influence of the charge of the fast particle when the relative velocity is $v < e^2/\hbar$.

The production of free electrons is connected with the probability of occurrence of various inelastic processes, and the character of the variation of the total ionization cross section σ_- with the charge n is determined by the relative role of the particular process. This is well illustrated by the data obtained for two groups of particles (Ne^{n+}—Xe, Xe^{n+}—Ne) which differ strongly in the binding energy of the electrons in the ionizing par-

*We do not consider here the charge exchange with total neutralization of the charge for the Ne^{3+} and Ne^{4+} ions, since it is known[6] that the charge-exchange cross section decreases strongly with an increasing number of captured electrons. Apparently, the main role in the further ionization of the Xe atoms is played by the processes of single-electron charge exchange (8) and (10).

*For the pairs Xe^{+}—Ne, the ionization cross section Ne practically coincides with the total production cross section of slow ions (σ_+), and the stripping cross section of Xe^{+} can be determined from the difference between the cross sections ($\sigma_- - \sigma_+$).[4]

ticle and in the gas atom. In this case, where the ionization processes with capture are exothermic, they can contribute greatly to the total ionization cross section σ_-, and an increase in σ_- with increasing charge is observed (Ne^{n+}—Xe pairs). On the contrary, for the pairs Xe^{n+}—Ne, the predominant role in the production of free electrons is due to the stripping processes, and the cross section σ_- decreases with increasing charge. When there is no sharp difference in the binding energy of the electrons in the shells of colliding atomic particles, there may be no regular variation of the cross section σ_- with the charge n.[3]

In the future, it would be of interest to carry out similar investigations with ions having larger charges and in the range of lower velocities, which might enable us to separate the field ionization in pure form (without the superposition of kinetic ionization). It would also be of basic interest to measure the energy of electrons produced in the ionization of the gas by ions with different charge.

In conclusion, the authors express their deep gratitude to Prof. V. M. Dukel'skii for valuable advice in discussing the results of the experiment.

[1] N. V. Fedorenko, Usp. Fiz. Nauk **58**, 481 (1959).

[2] O. B. Firsov, JETP **36**, 1517 (1959), Soviet Phys. JETP **9**, 1076 (1959).

[3] Fedorenko, Flaks, Filippenko, JETP **38**, 719 (1960), Soviet Phys. JETP **11**, 519 (1960).

[4] I. P. Flaks, ZhTF **31**, 367 (1961), Soviet Phys.-Tech. Phys. **6**, 263 (1961).

[5] Flaks, Ogurtsov, and Fedorenko, JETP **41**, 1094 (1961), Soviet Phys. JETP.

[6] I. P. Flaks and L. G. Filippenko, ZhTF **29**, 1100 (1959), Soviet Phys. Tech. Phys. **4**, 1005 (1960).

[7] Fedorenko, Filippenko, and Flaks, ZhTF **30**, 49 (1960), Soviet Phys. Tech. Phys. **5**, 45 (1960).

[8] I. P. Flaks, ZhTF **25**, 2463 (1955).

Translated by H. Kasha
246

WHICH IS RESPONSIBLE FOR THE DESTRUCTION OF SUPERFLUIDITY, v_s OR $v_s - v_n$

V. P. PESHKOV and V. B. STRYUKOV

Institute for Physics Problems, Academy of Sciences, U.S.S.R.

Submitted to JETP editor June 10, 1961

J. Exptl. Theoret. Phys. (U.S.S.R.) **41**, 1443-1448 (November, 1961).

The critical velocities for the flow of the superfluid component alone, within a capillary 0.385 cm in diameter, and for movement in opposite directions of the superfluid and normal components, have been determined from the attenuation of second sound. It is shown that the determining factor in the destruction of superfluidity is the motion of the superfluid component relative to the wall.

THE concept of a critical velocity in flowing helium II was originally introduced by Kapitza, on the basis of his experiments in 1941.[1] Since that time, many experiments have been designed for the observation of critical phenomena in helium. Up to the present, however, it has remained unclear whether the destruction of superfluidity in helium II is governed by its internal properties—i.e., the relative motion of the superfluid (v_s) and normal (v_n) components—or by the movement of the superfluid component relative to the walls. The experiments of Hung, Hunt, and Winkel[2] with a slit of width $d \sim 1\mu$ indicate that the critical quantity is the velocity v_s relative to the walls. However, a number of authors, such as Vinen[3] and Kramers,[4] point out that for wide channels the question of whether $v_s - v_n$ or v_s is the critical factor is not clear, since the destruction of superfluidity in wide channels can take place in a different manner than in narrow ones. No specific experiments have been performed in this field, a fact explained by the difficulty of measuring the temperature differences prevailing under slightly supercritical conditions (10^{-7} to 10^{-8} °K).

The experiment described below was proposed as a means of resolving the question of whether the destruction of superfluidity arises from the interaction of the superfluid current with the walls, or from an internal interaction between the normal and superfluid currents. Critical velocities were observed both for motion of the superfluid component alone and for the same superfluid component velocity with the normal component flowing in the opposite direction at a velocity several times higher (the counterflow case).

For the measurements we made use of a second-sound attenuation method similar to that of Vinen.[5] The apparatus in which the measurements were carried out is illustrated in Fig. 1. The entire system is of glass. Critical velocities were observed in the flow of helium within a tube 1 of diameter 0.385 ± 0.005 cm and 10 cm long. The superfluid and normal components were set into motion in opposite directions with the aid of a heater 2 having the form of a flat spiral with wide openings, made of 30 μ diameter constantan. The tube 1 was separated from the upper portion of the apparatus by means of a silk screen with openings of ~ 50 μ, above which was a densely-packed column of rouge 3, consisting of particles of Fe_2O_3 a few microns in size.

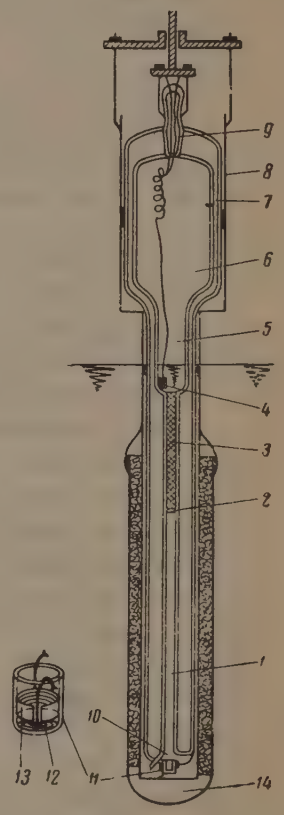

FIG. 1. Apparatus in which the measurements were performed. Scale 1:3. Cap shown in enlarged view.

Motion of the superfluid component alone was produced by means of the thermo-mechanical effect through the rouge, using the heater 4. The superfluid component velocity v_s was determined to an accuracy of 3% from measurements of the rise in the liquid level in the tubes 5 and 6, using a cathetometer and a stopwatch. To insure adiabatic conditions, the apparatus was enclosed in a vacuum jacket 7, and was surrounded by a copper screen 8. The plug 9, which can be lowered or raised, controlled the thermal contact between the helium within the apparatus and the external helium bath. The tube 1 and the cap 11, separated from the former by a broad ($h \approx 1.2$ mm) gap 10 formed a second sound resonator. The cap had a length $h' \approx 4.5$ mm. To insure maximum Q for the resonator, its length was determined from the condition

$$\lambda/4 = h' + h/2.$$

The second sound wavelength is $\lambda \approx 2.3$ cm; the width h of the gap was so chosen that the area of the gap was somewhat greater than the cross-section of the tube 1.

A second sound radiator 12 in the form of a flat spiral of 30 μ diameter constantan was situated at the bottom of the cap. The second sound receiver 13, of 40 μ diameter phosphor bronze, was cemented to a strip of thin paper and attached to the side wall of the cap, as close to the bottom as possible. The Q of the resonator was found to be of the order of 140, determined to an accuracy of 8%.

To reduce contact with the external volume, we made use of a container 14 filled with cotton. The temperature of the helium bath was automatically held constant to 10^{-5} °K. The second sound measuring apparatus was essentially the same as that used in the work of Peshkov.[6] The noise level was $\sim 0.3 \times 10^{-8}$ v, which is equivalent to reliable detection of a temperature difference of $\sim 3.5 \times 10^{-7}$ °K. The signal from the second sound receiver was applied, after amplification, to an ÉNO-1 oscilloscope.

In order to determine the critical velocity in the case of motion of the superfluid component alone, we carried out the following operations.

1. Flow of the superfluid component at velocities v_s' close to the critical value was induced in the quiescent helium above the rouge with the aid of the heater 4.

2. The heater 2, below the rouge, was turned on, producing a counter current of density W_2 which was known to be well into the supercritical range (by a factor of 7—8). Simultaneously with switching on the heater 2, a sweep was started across the oscilloscope, whose screen was of the long-persistence type. The time τ required for the second sound amplitude to fall half-way to its final value was measured on the oscilloscope. We then switched off both heaters and waited a sufficient time for the turbulence in the capillary to die down and the helium to come to rest.

The following experiment was conducted to determine the time required for the helium to come to rest. As in the preceding case, we switched on the heater 2, producing a certainly supercritical flux W_2. After equilibrium had become established, we turned off the heater; switching it on again after a time t, we determined τ as before.

The dependence of τ upon t at $T = 1.32°K$ and $W = 6.5 \times 10^{-2}$ w/cm^2 is presented in Figure 2. As is evident from this figure, the quiescence time of the helium was ~ 240 sec. During the experimental runs we allowed at least 300 sec for the helium to become quiet.

After the helium had come to rest, we again switched on heater 4, with a power input corresponding to another value of v_s and repeated the whole procedure for determining τ. Data on the variation of τ with v_s for motion of the superfluid alone are presented in Fig. 3. As is evident from the graph, a sharp decrease in τ is observed at $v_s \approx 3 \times 10^{-2}$ cm/sec, indicating that the supercritical mode has set in.

To determine the critical value v_s'' for the counterflow case, we carried out the following operations.

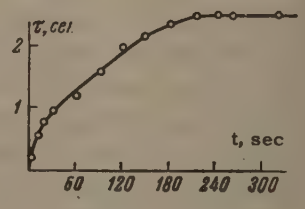

FIG. 2. Variation of τ with t. $T = 1.32°K$, $W_2 = 6.5 \times 10^{-2}$ w/cm^2.

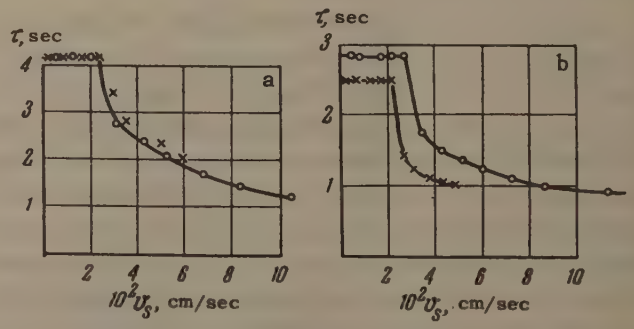

FIG. 3. Dependence of τ upon the velocity v_s: × — counterflow case, o — case of flow only of superfluid component. a — $T = 1.44°K$: for both cases $W_2 = 5.5 \times 10^{-2}$ w/cm^2, b — $T = 1,32°K$; $W_2 = 6.5 \times 10^{-2}$ w/cm^2 for counterflow and $W_2 = 5.5 \times 10^{-2}$ w/cm^2 for motion of the superfluid component alone.

1. A small thermal flux W_1, of the same order as the critical flux, was applied to the quiescent helium, using the heater 2.

2. After waiting for a time $t_2 = 60$ sec, sufficient for propagation of the turbulence along the length of the tube for supercritical values of v_s'', we applied via heater 2 a heat flux W_2 which was known to exceed the critical value. The time τ was then determined as before. Subsequently, heater 2 was turned off, the helium was allowed to come to rest (by waiting at least 300 sec), and the operation was repeated for a new value of W_1.

In the counterflow case, the mean mass current density is zero; i.e.,

$$\bar{j} = \rho_s \bar{v}_s + \rho_n \bar{v}_n = 0, \qquad \bar{v}_s = -\rho_n \bar{v}_n / \rho_s, \tag{1}$$

where ρ_s and ρ_n are the superfluid and normal component densities, respectively, and $\bar{v}_s$ and $\bar{v}_n$ are the corresponding velocities, averaged over the cross section of the tube. Since the thermal current density in superfluid helium is $W = \rho Q \bar{v}_n$, where Q is the heat content of the helium, we have, using (1)

$$W = \rho \frac{\rho_s}{\rho_n} Q \bar{v}_s = \rho_s Q (\bar{v}_n - \bar{v}_s). \tag{2}$$

In the subcritical regime $\bar{v}_s = v_s$. Knowing W_1, one can, with the aid of (2) find v_s''. The dependence of τ upon v_s'', with the latter determined in this manner, is also shown in Fig. 3. At $T = 1.44°$ K, the flux $W_2 = 5.5 \times 10^{-2}$ w/cm^2, while at $T = 1.32°$ K, $W_2 = 6.5 \times 10^{-2}$ w/cm^2. Different values for W_2 were used in the counterflow case and in the case of motion of the superfluid component alone in order to demonstrate that the values obtained for $v_{s\,cr}$ are independent of W_2.

It must be mentioned that a parasitic thermal flux from the second sound radiator and receiver, amounting to approximately half the value of the critical flux $W_{1\,cr}$, introduces an uncertainty in the numerical value of $v_{s\,cr}$ as determined from Fig. 3. The effect of this parasitic flux is small, however, since due to the laminar character of the flow, the presence of the broad gap 10 prevents the propagation of the disturbances into the body of the tube. In control experiments, we turned on the second sound receiver and radiator and then turned them off a few seconds before applying the flux W_2. This had no effect; i.e., the influence of the parasitic flux is small. Moreover, in determining the critical velocity for the case of motion of the superfluid alone, we waited for a longer time than usual (up to 150 sec) after turning heater 4 on, and then switched it off at the same time heater 2 was turned on. This did not affect the data on $v_{s\,cr}$.

Let us analyze our experiments on the basis of the hypothesis that excitations arise during the destruction of superfluidity by vortex rings. This viewpoint makes it possible to explain a whole series of experiments (Atkins[7], Peshkov and Tkachenko[8]). If one assumes that the quantity $v_s - v_n$ is the determining factor in the onset of criticality, then it is natural to consider that the vortex ring arises somewhere within the tube. We then have, according to Landau's relation

$$\varepsilon/p < |v_s - v_n|.$$

Using the relationship between ε and p

$$\frac{\varepsilon}{p} = \frac{\hbar}{mr'} \ln \frac{r'}{a}$$

for a vortex ring of unknown radius r' (Atkins[7]), and taking into account the parabolic profile of the normal component velocity, one can readily demonstrate that the formation of a vortex ring of radius $r' = R/\sqrt{3}$ is the most profitable, where R is the radius of the tube. Then

$$(v_s - v_n)_{cr} = (\varepsilon/p)_{r'=R/\sqrt{3}} \approx 3 \cdot 10^{-2} \text{ cm/sec}.$$

Experimentally, in the counterflow case at $T = 1.32°$ K, the value of $(v_s - v_n)_{cr}$ at $r = R/\sqrt{3}$ is 0.6 cm/sec. This is higher by a factor of 20 than the theoretical value, which indicates that the assumption that $v_n - v_s$ is the critical velocity, and, consequently, that the vortices are formed within the tube, is incorrect.

A second viewpoint, which makes the velocity of the superfluid component relative to the walls the critical one, appears to be the correct one. In this case the formation of vortices of maximum radius, close to that of the tube, is the most favored. There must, then be agreement between the values of the critical velocity $v_{s\,cr}$ obtained for v_s and v_n oppositely directed, and for movement of the superfluid component alone, as is, indeed, observed experimentally. As can be seen from Fig. 3, these velocities do agree, and we find $v_{s\,cr} \approx 0.3 \times 10^{-1}$ cm/sec. This is close to the value $v_{s\,cr} \approx 0.35 \times 10^{-1}$ cm/sec obtained by use of the semiempirical formula derived by Peshkov[9] on the basis of certain assumptions regarding vortex rings.

In addition to finding the critical velocity, we also determined the character of the attenuation of second sound with the superfluid component alone in motion. The smallest value for the attenuation, limited by the sensitivity of the apparatus, was found at $\bar{v}_s = 0.2$ cm/sec. The attenuation coefficient was determined from

$$\gamma = \frac{\pi\nu}{Q(0)\,u_2}\left(\frac{A_0}{A_1} - 1\right),$$

where ν is the resonance frequency ($\nu \approx 850$ cps), $Q(0)$ is the quality factor of the resonator, and A_0 and A_1 are the amplitudes before and after the onset of the attenuation. The dependence of γ upon $\bar{v}_s$ was found to be quadratic, and is illustrated in Fig. 4.

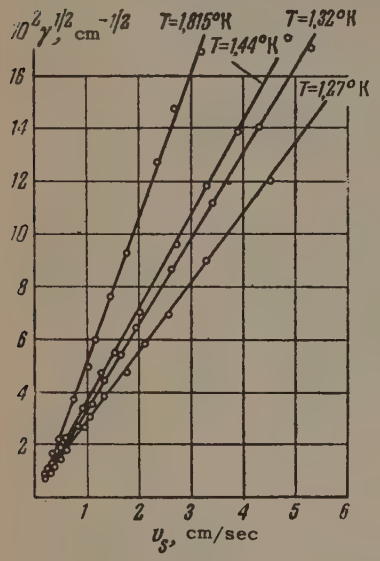

FIG. 4. Attenuation of second sound for the case of movement of superfluid component alone.

The value of γ does not change as the second sound amplitude is varied. The force F_{sn} developed per unit volume may be represented (Vinen,[10] Atkins[7]) in the form

$$F_{sn} = A\rho_n\rho_s\bar{v}_s^2(v_s - v_n),$$

The constant A in this formula is found from the expression $\gamma = A\rho v_s^2/2u_2$, where u_2 is the second sound velocity; it has, at various temperatures, the following values:

T, °K	=	1.27	1.32	1.444	1.815
A, cm sec g^{-1}	=	20	28.4	35	73

The accuracy of determination of the constant is 15—20%, due to the fact that contact between the internal resonator and the external helium bath was not completely eliminated in our system.

The existence of the force F_{sn}, as Vinen[11] has shown, may be explained by the appearance in moving helium of well-developed turbulence. Comparison of the results of Kidder and Fairbank,[12] which cannot be explained by the existence of well-developed turbulence leading to the generation of the force F_{sn}, with our data, indicates the presence in broad channels of a transition from "small-scale" to "large-scale" turbulence. In narrow channels (Hung, Hunt and Winkel[2]) the "small-scale" turbulence region is evidently either absent or extremely short, due to the large critical values for v_s.

The experiments which we have performed thus support the viewpoint that the destruction of superfluidity is a consequence of the formation of vortex rings of the Onsager-Feynman type. The critical velocity, moreover, appears to be v_s and not $v_s - v_n$; i.e., vortices are formed, not as a result of counterflow within the helium, but due to the interaction of the superfluid motion with the wall of the capillary.

In conclusion, the authors take the opportunity to express their gratitude to P. L. Kapitza for his unfailing interest in and attention to this work.

[1] P. L. Kapitza, JETP **11**, 581 (1941).
[2] Hung, Hunt and Winkel, Physica **18**, 629 (1952).
[3] W. F. Vinen, Proc. Roy. Soc. **A243**, 400 (1958), p. 412.
[4] H. C. Kramers, Proc. VII Internat. Conf. on Low Temp. Phys. 1960; p. 94.
[5] W. F. Vinen, Proc. Roy. Soc. **A240**, 128 (1957).
[6] V. P. Peshkov, JETP **38**, 799 (1960), Sov. Phys. JETP **11**, 580 (1960).
[7] K. R. Atkins, Liquid Helium, Cambridge, 1959.
[8] V. P. Peshkov and V. K. Tkachenko, JETP **41**, 1427 (1961), this issue, p. 1019.
[9] V. P. Peshkov, Proc. VII Internat, Conf. on Low Temp. Phys. 1960, p. 89; JETP **40**, 379 (1961); Sov. Phys. JETP **13**, 259 (1961).
[10] W. F. Vinen, Proc. Roy. Soc. **A240**, 114 (1957).
[11] W. F. Vinen, Proc. Roy. Soc. **A242**, 493 (1957).
[12] J. N. Kidder and W. M. Fairbank, Proc. VII Internat, Conf. on Low Temp. Phys. 1960, p. 91.

Translated by S. D. Elliott
247

QUANTUM CHARACTERISTICS OF THE 6.847-Mev LEVEL OF P^{30} *OBSERVED IN THE REACTION* $Si^{29}(p, \gamma)P^{30}$

A. K. VAL'TER, Yu. P. ANTUF'EV, E. G. KOPANETS, A. N. L'VOV, and S. P. TSYTKO

Physico-Technical Institute, Academy of Sciences, Ukranian S.S.S.R.

Submitted to JETP editor June 15, 1961

J. Exptl. Theoret. Phys. (U.S.S.R.) 41, 1449-1453 (November, 1961)

Resonance at an energy of 1330 kev was investigated in the reaction $Si^{29}(p, \gamma)P^{30}$. The magnetically separated isotope Si^{29} was used as a target and a γ-spectrometer with a NaI(Tl) crystal of 70 mm diameter and 50 mm height was used for the measurements. Quantum characteristics $J^{\pi} = 2^{+}$ and $T = 1$ were obtained for the P^{30} 6.847-Mev resonance level on the basis of measurements of the γ-ray spectra and of the angular distributions. A scheme is proposed for the γ-transitions from the given resonance level.

INTRODUCTION

THE first researches on the reaction $Si^{29}(p, \gamma)P^{30}$ ($Q = 5.562$ Mev) using targets made of magnetically separated Si^{29} were carried out in 1954 by Endt, Kluyver, and Van der Leun.[1] By magnetic analysis of the α particles from the reaction $S^{32}(d, \alpha)P^{30}$ ($Q = 4.887$ Mev), Endt and Paris[2] observed that P^{30} has not one 0.688-Mev level as indicated by Endt et al,[1] but two closely-lying levels with energies 0.684 and 0.706 Mev. Van der Leun and Endt[3] again investigated the γ spectra in the $Si^{29}(p, \gamma)P^{30}$ reaction at resonant energies $E_p = 326$, 414, 696, and 729 kev, and determine the spins and parities and also the isobaric spins of certain low-lying and resonant levels of P^{30}.

In the present investigation we continue the study of the $Si^{29}(p, \gamma)P^{30}$ reaction at higher bombarding-proton energies and measure the spectra and angular distribution of the γ rays for one of the observed resonances ($E_p = 1330$ kev).

APPARATUS, METHOD, AND PROCEDURE OF MEASUREMENTS

The source of the bombarding protons was the 4-Mev electrostatic generator of the Physico-Technical Institute of the Ukranian Academy of Sciences, which was described earlier.[4]

The isotopic target was prepared directly in an electromagnetic separator, by "hammering" the Si^{29} ions into a tantalum base.[5] The energy losses in the target used in these experiments were approximately 5 kev for 1.3-Mev protons.

To measure the spectra of the γ rays we used a NaI(Tl) crystal 70 mm in diameter and 50 mm high, mounted on an FÉU-43 photomultiplier. The preamplifier was placed next to the photomultiplier and was connected to the main amplifier through a long cable, the output of the main amplifier being fed to a 100-channel AI-100-1 pulse-height analyzer. The crystal with the photomultiplier could be rotated about the center of the target, and the angles to the proton beam could be set at values from 0 to 145°, right or left.

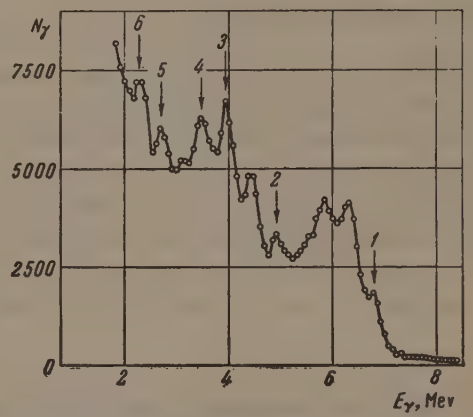

FIG. 1. Hard part of the γ-ray spectrum for the resonance at $E_p = 1330$ kev in the reaction $Si^{29}(p, \gamma)P^{30}$.

In the measurement of the angular distribution of the γ rays, the target was mounted such that its normal made an angle of 30° with the direction of the proton beam. Consequently, for angles less than 90°, a correction was introduced for the absorption of γ rays in the tantalum base. The correction for absorption did not exceed 5% with a 3% average.

The measured angular distribution of the γ rays was processed by the least-squares method and the coefficient A_2 in the angular distribution

Table I.

No.	γ lines observed in the spectrum, Mev	Level of P^{30} nucleus		Energy of γ transition and relative intensity*
		initial	final	
1	6.84±0.08	6,847	0	6,847; 70%
2	4.90±0.08	6.847	1,97	4,877; 10%
3	3.90±0.08	6.847	2,94	3,907; 15%
4	3,50±0.08	4,18	0,684	3,496; 5%
5	2,70±0,08	6.847	4.18	2,667
6	2.25±0,08	2.94	0,684	2,256
7	1.97±0.08	1,97	0	1.97
8	1,65±0.08	4,18	2,54	1.64
9	1.45±0.08	2.94	1,45	1,49
10	0,68±0,05	0,684	0	0,684

*The sum of all the transitions from the resonant level is taken to be 100 percent.

was corrected for the finite angle subtended by the crystal.

EXPERIMENTAL RESULTS

The relative γ-ray yield due to proton capture was measured at 90° to the proton beam. Two γ resonances belonging to this reaction were observed at E_p values of 1308 and 1330 kev.

Figure 1 shows the hard part of the γ-ray spectrum, measured for the 1330-kev resonance. All the observed γ lines and the corresponding γ transitions between the P^{30} levels are listed in Table I.

The angular distribution for the γ transition from the 6.847-Mev resonant level to the ground state of P^{30} (γ line 1) is shown in Fig. 2. As can be seen from the figure, the angular distribution has good symmetry relative to the 90° angle. We can therefore assume that at the 1330-kev resonance this γ-ray angular distribution is due to the capture of protons with one value of the orbital momentum l^p.

The experimentally obtained angular γ-ray distribution for the 6.847-Mev γ line, reduced by the least-squares method and corrected for the finite solid angle subtended by the crystal, had the form

$$W_{exp.}(\theta) = 1 - (0{,}485 \pm 0{,}015)\cos^2\theta. \quad (1)$$

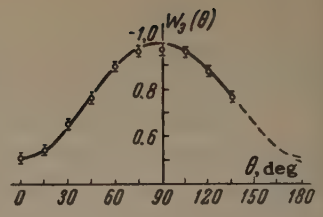

FIG. 2. Experimental angular distribution of the γ rays for the γ transition from the 6.847-Mev level to the ground state of P^{30} [see (1)].

This value was compared with all the theoretical angular distributions possible for γ transitions to the level with spin 1. From Table II it is easy to see that this comparison makes it possible to assign to the 6.847-Mev resonant level only one spin value, namely 2. The parity still remains indeterminate, however, since the coefficient A_2 in the experimentally-obtained angular distribution can correspond either to one of the calculated angular distributions (– 0.50), or to multipole mixtures ($M_1 + E_2$), or to channel-spin mixtures ($J_c = 1$ and 0).

GAMMA-TRANSITION SCHEME FOR P^{30} AND DISCUSSION OF THE RESULTS

The analysis of the measurement results in a proposed γ-transition level scheme for the 6.847-Mev level of P^{30} is shown in Fig. 3. From an examination of this scheme we can draw certain conclusions concerning the parity of the 6.847-Mev resonant level and its isobaric spin T. For the given resonant level, generally speaking, there exist four possible estimates of the quantum characteristics, namely: 2^+, T = 0; 2^+, T = 1; 2^-, T = 0 and 2^-, T = 1. Recognizing, however, that the direct transition to the ground state of P^{30} from the resonant level is a dipole transition and is the most intense of all other γ transitions, and that E1 and M1 transitions with ΔT = 0 are apparently forbidden by the selection rules in T, we must assign to the 6.847-Mev resonant level a value of T = 1. It remains therefore to examine two possible estimates: 2^+, T = 1 and 2^-, T = 1.

The γ transitions to the ground state and the intermediate levels should be classified as M1 and E2 in the former case and E1 and M2 in the latter case. But since the probability of observing M2

Table II.

Spin of initial state								
0			1			2		
l_p	J_c	A_2	l_p	J_c	A_2	l_p	J_c	A_2
0	0	0	0	1	0	2	0	–0,60
1	1	0	2	1	+0.43	2	1	–0,33
			1	0	+1.00	1	1	–0,45
			1	1	–0,33	3	1	–0,50

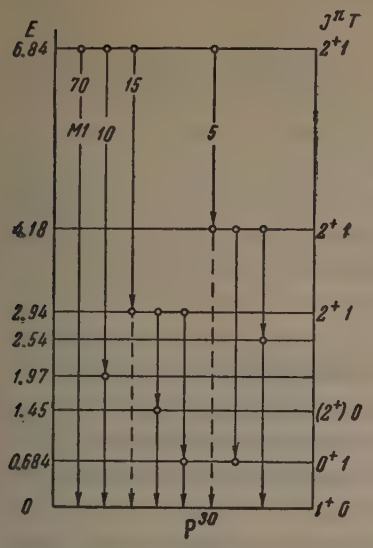

FIG. 3. γ-transition scheme in P^{30} from the 6.847-Mev resonant level.

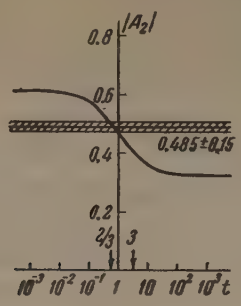

FIG. 4. The coefficient A_2 in the angular distribution of the γ rays for a channel-spin mixture as a function of the mixture coefficient t. The hatched strip corresponds to the experimental value of A_2 (with the error in its determination). The arrows indicate the values of t_{jj} predicted by the theory.

transitions in parallel with an E1 transition is negligibly small compared with the probability of observing the corresponding M1 and E2 transitions, a positive parity of the resonant level is the more probable. Thus, the resonant level must be assigned values 2^+ and $T = 1$.

Since the value $A_2 = -0.485 \pm 0.015$ obtained in the experimental angular distribution differs appreciably from the calculated values (– 0.60 and – 0.33), it is of interest to discuss possible mixtures of multipoles and channel spins.

For the multipole mixture M1 + E2 we can obtain good agreement with experiment if we add to the pure M1 transition [with angular distribution $W(\theta) = 1 - 0.60 \cos^2\theta$] an E2 transition mixture with coefficient $\delta = (2|E2|1)/(2|M1|1) = 0.1$ or $\delta^2 = 0.01$.

For the mixture in channel spin, the coefficient in the angular distribution of the γ rays is given by the relation

$$A_2 = -(0.60 + 0.33)/(1 + t),$$

where t is the channel-spin mixture coefficient.

It is of interest in this case to compare with experiment the values of the coefficient t, predicted by the theory for two limiting cases of jj and ls couplings. The analysis shows that in the case of an ls coupling there is no agreement with experiment, since the theoretically predicted values of t_{ls} are 0 and ∞, i.e., there are no channel spin mixtures for the ls coupling. In the case of jj coupling, t_{jj} has two values[6], $\frac{2}{3}$ and 3.

Figure 4 shows a comparison of the theoretical values of t for the jj coupling with the experimentally obtained value based on measurement of the angular distribution of the γ rays. As can be seen from the plots of A_2 vs. t, only one of the values predicted by the theory for the jj coupling is in good agreement with the experimental value $A_2 = -0.485 \pm 0.015$.

[1] Endt, Kluyver, and Van der Leun. Phys. Rev. 95, 580 (1954).

[2] P. M. Endt and C. H. Paris. Phys. Rev. **110**, 89 (1958).

[3] C. Van der Leun and P. M. Endt. Phys. Rev. **110**, 96 (1958).

[4] A. K. Val'ter and A. A. Tsygikalo, PTÉ No. 4, 3 (1957).

[5] M. I. Guseva, ibid, No 5, 112 (1957).

[6] Nuclear Reactions, **1**, edited by P. M. Endt and M. Demeur, Amsterdam (1959), p. 312.

Translated by J. G. Adashko
248

DEFORMATION OF THE NaCl *LATTICE BY* Ag^+, Br^-, *AND* K^+ *IMPURITY IONS*

M. I. KORNFEL'D and V. V. LEMANOV

Semiconductor Institute, Academy of Sciences, U.S.S.R.

Submitted to JETP editor June 17, 1961

J. Exptl. Theoret. Phys. (U.S.S.R.) 41, 1454-1460 (November, 1961)

The lattice constant and the intensity of the Na^{23} nuclear magnetic resonance absorption line were studied as functions of the impurity concentration in NaCl crystals containing AgCl, NaBr, and KCl impurities. A clear correlation was observed between decrease of the absorption line intensity and variation of the lattice constant. Both the intensity and the lattice constant are unique functions of n and c not depending on the kind of impurity. (c is the impurity concentration and n is the number of Na^{23} nuclei within the "critical" sphere.) The degree of elastic deformation of the lattice near an impurity ion is estimated. At distances of 8.9, 12.4, and 16.7 A from Ag^+, Br^-, and K^+ ions, respectively, the degree of deformation was approximately 10^{-3}.

1. INTRODUCTION

CRYSTAL lattices are deformed in the vicinity of impurity atoms and ions. However, very little is known regarding the nature and degree of this deformation. X-ray analysis shows that impurities change the average atomic separation (the lattice constant), but does not supply information regarding local deformations near impurity ions or atoms. The latter type of information can be obtained by means of nuclear magnetic resonance. The investigation of quadrupole effects in the nuclear magnetic resonance of impure crystals can be used to determine the character and degree of local lattice deformations. However, the results obtained by this method are still very incomplete.*[1,2]

Let us consider the method as applied to the simplest case of a cubic crystal. The high lattice symmetry of a pure and nearly perfect crystal makes the electric field gradient zero at all nuclei. Therefore the central line component (the transition $m = \frac{1}{2} \rightarrow m = -\frac{1}{2}$, where m is the magnetic quantum number) and satellites ($m \rightarrow m - 1$ transitions with $m \neq \frac{1}{2}$) coincide in frequency, forming a single combined absorption line. The introduction of an impurity induces electric field gradients at the nuclei. These gradients can result both from the electric field of an impurity atom or ion and from elastic deformations, i.e., local changes of lattice symmetry. A charged impurity is accompanied by both effects, while only the second effect occurs in the case of a neutral impurity.

Satellite frequencies are shifted by an interaction between nuclear quadrupole moments and the electric field gradient. The maximum shift will obviously occur for nuclei in the immediate vicinity of an impurity ion, where the gradient is especially large; the shift will diminish with increasing distance between the nuclei and the impurity. We therefore introduce the concept of a critical sphere around an impurity ion. The radius of this sphere is defined as such that for all nuclei within the sphere the satellite frequency shift exceeds the half-width of the absorption line at its base, i.e., at the instrumental noise level. The satellites of these nuclei are smeared out within a broad frequency interval and are lost in the noise background, so that an apparent reduction of absorption line intensity is observed. The reduction of intensity becomes more marked as the impurity concentration increases and thus puts more nuclei within critical spheres.

At low concentrations, however, when there is only a small probability that critical spheres intersect, the contribution of satellites to the absorption line intensity is

$$J = J_0(1 - nc), \tag{1}$$

where J_0 and J are the satellite intensity in a pure and impure crystal, respectively, n is the number of nuclei within a critical sphere, and c is the impurity concentration. The slope of the first segment of the curve of J/J_0 as a function of

*This does not apply to Rowland's very thorough study[3] of impurities in copper, where it was shown that in this case charge effects, rather than lattice deformations, are responsible for the quadrupole interaction.

c can be used to determine n and thus also the radius R of the critical sphere.*

The critical radius determined in the foregoing manner is, of course, arbitrary since the width of the absorption line at its base depends on the noise level. However, this width can be used to determine the electric field gradient for nuclei at a distance R from an impurity ion, thus imparting a definite quantitative meaning to the concept of a critical sphere.

As a basis for a systematic study of the different impurities in NaCl crystals we had first determined the components of the tensor relating the electric field gradient at a Na^{23} nucleus to the elastic deformation of the NaCl lattice.[6] When these tensor components are known the degree of lattice deformation at the boundary of a critical surface can be computed.

In the present work we investigated NaCl crystals with neutral impurities containing Ag^+, Br^-, and K^+. The dependence of the Na^{23} absorption line intensity on impurity concentration was measured along with x-ray measurements of the lattice constant.

2. PREPARATION OF SAMPLES

Pure NaCl crystals and crystals doped with AgCl, NaBr, or KCl were grown by the Kyropoulos method from a melt containing chemically pure materials. The impurity content was determined by chemical analysis—by weighing in the case of Ag, by the iodometric method in the case of Br, and by the cobaltinitrite method in the case of K.†

The largest concentrations of AgCl, NaBr, and KCl in the crystals were 4, 11, and 3% mole, respectively. All crystals grew well within these limits. An attempt to grow NaCl-AgCl crystals containing above 5% AgCl was unsuccessful; the growth rate decreased sharply and the crystals were unsatisfactory.

It should be noted that the impurity concentration in the NaCl-NaBr system was almost identical with the concentration in the melt, but that there were considerable differences in the other two systems.

Samples for both x-ray structural measurements and nuclear magnetic resonance measurements were cut from single crystals grown to a diameter of about 50 mm and height of 30 mm. The average dimensions of the samples were $5 \times 5 \times 10$ mm and $9 \times 9 \times 20$ mm, respectively. Samples for chemical analysis were taken from the same portions of the respective crystals. In order to allow for a possible nonuniform impurity distribution many samples were analyzed chemically following the completion of the other measurements. It was found that the nonuniformity of impurity distribution within a sample did not exceed 10% of the mean concentration. In most instances the nonuniformity was at a satisfactory level of about 5%.

It is known from the literature that some mixed alkali halide crystals contain a large number of vacancies (see[7], for example). To determine the vacancy concentration, the density of our samples was measured by flotation, and the results were compared with the densities calculated from x-ray data. The discrepancy found in the case of NaCl crystals containing NaBr indicates that one vacancy exists for every seven Br^- ions. In the case of crystals doped with AgCl and KCl the disagreement between the computed and measured densities did not exceed the experimental error limit. On the basis of the measurements we conclude that not more than one vacancy exists for every 15 Ag^- ions or every 25 K^+ ions.

We have thus found that crystals containing NaBr have the largest number of vacancies, while those containing KCl have the smallest number. Our results will show that vacancies do not appreciably influence the intensity reduction of the nuclear magnetic resonance line.

3. MEASUREMENT OF THE LATTICE CONSTANT

The lattice constants were measured by A. I. Zaslavskii and T. B. Zhukova, using K_α emission from copper in a RKU-114 camera. Preliminary adjustment of the samples was performed in a RKSO camera. The lattice constant was determined to within $\pm 3 \times 10^{-4}$ A from the distance between reflections from (640) planes. The results are seen in Fig. 1, which also gives the relative change $\Delta a/a_0$ of the lattice constant as a function of impurity concentration for each of the three systems. $\Delta a/a_0$ is seen to be a linear function of concentration within the given limits. The lattice constant changes most markedly in NaCl-KCl crystals. Changes in the NaCl-AgCl system are small, and the NaCl-NaBr system occupies an intermediate position.

*In earlier work[4,5] we determined the number of atoms in a critical sphere from the expression $J/J_0 = (1-c)^n$, which was derived from probability considerations.[1] It is easily seen that at low concentrations this expression is equivalent to the simpler formula (1).

†We take this opportunity to thank I. A. Amantova, N. S. Volosatova, P. V. Usachev, and G. I. Bel'kov for performing careful analyses.

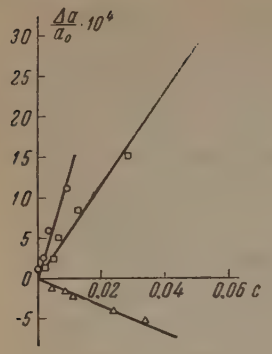

FIG. 1. Relative variation of lattice constant as a function of impurity concentration. Δ – Ag^+, □ – Br^-, ○ – K^+.

4. MEASUREMENT OF NUCLEAR MAGNETIC RESONANCE

The Na^{23} absorption line in pure and impure NaCl crystals was measured with the apparatus described in[8], using both a Franklin oscillator and one of the type described by Gutowsky et al. in in[9]. The latter differed from the original design in that prior to detection the signal was amplified at high frequency, thus somewhat improving the signal-to-noise ratio. In order to avoid saturation of the absorption line, measurements were performed at low voltages of the order 0.03 and 0.01 volt, respectively, in the Franklin and Gutkowsky oscillator circuits. For all measurements the magnetic field strength was 45 oe with 0.5 oe modulation amplitude.

The measurements showed that with increasing impurity concentration the absorption line intensity is reduced, approaching that of the central component, which in the case of Na^{23} with spin $^3/_2$ is four-tenths of the total intensity.[10] With further increase of the impurity concentration a reduction of central line intensity is observed; this corresponds to a second-order quadrupole effect.[10] The concentration at which this reduction begins is 3% mole in KCl and 10% mole in NaBr. Reduced central line intensity was not observed for crystals containing AgCl since, as already mentioned, crystals could not be grown with a sufficient AgCl content.

Figure 2 shows the relative intensity of satellites as a function of impurity concentration. Satellite intensity was taken as the difference between the measured intensity and that of the central component. The steepest reduction of satellite intensity is seen to occur for NaCl-KCl, where the intensity is reduced to approximately one-fifth for 1% mole KCl. The NaCl-AgCl system exhibits the smallest intensity reduction, while NaCl-NaBr occupies an intermediate position.

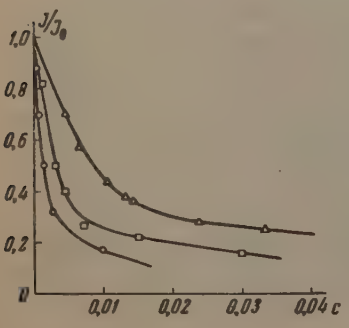

FIG. 2. Relative intensity of satellites as a function of impurity concentration. (Notation as in Fig. 1).

It should be noted here that the measure of satellite intensity in Fig. 2 is the amplitude of the derivative of the absorption line, since no changes of line width and shape were observed within experimental error limits. However, the absorption line area was calculated for individual samples, as a check. The intensities obtained in this way showed that the amplitude of the derivative is an exact measure of intensity only at low impurity concentration, but gives slightly overestimated intensities at high concentrations, when the satellite intensity approaches zero. This can account for some narrowing of the central line as the satellites are smeared out.[10] However, since the general character of the dependence of intensity on impurity concentration does not vary and only low concentrations are important for our quantitative purposes, the amplitudes of the derivative of the absorption line have been used as a measure of intensity for all points in Fig. 2.

It is seen from Fig. 2 that the first portion of the satellite intensity vs impurity concentration curve is a straight line for each of the three systems. The slope of each line gives the number n of Na^+ ions within the critical sphere and thus the radius R of the critical sphere. The values of n and R obtained in this manner are shown in the table.

Impurity ion	n	R, Å
Ag^+	76	8,9
Br^-	200	12,4
K^+	460	16,7

5. DISCUSSION OF RESULTS

1. From the determination of the critical sphere in accordance with Eq. (1) it follows that at low impurity concentrations the satellite intensity is a unique function of the total volume nc of critical spheres, independently of the kind of impurity. Experiment shows (Fig. 3) that this also occurs at high concentrations, when the critical spheres must intersect. This intersection only causes the given dependence to depart from linearity, beginning at $nc \approx 1$, as was to be expected.

Another interesting result is that the absolute value $|\Delta a|/a_0$ of the relative change of the lattice

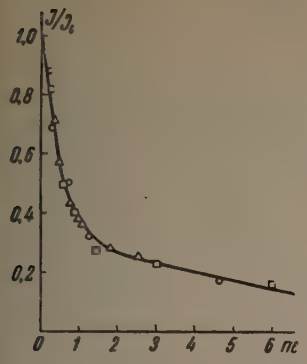

FIG. 3. Satellite intensity vs. total volume of critical spheres. (Notation as in Fig. 1).

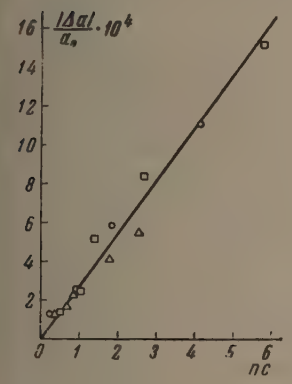

FIG. 4. Relative change of lattice constant vs. total volume of critical spheres. (Notation as in Fig. 1).

constant is also a unique function of nc, independently of the kind of impurity (Fig. 4).

A clear correlation, independent of the kind of impurity, therefore exists between the change of atomic separation determined by x-ray analysis and the departure from cubic symmetry detected by means of nuclear magnetic resonance.

2. We now compute the plastic deformation of the NaCl lattice caused by impurity ions. For this purpose we use the previously[6] determined components of the tensor S ($S_{11} = 2 \times 10^{15}$ and $S_{44} = 0.5 \times 10^{15}$ in cgs electrostatic units) which relate the electric field gradient at a nucleus to the elastic deformation of the lattice. When the field gradient at the nucleus is known the degree of deformation can be evaluated from a knowledge of these tensor components.

By perturbation theory the satellite frequency shift associated with quadrupole interaction is given by[10]

$$\Delta\nu = \frac{3eQ(2m-1)}{4I(2I-1)h}\varphi_{HH}, \qquad (2)$$

where I is the nuclear spin, Q is the nuclear quadrupole moment, and φ_{HH} is the component of the gradient along the magnetic field.

Equation (2) enables us to determine the gradient φ_{HH} for nuclei located at the critical sphere boundary. As already stated, the critical sphere is defined in such a manner that for nuclei situated at the critical radial distance from impurity ions the frequency shift $\Delta\nu$ equals one-half the experimental line width at its base. Equating the right-hand side of (2) to the half-width, which in our case is ~ 5 kc, we determine the gradient at the critical sphere boundary. Our result, $\varphi_{HH} \approx 10^{12}$ cgs esu, leads to a deformation of the order 10^{-3} at the critical sphere boundary.

This deformation occurs at distances of 8.9, 12.4, and 16.7 A from Ag^+, Br^-, and K^+ ions, respectively. This large deformation at such large distances from impurity ions shows how strongly the lattice is deformed by impurities. Even at low impurity concentrations a cubic crystal is actually cubic only "on the average" and departs from cubic symmetry at every individual point.

3. The theory of elasticity for an isotropic continuum is conventionally used to determine lattice deformations induced by impurities. The relative deformation ε at a distance r from an impurity ion is taken to be

$$\varepsilon = (a_n - a_0)\, a_0^2 r^{-3}, \qquad (3)$$

where a_0 and a_n are the radius of the host ion and impurity ion, respectively. It is interesting to check the consistency of this formula with our experimental data.

It follows from the definition of the critical sphere that the relative deformation ε_{cr} at the critical sphere boundary should be a constant that is independent of the kind of impurity. We obtained the following values of $\varepsilon_{cr} = (a_n - a_0) \cdot a_0^2 R^{-3}$ for each of the impurities:

	Ag^+	Br^-	K^+
$\varepsilon_{cr} \cdot 10^4 =$	3,95	2,40	0.73.

Pauling's values of the ionic radii have been used: Na^+ – 0.95, Cl^- – 1.81, Ag^+ – 1.26, Br^- – 1.95, and K^+ – 1.33 A.

Very different values of ε_{cr} are therefore associated with the different ions. This result probably ensues mainly from the fact that ions do not actually resemble solid spheres with well defined radii, as was assumed in deriving (3).

In conclusion the authors wish to thank O. M. Nilov and V. V. Sokolov for assistance.

[1] N. Bloembergen, Report of the Conference on Defects in Crystalline Solids, Bristol, 1954 (The Physical Society, London, 1955), p. 1.

[2] Kawamura, Otsuka, and Ishiwatari, J. Phys. Soc. Japan 11, 1064 (1956); E. Otsuka and H. Kawamura, J. Phys. Soc. Japan 12, 1071 (1957).

[3] T. J. Rowland, Phys. Rev. 119, 900 (1960).

[4] M. I. Kornfel'd and V. V. Lemanov, JETP 39, 53 (1960), Soviet Phys. JETP 12, 38 (1961).

[5] M. I. Kornfel'd and V. V. Lemanov, JETP 39, 262 (1960), Soviet Phys. JETP 12, 188 (1961).

[6] V. V. Lemanov, JETP 40, 775 (1961), Soviet Phys. JETP 13, 543 (1961).

[7] W. E. Wallace and R. A. Flinn, Nature 172, 681 (1953).

[8] V. V. Lemanov, PTÉ (Instrum. and Exptl. Techniques) 1, 126 (1961).

[9] Gutowsky, Meyer, and McClure, Rev. Sci. Instr. 24, 644 (1953).

[10] M. H. Cohen and F. Reif, Solid State Physics, edited by F. Seitz and D. Turnbull (Academic Press, New York, 1957), Vol 5, p. 321.

Translated by I. Emin
249

*INELASTIC INTERACTIONS BETWEEN 6.8 Bev/c π^- MESONS AND NUCLEONS**

N. G. BIRGER, WANG KANG-CH'ANG, WANG TS'U-TSENG, TING TA-TS'AO, YU. V. KATYSHEV, E. N. KLADNITSKAYA, D. K. KOPYLOVA, V. B. LYUBIMOV, NGUYEN DINH TU, A. V. NIKITIN, M. I. PODGORETSKII, YU. A. SMORODIN, M. I. SOLOV'EV, and Z. TRKA

Joint Institute for Nuclear Research

Submitted to JETP editor May 18, 1961

J. Exptl. Theoret. Phys. (U.S.S.R.) **41**, 1461-1474 (November, 1961)

An analysis was made of 355 interactions between π^- mesons and nucleons. The momentum and angular distributions of the secondary charged particles were measured. Information on π^0 mesons produced in the interactions has been obtained. The experimental data are compared with the statistical theory. The results suggest that peripheral interactions may exist. In events of low multiplicity (two-prong cases) "one-meson" peripheral interactions play an important role, while in events of large multiplicity an important role is played by interactions not of the one-meson type, among which also central collisions are possible.

I. EXPERIMENTAL RESULTS

IN this experiment we used photographs obtained with a 24-liter propane bubble chamber[2] placed in a magnetic field of 13 700 oe. The arrangement in which the chamber was located in a beam of (6.8 ± 0.6) Bev/c negative pions from the proton synchrotron of the Joint Institute for Nuclear Research has been described previously.[3] We scanned 870 pictures, on which we found 777 interactions of π^- mesons with hydrogen and carbon nuclei. The pictures were scanned twice. The overall efficiency of the scanning was close to unity.

1. To measure the momenta and angles we selected visually 456 interactions. The remaining 321 events were rejected on the basis of the following criteria: a) the sum of the charges of the secondary particles was not equal to 0 or −1; b) the presence of a short track of length $\lesssim$ 2 mm; c) the number of slow-particle tracks stopping in the chamber was $\geq$ 2.

Moreover, we discarded 28 elastic π^-p scatterings which were used in[3].

On stereoscopic pairs of pictures of the selected events we measured under a microscope the coordinates of 8—20 points of each track. From the coordinates we calculated the momenta of the particles, the error of the momentum measurement, and also the direction cosines of the track at the point of interaction. The calculations were made on an electronic computer. For tracks of primary pions producing the interactions we obtain a mean momentum $\bar{p}_{\pi^-} = 6.9 \pm 0.4$ Bev/c, which agrees, within the limits of error, with the mean momentum calculated from the data of[3] (6.7 ± 0.2 Bev/c).

2. All secondary negative particles were assumed to be π^- mesons. For positive particle tracks we measured the ionization by a gap-counting method similar to that used in[4]. For each interaction we measured the ionization of the primary pion, and the ionization of all secondary particles was referred to this value. We separated the protons and π^+ mesons for the momenta up to 1.2 Bev/c. In addition, part of the particles were also identified by their range. In all, it proved to be possible to identify 99% of the positive particle tracks of momentum $\leq$ 1.2 Bev/c.

3. As a result of the momentum and ionization measurements, we discarded 37 cases not satisfying the foregoing criteria and also cases of "scattering" by angles < 5°.

As was shown earlier in[5], for each πN interaction the relation

$$\sum \Delta_i \equiv \sum (E_i - p_i \cos\theta_i) \leqslant M$$

should be satisfied, where M is the nucleon mass.* The summation is carried out over all secondary particles of total energy E_i, momentum p_i, and angle θ_i relative to the direction of motion of the

*The value of M is equal to the nucleon mass for interactions with a free nucleon. For interactions with quasi-free nucleons, the value of M depends on the state of motion of the target nucleon and lies within the limits 0.76–1.16 Bev. The events were considered to be πN interactions if $\Sigma\Delta_i \leqslant 1.16$ Bev.

*Similar interactions with neutrons are included in the group of "scatterings" by an angle < 5°, and therefore were also excluded from the final statistics.

Table I

Reference	Primary π^- energy, Bev	$\sigma_{tot}(\pi^-p)$, mb
[9]	9.2	25±4
Present expt.	6.8	~31
[7]	5.2	29.1±2.9
[8]	4.7	28
[5]	4.4	30±5
[10]	4.3	30±5

primary particle. The inequality sign refers to cases in which not all neutral secondary particles are known. We discarded another 24 cases as a result of the application of this relation.

Moreover we discarded 12 two-prong events whose kinematics corresponded to cases of elastic interactions of a π^- meson with a quasi-free proton.*

4. We ultimately selected 262 cases of inelastic interactions of a π^- meson with a proton and 93 cases of interaction with a neutron. We estimated the inelastic π^-p interaction cross section and obtained the value $\sigma_{in}(\pi^-p) = 25 \pm 3$ mb. In the calculation of the cross section we assumed that the interactions with quasi-free protons and quasi-free neutrons are of the same frequency. The corresponding value for inelastic interactions of a π^- meson with a carbon nucleus turned out to be $\sigma_{in}(\pi^-C) = 194 \pm 13$ mb. The elastic π^-p cross section obtained in[3] was 5.5 mb. Hence the total π^-p interaction cross section was $\sigma_{tot}(\pi^-p) = 31$ mb. Tables I and II give a summary of the data on the cross sections $\sigma_{tot}(\pi^-p)$ and $\sigma_{in}(\pi^-C)$ obtained in our and other experiments.

Table II

Reference	Primary π^- energy, Bev	$\sigma_{in}(\pi^-C)$, mb
[11]	1.5	219 ± 11
[12]	4.2	218 ± 7
[13]	2—4	210^{+59}_{-68}
	4—66	208^{+97}_{-120}
Present expt.	6.8	194±13*

*Only the statistical error is shown. No special estimate of possible systematic errors was made.

*We estimated only the statistical error. No special estimate of systematic errors was made.

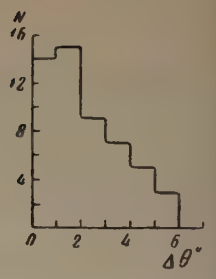

FIG. 1. Distribution of angles between electron and positron tracks.

Tables III and IV show the distributions of the observed cases for different values of the multiplicity n of charged particles and the values of the mean multiplicity $\bar{n}$ of charged particles. Also shown are the emulsion data[14] and the results of calculations made with the statistical theory in which the isobaric states[15,16] were taken into account.

As seen from these tables, the charged-particle multiplicity distribution is in agreement with the results obtained by the emulsion technique. The calculations with the statistical theory give values close to the experimental.

5. During the scanning, we recorded all electron-positron pairs which appeared to be emitted from the point of interaction.* After the measurements, we separated 74 γ quanta (for a total number of 355 π^-N interactions) which gave pairs satisfying the condition

$$|\theta_\gamma - \theta_i| \leqslant 2\Delta\theta \quad (i = 1, 2).$$

Here θ_γ, θ_1, θ_2 are the angles between the direction of flight of the γ quantum, electron, positron, respectively, and the direction of the primary track; $\Delta\theta$ is the angle between the electron and positron tracks. The quantity $\Delta\theta$ characterizes the accuracy in the measurement of the angles for a given event; the distribution of these values is shown in Fig. 1.

Fulfillment of this condition did not exclude the possibility of recording γ quanta from background interactions. However, it was estimated that the number of such γ quanta cannot exceed 2%.

We determined for each γ quantum the "potential" range in the effective region of the chamber and calculated the "statistical" weight

$$W_i = (1 - \exp[-l_i \mu(E_\gamma)])^{-1}.$$

Here l_i is the "potential" range of the γ quantum in radiation lengths (100 cm for propane of density 0.43 g/cm^3), W_i is the total probability for the production of pairs per radiation length. The sum of all values of W_i is equal to the total num-

*A special check showed that the efficiency of detection of pairs was close to 100%.

Table III.

Multiplicity, n	Present experiment		[14]		Statistical theory
	Number of interactions	%	Number of interactions	%	%
0	7	2.7±1.0	13	4.4±1.2	3.7
2	119	45.4±4.2	142	48.5±4.1	45.1
4	115	43.9±4.3	122	41.6±3.8	46.5
6	20	7.7±1.7	14	4.8±1.3	4.7
8	1	0.4±0.4	2	0.7±0.5	0.05
0—8	262		293		
$\bar{n}$	3.15±0.09		2.98±0.08		3.05

Table IV.

Multiplicity, n	Present experiment		[14]		Statistical theory
	Number of interactions	%	Number of interactions	%	%
1	16	17.2±4.6	56	23.1±3.1	18.5
3	53	57±9.8	143	59.1±4.9	59.5
5	21	22.6±5.4	36	14.9±2.5	20
7	3	3.2±1.9	7	2.9±1.1	2.0
1—7	93		242		
$\bar{n}$	3.24±0.15		2.95±0.09		3.0

ber of γ quanta emitted in the observed interactions. It turned out that $\sum_{i=1}^{74} W_i = 743 \pm 90$ γ quanta, i.e., the mean efficiency of recording γ quanta under our conditions was $(10 \pm 1)\%$.

6. The most complete information is obtained for the properties of the secondary π^- mesons. Figure 2 shows the c.m.s. angular distribution of π^- mesons from all π^-p and π^-n interactions. It proved to be asymmetric with respect to the angle $\theta^* = \frac{1}{2}\pi$. The forward-peaked anisotropic part of the angular distribution is associated primarily with fast π^- mesons ($P_{lab} \geq 2$ Bev/c. Angular distributions of such a nature are in sharp contradiction with the statistical theory. It is natural to associate the "anisotropic" π^- mesons with peripheral interactions (see, for example,[14,15]). The percentage of such π^- mesons decreases with the multiplicity (see Fig. 3).

Figure 4 shows the c.m.s. momentum distribution of π^- mesons for different multiplicities and

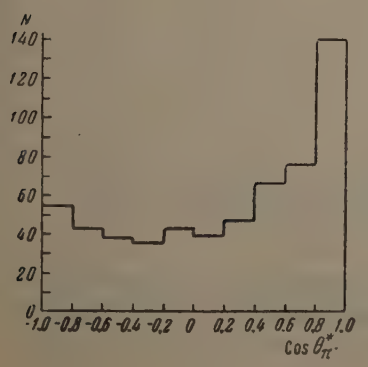

FIG. 2. C.m.s. angular distribution of π^- mesons from all π^-p and π^-n interactions.

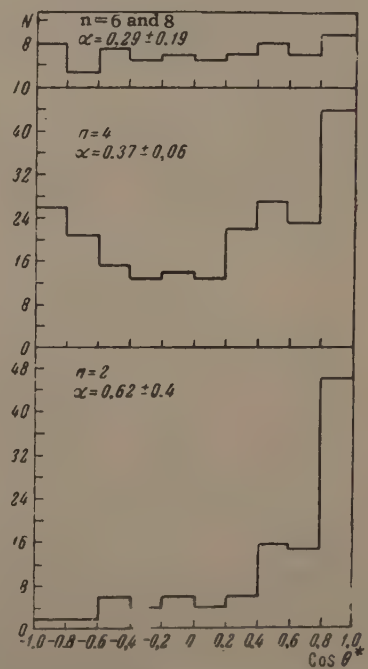

FIG. 3. C.m.s. π^--meson angular distribution for interactions of even multiplicity; $\alpha = (N_2 - N_1)n_{int}$, where N_2 and N_1 are the number of π^- mesons emitted forward and backward, n_{int} is the number of interactions.

Table V. Mean Value of $p_\perp$ (Bev/c)

Particles	$n=2$	$n=4$	$n=6, 8$	$n=2, 4, 6, 8$
π^- mesons	0.38±0.03	0.38±0.02	0.28±0.03	0.36±0.01
All positive particles	0.42±0.03	0.36±0.02	0.28±0.03	0.36±0.01
Identified π^+ mesons	0.35±0.04	0.26±0.01	0.19±0.02	0.26±0.04
Identified protons	0.26±0.03	0.37±0.04	0.28±0.07	0.31±0.04
π^0 mesons	—	—	—	0.34±0.07

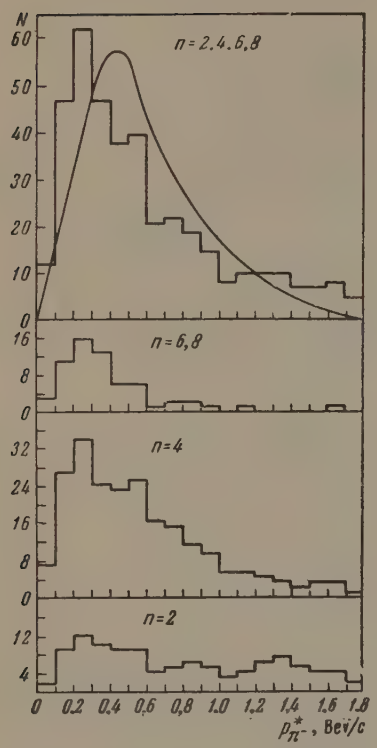

FIG. 4. C.m.s. π^--meson momentum distribution for π^-p interactions of even multiplicity. The smooth curve was calculated from statistical theory.[15]

the overall distribution together with the theoretical curve calculated from statistical theory.[15] As we see, the calculations based on statistical theory are not in qualitative contradiction with the experimental histogram.

Shown in Fig. 5 are the l.s. momentum distributions of the π^- mesons. The theoretical distributions were obtained from tables of random stars.[18]

The c.m.s γ-quantum angular distribution (from π^-p and π^-n interactions), which reflects the angular distribution of π^0 mesons is asymmetric (Fig. 6), i.e., it is apparently similar to the angular distribution of the charged π^- mesons. The mean number of π^0 mesons in π^-p interactions is 1.3 ± 0.2 and agrees with the calculations based on statistical theory.[16]

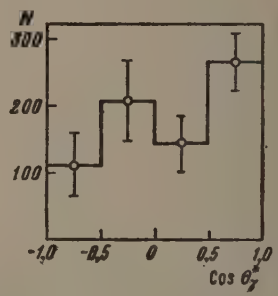

FIG. 6. C.m.s. angular distribution of γ quanta from all π^-n and π^-p interactions.

The observed l.s. γ quantum energy distribution is shown in Fig. 7. The mean π^0 energy for one π^-p interaction is 1.12 ± 0.15 Bev. This is less than the mean energy of the π^- mesons E_{π^-} = 2.7 ± 0.15 Bev.

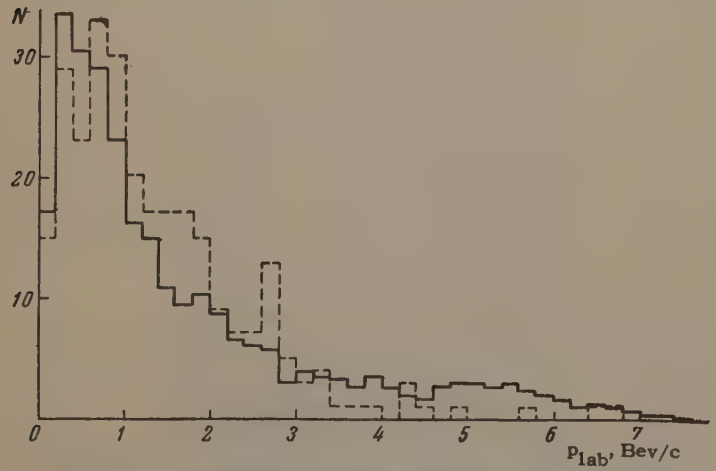

FIG. 5. L.s. π^--meson momentum distribution for π^-p interactions. The dotted-line histogram represents the statistical theory distribution obtained with the aid of tables of random stars.[18]

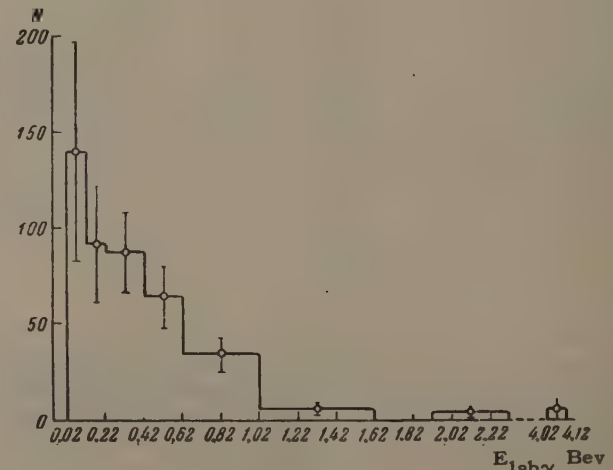

FIG. 7. L.s. energy distribution of γ quanta from all π^-n and π^-p interactions. The ordinate axis gives the number of γ quanta for intervals of $E_{lab,\gamma}$ = 0.10 Bev.

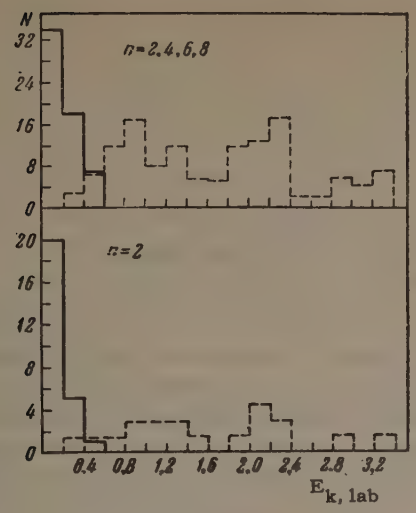

FIG. 8. L.s. energy distribution of protons in π^-p interactions; the histograms expected from statistical theory (table of random stars[18]) are shown dotted.

7. Table V lists the mean values of the transverse momenta calculated for particles produced in π^-p interactions of different multiplicity. The observed mean transverse momenta are close to the mean transverse momenta of Λ^0 and K^0 particles produced in π^-p interactions for the same primary π^--meson energy.[17] The value of the transverse momenta for π^- mesons, within the limits of error, depends weakly on the multiplicity, which, perhaps, reflects the approximate equality of the interaction range

$$\overline{(\Delta r^2)}^{1/2} \geqslant \hbar/2\,(\overline{p_\perp^2})^{1/2} = 3.2\cdot 10^{-14}\ \text{cm}.$$

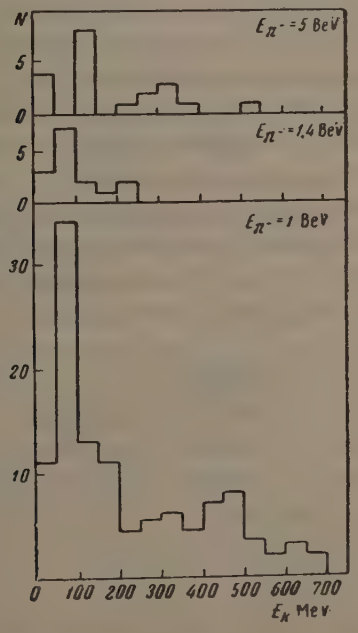

FIG. 9. L.s. proton energy distribution for π^-p interactions produced by π^- mesons of energy 1, 1.4, and 5.0 Bev. The distributions were constructed from the data of[22-24].

Table VI.

n	Number of cases	$\bar{p}_{lab}$, Bev/c	$\bar{\bar{\theta}}_{lab}$, deg
2	26	0.41±0.05	53±5
4	26	0.62±0.05	42±4
6; 8	7	0.88±0.08	19±4
2—8	59	0.56±0.04	44±3

8. Figure 8 shows the experimental l.s. energy distribution of the identified protons and the distribution of protons of any momentum expected from statistical theory for the observed interactions (obtained with the aid of tables of random stars[18]). As seen from the figure, a maximum in the proton distribution occurs for energies of 100—200 Mev, while in the case of statistical theory hardly any such protons should occur.

The presence of a maximum indicates that there is a definite group of interactions in which there is a small energy transfer to the target nucleon. One may suspect that these cases are connected mainly with peripheral interactions of the incident π^- mesons. Theoretical investigations of peripheral interactions[19-21] also predict the existence of such a maximum in the region of low proton kinetic energies. Similar results were also obtained in[22-24] for primary π^--meson energies of 1, 1.4, and 5 Bev (see Fig. 9). The fraction of cases with a very slow proton (E_k < 200 Mev) at each of these energies (1, 1.4, 5.0, 6.8 Bev) is approximately constant and equal to ~10% of the total

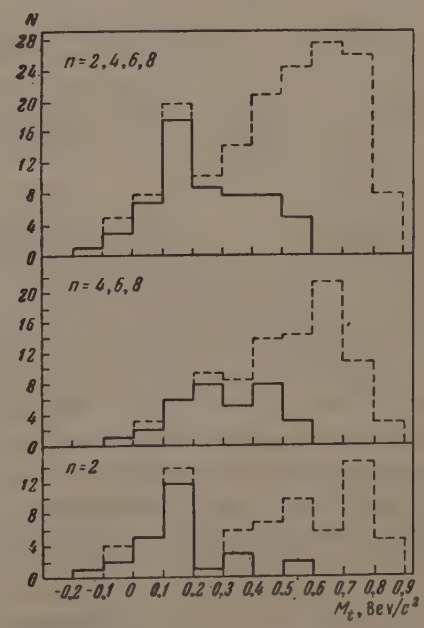

FIG. 10. Distribution of the "target mass" M_t for π^-p interactions in which an identified proton is among the secondary particles. The dotted-line histograms represent events with an unknown positive particle, which is assumed to be a proton.

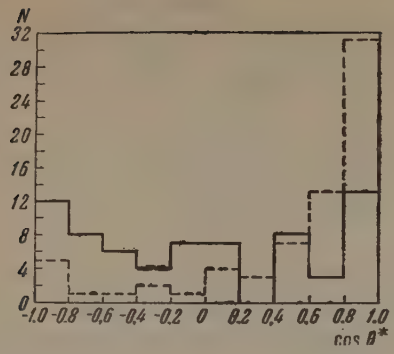

FIG. 11. Angular distribution of charged pions in the system of two pions for π^-p interactions with a "target mass" $M_t < 0.3$ Bev/c² calculated from the identified proton. The dotted-line histogram represents the distribution of these pions in the c.m.s. (pion-nucleon system).

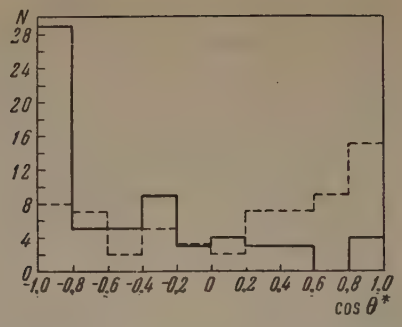

FIG. 12. Angular distribution of charged pions in the system of two-pions from π^-p interactions in which the "target mass" M_t calculated from the identified proton was greater than 0.3 Bev/c². The dotted-line histogram represents the angular distribution of these pions in the pion-nucleon c.m.s.

π-nucleon cross section. This is also in qualitative agreement with the picture of peripheral interactions.

In the present experiment a maximum occurs in the proton energy distribution from two-prong interactions and is not evident in interactions of large multiplicity. This can be connected with a decrease in the fraction of peripheral interactions as the multiplicity increases. Shown in Table VI are the values of the mean momentum and mean angle of emission of the protons in the l.s. for cases of different multiplicity. It is seen that both the energy characteristics and the mean angle of emission of the proton change with the multiplicity.

II. ANALYSIS OF EXPERIMENTAL DATA

N. G. BIRGER, Yu. V. KATYSHEV, D. K. KOPYLOVA, V. B. LYUBIMOV, A. V. NIKITIN, Yu. A. SMORODIN, and Z. TRKA

THE data obtained on π^--meson interactions with nucleons at 6.8 Bev and the data at lower energies lead to the conclusion that the statistical theory cannot explain a number of important characteristics of the angular and momentum distributions of the secondary particles. In this connection, one can conclude that an appreciable role is played by the so-called peripheral interactions.

We shall consider this question from a somewhat different viewpoint. We introduce the quantity[25]

$$M_t = M - (E_p - p_p \cos\theta_p),$$

where M is the nucleon mass, E_p and p_p are total energy and momentum of the secondary proton in the l.s., θ_p is its angle of emission. It is known that, qualitatively, M_t can be regarded as the "effective mass" of that part of the target nucleon with which the primary meson collides. Figure 10 shows the experimental distribution of M_t for π^-p interactions of different multiplicity and calculated for the group of interactions in which there is either a secondary proton or an unidentified positive particle of momentum > 1.2 Bev/c, which we shall assume to be a proton.

As seen from Fig. 10, there is a maximum at the mass M_t close to the pion mass in the case of two-prong interactions. One may therefore assume that among the two-prong events is a sizable group of so-called one-meson interactions corresponding to the collision of a primary π^- meson with a single virtual pion emitted by the target nucleon. Interactions of this type associated with small values of M_t possibly occur also in events of large multiplicity.

Figure 11 shows the angular distributions of charged pions from interactions in which the mass M_t calculated from the identified proton was less than 0.3 Bev/c². The distributions are shown in the c.m.s. of two pions ($\pi\pi$ system) and in the pion-nucleon c.m.s. The first angular distribution is symmetric with respect to the angle 90° and the second is asymmetric. This result appears to agree with the suggestion that the primary π^-

Table VII.

	Events with $M_t < 0.3$ Bev/c²	Events with $M_t \gg 0.3$ Bev/c²	Total
Number of cases	38	21	59
Number of cases with $p_{lab} \geq 0.3$ Bev/c	19	5	24
Mean momentum of π^- mesons in l.s., Bev/c	2.6±0.3	1.3±0.2	2.0±2.0

meson interacts with a virtual pion of the nucleon. In this connection, it is interesting to note that, in cases with $M_t > 0.3$ Bev/c^2, the angular distribution of the secondary pions in the $\pi\pi$ system is strongly asymmetric, with a predominance of angles greater than 90° (see Fig. 12).

There is also a clear correlation between the value of M_t and the number of high-momentum secondary pions (see Table VII). It is possible that the π^- mesons are associated with elastic scattering of a primary π^- meson on a virtual target pion.

It is interesting to note that the ratio of the number of π^- mesons to the number of positive particles changes rapidly with the momentum. Thus, for example, among positive particles with $p_{lab} \geq 2.0$ Bev/c the ratio of the number of positive particles to the number of negative particles is $n_+/n_- = 0.6 \pm 0.1$, while for $p_{lab} \geq 4.5$ Bev/c we have $n_+/n_- = 0.2 \pm 0.1$. The number of π^+ mesons apparently decreases still more rapidly. Comparison of the energy characteristics of the π^-, π^+, and π^0 mesons leads to the same qualitative result. In particular, the mean energy of the π^- mesons in π^-p interactions is $\bar{E}_{lab\,\pi^-} = 1.69 \pm 0.08$ Bev, while for π^0 mesons this value is $\bar{E}_{lab\,\pi^0} = 0.90 \pm 0.12$ Bev. For π^-p interactions in which slow protons are produced, the mean π^- momentum is $\bar{p}_{lab} = 2.04 \pm 0.19$ Bev/c, while for π^+ mesons $\bar{p}_{lab} = 1.2 \pm 0.16$ Bev/c. Thus the secondary π^- mesons stand out with respect to the π^+ and π^0 mesons. This circumstance cannot be explained from the viewpoint of statistical theory and is in good agreement with the views on the important role of peripheral interactions. In pp interactions no such difference among π^-, π^0, and π^+ mesons is observed.*

In this connection, one might suppose that the greater part of the high-momentum π^- mesons (say, for $p_{lab} > 4.0$ Bev/c) is produced as a result of $\pi\pi$ diffraction scattering. Such a conclusion appears to correspond fully with the general views on the mechanism of elementary particle interactions at high energies (see[26-28]). If this is so, then the cross sections for elastic and inelastic $\pi\pi$ interactions should not depend on the charge state of the colliding pions. It thus follows that the number of fast π^- mesons in π^-p interactions should, on the average, be the same as for π^-n interactions. The experimental data does not contradict this statement. For example, for $p_{lab} \geq 4.0$ Bev/c the corresponding ratio is

$$n_{\pi^-}(\pi^- n)/n_{\pi^-}(\pi^- p) = 0.9 \pm 0.3.$$

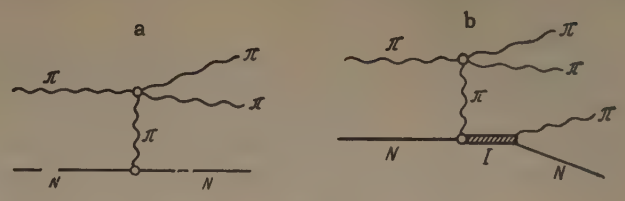

FIG. 13

The mean value of the transverse momentum $p_\perp$ in diffraction scattering directly characterizes the range of interaction. For π^- mesons with $E_{\pi^-} \geq 4$ Bev produced in two-prong events, the mean value of the transverse momentum is $\bar{p}_\perp = 0.44 \pm 0.05$ Bev/c. It should be borne in mind here that the virtual pion, before the collision with the primary pion, also has a transverse momentum which is reasonably taken equal to the transverse momentum of the recoil protons in the considered group of interactions ($\sim 0.26 \pm 0.03$ Bev/c). If we take this into account, the interaction range in $\pi\pi$ diffraction scattering* proves to be $(1-2)\hbar/m_\pi c$.

We shall now present some remarks with a view to establishing more accurately the character of the peripheral interactions. The possibility of the existence of a group of interactions described by the diagram of Fig. 13a has been indicated several times. In this case we shall speak of "nucleonic dissociation" of the target nucleon. On the other hand, Gramenitskii, Dremin, and Chernavskii[21] have indicated the important role played by processes with the so-called "isobaric dissociation" of the nucleon (see Fig. 13b). For the following analysis we shall consider only events in which a fast π^- meson is produced ($p_{lab} \geq 3.0$ Bev/c),† and assume that in these cases the upper vertex of each diagram corresponds to $\pi\pi$ diffraction scattering. Under these conditions, there are, within the framework of each of the schemes, single-valued isotopic relations connecting the cross sections of these reactions. One may expect that a

*Similar conclusions can be made on the basis of an analysis of the angular distribution of secondary protons, which are emitted primarily backward in the c.m.s. (see, for example,[29,10,14]).

*It should be noted that the entire picture of $\pi\pi$ diffraction scattering has not been fully established. In particular, one cannot exclude the possibility that part of the $\pi\pi$ scattering is accompanied by charge exchange. This can be connected with the existence of a certain amount of fast π^0 mesons as well as π^+ mesons.

†Such a choice is partly connected with the absence of interactions with 5, 6, 7, and 8 prongs in which a π^- meson with $p_{lab} \geq 3.0$ Bev/c is produced. The presence of such interactions would be in contradiction with the scheme being considered.

Table VIII.

Multiplicity n	$\overline{M}_t$, Bev/c²—calculated only from charged secondary particles		$\overline{M}_t$, Bev/c²—calculated with allowance for the contribution from π^0 mesons		$\overline{k}$	
	min	max	min	max		
2	0.18	0.41	0.30±0.06	0.44±0.06	0,32±0,06	0,47±0,06
4	0.38	0,53	0,54±0,12	0,59±0.09	0,57±0,13	0,63±0.09
6; 8	0.49	0.58	0,71±0.30	0,80±0,30	0.76±0,32	0,85±0,32
2—8	0.30	0.48	0,44±0.06	0,54±0,05	0.47±0,07	0,57±0,05

comparison of these relations with the experimental data will permit some conclusions on the relative role of peripheral interactions with nucleonic and isobaric dissociation (if, of course, we are dealing with $\pi\pi$ diffraction scattering).

It is readily shown that in the case of isobaric dissociation the number of slow protons in π^-p interactions should be 3.5 times as great as in π^-n interactions; on the other hand, in the case of nucleonic dissociation, slow protons should be encountered in π^-n interactions twice as often as in π^-p interactions. Experimentally, we observe in 51 two- and four-prong π^-p interactions containing π^- mesons of momentum ≥ 3.0 Bev/c a total of 24 slow protons (with $p \leq 1.2$ Bev/c) and only two slow protons in 17 three-prong π^-n interactions.

The number of slow π^+ mesons in π^-n interactions should be $^5/_7$ of the number of slow π^+ mesons in π^-p interactions if the dissociation is isobaric. Experimentally, this ratio is 0.9 ± 0.5 for π^+ mesons of momentum ≤ 1.2 Bev/c, while for the case of nucleonic dissociation in π^-n interactions, the slow π^+ mesons should be entirely absent. On the other hand, for two-prong interactions in which π^- mesons are produced with energy near the upper limit, there is an appreciable mixture of nucleonic dissociation. If fact, for isobaric dissociation the ratio of the number of two-prong interactions with fast π^- mesons to the number of analogous four-prong interactions should be $^4/_5$. Actually, this ratio turns out to be dependent on the π^--meson energy, as is seen from the following data:

E_{π^-}, Bev:	2,0	3,0	4,0
$N_{n=2}/N_{n=4}$:	1,4±0.3	2.6±0,8	3,2±1,3

If the dissociation were to take place only by the nucleonic scheme, then the ratio would be infinite, since the four-prong interactions cannot occur.*

Apart from the one-meson interactions considered above, an important role is apparently played by interactions with a larger number of virtual pions. As has already been noted, the momentum and angular distributions of the secondary protons change with an increase in multiplicity. Table VIII lists the estimates of the value of $\overline{M}_t$ for π^-p interactions of different multiplicity. For events in which there are no identified protons and all positive particles are assumed to be π^+ mesons, the value of M_t was calculated from the formula

$$M_t = \Sigma (E_i - p_i \cos\theta_i).$$

Here the summation is carried out over all charged pions and γ quanta from the π^0-meson decay for a given event. The minimum and maximum estimates of M_t are obtained under the assumption that the unidentified positive particles are π^+ mesons or protons, respectively.* It is known that the quantity M_t/M is equal to the fraction of energy k lost by a proton in a collision with a π^- meson if we consider the π^-p interaction in the S system, in which the initial π^- meson is at rest.[5] (The proton energy in this system is ~46 Bev.) The values obtained for the mean loss $\overline{k}$ are also shown in Table VIII. As seen from this table, the quantities $\overline{M}_t$ and $\overline{k}$ evidently depend on the multiplicity, which indicates the different nature of the interaction (decrease in the "degree of peripheralness" with an increase in the multiplicity). For the π^-p interactions considered as a whole, the quantity $\overline{M}_t(\overline{k})$ proves to be rather large. It thus apparently follows that there is a large group of interactions which are not of the one-meson type. In fact, it follows from the consideration of a very rough model that for one-meson interactions the energy losses in the S system should be close to the value $m_\pi/M \approx 0.15$,

*If "nucleonic dissociation" were to play the basic role in peripheral interactions, then the foregoing conclusion on the absence of slow protons in π^- n interactions could be understood if it were assumed that $\sigma(\pi^-\pi^0) > \sigma(\pi^-\pi^-)$ and, consequently, that charge-exchange scattering occurs in $\pi\pi$ interactions.

*The errors in Table VIII were calculated directly only for the resultant mean numbers. From the values obtained with allowance for the observed number of γ quanta, we estimated the errors of the quantities corresponding to each multiplicity.

while the experimental value is $\bar{k} = 0.47 - 0.57$.* As regards "truly central" interactions accompanied by the production of a very high energy secondary nucleon (in the l.s.) we cannot, at present, say anything definite about their relative role and properties.

One may, however, estimate the l.s. nucleon energy from the mean energy loss in the S system for all π^-p interactions, apart from those for which M_t determined from the slow proton is ≤ 0.3 Bev/c^2 (i.e., for 87% of the interactions). In this case $\bar{k} = 0.54-0.66$, and for the mean l.s. nucleon energy we obtain the estimate $\bar{E}_{labp} = 1.2-1.8$ Bev if we assume that for nucleons $p_\perp = 0.31-0.47$ Bev/c. In this connection it is interesting to note that the energy of the nucleon which, after interaction, comes to rest in the c.m.s. is $E_{lab} = 2.0$ Bev.

It is known (see, for example[31,32] that in the interaction of a fast proton with a proton the energy loss is $k_{pp} \approx 0.4$; in any case it does not exceed the value of the energy loss in collisions of a fast proton with a π^- meson ($\bar{k}_p = 0.47-0.57$). If we roughly represent each of the nucleons as consisting of a "core" and a pion cloud, then the above-mentioned circumstance can be considered to mean that the basic role in pp interactions is played by collisions of the "cloud"-"core" type, while there are practically no collisions of the "core"-"core" type, which, of course, lead to a large energy loss (see also[25]). Further investigations are necessary before a more accurate picture can be formed.

In conclusion, the authors express their gratitude to V. I. Veksler for his interest in this work and for helpful advice, to D. S. Chernavskii for discussions of the results, to M. Danysz for taking part in the development of the ionization measurement method and for helpful discussions, to the proton synchrotron crew for making the exposure, and to the laboratory staff for performing measurements and calculations.

[1] V. Petrzilka, Proc. of the 1960 Ann. Intern. Conf. on High Energy Physics at Rochester, Interscience Publ. 1960, p. 82.

[2] Wang, Solov'ev, and Shkobin, PTÉ (Instruments and Measurement Techniques) No. 1, 41 (1959); Wang, Ting, Ivanov, Kladnitskaya, Nguyen, Saitov, Solov'ev, and Shafranov, Report, High Energy Laboratory of the Joint Institute for Nuclear Research, 1959.

[3] Wang, Wang, Ting, Ivanov, Katyshev, Kladnitskaya, Kulyukina, Nguyen, Nikitin, Otwinowski, Solov'ev, Sosnovskii, and Shafranov, JETP **38**, 426 (1960), Soviet Phys. JETP **11**, 313 (1960).

[4] Blinov, Krestinkov, and Lomanov, JETP **31**, 762 (1956), Soviet Phys. JETP **4**, 661 (1957).

[5] N. G. Birger and Yu. A. Smorodin, JETP **36**, 1159 (1959), Soviet Phys. JETP 9, 823 (1959).

[6] Vovenko, Kulakov, Lubimov, Matulenko, Savin, Smirnov, and Shafranov, Proc. of the 1960 Ann. Int. Conf. on High Energy Phys. at Rochester, Interscience Publ., 1960, p. 443.

[7] R. G. Thomas, Phys. Rev. **120**, 1015 (1960).

[8] G. Maenchen et al., CERN Symposium, 1958. Cited by V. S. Barashenkov, UFN **72**, 53 (1960), Soviet Phys.-Uspekhi **3**, 689 (1960).

[9] Bandtel, Bostick, Moyer, Wallace and Wikner, Phys. Rev. 99, 673 (1955).

[10] N. F. Wikner, UCRL-3639, 1957. Cited by Barashenkov, op. cit. ref. 8.

[11] Bowen, Di Corato, Moore, and Tagliarferri, Nuovo cimento 9, 908 (1958).

[12] Wikner, Bostick, and Moyer, Bull. Am. Phys. Soc. **1**, 252 (1956).

[13] Kocharyan, Saakyan, and Kirakosyan, JETP **35**, 1335 (1958), Soviet Phys. JETP **8**, 933 (1959).

[14] Belyakov, Wang, Glagolev, Dalkhazhav, Lebedev, Mel'nikova, Nikitin, Petrzilka, Sviridov, Suk, and Tolstov, JETP **39**, 937 (1960), Soviet Phys. JETP **11**, 675 (1960).

[15] V. S. Barashenkov, UFN **72**, 53 (1960), Soviet Phys.-Uspekhi **3**, 689 (1960).

[16] V. M. Maksimenko, Dissertation, Joint Institute for Nuclear Research, 1961.

[17] Wang, Wang, Veksler, Vrana, Ting, Ivanov, Kladnitskaya, Kuznetsov, Nguyen, Nikitin, Solov'ev, and Ch'eng, JETP 40, 464 (1961), Soviet Phys. JETP **13**, 323 (1961).

[18] M. I. Dyment and G. I. Kopylov, Preprint, Joint Institute for Nuclear Research, 1960.

[19] G. F. Chew and F. E. Low, Phys. Rev. **113**, 1640 (1959).

[20] F. Selleri, Phys. Rev. Lett. **6**, 64 (1960).

[21] Gramenitskii, Dremin, and Chernavskii, JETP **41**, 856 (1961), Soviet Phys. **14**, 613 (1962).

[22] J. Derado, Nuovo cimento **15**, 853 (1960).

[23] Eisberg, Fowler, Lea, Shephard, Shutt, Thorndike, and Whittemore, Phys. Rev. **97**, 796 (1955).

*In correspondence with the presently accepted phenomenological classification, we consider as peripheral interactions those accompanied by a small energy loss and strongly anisotropic secondary particles. From this point of view, peripheral collisions can include many interactions other than those of the one-meson type. In particular, one may note in this connection that, for interactions with $M_t > 0.3$ Bev/c^2 in the c.m.s., the angular distribution of π^- mesons turns out to be anisotropic.

[24] Maenchen, Fowler, Powell, and Wright, Phys. Rev. 108, 850 (1957).
[25] N. G. Birger and I. Ya. Smorodin, JETP 37, 1355 (1959), Soviet Phys. JETP 10, 964 (1960).
[26] L. B. Okun' and I. Ya. Pomeranchuk JETP 30, 424 (1956), Soviet Phys. JETP 3, 307 (1956).
[27] S. Z. Belen'kii, JETP 33, 1248 (1957), Soviet Phys. JETP 6, 960 (1958).
[28] V. N. Strel'tsov, Preprint D-472, Joint Institute for Nuclear Research, 1959.
[29] Grote, Krecker, Kundt, Lanius, Manske, and Meier, Nuclear Phys. 24, 300 (1961).
[30] W. D. Walker, Phys. Rev. 108, 872 (1957).
[31] Viski, Gramenitskii, Korbel, Nomofilov, Podgoretskii, Rob, Strel'tsov, Tuvdéndorzh, and Khvastunov, JETP 41, 1069 (1961), Soviet Phys. JETP 14, 763 (1962).
[32] Kalbach, Lord, and Tsao, Phys. Rev. 113, 330 (1959).

Translated by E. Marquit
250

FINE STRUCTURE OF THE Pa^{231} *ALPHA RADIATION AND THE ENERGY LEVEL SCHEME OF THE* Ac^{227} *NUCLEUS*

S. A. BARANOV, V. M. KULAKOV, P. S. SAMOĬLOV, A. G. ZELENKOV, Yu. F. RODIONOV, and S. V. PIROZHKOV

Submitted to JETP editor June 21, 1961

J. Exptl. Theoret. Phys. (U.S.S.R.) 41, 1475-1483 (November, 1961)

Results of an investigation of the radioactive decay of Pa^{231} are presented. The measurements were performed with magnetic α and β spectrometers and a spectrometric arrangement for γ-radiation measurements. Twenty monoenergetic α lines were detected in the α-ray spectrum. Ten of these lines have been established for the first time. From an analysis of the electron and γ spectra it has been possible to detect some new conversion lines and identify the multipolarity of the γ transitions in the Ac^{227} nucleus. A more complete energy level scheme of the Ac^{227} nucleus is constructed on the basis of all available data.

1. INTRODUCTION

THE radioactive nucleus Pa^{231} is converted via α decay into the α-active isotope Ac^{227}. The half-life of Pa^{231} is 3.4×10^4 years. Some information on the radiation emitted in the decay of this nucleus and on the levels of the Ac^{227} nucleus were presented in several papers [1-8]. These investigations did not make it possible to resolve some contradictions in the level scheme of Ac^{227}. We have therefore undertaken a further more careful investigation of the α spectrum of Pa^{231} and of the conversion-electron and γ-radiation spectra of Ac^{227}.

2. APPARATUS AND PREPARATION OF RADIOACTIVE Pa^{231} SOURCE

To study the electron and α spectrum we used magnetic α and β spectrometers with double focusing of a beam of charged particles at an angle $\pi\sqrt{2}$.[9,10] In these experiments the relative resolution of the instruments was respectively several hundredths and several tenths of one percent at solid angles on the order of $10^{-3} \times 4\pi$. The γ radiation was investigated with ordinary γ-spectrometric apparatus.

Prior to the direct preparation of the sources for the α, β, and γ spectroscopic measurements, the protactinium was thoroughly purified to remove extraneous impurities, primarily actinium.

The source for the α-spectroscopic measurements was prepared by evaporating protactinium chloride in vacuum on a glass base. The surface density of the active layer of the source was 1 $\mu g/cm^2$. The effective areas of the sources used in the series of experiments on the fine structure of the α radiation were 0.5, 1.0, and 3.0 cm^2.

For electronic and γ-spectrometric measurements, the sources were prepared by the method described in our earlier papers (see, for example, [11]).

3. EXPERIMENTAL RESULTS

A. Investigation of the α spectrum of Pa^{231}. In the investigation of the α spectrum we confined ourselves to the energy interval 4450—5050 kev, with intensity $I \geq 2 \times 10^{-3}$ percent. As was shown earlier,[12] the energy calibration of the spectrometer remains unchanged in this energy interval. The standard line used in these experiments was the known group of Pa^{231} 4938.0-kev α particles.[4] The accuracy in the determination of the energies of the remaining α groups was ~ 2 kev. The background of scattered particles in these experiments did not exceed 4×10^{-4} percent, and was therefore outside the limits of the investigated intensities. To investigate a relatively broad portion of the spectrum (600 kev), several exposures were necessary.

Figure 1 shows the apparatus spectra of the α radiation from Pa^{231}, obtained in three different exposures. The minimum half-width attained was 3 kev (T_{exp} = 12 hours). We observed 20 α-radiation fine-structure groups, of which the groups α_X, α_Z (?), α_4, α_Y, α_8, and α_{12}—α_{16} were found for the first time.

Table I summarizes the data of three experiments. We give here the values of the energy (in kev) and the intensity (percent) of individual groups of α particles, along with the calculated values of

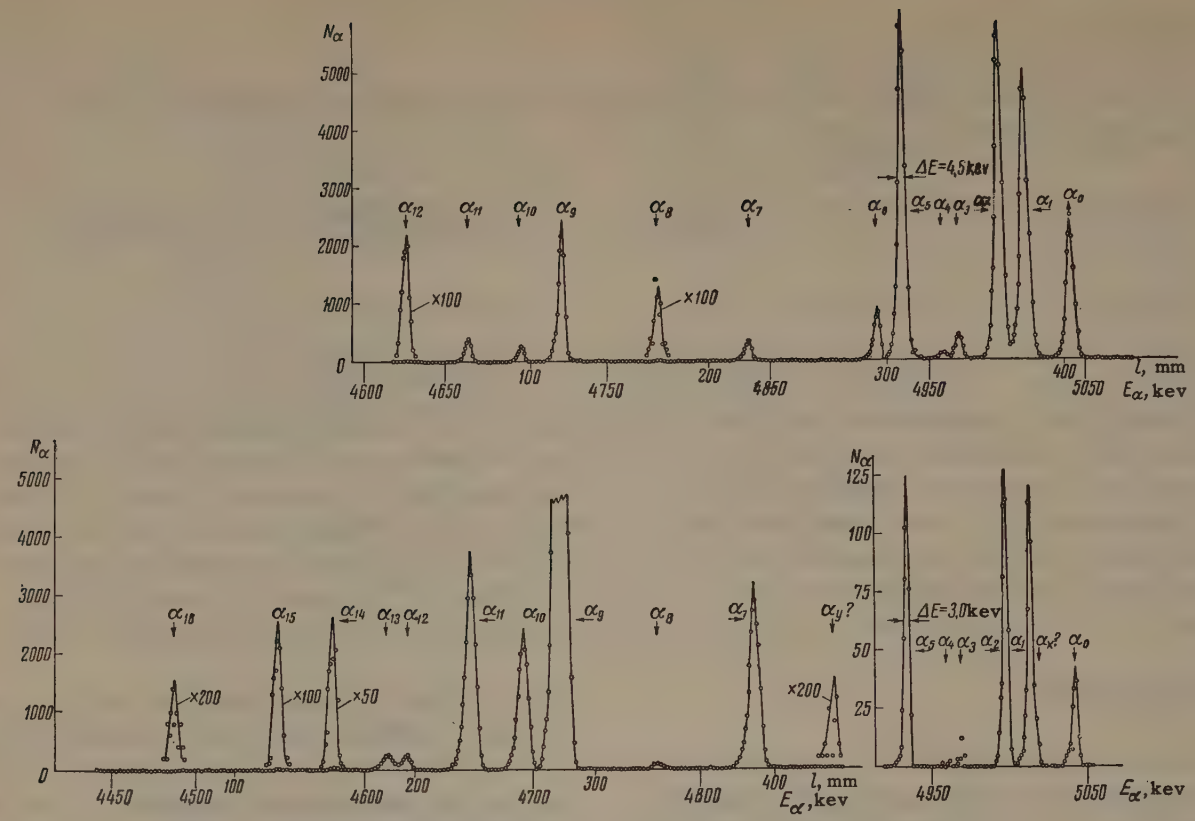

FIG. 1. Apparatus spectrum of the fine structure of the α radiation of Pa^{231}.

Table I. Fine structure of α spectrum of Pa^{231}

α group	Energy* of α particles, kev	Intensity**, percent	Hindrance coefficient, m	Level energy, kev	α group	Energy* of α particles, kev	Intensity**, percent	Hindrance coefficient, m	Level energy, kev
α_0	5045,3	11.0	205	0	α_7	4839,4	1.4	75	209.5
α_x	5018,5	∼2.5	640	27.4	α_8	4781,7	$4\cdot10^{-2}$	1050	268.2
α_1	5016,4	⩽20.0	70	29.4	α_9	4724,0	8.4	2	327.0
α_z?	5012 5010			∼34?	α_{10}	4699,7	∼1	12	351.7
					α_{11}	4667,5	1,5	5	384,5
α_2	4999,3	25.4	45	45.9	α_{12}	4630,2	$\sim10^{-1}$	∼40	422.4
α_3	4972,2	1,4	525	73.1	α_{13}	4618,7	$\sim10^{-1}$	30	434.0
α_4	4961,5	0.4	1600	84.4	α_{14}	4586,0	$1,5\cdot10^{-2}$	120	467.4
α_5	4938,0	22.8	20	107.1	α_{15}	4553,3	$8\cdot10^{-3}$	120	501.0
α_6	4920,7	3.0	120	126.8	α_{16}	4494,8	$3\cdot10^{-3}$	135	560.0
α_y	4887,0	$2\cdot10^{-3}$	$\sim10^5$	∼160					

*The standard line used was the 4938.0-kev α_5 group.

**Data from three experiments were included in the estimate of the α-group intensity.

the hindrance coefficients m and the level energies.

The experimental values of the energy and intensity which we have obtained for the ten known α groups differ somewhat from the corresponding values quoted in the literature.[4-8] This discrepancy lies apparently within the limits of experimental error.

It is highly interesting to consider separately the α-spectrum shown in the lower right of Fig. 1. It is easily seen that the form of the α_1 line, and

particularly the width of its base and the fall-off on the high-energy side differ from the forms of the groups α_2 and α_5, which have almost the same intensity. This gives grounds for assuming the α_1 line to have a complex structure. The groups α_X, α_1, and α_Z in Table I are the components of this complex α line. Naturally, the intensities of these groups cannot be determined with sufficient accuracy.

B. Investigation of the electron and γ spectra. These spectra were studied in several investigations, but not the low-energy region of the electron spectrum of Ac^{227}. Using very thin organic films for the window of the Geiger-counter (the electron indicator in the β spectrometer), we could study the electron spectrum, starting with low energies (1.5—2.0 kev).

Table II. Interpretation of electron lines produced in the decay of Pa^{231}

Number of electron line	Observed electron energy, kev	Conversion shell	Transition energy, kev	Intensity of conversion lines (relative units)
3	5.9	M	~11.0	70 L_I (25)+M(11)
11	11.5	M_I	16.5	130
14	15.1	N_I	16.3	40
		average	16.4	
2	3.8	L_{III}	19.6	~10
1	2	L_I	22.7	~25
10	2.7	L_{II}	22.7	~25
4	6.9	L_{III}	22.7	~25
		average	22.7	
3	5.6	L_I	25.4	70 L_I(25)+M(11)
19	20.2	M_I	25.2	25
20	20.8	M_{II}	25.4	2
21	21.5	M_{III}	25.4	1
		average	25.4	
6	8.1	L_{II}	27.2	
10	10.8	L_{III}	26.7	
15	21.9	M_I	26.9	
	23.0	M_{II}	26.9	
		average	27.0	
5	7.6	L_I	27.4	70
7	8.4	L_{II}	27.5	100
12	11.5	L_{III}	27.4	120
23	22.4	M_I	27.4	30
24	22.7	M_{II}	27.3	15
26	23.4	M_{III}	27.3	30
27	24.0	$M_{IV,V}$	27.3	5
30	26.2	N	27.4	16
31	27.2	O	27.4	
		average	27.4	
8	9.5	L_I	29.5	90
9	10.2	L_{II}	29.3	90
13a	13.7	L_{III}	29.5	~40
28	24.2	$M_{I,II}$	29.8	~35
29	25.2	$M_{III,IV}$	29.2	~35
32	28.5	N	29.7	
		average	29.4	
13	14.1	L_I	34.1	~100
33	29.0	M_I	34.0	
		average	34.0	

Table II (continued)

Number of electron line	Observed electron energy, kev	Conversion shell	Transition energy, kev	Intensity of conversion lines (relative units)
17	18.4	L_{I}	38,2	60
18	19.1	L_{II}	38.2	15
23	22.4	(L_{III})	38.2	~15
35	33.0	M_{I}	38.0	$\Sigma M=30$
36	33.3	M_{II}	38.1	
37	33.6	M_{III}	38.0	
38	36.8	$N_{I,II}$	~38.0	$\Sigma N=16$
39	37.1	N_{III-V}	~38.0	
40	37.5	O	~38.0	
		average	38.2	
41	37.9	L_{II}	57.0	26
43	41.2	L_{III}	57.1	23
47	52.4	$M_{II, III}$	57.0	$\Sigma M=14$
48	56.2	N, O	~57.0	
		average	57.0	
44	43.4	L_{I}	63.2	3
45	44.2	L_{II}	63.3	22
46	47.5	L_{III}	63.5	21
51	58.4	M_{II}	63.4	$\Sigma M=12$
52	59.0	M_{III}	~63.1	
		average	63.3	
55	77.0	L_{II}	~96.0	
57	80.0	L_{III}	96.0	
		average	96.0	
56	78.0	L_{II}	97.1	5,5
58	81.2	L_{III}	97.0	4
62	92.0	M	97.0	$\Sigma M=3$
63	96.0	N, O	~97	
		average	97,0	
59	83.6	L_{II}	102.7	2
60	86.6	L_{III}	102.5	1,5
64	98.1	M	102.7	
65	101.2	N, O	102.5	
		average	102.5	
19	20.0	K	126.8	
66	107.1	L	126.8	
		average	126.8	
67	153.8	K	260.5	
75	240.0	L	260.5	
		average	260.5	
68	178.3	K	285.0	1
77	265.2	L	285.1	~0,2
79	280	M	~285.0	
		average	285,0	

Table II shows the calculated energies of the conversion electrons, the intensities, and the values of the γ-transition energies. The data of Table II show that the observed conversion lines are due to at least twenty γ transitions in the Ac^{227} nucleus.

Figure 2 shows the apparatus spectra of the x-ray and γ radiation of Ac^{227}. The ordinates represent the number of pulses per channel of the pulse-height analyzer, while the abscissas represent the energies of the x rays and γ rays.

The experimental data obtained in the investigation of the e_K and γ spectra of Ac^{227} made it possible to determine the multipolarity class for twelve γ transitions in this nucleus (see Table III).

Table II (continued)

Number of electron line	Observed electron energy, kev	Conversion shell	Transition energy, kev	Intensity of conversion lines (relative units)
71	193,5	*K*	300	12,5
80	279,3	*L*	300	2,8
81	295,1	*M*	300	0,6
		average	300	
72	196,0	*K*	303	
		average	303	
74	223,2	*K*	330	5.0
83	310	*L*	330	1.3
	325	*M*	330	~0.3
		average	330	
76	248.7	*K*	354,5	0.4
		average	354.5	
78	274	*K*	380	
		average	380	

Table III

Number	E_γ, kev	Multipolarity	Reduced intensity of γ transitions, %
1	11,0		11 ($\Sigma\gamma_1$, γ_8)
2	16,5	*M*1	~20
3	19,6		~ 2
4	22,7		~ 2
5	25.4	*M*1	11 ($\Sigma\gamma_1$, γ_8)
6	27,0		< 2
7	27.4	*E*1	~50
8	29.4	*M*1+*E*2	40 $\Sigma(\gamma_8,\gamma_9)$
9	34,0	*M*1	
10	38.2	*E*1+*M*2?	~15
11	57,0	*E*2	13 $\Sigma(\gamma_{11}, \gamma_{12})$
12	63,3	*E*1	
13	96.0	*E*2?	weak
14	97.1		~1,5
15	102,5	*E*2	~0.5
16	126,8		weak
17	260.5		weak
18	285		weak
19	300	*M*2	2.2
20	303		weak
21	330	*M*2	1
22	354		weak
23	~380		weak

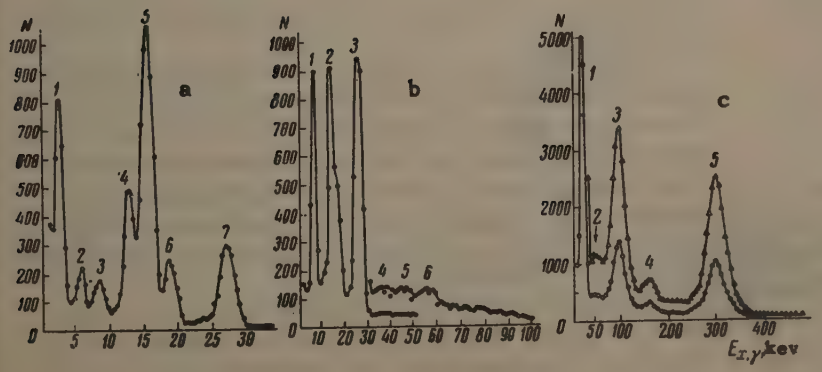

FIG. 2. X-ray and soft γ-ray spectrum of Ac^{227}, obtained with the aid of a proportional counter:
a) counter filled with mixture of Kr and CH_4,
b) counter filled with mixture of Xe and CH_4,
c) x-ray and γ-ray spectrum of Ac^{227}, obtained with scintillation spectrometer.

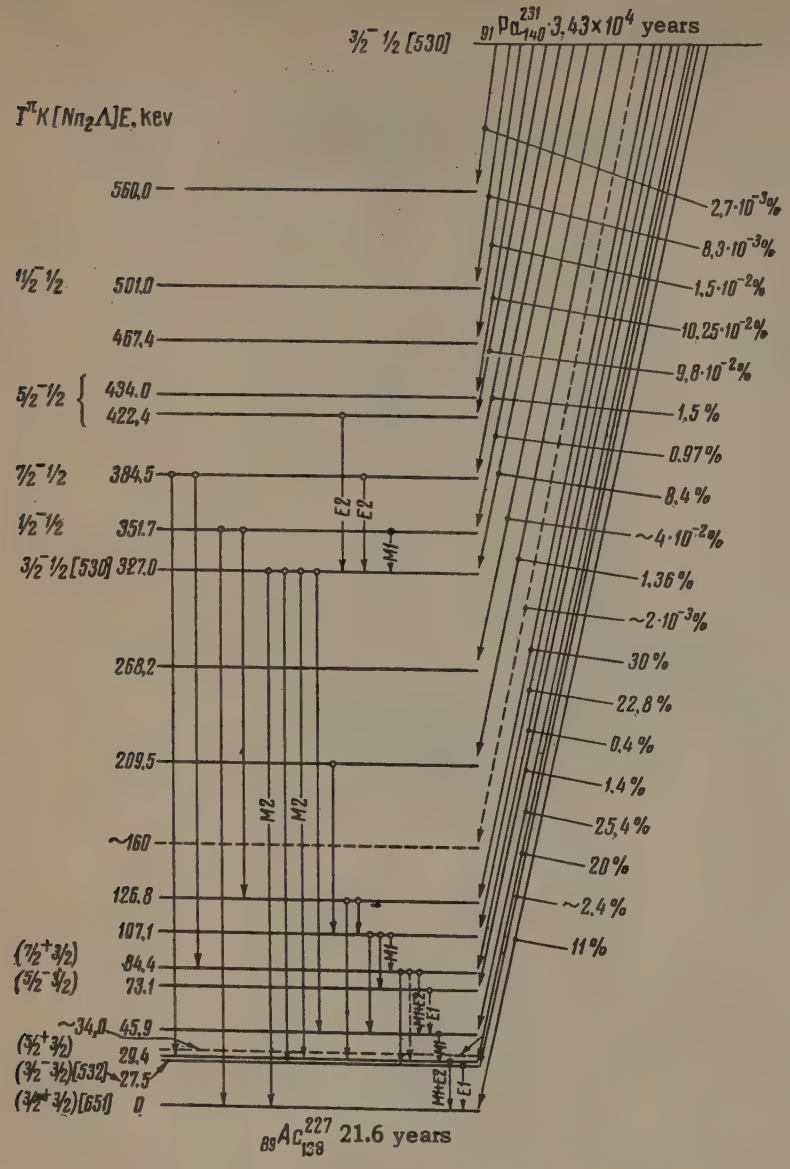

FIG. 3. Level scheme of Ac^{227}.

With the aid of a calibrated proportional counter it was also established that the γ-ray yield of 27.4-kev γ rays is $(10 \pm 2)\%$ of the total α decay. This is in good agreement with the value given in [6].

Taking account of this result and of the data Tables II and III, we calculated the intensities of the strongest γ transitions between the levels, referred to the total number of α decays. The results of the calculations are listed in the last column of Table III.

4. LEVEL SCHEME OF Ac^{227}

An analysis of all the experimental data obtained indicates that the level scheme of Ac^{227} contains at least 4—5 rotational bands. (see Fig. 3). The most clearly distinguishable is the rotational band located in the upper part of the scheme, in the energy interval 327—501 kev. Actually, as can be seen from Table I, the smallest hindrance coefficient is possessed by the group α_9. This favored transition is to a single-particle level with energy ~327 kev, which should have the same characteristics as the ground state of the decaying nucleus $3/2-1/2$ [530]* (see [13,3]). In view of their hindrance coefficients, the α_{10}, α_{11}, and α_{15} transitions can go to the next levels of this rotational band (U_{lev} = 352, 385, 434 kev).** The experimentally obtained ratio of the reduced intensi-

*The quantum numbers $I\pi K[Nn_z\Lambda]$, which characterize the state of the deformed nucleus, are defined as follows: I – spin, π – parity, K – projection of spin on the symmetry axis of the nucleus, $Nn_z\Lambda$ – asymptotic quantum numbers introduced by Nilsson, N – principal quantum number of the oscillator, n_z – quantum number of the oscillations along the symmetry axis, Λ – projection of orbital angular momentum on the symmetry axis of the nucleus.

**It must be noted that, like the rotational band of Pa^{231}, which belongs to the ground state, the spin sequence should apparently be reversed here, too ("inverted doublets"), i.e., $3/2^-$, $1/2^-$, $7/2^-$, $5/2^-$ etc.

ties of these α transitions to the levels 327, 352, 385 and 434 kev is 100: 17.1, 44.8: 6.8, which is in good agreement with the theoretical estimate for the intensity of the transitions to the levels with characteristics $I = 3/2, 1/2, 7/2$, and $5/2$, namely 100, 17.2, 44.4, and 7.4. Nor is assignment of the 501-kev level to this rotational band excluded ($I = 11/2$).

The most reliably established levels in this band are 327, 352, and 385 kev. Taking into consideration the spins and spacings of these levels, we obtained $\hbar^2/2J = 7.5$ kev and $a = -2.1$. Thus, the moment of inertia in this case differs insignificantly from the moments of inertia of the neighboring even-even nuclei.

An analysis of the lower part of the level scheme, located in the narrow energy interval 0—100 kev, shows that it is very difficult to identify these levels from the point of view of the existing theories. In this narrow interval are concentrated almost half the observed levels, and it is therefore natural to assume that several rotational bands are present here. Although some of these levels belong to different rotational bands, they probably have identical spins and parities. This results in an "interaction between levels",[14] which leads to violation of O. Bohr's known interval rule for rotational bands and can distort the expected distribution of the intensities of the α transitions[15] to levels of the same band. Consequently, a reliable interpretation of these levels cannot be made without taking these singularities into account. However, allowing a certain leeway, we can draw the following rough conclusions from the experimental facts. The ground state of Ac^{227} is $3/2^+$ [651]. The rotational band of this state apparently contains the levels 0 kev ($3/2^+$), 34 kev ($5/2^+$), and 84 kev ($7/2^+$).

The level with energy ~34 kev must be introduced to conserve the balance of the intensities in the proposed scheme, and is also due to the probable existence of the α_Z group in the α-particle spectrum of Pa^{231}.

The 27.4-kev level, the existence of which is not subject to doubt according to our data (see Tables I and III), has also been proposed by others (see[16]). Apparently an orbit $3/2^-$ [532] must be ascribed to it. It is possible that the next term in this new rotational band is the 73-kev level.

Nor is it excluded, finally, that the levels with energy 29 and 46 kev are terms of a different rotational band, the start of which is the hole level (from the point of view of the Nilsson diagram) with characteristics $1/2^+$ [660] and an energy 29.4 kev.

We shall not stop to explain the other levels of the scheme, since their interpretation cannot be made unambiguous as yet.

In conclusion we thank S. N. Belen'kii, A. A. Arutyunov, K. I. Merkulova, Yu. N. Dmitriev, and G. V. Shishkin for help with the measurements.

[1] L. Z. Neitner. Physica, **50**, 15 (1928).

[2] J. P. Butler and J. S. Adam. Phys. Rev. **91**, 1219 (1953).

[3] Stephens, Asaro and Perlman. Phys. Rev. **113**, 212 (1959).

[4] Rosenblum, Cotton, and Bouissieres. Compt. rend. **229**, 825 (1949).

[5] Gol'din, Tret'yakov, and Novikova, Materials of the U.S.S.R. Academy of Sciences Session on Peaceful Uses of Atomic Energy, Moscow, July 1955. AN SSSR.

[6] P. Falk-Vairant and M. Riou. J. Phys. Radium, 14, 65 (1953).

[7] A. Manhasser and R. Riou. Compt. rend. 237, 2520 (1954).

[8] Teillac, Riou, and Desneiges. ibid. 237, 41 (1953).

[9] Baranov, Zelenkov, Shchepkin, Beruchko, and Malov, Izv. AN SSSR, ser. fiz. **23**, 1402 (1959), Columbia Tech. Transl. p. 1389.

[10] P. S. Samoĭlov, PTÉ No 6, 33 (1959).

[11] G. I. Khlebnikov and E. P. Dergunov, Atomn. energ. **4**, 376 (1958).

[12] Baranov, Zelenkov, and Kulakov, Izv. AN SSSR, ser. fiz. **24**, 1035 (1960), Columbia Techn. Transl. p. 1045.

[13] B. Mottelson and S. Nielsson. Mat.-Fys. Medd. Adn. Vid. Selsk. **1**, No. 8 (1959).

[14] A. Kerman. Mat-Fys. Medd. Dan. Vid. Selsk. **30**, No. 15 (1955).

[15] O. Prior. Arkiv Fys. **16**, 15 (1959).

[16] Strominger, Hollander, and Seaborg. Revs. Modern Phys. **30**, 585 (1958).

Translated by J. G. Adashko
251

DECAY SCHEME FOR Br^{75}

K. A. BASKOVA, S. S. VASIL'EV, NO SENG CH'ANG, and L. Ya. SHAVTVALOV

Institute of Nuclear Physics, Moscow State University

Submitted to JETP editor June 26, 1961

J. Exptl. Theoret. Phys. (U.S.S.R.) 41, 1484-1486 (November, 1961)

The β^+ and γ spectra of Br^{75} with half-life of 100 ± 5 min are investigated. The β^+ spectrum consists of three components with end-point energies 1720, 1100, and 650 kev. Gamma transitions with energies 285 and 620 kev are observed. A study of $\beta^+\gamma$ coincidences indicates the existence of a temporal correlation between the β^+ transition (1720 kev) and γ transition (285 kev). A probable decay scheme is suggested for Br^{75}.

THE single-particle model of the nucleus describes well such quantum characteristics as the total angular momentum and the parity of the ground state of odd nuclei [1]. For certain nuclei, however, the values of the angular momentum do not agree with experiment. One such nucleus is $_{34}Se^{75}_{41}$, with a ground-state total momentum of $^5/_2$. [2] In addition, Se^{75} has an anomalously large quadrupole moment. Nemirovskii [3] noted in his book that the deformation of the nuclear surface plays an appreciable role here.

The present investigation was devoted to a study of β^+ and γ radiation from Br^{75}, which decays to Se^{75}. In an investigation of the activities induced in enriched Se^{75} bombarded by protons and deuterons in a cyclotron, Woodward, McCown, and Pool first succeeded in observing the radioactive isotope Br^{75} with a half life of 102 minutes. A magnetic-spectrometer investigation [5] of the β^+ radiation from Br^{75} disclosed the existence of four partial β^+ transitions with end-point energies 1700 ± 20, 800, 600, and 300 kev. The γ spectrum of Br^{75} was investigated by Beydon et al. [6] with the aid of a luminescent γ spectrometer, in which an investigation of the products of the reaction Cu + C^{12} disclosed a 285-kev γ transition. The intensity of this γ transition decreased with a half life of 95 ± 5 minutes.

In the present investigation, the Br^{75} was obtained by bombarding Se^{74} (enriched to 40.9%) with deuterons in the 120-cm cyclotron of the Nuclear Physics Research Institute of the Moscow State University. The targets were exposed for about 3 hours. The β^+ spectrum of Br^{75} was investigated in a thin-lens magnetic β spectrometer. An analysis of the Fermi plot of the resultant β^+ spectrum yielded two partial β^+ transitions with end-point energies 1720 ± 50, 1100, and 650 kev

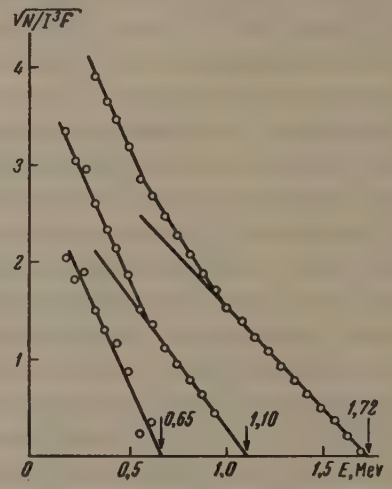

FIG. 1. Fermi plot of β^+ spectrum of Br^{75}.

(Fig. 1) and with respective intensities 80, 15 and 5%.

The γ spectrum was investigated with a luminescent γ spectrometer with a 100-channel analyzer. The resolution of the γ spectrometer was 8.7% for the Cs^{137} 662-kev γ transition. The initial measurement of the γ spectrum of Br^{75} disclosed the presence of a single γ transition with energy 285 kev. The β^+ spectrum, however, indicates that a 1720 − 1100 = 620 kev γ transition is possible on the skirt of the powerful annihilation peak. To observe the γ transition it was necessary to reduce the intensity of the annihilation peak. For this purpose we used a conical lead collimator [7] and a thin source, so as to be able to neglect the annihilation in the source itself.

The γ spectrum thus obtained is shown in Fig. 2. We see in this spectrum a strong 285-kev γ and a weak 620-kev γ transition. The low-intensity γ radiation with energy $E_\gamma > 700$ kev is due to long-lived activity of Br^{82} (T = 36 hours). The

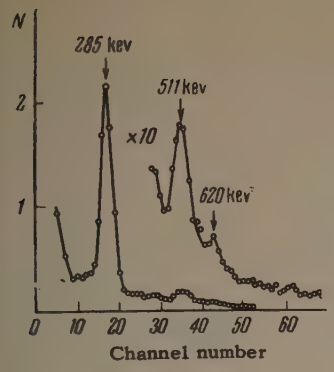

FIG. 2. γ spectrum of Br^{75}, measured with conical lead collimator.

half-life of the Br^{75} is determined from the change in the intensity of the 285-kev γ line and the annihilation peak, and was found to be 100 ± 5 minutes. The 620-kev γ-line had the same half life.

The $\beta^+\gamma$ coincidences were investigated with a magnetic-lens β spectrometer and with a luminescent spectrometer, connected for coincidence. The resolution time was determined periodically during the measurement of the true coincidences, and was found to be 0.25 μsec. Figure 3 shows the Fermi plot of the β^+ spectrum, which is in correlation with the 285-kev γ quanta. It is seen from Fig. 3 that the points lie sufficiently close to a straight line. The end-point energy was found in this case to be 1700 ± 100 kev. The 285-kev transition thus follows the 1720-kev β^+ transition. This result contradicts the Br^{75} decay scheme given by Dzhelepov and Peker,[8] who assumed the 1720-kev β^+ transition to go to the ground state of Se^{75}.

We have therefore drawn a probable decay scheme for Br^{75} (Fig. 4), in which the 1335-kev level expected from the 650 kev β^+ transition is shown dotted. From measurements of the 285-kev γ-transition intensity and of the annihilation peak we estimated the relative K-capture probability, compared with β^+ decay. This was found to be approximately 10%, which does not contradict the paper by Kuznetsova and Mekhedov[9] where a value ~15% is cited. The total Br^{75}—Se^{75} decay energy resulting from the proposed Br^{75} decay scheme is 3025 kev, which is closer to the 3236 kev calculated by the Cameron formula.[10] The cause of the excited states of the nucleus is difficult to establish without data on the total angular

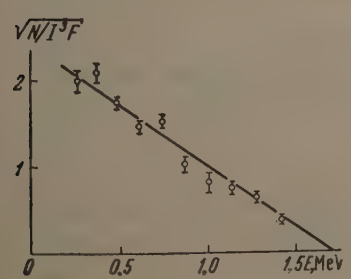

FIG. 3. Fermi plot of β^+ spectrum of Br^{75}, which correlates with the 285-kev quanta.

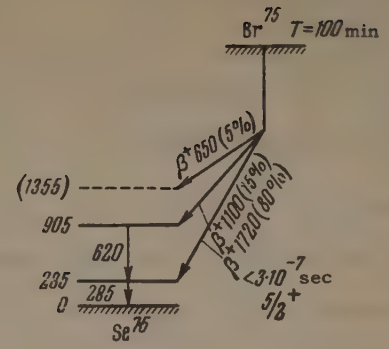

FIG. 4. Probable decay scheme of Br^{75}.

momenta. However, the observed excited levels are apparently not rotational.

The authors are grateful to Yu. A. Vorob'ev and V. S. Zazulin for help with the work.

[1] M. Goeppert Mayer and J. H. D. Jensen, Elementary Theory of Nuclear Shell Structure, Wiley, N. Y., 1955.

[2] L. C. Aamodt and P. C. Fletcher Phys. Rev. 98, 1224 (1955).

[3] P. É. Nemirovskii, Sovremennye modeli atomnogo yadra (Modern Models of the Atomic Nucleus), Atomizdat, 1960.

[4] Woodward, McCown, and Pool. Phys. Rev. **74**, 870 (1948).

[5] S. C. Fultz and M. L. Pool. Phys. Rev. **86**, 347 (1952).

[6] Beydon, Chaminade, Dru, Farragi, Olkowsky, and Papineau. Nucl. Phys. **2**, 593 (1957).

[7] Konijn, van Nooijen, Mostert, and Endt. Physica **22**, 887 (1956).

[8] B. S. Dzhelepov and A. K. Peker, Skhemy raspada radioaktivnykh yader (Decay Schemes of Radioactive Nuclei), An SSSR, 1958.

[9] M. Kuznetsova and V. Mekhedov. Izv. AN SSSR, ser. fiz. **21**, 1020 (1957), Columbia Tech. Transl. p. 1021.

[10] B. S. Dzhelepov and G. F. Dranitsina, Sistematika energii β-raspada (Systematics of β-Decay Energies), AN SSSR, 1960.

Translated by J. G. Adashko
252

EFFECT OF POLARIZATION OF THE MEDIUM ON THE DEVELOPMENT OF ELECTRON-PHOTON SHOWERS

G. A. TIMOFEEV

Institute of Nuclear Physics, Moscow State University

Submitted to JETP editor March 9, 1961

J. Exptl. Theoret. Phys. (U.S.S.R.) **41**, 1487-1492 (November, 1961)

A one-dimensional cascade theory of electron-photon showers is developed in the A-approximation with account of polarization for a dense medium. The integral energy spectra of shower particles at depths $t = 1$ and $t = 2$ in lead and air are computed. The results of the calculations are compared with the data of the usual cascade theory.

HIGH-ENERGY electron-photon showers in a dense medium exhibit many properties that are due to the character of the electromagnetic interaction in the medium. If the particle energy exceeds 10^{12} ev, then the cross sections for bremsstrahlung and pair production in the dense medium are greatly influenced by multiple scattering of the shower particles by the atoms of the medium. The theory of this phenomenon was developed by Landau and Pomeranchuk [1] and also by Migdal. [2] The differential cross sections for bremsstrahlung and pair production were calculated by Migdal [3] with account of multiple scattering. These proved to be not homogeneous functions of the energy, as were the Bethe-Heitler cross sections [4] that describe the interaction between the particles and the individual atoms. The cascade-theory formalism is therefore not suitable for the analysis of high-energy showers in a condensed medium. High-energy showers in the first few t-units of matter were investigated by the Monte Carlo method. [5-8]

The polarization of the medium plays an important role in the interaction between charged particles and matter. The differential cross section of the bremsstrahlung of an electron in the medium, with account of polarization, was found by Ter-Mikaélyan [9] to be

$$W_e(E, E') = E^{-2}E'^{-1}\left(\tfrac{4}{3}E^2 - \tfrac{4}{3}EE' + E'^2\right)\left[1 + \omega^2(E/E')^2\right]^{-1}. \quad (1)$$

Here $\omega = \sqrt{4\pi NZe^2\hbar^2/m^3c^4}$, N—number of atoms per cm^3 of the medium, Z—charge of the nuclei of the medium, m and e—mass and charge of the electron, $\hbar$—Planck's constant, c—velocity of light.

Ter-Mikaélyan's cross section (1) differs from the Bethe-Heitler cross section by a factor $[1 + \omega^2(E/E')^2]^{-1}$. If the ratio E'/E of the emitted photon energy to the electron energy is of the same order as or less than ω, this factor is appreciably smaller than unity. This means that the probability of an electron emitting a low-energy photon in the medium is much less than in the interaction with the individual atom. We note that the cross section for electron bremsstrahlung in the medium tends to zero if the energy of the emitted photon tends to zero.

Our problem is to obtain the integral spectra of the electrons and photons in showers that develop in lead and air. The value of ω is 1.9×10^{-4} for lead and 7.5×10^{-5} for air. When $E'/E < 10^{-4}$, the integral number of shower particles in these media should be less than usual. [10] The development of a shower in a dense medium is described in the A approximation by the usual cascade equations. The bremsstrahlung cross section is given by expression (1), and the pair-production cross section is taken from the book by Belen'kii. [10] Since the cross sections of all the processes are functions of the ratio E'/E, we can use the method of functional transformations [10] to solve the problem.

Going from the transforms $P(t, s)$ and $\Gamma(t, s)$ to the originals $P(t, E)$ and $\Gamma(t, E)$ [5] and integrating with respect to the energy we obtain the expressions for the integral spectrum of the electrons and photons

$$N_P(t, E) = \frac{1}{2\pi i}\int_{\delta-i\infty}^{\delta+i\infty}\left[\left(\frac{E_0}{E}\right)^s - 1\right]\left\{\frac{\sigma_0 + \lambda_1(s)}{\lambda_1(s) - \lambda_2(s)}e^{\lambda_1(s)t} - \frac{\sigma_0 + \lambda_2(s)}{\lambda_1(s) - \lambda_2(s)}e^{\lambda_2(s)t}\right\}ds,$$

$$N_\Gamma(t, E) = \frac{1}{2\pi i}\int_{\delta-i\infty}^{\delta+i\infty}\left[\left(\frac{E_0}{E}\right)^s - 1\right]C(s)\left\{\frac{\sigma_0 + \lambda_1(s)}{\lambda_1(s) - \lambda_2(s)}e^{\lambda_1(s)t} - \frac{\sigma_0 + \lambda_2(s)}{\lambda_1(s) - \lambda_2(s)}e^{\lambda_2(s)t}\right\}ds. \quad (2)$$

s	A(s)	B(s)	Air					Lead				
			C(s)	$\lambda_1(s)$	$\lambda_1'(s)$	$-\lambda_2(s)$	$H_1(s)\cdot 10$	C(s)	$\lambda_1(s)$	$-\lambda_1'(s)$	$-\lambda_2(s)$	$H_1(s)\cdot 10$
−1.0	−∞	∞	$2.06\cdot 10^6$	∞	∞	∞	5.00	$1.75\cdot 10^5$	∞	∞	∞	5.00
−0.9	−9.73	18.8	$5.24\cdot 10^5$	3150	32800	3140	5.01	7170	372	3600	360	5.07
−0.8	−4.63	8.97	$1.37\cdot 10^5$	1110	10500	1100	5.01	3010	166	1160	163	5.08
−0.7	−2.86	5.76	$3.68\cdot 10^4$	461	3840	459	5.02	579	87.6	522	85.6	5.11
−0.6	−1.94	4.19	$1.02\cdot 10^4$	207	1690	206	5.03	266	49.9	267	48.7	5.14
−0.5	−1.36	3.27	$2.93\cdot 10^3$	98.3	711	97.7	5.05	127	28.8	147	29.2	5.18
−0.4	−0.950	2.68	884	48.8	331	48.6	5.09	63.5	18.5	84.8	18.4	5.23
−0.3	−0.637	2.26	284	25.3	160	26.4	5.14	33.5	11.9	63.1	12.1	5.29
−0.2	−0.389	1.96	99.3	13.8	80.1	14.2	5.21	18.7	7.93	31.3	8.31	5.36
−0.1	−0.185	1.73	38.9	7.92	41.4	8.51	5.29	11.2	5.42	23.4	6.01	5.42
0	0	1.55	17.6	4.84	22.2	5.61	5.37	11.2	3.79	12.9	4.57	5.46
0.1	0.162	1.40	9.23	3.15	12.6	4.07	5.43	7.17	2.72	8.77	3.65	5.49
0.2	0.286	1.28	5.58	2.15	7.69	3.21	5.45	4.90	1.99	6.12	3.05	5.48
0.3	0.407	1.18	3.78	1.53	5.17	2.71	5.43	3.55	1.46	4.42	2.64	5.45
0.4	0.515	1.10	2.78	1.11	3.55	2.39	5.37	2.70	1.08	3.31	2.37	5.37
0.5	0.615	1.02	2.17	0.803	2.65	2.19	5.27	2.14	0.79	2.55	2.18	5.27

The poles of the Mellin transforms $P(t, s)$ and $\Gamma(t, s)$ coincide with the poles of the functions $A(s)$, $B(s)$, $C(s)$, and σ_0. Thus, the region of existence $P(t, s)$ and $\Gamma(t, s)$ can be determined if we know which of the functions $A(s)$, $B(s)$, $C(s)$ and σ_0 has the pole with the largest real part.

In the case of the Bethe-Heitler cross section, the pole with the largest real part $s = 0$ belongs to $C(s)$. This means that $P(t, s)$ and $\Gamma(t, s)$ exist when $s > 0$ and when $\delta > 0$ in (2). The numerical values of $A(s)$, $B(s)$, $C(s)$, and σ_0 are given by Belen'kii.[10] The use of bremsstrahlung cross sections in the form (1) results in different expressions for $A(s)$ and $C(s)$, while $B(s)$ and σ_0 remain unchanged:

$$A(s) = \int_0^1 \left[\tfrac{4}{3}(1-x) + x^2\right]\left[1-(1-x)^s\right]\frac{x}{x^2+\omega^2}\,dx,$$

$$C(s) = \int_0^1 \left[\tfrac{4}{3}(1-x) + x^2\right]\frac{x^{s+1}}{x^2+\omega^2}\,dx. \qquad (3)$$

Using the smallness of ω, we can show that $A(s)$ coincides within 1% with the value obtained from the Bethe-Heitler cross sections. The integral (3) can be reduced to a sum of integrals of the type

$$\int_0^{\omega^{-2}} u^{\nu}\frac{1}{1+u}\,du, \qquad 0 < \operatorname{Re}\nu < 1.$$

In the evaluation of this integral it is convenient to divide the integration region into two parts, $0 < u < 1$ and $1 < u < \omega^{-2}$. Since ω^{-2} is of the order of 10^8, the upper limit of integration in the second region can be set equal to infinity. Then the integrals in both regions are expressed in terms of the Euler β function. The approximate expressions obtained in this fashion

$$C(s) = \begin{cases} \frac{4}{3}\omega^s\frac{\pi(s+2)}{2}\sin^{-1}\frac{\pi(s+2)}{2}\frac{1}{s+2} + \frac{1}{s+2} \\ \quad\times\left[1-\omega^{s+2}\frac{\pi(s+2)}{2}\sin^{-1}\frac{\pi(s+2)}{2}\right] \\ -\frac{4}{3(s+1)}\left[1-\omega^{s+1}\frac{\pi(s+1)}{2}\sin^{-1}\frac{\pi(s+1)}{2}\right]+\frac{4}{3s}, \\ \quad -1 \geqslant \operatorname{Res} > -2 \\ \frac{1}{s+2}-\frac{4}{3(s+1)}\left[1-\omega^{s+1}\frac{\pi(s+1)}{2}\sin^{-1}\frac{\pi(s+1)}{2}\right] \\ +\frac{4}{3s}\left[1-\omega^s\frac{\pi s}{2}\sin^{-1}\frac{\pi s}{2}\right], \qquad 0 \geqslant \operatorname{Res} \geqslant -1 \\ \frac{1}{s+2}-\frac{4}{3(s+1)}+\frac{4}{3s}\left[1-\omega^s\frac{\pi s}{2}\sin^{-1}\frac{\pi s}{2}\right], \\ \qquad 1 \geqslant \operatorname{Res} \geqslant 0 \\ \frac{1}{s+2}-\frac{4}{3(s+1)}+\frac{4}{3s}, \qquad \operatorname{Res} \geqslant 0 \end{cases}$$

differ from the exact ones by terms of order ω^2. The pole having the largest real part $s = -1$ belongs to the functions $A(s)$ and $B(s)$, and the Mellin transforms exist when $s > -1$. The table lists the values of the functions, necessary for numerical calculations, for real $-1 < s \leq 0.5$ in the case of lead and air.

We note that when $0 < \operatorname{Re} s < 0.5$, $C(s)$ (and hence $\lambda_1(s)$) is smaller than the corresponding functions obtained by Belen'kii[10] with Bethe-Heitler cross sections. When $s \geq 0.5$ the functions $C(s)$ and $\lambda_1(s)$, which pertain to cross sections, are practically identical.

When $t > 1$ we can neglect the second term in the intergrand of (2). We then have approximately

$$N_P(t, E) = \frac{1}{2\pi i}\int_{\delta-i\infty}^{\delta+i\infty}\left[\left(\frac{E_0}{E}\right)^s - 1\right]H_1(s)\,e^{\lambda_1(s)\,t}\,ds,$$

$$N_\Gamma(t, E) = \frac{1}{2\pi i}\int_{\delta-i\infty}^{\delta+i\infty}\left[\left(\frac{E_0}{E}\right)^s - 1\right]C(s)\,H_1(s)\,e^{\lambda_1(s)\,t}\,ds. \qquad (4)$$

We have evaluated the integrals in (4) by the saddle-point method, using for the exponent the function

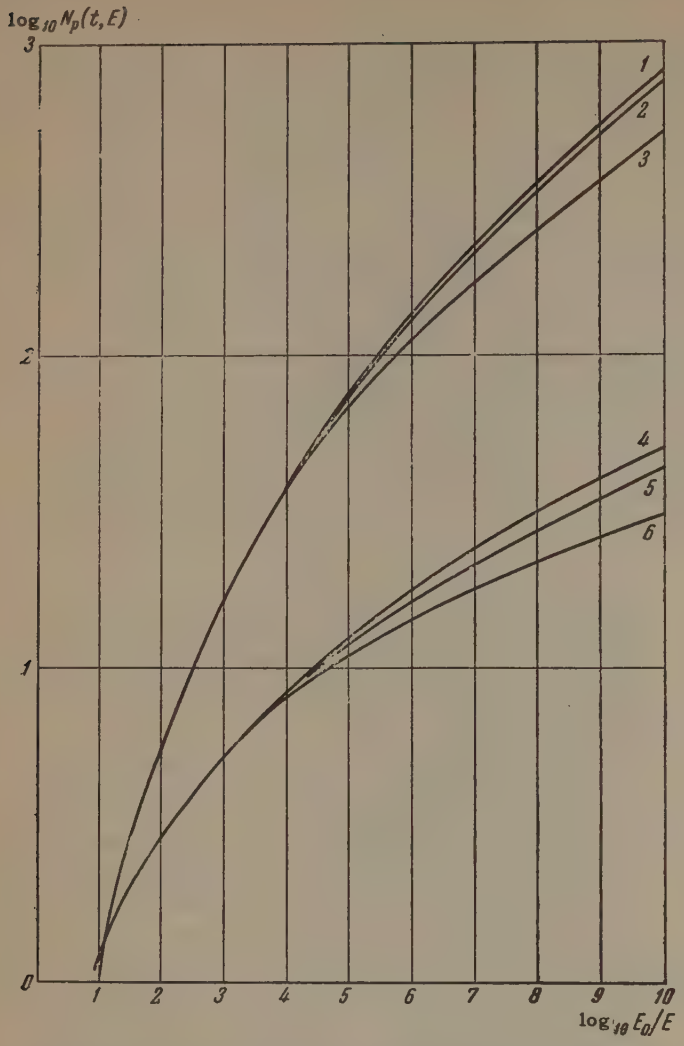

FIG. 1. Integral spectrum of electrons: 1 – t = 2, Bethe-Heitler cross section; 2 – t = 2, Ter-Mikaélyan cross sections (in air); 3 – t = 2, Ter-Mikaélyan cross sections (in lead); 4 – t = 1, Bethe-Heitler cross sections; 5 – t = 1, Ter-Mikaélyan cross sections (in air); 6 – t = 1, Ter-Mikaélyan cross sections (in lead).

$$\varphi(s) = \lambda_1(s)\, t + \ln \frac{(E_0/E)^s - 1}{s}.$$

The calculated formulas are

$$\begin{aligned} N_P(t, E) &= H_1(s)\, e^{\lambda_1(s)\, t}\, (u-1)/s \sqrt{2\pi d^2\varphi/ds^2}, \\ N_\Gamma(t, E) &= C(s)\, H_1(s)\, e^{\lambda_1(s)\, t}\, (u-1)/s \sqrt{2\pi d^2\varphi/ds^2}, \end{aligned} \qquad (5)$$

where

$$H_1(s) = \frac{\sigma_0 + \lambda_1(s)}{\lambda_1(s) - \lambda_2(s)}, \quad \frac{d^2\varphi}{ds^2} = \frac{1}{s^2}\left\{1 - \frac{u \ln^2 u}{(u-1)^2}\right\} + t\,\frac{d^2\lambda_1(s)}{ds^2},$$

and $u = (E_0/E)^s$ is determined from the equation

$$\frac{u \ln u}{u-1} = 1 - ts\frac{d\lambda_1(s)}{ds}.$$

We have calculated the integral spectrum of the electrons and photons due to a primary electron in lead or air at depths t = 1 and t = 2. The results are illustrated in Figs. 1 and 2, which also show (curves 1 and 4) the results obtained by Messel et al [11] using Bethe-Heitler cross sections.

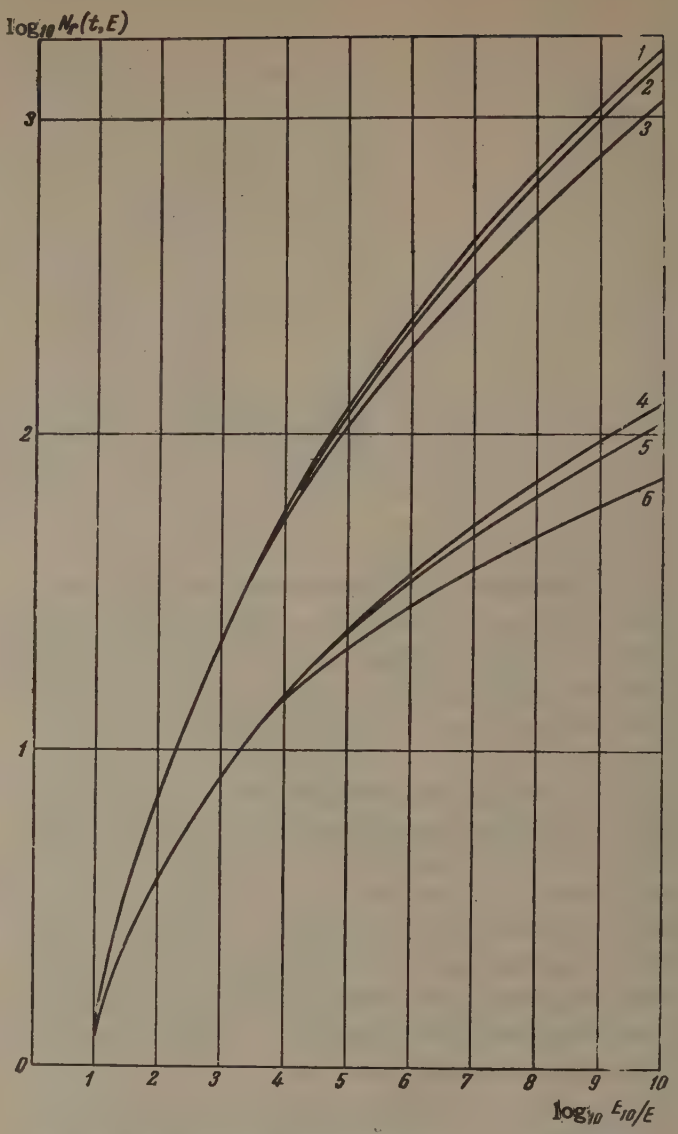

FIG. 2. Integral spectrum of photons: 1 – t = 2, Bethe-Heitler cross section; 2 – t = 2, Ter-Mikaélyan cross sections (in air); 3 – t = 2, Ter-Mikaélyan cross sections (in lead); 4 – t = 1, Bethe-Heitler cross section; 5 – t = 1, Ter-Mikaélyan cross sections (in air); 6 – t = 1, Ter-Mikaélyan cross sections (in lead).

The integral spectra of the sharp particles become different when $E_0/E > 10^{-4}$, the difference increasing with the ratio E_0/E. This difference, however, is quite small. Even when $E_0/E = 10$ the shortage of shower particles in lead, for the spectra calculated by us, amounts to 10% of Messel's spectrum. By virtue of the multiple scattering of the particles we should confine ourselves to an examination of showers generated by a primary of energy $E_0 < 10^{12}$. It is therefore advantageous to consider only the results pertaining to $E_0/E \leq 10^6$. In the case of lead, the difference in the spectra is only 5% of the Messel spectrum when $E_0/E = 10^6$. We can therefore state that the polarization of the medium hardly influences the integral spectrum

of the shower particles. Polarization in a less dense medium, such as in air, is even less effective. As the depth of shower observation increases, the integral spectrum in the dense medium becomes equal to the ordinary spectrum. We have disregarded the fact that the electrons lose energy to ionization. This process will decrease the polarization effect for the observed showers. Our results pertain to integral spectra. The influence of polarization on the differential spectra is apparently more appreciable.

The author is grateful to I. P. Ivanenko for guidance and constant help with the work, and to I. I. Knyazev for help with the numerical calculations.

Note added in proof (October 30, 1961). Supplementing the table, we give the following values of $\lambda_1''(s)$ for several values of s:

s	−0.9	−0.7	−0.5	−0.3	−0.2	−0.1	0	0.1	0.2	0.3
λ_1'' (air)	$5.47 \cdot 10^5$	35500	5580	1140	541	267	132	68.1	35.9	19.7
λ_1'' (lead)	54400	3760	842	254	147	75.6	52.5	33.5	21.3	13.9

[1] L. D. Landau and I. Ya. Pomeranchuk, DAN SSSR **92**, 535 and 735 (1953).

[2] A. B. Migdal, DAN SSSR **96**, 49 (1954) and **105**, 77 (1955).

[3] A. B. Migdal, JETP **32**, 633 (1957), Soviet Phys. JETP **5**, 527 (1957).

[4] H. A. Bethe and W. Heitler, Proc. Roy. Soc. **A146**, 83 (1934).

[5] A. A. Varfolomeev and I. A. Svetlolobov, JETP **36**, 1771 (1959), Soviet Phys. JETP **9**, 1263 (1959).

[6] A. A. Varfolomeev, and I. A. Svetlolobov, Trans. Internat. Cosmic Ray Conference IUPAP, Moscow 1959, vol 2, p. 292.

[7] Volkonskaya, Ivanenko, and Timofeev, JETP **35**, 293 (1958), Soviet Phys. JETP **8**, 202 (1959).

[8] Volkonskaya, Ivanenko, and Timofeev, op. cit.[6], p. 269.

[9] M. L. Ter-Mikaélyan, Izv. An SSSR ser. fiz. **19**, 657 (1955), Columbia Tech. Transl. p. 595.

[10] S. Z. Belen'kii, Lavinnye protsessy v kosmicheskikh luchakh (Cascade Showers in Cosmic Rays), Gostekhizdat 1948.

[11] Butcher, Chartress, and Messel, Nucl. Phys. **6**, 271 (1958).

Translated by J. G. Adashko
253

HIGH ENERGY PHOTODISINTEGRATION OF Be^9 *AND* C^{12} *NUCLEI*

V. I. MAMASAKHLISOV and R. I. JIBUTI

Tbilisi State University

Submitted to JETP editor April 3, 1961; revised June 29, 1961

J. Exptl. Theoret. Phys. (U.S.S.R.) 41, 1493-1497 (November, 1961)

Photo-absorption by Be^9 and C^{12} nuclei accompanied by the emission of protons is investigated on the basis of the α-particle model of these nuclei. The results are compared with the experimental results.

RECENTLY, a number of experimental and theoretical works[1-4] have indicated the possibility of the existence of clusters of nucleons in light nuclei. Moreover, the analysis of experimental data on photodisintegration of light nuclei leads to the conclusion that these clusters play an important role in radiative transitions. In particular, the characteristics (threshold and energy corresponding to the giant resonances) of the cross sections for the $C^{12}(\gamma, n)$ and $O^{16}(\gamma, n)$ reactions are close to the characteristics of the $He^4(\gamma, n)$ reaction cross section, and in addition to the first maximum (apparently corresponding to the unpaired neutron) of the cross section curve for the $Be^9(\gamma, n)$ and $C^{13}(\gamma, n)$ reactions, one also observes other maxima which lie close to the energy corresponding to the giant resonance in the $He^4(\gamma, n)$ reaction.

These facts indicate that in the above-mentioned light nuclei the photoabsorption occurs primarily in substructures similar to α particles. If clusters of nucleons actually exist in light nuclei, then their role should be especially important at high energies above the giant resonances and lead to considerable yields of high-momentum nucleons. Since the photon carries a small momentum into the nucleus, then such nucleons should already have a high momentum in the initial state, and the nucleons possessing high momenta in the nucleus should be strongly correlated with a less-than-average distance between them, so that they interact and form separate substructures.

1. The experimental data[5] on photoprotons emitted from the Be^9 and C^{12} nuclei by γ quanta of maximum energy 84 Mev show that these nuclei have very similar properties. For example, the angular distributions of photoprotons from Be^9 and C^{12} nuclei are the same within the limits of experimental error. They have a large asymmetry with respect to 90° with a maximum at 50° and a strongly diminished isotropic part. The total cross sections for the reaction at high energies in both cases drop exponentially with the γ-quantum energy and have a value of the order 10^{-28} cm^2 at an energy $\hbar\omega = 80$ Mev. If we compare these experimental results with the data on the photodisintegration of α particles,[6] then we readily note that there is a strong similarity between the properties of the Be^9 and C^{12} nuclei on the one hand and α particles on the other, which they display in interactions with γ quanta.

The foregoing discussion gives a basis for the suggestion that the photoreactions occur in Be^9 and C^{12} nuclei mainly through the interaction of γ quanta with individual quasi-α particles which are apparently formed by the clustering of nucleons in these light nuclei.

The present article is devoted to the study of the photodisintegration of the Be^9 and C^{12} nuclei on the basis of the mechanism of the absorption of γ quanta by α particles.

2. Under the assumption that the photonucleon is emitted from a bound quasi-α particle and the remaining nucleons are not disturbed by the radiation, we can write the wave function for the initial and final states as follows:

$$\Psi_i = \Phi\Psi_c(\alpha)\varphi_i, \qquad \Psi_f = \Phi\Psi_c(H^3)\varphi_f,$$

where Φ describes the motion of the undisturbed nucleons, $\Psi_c(\alpha)$ is the motion of the center-of-mass of the quasi-α particle in the field of the undisturbed nucleons of the nucleus, φ_i is the internal state of the quasi-α particle, $\Psi_c(H^3)$ is the motion of the center of mass of H^3 (or He^3), φ_f is the motion of the emitted nucleon relative to the residual nucleus.

To describe the internal motion of the quasi-α particle we employ a model which was used earlier[7] to describe the $He^4(\gamma, p)$ and $He^3(\gamma, n)$ reactions.

We assume that the interaction potential of γ quanta with the quasi-α particle contains all multipoles, both electric and magnetic. The motion of the center of mass of the quasi-α particle and the triton (or He^3) is described by Gaussian-type wave functions, and the motion of the emitted nucleon by a plane wave. Using the mechanism of the $He^4(\gamma, N)$ reaction (cf. [7]), we obtain for the differential cross section of the photodisintegration of α nuclei

$$\frac{d\sigma}{d\Omega} = B_0 n \frac{A-1}{A} \frac{k^3}{\omega} \sin^2\theta \exp[-2\alpha_0 k'^2 + 2\beta_0 kk' \cos\theta - 2\gamma_0 k^2]\{\delta' - \eta B_1 \exp[\alpha_1 k'^2 - \beta_1 kk' \cos\theta] - \eta B_2 \exp[-(\alpha_2 - \alpha_0) k'^2 - (\beta_0 - \beta_2) kk' \cos\theta - (\gamma_2 - \gamma_0) k^2]\}^2 + \frac{1}{2} B_0 n \frac{A-1}{A} \frac{\mu_{n,p}^2}{c^2} \omega k \exp[-2\alpha_0 k'^2 + 2\beta_0 kk' \cos\theta - 2\gamma_0 k^2]\{1 - \exp[\alpha_1 k'^2 - \beta_1 kk' \cos\theta]\}^2, \quad (1)$$

where ω and $\mathbf{k}'$ are the frequency and wave vector of the incident quantum, $\mathbf{k}$ is the wave vector of the emitted nucleon, n is the number of quasi-α particles in the nucleus, A is the mass number of the initial nucleus, $\mu_{n,p}$ is the magnetic moment of the neutron or proton in nuclear magnetons, $\delta' = 1$ or 0 and $\eta = 1$ or 2, depending on whether a proton or neutron is emitted. The constants occurring in formula (1) are

$$B_0 = \frac{2^{13}\pi^{1/2}\gamma^3\beta^3\delta^3 l^2}{p^3 Mc}, \quad B_1 = \frac{3p - \beta^2 q}{3(A-1)p}, \quad B_2 = \frac{s\beta^2}{3(A-1)p},$$

$$\alpha_0 = \frac{p + (3\delta^2 + 4\beta^2)^2}{4p(\delta^2 + \beta^2)}, \quad \beta_0 = \frac{(A-4)p + (3\delta^2 + 4\beta^2)q}{2(A-1)p(\delta^2 + \beta^2)},$$

$$\gamma_0 = \frac{(A-4)^2 p + q^2}{4(A-1)p(\delta^2 + \beta^2)}, \quad \alpha_1 = \frac{2(\delta^2 + 2\beta^2)}{p},$$

$$\beta_1 = \frac{2q}{(A-1)p}, \quad \alpha_2 = \frac{p + 64\gamma^4}{4pl}, \quad \beta_2 = \frac{16\gamma^2 s - 6Ap}{4(A-1)pl},$$

$$\gamma_2 = \frac{s^2 + 9A^2 p}{4(A-1)pl},$$

where M is the nucleon mass, c is the velocity of light,

$$p = 8\gamma^2(\delta^2 + \beta^2) + \delta^2\beta^2, \quad q = 4(A-1)\beta^2 + 3A\delta^2,$$
$$l = 8\gamma^2 + \beta^2, \quad s = 8(A-4)\gamma^2 + 4(A-1)\beta^2.$$

In these formulas δ and β the parameters of the wave functions describing the motion of the center of mass of the quasi-α particle and center of mass of the triton (or He^3), respectively. The parameter γ corresponds to the internal state of the quasi-α particle.

Integrating expression (1) over the angular variable, we readily obtain the total cross section for the process. Thus

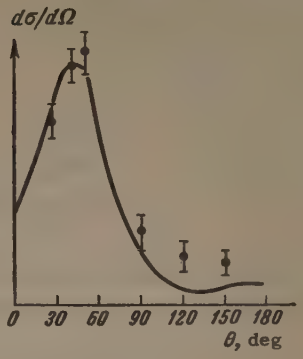

FIG. 1. Angular distribution of photoprotons in the $Be^9(\gamma, p)$ reaction for 80-Mev γ quanta.

$$\sigma = 8\pi B_0 n \frac{A-1}{A} \frac{k^3}{\omega} \exp(-\varphi_1)\{\delta'\Phi_1[\xi_1] + \eta^2 B_1^2 \exp(\varphi_2)\Phi_1[\xi_2] + \eta^2 B_2^2 \exp(\varphi_3)\Phi_1[\xi_3] - 2\delta'\eta B_1 \exp(\varphi_2/2)\Phi_1[\xi_4] - 2\delta'\eta B_2 \exp(\varphi_3/2)\Phi_1[\xi_5] + 2\eta^2 B_1 B_2 \exp(\varphi_4)\Phi_1[\xi_6]\} + 2\pi B_0 n \frac{A-1}{A} \frac{\mu_{n,p}^2}{c^2} \omega k \exp(-\varphi_1)\{\Phi_2[\xi_1] + \exp(\varphi_2)\Phi_2[\xi_2] - 2\exp(\varphi_2/2)\Phi_2[\xi_4]\}, \quad (2)^*$$

where

$$\varphi_1 = 2\alpha_0 k'^2 + 2\gamma_0 k^2, \quad \varphi_2 = 2\alpha_1 k'^2,$$
$$\varphi_3 = 2(\alpha_0 - \alpha_2) k'^2 + 2(\gamma_0 - \gamma_2) k^2,$$
$$\varphi_4 = (\alpha_0 - \alpha_2 + \alpha_1) k'^2 + (\gamma_0 - \gamma_2) k^2,$$
$$\xi_1 = 2\beta_0 kk', \quad \xi_2 = 2(\beta_0 - \beta_1) kk', \quad \xi_3 = 2\beta_2 kk',$$
$$\xi_4 = (2\beta_0 - \beta_1) kk', \quad \xi_5 = (\beta_0 + \beta_2) kk',$$
$$\xi_6 = (\beta_0 + \beta_2 - \beta_1) kk', \quad \Phi_1[\xi] = \frac{1}{\xi^2}\left(\mathrm{ch}\,\xi - \frac{\mathrm{sh}\,\xi}{\xi}\right),$$
$$\Phi_2[\xi] = \frac{\mathrm{sh}\,\xi}{\xi}.$$

3. The numerical calculation of the angular distribution of the photoprotons was carried out for the $Be^9(\gamma, p)$ reaction for an incident γ-quantum energy $\hbar\omega = 80$ Mev. The result is shown in Fig. 1. Also shown are the experimental points obtained by Chuvilo and Shevchenko.[5] The curve for the total cross section calculated on the basis of formula (2) is shown in Fig. 2.

The parameters of the wave functions describing the motion of the center of mass of the quasi-α particle and of the center of mass of the triton were determined with the use of the electromagnetic radius of the nucleus, while the value of the parameter γ was taken from [7] ($\gamma = 8 \times 10^{12}$ cm^{-1}, $\beta = 4.20 \times 10^{12}$ cm^{-1}, $\delta = 4.17 \times 10^{12}$ cm^{-1}).

The data of [5] on Be^9 concerns the bremsstrahlung spectrum. To determine from these data the dependence of the $Be^9(\gamma, p)$ reaction cross section on the incident γ-quantum energy, we used the relation obtained by Chuvilo and Shevchenko

*sh = sinh, ch = cosh.

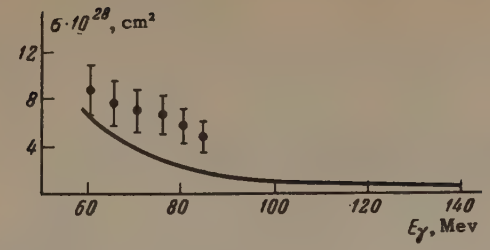

FIG. 2. Total cross section of the $Be^9(\gamma, p)$ reaction as a function of the incident γ-quantum energy.

$$\int_{\omega_{min}}^{\omega_{max}} \sigma_{Be^9}(\omega) I(\omega) d\omega = (1.0 \pm 0.2) A \int_{\omega_{min}}^{\omega_{max}} \sigma_d(\omega) I(\omega) d\omega,$$

where $I(\omega)$ is the bremsstrahlung intensity, $\sigma_d(\omega)$ is the photodisintegration cross section of the deuteron. According to [5], this relation does not depend, within the limits of experimental error, on the value of the maximum energy of the radiation ω_{max} (in the 50 — 85 Mev interval). This permits us to write

$$\sigma_{Be^9}(\omega) = (1.0 \pm 0.2) A \sigma_d(\omega).$$

The experimental points for σ_{Be^9} determined in this way are shown in Fig. 2, where the values of $\sigma_d(\omega)$ were determined from the curve given by Hulthén and Sugawara.[9]

As regards the $C^{12}(\gamma, p)$ reaction, the calculation [see (1)] shows that the character of the angular distribution is similar to the $Be^9(\gamma, p)$ reaction, which is in agreement with the experimental data.[10]

As seen from Figs. 1 and 2, the shape of the angular distribution is in good agreement with the theoretical curve, and the curve of the total cross section runs only slightly below the experimental points. These results allow us to conclude that in the energy interval under consideration the quasi-α particle absorption of γ quanta plays the basic role in the photodisintegration of the Be^9 and the C^{12} nuclei ($\sim 70\%$). Along with this, there are apparently other absorption mechanisms whose contributions to the photoabsorption cross section are evidently small.

Let us consider, for example, the photodisintegration of α nuclei from the viewpoint of the shell model. It is known (see, for example, Wilkinson[11]) that, according to this model, the angular distribution of the photoprotons strongly depends on initial angular momentum of the proton in the nucleus. Therefore, if the reaction takes place in accordance with the independent-particle model, one should observe a distinct difference in the angular distribution of the protons from the Be^9 and C^{12} nuclei, since the ratio of the number of protons in the p state to the number in the s state is 2:1 for carbon and 1:1 for beryllium. Feld et al[10] have drawn attention to this. Actually, the experimental angular distribution of the protons from the Be^9 and the C^{12} nuclei are almost identical.[5]

We note that on the basis of the α-particle absorption model one should expect the existence of the photonuclear reaction with the simultaneous emission of the proton and triton. Such a reaction has actually been observed by Maĭkov[12] in the case of the C^{12} nucleus in the energy interval 30 — 150 Mev, but no detailed investigation was made in view of the poor statistical accuracy. It is therefore best to defer the theoretical consideration of this reaction, which can be made in analogy with the theory developed above, until reliable experimental data have been accumulated.

We thank T. I. Kopaleĭshvili for helpful discussions.

[1] P. E. Hodgson, Nuclear Phys. 8, 1 (1958).
[2] V. G. Solov'ev, DAN SSSR 131, 286 (1960), Soviet Phys.-Doklady 5, 298 (1960).
[3] Vashakidze, Kopaleĭshvili, Mamasakhlisov, and Chilashvili, JETP 38, 937 (1960), Soviet Phys. JETP 11, 675 (1960).
[4] P. D. Kunz, Ann. Phys. 11, 275 (1960).
[5] N. V. Chuvilo and V. G. Shevchenko, Yadernye reaktsii pri malykh i srednikh énergiyakh (Low and Medium Energy Nuclear Reactions), AN SSSR, 1958, p. 435.
[6] A. N. Gorbunov and V. M. Spiridonov, JETP 33, 21 (1957), Soviet Phys. JETP 6, 16 (1958).
[7] R. I. Jibuti and A. V. Tagviashvili, JETP 39, 1756 (1960), Soviet Phys. JETP 12, 1225 (1961).
[8] R. Hofstadter, Revs. Modern Phys. 28, 214 (1956).
[9] L. Hulthén and M. Sugawara, Handbuch der Physik, Band 39, 1957.
[10] Feld, Godbole, Odian, Scherb, Stein, and Wattenberg, Phys. Rev. 94, 1000 (1954).
[11] D. H. Wilkinson, Physica 22, 1039 (1956).
[12] V. H. Maĭkov, Yadernye reaktsii pri malykh i srednikh énergiyakh (Low and Medium Energy Nuclear Reactions), AN SSSR, 1958, p. 414.

Translated by E. Marquit
254

THE CONDITION FOR SELF-EXCITATION OF A LASER

V. M. FAĬN and Ya. I. KHANIN

Gor'kii Radiophysical Institute

Submitted to JETP editor April 22, 1961

J. Exptl. Theoret. Phys. (U.S.S.R.) 41, 1498-1502 (November, 1961)

The problem of the conditions for self-excitation is considered for devices of the type of a molecular generator with a resonating cavity with dimensions much larger than the generated wavelength. The problem is solved by the method of expansion in terms of eigenfunctions of the cavity with ideally conducting walls. The limits of applicability of the results to real cavities are estimated.

THE study of features of the operation of quantum-mechanical generators and amplifiers that use resonating cavities of dimensions much larger than the wavelength has become interesting because of the practical development of such devices in the optical range of wavelengths (lasers).[1,2] One particularly important question is that of the conditions for self-excitation of a laser. Calculations on this have been made by Schawlow and Townes.[3] The problem can, however, be treated by much more rigorous methods than those used by the authors of [3].

Let us consider a system of weakly interacting molecules* with two energy levels, which completely fills the resonating cavity.† The state of the system is characterized by the density of the energy spin $\mathbf{s}(\mathbf{r},t)$, whose components s_1, s_2, and s_3 obey the following equations of motion[5]:

$$\begin{aligned}
&\dot{s}_1+\omega_0 s_2+\frac{1}{T_2}s_1+\frac{1}{\hbar}\sum_\lambda \mathbf{A}_\lambda(\mathbf{r})\,\mathbf{e}_2 s_3 q_\lambda=0,\\
&\dot{s}_2-\omega_0 s_1+\frac{1}{T_2}s_2-\frac{1}{\hbar}\sum_\lambda \mathbf{A}_\lambda(\mathbf{r})\,\mathbf{e}_1 s_3 q_\lambda=0,\\
&\dot{s}_3=\frac{1}{T_1}(s_3^0-s_3)-\frac{1}{\hbar}\sum_\lambda \mathbf{A}_\lambda(\mathbf{r})\,(\mathbf{e}_1 s_2-\mathbf{e}_2 s_1)\,q_\lambda;\\
&\ddot{q}_\lambda+\frac{\omega_\lambda}{Q_\lambda}\dot{q}_\lambda+\omega_\lambda^2 q_\lambda=\int_{V_c}\mathbf{A}_\lambda(\mathbf{r})\,(\mathbf{e}_1 s_1+\mathbf{e}_2 s_2)\,dV.
\end{aligned}\tag{1}$$

Here ω_0 is the frequency of the molecular transition, ω_λ are the natural frequencies of the resonator, Q_λ are the quality factors corresponding to these frequencies, T_1 and T_2 are the Bloch relaxation times, and $\mathbf{e}_1$ and $\mathbf{e}_2$ are vector molecular constants. These constants can be expressed in terms of the matrix elements of the dipole moment. According to [5]

$$\frac{1}{c}\frac{d\hat{\mu}}{dt}=\mathbf{e}_1 r_1+\mathbf{e}_2 r_2,\tag{2}$$

where $\hat{\mu}$ is the operator for the dipole moment of the molecule, and r_1 and r_2 are spin matrices. In the representation in which the energy operator of the isolated molecule is diagonal we have

$$r_1=\frac{1}{2}\begin{pmatrix}0&1\\1&0\end{pmatrix},\quad r_2=\frac{1}{2}\begin{pmatrix}0&-i\\i&0\end{pmatrix}.$$

The relation (2) gives the connection between $\mathbf{e}_1$ and $\mathbf{e}_2$ and the matrix elements of $\hat{\mu}$ calculated with the eigenfunctions of the energy operator of the isolated molecule:

$$\mathbf{e}_1+i\mathbf{e}_2=(2i\omega_0/c)\,\mu_{21},\qquad \mathbf{e}_1-i\mathbf{e}_2=(-2i\omega_0/c)\,\mu_{12}.\tag{3}$$

We note by the way that the oscillating part of the mean dipole moment is linearly polarized only in cases in which $\mathbf{e}_1$ and $\mathbf{e}_2$ are collinear. In fact,

$$\begin{aligned}\langle\psi|\hat{\mu}|\psi\rangle_{osc}&=\langle c_1\psi_1+c_2\psi_2|\hat{\mu}|c_1\psi_1+c_2\psi_2\rangle\\&=c_1^*c_2\mu_{12}e^{-i\omega_0 t}+c_1c_2^*\mu_{21}e^{i\omega_0 t},\end{aligned}\tag{4}$$

and it becomes obvious that our assertion is correct when one substitutes μ_{12} and μ_{21} from Eq. (3) into Eq. (4).

In writing out the system (1) we have used the expansion of the vector potential of the electromagnetic field in terms of the eigenfunctions of the resonator:

$$\mathbf{A}(\mathbf{r},t)=\sum_\lambda \mathbf{A}_\lambda(\mathbf{r})\,q_\lambda(t),\qquad \int_{V_c}\mathbf{A}_\lambda^2\,dV=4\pi c^2.\tag{5}$$

Let us introduce the notation

$$\mathbf{A}_\lambda\mathbf{e}_1/\hbar=\alpha_{1\lambda},\qquad \mathbf{A}_\lambda\mathbf{e}_2/\hbar=\alpha_{2\lambda},\qquad \alpha_{2\lambda}-i\alpha_{1\lambda}=\alpha_\lambda\tag{6}$$

and make the change of variables $s_1+is_2=P_1$, $s_1-is_2=P_2$; the system (1) then takes the form

*By molecules we here mean any quantum-mechanical objects with two levels.

†The disk type of resonator used in practice is not a closed system, but for the main modes of oscillation the field is practically all concentrated in the space between the disks. This is confirmed by calculations made by Fox and Li[4]. Therefore our analysis includes the case of disk resonators.

$$\dot{P}_1 + (T_2^{-1} - i\omega_0) P_1 + \sum_\lambda \alpha_\lambda q_\lambda s_3 = 0, \quad (7a)$$

$$\dot{P}_2 + (T_2^{-1} + i\omega_0) P_2 + \sum_\lambda \alpha_\lambda^* q_\lambda s_3 = 0, \quad (7b)$$

$$\dot{s}_3 = \frac{1}{T_1}(s_3^0 - s_3) + \frac{1}{2}\sum_\lambda (P_1\alpha_\lambda^* + P_2\alpha_\lambda) q_\lambda, \quad (7c)$$

$$\ddot{q}_\lambda + \frac{\omega_\lambda}{Q_\lambda}\dot{q}_\lambda + \omega_\lambda^2 q_\lambda = -\frac{i\hbar}{2}\int_{V_c} (P_1\alpha_\lambda^* - P_2\alpha_\lambda)\, dV. \quad (7d)$$

Since, by hypothesis, the working substance uniformly fills the entire volume of the resonating cavity, it is convenient to make an expansion of $P_1(\mathbf{r},t)$ and $P_2(\mathbf{r},t)$ in terms of the system of functions α_λ and α_λ^*:

$$P_1(\mathbf{r},t) = \sum_\lambda \alpha_\lambda(\mathbf{r})\, P_{1\lambda}(t), \qquad P_2(\mathbf{r},t) = \sum_\lambda \alpha_\lambda^*(\mathbf{r})\, P_{2\lambda}(t). \quad (8)$$

The completeness and orthogonality of the system α_λ follows from the properties of the system $\mathbf{A}_\lambda$.*

Our set problem of finding the conditions of self-excitation of the generator presupposes an analysis of (7) for stability. Let us assume that at the initial time the quantities $P_{1\lambda}$, $P_{2\lambda}$, and q_λ are close to 0 and $s_3 = s_3^0$ does not depend on the space coordinates.† The replacement of s_3 by s_3^0 in (7a) and (7b) linearizes these equations and allows us to go from a system of an infinite number of coupled equations to a finite system. Multiplying both sides of (7a) by α_λ^* and both sides of (7b) by α_λ and integrating them over the cavity volume V_c, we get

$$\dot{P}_{1\lambda} + (T_2^{-1} - i\omega_0) P_{1\lambda} + s_3^0 q_\lambda = 0, \quad (9a)$$

$$\dot{P}_{2\lambda} + (T_2^{-1} + i\omega_0) P_{2\lambda} + s_3^0 q_\lambda = 0. \quad (9b)$$

Integrating both sides of (7c) and the right side of (7d), we arrive at the equations

$$V_c \dot{s}_3 = \frac{a^2}{2}\sum_\lambda (P_{1\lambda} + P_{2\lambda}) q_\lambda, \quad (9c)$$

$$\ddot{q}_\lambda + \frac{\omega_\lambda}{Q_\lambda}\dot{q}_\lambda + \omega_\lambda^2 q_\lambda = \frac{i\hbar a^2}{2}(P_{2\lambda} - P_{1\lambda}), \quad a^2 = \int_{V_c} \alpha_\lambda \alpha_\lambda^*\, dV. \quad (9d)$$

Let us now assume that there is a small perturbation of the form

$$P_{1\lambda}^0 e^{i\xi_\lambda t}, \qquad P_{2\lambda}^0 e^{i\xi_\lambda t}, \qquad q_\lambda^0 e^{i\xi_\lambda t}, \quad (10)$$

where $\xi_\lambda = \Omega_\lambda + i\delta_\lambda$. Substitution of (10) in (9a)–(9c) leads to a system of homogeneous algebraic equations, which has a non-trivial solution when the determinant is equal to zero:

$$\xi_\lambda^4 - i\xi_\lambda^3(\omega_\lambda/Q_\lambda + 2/T_2) - \xi^2(\omega_\lambda^2 + \omega_0^2 + T_2^{-2} + 2\omega_\lambda/Q_\lambda T_2) + i\xi_\lambda\omega_\lambda[2\omega_\lambda/T_2 + (\omega_0^2 + T_2^{-2})/Q_\lambda] + \omega_\lambda^2(\omega_0^2 + T_2^{-2}) + \hbar a^2\omega_0 s_3^0 = 0. \quad (11)$$

Confining ourselves to the case $|\delta_\lambda| \ll \Omega_\lambda$ and neglecting terms in δ_λ^2, δ_λ^3, and δ_λ^4, we can write instead of Eq. (11) two real equations which determine Ω_λ and δ_λ as functions of ω_λ, s_3^0, and so on. We shall be interested in the occurrence of solutions of the system (9) that increase with the time. From physical considerations it is clear that for $s_3^0 > s_{3\,cr}^0$ there must be increasing solutions characterized by $\delta_\lambda < 0$.* The condition $\delta_\lambda < 0$ leads to the following relations:

$$\Omega_{\lambda\,cr}^2 = \frac{\omega_\lambda(\omega_0^2 T_2 + T_2^{-1} + 2Q_\lambda\omega_\lambda)}{\omega_\lambda T_2 + 2Q_\lambda}, \quad (12)$$

$$s_{3\,cr}^0 = \frac{\omega_\lambda[(\omega_0^2 - \Omega_{\lambda\,cr}^2 + T_2^{-2})^2 + 4T_2^{-2}\Omega_{\lambda\,cr}^2]}{2Q_\lambda T_2^{-1}\omega_0\hbar a^2}. \quad (13)$$

The quantity $s_{3\,cr}^0$ depends on ω_λ, and to a certain characteristic frequency of the cavity there corresponds a value $(s_{3\,cr}^0)_{min}$ below which there is no instability in the system. The quantity $(s_{3\,cr}^0)_{min}$ can be determined from Eq. (13), and the corresponding oscillation frequency is given approximately by $\Omega_\lambda^2 = \omega_0^2 - T_2^{-2}$. If we use the fact that $T_2^{-2} \ll \omega_0^2$, so that without much error we can set $\omega_\lambda = \Omega_\lambda = \omega_0$, we get a simple formula for the boundary of the region of self-excitation:

$$(s_{3\,cr}^0)_{min} \approx 2\omega_0^2/\hbar a^2 Q_\lambda T_2. \quad (14)$$

The quantity a^2 that appears here is given by

$$a^2 = \frac{1}{\hbar^2}\int_{V_c} [(\mathbf{A}_\lambda\mathbf{e}_1)^2 + (\mathbf{A}_\lambda\mathbf{e}_2)^2]\, dV. \quad (15)$$

The simplest special case is that in which $\mathbf{A}_\lambda$ are plane waves and the vectors $\mathbf{e}_1$ and $\mathbf{e}_2$ are collinear. Then the optimal mode, in the sense of its polarization, is that for which $\mathbf{A}_\lambda \parallel \mathbf{e}_1$, and by using the normalization conditions and Eq. (3) one verifies without difficulty that $a^2 = (16\pi\omega_0^2/\hbar^2)|\mu_{12}|^2$. From this we have

$$N_{min} = 2(s_{3\,cr}^0)_{min} = \hbar/4\pi|\mu_{12}|^2 Q_\lambda T_2. \quad (16)$$

Comparing Eq. (16) with the condition for self-excitation of an ordinary molecular generator obtained by Basov and Prokhorov,[6] one readily verifies that they are identical. This fact is not unexpected, since the calculation of Basov and Prokhorov was made on the same assumptions about the character of the polarization of the field in the cavity and about the properties of the dipole

*We are confining ourselves to the case of greatest practical importance, for which $\mathbf{A}_\lambda/|\mathbf{A}_\lambda|$ is a constant vector.

†$2s_3$ has the meaning of the number of active molecules per unit volume, and $s_3 > 0$ describes a state with a preponderance of molecules in the upper level.

*This can be shown directly, because $d\delta/ds_3^0 < 0$.

moment as have been used in obtaining Eq. (16), and is due to the fact that the minimum point on the curve of $s_{3\,cr}^{0}(\omega_\lambda)$ corresponds to the excitation of only one mode of the cavity. For $s_3^0 > (s_{3\,cr}^0)_{min}$ adjacent modes also become unstable.

In conclusion we remark that the treatment given here has been based essentially on the assumption that the volumes of the matter and the field are the same. It is just owing to this that we could go from the system (7) to the system (9). If we take into account the finite conductivity of the walls of the cavity this assumption is incorrect, owing to the penetration of the field into the metal to the extent of the skin depth. In this case our derivation remains valid, though only approximately, provided a condition which will now be indicated is satisfied.

Let A_λ be the eigenfunctions of a hypothetical cavity with ideally conducting walls and with the same geometry as the actual cavity. Then we have the equation

$$\int\limits_{V_c+V_{sk}} \sum_\mu A_\lambda A_\mu\, dV = \int\limits_{V_c} \sum_\mu A_\lambda A_\mu\, dV + \int\limits_{V_{sk}} \sum_\mu A_\lambda A_\mu\, dV, \quad (17)$$

in which V_c is the volume of the cavity and V_{sk} is the volume of the skin-depth layer. It follows from Eq. (17) that the system of functions A_λ can be used if

$$\int\limits_{V_c} \sum_\mu A_\lambda A_\mu\, dV \equiv \int\limits_{V_c} A_\lambda^2\, dV \gg \int\limits_{V_{sk}} \sum_\mu A_\lambda A_\mu\, dV. \quad (18)$$

Since

$$\sum_\mu \int\limits_{V_{sk}} A_\lambda A_\mu\, dV \leqslant \sum_\mu \int\limits_{V_{sk}} \{\max A_\mu\}^2\, dV = n\{\max A_\mu\}^2 V_{sk},$$

we can replace Eq. (18) by the stronger inequality

$$\int\limits_{V_c} A_\lambda^2\, dV \gg n\{\max A_\lambda\}^2 V_{sk}. \quad (19)$$

It is natural to take n to mean the total number of characteristic frequencies of the cavity that fall within the line width of the molecules. Violation of the inequality (19) is to be expected only in the case of large n, i.e., when the dimensions of the cavity are much larger than the wavelength. Furthermore, according to the normalization condition, $\{\max A_\lambda\}^2 \sim 4\pi c^2/V_c$. Using the fact that the ratio V_c/V_{sk} is approximately equal to the quality figure (cf., e.g., [7]), we finally get the condition for the validity of our approximation in the form

$$Q \gg n. \quad (20)$$

The criterion (20) is satisfied clear up to the optical region. In fact, the number of types of vibrations of a resonator such as a Fabry-Perot interferometer which have sufficiently high values of Q is given, according to [8], by the formula

$$n = LD^4\omega^4\Delta\omega/2\pi^2c^5Q^2.$$

Here $Q = L\omega/c(1-\alpha)$, L is the distance between the plates and D their diameter, and α is the reflection coefficient. For L = 4 cm, D = 0.5 cm, $\omega \approx 3 \times 10^{15}$, $\Delta\omega/\omega = 10^{-3}$, $\alpha = 0.95$, we get $n/Q \approx 0.2$.

[1] H. Lyons, Astronautics 5, 39 (1960).

[2] Collins, Nelson, Schawlow, Bond, Garrett, and Kaiser, Phys. Rev.Letters 5, 303 (1960).

[3] A. L. Schawlow and C. H. Townes, Phys. Rev. 112, 1940 (1958).

[4] A. G. Fox and T. Li, Proc. IRE 48, 1904 (1960).

[5] V. M. Faĭn, Izv. Vuzov, Radiofizika (News of the Universities, Radiophysics) 2, 167 (1959).

[6] N. G. Basov and A. M. Prokhorov, JETP 30, 560 (1956), Soviet Phys. JETP 3, 426 (1956).

[7] A. G. Gurevich, Polye rezonatory i volnovody (Cavity Resonators and Waveguides), Moscow, Sov. Radio, 1952.

[8] Basov, Krokhin, and Popov, UFN 72, 161 (1960), Soviet Phys.-Uspekhi 3, 702 (1961).

Translated by W. H. Furry.
255

THE SIGN OF THE MASS DIFFERENCE OF K_1^0 AND K_2^0 AND THEIR LEPTONIC DECAYS

S. G. MATINYAN

Physics Institute, Academy of Sciences, Georgian S.S.R.

Submitted to JETP editor May 10, 1961

J. Exptl. Theoret. Phys. (U.S.S.R.) 41, 1503-1506 (November, 1961)

Interference of leptonic decays of K^0 mesons during the transversal through matter of K_2^0 mesons is studied as a possible method for the determination of the sign of the K_1^0-K_2^0 mass difference.

KOBZAREV and Okun' [1] have proposed a method for the determination of the sign of the mass difference $\Delta m = m_1 - m_2$ of the K_1^0 and K_2^0, based on the interference phenomena that take place when a beam of K_2^0 mesons passes through a pair of plates made of different substances. The K_1^0 waves produced in each of these plates are out of phase by an amount $\Delta\varphi$ and therefore one can, in principle, determine the sign of Δm by studying the oscillation of the two-pion mode of decay of the K_1^0 as a function of the distance between the plates. In a paper by the author [2] this phenomenon was analyzed in detail and optimum conditions for performing the experiment were found. The analysis showed that it would be advisable to use two thick plates located next to each other provided that $|\Delta\varphi|$ was not very small ($\geq \pi/8$).

However it is not clear a priori what magnitudes of $\Delta\varphi$ can be expected for various pairs of plates, not to mention the extremely complicated problem of determining the sign of $\Delta\varphi$, which is essential in this method. It is not out of the question that $\Delta\varphi$ could be so small that curves with opposite signs of Δm could not be resolved. In view of these considerations it does not seem likely that an experiment to determine the sign of Δm by the two-plates method will be carried out in the near future.

It is therefore of considerable interest to investigate the possibility of determining the sign of Δm by utilizing just one plate placed in the K_2^0 beam. This could be done by studying the number of hyperons produced in a thin plate, placed at a distance x_0 from the main plate, as a function of x_0, [1,2] and by studying the leptonic decays K_{e3}^0 and $K_{\mu 3}^0$ in the part of the beam that goes through without deviation as a function of the distance x_0 between the point of decay and the plate. [2]*

*The possibility of utilizing interference effects in leptonic decays for the purposes of determining the sign of Δm was already pointed out by Biswas [3] in the case of single scattering of the K^0 beam. In contrast to Biswas we consider phenomena arising from the transmission of the K_2^0 through matter.

The obvious drawback of these methods of determining the sign of Δm in contrast to the two-plate method lies in the fact that the effect under study (hyperon production, leptonic decays) occurs not only because and not so much because of the presence of the "regenerated" K_1^0 wave, as because of the presence of the here predominating K_2^0 component. Therefore the distribution of the number of observed events will be given by a term large in magnitude, on which there will be superimposed an oscillation of small amplitude, connected with the sign of Δm. At the same time one should keep in mind that the use of a thick plate substantially increases the amplitude of this oscillation (by increasing the fraction of "regenerated" K_1^0 mesons [2]); furthermore, in the case of leptonic decays the amplitude of oscillations can be doubled by making use of the difference effect (see below) which is absent in the hyperon case.

These considerations make it necessary to investigate in detail leptonic decays in a beam of K^0 mesons that has traversed a plate.* As was shown by the author, [2] the number of leptonic decays $N_+(N_-)$ in a beam transmitted without deviation through a plate of thickness $t = x/v$ (v — velocity of the K_2^0 beam) per unit time at a distance $t_0 = x_0/v$ from the plate, relative to the initial number of mesons in the beam, for decays into π^+ mesons and leptons (π^- mesons and leptons) is equal to

*The fact that when leptonic decays are used to determine the sign of Δm it is sufficient, in principle, to transmit the K_2^0 through one plate is directly related to the fact that the decays $K^0 \to e^+(\mu^+) + \nu + \pi^-$ and $\bar{K}^0 \to e^-(\mu^-) + \nu + \pi^+$ are allowed, whereas $K^0 \to e^-(\mu^-) + \nu + \pi^+$ and $\bar{K}^0 \to e^+(\mu^+) + \nu + \pi^-$ are forbidden by the $\Delta Q = \Delta S$ rule, where Q and S are the charge and strangeness of the strongly interacting particles. [4] We note that the magnitude of Δm can be determined through leptonic decays from the free K^0 beam, whereas its determination from two-pion decays of K_1^0 requires the transmission of the K_2^0 beam through one plate. In order to determine the sign of Δm one more plate is required (of a different substance).

$$\binom{N_+}{N_-} = \Gamma_l \exp\left(-\frac{N}{2}(\bar{\sigma}+\sigma)x\right)\left\{\frac{1}{2}\exp\left(-\frac{t_0}{\gamma\tau_2}\right) \pm r\exp\left(-\frac{t_0}{2\gamma\tau_1}-\frac{t_0}{2\gamma\tau_2}\right)\left[\sigma(t)\sin\left(\varphi-\frac{\Delta m}{\gamma}t_0\right) - \varkappa(t)\cos\left(\varphi-\frac{\Delta m}{\gamma}t_0\right)\right]\right\}\exp\left(-\frac{t}{\gamma\tau_2}\right). \quad (1)$$

The notation in Eq. (1) is the same as in [2]; in contrast to the corresponding formula (15) of [2] we have taken here into account the finite lifetime τ_2 of the K_2^0 meson; $\sigma(t)$ and $\kappa(t)$ are respectively even and odd functions of Δm, given by Eq. (16) of [2].

Equation (1), as well as the entire theory developed earlier in [2], is valid provided that the condition of preponderance of K_1^0 decays over effects due to their regeneration in matter is well satisfied [condition (4) in [2]].

Taking into account that the introduced in [2] modulus r of a quantity proportional to the amplitude for the transition $K_2^0 \to K_1^0$ may be written with the help of the optical theorem in the form $r = N(\bar{\sigma}-\sigma)/4\,|\sin\varphi|$ $(0 < \varphi < \pi)$ we find that the condition (4) of [2] reduces to a condition whose left side has an obvious physical meaning

$$N(\bar{\sigma}-\sigma)\gamma\tau_1 v \ll 2\,|\sin\varphi|. \quad (2)$$

Let us note that $\varphi = \tan^{-1}(\rho_2/\rho_1)$, where $\bar{f}(0) - f(0) \equiv \rho_1 + i\rho_2$, with $\rho_2 > 0$ in the entire so far investigated large energy interval. On the other hand, Eq. (1) is invariant under simultaneous replacements $\Delta m \to -\Delta m$ and $\varphi \to \pi - \varphi$, so that it is necessary to know the sign of ρ_1 in order to be able to determine the sign of Δm. [In the two-plate case one was faced with the more complex problem of determining the sign of the difference of the real parts of $\bar{f}(0) - f(0)$ in the two plates.]

Information on the sign of ρ_1 may be obtained from the results of the analysis of experiments on elastic scattering of K^+ and K^- mesons with energies ~ 100 Mev on photoemulsion nuclei on the basis of the optical model of the nucleus with a diffuse edge.[5,6] This analysis leads to a negative real part for the interaction potential between K^- mesons and photoemulsion nuclei (about −30 Mev) corresponding to attraction, whereas for K^+ scattering the nuclear potential corresponds to a repulsion (its real part is approximately +20 Mev for photoemulsion nuclei).

These data lead to the conclusion that $\mathrm{Re}\,[\bar{f}(0) - f(0)]$ is positive for K^+ and K^- scattering on photoemulsion nuclei. It is to be expected that a similar relation holds true for K^0 and $\bar{K}^0$ mesons; also it is hardly to be expected that the sign of the real part of the potential would change upon passing from one nucleus to another.

At this time, however, it is not possible to arrive at any conclusions on the sign of the difference of the real parts of $\bar{f}(0) - f(0)$ for different nuclei, which requires the precise knowledge of the actual size of the real parts of the scattering amplitudes. This problem is not likely to be solved in the near future. From this point of view methods for determining the sign of Δm using one plate have an incomparable advantage over two-plate methods.

It should be noted that the experiment is impossible if φ is close to $\pi/2$. However the data on K^+ and K^- scattering[5,6] definitely indicate that $\varphi \neq \pi/2$. At the same time they indicate that φ is not near zero,* so that the condition (2) for the applicability of Eq. (1) is always satisfied, even if not with quite the margin that would be expected from the approximate condition (4′) of [2].

Before carrying out a quantitative analysis of Eq. (1) let us indicate how it is possible, in principle, to estimate $|\sin\varphi|$, i.e. φ, given the sign of ρ_1, by studying the dependence of the number N_1 of K_1^0 decays into two pions in the undeviated beam on the distance t_0 when $|\Delta m|$, v, t, $\bar{\sigma}$ and σ are given. This dependence is given by the formula

$$N_1 = \frac{N^2(\bar{\sigma}-\sigma)^2}{16\sin^2\varphi}\exp\left\{-\frac{N}{2}(\bar{\sigma}+\sigma)x\right\}e^{-t_0/\gamma\tau_1} \times \frac{1 - 2\cos(\Delta m t/\gamma)\exp(-t/2\gamma\tau_1) + \exp(-t/\gamma\tau_1)}{(\Delta m/\gamma v)^2 + (1/2\,\gamma\tau_1 v)^2} \quad (3)$$

(see also [7]).

Turning to our problem with leptonic decays we introduce the ratio

$$R(t, t_0) \equiv \frac{N_+ - N_-}{N_+ + N_-} = 2r\left[\sigma(t)\sin\left(\varphi-\frac{\Delta m}{\gamma}t_0\right) - \varkappa(t)\cos\left(\varphi-\frac{\Delta m}{\gamma}t_0\right)\right]e^{-t_0/2\gamma\tau_1}. \quad (4)$$

A study of this ratio as a function of t_0 at an optimal thickness of the plate t permits the determination, in principle (given the sign of ρ_1, i.e., information about what quadrant φ is in—the first or second), of the sign of Δm.

In the figure are shown curves giving the dependence of R on $x_0 = vt_0$ for an optimal thickness of a copper plate $x \equiv vt = 3.5$ cm (the energy of the K_2^0 mesons is equal to 100 Mev; the decay length of K_1^0 mesons $\gamma\tau_1 v$ is equal to 2.2 cm). The curves a, b, c correspond to the values $\varphi = \pi/8, \pi/6, \pi/4$ for $\Delta m < 0$, and $\varphi = \pi - \pi/8, \pi - \pi/6, \pi - \pi/4$ for $\Delta m > 0$. The curves a_1, b_1

*An estimate of f(0) and $\bar{f}(0)$, based on the nuclear potentials of K^+ and K^- mesons given in[5,6], results in a value of φ of approximately $\pi/6$.

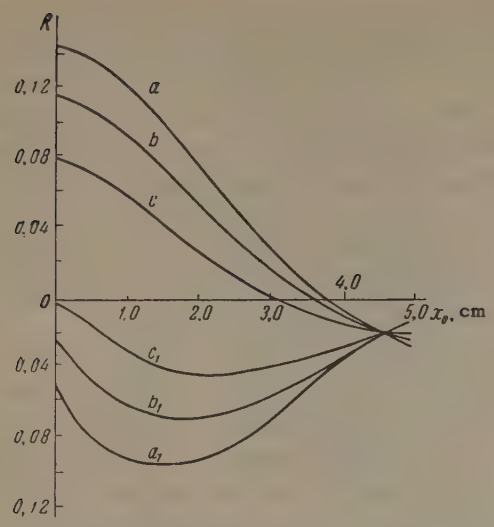

Sign of the mass difference of K_1^0 and K_2^0 mesons and their leptonic decays.

and c_1 correspond to the same choice of φ for opposite sign of Δm. The magnitude of Δm was taken to be 10^{10} sec^{-1}.[8,9]

It is seen from the figure that, given the information on the sign of ρ_1, it is possible in principle to determine the sign of Δm from the sign of R near the plate on the basis of even a single point at some arbitrary x_0. For $\varphi \approx \pi/6$ the ratio R amounts to ~ 0.08. In other words, given approximately 350 leptonic decays we should get 190 decays into leptons of one sign and 160 decays into leptons of the other sign, which insures a statistically reliable determination of the sign of R, hence of Δm.

It must, however, be kept in mind that the events of interest take place at a distance from the plate of the order of a decay length $\gamma\tau_1 v$ of the K_1^0, so that all leptonic decays in that distance will be rare. In order to obtain 350 leptonic decays in the region of interest it is necessary to transmit $\sim (\tau_2/\tau_1) \cdot 350 = 175{,}000$ K_2^0 mesons. However one should not forget that in the proposed experiment for the determination of the sign of Δm it is not necessary to observe the oscillation, it being sufficient to determine the sign of R at one point. We note that with increasing energy of the K_2^0 mesons the ordinates of the curves increase as well as the region near the plate, in which for a given φ the ratios R differ in sign for opposite signs of Δm.

If one takes into account the difficulties connected with the sign of the difference of the real parts of $\bar{f}(0) - f(0)$ for two plates and of the quantity $\Delta\varphi$, then one might conclude that the utilization of interference phenomena in leptonic decays of K^0 mesons represents a real possibility for the determination of the sign of Δm.

In order to improve the statistics one could integrate the ratio R, Eq. (4), over x_0 between 0 and $\sim\gamma\tau_1 v$, where the sign effect is most pronounced, and study the dependence of the resultant quantity on the plate thickness x. In that case the integral of R, corresponding to the curves a, b and c in the figure, will be for x less than optimal a positive increasing function of x, whereas for the curves a_1, b_1 and c_1 the integral will be negative and increasing in absolute magnitude with the plate thickness.

The author is indebted to I. Yu. Kobzarev, Z. Sh. Mandzhavidze, L. B. Okun', B. M. Pontecorvo, K. A. Ter-Martirosyan and G. E. Chikovani for a number of valuable remarks and discussion of theoretical and experimental problems, connected with this work.

I express gratitude to G. I. Lebedevich for carrying out numerical calculations.

[1] I. Yu. Kobzarev and L. B. Okun', JETP **39**, 605 (1960), Soviet Phys. JETP **12**, 426 (1960).

[2] S. G. Matinyan, JETP **39**, 1747 (1960), Soviet Phys. JETP **12**, 1219 (1960).

[3] N. Biswas, Phys. Rev. **118**, 866 (1960).

[4] L. B. Okun', JETP **34**, 469 (1958), Soviet Phys. JETP **7**, 322 (1958).

[5] Melkanoff, Price, Stork, and Ticho, Phys. Rev. **113**, 1303 (1959).

[6] Melkanoff, Prowse, and Stork, Phys. Rev. Lett. **4**, 183 (1960).

[7] M. L. Good, Phys. Rev. **106**, 591 (1957).

[8] F. Muller et al., Phys. Rev. Lett. **4**, 418 (1960).

[9] R. W. Birge, Proc. of the Tenth Rochester Conf. on High Energy Physics (1961).

Translated by A. M. Bincer
256

A NEW METHOD OF CALCULATING THE ENERGY SPECTRUM OF CARRIERS IN SEMICONDUCTORS. II. ACCOUNT OF SPIN-ORBIT INTERACTION

G. E. PIKUS

Institute of Semiconductors, U.S.S.R. Academy of Sciences

Submitted to JETP editor, May 11, 1961

J. Exptl. Theoret. Phys. (U.S.S.R.) 41, 1507-1521 (November, 1961)

The method previously developed for constructing the Hamiltonian in the effective-mass approximation is generalized for the cases when spin-orbit interaction must be taken into account. This method is used to calculate the change of the energy spectrum when semiconductors with wurtzite or germanium lattices are deformed.

1. INTRODUCTION

In the first part of the present work,[1] a general method was developed for constructing the Hamiltonian $\mathcal{D}$ in the effective mass approximation; the method was based directly on the symmetry conditions and the invariance of the Schrödinger equation to time inversion. We shall consider how spin-orbit interaction can be accurately included in the framework of this method. We retain the notation of[1], and when referring to formulae from it we use the prefix I before the number of the formula.

To calculate $\mathcal{D}$ including spin-orbit interaction two procedures are possible: in the Hamiltonian $\hat{\mathcal{H}}$ the term describing the spin-orbit interaction for $V(\mathbf{r}) = V_0(\mathbf{r})$

$$\hat{\mathcal{H}}_{s.o.} = -(i/4m^2c^2)([\nabla V_0, \nabla]\hat{\sigma}),$$

can, on the one hand, be included in $\hat{\mathcal{H}}_1$, i.e., considered as a perturbation, since the interaction is relatively small; on the other hand, since $\hat{\mathcal{H}}_{s.o.}$ does not depend on $\mathcal{K}$ and has the same symmetry as $\hat{\mathcal{H}}_0$, this term can be immediately included in $\hat{\mathcal{H}}_0$, and only those terms describing the spin-orbit interaction which included $\mathcal{K}$ are retained in $\hat{\mathcal{H}}_1$.

In the first case the spin functions will appear in the smooth functions F_i in (I.2), and the basis functions $\varphi_{i\mathbf{k}_0}$ will, as before, depend only on the coordinates. In the second case, however, $\varphi_{i\mathbf{k}_0}$ will include functions of the spin variables, and F_i will not.

We shall consider both these methods.

2. $\hat{\mathcal{H}}_{s.o.}$ INCLUDED IN $\hat{\mathcal{H}}_1$

In this case the functions F_i depend both on the coordinates and on the spin variable α, which can take the two values $\pm 1/2$. Correspondingly, $\mathcal{D}$ depends both on the operators $\hat{\mathcal{K}}$, which act on the coordinate functions, and on the operators $\hat{\sigma}_i$, which act on the spin functions. The operator $\mathcal{D}$ can, as previously, be expressed in terms of basis matrices and written in the form (I.9), but now $f(\mathcal{K})$ will contain not only functions of the quantities k_i, H_i, ϵ_{ij}, etc., and their products, but also linear functions of $\hat{\sigma}_i$, which describe the spin-orbit splitting at the point $\mathbf{k}_0$, and functions of the products of $\hat{\sigma}_i$ and the remaining variables. In accord with (I.11) all these functions must be chosen so that they transform according to the irreducible representations of the point group $\bar{G}$, corresponding to the wave vector group $G_{\mathbf{k}_0}$. It is clear that the $\hat{\sigma}_i$ themselves transform as the components of an axial vector, and $\mathcal{D}$ must be constructed so that the terms entering in it satisfy condition (I.10). The constants C_s^{rt} for the terms containing $\hat{\sigma}_i$ are then small quantities relative to the other corresponding constants—of the order β^2, where $\beta = v/c$. Since in[1] the form of the operators appearing in $\mathcal{D}$ was nowhere precisely specified, but was denoted by the general symbol $\mathcal{K}$, it is clear that all the results of[1], in particular the formula for determining n_s taking into account the invariance to time inversion, and the methods for constructing $\mathcal{D}$, remain valid in the present case also. When determining γ in (I.18) it must be remembered that $\hat{\sigma}_i$ are odd functions, since, when changing t into $-t$ in $\hat{\mathcal{H}}$ it is necessary to change $\hat{\sigma}_i$ into $-\hat{\sigma}_i$.[2]

To construct $\mathcal{D}$ it is convenient to choose at once $F_i(\mathbf{r}, \alpha, t)$ in the form of products of coordinate functions $F_{i,\alpha}(\mathbf{r}, t)$ and spin functions α. Then the system (I.3) takes the form

$$\mathcal{D}_{ij}(\mathcal{K})F_{j,\beta}\cdot\beta = i\hbar\alpha\partial F_{i,\alpha}/\partial t.$$

Hence we obtain the system of equations determining the coordinate functions $F_{i,\alpha}$:

$$\mathcal{D}_{i\alpha,j\beta}(\mathcal{K}')F_{j,\beta} = i\hbar\partial F_{i,\alpha}/\partial t, \quad (1)$$

where

$$\mathcal{D}_{i\alpha,j\beta}(\mathcal{K}') = \langle\alpha|\mathcal{D}_{ij}(\mathcal{K})|\beta\rangle.$$

In $\mathcal{K}'$ in (1) the operators $\hat{\sigma}$ are, of course, not included.

If the matrices A^t_{sl} are formed by one of the methods given in [1], it is easy to set up $\mathcal{D}$ in (1). The functions $f^r_{sl}(\mathcal{K})$ in $\mathcal{D}$ are now products of functions of all the operators $\mathcal{K}'$, including unity, and the spin operators $\hat{\sigma}_r$, which are linear combinations of the Pauli operators or the unit operator, i.e.,

$$f^r_{sl}(\mathcal{K}) = f^r_{sl}(\mathcal{K}')\,\hat{\sigma}_r. \quad (2)$$

Therefore, if

$$\mathcal{D}(\mathcal{K}) = \sum_{t,r,s,l} C^{tr}_s A^t_{sl} f^r_{sl}(\mathcal{K}),$$

then

$$\mathcal{D}(\mathcal{K}') = \sum_{t,r,s,l} C^{tr}_s A^{tr}_{sl} f^r_{sl}(\mathcal{K}'). \quad (3)$$

Here $\mathcal{D}(\mathcal{K}')$ is expressed in terms of matrices A^{tr}_{sl} of rank $2n \cdot 2n$, which are constructed in the basis $\varphi_{i\mathbf{k}_0} \cdot \alpha$, with the matrix elements

$$A^{tr}_{sl,i\alpha,j\beta} = A^t_{sl,ij}\,\hat{\sigma}_{r\alpha\beta}. \quad (4)$$

Knowing the matrices A^t_{sl} it is possible to construct at once these matrices also, since $\hat{\sigma}_r$ is either a unit matrix or a combination of Pauli matrices determined from (2).

3. $\hat{\mathcal{H}}_{s.o.}$ INCLUDED IN $\hat{\mathcal{H}}_0$

The functions $\varphi_{i\alpha} = \varphi_{i\mathbf{k}_0} \cdot \alpha$ which are the basis of the matrices $\mathcal{D}(\mathcal{K}')$ in (3) transform according to the double-valued representation T', which is the direct product of the representation T_0 and the double-valued representation $T'_{1/2}$, according to which the spin functions α transform: $T' = T_0 \times T'_{1/2}$. This representation T' is in general reducible, and decomposes into the irreducible representations T'_0. If the spin-orbit splitting is sufficiently large, it is often not necessary to consider together all these representations, and it is sufficient to set up $\mathcal{D}$ only for one of the irreducible double-valued representations T'_0 corresponding to the extremum point. Of course, this matrix can also be obtained from (3); however, in the present case it is simpler to include at once $\hat{\mathcal{H}}_{s.o.}$ in $\hat{\mathcal{H}}_0$, and to choose as basis the eigen functions $\varphi'_{i\mathbf{k}_0}(\mathbf{r},\alpha)$ of the Hamiltonian $\hat{\mathcal{H}}'_0 = \hat{\mathcal{H}}_0 + \hat{\mathcal{H}}_{s.o.}$, which transform according to the representation T'_0. As before $\mathcal{D}$ can be written in the form (I.9), where $\mathcal{K}$ does not, of course, contain the operators $\hat{\sigma}$. Obviously, it is also possible to proceed when the representation $T' = T_0 \times T'_{1/2}$ is irreducible. In this case the n^2 linearly independent matrices A^t_{sl} are the basis for constructing $\mathcal{D}$, where n is the dimension of a representation T'_0. It is obvious here that Eq. (I.8) remains in force, i.e., these matrices transform according to the representations T_s contained in the product $T'_0 \times T'^*_0$. For $\chi_0(G)$ in (I.8) must now be understood the characters of the double-valued representation T'_0. If, as usual,[3] a new element $Q = C_{2\pi}$ is introduced to the group $G_{\mathbf{k}_0}$, in order to change it from a double-valued representation to a single-valued, the summation in (I.8) must be made over all the elements of this new group $G'_{\mathbf{k}_0}$, and h is to be understood as the number of elements in it. The characters of the corresponding representation of this group will be denoted below by $\chi'_0(G)$. The result of the calculations will, of course, be the same as when the double-valued representations of the group $G_{\mathbf{k}_0}$ are used. It is clear that the matrices A_{sl} and $f_{sl}(\mathcal{K})$ transform according to single-valued representations, i.e., the representations T_s of the point group $\bar{G}$, for which $Q = E$, while for the representations T'_0 we have $\chi'(Q) = -\chi'(E)$.

We now consider the additional conditions imposed on $\mathcal{D}$ in the present case by the time inversion invariance conditions. In distinction from (I.1), we now have $\hat{\mathcal{H}}_0^* \neq \hat{\mathcal{H}}_0$, since $\hat{\mathcal{H}}_0$ now includes an imaginary term $\hat{\mathcal{H}}_{s.o.}$. In order to obtain from $\hat{\mathcal{H}}^*$ a Hamiltonian coinciding with $\hat{\mathcal{H}}$, it is now inadequate to replace H_i by $-H_i$ and k_i by $-k_i$, and it is necessary to perform a unitary transformation[2] S', so that $S'\hat{\mathcal{H}}^*_{s.o.}S'^{-1} = \hat{\mathcal{H}}_{s.o.}$, or $\hat{S}'\hat{\sigma}_i^*S'^{-1} = -\hat{\sigma}_i$; consequently $\hat{S}' = \hat{\sigma}_y$. Here, as in [1], the Hamiltonian $S\hat{\mathcal{H}}'S^{-1} = \hat{\mathcal{H}}$. Here $\hat{S}$ is the Wigner operator, $\hat{S} = \hat{S}_0\hat{S}'$, where $\hat{S}_0$ is the complex conjugate operator. Therefore, the functions $\hat{S}\Psi'$, as well as the functions Ψ, are eigen functions of $\hat{\mathcal{H}}$, corresponding to the same eigen values E and k. The stroke denotes, as in (I.12) the replacement of H_i by $-H_i$ and of k_i by $-k_i$; the change of sign for $\hat{\sigma}_i$ in $\hat{\mathcal{H}}^*$ is now performed by the unitary transformation S'.

From the conjugate equation we again obtain the system (I.12), but now the functions $\hat{S}\varphi_{i\mathbf{k}_0}(\mathbf{r},\alpha) = \hat{\sigma}_y\varphi^*_{i\mathbf{k}_0}(\mathbf{r},\alpha)$ are the basis of $\mathcal{D}^*$ in (I.12), whilst the functions $\varphi_{i\mathbf{k}_0}(\mathbf{r},\alpha)$ are the basis of $\mathcal{D}$ in (I.3). For brevity in what follows,

we shall not write out the arguments of these functions.

If a linear relationship exists between the functions $\hat{S}\varphi_i$ and φ_i, then, as previously, additional conditions are imposed on $\mathcal{D}$. According to,[2] for double-valued representations such a relationship occurs in case c; in cases a and $b_{1,2}$ additional degeneracy occurs. If $\mathbf{k}_0$ and $-\mathbf{k}_0$ belong to different stars (i.e., in case b_3), then, as previously, no additional conditions, apart from (I.6), are imposed on $\mathcal{D}$.

We now consider separately all the cases when time inversion imposes new conditions on $\mathcal{D}$.

The methods of derivation are basically the same as in Sec. 3[1]; without presenting details we emphasize only the points where there are differences.

Case c: the representations T_0' and $T_0'^*$ complex and equivalent.

1) c_1; $\mathbf{k}_0$ equivalent to $-\mathbf{k}_0$.

In this case, analogously to (I.14), the functions $\hat{S}\varphi_i$ can be expressed linearly in terms of φ_i:

$$\hat{S}\varphi_i = \hat{\sigma}_y\varphi_i^* = S_{i'i}\varphi_{i'}. \tag{5}$$

However, in distinction from (I.15) we now have $\hat{S}\hat{S} = -1$; therefore,

$$S = -S^{*-1} = -\tilde{S}. \tag{6}$$

Hence, it is apparent that in the present case $\mathcal{D}$ satisfies the relations (I.16) and (I.17), and A^t_{sl} the relation (I.19). However, since now, according to (6), $SG^*S^* = -SG^*S^{-1} = -G$, then from (I.19), instead of (I.20), we obtain

$$n_s = \frac{1}{2h}\sum_{G\in\bar{G}'_{\mathbf{k}_0}}\chi_l(G)\,[\chi_0'^2(G) - \gamma\chi_0'(G^2)]. \tag{7}$$

Consequently, for even functions ($\gamma = 1$) the quantity n_s is equal to the number of representations T_s contained in the antisymmetric product $\{T_0'^2\}$, and for odd ($\gamma = -1$) in the symmetric product $[T_0'^2]$.

2) c_2; $\mathbf{k}_0$ not equivalent to $-\mathbf{k}_0$.

In this case, analogously to (I.21a), the functions $\hat{R}\hat{S}\varphi_i$ are linearly expressed in terms of φ'_i, and since $\hat{R}$ commutes with S, and $\hat{S}^2 = -1$, then $RS\varphi_i = R_{i'i}\varphi_{i'}$; but

$$R\varphi_i = -R^*_{i'i}\hat{S}\varphi_{i'}. \tag{8}$$

Now, therefore, in distinction from (I.23),

$$(R^{-1})_{ij} = -R_{ij}^{*-1} = -R_{ji}. \tag{9}$$

Consequently, $\mathcal{D}$, as previously, satisfies (I.22), and A^t_{sl} satisfies (I.24), but, since now $(R^2)_{ii} = R_{iJ}R_{Ji} = -R_{ij}R^*_{ji}$, the quantity n_s, in distinction from (I.25), is equal to

$$n_s = \frac{1}{2h}\sum_{G\in\bar{G}'_{\mathbf{k}_0}}[\chi_s(G)\,|\,\chi'_{\delta_0}(G)\,|^2 - \gamma\chi_s(R_0G)\,\chi'_0(R_0G)^2]. \tag{10}$$

Cases a and b: the representations T_0' and $T_0'^*$ real or complex non-equivalent.

1) a_1 and b_1; $\mathbf{k}_0$ equivalent to $-\mathbf{k}_0$

In these cases the functions φ_i and $\hat{S}\varphi_i$ are linearly independent and are united in a single representation. The matrix D is constructed on the basis φ_i and $\varphi_I = \hat{S}\varphi_i$, but D'^* is constructed on the basis $\bar{\varphi}_i = \hat{S}\varphi_i$ and $\bar{\varphi}_I = \hat{S}\varphi_I = \hat{S}^2\varphi_i = -\varphi_i$. Therefore, in distinction from (I.26b), now

$$\mathcal{D}'_{Ji} = -\mathcal{D}_{Ij}. \tag{11}$$

Correspondingly, instead of (I.27)

$$A_{sl,\,Ij} = -\gamma A_{sl,\,Ji}. \tag{12}$$

Therefore, for the "non-diagonal" terms n_s is now determined by (7), and for the diagonal ones, as before, by (I.8).

2) a_2 and b_2; $\mathbf{k}_0$ not equivalent to $-\mathbf{k}_0$

Here the functions φ_i and $\varphi_I = R_0S\varphi_i$ are united into a single representation. The matrix $\mathcal{D}$ is also written in this basis. Then $\mathcal{D}'^*$ is written in the basis $\bar{\varphi}_i = \hat{S}\varphi_i$ and $\bar{\varphi}_I = \hat{S}\varphi_I = -R_0\varphi_i$; therefore, instead of (I.29), $\bar{\varphi}_I = (R_0R)_{i'i}\,\bar{\varphi}_{i'}$, and $\varphi_i = -(RR^{-1})_{i'i}\,\bar{\varphi}_{I'}$. Correspondingly, instead of (I.30b) and (I.31), we obtain

$$\mathcal{D}_{Ij}(\mathcal{K}) = -(RR_0^{-1})_{j'j}\,\mathcal{D}'_{J'I'}(\hat{R}\mathcal{K})\,(R_0R)_{i'i} \tag{13}$$

and

$$A^t_{sl,\,Ij} = -\gamma\,(RR_0^{-1})_{i'j}\,(R_0R)_{j'j}\,R^{*s}_{i'i}A^t_{sl',\,i'j'}. \tag{14}$$

Hence, it follows that for the "non-diagonal" elements n_s is determined from (10), while for diagonal elements (I.8) is retained.

From (I.8), (7), and (10) the formulae derived previously by Sheka[4] are obtained for determining the points of zero slope for the double-valued representations.

We shall deal briefly with the methods of constructing the basis matrices $A^t_{s,l}$ and the matrix $\mathcal{D}$ for double-valued representations.

These methods do not differ from those described in[1], Sec. 4. It is clear that each of the terms in $\mathcal{D}$ must satisfy condition (I.10). If the group $G_{\mathbf{k}_0}$ is equivalent to the point group $\bar{G}$, the basis for A^t_{sl} can be chosen to be the eigen functions of this group, which can consist of the eigen functions of the space group $D^{\pm}_j$ with the

Table I. The distribution of $f(\mathcal{K})$ and $\varphi(J)$ over the representations Γ and K (wurtzite)

Representation		$f(\mathcal{K})$		$\varphi(J)$	
Γ	K	Odd	Even	For equation (15)	For equation (20)
Γ_1	K_1	k_z	$k_z^2;\ k_\perp^2;\ \varepsilon_{zz};\ \varepsilon_\perp;\ \sigma_+ k_- - \sigma_- k_+$	$I,\ J_z^2$	—
Γ_4		—	—	—	$J_+^3 - J_-^3$
Γ_2	K_2	σ_z	$\sigma_z k_z,\ \sigma_+ k_- + \sigma_- k_+$	J_z	J_z^3
Γ_3		—	—	—	$J_+^3 - J_-^3$
Γ_5	K_3	—	$k_+^2, k_-^2;\ \varepsilon_+, \varepsilon_-;$ $\sigma_+ k_+,\ \sigma_- k_-$	J_+^2, J_-^2	$[J_z J_+^2], [J_z J_-^2]$
Γ_6		σ_+, σ_- k_+, k_-	$k_+ k_z, k_- k_z;\ \varepsilon_{+z}, \varepsilon_{-z};$ $\sigma_+ k_z, \sigma_- k_z;\ \sigma_z k_-, \sigma_z k_-$	J_+, J_- $[J_+ J_z], [J_- J_z]$	$[J_+ J_z^2], [J_- J_z^2]$

Note: $k_\pm = k_x \pm i k_y$, $J_\pm = (J_x \pm i J_y)/\sqrt{2}$, $\varepsilon_\pm = \varepsilon_{xx} \pm 2i\varepsilon_{xy} - \varepsilon_{yy}$, $\varepsilon_{\pm z} = \varepsilon_{xz} \pm i\varepsilon_{yz}$, $\varepsilon_\perp = \varepsilon_{xx} + \varepsilon_{yy}$.

corresponding half-integral values of j, and the matrices A_{sl} can be chosen to be the matrices of the functions of the components of the axial vector $\varphi_{sl}(\hat{J}_i)$, which transform according to the representation T_s, constructed in this basis as was shown in Part 1, Sec. 3 of [1]. The additional conditions associated with time inversion must be included separately. In case c_1, (I.38) is now satisfied, since here also $\hat{S}^4 = 1$; consequently, $\hat{\mathcal{D}}$ can contain only even products of $f(\mathcal{K})$ and $\varphi(\hat{J})$, which do not change sign when changing the signs of k_i, H_i and J_i. In the other cases it is necessary to use the general formulae given above.

If the representation T_0' is two-dimensional, $\mathcal{D}$ can be constructed by the method discussed in Part 4, of Sec. 4 of [1]. When necessary, D can also be constructed here for a combined representation which includes several irreducible representations. However, if all these representations arise as a result of the spin-orbit splitting of one representation T_0, i.e., are contained in $T' = T_0 \times T_{1/2}$, then the first method is more convenient for their simultaneous consideration. This method is especially convenient when the double-valued representation—reducible or irreducible—arises from a two-dimensional single-valued representation, since then the construction of the matrices A_{sl} is performed in the simple way as described in Part 4 of Sec. 4[1]. The defect of the second method is the difficulty in determining the order of the coefficients C_s^{tr}. Whereas in the first method the coefficients of the first order of smallness in β^2 are determined at once (the coefficients in $f(\mathcal{K})$ containing σ_i), to do this by the second method requires as a rule additional comparison. To do this, for example, one can compare the general expressions for $\mathcal{D}$, obtained by both methods, and consider how they turn into one another for weak spin-orbit interaction, as is done, for example, in[5] (Appendix B). It is not, of course, necessary to write out in explicit form the matrices $\varphi_{sl}(J)$ for both cases.

Below we consider a number of examples where both methods are used.

4. THE EFFECT OF DEFORMATION ON THE ENERGY SPECTRUM OF WURTZITE-TYPE CRYSTALS

In[1] we considered the effect of deformation on the spectrum of wurtzite-type crystals ignoring spin-orbit interaction. The formulae obtained are valid when the splitting of the bands due to spin-orbit interaction is small in comparison with both kT and the splitting caused by the deformation.

Of the crystals in this group CdS has been studied best. By analyzing experimental data on the absorption and reflection of light in these crystals, Birman[6] and Thomas and Hopfield[7] con-

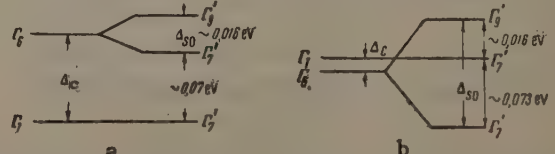

Genesis of the bands: a – according to Birman[6], b – according to Thomas and Hopfield.[7]

cluded that the extremum of the valence band in CdS lies on the Δ axis, apparently at the point Γ ($k = 0$), where the wave functions at the extremum point, ignoring spin-orbit interaction, transform according to the representation Γ_6 (in the notation of[8]).

However, the representation Γ_1 also lies close to the edge of the band at a distance Δ_C from it. Owing to spin-orbit interaction, the representation Γ_6 is split into two double-valued representations Γ_7' and Γ_9', where Γ_9' corresponds to the maximum energy of the electrons, and Γ_1 goes over to Γ_7'. According to[6], the spin-orbit splitting Δ_{S0} is smaller than Δ_C but comparable with it, whereas, according to[7], Δ_{S0} is greater than Δ_C. The geneses of the bands according to[6,7] are shown schematically in the figure. We consider the effect of deformation on the spectrum of CdS for both these models. Thus, we must construct $\mathscr{D}$ simultaneously for both the representations Γ_1 and Γ_6. We first write down $\hat{\mathscr{D}}$, using the first method. The characters of the single-valued representations at the point Γ calculated by Rashba[8] are given in Table I in[1]. Both the representations Γ_1 and Γ_6 belong to case a_1; therefore, according to (I.20), there must appear in $\hat{\mathscr{D}}$ even functions of $\mathscr{K}$ which transform according to the representations $\left[(\Gamma_1 + \Gamma_6)^2\right] = 2\Gamma_1 + \Gamma_5 + \Gamma_6$, and odd functions which transform according to $\{(\Gamma_1 + \Gamma_6)^2\} = \Gamma_2 + \Gamma_6$.

In addition to the functions given in Table III of[1], we now include in $\mathscr{D}$ terms with $\hat{\sigma}_i$ not dependent on $\mathbf{k}$ and linear in $\mathbf{k}$. All these functions are given in Table I. Also given are nine functions $\varphi(\hat{\mathbf{J}})$ transforming according to the representations quoted above. Using these functions, we form $\hat{\mathscr{D}}$ in accord with the requirements of Part 1 of Sec. 4[1]:

$$\begin{aligned}\hat{\mathscr{D}} = {} & \Delta_1 J_z^2 + \Delta_2 J_z \hat{\sigma}_z + \Delta_3 (\hat{\sigma}_+ J_- + J_- \hat{\sigma}_+) + B_1 k_z^2 + B_2 k_\perp^2 \\ & + B_3 (J_+^2 k_-^2 + J_-^2 k_+^2) + B_4 J_z^2 k_z^2 + B_5 J_z^2 k_\perp^2 \\ & + B_6 k_z ([J_z J_+] k_- + [J_z J_-] k_+) + iB_7 (k_+ J_- - k_- J_+) \\ & + i(\beta_1 + \beta_3 J_z^2)(\hat{\sigma}_+ k_- - \hat{\sigma}_- k_+) + i\beta_2 (J_+^2 k_- \hat{\sigma}_- - J_-^2 k_+ \hat{\sigma}_+) \\ & + i\beta_4 \hat{\sigma}_z ([J_z J_+] k_- - [J_z J_-] k_+) + i\beta_5 k_z ([J_z J_+] \hat{\sigma}_- \\ & - [J_z J_-] \hat{\sigma}_+) + C_1 \varepsilon_{zz} + C_2 \varepsilon_\perp + C_3 J_z^2 \varepsilon_{zz} + C_4 J_z^2 \varepsilon_\perp \\ & + C_5 (J_-^2 \varepsilon_+ + J_+^2 \varepsilon_-) + C_6 ([J_z J_+] \varepsilon_{+z} + [J_z J_-] \varepsilon_{-z}).\end{aligned} \tag{15}$$

Here

$$2[J_i J_j] = J_i J_j + J_j J_i, \qquad \varepsilon_{\pm z} = \varepsilon_{xz} \pm i\varepsilon_{yz},$$

$$\varepsilon_+ = \varepsilon_{xx} \pm 2i\varepsilon_{xy} - \varepsilon_{yy}, \qquad \varepsilon_\perp = \varepsilon_{xx} + \varepsilon_{yy},$$

$$k_\pm = k_x \pm ik_y, \qquad k_\perp^2 = k_x^2 + k_y^2.$$

We shall not write out $\mathscr{D}$ in a general form, but consider limiting cases.

1. $\Delta_C \gg \Delta_{S0}$. In this case it is possible to ignore the representation Γ_1. Then $\hat{\mathscr{D}}$ must contain only matrices which transform according to the representations $\Gamma_6 \times \Gamma_6 = \Gamma_1 + \Gamma_2 + \Gamma_5$, i.e., 1, J_z^2, J_+^2 and J_-^2. Since the representation Γ_6 is twofold degenerate, and the functions $f(\mathscr{K})$ were chosen in accordance with the requirements of Part 4 of Sec. 4[1], the matrices of these operators, according to (I.46), can be put, respectively, equal to I, σ_z, σ_+, and σ_-. (In fact, this corresponds to a choice of the basis functions in the form $u_\pm = (\pm x - iy)/\sqrt{2}$.)

If we now write, in accordance with (I.4), the matrix $\mathscr{D}$ in the basis $u_-\alpha_+$, $u_+\alpha_-$, $u_+\alpha_+$, $u_-\alpha_-$, we obtain

$$\mathscr{D} = \begin{vmatrix} \lambda - \Delta_2 & F & G & I \\ F^* & \lambda - \Delta_2 & I^* & G^* \\ G^* & I^* & \lambda + \Delta_2 & 0 \\ I^* & G & 0 & \lambda + \Delta_2 \end{vmatrix}, \tag{16}$$

where $\lambda = B_1 k_z^2 + B_2 k_\perp^2 + C_1 \epsilon_{zz} + C_2 \epsilon_\perp$, $F = -i\beta_2 k_+$, $G = B_3 k_+^2 + C_3 \epsilon_+$, $I = i\beta_1 k_-$, $\Delta_2 = \Delta_{S0}/2$. Here the constants β_i are of the first order of smallness with respect to β^2, and the remaining constants of zero order. If we omit the terms associated with the deformation, this matrix coincides with that obtained previously by Rashba and Sheka.[9]

The secular equation $\|\mathscr{D} - E\| = 0$ according to (16) has the form

$$\begin{aligned}(\lambda - E')^2 [(\lambda - E' - 2\Delta_2)^2 - |F|^2] - 2(\lambda - E')[(\lambda - E' \\ - 2\Delta_2)(|I|^2 + |G|^2) - I^* F G^* - I F^* G] \\ + (|G|^2 - |I|^2)^2 = 0.\end{aligned} \tag{17}$$

Here $E' = E - \Delta_2$, i.e., the energy of the electrons measured relative to the edge of the valence band.

If, in this equation, of the terms proportional to β^2, only those not dependent on $\mathbf{k}$ are retained, its solution will be

$$\begin{aligned}E' = \lambda - \Delta \pm \{\Delta^2 + B_2^2 k_\perp^4 + 2B_3 C_3 [(k_x^2 - k_y^2)(\varepsilon_{xx} - \varepsilon_{yy}) \\ + 4\varepsilon_{xy} k_x k_y] + B_3^2 [(\varepsilon_{xx} - \varepsilon_{yy})^2 + 4\varepsilon_{xy}^2]\}.\end{aligned} \tag{18}$$

Close to the extremum, i.e., for $E' \ll \Delta_{S0}$

$$E = \lambda + 2B_3 C_3 [(k_x^2 - k_y^2)(\varepsilon_{xx} - \varepsilon_{yy}) + 4\varepsilon_{xy} k_x k_y]/\Delta_{S0}. \tag{19}$$

It follows from (18) that when Δ_{S0} exceeds both kT and the splitting of the bands due to the deformation, the deformation causes only a change of the effective masses. These changes are relatively large—of the order $C_3\epsilon/\Delta_{S0}$; comparatively large values of the piezo-resistance constants Π_{xxxx}, Π_{xxyy}, and Π_{xyxy}, can therefore be expected here; however, in distinction from the case considered in Sec. 5 of[1], these coefficients are now proportional to C_3/Δ_{S0}, i.e., they do not depend on temperature.

Table II. Characters of the double-valued representations for the point Δ (wurtzite)

Number of elements	Elements of the class	Δ_7'	Δ_8'	Δ_9'
1	$(\varepsilon\|0)$	2	2	2
1	$(\bar{\varepsilon}\|0)$	−2	−2	−2
2	$\left(\delta_6, \bar{\delta}_6^5 \middle\| \frac{t_0}{2}\right)$	$\sqrt{3}\,\eta_k$	$-\sqrt{3}\,\eta_k$	0
2	$(\delta_6^2, \bar{\delta}_6^4\|0)$	1	1	−2
2	$(\delta_6^4, \bar{\delta}_6^2\|0)$	−1	−1	2
2	$\left(\delta_6^5, \bar{\delta}_6 \middle\| \frac{t_0}{2}\right)$	$-\sqrt{3}\,\eta_k$	$\sqrt{3}\,\eta_k$	0
2	$\left(\delta_6^3, \bar{\delta}_6^3 \middle\| \frac{t_0}{2}\right)$	0	0	0
6	$(\sigma_1, \sigma_2, \sigma_3\|0), (\bar{\sigma}_1, \bar{\sigma}_2, \bar{\sigma}_3\|0)$	0	0	0
6	$(\sigma_1', \sigma_2', \sigma_3'\|\frac{t_0}{2}), (\bar{\sigma}_1', \bar{\sigma}_2', \bar{\sigma}_3'\|\frac{t_0}{2})$	0	0	0

Note: $\eta_k = \exp\{ik_{z0}t_0/2\}$; for the point Γ the quantity $\eta_k = 1$.

2. $\Delta_{so} \gg \Delta_c$. In this case we can consider only the two split-off half-integral representations Γ_9' and Γ_7'. The corresponding expression for $\mathcal{D}$ can be obtained from (15); it is, however, more convenient here to use the second method, and to consider only these two representations. In Table II are given the characters of the double-valued representations at the point Δ, calculated by Rashba and Sheka.[9]*

The representations Γ_9' and Γ_7' belong to case c_1, and therefore, according to (7), $\mathcal{D}$ contains even functions of $\mathcal{K}$ which transform according to the representations $\{(\Gamma_7' + \Gamma_9')^2\} = 2\Gamma_1 + \Gamma_5 + \Gamma_6$, and odd functions which transform according to $[(\Gamma_7' + \Gamma_9')^2] = 2\Gamma_2 + \Gamma_3 + \Gamma_4 + \Gamma_5 + \Gamma_6$. These functions can be chosen from Table I. In the same table are given sixteen corresponding functions $\varphi(\mathbf{J})$ that transform according to these representations. Here, as shown above, can appear in $\mathcal{D}$ in case c_1 products only of even functions of $\mathcal{K}$ and $\mathbf{J}$, or only of odd.

We construct $\hat{\mathcal{D}}$ following Part 1 of Sec. 4 of [1]:

$$\begin{aligned}\hat{\mathcal{D}} = {} & \delta_1 J_z'^2 + B_1 k_z^2 + B_2 k_\perp^2 + \frac{2B_3}{\sqrt{3}}(J_+^2 k_-^2 + J_-^2 k_+^2) + B_4 J_z'^2 k_z^2 \\ & + B_5 J_z'^2 k_\perp^2 + \sqrt{\frac{2}{3}} B_6 J_z k_z ([J_z J_+] k_- + [J_z J_-] k_+) \\ & + i\sqrt{\frac{2}{3}} B_7 (J_+ k_- - J_- k_+) + i\sqrt{\frac{2}{3}} \beta_1 ([J_z''^2 J_+] k_- \\ & - [J_z''^2 J_-] k_+) + C_1 \varepsilon_{zz} + C_2 \varepsilon_\perp + \frac{2}{\sqrt{3}} C_3 (J_+^2 \varepsilon_- + J_-^2 \varepsilon_+) \\ & + C_4 J_z'^2 \varepsilon_{zz} + C_5 J_z'^2 \varepsilon_\perp + \sqrt{\frac{2}{3}} C_6 ([J_z J_+] \varepsilon_{-z} \\ & - [J_z J_-] \varepsilon_{z+}).\end{aligned} \tag{20}$$

Here

$$J_z'^2 = \tfrac{1}{2}\left(\tfrac{9}{4} - J_z^2\right), \qquad J_z''^2 = \tfrac{5}{4} - J_z^2,$$
$$2[J_i J_k] = J_i J_k + J_k J_i.$$

This choice of the numerical coefficients in (20) is made with the aim of obtaining a matrix $\mathcal{D}$ closest to (16), to simplify the comparison of the two cases. The constants B_i and C_i in (16) and (20) are not, of course, identical. In the approximation of weak spin-orbit coupling, these constants can be expressed in terms of one another by the use, for example, of the method mentioned above due to Luttinger.[5]

We shall not make such a comparison, but only point out that from (15) and (20) it follows at once that all the constants B_i and C_i in (20) are of zero order in β^2. Only the constant β_1 for the cubic term in J_i is of the first order of smallness in β^2. Of course, the remaining constants can also include contributions of the same order. The complete set of functions Y_m^j with $j = 3/2$ are the basis for $\mathcal{D}$. Therefore the actual choice of the representation for $\varphi(\mathbf{J})$ can be arbitrary here. The corresponding matrices are given, for example, in,[10] p. 171. In the representation $Y_{-1/2}^{3/2}$, $Y_{+1/2}^{3/2}$, $Y_{+3/2}^{3/2}$, $Y_{-3/2}^{3/2}$, the matrix $\mathcal{D}$ takes the form

$$\mathcal{D} = \begin{vmatrix} \lambda + \theta & F & G & I + H \\ F^* & \lambda + \theta & I^* - H^* & G^* \\ G^* & I - H & \lambda & 0 \\ I^* + H^* & G & 0 & \lambda \end{vmatrix}, \tag{21}$$

where

$$\lambda = B_1 k_z^2 + B_2 k_\perp^2 + C_1 \varepsilon_{zz} + C_2 \varepsilon_\perp,$$
$$\theta = \delta_1 + B_4 k_z^2 + B_5 k_\perp^2 + C_4 \varepsilon_{zz} + C_5 \varepsilon_\perp,$$
$$F = -\frac{2}{\sqrt{3}} i (B_7 + \beta_1) k_+, \qquad G = B_3 k_+^2 + C_3 \varepsilon_+,$$
$$I = iB_7 k_-, \qquad H = B_6 k_- k_z + C_6 \varepsilon_{-z}.$$

*Throughout the tables of the groups the following notation is used for the operators: δ – rotation, ρ – reflection rotation, σ – reflection.

The secular equation $\| \mathcal{D} - E \| = 0$ has the form

$$(\lambda - E)^2 [(\lambda + \theta - E)^2 - |F|^2] - 2(\lambda - E) \times [(\lambda + \theta - E)(|I|^2 + |H|^2 + |G|^2) - FG^*I^* - F^*GI] + |G|^4 - 2|G_*|^2 (|I|^2 - |H|^2) + (I^2 - H^2)(I^{*2} - H^{*2}) = 0. \quad (22)$$

It is not difficult to verify that here, just as in (17), k_x and k_y appear in the terms not containing ϵ only in the combination $k_\perp^2 = k_x^2 + k_y^2$. This means that in the undeformed crystal the extremum in the lowest band Γ_7', is in both cases a ring—with $k_\perp$ = const. However, in distinction from (17), the term in (20) linear in k is not small, since it arises, not due to the spin-orbit interaction, but as a result of the interaction of the two bands Γ_1 and Γ_6. Therefore the extremum can be far from the point k = 0, where terms of the fourth order in k, not included in (20), play an important part.

In the uppermost band Γ_9', which corresponds to the minimum energy of holes, the extremum is at the point k = 0. Close to this point for $E(\mathbf{k}, \epsilon) \ll \delta_1$ we have

$$E = \lambda + \frac{B_7^2}{\delta}\left\{k_\perp^2 + \frac{4C_3}{\sqrt{3}\,\delta}[(k_x^2 - k_y^2)(\varepsilon_{xx} - \varepsilon_{yy}) + 4k_xk_y\varepsilon_{xy}]\right\} + \frac{2}{\delta}\{B_3C_3[(k_x^2 - k_y^2)(\varepsilon_{xx} - \varepsilon_{yy}) + 4k_xk_y\varepsilon_{xy}] + B_6C_6(k_xk_z\varepsilon_{xz} + k_yk_z\varepsilon_{yz})\}. \quad (23)$$

Here we neglect terms of the order $\beta^2 k$, and also ignore the splitting of the bands caused by the deformation and proportional to ϵk, since this splitting leads to effects of higher order in ϵ. It can be expected that the coefficient B_7^2/δ in (23) greatly exceeds B_2. In this case the principal contribution to $m_\perp^* = \hbar^2/2(B_2 + B_7^2/\delta)$ is provided by the interaction of the bands Γ_6 and Γ_1, and the change of the corresponding effective masses under deformation in the plane xy is basically determined by the first term in (23) proportional to $B_7^2C_3/\delta^2$.

We note that, in distinction from (19), a large change of the effective mass and, consequently, of the conductivity also, can occur not only under deformations ϵ_{xx}, ϵ_{yy}, and ϵ_{xy}, but, as seen from (23), also under deformation ϵ_{xz} and ϵ_{yz}.

By the use of Table I it is also easy to construct the operator $\mathcal{D}$ for an arbitrary point on the Δ axis, where an extremum can also exist. At these points time inversion imposes no additional conditions on $\mathcal{D}$, and in it there can appear products of any even and odd functions of $\mathcal{K}$ and J which transform according to conjugate (equivalent) representations.

We shall not linger on this, but consider the spectrum at the point H_3, where there is also a point of zero slope in wurtzite.

3. Spectrum for the representation H_3. To construct $\mathcal{D}$ we use the first method. The characters of the single-valued representations at the point H are given in Table II of [1]. As shown in [1], the representation H_3 belongs to the case a_2, and, according to (I.25), there can appear in $\mathcal{D}$ odd functions transforming according to the representations Γ_2 and Γ_5, and even functions transforming according to Γ_1 and Γ_6.

These functions are given in Table I. The matrices A_{sl} can be chosen according to (I.46). The basis of these matrices will be denoted as φ_1, φ_2.

$$\mathcal{D} = A_1[B_1k_z^2 + B_2k_\perp^2 + i\beta_1(\hat\sigma_+k_- - \hat\sigma_-k_+) + C_1\varepsilon_{zz} + C_2\varepsilon_\perp] + A_2\Delta\hat\sigma_z + A_{31}[B_3k_zk_+ + C_3\varepsilon_{+z} + i\beta_2\hat\sigma_zk_+ + i\beta_3\hat\sigma_+k_z] + A_{32}[B_3k_zk_- + C_3\varepsilon_{-z} - i\beta_2\hat\sigma_zk_- - i\beta_3\hat\sigma_-k_z]. \quad (24)$$

In the basis $(\varphi_1\alpha_+, \varphi_2\alpha_-, \varphi_1\alpha_-, \varphi_2\alpha_+)$ the matrix $\mathcal{D}$ is

$$\mathcal{D} = \begin{vmatrix} \lambda+\Delta & F & G & I+H \\ F^* & \lambda+\Delta & I^*-H^* & G^* \\ G^* & I-H & \lambda-\Delta & 0 \\ I^*+H^* & G & 0 & \lambda-\Delta \end{vmatrix}, \quad (25)$$

where

$$\lambda = B_1k_z^2 + B_2k_\perp^2 + C_1\varepsilon_{zz} + C_2\varepsilon_\perp,$$
$$I = B_3k_zk_+ + C_3\varepsilon_{z+}, \qquad H = i\beta_2k_+,$$
$$F = i\beta_3k_z, \qquad G = i\beta_1k_-.$$

When the terms proportional to ϵ are ignored, this matrix agrees with that obtained previously in [9]. In form (25) is similar to (21), and the secular equation $\| \mathcal{D} - E \| = 0$ is similar to (22). Of course, the explicit form of the matrix elements in (25) and (21) is different. If, of the terms proportional to β^2 in $\mathcal{D}$, we retain only those independent of k, the solution of the secular equation is of the form

$$E = \lambda \pm \{\Delta + B_3^2k_\perp^2k_z^2 + 2B_3C_3(\varepsilon_{xz}k_xk_z + \varepsilon_{yz}k_yk_z) + B_3^2(\varepsilon_{xz}^2 + \varepsilon_{yz}^2)\}^{1/2}. \quad (26)$$

Close to the extremum point for $E' \ll \Delta$

$$E' = E - \Delta = \lambda \pm (B_3C_3/\Delta)(k_xk_z\varepsilon_{xz} + k_yk_z\varepsilon_{yz}). \quad (27)$$

Thus, in distinction from (23) and (19), a significant change of the effective masses occurs here only for deformations ϵ_{xz} and ϵ_{yz}, and large values of the constants $\Pi_{xzxz} = \Pi_{yzyz}$ can be expected.

Consequently, the study of the effects of piezoresistance in these crystals can serve as one of

Table III. Characters of the irreducible representations for the point Γ (germanium)

Number of elements	Elements of the class	Single-valued					Double-valued		
		$\Gamma_1^\pm$	$\Gamma_2^\pm$	$\Gamma_{12}^\pm$	$\Gamma_{15}^\pm$	$\Gamma_{25}^\pm$	$\Gamma_6'^\pm$	$\Gamma_7'^\pm$	$\Gamma_9'^\pm$
1	$(\varepsilon\|0)$	1	1	2	3	3	2	2	4
1	$(\bar{\varepsilon}\|0)$						−2	−2	−4
6	$(\delta_4^2\|0)$, $(\bar{\delta}_4^2\|0)$	1	1	2	−1	−1	0	0	0
6	$(\delta_4\|\tau)$, $(\delta_4^3\|\tau)$	1	−1	0	1	−1	$\sqrt{2}$	$-\sqrt{2}$	0
6	$(\bar{\delta}_4\|\tau)$, $(\bar{\delta}_4^3\|\tau)$						$-\sqrt{2}$	$\sqrt{2}$	0
12	$(\delta_2\|\tau)$, $(\bar{\delta}_2\|\tau)$	1	−1	0	−1	1	0	0	0
8	$(\delta_3\|0)$, $(\delta_3^2\|0)$	1	1	−1	0	0	1	1	−1
8	$(\bar{\delta}_3\|0)$, $(\bar{\delta}_3^2\|0)$						−1	−1	1
48	$(i\|\tau)\times z$	$\pm\chi(z)$							

the methods for determining the positions of the extremum points.

5. THE CHANGE OF THE ENERGY SPECTRUM DUE TO DEFORMATION IN LATTICES OF THE GERMANIUM TYPE

We shall not consider here the spectrum at all the points of zero slope where there are degenerate representations, but limit ourselves to two of them only: the points Γ at the center of the Brillouin zone, and X at its edge on the [001] axis.

1) The point Γ. The characters of the single-valued and double-valued representations of Γ are given in Table III.[11] At this point there are three pairs of degenerate single-valued representations. Two of them, $\Gamma_{15}^\pm$ and $\Gamma_{25}^\pm$, are threefold degenerate (without spin); due to spin-orbit interaction, these representations break up, respectively, into $\Gamma_6^\pm + \Gamma_8^\pm$ and $\Gamma_7^\pm + \Gamma_8^\pm$. To construct the spectrum for the fourfold degenerate representations $\Gamma_8^\pm$, derived from $\Gamma_{15}^\pm$ or $\Gamma_{25}^\pm$, it is more convenient to use the second method. The functions $f(\mathcal{K})$ and $\varphi(\mathbf{J})$ transforming according to the corresponding representations Γ are given in Table IV. Since the representations $\Gamma_8^\pm$ belong to case c_1, then there appear in $\mathcal{D}$, according to Sec. 3, only products of even functions which transform according to the representations $\{\Gamma_8^{\pm 2}\} = \Gamma_1^+ + \Gamma_{12}^+ + \Gamma_{25}^+$, and odd functions which transform according to $[\Gamma_8^{\pm 2}] = \Gamma_2^+ + 2\Gamma_{15}^+ + \Gamma_{25}^+$.

Therefore $\mathcal{D}$ will have the form

$$\hat{\mathcal{D}} = B_1 k^2 + B_2 (J_1 k_2 + J_2 k_1) + B_3 ([J_x J_y] k_x k_y + [J_x J_z] k_x k_z + [J_y J_z] k_y k_z) + C_1 \varepsilon + C_2 (J_1 \varepsilon_2 + J_2 \varepsilon_1) + C_3 ([J_x J_y] \varepsilon_{xy} + [J_x J_z] \varepsilon_{xz} + [J_y J_z] \varepsilon_{yz}), \quad (28)$$

where $R_1 = R_X^2 + \omega R_Y^2 + \omega^2 R_Z^2$, $R_2 = R_1^*$ ($R_i^2 \to J_i^2$, k_i^2 or ϵ_{ii} and $\omega = e^{2\pi i/3}$).

As is well known, the wave functions in germanium and silicon at the extremum point of the valence band transform according to the representation Γ_{25}^+, where the upper of the split-off representations is $-\Gamma_8^+$. Thus (28) describes the

Table IV. The distribution of $f(\mathcal{K})$ and $\varphi(\mathbf{J})$ over the representations Γ (germanium)

Representation	$f(k)$	$f(\varepsilon)$	$f(\sigma)$	$f(\sigma, k)$	$\varphi(\mathbf{J})$	
					Odd	Even
Γ_1^+	k^2	ε	—	—	—	I
Γ_1^-	—	—	—	$k_x\sigma_x + k_y\sigma_y + k_z\sigma_z$	—	—
Γ_2^+	—	—	—	—	$J_xJ_yJ_z + J_zJ_yJ_x$	—
Γ_2^-	—	—	—	—	—	—
Γ_{12}^+	k_1, k_2	ε_1, ε_2	—	—	—	J_1, J_2
Γ_{12}^-	—	—	—	$(k\sigma)_1$, $(k\sigma)_2$	—	—
Γ_{15}^+	—	—	σ_x, σ_y, σ_z	—	J_x, J_y, J_z, J_x^3, J_y^3, J_z^3	—
Γ_{15}^-	k_x, k_y, k_z	—	—	$\{k_x\sigma_y\}$, $\{k_y\sigma_z\}$, $\{k_x\sigma_z\}$	—	—
Γ_{25}^+	k_xk_y, k_xk_z, k_yk_z	ε_{xy}, ε_{xz}, ε_{yz}	—	—	V_x, V_y, V_z	$[J_xJ_y]$, $[J_xJ_z]$, $[J_yJ_z]$
Γ_{25}^-	—	—	—	$[k_x\sigma_y]$, $[k_x\sigma_z]$, $[k_y\sigma_z]$	—	—

Note: $R_1 = R_x + \omega R_y + \omega^2 R_z$, $R_2 = R_1^*$ and $R_i \to k_i^2$, ε_{ii}, $k_i\sigma_i$, J_i^2, $\omega = e^{2\pi i/3}$, $V_x = [J_x(J_y^2 - J_z^2)]$ etc.

Table V. Characters of the representations for the point X (germanium)

Number of elements	Elements of the class	$X_{1,2}$	$X_{3,4}$	Number of elements	Elements of the class	$X_{1,2}$	$X_{3,4}$
1	$(\varepsilon \mid 0)$	2	2	2	$(\sigma_{xy}, \sigma_{x\bar{y}} \mid t)$	±2	0
1	$(\varepsilon \mid t)$	−2	−2	2	$(i \mid \tau, \tau+t)$	0	0
1	$(\delta_{2z} \mid 0)$	2	−2	2	$(\sigma_z \mid \tau, \tau+t)$	0	0
1	$(\delta_{2z} \mid t)$	−2	2	4	$(\delta_{4z}, \delta_{4z}^{-1} \mid \tau, \tau+t)$	0	0
4	$(\rho_{4z}, \rho_{4z}^{-1} \mid 0,t)$	0	0	4	$(\sigma_x, \sigma_y \mid \tau, \tau+t)$	0	0
4	$(\delta_{2x}, \delta_{2y} \mid 0,t)$	0	0	2	$(\delta_{2xy} \mid \tau), (\delta_{2x\bar{y}} \mid \tau+t)$	0	±2
2	$(\sigma_{xy}, \sigma_{x\bar{y}} \mid 0)$	±2	0	2	$(\delta_{2x\bar{y}} \mid \tau), (\delta_{2xy} \mid \tau+t)$	0	∓2

spectrum obtaining in these crystals. Ignoring terms proportional to ϵ, for germanium $\hat{\mathcal{D}}$ in operator form has been given in [5], where all the coefficients B_i are of zero order in β^2; it is not difficult to show that this is also true for the coefficients C_i. The change of the energy spectrum of p germanium under deformation has been considered in detail in [12], where the matrix $\mathcal{D}$ was obtained with the aid of perturbation theory (equation (13)). The same results are, of course, obtained from (28). We shall not, therefore, consider this question in detail here. We merely establish the correspondence between the coefficients in (28) and in [12]

$$B_1 = {}^1/_4\,(4A - 9B), \qquad B_2 = B,$$
$$B_3 = 2/\sqrt{3}D, \qquad C_1 = {}^1/_4\,(4a - 9b), \tag{29}$$
$$C_2 = b, \qquad C_3 = 2/\sqrt{3}d.$$

We now consider the spectrum for the twofold degenerate representation $\Gamma_{12}^{\pm}$. Taking into account spin-orbit interaction, this representation goes over to $\Gamma_8^{\pm}$, i.e., in principle $\mathcal{D}$ is also given here by expression (28). But now some of the coefficients are of order β^2. It is better, therefore, to use the first method: $\mathcal{D}$ will contain even functions of $\mathcal{K}$ transforming according to $[\Gamma_{12}^{\pm 2}] = \Gamma_1^+ + \Gamma_{12}^+$, and odd ones transforming according to $\{\Gamma_{12}^{\pm 2}\} = \Gamma_2^+$.

It is apparent that $\mathcal{D}$ contains no terms of order β^2 which do not depend on $\mathbf{k}$ or are linear in $\mathbf{k}$. Quadratic terms of this order we shall ignore. Then $\hat{\mathcal{D}}$ is

$$\hat{\mathcal{D}} = B_1 k^2 + B_2\,(J_1 k_2 + J_2 k_1) + C_1 \varepsilon + C_2\,(J_1 \varepsilon_2 + J_2 \varepsilon_1). \tag{30}$$

Since this representation is two-dimensional, the matrices J_1 and J_2 in accordance with (I.46) can be chosen to be equal to σ_+ and σ_-. Hence,

$$E = B_1 k^2 + C_1 \varepsilon \pm \Big\{ B_2 \Big(k^4 - 3 \sum_{i>j} k_i^2 k_j^2 \Big) + B_2 C_2 \Big(3 \sum_i k_i^2 \varepsilon_{ii} - k^2 \varepsilon \Big) + {}^1/_2 C_2 \sum_{i>j} (\varepsilon_{ii} - \varepsilon_{jj})^2 \Big\}^{1/2} \tag{31}$$

This differs from Eqs. (14)—(17) of [12] only in the absence of terms containing the constants D and d. Therefore, according to [13], in this case the piezo-resistance coefficients Π_{1111} and Π_{1122} will be large, but the coefficient Π_{1212} will be small. It is interesting that for the representation $\Gamma_{12}^{\pm}$ in the undeformed crystal the degeneracy is not lifted along the [111] axes, where the term in B_2 in (31) goes to zero.

2) The point X. In conclusion, in order to illustrate the ways of constructing $\mathcal{D}$ in cases when the wave vector group is not equivalent to the point group, we consider the point X. The characters of the representations in this group are given in

Table VI. Characters of the representations of the groups $D_{2d}I$ and D_{2d}

Number of elements	Elements of the class	$A_1^{\pm}$ A_1	$A_2^{\pm}$ A_2	$B_1^{\pm}$ B_1	$B_2^{\pm}$ B_2	$E^{\pm}$ E
1	ε	1	1	1	1	2
1	δ_{2z}	1	1	1	1	−2
2	$\rho_{4z}, \rho_{4z}^{-1}$	1	1	−1	−1	0
2	δ_{2x}, δ_{2y}	1	−1	1	−1	0
2	$\sigma_{xy}, \sigma_{x\bar{y}}$	1	−1	−1	1	0
8	$i \times z$ (only for $D_{2d}I$)	$\pm\chi(z)$				

Table VII. The distribution of $f(\mathcal{X})$ and $\varphi(J)$ over the representations $D_{2d}I$ and D_{2d}

Representation		$f(k, \varepsilon, \sigma)$	$\varphi(J)$
$D_{2d}I$	D_{2d}		
A_1^+	A_1	$k_z^2,\ k_\perp^2,\ \varepsilon_{zz},\ \varepsilon_\perp$	I
A_1^-		$\sigma_z k_z,\ \sigma_x k_x + \sigma_y k_y$	
A_2^+	A_2	σ_z	J_z
A_2^-		$\sigma_x k_y - \sigma_y k_x$	
B_1^+	B_1	$k_x^2 - k_y^2,\ \varepsilon_{xx} - \varepsilon_{yy}$	$J_x^2 - J_y^2$
B_1^-		$\sigma_x k_x - \sigma_y k_y$	
B_2^+	B_2	$k_x k_y,\ \varepsilon_{xy}$	$\{J_x J_y\}$
B_2^-		$k_z,\ \sigma_x k_y + \sigma_y k_x$	
E^+	E	$k_x k_z,\ k_y k_z;\ \varepsilon_{xz},\ \varepsilon_{yz};\ \sigma_x,\ \sigma_y$	
E^-		$k_x,\ k_y;\ \sigma_z k_x,\ \sigma_z k_y;\ \sigma_x k_z,\ \sigma_y k_z$	—

Table V.[11] The point X is the point of zero slope for the representations $X_{3,4}$. These representations belong to the case a_1, and for them there appear in $\mathcal{D}$ even functions which transform according to the representations $\bar{\bar{X}}$, coinciding with the representations of the corresponding point group $\bar{\bar{X}} = D_{2d}I$, appearing in $[\bar{\bar{X}}_{3,4}^2] = A_1^+ + B_1^- + B_2^+$, and odd functions transforming according to $\{X_{3,4}^2\} = A_2^-$.

The characters of the representations of the group $D_{2d}I$ are given in Table VI, and the distribution of $f(\mathcal{X})$ over these representations in Table VII.

Then

$$\mathcal{D} = A_1\lambda + iA_3\beta_1(\hat{\sigma}_x k_x - \hat{\sigma}_y k_y) + A_4(B_3 k_x k_y + C_3\varepsilon_{xy}), \quad (32)$$

where $\lambda = B_1 k_z^2 + B_2 k_\perp^2 + C_1\epsilon_{zz} + C_2\epsilon_\perp$.

In the case considered, since the representations $X_{3,4}$ are two-dimensional, according to (I.43) the matrix $A_1 = 1$, and A_3 and A_4 can be chosen to be, respectively, σ_x and σ_y.

For comparison, we write down $\mathcal{D}$, using the general method given in Part 3 of Sec. 4 of [1]. By excluding the element (i/τ) we obtain, in place of the group X, the point group D_{2d}, of which the characters of the representations are given in Table VI. The representations $X_{3,4}$ go over into E; therefore $\mathcal{D}$ contains $f(\mathcal{X})$ and $\varphi(J)$, transforming according to $E \times E = A_1 + A_2 + B_1 + B_2$.

We take these functions from Table VII, where the correspondence of the representations of the point group $D_{2d}I$ and the group D_{2d} is shown. We at once include in $\mathcal{D}$ only those $f(\mathcal{X})$ which appear in (28), and then obtain

$$\hat{\mathcal{D}} = \lambda + i\beta_1(\hat{J}_x^2 - \hat{J}_y^2)(\hat{\sigma}_x k_x - \hat{\sigma}_y k_y) + 2[J_x J_y](B_3 k_x k_y + C_3\varepsilon_{xy}). \quad (32a)$$

The matrices $J_x^2 - J_y^2$ and $2[J_x J_y] = J_x J_y + J_y J_x$ in the representation $u_\pm = (1/\sqrt{2})(\mp x - iy)$ are once again equal to σ_x and σ_y.

The solution of the equation $\| \mathcal{D} - E \| = 0$ has the form

$$E(k, \varepsilon) = \lambda \pm \{(B_3 k_x k_y + C_3\varepsilon_{xy})^2 + \beta_1^2 k_\perp^2\}^{1/2}, \quad (33)$$

i.e., the twofold degeneracy is retained. Close to the extremum in the undeformed crystal the surfaces of constant energy have the form of a torus:

$$E(k) = B_1 k_z^2 + B_2(k_\perp \pm k_\perp^0)^2, \quad (34)$$

where $k_\perp^0 = \beta_1/2B_2$. As Rashba[14] showed, semiconductors with bands of this type have a number of interesting peculiarities. For large k terms with β_1^2 can be neglected. Then

$$E(k, \varepsilon) = \lambda \pm (B_3 k_x k_y + C_3\varepsilon_{xy}). \quad (35)$$

Here the surfaces of constant energy are ellipsoids, where deformation causes splitting of the band at $k = 0$, i.e., the relative displacement of these ellipsoids. Large changes of resistance under shear deformations can, therefore, be expected. In addition, due to the relative displacement of the extrema situated at non-equivalent points of the star k_0, i.e., on the axes x, y, and z, there will be large effects also for the deformations ϵ_{xx}, ϵ_{yy} and ϵ_{zz}.

As is well known, the extrema in n-Si are disposed along the [100] axes, but in the interior of the zone. Thus, there should be observed only effects associated with the displacement of the extrema, and shears ϵ_{xy}, ϵ_{xz}, and ϵ_{yz} should not cause resistance changes. Experimentally the value of the constant $\frac{1}{2}(\Pi_{1111} - \Pi_{1212})$ in n-Si is, in fact, approximately eight times larger than Π_{1212}.[15]

In conclusion, the author expresses his deep gratitude to L. D. Landau for valuable discussions, to A. I. Ansel'm, E I. Rashba and G. L. Bir for numerous very valuable discussions, and also to V. I. Sheka for sending the manuscript of his paper.

[1] G. E. Pikus, JETP 41, 1258 (1961), Soviet Phys. JETP 41, 898 (1962).

[2] E. Wigner, Nachr. Akad. Wiss. Göttingen, Math.-Physik. Kl. 5, 546 (1932).

[3] L. D. Landau and E. M. Lifshitz, Quantum Mechanics, Pergamon Press, 1958, Chap. 12.

[4] V. I. Sheka, FTT 2, 1211 (1960), Soviet Physics -Solid State 2, 1096 (1960).

[5] J. M. Luttinger, Phys. Rev. 102, 1030 (1956).

[6] J. L. Birman, Phys. Rev. 114, 1490 (1959).

[7] D. G. Thomas and J. J. Hopfield, Phys. Rev. 116, 573 (1959); Thomas, Hopfield and Power, Phys. Rev. 119, 570 (1960).

[8] É. I. Rashba, FTT 1, 407 (1959), Soviet Physics -Solid State 1, 368 (1959).

[9] É. I. Rashba and V. I. Sheka, FTT 1, 162 (1959), Soviet Physics -Solid State 1, 143 (1959).

[10] L. I. Schiff, Quantum Mechanics, McGraw-Hill, N. Y., 1955.

[11] W. Döring and V. Zehler, Ann. Physik 13, 214 (1953); V. Zehler, Ann. Physik 13, 229 (1953).

[12] G. E. Pikus and G. L. Bir, FTT 1, 1642 (1959), Soviet Physics -Solid State 1, 1502 (1960).

[13] G. E. Pikus and G. L. Bir, FTT 1, 1828 (1959), Soviet Physics -Solid State 1, 1675 (1960).

[14] É. I. Rashba, FTT 2, 1224 (1960); Soviet Physics -Solid State 2, 1109 (1960); I. I. Boĭko and É. I. Rashba, FTT 2, 1874 (1960); Soviet Physics -Solid State 2, 1692 (1961).

[15] C. Smith, Phys. Rev. 94, 42 (1954).

Translated by K. F. Hulme
257

LINE WIDTH IN ANTIFERROMAGNETIC RESONANCE

V. N. GENKIN and V. M. FAĬN

Radiophysics Institute, Gor'kii State University

Submitted to JETP editor May 16, 1961

J. Exptl. Theoret. Phys. (U.S.S.R.) 41, 1522-1526 (November, 1961)

Relaxation of the uniform precession of the magnetization of an antiferromagnetic substance due to the interaction between the uniform precession and spin waves is considered. The model of localized spins with exchange interaction was employed in the calculations. Terms of the fourth order in the creation and annihilation operators were taken into account in the Hamiltonian. The relaxation time for uniform precession at low temperatures has been derived.

1. INTRODUCTION

WHILE the theory of line width in ferromagnetic resonance has progressed considerably,[1,2] the line width in antiferromagnetic resonance has not to date received any explanation that is at all satisfactory.

The object of the present paper consists of evaluating the linewidth (or the relaxation time associated with it) resulting from the interaction of the uniform precession of the magnetization with spin waves. A similar interaction in the case of ferromagnetic substances has been discussed in the papers by Akhiezer and co-workers.[2] However, the line width in the case of ferromagnetic substances turns out to be very small. This is associated with the fact that the interaction of spin waves with uniform precession (in the ferromagnetic case) is due to comparatively small relativistic effects, while the exchange interaction does not affect uniform precession. In the case of an antiferromagnetic substance the exchange interaction turns out to be the dominant one in the calculation of the relaxation brought about by the interaction between the uniform precession and spin waves, and, as will be seen from our estimates, leads to an appreciable line width.

2. THE INTERACTION HAMILTONIAN

We shall write the Hamiltonian for a system of spins in an antiferromagnetic substance in the following form* (cf., for example, [3])

$$\mathcal{H} = 2J \sum_{\langle lm \rangle} \mathbf{S}_l \mathbf{S}_m + g\beta H_A \Big(\sum_l S_l^z - \sum_m S_m^z \Big). \qquad (1)$$

Here $\mathbf{S}_l$ and $\mathbf{S}_m$ are spin operators of the first and the second sublattices respectively, $\langle lm \rangle$ denotes summation over the nearest neighbors, the exchange integral is $J > 0$, H_A is the effective anisotropic field (for simplicity we shall assume that there is no external magnetic field).

Further, we express $\mathbf{S}_l$ and $\mathbf{S}_m$ in the usual manner in terms of the spin deviation operators, restricting ourselves to terms of order not higher than the third:

$$S_l^+ = (2S)^{1/2} (1 - a_l^* a_l / 4S)\, a_l, \quad S_l^- = (2S)^{1/2} a_l^* (1 - a_l^* a_l / 4S),$$
$$S_l^z = S - a_l^* a_l, \quad S_m^+ = (2S)^{1/2} b_m^* (1 - b_m^* b_m / 4S),$$
$$S_m^- = (2S)^{1/2} (1 - b_m^* b_m / 4S)\, b_m, \quad S_m^z = -S + b_m^* b_m,$$
$$S_{lm}^{\pm} = S_{lm}^x \pm i S_{lm}^y. \qquad (2)$$

After these operators have been substituted into (1) the Hamiltonian can be separated into a sum of second- and fourth-order terms in the operators a and b. The second-order terms are subsequently diagonalized. They represent the unperturbed Hamiltonian for the spin waves. The fourth-order terms represent the interaction energy of the spin waves:

$$\mathcal{H}' = -2J \sum_{\langle lm \rangle} \Big\{ \tfrac{1}{4} (a_l^* a_l a_l b_m + a_l b_m^* b_m b_m + b_m^* a_l^* a_l^* a_l + b_m^* b_m^* b_m a_l^*) + a_l^* a_l b_m^* b_m \Big\}.$$

We next transform to the Fourier components of the operators a and b:

*We note that if the energy associated with the anisotropy is taken into account in a more general form (cf., for example,[2]) than in (1), then this leads to the appearance in (4) of a number of additional terms. However, it can be easily seen that some of these terms describe processes for which the law of conservation of energy does not hold, while the others have no effect on the uniform precession. From this it is clear that a more complete method of taking anisotropy into account, as has been done, in particular, by Akhiezer et al,[2] turns out to be superfluous in our calculation.

$$a_l = (2/N)^{1/2}\sum_k a_k e^{-ikl}, \quad a_l^* = (2/N)^{1/2}\sum_k a_k^* e^{+ikl},$$

$$b_m = (2/N)^{1/2}\sum_k b_k e^{ikm}, \quad b_m^* = (2/N)^{1/2}\sum_k b_k^* e^{-ikm}.$$

The Hamiltonian $\mathcal{H}'$ can be put in the form

$$\mathcal{H}' = -\frac{Jz}{N}\sum_{1,2,3,4}\{\gamma_4[b_1^*b_2b_3a_4 + b_3^*b_2^*b_1a_4^* + a_1^*a_2a_3b_4 + a_3^*a_2^*a_1b_4] + 4\gamma_{(k_1-k_2)}a_1^*a_2b_3^*b_4\}\Delta(k_1 + k_4 - k_2 - k_3),$$

$$\gamma_k = \frac{1}{z}\sum_{\langle lm\rangle} e^{ik(l-m)},$$

where 2z is the number of nearest spins.

We diagonalize the second order terms by introducing new variables:

$$a_k = \alpha_k \operatorname{ch}\theta_k - \beta_k^* \operatorname{sh}\theta_k, \quad b_k = -\alpha_k^* \operatorname{sh}\theta_k + \beta_k \operatorname{ch}\theta_k, \tag{3}$$

where $\tanh 2\theta_k = \gamma_k/D$; $D = 1 + g\beta H_A/zJS$. This operation, analogous to the Holstein-Primakoff[4] transformation brings the interaction Hamiltonian into the form

$$\mathcal{H}' = \frac{Jz}{N}\sum_{1,2,3,4}\{\Phi_{1(23)4}\alpha_1\alpha_2^*\alpha_3^*\alpha_4 + \Psi_{1(23)4}\beta_1\beta_2^*\beta_3^*\beta_4 + \lambda_{1234}\alpha_1^*\alpha_2\beta_3^*\beta_4 - \Phi_{1234}\alpha_1^*\alpha_2\alpha_3\beta_4 - \Psi_{1234}\beta_1^*\beta_2\beta_3\alpha_4\}\Delta(k_1 - k_2 - k_3 + k_4). \tag{4}$$

Here we have omitted terms of the type $\alpha_1\alpha_2\beta_1\beta_2$ which cannot correspond to processes in which the energy of the spin waves is conserved. In formula (4) we have introduced the notation

$$\lambda_{1234} = \lambda'_{(1)2(3)4} + \lambda''_{42(31)} + \lambda'_{13(24)} + \lambda''_{(4)3(2)1}.$$

We shall not in future need the specific form of the coefficients Φ and Ψ, and, therefore, we do not give them here. We merely note that the omitted coefficients do not exceed λ in order of magnitude.

The quantities $\lambda_{(1)2(3)4}$ and $\lambda'_{12(34)}$ are of the form

$$\lambda'_{(1)2(3)4} = \gamma_4(\operatorname{sh}\theta_1\operatorname{sh}\theta_2\operatorname{ch}\theta_3\operatorname{sh}\theta_4 + \operatorname{ch}\theta_1\operatorname{ch}\theta_2\operatorname{sh}\theta_3\operatorname{ch}\theta_4) - 2\gamma_{1-2}\operatorname{ch}\theta_1\operatorname{ch}\theta_2\operatorname{ch}\theta_3\operatorname{ch}\theta_4,$$

$$\lambda'_{12(3)(4)} = \gamma_4(\operatorname{sh}\theta_1\operatorname{ch}\theta_2\operatorname{sh}\theta_3\operatorname{sh}\theta_4 + \operatorname{ch}\theta_1\operatorname{sh}\theta_2\operatorname{ch}\theta_3\operatorname{ch}\theta_4) - 2\gamma_{1-2}\operatorname{ch}\theta_1\operatorname{ch}\theta_2\operatorname{sh}\theta_3\operatorname{ch}\theta_4,$$

where $\gamma_{1-2} \equiv \gamma_{k_1-k_2}$; λ'' are obtained from the corresponding λ' by the substitutions $\cosh\theta_i \to \sinh\theta_i$ and $\sinh\theta_i \to \cosh\theta_i$.

3. RELAXATION PROCESSES

The Hamiltonian (4) is responsible for the interaction of the spin waves. We note that this Hamiltonian satisfies Van Hove's condition of diagonal singularity.[5] This enables us in discussing the relaxation processes to utilize the ordinary method involving probabilities per unit time. We shall now consider the relaxation of the uniform precession of the magnetization which is, in particular, represented by the operators α_0 and α_0^*. In carrying this out we assume that the spin waves are in the state of thermodynamic equilibrium at the temperature T. We obtain the probabilities for the occurrence of processes involving a change in the number of spin waves and containing the operator α_k:

$$W(n_1, n_2, n_3, n_4 \to n_1 - 1, n_2 + 1, n_3 + 1, n_4 - 1) = \frac{2\pi}{\hbar}\frac{\varepsilon_{ex}^2}{4N^2}|\Phi_{1(23)4} + \Phi_{1(32)4} + \Phi_{4(23)1} + \Phi_{4(32)1} + \Phi_{3(14)2} + \Phi_{2(14)3} + \Phi_{2(41)3} + \Phi_{3(41)2}|^2\Delta(k_1 + k_4 - k_2 - k_3)\,\delta(\varepsilon_1 + \varepsilon_4 - \varepsilon_2 - \varepsilon_3)(n_2 + 1)(n_3 + 1)n_1n_4, \tag{5}$$

$$W(n_1, n_2, n_3, n_4' \to n_1 + 1, n_2 - 1, n_3 - 1, n_4' - 1) = \frac{2\pi}{\hbar}\frac{\varepsilon_{ex}^2}{4N^2}|\Phi_{1234}|^2\Delta(k_1 + k_4 - k_2 - k_3)\,\delta(\varepsilon_1 - \varepsilon_2 - \varepsilon_3 - \varepsilon_4')(n_1 + 1)n_2n_3n_4', \tag{6}$$

$$W(n_1, n_2, n_3', n_4' \to n_1 + 1, n_2 - 1, n_3' + 1, n_4' - 1) = \frac{2\pi}{\hbar}\frac{\varepsilon_{ex}^2}{4N^2}|\lambda_{1234} + \lambda_{2143}|^2\Delta(k_1 + k_4 - k_2 - k_3)\,\delta(\varepsilon_1 - \varepsilon_2 - \varepsilon_3' - \varepsilon_4')(n_1 + 1)n_2(n_3' + 1)n_4'. \tag{7}$$

Here $\epsilon_{ex} = 2Jz$, the primed quantities refer to spin waves described by the operators β; n_k and n_k' are the mean numbers of α- and β-spin waves in the state of momentum k; ϵ_k and ϵ_k' are the energies of magnons of momentum k.

In the rest of the paper we restrict ourselves to the low temperature case

$$kT < \varepsilon_0. \tag{8}$$

In this case we can neglect processes of type (5) since the corresponding matrix elements vanish. The contribution made by processes (6) will be small, since in order to satisfy the law of conservation of energy it is necessary that one of the ϵ_k should be greater than $3\epsilon_0$, and this corresponds to a relatively small value of n_k if condition (8) is satisfied. Thus, the principal contribution to the line width is made by processes of type (7). This leads to the following equation for the relaxation of the uniform precession of the magnetization:

$$\dot{n}_0 = \sum_{234}[W(n_0, n_2, n_3', n_4' \to n_0 + 1, n_2 - 1, n_3' - 1, n_4' - 1) - W(n_0, n_2, n_3', n_4' \to n_0 - 1, n_2 + 1, n_3' - 1, n_4' + 1)] + \sum_{134}[W(n_1 - 1, n_0, n_3' - 1, n_4' + 1 \to n_1, n_0 + 1, n_3', n_4') - W(n_1, n_0, n_3', n_4' \to n_1 + 1, n_0 - 1, n_3' + 1, n_4' - 1)]. \tag{9}$$

*ch = cosh, sh = sinh.

Here we have everywhere taken $n_{k\neq 0} = \bar{n}_k = 1/[\exp(\epsilon_k/kT) - 1]$.

Equation (9) can be written in the form

$$\dot{n}_0 = -\lambda (n_0 - \bar{n}_0).$$

λ^{-1} is equal to the average relaxation time of uniform precession. It can be easily obtained from (7) and (9) that

$$\lambda = \frac{\pi}{\hbar}\frac{\varepsilon_{ex}^2}{N^2}\sum_{234}|\lambda_{0234} + \lambda_{2043}|^2 \Delta(\mathbf{k}_4 - \mathbf{k}_3 - \mathbf{k}_2)\,\delta(\varepsilon_0 - \varepsilon_2 + \varepsilon_3' - \varepsilon_4')(n_3' - n_2 n_4' + n_2 n_3' + n_3' n_4'). \quad (10)$$

By utilizing the expression for λ_{iklm}, we obtain

$$|\lambda_{0234} + \lambda_{2043}|^2 = D^2 \varepsilon_{ex}^4 |\mathbf{k}_1\mathbf{k}_2 l^2|^2 / \varepsilon_0\varepsilon_2\varepsilon_3\varepsilon_4, \quad (11)$$

where $\epsilon_k^2 = \epsilon_{ex}^2(h_A + k^2 l^2/3)$; $h_A = g\beta H_A/zJS$, l is the lattice constant, and we have taken into account the fact that $\mathbf{k}\cdot\mathbf{l} \ll 1$.

We carry out the summation over $\mathbf{k}_4$, replace the summation over $\mathbf{k}_2$ and $\mathbf{k}_3$ by integration, substitute (11), integrate over the angles θ_2, φ_1, φ_2, and as a result obtain

$$\lambda = \frac{27}{\hbar(2\pi)^3 \varepsilon_{ex}^4}\int \frac{(\varepsilon_2^2 - \varepsilon_0^2)^{3/2}(\varepsilon_3^2 - \varepsilon_0^2)^{3/2}\cos^2\theta\, d\theta \sin\theta}{\varepsilon_0\varepsilon_{3+2}} \times e^{-\varepsilon_3/kT}\delta(\varepsilon_0 - \varepsilon_2 + \varepsilon_3 - \varepsilon_{3+2})\, d\varepsilon_3\, d\varepsilon_2. \quad (12)$$

Here $\epsilon_{3+2} \equiv \epsilon_{\mathbf{k}_3+\mathbf{k}_2}$ and $D^2 \approx 1$. In going over from formula (10) to formula (12) we have taken into account condition (8), and we have retained only the term $n_3' \approx \exp(-\epsilon_3/kT)$. Integration over ϵ_2 reduces, as follows from the presence of the δ-function, to the replacement

$$\varepsilon_2 = \varepsilon_0\frac{\varepsilon_3 + \varepsilon_0 + \cos^2\theta(\varepsilon_3 - \varepsilon_0)}{\varepsilon_3 + \varepsilon_0 - \cos^2\theta(\varepsilon_3 - \varepsilon_0)},$$

$$\varepsilon_{3+2} = \frac{\varepsilon_3(\varepsilon_0 + \varepsilon_3)\sin^2\theta + 2\varepsilon_0^2\cos^2\theta}{\varepsilon_3 + \varepsilon_0 - \cos^2\theta(\varepsilon_3 - \varepsilon_0)}.$$

From the condition $\epsilon_{2+3} < \epsilon_3$ (since $\epsilon_0 < \epsilon_2$) we obtain

$$\pi/2 < \theta < \pi.$$

After integrating over θ and ϵ_3 we finally obtain

$$\frac{\lambda}{\omega_0} = h_A^2\frac{e^{-\varkappa_0}}{\varkappa_0^5}(16\varkappa_0^4 + 30\varkappa_0^3 + 46\varkappa_0^2 + 54\varkappa_0 + 37),$$

where $\varkappa_0 = (\epsilon_0/kT)$, $h_A = g\beta H_A/zJS = H_A/H_E$, H_E is the intensity of the "exchange force field," $\omega_0 = \epsilon_0/\hbar$ is the antiferromagnetic resonance frequency.

We give estimates of λ for the case of MnF_2. In this case[6] $H_A = 9 \times 10^3$ gauss; $H_E = 6 \times 10^5$ gauss, and at $T = 6°K$, $\lambda = 160$ gauss, at $T = 4°K$, $\lambda = 12$ gauss, i.e., even at such low temperatures considerable broadening is present. It is obvious that at higher temperatures the line width increases.

[1] Clogston, Suhl, Walker, and Anderson, J. Phys. Chem. Solids **1**, 129 (1956).

[2] A. I. Akhiezer, J. Phys. (U.S.S.R.) **10**, 217 (1946). Akhiezer, Bar'yakhtar, and Peletminskii, JETP **36**, 216 (1959), Soviet Phys. JETP **9**, 146 (1959). Akhiezer, Bar'yakhtar, and Kaganov, UFN **72**, 3 (1960), Soviet Phys. Uspekhi **3**, 661 (1961).

[3] J. Van Kranendonk and J. H. Van Vleck, Revs. Modern Phys. **30**, 1 (1958).

[4] T. Holstein and H. Primakoff, Phys. Rev. **58**, 1908 (1940).

[5] L. Van Hove, Physica **21**, 517 (1955).

[6] F. M. Johnson and A. H. Nethercot, Phys. Rev. **114**, 705 (1959).

Translated by G. Volkoff
258

THE DISPERSION EQUATION FOR AN EXTRAORDINARY WAVE MOVING IN A PLASMA ACROSS AN EXTERNAL MAGNETIC FIELD

Yu. N. DNESTROVSKIĬ and D. P. KOSTOMAROV

Moscow State University

Submitted to JETP editor May 17, 1961

J. Exptl. Theoret. Phys. (U.S.S.R.) 41, 1527-1535 (November, 1961)

A general qualitative study has been carried out on the non-relativistic dispersion equation for extraordinary and plasma waves propagating in a plasma transversely to an external magnetic field. Frequency regions are established in which these waves can propagate without damping. An error is pointed out in the conclusion drawn by a number of authors that gaps of zero transmission can exist for waves of a given type in the vicinity of each cyclotron resonance. The laws of behavior that are established are illustrated by the results of a numerical solution of the dispersion equation.

INTRODUCTION

IT is well known that two types of waves can exist in a homogeneous unbounded plasma located in a homogeneous external magnetic field $\mathbf{H}_0$. The propagation direction of these waves is perpendicular to the field $\mathbf{H}_0$. In the first place, one has a purely transverse wave with its electric vector polarized along the field $\mathbf{H}_0$ (the ordinary wave) and, in the second place, one has waves in which the electric vector is polarized perpendicular to $\mathbf{H}_0$ (the extraordinary and plasma waves). In our previous research,[1] a general qualitative study was carried out on the dispersion equation for the ordinary wave. The present work is devoted to the investigation of the dispersion equation for the extraordinary and plasma waves.

The equation that connects the frequency ω with the propagation constant k has the following form:

$$D(k, \omega) = k^2\varepsilon_{11} - \omega^2 c^{-2}(\varepsilon_{11}\varepsilon_{22} - \varepsilon_{12}\varepsilon_{21}) = 0. \quad (1)$$

Here $\epsilon_{ij}(\mathbf{k}, \omega)$ are the components of the dielectric permittivity tensor. In the non-relativistic case and for the unperturbed Maxwellian electron distribution function,

$$\varepsilon_{11} = 1 + \tfrac{1}{4}(A + 2B + C),$$

$$\varepsilon_{22} = 1 + \tfrac{1}{4}(A - 2B + C),$$

$$\varepsilon_{12} = -\varepsilon_{21} = \tfrac{1}{4} i (A - C); \quad (2)$$

$$A(k, \omega) = C(k, -\omega)$$

$$= \frac{2\omega_0^2}{\omega\omega_H} \sum_{n=-\infty}^{\infty} (\zeta_{n-1}(\mu) + \mu\zeta'_{n-1}(\mu)) \left(n - \frac{\omega}{\omega_H}\right)^{-1}$$

$$= \frac{\omega_0^2}{\omega\omega_H \sin(\omega\pi/\omega_H)} \int_0^{2\pi} e^{-\mu(1-\cos\tau)} [1 - \mu(1 - \cos\tau)]$$

$$\times \cos\left[\left(\frac{\omega}{\omega_H} - 1\right)(\tau - \pi)\right] d\tau, \quad (3)$$

$$B(k, \omega) = \frac{2\omega_0^2}{\omega\omega_H} \mu \sum_{n=-\infty}^{\infty} \zeta'_n(\mu) \left(n - \frac{\omega}{\omega_H}\right)^{-1}$$

$$= \frac{\omega_0^2 \mu}{\omega\omega_H \sin(\omega\pi/\omega_H)} \int_0^{2\pi} e^{-\mu(1-\cos\tau)} (1 - \cos\tau)$$

$$\times \cos\frac{\omega}{\omega_H}(\tau - \pi)\, d\tau, \quad (4)$$

where $\omega_0 = \sqrt{4\pi N_0 e^2/m}$ is the plasma frequency, $\beta = eH_0/mc$ is the Larmor frequency, $\mu = Tk^2/m\omega_H^2$, T is the electron temperature in energy units, $\zeta_n(\mu) = e^{-\mu} I_n(\mu)$, and $I_n(\mu)$ is the Bessel function of imaginary argument.

Equation (1) was first obtained by Gross[2] on the basis of simultaneous consideration of the non-relativistic kinetic equation for electrons and the set of Maxwell equations. It has since been studied by many authors.[4-10] A characteristic feature of the method employed was the preliminary expansion of the equation in powers of some parameter, assumed to be small. It is usually assumed that $\mu \ll 1$. However, such an approach has a number of important weaknesses, the most

important of which are the following: 1) in replacing the transcendental equation (1) by a simplified algebraic equation, certain roots are lost; 2) the expansions in a small parameter in the vicinity of cyclotron resonances are non-uniform; therefore, the behavior of the roots of the complete and simplified equations can differ significantly in the neighborhood of the resonances. The higher cyclotron resonances are not generally taken into account in the simplified equations.

The analytic formulas thus obtained from the simplified equation have at best a limited region of application, and are seen to be invalid as a rule in the neighborhood of resonances. In attempting to draw general conclusions on the properties of Eq. (1) with the help of formulas of an appropriate type, it is easy to make a mistake. As an example, we shall point out an incorrect conclusion of a number of authors[2,5] as to the existence (in the neighborhood of a cyclotron resonance) of gaps of zero transmission for the extraordinary and plasma waves. This conclusion is based on the incorrect use (in the neighborhood of the resonance) of formulas obtained by an expansion in terms of some small parameter. In the same way, the curves for the index of refraction of the extraordinary wave, found by Drummond[8] as a result of numerical solution of the simplified equation, are valid only far from cyclotron resonance.

In particular, the problem of plasma waves should be considered in some detail. By taking it into account that k^2 is generally large for these waves, one can write down the following approximate equation for them:[2,3]

$$\varepsilon_{11}(k, \omega) = 0 \qquad (5)$$

(it can be shown that the transition from Eq. (1) to Eq. (5) corresponds to the assumption of a purely longitudinal character for the plasma wave). For plasma waves, $k \to \infty$ as $T \to 0$; in this case, the parameter μ is, for all frequencies, a quantity either of the order of, or larger than, unity. Therefore, the results of the study of plasma waves by expansion of Eq. (1) in powers of μ have a very limited region of application. Thus the formula for the index of refraction of the plasma wave obtained by this method in a number of works[4-6] is qualitatively valid for $\omega_H < \omega < 2\omega_H$ and is shown to be completely invalid for $\omega > 2\omega_H$.

In the work of Bernstein,[7] an attempt was made to show the existence of gaps of zero transmission for the plasma wave in the vicinity of each cyclotron resonance, by working with the abbreviated Eq. (5) without having recourse to other simplifying assumptions. However, in the course of the proof, the author made the following logical error. Equation (5) can be written in the form $k^2 = F(k, \omega)$ [Eq. (48) in [7]]. For fixed k, the function F is an alternating function of ω, negative in a certain neighborhood of the resonance. Therefore, Bernstein[7] drew the conclusion that these regions are zero-transmission gaps for the plasma wave, inasmuch as for such frequencies, as it were, Eq. (5) cannot have real roots in k. However, the parameter k in Eq. (5) is in fact not fixed, but is a function of ω, defined by the same dispersion equation (5). The function $F(k(\omega), \omega)$ can remain positive in any arbitrary neighborhood of resonance. Thus the discussions of Bernstein prove nothing.

In the present paper, the authors aimed at carrying out a detailed qualitative study of Eqs. (1) and (5) without additional simplifying assumptions other than the non-relativistic condition. Initially, Eq. (1) is considered from the viewpoint of the determination of the propagation constant k for a given real frequency ω. Regions of the frequency ω are established in which there exist real roots $k = k(\omega)$ (the transmission region of the plasma for waves of a given type). In particular, it is shown that for $\omega_H < \omega < \omega^* < \sqrt{\omega_H^2 + \omega_0^2}$ the dispersion equation has a real root $k(\omega)$, to which corresponds a plasma wave propagating without absorption (ω^* is the point of coincidence of the roots for the extraordinary and plasma waves, located somewhat to the left of the hybrid frequency $\sqrt{\omega_H^2 + \omega_0^2}$). The established rules are illustrated by the results of a numerical solution of Eq. (1) for different values of the electron temperature and the plasma density. It is seen from a numerical calculation that the plasma roots of Eq. (1) can be formed from a solution of the abbreviated Eq. (5) with a high degree of accuracy. The results become invalid only in the vicinity of the hybrid frequency $\sqrt{\omega_H^2 + \omega_0^2}$. It is established that Eq. (1) has an infinite set of complex roots $k = k(\omega)$ in addition to the real roots. In Eq. (5) of the present work, the dispersion equation is considered as an equation which determines the frequency ω as a function of the wave number k. It is shown that there exists an infinite set of real roots $\omega = \omega(k)$, while the complex roots $\omega = \omega(k)$ are lacking in Eq. (1).

1. PRELIMINARY INVESTIGATION OF THE DISPERSION EQUATION

We shall begin our study of Eq. (1) with the study of the case in which one is required to deter-

mine the propagation constant k for a given frequency ω. We introduce the dimensionless variables: $s = k^2c^2/\omega^2 = N^2$ is the square of the index of refraction, $\alpha = \omega/\omega_H$, $\beta = \omega_0/\omega_H$, $\gamma = T/mc^2$; then Eq. (1) takes the form

$$D(s, \alpha, \beta, \gamma) = s[1 + \tfrac{1}{4}(a + 2b + c)]$$
$$- [1 + \tfrac{1}{2}(a + c) + \tfrac{1}{4}(ac - b^2)] = 0, \quad (6)$$

where $a = a(s, \alpha, \beta, \gamma)$, $b = b(s, \alpha, \beta, \gamma)$, $c = c(s, \alpha, \beta, \gamma)$ are the functions (3) and (4) in the new variables.

We shall seek roots of Eq. (6), $s = s(\alpha, \beta, \gamma)$, for all possible real values of α ($\alpha \neq n$). To begin with, we analyze the real roots (Secs. 1–3), which we do in a fashion similar to [1]. For this purpose we first compare the signs of the function D for $s = 0$ and $s = \pm\infty$, and then compare Eq. (6) and the degenerate equation corresponding to zero temperature of the electrons ($T = 0$, $\gamma = 0$).

1. By direct calculation, we find that

$$D(0, \alpha, \beta, \gamma) = -\left(1 - \frac{\beta^2}{\alpha(\alpha-1)}\right)\left(1 - \frac{\beta^2}{\alpha(\alpha+1)}\right). \quad (7)$$

At the same time, we can show that the behavior of the function D as $|s| \to \infty$ is determined by the asymptotic formula

$$D(s, \alpha, \beta, \gamma) \approx s - \frac{\pi\beta^4}{2\sin^2\alpha\pi} \frac{e^{-4s\alpha^2\gamma}}{(s\alpha^2\gamma)^2}. \quad (8)$$

Thus,

$$\lim_{s\to+\infty} D(s, \alpha, \beta, \gamma) = \infty, \qquad \lim_{s\to-\infty} D(s, \alpha, \beta, \gamma) = -\infty.$$

Taking this into account, we can conclude that when $D(0, \alpha, \beta, \gamma) < 0$ Eq. (6) has an odd number of positive roots and an even number of negative roots and, conversely, when $D(0, \alpha, \beta, \gamma) > 0$, Eq. (6) has an even number of positive and an odd number of negative roots.

2. Substituting $\gamma = 0$ ($T = 0$) in Eq. (6), we obtain the degenerate equation

$$D(s, \alpha, \beta, 0) = s\left[1 - \frac{\beta^2}{\alpha^2 - 1}\right]$$
$$- \left[1 - \frac{\beta^2}{\alpha(\alpha-1)}\right]\left[1 - \frac{\beta^2}{\alpha(\alpha+1)}\right] = 0. \quad (9)$$

We note three characteristic points of this equation, which correspond to the vanishing of each of the square brackets in (9):

$$\alpha' = -\tfrac{1}{2} + \tfrac{1}{2}\sqrt{1 + 4\beta^2}, \quad \alpha'' = \alpha' + 1, \quad \alpha^0 = \sqrt{1 + \beta^2}$$
$$(\alpha' < \alpha^0 < \alpha'', \ \alpha^0 > 1). \quad (10)$$

The root $s_0 = s_0(\alpha\beta)$ of Eq. (9) is positive for $\alpha' < \alpha < \alpha^0$ and $\alpha'' < \alpha$, negative for $0 < \alpha < \alpha'$ and $\alpha^0 < \alpha < \alpha''$. As $\alpha \to \alpha^0$, we have $|s_0| \to \infty$.

Equation (6) is non-relativistic, and is therefore meaningful only at sufficiently small values of γ. As $\gamma \to 0$, the roots of Eq. (6) either approach the root of the degenerate equation or diverge to infinity. The corresponding waves are called extraordinary in the first case and plasma in the second.[6]

2. POSITIVE ROOTS OF EQUATION (6) IN THE NON-RESONANT REGION

We shall investigate the positive roots of Eq. (6) for values of α far from the integral values (non-resonant regions of frequency). In accord with (7), the function $D(0, \alpha, \beta, \gamma)$ changes sign when $\alpha = 1$, $\alpha = \alpha'$, $\alpha = \alpha''$. Two cases are possible here, $\alpha' < 1$ and $\alpha' > 1$. We shall consider them separately.

1. $\alpha' < 1$ (i.e., $\omega_0^2 < 2\omega_H^2$). Comparing the data given in the first two rows of Table I, for $0 < \alpha < 1$ and $\alpha^0 < \alpha$, we see that the minimum possible number of positive roots of Eq. (6) coincides with the number of positive roots of Eq. (9). It is natural to expect that, at sufficiently small values of γ and values of α belonging to the intervals shown and far from the integral values, the transition from Eq. (9) to Eq. (6) does not lead to the appearance of new positive roots. This conclusion is supported by the results of a numerical solution of Eq. (6) (see Figs. 1–3). Thus, Eq. (6) has no positive roots for $0 < \alpha < \alpha'$ and $\alpha^0 < \alpha < \alpha''$, and has a single positive root (extraordinary wave) for $\alpha' < \alpha < 1$ and $\alpha'' < \alpha$.

We now turn to the interval $1 < \alpha < \alpha^0$. Equation (6) should have a positive root inside this range, close to the root of the degenerate equation (9) (extraordinary wave). Since the total number of positive roots of Eq. (6) is even in this interval, Eq. (6) should still have one positive root which goes to infinity as $\gamma \to 0$ (the plasma wave). The results of a numerical solution of Eq. (6) show that in the approach to the point α^0 from the left, the roots corresponding to the extraordinary and plasma waves combine. In this case, in the region between the point of coincidence of α^* and α^0, Eq. (6) no longer has positive roots. The number of positive roots of Eq. (6) is shown in the third row of Table I. The capital letters E and P denote the wave to which the root corresponds, extraordinary or plasma. It should be noted that the data of Table I (as also of Table II) are invalid for the immediate vicinity of integral values of α, at which the formulated conclusions do not follow. The problem of the number of roots and their behavior in the resonant regions will be discussed in Sec. 3.

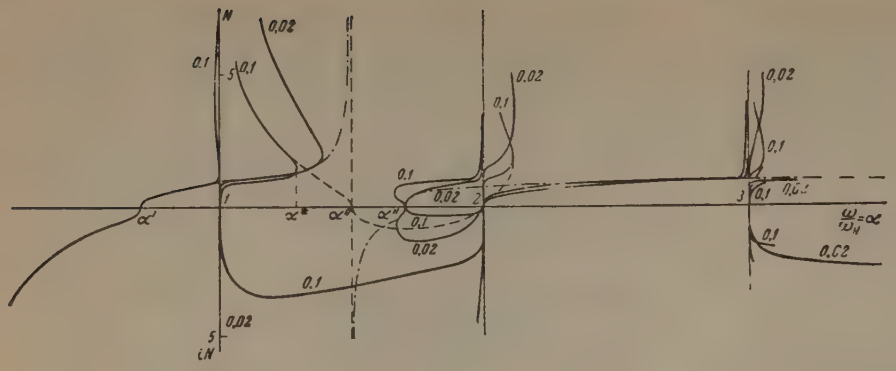

FIG. 1. Dependence of the index of refraction on the frequency for different values of γ with $\beta^2 = 1.2$.

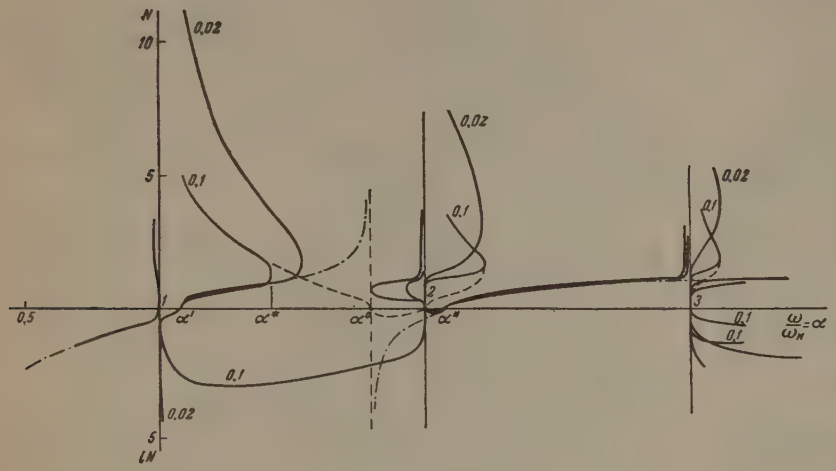

FIG. 2. Dependence of the index of refraction on the frequency for different values of γ with $\beta^2 = 2.25$.

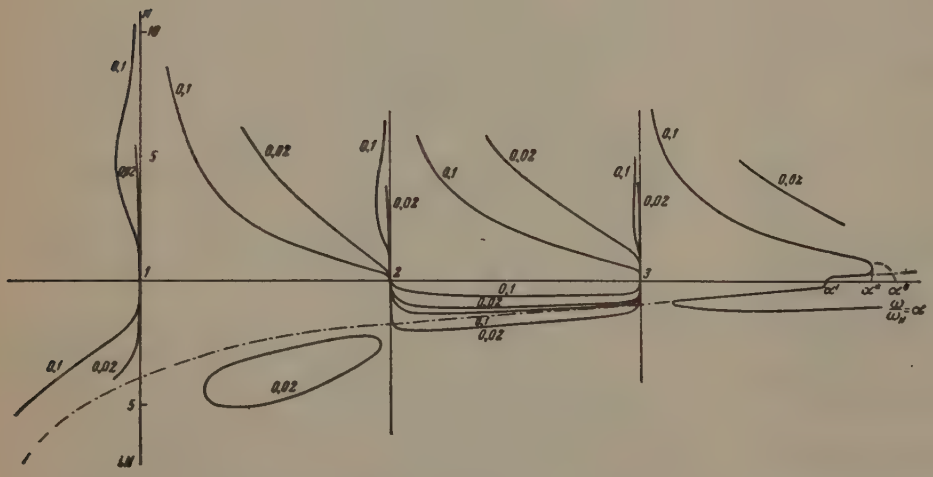

FIG. 3. Dependence of the index of refraction on the frequency for different values of γ with $\beta^2 = 17.6$.

2. $\alpha' > 1$ (i.e., $\omega_0^2 > 2\omega_H^2$). This case can be studied in a way similar to the above. The necessary data and the results of the investigation are given in Table II. As in the first case, propagation of the plasma wave is possible for $1 < \alpha < \alpha^* < \alpha^0$, while only the plasma wave is propagated in the portion $1 < \alpha < \alpha'$.

The results of a numerical solution of Eq. (6) are given in Figs. 1–3. The positive and negative ordinates correspond to $N = \sqrt{s}$ and $iN = \sqrt{-s}$, respectively. The results of numerical solution of the abbreviated dispersion equation for the plasma wave (5) are shown dotted. The equation is written in corresponding dimensionless variables. The positive root corresponding to the plasma wave and the point α^* where this root becomes equal to the root of the extraordinary wave are clearly seen in all the drawings. This point is located to the left of α^0. Calculations that have been carried out show that the plasma wave is "quasi-longitudinal" (the ratio of the longitudinal component of the electric field to the transverse component is of the order of $10-10^3$). In this way, the excellent agreement of the results of the solution of the complete and abbreviated equations is explained everywhere except in the vicinity of the point α^*, where the "quasi-longitudinal" character becomes worse.

Table I

Range of α	$0-\alpha'$	$\alpha'-1$	$1-\alpha^*$	$\alpha^*-\alpha^0$	$\alpha^0-\alpha''$	$\alpha''<\alpha$
Parity of the number of positive roots of Eq. (6)	even	odd	even	even	even	odd
Number of positive roots of (9)	0	1	1	1	0	1
Number of positive roots of (6)	0	1,E	2,E,P	0	0	1,E

Table II

Range of α	0–1	$1-\alpha'$	$\alpha'-\alpha^*$	$\alpha^*-\alpha^0$	$\alpha^0-\alpha''$	$\alpha>\alpha''$
Parity of the number of positive roots of Eq. (6)	even	odd	even	even	even	odd
Number of positive roots of (9)	0	0	1	1	0	1
Number of positive roots of (6)	0	1, P	2,E,P	0	0	1,E

The temperature of the electrons T and the wave number k enter into the equation for the plasma wave (5) only in the form of the combination $\mu = Tk^2/m\omega_H^2$. Therefore, for those values of α for which the plasma root of Eq. (6) is well described by Eq. (5), the index of refraction of the plasma wave is inversely proportional to the square root of the temperature:

$$N(\alpha, \beta, \gamma)/N(\alpha, \beta, \gamma') = \sqrt{T'/T}. \quad (11)$$

This fact can be employed for the experimental determination of the electron temperature in the plasma by measurement of the phase velocity of the plasma wave. We note that $dk/d\omega < 0$ for the plasma wave, i.e., it possesses anomalous dispersion.

The negative roots of Eq. (6) can be considered in an entirely similar manner. We shall not dwell on the details of this study, but shall limit ourselves to the results of a numerical calculation, which are given in Figs. 1–3.

3. THE BEHAVIOR OF THE POSITIVE ROOTS OF EQUATION (6) IN THE NEIGHBORHOOD OF RESONANCE

The resonance points $\alpha = n$ are the singularities of the function $D(s, \alpha, \beta, \gamma)$. It can be shown that as $\alpha \to n$ the real roots of Eq. (6) should tend either to zero or to $+\infty$. Proceeding to a more detailed study of the behavior of the roots near the resonances, we first note that when $\alpha \approx n$ the principal role in Eqs. (3) and (4) will be played by two types of terms: terms having a singularity when $\alpha = n$, and terms which vanish as $\mu \to 0$. Thus, when $\alpha \approx n$,

$$a \approx \frac{2\beta^2}{\alpha}\left[\frac{\zeta_{n-1}(\mu) + \mu\zeta'_{n-1}(\mu)}{n-\alpha} + \frac{\zeta_0(\mu)}{1-\alpha}\right],$$
$$c \approx \frac{2\beta^2}{\alpha}\left[\frac{\zeta_{n+1}(\mu) + \mu\zeta'_{n+1}(\mu)}{n-\alpha} - \frac{\zeta_0}{1+\alpha}\right],$$
$$b \approx \frac{2\beta^2}{\alpha}\frac{\mu\zeta'_n(\mu)}{n-\alpha}. \quad (12)$$

If $n = 1$, then the first term in the formula for a should be omitted.

Substituting (12) in (6), we get a simplified equation describing the behavior of the roots near the n-th resonance. We consider first the large positive roots. For this purpose, we replace the functions $\zeta_n(\mu)$ by their asymptotic forms as $\mu \to \infty$. As a result, the equation takes the form

$$z^2 + z - \gamma = 0, \quad (13)$$

where $z = \sqrt{2\pi}\beta^{-2}n^2(n-\alpha)\gamma^{3/2}s^{3/2}$. It then follows that on each side of the resonant point $\alpha = n$ there is a positive root that goes to infinity as $\alpha \to n$. Thus, for $\alpha < n$,

$$s \approx (\beta^2/\sqrt{2\pi}\, n^2(n-\alpha))^{2/3}\gamma^{-1/3}, \quad (14)$$

and for $\alpha > n$,

$$s \approx (\beta^2/\sqrt{2\pi}n^2(\alpha-n))^{2/3}/\gamma. \quad (15)$$

Inasmuch as the simplified Eq. (5) has a root with the asymptote (15), the plasma wave corresponds to this root. The extraordinary wave corresponds to the root with the asymptote (4), which is located to the left of the resonances (there are similar roots for the dispersion equation for the ordinary wave[1]).

We now turn to the investigation of the roots that tend to zero as $\alpha \to n$. For this purpose, we expand the function $\zeta_n(\mu)$ in the simplified equation in a power series in μ and keep only the principal terms. In the consideration of the small roots, it is convenient to distinguish six cases: 1) $\alpha' < 1$: a) $n = 1$, b) $n > 1$ (in this case, $n > \alpha''$); 2) $\alpha' > 1$: a) $n = 1$, b) $1 < n < \alpha'$, c) $\alpha' < n < \alpha''$, d) $\alpha'' < n$.

We shall not stop to study these individually, but only write out the final results. For $n = 1$, a positive root exists on one side of the resonance point, which tends to zero as $\alpha \to 1$. For $\alpha' > 1$, it is located to the left of the point $\alpha = 1$, for $\alpha' < 1$, to the right. For all the remaining resonant points $\alpha = n > 1$ there exist pairs of positive roots which tend to zero as $\alpha \to n$. In this case, both roots approach the resonant point from the left if $1 < n < \alpha'$ (case 2b); both roots approach from

the right if $\alpha'' < n$ (cases 1b and 2d); one root approaches from the left, and the other from the right if $\alpha' < n < \alpha''$ (case 2c).

The total number of positive roots near resonance, may exceed that shown in Tables I and II. For example, there are three positive roots [one large (15) and two small] to the right of the resonances located in the region $\alpha'' > \alpha$ instead of the one that follows from Tables I and II. Consequently, at large distances from the resonances, the extra roots should join together and vanish, producing a pair of complex roots.

The distribution of the additional roots is as follows. To the left of each resonance, located in the region of zero-transmission of the plasma for the extraordinary wave, which was shown in Tables I and II, there is a band of frequencies where Eq. (6) has a pair of positive roots for the extraordinary wave. As $\alpha \to n - 0$ one of these approaches zero while the other (14) goes to infinity. In the same way, to the right of each resonance located in the zero-transmission region of the plasma, for the plasma wave which was shown in Tables I and II, there is a band of frequencies where Eq. (6) has a pair of positive roots for the plasma wave. As $\alpha \to n + 0$, one of these approaches zero and the other (15) infinity.

It should be particularly noted that there are always regions on both sides of an arbitrary resonance in which Eq. (6) has at least one positive root. Thus the conclusion of Gross and a number of other authors[2,5,7] on the existence of gaps of zero transmission (for the non-relativistic dispersion equation) in the vicinity of each resonance appears to be in error. All the established laws are demonstrated in Figs. 1—3. The special features in the behavior of the negative roots in the vicinity of the resonances are also shown there.

In conclusion, we shall show that even at low electron temperatures relativistic effects begin to appear in the vicinity of the resonances. In the present paper we shall not concern ourselves with the detailed analysis of the relativistic dispersion equation obtained by Trubnikov.[11] We only note that if α belongs to the interval $(n-1) < \alpha < n$, then the order of the relativistic effects (for example, the absorption associated with the Doppler effect) is determined by a factor of the form $\exp\{-mc^2[(n\omega_H/\omega)^2 - 1]/T\}$. Thus, for non-relativistic plasma, the relativistic effects manifest themselves primarily in the appearance of a narrow band of strong absorption to the left of each resonance (of width $\Delta\alpha \sim \gamma$). For the remaining values of α, the relativistic corrections are exponentially small.

4. COMPLEX ROOTS OF EQUATION (6)

The study of the complex roots of Eq. (6) can be carried out by the method set forth in [1]. Applying the principle of the argument, and taking into account the asymptotic formula (8), it is easy to show that the function D has an infinite set of roots in the plane of the complex variable s. These roots are grouped into the second and third quadrants, near the imaginary axis. Each complex root of Eq. (6), together with the complex conjugate root corresponding to it, gives a quartet of complex roots of Eq. (1):

$$k = p(\omega) \pm iq(\omega), \quad k = -p(\omega) \pm iq(\omega).$$

5. DETERMINATION OF THE FREQUENCY AS A FUNCTION OF THE PROPAGATION CONSTANT FROM THE DISPERSION EQUATION (1)

We now consider the Eq. (1) from another point of view, when it is required to determine the frequency ω for a given real propagation constant k. The real roots of Eq. (1) $\omega = \omega(k)$ are found by the points of intersection of the line $N = kc/\omega_H\alpha$ with the graph of the function $N = \sqrt{s(\alpha, \beta, \gamma)}$: to each point of intersection (α_n, N_n) there corresponds a pair of roots $\omega_n = \pm\omega_H\alpha_n$. The analysis carried out in Secs. 2 and 3 shows that the number of points of intersection is infinitely great, while their abscissas α_n $(n = 1, 2, 3, \ldots)$ are distributed in the following fashion:

$$0 < \alpha_1 < 1, \quad n < \alpha_{2n} < \alpha_{2n+1} < n + 1 \quad (n > 1).$$

Making use of the argument principle, it is not difficult to show that Eq. (1) does not have complex roots $\omega = \omega(k)$. In proof of this assertion, one must keep it in mind that the function $D(k, \omega)$ is regular at the point $\omega = 0$, has a pole of second order at the points $\omega = \pm n\omega_H$ and that there are $4n + 2$ zeros on the real axis in the plane of the complex variable s inside a circle of sufficiently small radius.

The authors express their gratitude to A. A. Chechina for help in carrying out the calculations.

[1] Yu. N. Dnestrovskiĭ and D. P. Kostomarov, JETP 40, 1404 (1961), Soviet Phys. JETP 13, 986 (1961).

[2] E. P. Gross, Phys. Rev. 82, 232 (1951).

[3] G. V. Gordeev, JETP 24, 445 (1953).

[4] B. N. Gershman, JETP 24, 659 (1953).

[5] A. G. Sitenko and K. N. Stepanov, JETP 31, 642 (1956), Soviet Phys. JETP 4, 512 (1957).

[6] Gershman, Ginzburg, and Denisov, Usp. Fiz. Nauk 61, 561 (1957).

[7] J. Bernstein, Phys. Rev. 109, 10 (1958).

[8] J. E. Drummond, Phys. Rev. 110, 293 (1958).
[9] B. N. Gershman, JETP 37, 695 (1959), Soviet Phys. JETP 10, 497 (1960).
[10] B. N. Gershman, JETP 38, 912 (1960), Soviet Phys. JETP 11, 657 (1960).
[11] B. A. Trubnikov, in the collection Fizika plazmy i problema upravlyaemykh termoyadernykh reaktsiĭ (Plasma Physics and the Problem of Controlled Thermonuclear Reactions) Vol 3, AN SSSR, 1958, p. 104.

Translated by R. T. Beyer
259

ON THE KINETIC THEORY OF GASES WITH ROTATIONAL DEGREES OF FREEDOM

Yu. KAGAN and A. M. AFANAS'EV

Submitted to JETP editor May 17, 1961

J. Exptl. Theoret. Phys. (U.S.S.R.) 41, 1536-1545 (November, 1961)

The solution of the kinetic equation for molecules with rotational degrees of freedom (diatomic or linear molecules) is considered. The problem of the thermal conductivity and of the first and second viscosities is investigated.

1. INTRODUCTION

THE kinetic theory of gases with internal degrees of freedom is still in a rudimentary stage of development. The difficulties in setting up such a theory are mainly the sharp increase in the number of parameters characterizing the collisions between the molecules and the trouble in finding the explicit form of the collision integral taking into account inelastic processes. All these difficulties show up particularly clearly in a comparison with the kinetic theory developed for the monatomic gas.

The number of papers devoted to the study of the kinetic equation for molecules with internal degrees of freedom, in particular, rotational ones, is very small. Besides the traditional references to be found in the well known monographs,[1,2] the papers of Curtiss and Muckenfuss[3] deserve mention.

The papers in which the attempt is made to take account of the rotational degrees of freedom, start with assuming simple models of solid bodies for the description of the collisions and proceed then to translate the Chapman-Enskog-Barnett method, developed for the monatomic gas, to this case.

To which difficulties and actual errors this can give rise, may be seen by the example of the paper of Curtiss and Muckenfuss.[3] Regarding the molecule as a solid body with a center of symmetry, these authors keep as independent variables in the kinetic equation the phase angles, which vary strongly during the free flight. This leads, obviously, to an extremely complicated problem. On the other hand, when considering the problem of thermal conductivity and viscosity, the above-mentioned authors choose the solution in a form which contains tensors that are constructed entirely from components of the vector of the molecular velocity **V**. This is obviously wrong, since now the problem deals with two independent vectors, **V** and the angular momentum of the molecule **M** (more precisely, a vector and a pseudovector), and the general solution should contain all tensors of corresponding rank which can be formed from the components of these vectors.

In the present paper we investigate the kinetic theory of a diatomic gas in a region of temperatures where the vibrational degrees of freedom can be neglected. We make use of a kinetic equation which does not contain rapidly varying phases and solve the problem of thermal conductivity and of first and second viscosity.

2. KINETIC EQUATION

In the case of diatomic (linear) molecules the rotational motion is described by four quantities: two generalized momenta and the two corresponding generalized coordinates. However, it is convenient to choose as independent variables the three components of the angular momentum M_i and the angle ψ characterizing the position of the axis of the molecule in the plane perpendicular to **M**.

The classical kinetic equation in these variables is written in the form

$$\frac{\partial f}{\partial t}+\mathbf{V}\frac{\partial f}{\partial \mathbf{r}}+\dot{\mathbf{V}}\frac{\partial f}{\partial \mathbf{V}}+\frac{\partial}{\partial \psi}(\dot{\psi}f)+\frac{\partial}{\partial \mathbf{M}}(\dot{\mathbf{M}}f)=\left(\frac{\partial f}{\partial t}\right)_{\text{coll}}. \quad (2.1)$$

It is easy to show that the phase volume corresponding to these variables is equal to

$$M dM d\Omega_{\mathbf{M}}\, d\psi = d\Gamma\, d\psi. \quad (2.2)$$

The equilibrium distribution function is written as

$$f^0 = n\left(\frac{\mu}{2\pi kT}\right)^{3/2}\frac{1}{4\pi IkT}\exp\left\{-\frac{\mu V^2}{2kT}-\frac{M^2}{2IkT}\right\}, \quad (2.3)$$

where I is the moment of inertia (all the remaining notations are standard).

The function (2.3) is normalized such that

$$\int f^0\, d\mathbf{V}\, d\Gamma = n. \quad (2.4)$$

One estimates easily that $1/\dot{\psi}$ is of the order of the collision time. But in deriving the kinetic equa-

tion for a monatomic function in the usual form one assumes explicitly that the gas is sufficiently rarefied and that the collision time is small compared with the time of free flight. Therefore, Eq. (2.1) reduces in first approximation to

$$\dot{\psi}\partial f/\partial\psi = 0.$$

Thus the function f is practically independent of ψ, and we find by integrating (2.1) over $d\psi$

$$\frac{\partial f}{\partial t} + \mathbf{V}\frac{\partial f}{\partial \mathbf{r}} + \dot{\mathbf{V}}\frac{\partial f}{\partial \mathbf{V}} + \frac{\partial}{\partial \mathbf{M}}(\dot{\mathbf{M}}f)$$
$$= \int (f'f_1' - ff_1)\, W\, d\mathbf{V}_1 d\mathbf{V}' d\mathbf{V}_1' d\Gamma_1 d\Gamma' d\Gamma_1'. \qquad (2.5)$$

In writing down the righ-hand side of (2.5), we assumed that the collision probability is an even function of the angular momenta of the colliding molecules. We note that, if the model of a solid body is used in the description of the collisions of the molecules, W involves an average over ψ and ψ_1 and a sum over ψ' and ψ_1'.

Let us consider the case where there are no external forces. Assuming a small deviation from equilibrium, we shall seek the solution in the form

$$f = f^0(1+\chi), \qquad (2.6)$$

where we choose for f^0 a quasi-equilibrium local distribution of the form (2.3) with V replaced by $\mathbf{U} = \mathbf{V} - \mathbf{V}_0$ ($\mathbf{V}_0$ is the macroscopic velocity of the gas at the given point). For each point in space we assume that there is no rotation of the gas as a whole.

The total distribution function is subject to the conditions

$$\int f\, d\mathbf{V}\, d\Gamma = n, \qquad \int f\left(\frac{\mu U^2}{2} + \frac{M^2}{2I}\right) d\mathbf{V}\, d\Gamma = \frac{5}{2}kT,$$
$$\int f\mathbf{U}\, d\mathbf{V}\, d\Gamma = 0, \qquad \int f\mathbf{M}\, d\mathbf{V}\, d\Gamma = 0. \qquad (2.7)$$

Let us substitute (2.6) in (2.5). Keeping, as usual, only f^0 on the left and linearizing the collision integral, we find with the help of the conservation laws

$$f^0\left\{\left(u^2 + m^2 - \frac{7}{2}\right)\mathbf{U}\frac{\partial \ln T}{\partial \mathbf{r}} + u_i u_k\left(\frac{\partial V_{0l}}{\partial x_k} + \frac{\partial V_{0k}}{\partial x_i}\right.\right.$$
$$\left.\left. - \frac{2}{3}\delta_{ik}\frac{\partial V_{0l}}{\partial x_l}\right) + \frac{2}{5}\left(\frac{2}{3}u^2 - m^2\right)\frac{\partial V_{0l}}{\partial x_l}\right\}$$
$$= \int f^0 f_1^0 \{\chi\}\, W\, d\mathbf{V}_1 d\mathbf{V}' d\mathbf{V}_1' d\Gamma_1 d\Gamma' d\Gamma_1'. \qquad (2.8)$$

Here

$$\mathbf{u} = \sqrt{\mu/2kT}\,\mathbf{U}, \qquad \mathbf{m} = \mathbf{M}/\sqrt{2IkT}, \qquad (2.9)$$
$$\{\chi\} = \chi' + \chi_1' - \chi - \chi_1. \qquad (2.10)$$

3. THERMAL CONDUCTIVITY

Let us now consider the problem of thermal conductivity. If the gradient of the macroscopic velocity vanishes, Eq. (2.8) reduces to

$$f^0\left(u^2 + m^2 - \frac{7}{2}\right)\mathbf{U}\nabla \ln T = J_{\text{coll}}(\chi). \qquad (3.1)$$

We write the solution of this equation in the form

$$\chi = -\mathbf{A}\nabla \ln T. \qquad (3.2)$$

Substituting (3.2) in (3.1), we find

$$f^0\left(u^2 + m^2 - \frac{7}{2}\right)\mathbf{U} = -J_{\text{coll}}(\mathbf{A}). \qquad (3.3)$$

In the case of a monatomic gas only the vector u is available for constructing the vector A, and we therefore seek the solution in the form $\mathbf{A} = \mathbf{u}S$, where S is a scalar function of u^2. In the case of a gas with rotational degrees of freedom we have three independent vectors: u, $\mathbf{m}(\mathbf{m}\cdot\mathbf{u})$, and $\mathbf{m}\times\mathbf{u}$. Therefore A is in general written as

$$\mathbf{A} = \mathbf{u}S_1(u^2, m^2, t^2) + \mathbf{m}(\mathbf{mu})\, S_2(u^2, m^2, t^2)$$
$$+ [\mathbf{mu}]\, S_3(u^2, m^2, t^2), \qquad (3.4)^*$$

where

$$t^2 = (\mathbf{mu})^2/m^2u^2. \qquad (3.5)$$

The left-hand side of (3.1) and the kernel of the collision integral are even functions of M. It is easy to show that then

$$S_3 \equiv 0. \qquad (3.6)$$

Thus the problem of the thermal conductivity is determined by the two scalar functions S_1 and S_2.

Let us expand these functions in terms of orthogonal functions in the following way:

$$S_1 = \sum_{ikl} a_1^{ikl} S_i^{3/2}(u^2)\, S_k^0(m^2)\, P_l^0(t^2) \equiv \sum_{ikl} a_1^{ikl} R_{ikl}^1,$$
$$S_2 = \sum_{ikl} a_2^{ikl} S_i^{3/2}(u^2)\, S_k^1(m^2)\, P_l^1(t^2) \equiv \sum_{ikl} a_2^{ikl} R_{ikl}^2, \qquad (3.7)$$

where the S_i^α are Sonine polynomials with the corresponding indices and the $P_l^{0,1}$ are polynomials which are orthogonal in the interval $(-1, 1)$, with weights 1 and t^2, respectively:

$$\int_{-1}^{1} P_l^0(t^2)\, P_{l'}(t^2)\, dt = \delta_{ll'}, \qquad \int_{-1}^{1} t^2 P_l^1(t^2)\, P_{l'}(t^2)\, dt = \delta_{ll'}.$$

If we consider only a finite number of terms in (3.7), the best variational solution is found from a system of algebraic equations which is obtained by multiplying (3.1) successively by $\mathbf{u}R_{ikl}^1$ and $\mathbf{m}(\mathbf{m}\cdot\mathbf{u})R_{ikl}^2$ and integrating over $d\mathbf{V}\,d\Gamma$.

We note that the choice of polynomials for the expansion of S_1 and S_2 is arbitrary and is dictated only by numerical simplicity. This arbitrariness stems from the fact that the variational principle does not even presuppose orthogonal polynomials.

The conditions (2.7) imply that not all coefficients in the expansion (3.7) are independent. Using (3.2), (3.4), and (3.7), we find

*$[\mathbf{mu}] = \mathbf{m}\times\mathbf{u}$.

$$a_1^{000} + \tfrac{1}{3} a_2^{000} = 0. \tag{3.8}$$

Let us now define the heat current:

$$\mathbf{q} = \int f^0 \chi \mathbf{U} \left(\frac{\mu U^2}{2} + \frac{M^2}{2I} \right) d\mathbf{V}\, d\Gamma \equiv -\lambda \nabla T.$$

Substituting in this the value of χ, we obtain

$$\lambda = \frac{nk}{3} \left(\frac{2kT}{\mu} \right)^{1/2} \left[\frac{15}{4} a_1^{100} + \frac{3}{2} a_1^{010} + \frac{1}{2} a_2^{000} + \frac{5}{4} a_2^{100} + a_2^{010} \right]. \tag{3.9}$$

4. FIRST AND SECOND VISCOSITY

Assume now that $\nabla T = 0$. The solution of the general kinetic equation (2.8) will then be sought in the form

$$\chi = -B_{ik} \left(\frac{\partial V_{0l}}{\partial x_k} + \frac{\partial V_{0k}}{\partial x_l} - \frac{2}{3} \delta_{ik} \frac{\partial V_{0l}}{\partial x_l} \right) - C \frac{\partial V_{0l}}{\partial x_l}, \tag{4.1}$$

where B_{ik} is a symmetric tensor with vanishing trace. Substituting (4.1) in (2.8), we find

$$f^0 \left(u_i u_k - \tfrac{1}{3} \delta_{ik} u^2 \right) = -J_{\text{coll}} (B_{ik}), \tag{4.2}$$

$$f^0 \left(\tfrac{4}{15} u^2 - \tfrac{2}{5} m^2 \right) = -J_{\text{coll}} (C). \tag{4.3}$$

In the most general case the tensor B_{ik} can be written as

$$\begin{aligned} B_{ik} = {} & B_1 \left(u_i u_k - \tfrac{1}{3} \delta_{ik} u^2 \right) + B_2 \left(m_i m_k - \tfrac{1}{3} \delta_{ik} m^2 \right) \\ & + B_3 \left([\mathbf{mu}]_i [\mathbf{mu}]_k - \tfrac{1}{3} \delta_{ik} [\mathbf{mu}]^2 \right) + B_4 (\mathbf{mu}) \left(m_i u_k \right. \\ & \left. + u_i m_k - \tfrac{2}{3} \delta_{ik} (\mathbf{mu}) \right) + B_5 \left(u_i [\mathbf{mu}]_k + u_k [\mathbf{mu}]_i \right) \\ & + B_6 (\mathbf{mu}) \left(m_i [\mathbf{mu}]_k + m_k [\mathbf{mu}]_i \right). \end{aligned} \tag{4.4}$$

Here the B_i are scalar functions of u^2, m^2, and t^2. Since the left-hand side of (4.2) is again an even function of $\mathbf{M}$, the evenness of the kernel of the collision integral leads to the relations

$$B_5 \equiv 0, \qquad B_6 \equiv 0. \tag{4.5}$$

We expand the quantities B_i in terms of orthogonal polynomials:

$$B_1 = \sum_{ikl} b_1^{ikl} S_i^{5/2} (u^2)\, S_k^0 (m^2)\, P_l^0 (t^2), \tag{4.6}$$

$$B_2 = \sum_{ikl} b_2^{ikl} S_i^{3/2} (u^2)\, S_k^1 (m^2)\, P_l^0 (t^2), \tag{4.7}$$

$$B_3 = \sum_{ikl} b_3^{ikl} S_i^{3/2} (u^2)\, S_k^1 (m^2)\, P_l^{(0,1)} (t^2), \tag{4.8}$$

$$B_4 = \sum_{ikl} b_4^{ikl} S_i^{3/2} (u^2)\, S_k^1 (m^2)\, P_l^1 (t^2). \tag{4.9}$$

The $P_l^{(0,1)}$ are orthogonal with weight $1 - t^2$. With B_{ik} defined as in (4.4), the conditions (2.7) are satisfied automatically.

We write the scalar function C which solves (4.3) in such a form that the conditions (2.7) are automatically fulfilled:

$$C = c_0 \left(\tfrac{2}{3} u^2 - m^2 \right) + \sum_{ikl} c^{ikl} S_i^{1/2} (u^2)\, S_k^0 (m^2)\, P_l^0 (t^2),$$

$$c^{000} = c^{100} = c^{010} = 0. \tag{4.10}$$

Let us now determine the expression for the stress tensor:

$$\sigma_{ik} = -\mu \int f^0 \chi\, U_i U_k\, d\mathbf{V}\, d\Gamma.$$

Substituting (4.1) and taking account of (4.4) to (4.10), we find

$$\sigma_{ik} = \eta \left(\frac{\partial V_{0i}}{\partial x_k} + \frac{\partial V_{0k}}{\partial x_i} - \frac{2}{3} \delta_{ik} \frac{\partial V_{0l}}{\partial x_l} \right) + \zeta \delta_{ik} \frac{\partial V_{0l}}{\partial x_l}, \tag{4.11}$$

where the first viscosity coefficient η is given by the expression

$$\eta = nkT \left(b_1^{000} + \left(\tfrac{2}{5} \right)^{3/2} b_2^{001} - \tfrac{1}{3} b_3^{000} + \tfrac{2}{3} b_4^{000} \right), \tag{4.12}$$

and the coefficient of second viscosity ζ by

$$\zeta = 2kT c_0 / 3. \tag{4.13}$$

The coefficients entering in (4.12) and (4.12) are determined approximately from a system of algebraic equations obtained from (4.2) and (4.3) by making use, as in the case of the thermal conductivity, of the usual variation procedure.

5. ON THE COLLISION INTEGRAL FOR THE MODEL OF SOLID BODIES

The results obtained in the preceding sections are very general and can be used for any type of interaction between the molecules.

In calculating the kinetic coefficients in the present paper, we describe the collisions between the molecules with the help of the model of elastic cylinder-spheres (see the following section). However, the use of the model of solid bodies necessitates a careful analysis of the collision integral. This is the more imperative as the expression for the collision integral given as exact in [3,4] is actually highly approximate and can in extreme cases lead to absurd results (see below).

For a complete description of the collision between two molecules with definite velocities $\mathbf{V}$, $\mathbf{V}_1$ and angular momenta $\mathbf{M}$, $\mathbf{M}_1$ we need only four variables: X, Y, the coordinates of the center of gravity of the incoming molecule in the plane perpendicular to the relative velocity $\mathbf{g} = \mathbf{V}_1 - \mathbf{V}$, and ψ_0, ψ_{01}, the values of the angles ψ, ψ_1 when the centers of gravity of the molecules are located at

some fixed distance a from one another. Then we have for the part of the collision integral corresponding to emission from a given element of the phase volume

$$-\int f(\mathbf{VM})\, f(\mathbf{V}_1\mathbf{M}_1)\, g\, dX\, dY \frac{d\psi_0}{2\pi}\frac{d\psi_{01}}{2\pi}\, d\mathbf{V}_1 d\Gamma_1. \qquad (5.1)$$

The corresponding limits of integration are evidently closely connected with the geometry of the molecules. For molecules with a center of symmetry it is easy to obtain an expression for the inverse transitions. For this purpose we must use the connection between quantities before and after the collision (see [3]):

$$\begin{aligned} \mathbf{V}_1' &= \mathbf{V}_1 - \xi(\mathbf{kG})\,\mathbf{k}, \qquad \mathbf{V}' = \mathbf{V} + \xi(\mathbf{kG})\,\mathbf{k}, \\ \mathbf{M}_1' &= \mathbf{M}_1 - \xi(\mathbf{kG})\,[\sigma_1\mathbf{k}], \quad \mathbf{M}' = \mathbf{M} + \xi(\mathbf{kG})\,[\sigma\mathbf{k}], \\ \xi &= [1 + (m/2I)\{[\sigma\mathbf{k}]^2 + [\sigma_1\mathbf{k}]^2\}]^{-1}. \end{aligned} \qquad (5.2)$$

Here $\mathbf{k}$ is a unit vector normal to the surface of the molecules at the point of contact, σ and σ_1 are the vectors from the centers of the corresponding molecules to the point of contact, and $\mathbf{G}$ is the relative velocity of the colliding molecules at the point of contact:

$$\mathbf{G} = \mathbf{V}_1 - \mathbf{V} + \left[\frac{\mathbf{M}_1}{I}\sigma_1\right] - \left[\frac{\mathbf{M}}{I}\sigma\right]. \qquad (5.3)$$

Let us now go over from the variables X, Y, ψ_0, ψ_{01} to the variables $\mathbf{k}$, ψ, ψ_1 (ψ, ψ_1 are the angles at the time of collision), using the relations

$$\psi_0 = \psi - Mt_0/I, \qquad (5.4)$$

$$\psi_{01} = \psi_1 - M_1 t_0/I, \qquad (5.5)$$

$$\mathbf{R} = \mathbf{R}(\mathbf{k}, \psi, \psi_1, \mathbf{M}, \mathbf{M}_1), \qquad (5.6)$$

$$t_0 = (\mathbf{a} - \mathbf{R})\,\mathbf{g}/g^2, \qquad (5.7)$$

where $\mathbf{R}\{X, Y, Z\}$ is the radius vector connecting the centers of the molecules at the moment of the collision and $\mathbf{a}$ is an arbitrary vector. The form of (5.6) can be established immediately for any given geometry.

The Jacobian for making the transition from the old to the new variables is equal to (see the Appendix)

$$\partial(X, Y, \psi_0, \psi_{01})/\partial(\mathbf{k}, \psi, \psi_1) = \frac{\mathbf{kG}}{g} S(\mathbf{k}); \qquad (5.8)$$

$S(\mathbf{k})\,d\mathbf{k}$ is the surface element of the surface defined by (5.6) with constant ψ, ψ_1, $\mathbf{M}$, and $\mathbf{M}_1$.

The expression for the collision integral in the new variables is

$$\int (f'f_1' - ff_1)\,|\mathbf{kG}|\, S(\mathbf{k})\, d\mathbf{k} \frac{d\psi}{2\pi}\frac{d\psi_1}{2\pi}\, d\mathbf{V}_1\, d\Gamma_1. \qquad (5.9)$$

It is easily seen that the region of integration is bounded by the condition

$$\mathbf{kG} < 0 \qquad (5.10)$$

(only those parts of the surface collide which move toward one another). However, condition (5.10) is not the only restriction on the region of possible values of $\mathbf{k}$, ψ, and ψ_1. This has to do with the fact that in general $\mathbf{k}$, ψ, and ψ_1 are multivalued functions of X, Y, ψ_0, and ψ_{01}. Of all the possible values one must evidently choose only that which corresponds to the smallest t_0. This implies a further restriction on the region of possible values of $\mathbf{k}$, ψ, and ψ_1.

It is easily seen that the formula (5.9) with only the condition (5.10) is completely useless for $\dot{\psi} \gg g/l$, where l is a characteristic dimension of the molecules. [For $g = 0$ the molecules do not collide at all, while there is a nonvanishing contribution according to (5.9).] In the opposite limiting case the multivaluedness does not play a role, and we can use the formulas (5.9) and (5.10).

Thus it is clear that using a collision integral of the form (5.9) with the restriction (5.10) is in general only an approximate procedure. The determination of the exact region of integration in (5.9) for arbitrary $\dot{\psi}$ is a complicated problem. In view of the fact that in many actual cases $\dot{\psi} \lesssim g/l$, we have used (5.9) and (5.10) in all specific calculations.

In this case the use of a more exact region of integration should lead only to relatively small corrections.

6. CALCULATION OF THE KINETIC COEFFICIENTS. THE MODEL OF CYLINDER-SPHERES

Let us now go over to the direct determination of the kinetic coefficients, using the results of Secs. 3 and 4 with a collision integral of the form (5.9) and (5.10).

In calculating the coefficient of thermal conductivity, we restrict ourselves to the first three terms in the expansion of S_1 and to the first term in the expansion of S_2 [see (3.7)]:

$$S_1 = a_1^{000} + a_1^{100}(u^2 - \tfrac{5}{2}) + a_1^{010}(m^2 - 1), \qquad S_2 = a_2^{000}. \qquad (6.1)$$

Multiplying (3.1) by $\mathbf{u}(u^2 - 5/2)$, $\mathbf{u}(m^2 - 1)$, and $\mathbf{m}(\mathbf{m}\cdot\mathbf{u})$ and integrating over $d\mathbf{V}d\Gamma$, we obtain a system of equations for the determination of the coefficients a_1^{100}, a_1^{010}, and a_2^{000}:

$$\begin{aligned} C_1 &= c_{11}a_1^{100} + c_{12}a_1^{010} + c_{13}a_2^{000}, \quad C_2 = c_{21}a_1^{100} + c_{22}a_1^{010} \\ &+ c_{23}a_2^{000}, \quad C_3 = c_{31}a_1^{100} + c_{32}a_1^{010} + c_{33}a_2^{000}. \end{aligned} \qquad (6.2)$$

The coefficient a_1^{000} is determined by condition (3.8).

The computation of the coefficients C_i is elementary. The determination of the c_{ik} involves an integration over 16 variables. However, through a series of linear substitutions we can carry out the integration over 10 variables without reference to a particular model. The expression for c_{ik} is of the form

$$c_{ik} = \frac{V\bar{2}\, n^2}{8\pi^2} \int \Phi_1^0 \Phi^0 A_i \{A_k\} \,|\, kw \,|\, S(k)\, dk\, du_1\, du\, d\tilde{\Gamma}_1\, d\Gamma, \quad kw < 0, \tag{6.3}$$

where

$$A_1 = \left(u^2 - \tfrac{5}{2}\right) u, \quad A_2 = (m^2 - 1)\, u, \quad A_3 = m\,(mu),$$

$$w = \left(\frac{2kT}{\mu}\right)^{1/2} G, \quad d\tilde{\Gamma} = m dm\, d\Omega_m, \quad \Phi^0 = \pi^{-3/2} e^{-u^2 - m^2}.$$

Let us first go over from the variables $\mathbf{m}$, ψ, $\mathbf{m}_1$, ψ_1 to the variables $\mathbf{l}$, m_n, m_τ, $\mathbf{l}_1$, m_{n_1}, m_{τ_1}, where $\mathbf{l}$ and $\mathbf{l}_1$ are unit vectors defining the direction of the axes of the molecules in space, m_n and m_{n_1} are the projections of the vectors $\mathbf{m}$ and $\mathbf{m}_1$ on the vector $\mathbf{l} \times \mathbf{l}_1$, m_τ is the projection of $\mathbf{m}$ on the vector $\mathbf{n} \times \mathbf{l}$, and m_{τ_1} is the projection of $\mathbf{m}_1$ on the vector $\mathbf{n} \times \mathbf{l}_1$.

It is easy to show that

$$d\tilde{\Gamma}\, d\psi = dm_n\, dm_\tau\, dl. \tag{6.4}$$

Then we make the following substitutions:

$$u = (Q - \gamma)/V\bar{2}, \quad u_1 = (Q + \gamma)/V\bar{2}, \tag{6.5}$$

$$m_{\tau_1} = (r_1 x + r y)/\sqrt{r_1^2 + r^2}, \quad m_\tau = (-r x + r_1 y)/\sqrt{r_1^2 + r^2},$$

$$\gamma_3 = (t - \sqrt{r_1^2 + r^2}\, z)/\sqrt{1 + r_1^2 + r^2}, \tag{6.6}$$

$$x = (\sqrt{r_1^2 + r^2}\, t + z)/\sqrt{1 + r_1^2 + r^2}, \tag{6.7}$$

where

$$r^2 = \frac{\mu}{2I}[\sigma k]^2, \quad r_1^2 = \frac{\mu}{2I}[\sigma_1, k]^2, \quad \gamma_3 = k\gamma.$$

The product $\Phi^0 \Phi_1^0$ can be written in terms of the new variables:

$$\Phi^0 \Phi_1^0 = \pi^{-5} \exp\{-Q^2 - \gamma_1^2 - \gamma_2^2 - y^2 - t^2 - z^2 - m_n^2 - m_{n_1}^2\}, \tag{6.8}$$

where γ_1 and γ_2 are the projections of the vector γ on two mutually orthogonal axes perpendicular to the vector $\mathbf{k}$.

Taking account of the fact that $A_i\{A_k\}$ can be expressed as a sum of products of the type [we use (6.5) to (6.7) and (5.2)]

$$F(k, ll_1)\, Q^n \gamma_1^m \gamma_2^l y^p t^q z^s m_n^t m_{n_1}^d \tag{6.9}$$

and that the region of integration (5.10) goes over into the region $t > 0$, we see easily that the integration over the variables

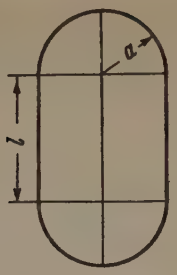

$$dQ\, d\gamma_1\, d\gamma_2\, dm_n\, dm_{n_1}\, dy\, dt\, dz$$

is completely trivial, and the final result can be expressed as a product of Γ functions.

Only the integration over $dk\, dl\, dl_1$ remains to be done in (6.3). In order to carry out this integration, we must know the explicit form of $S(k)$.

We shall use the model of cylinder-spheres. In this model the collision of the molecules is described by the collision of solid bodies of cylindrical shape with hemispheres at each end (see the figure). Our model has some peculiarities which have to do with the fact that the vector $\mathbf{k}$ cannot define a point on the cylindrical surface uniquely. For collisions involving the cylindrical surfaces it is therefore advantageous to define the point of contact by two other parameters α_1 and α_2.

In collisions involving the cylindrical surfaces we can take for these parameters $\sigma_l = \sigma \cdot \mathbf{l}$ and $\sigma_{l_1} = \sigma_1 \cdot \mathbf{l}_1$, which define the point of contact for a given position of the molecules (except for the distinction between "from above" and "from below"). In this case $S(k)\, dk$ goes over into

$$S(\sigma_l, \sigma_{l_1})\, d\sigma_l\, d\sigma_{l_1} = 2 \sin\Phi\, d\sigma_l\, d\sigma_{l_1}, \tag{6.10}$$

where

$$\sin\Phi = [ll_1].$$

For collisions involving the spherical surfaces we have

$$S(k)\, dk = 4a^2\, dk. \tag{6.11}$$

For mixed collisions we must write instead of $S(k)\, dk$

$$S(z, \tilde{\varphi})\, dz\, d\tilde{\varphi} = 2a dz\, d\tilde{\varphi}, \tag{6.12}$$

where z and $\tilde{\varphi}$ are the cylindrical coordinates of the point of contact in a coordinate system with a Z axis along the axis of the molecule which collides at a point of its cylindrical surface.

The integral (6.3) thus separates into three integrals. All integrals are evaluated completely.*

*We note that some of the resulting integrals have been computed in[3].

We shall not quote here the resulting complicated formulas for the c_{ik}. We give only the final expressions for the coefficients a_1^{100}, a_1^{010}, and a_2^{000} obtained as a solution of the system (6.2):

$$a_1^{100} \approx 0.34 \frac{1}{nl^2} \frac{1}{\beta^2+\beta+0.12}, \quad (6.13)$$

$$a_1^{010} \approx 0.48 \frac{1}{nl^2} \frac{1}{\beta^2+\beta+0.12}, \quad (6.14)$$

$$a_2^{000} \approx -0.17 \frac{1}{nl^2} \frac{1}{\beta^2+\beta+0.12}, \quad (6.15)$$

where $\beta = 2a/l$. These results refer to the case $\beta \gtrsim 1$, $\alpha = 4I/\mu l^2 = 1/2$. This value of the coefficient α corresponds to a diatomic molecule of the type A–A in which the atoms are located at a distance l from one another.

Information on the geometry of the molecules can be obtained if the virial coefficients are known.[2] It turns out that $\beta > 1$ in most cases.

Expressions for the coefficients a_1^{100}, a_1^{010}, and a_2^{000} can be found for arbitrary values of α and β. However, the general expressions are very complicated, and we shall be content with quoting only a particular example.

Substituting (6.13) to (6.15) in (3.9), we obtain an expression for the coefficient of thermal conductivity:

$$\lambda \approx 1.6\, k\left(\frac{kT}{\pi\mu}\right)^{1/2} \frac{1}{l^2} \frac{1}{\beta^2+\beta+0.12}. \quad (6.16)$$

It is interesting to note that all coefficients (6.13) to (6.15) are of the same order of magnitude, although their contributions to the coefficient of thermal conductivity are quite different [see formula (3.9)].

Finally, we give the final expressions for the first and second viscosity, obtained under the simplest assumptions:

$$B_1 = b_1^{000}, \qquad B_2 = B_3 = B_4 = 0, \qquad C = \left(\frac{2}{3}u^2 - m^2\right)c_0$$

[see formulas (4.6) to (4.9) and (4.10)]. For $\alpha = 1/2$ and $\beta \gtrsim 1$ we have

$$\eta \approx 0.32\, \mu\left(\frac{kT}{\pi\mu}\right)^{1/2} \frac{1}{l^2} \frac{1}{\beta^2+\beta+0.12}, \quad (6.17)$$

$$\zeta \approx 0.067\, \mu\left(\frac{kT}{\pi\mu}\right)^{1/2} \frac{1}{l^2} \frac{1}{\beta^2+0.87\beta+0.12}. \quad (6.18)$$

APPENDIX

Here we determine the value of the Jacobian

$$J_3 = \partial(X, Y, \psi_0, \psi_{01})/\partial(\cos\theta, \varphi, \psi, \psi_1), \quad (A.1)$$

where θ, φ are the angles which define the unit vector $\mathbf{k}$ in some coordinate system.

Using (5.4) to (5.6), we find easily

$$J = \frac{S(\mathbf{k})}{g}\left[\mathbf{gk} - \mathbf{k}\left(\frac{M}{I}\frac{\partial \mathbf{R}}{\partial \psi} + \frac{M_1}{I}\frac{\partial \mathbf{R}}{\partial \psi_1}\right)\right]. \quad (A.2)$$

We have made use of the fact that

$$S(\mathbf{k}) = \left[\left(\frac{\partial(XY)}{\partial(\cos\theta, \varphi)}\right)^2 + \left(\frac{\partial(Z, X)}{\partial(\cos\theta, \varphi)}\right)^2 + \left(\frac{\partial(Y, Z)}{\partial(\cos\theta, \varphi)}\right)^2\right]^{1/2},$$

$$k_x = \frac{1}{S(\mathbf{k})}\frac{\partial(Y, Z)}{\partial(\cos\theta, \varphi)}$$

and analogously for the other projections.

Let us now determine $(\partial \mathbf{R}/\partial\psi)_{\psi_1, \mathbf{k}}$. We see immediately that in general

$$\left(\frac{\partial \mathbf{R}}{\partial \psi}\right)_{\mathbf{k}, \psi_1} = \left[\frac{\mathbf{M}}{M}\sigma\right] + \mathbf{a}, \quad \left(\frac{\partial \mathbf{R}}{\partial \psi_1}\right)_{\mathbf{k}, \psi} = -\left[\frac{\mathbf{M}_1}{M_1}\sigma_1\right] + \mathbf{a}_1, \quad (A.3)$$

where $\mathbf{a}$ and $\mathbf{a}_1$ are vectors perpendicular to $\mathbf{k}$ which depend on the type of surface. Substituting (A.3) in (A.2), we find

$$J = \frac{S(\mathbf{k})}{g}\left\{\mathbf{gk} + \mathbf{k}\left(\left[\frac{\mathbf{M}_1}{I}\sigma_1\right] - \left[\frac{\mathbf{M}}{I}\sigma\right]\right)\right\}.$$

Using (5.3), we obtain (5.8).

[1] S. Chapman and T. G. Cowling, The Mathematical Theory of Non-Uniform Gases, Cambridge (1939).

[2] Hirschfelder, Curtiss, and Bird, Molecular Theory of Gases and Liquids, J. Wiley and Sons, Inc., N. Y. (1954).

[3] C. F. Curtiss, J. Chem. Phys. 24, 225 (1956). C. F. Curtiss and C. Muckenfuss, J. Chem. Phys. 26, 1619 (1957).

[4] Y. Ishida, Phys. Rev. 10, 305 (1917).

Translated by R. Lipperheide
260

SCATTERING OF PHOTONS BY NUCLEONS

L. I. LAPIDUS and CHOU KUANG-CHAO

Joint Institute for Nuclear Research

Submitted to JETP editor May 18, 1961

J. Exptl. Theoret. Phys. (U.S.S.R.) 41, 1546-1555 (November, 1961)

An analysis of elastic scattering of photons with energies up to 300 Mev by protons is carried out by making use of the dispersion relations method. Six dispersion relations are utilized to estimate the real parts of the amplitudes at $Q^2 = 0$. Photoproduction of pions is taken into account in a larger energy region than was done previously. Five subtraction constants are determined from the long wavelength limit and expressed in terms of the nucleon charge and magnetic moment. Differential cross sections and polarizations of the recoil nucleons are estimated. Photon-nucleon scattering at high energies is discussed.

1. Following the work of Gell-Mann, Goldberger, and Thirring[1] dispersion relations for photon-nucleon scattering, whose validity in the e^2-approximation has been rigorously proved by Logunov,[2] have been applied to the analysis of experimental data by a number of workers.[3-7] Cini and Stroffolini[3] were the first to calculate forward scattering cross sections for photons with energies up to 210 Mev. Certain qualitative peculiarities in the energy dependence of the forward scattering cross section were indicated earlier in[1], and also in[8].

Capps[4] has considered γN scattering through an arbitrary angle by taking into account a minimal number of states. In so doing he made use of some unpublished results of Gell-Mann and J. Mathews.

Akiba and Sato[5] considered scattering through nonzero angles. In order to evaluate the subtraction constants in some of the dispersion relations they made use of perturbation theory.

The authors have previously[6] considered in detail dispersion relations for all six invariant functions, that characterize the γN-scattering amplitude, and have carried out a dispersion analysis in the energy region up to 200 Mev in an approximation in which certain recoil effects were ignored. It was shown that if photoproduction of pions in S states is taken into account significant modifications are introduced in the near threshold region. These changes are such as to improve the aggreement between the dispersion analysis and experiment. Near threshold the energy dependence of the amplitudes and cross sections becomes nonmonotonic.

Aside from certain differences, connected with what assumptions were made regarding the number of subtraction constants in the dispersion relations and the maximum angular momentum of the states taken into account, all the published papers turned out to have in common the inability to obtain good agreement with experimental data in the energy region near 160—200 Mev.

In a number of papers[9,7,10] an attempt was made to eliminate this discrepancy by taking into account the contribution from Low's diagram.[11] However a direct measurement of the lifetime of the π^0 meson[12] together with an analysis of the question of the sign of the pole amplitude[13] have led to the conclusion, that the inclusion of Low's amplitude cannot substantially affect the results of the analysis. In connection with these discrepancies between the analysis and the existing experimental data we carry out in this work an analysis of γN scattering based on dispersion relation, in which we take into account in addition to photoproduction of pions in S states the contribution from the high energy regions in a more careful manner; we also analyze the question of the number of subtractions in the dispersion relations and, taking nucleon recoil fully into account, estimate the previously introduced quantities $R_i(\nu)$ at $Q^2 = 0$.

2. The connection between the invariant functions $T_i(\nu, Q^2)$ and the amplitudes $R_i(\nu, Q^2)$ in the barycentric system is given by Eq. (1) of[14] (in the following[14] will be referred to as A). For the definitions of $T_i(\nu, Q^2)$ and $R_i(\nu, Q^2)$ see[13] (in the following[13] will be referred to as B). The notation in the present paper is the same as the notation in A and B. By R_i without additional marks we will understand here the amplitudes in the barycentric frame.

Since according to the optical theorem

$$\mathrm{Im}\,(R_1+R_2)=\frac{v_c\sigma_t}{4\pi}=\frac{w^2-M^2}{2w}\frac{\sigma_t}{4\pi} \qquad (1)$$

(w is the total energy in the barycentric frame) it follows that under the assumption

$$\sigma_t(w)\to\text{const as } w\to\infty$$

we have asymptotically as $w\to\infty$

$$R_1+R_2\to w^2\sim\nu. \qquad (2)$$

Assuming further that as $w\to\infty$ all $R_i\sim\nu$, we get from A, Eq. (1) that as $w\to\infty$

$$T_1-T_3\to w^2,\quad T_1+T_3\to w^2,\quad T_5\to w^2,$$
$$T_2-T_4\to w,\quad T_2+T_4\to\text{const},\quad T_6\to w. \qquad (3)$$

Consequently, under the assumptions here made, the dispersion relations for T_1, T_3 and T_5 should contain one subtraction, whereas the dispersion relations for the quantities T_2, T_4 and T_6 may be written with no subtractions.

In order to estimate the amplitudes R_1+R_2, R_3, R_4, and R_5+R_6 it is sufficient to write dispersion relations for T_1, T_3 and T_5 at $Q^2=0$. At $Q^2=0$ the invariant

$$\nu=\nu_{\text{lab}}-Q^2/M$$

becomes, as is well known, the photon energy in the laboratory frame ν_{lab} (denoted in the following by ν).

3. As can be seen from A, Eq. (1), for forward scattering the functions T_5 and T_2+T_4 reduce to R_4-R_3, so that at $Q^2=0$ the dispersion relations for T_5 and T_2+T_4 are equivalent.

Let us consider the functions

$$F_1(\nu_0)=\tfrac{1}{2}[T_1-T_3-\nu_0(T_2-T_4)]=w_0(R_1+R_2)/M,$$
$$F_2(\nu_0)=\nu_0T_6=w_0[R_3+R_4+2R_5+2R_6]/M,$$
$$F_3(\nu_0)=\nu_0(T_1+T_3)/2M=(w_0/M)^2(R_3-R_4),$$
$$F_4(\nu_0)=\tfrac{1}{2}(T_1-T_3)$$
$$=w_0^2(R_3+R_4)/M\nu_0-2w_0(R_1+R_2)/(M+w_0). \qquad (4)$$

It is clear from the discussion above that the dispersion relations for the functions $F_1,\ldots,F_4$ should contain one subtraction. All quantities on the right side of Eq. (4) are in the barycentric frame. If one takes into account that (for $Q^2=0$) the amplitudes in the laboratory system are connected to the corresponding quantities in the barycentric system by

$$(R_1+R_2)^{\pi}=w_0(R_1+R_2)/M,$$
$$(R_4-R_3)^{\pi}=(w_0/M)^2(R_4-R_3), \qquad (5)$$
$$[R_3+R_4+2R_5+2R_6]^{\pi}=w_0[R_3+R_4+2R_5+2R_6]/M,$$

then one obtains from the dispersion relations for $F_1,\ldots,F_4$

$$D_{1,4}^{\text{lab}}(\nu_0)-D_{1,4}(0)=\frac{2\nu_0^2}{\pi}\int_{\nu_t}^{\infty}\frac{d\nu}{\nu^2-\nu_0^2}\frac{A_{1,4}(\nu)}{\nu},$$
$$D_{2,3}^{\text{lab}}(\nu_0)-\nu_0D'_{2,3}(0)=\frac{2\nu_0^3}{\pi}\int_{\nu_t}^{\infty}\frac{A_{2,3}(\nu)\,d\nu}{\nu^2(\nu^2-\nu_0^2)}, \qquad (6)$$

where

$$D_1^{\pi}=\mathrm{Re}\,(R_1+R_2)^{\text{lab}},\quad D_2^{\text{lab}}=\mathrm{Re}\,[R_3+R_4+2R_5+2R_6]^{\text{lab}},$$
$$D_3^{\text{lab}}=\mathrm{Re}\,(R_4-R_3)^{\text{lab}},\quad D_4^{\text{lab}}=\mathrm{Re}\,F_4(\nu);$$
$$D_1(0)=-e^2/M,\quad D'_2(0)=-2\mu^2_a,$$
$$D'_3(0)=-2[\mu^2-(e/2M)^2],\quad D_4(0)=-(e^2/2M)\lambda(2+\lambda),$$

and where $A_i(\nu_0)$ stands for the imaginary part of the corresponding amplitude; $\mu=e(1+\lambda)/2M$ stands for the magnetic moment and μ_a for the anomalous magnetic moment of the nucleon.

If the elements of the amplitude for the photoproduction of pions in states with $J\le{}^3/_2$ in the barycentric frame are denoted by E_1, E_2, E_3 (electric transitions into ${}^1/_2{}^-$, ${}^3/_2{}^+$ and ${}^3/_2{}^-$ respectively), M_1, M_2, M_3 (magnetic transitions into ${}^1/_2{}^+$, ${}^3/_2{}^-$ and ${}^3/_2{}^+$ respectively), then the unitarity relations lead to the equalities

$$\mathrm{Im}\,R_1=\nu_c\left\{|E_1|^2+2|E_3|^2+\tfrac{1}{3}|E_2|^2\cos\theta-\tfrac{1}{6}|M_2|^2\right\},$$
$$\mathrm{Im}\,R_3=\nu_c\left\{|E_1|^2+\tfrac{1}{3}|E_2|^2\cos\theta\right.$$
$$\left.-|E_3|^2+\tfrac{1}{12}|M_2|^2+\mathrm{Re}\,(E_3^*M_2)\right\},$$
$$\mathrm{Im}\,R_5=-\nu_c\left\{\tfrac{1}{6}|E_2|^2+\mathrm{Re}\,(E_2^*M_3)\right\}, \qquad (7)$$

which represent the generalization of the corresponding equalities in[6]. The expressions for Im R_2 differ from those for Im R_1 by the exchange $E_i\rightleftarrows M_i$. Analogously, the expression for Im R_4 may be obtained from that for Im R_3, and for Im R_6 from Im R_5.

In Eq. (7) we mean by the modulus of the amplitude on the right side the sum of the contributions from photoproduction of π^+ and π^0 mesons. We note that if the mass differences between mesons and between nucleons are ignored then a cancellation in the interference terms, for example in $|E_{\pi^0}|^2+|E_{\pi^+}|^2$, occurs as a consequence of isotopic symmetry in the pion photoproduction process. At that

$$A_1(\nu)=\nu\sigma_t/4\pi=\nu\left\{|E_1|^2+|M_1|^2\right.$$
$$\left.+2|E_3|^2+2|M_3|^2+\tfrac{1}{6}|M_2|^2+\tfrac{1}{6}|E_2|^2\right\},$$
$$A_2(\nu)=\nu\left\{|E_1|^2+|M_1|^2+\tfrac{1}{3}|M_2|^2+\tfrac{1}{3}|E_2|^2\right.$$
$$\left.-|M_3+\tfrac{1}{2}E_2|^2-|E_3+\tfrac{1}{2}M_2|^2\right\},$$

$$A_3(\nu) = -\nu(w/M)\left\{|E_1|^2 - |M_1|^2 + |M_3 - \tfrac{1}{2}E_2|^2 - |E_3 - \tfrac{1}{2}M_2|^2\right\},$$

$$A_4(\nu) + (w - M)\sigma_t/4\pi = w\left\{|E_1|^2 + |M_1|^2 + \tfrac{2}{3}|M_2|^2 + \tfrac{2}{3}|E_2|^2 - |E_3 - \tfrac{1}{2}M_2|^2 - |M_3 - \tfrac{1}{2}E_2|^2\right\}. \quad (8)$$

4. As was shown by Goldberger,[1] the sum rule that follows from the nonsubtracted dispersion relations:

$$\mathrm{Re}(R_1 + R_2) \to + \frac{1}{2\pi^2}\int_{\nu_t}^{\infty} \sigma_t(\nu)\, d\nu > 0 \quad (9)$$

is in contradiction with the long wavelength limit

$$R_1 + R_2 \to -e^2/M < 0. \quad (10)$$

Consequently, nonsubtracted dispersion relations for the amplitude $R_1 + R_2$ violate the requirements of relativistic and gauge invariance on which the long wavelength limit is based.

Let us remark that possible sum rules involving the square of the magnetic moment are not in direct contradiction with the long wavelength limit when nonsubtracted dispersion relations are assumed for $F_2(\nu)$. As can be seen from Eqs. (6) and (8), of particular importance here is the contribution of the resonant state, proportional to $|M_3|^2$. The result is unchanged if one takes into account the (numerically important) contribution from photoproduction in S states, which decreases the effective contribution of $|M_3|^2$.

The sum rule for the square of the magnetic moment is very sensitive to the ratio of the photoproduction amplitudes E_2 and M_3. For certain ratios (for example for $E_2 = M_3$[5]) one can arrive at a contradiction. At the present time, however, the analysis of photoproduction is not sufficiently precise to permit the assertion that the experimental data are in contradiction with the sum rule. An increase in the accuracy of the photoproduction analysis, aimed at obtaining information about the amplitudes E_2, M_2 and E_3, would be most welcome.

The fact that unsubtracted dispersion relations give rise to definite sum rules may be of particular interest in certain processes. Thus, in the case of $\pi\pi$ scattering analogous considerations (applied to dispersion relations at $Q^2 = 0$) lead to the conclusion that the S-state scattering lengths a_0 and a_2 are positive at low energies. The same holds for πK and KK scattering.

5. If in addition to the functions introduced previously one studies properties of the functions*

$$F_5(\nu_0) = (T_2 - T_4)', \quad (11)$$

$$F_6(\nu_0) = (T_2 + T_4)', \quad (12)$$

$$F_7(\nu_0) = T_6', \quad (13)$$

one concludes that $F_{5,6}(\nu)$ are odd functions of ν and contain no poles, whereas $F_7(\nu)$ is an even function of ν with a second order pole. As $\nu \to \infty$

$$F_{5,6,7} \to \nu^{-1/2},$$

so that the dispersion relations for these functions need no subtractions.

These dispersion relations may turn out to be useful since when photoproduction in states with $J \leq 3/2$ is taken into account the angular dependence of the amplitudes $R_i(\nu, Q^2)$ in the barycentric frame takes the form (cf.[6])

$$R_3 = \mathscr{E}_1 - \mathscr{E}_3 + 2\mathscr{E}_2\cos\theta + \tfrac{1}{2}\mathfrak{m}_2 + C(\mathscr{E}_3\mathfrak{m}_2),$$
$$R_4 = \mathfrak{m}_1 - \mathfrak{m}_3 + 2\mathfrak{m}_2\cos\theta + \tfrac{1}{2}\mathscr{E}_2 + C(\mathfrak{m}_3\mathscr{E}_2),$$
$$R_5 = -\mathscr{E}_2 - C(\mathfrak{m}_3\mathscr{E}_2), \qquad R_6 = -\mathfrak{m}_2 - C(\mathscr{E}_3\mathfrak{m}_2), \quad (14)$$

and is characterized by eight functions of energy $\mathscr{E}_{1,2,3}$, $\mathfrak{m}_{1,2,3}$, $C(\mathscr{E}_3\mathfrak{m}_2)$ $C(\mathfrak{m}_3\mathscr{E}_2)$, which can be expressed in terms of $R_i(\nu, 0)$ and $R_i'(\nu, 0)$.

It follows from Eq. (14) that if we restrict ourselves to contributions from states with $J \leq 3/2$

$$R_1' = R_3' = 2\mathscr{E}_2(\partial\cos\theta/\partial Q^2)_{Q^2=0} = -4\mathscr{E}_2 w_0^2/M^2\nu_0^2,$$
$$R_2' = R_4' = -4\mathfrak{m}_2 w_0^2/M^2\nu_0^2, \qquad R_5' = R_6' = 0,$$

so that

$$(R_1 + R_2)' = (R_3 + R_4)' = [R_3 + R_4 + 2(R_5 + R_6)]'. \quad (15)$$

In the long wavelength limit[14]

$$(R_1 + R_2)' = -2e^2/M^2\nu + O(1),$$
$$(R_3 + R_4)' = -e^2[3 + 2(1 + \lambda)^2]/2M^3 + O(\nu),$$
$$(R_3 + R_4 + 2R_5 + 2R_6)' = -e^2(2\lambda^2 - 2\lambda - 1)/2M^3 + O(\nu). \quad (16)$$

The fact that Eq. (15) is in contradiction with the long wavelength limit (16) means that the restriction to states with $J \leq 3/2$ is not a good approximation even in the low energy region. The crossing symmetry conditions introduce kinematic corrections of the order of ν/M, which corresponds to inclusion of states with higher values of J. The carrying out of the analysis with this high a precision requires the introduction of additional functions of energy and discussion of a larger number

*The prime denotes differentiation with respect to Q^2 and subsequent passage to $Q^2 = 0$.

of dispersion relations. Introduction of the Low diagram does not resolve the indicated contradiction. All estimates of the amplitudes given here were obtained with the neglect of $R_i'(\nu, 0)$.

6. The results of the calculations of the amplitudes $R_i(\nu_0)$ at $Q^2 = 0$ are shown in the figures. The energy of the photons ν_0 is given in units of the threshold energy $\nu_t = 150$ Mev, and the values of the amplitudes in units of e^2/Mc^2.

For the calculation of the forward differential scattering cross section

$$\sigma(0°) = |R_1 + R_2|^2 + |R_3 + R_4 + 2R_5 + 2R_6|^2$$

the amplitudes $R_1 + R_2$ and $R_3 + R_4 + 2R_5 + 2R_6$ are sufficient.

To estimate $D_1(\nu_0)$ use was made of the data on the total cross section for the interaction of photons with protons, including the second maximum and the cross section for pion pair production. The dependence of $A_1(\nu_0)$ is shown in Fig. 1. Previously we have neglected contributions from the energy region above 500 Mev. The result of estimating the amplitude $R_1 + R_2$ is shown in Fig. 2. The main difference between this and previous results appeared in the region $1 < \nu_0 < 2$, where as a consequence of a cancellation between the long wavelength limit and dispersion terms the value of $D_1(\nu_0)$ is significantly decreased. Let us note that this is precisely the energy region that is sensitive to a change in $A_1(\nu_0)$. The second maximum in $A_1(\nu_0)$ corresponds to the second maximum in photoproduction.

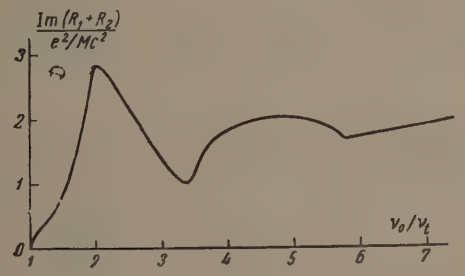

FIG. 1

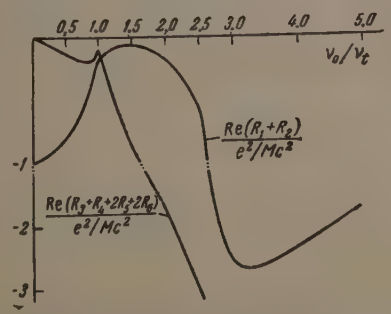

FIG. 2

For estimating real parts of the amplitudes, other than $R_1 + R_2$, which require much more detailed experimental data on photoproduction, we limit ourselves to the energy region up to 300 Mev. For the amplitude $R_1 + R_2$ it turns out to be possible to go much further, although with increasing energy the indeterminacy in the contribution from photoproduction of pairs (and larger numbers) of pions becomes appreciable.

In a number of papers[15,16] the γp scattering at 300—800 Mev has been looked upon as a diffraction process with $\mathrm{Re}\, R_i \ll \mathrm{Im}\, R_i$. The experimental study of γp scattering in the region of the second resonance is of interest as a sensitive method of investigation of the maximum itself.

If, ignoring all $\mathrm{Re}\, R_i$, we restrict ourselves to the imaginary parts of the amplitudes alone and consider only the contribution proportional to $|E_3|^2$, then we find immediately from Eq. (7) that

$$R_2 = R_4 = R_5 = R_6 = 0,$$

$$R_1 = \mathrm{Im}\, R_1 = -2\mathrm{Im}\, R_3 = 2v_c |E_3|^2,$$

whereas the differential cross section[6] is equal to

$$\sigma(\theta) = \tfrac{1}{8} R_1^2 (7 + 3\cos^2\theta) = \tfrac{1}{2} R_3^2 (7 + 3\cos^2\theta), \qquad (17)$$

in agreement with the results of Minami.[16] The same result for the form of the angular distribution remains valid if in Eq. (7) only M_3 ($R_1 \to R_2$, $R_3 \to R_4$) is different from zero. If simultaneously E_3 and M_3 (with $\mathrm{Re}\, R_i = 0$) are different from zero then we have

$$\sigma(\theta) = \tfrac{1}{2}(R_3^2 + R_4^2)(7 + 3\cos^2\theta) + 10 R_3 R_4 \cos\theta. \qquad (18)$$

However, as our estimates indicate, the quantities $\mathrm{Re}(R_1 + R_2)$ are large in the region of the second resonance and cannot be ignored. From this point of view the second resonance differs drastically from the $^3/_2$, $^3/_2$ resonance, in whose energy region

$$\mathrm{Re}(R_1 + R_2) \ll \mathrm{Im}\,(R_1 + R_2).$$

The results of the calculations for $R_3 \pm R_4$, $R_3 + R_4 + 2R_5 + 2R_6$ and $R_5 + R_6$ are shown in Figs. 2—4. In the evaluation of dispersion inte-

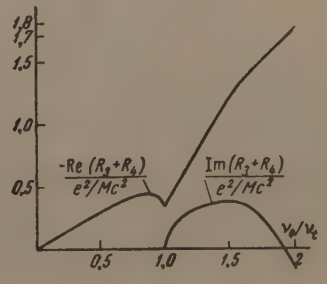

FIG. 3

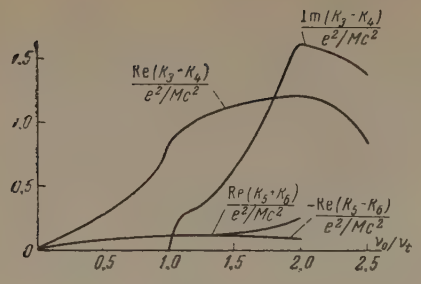

FIG. 4

grals $|E_1|^2$, $|M_3|^2$ and $|E_3|^2$ were assumed to be different from zero, and the energy dependence of $|E_1|^2$ and $|M_3|^2$ was taken from[6], whereas $|E_3|^2$ was assumed to be different from zero in the energy region $3.1 < \nu_0 < 5.8$. Let us remark that even in the absence of an imaginary part for $R_5 + R_6$ the real part of this quantity differs from its long wavelength limit, since the dispersion relations are satisfied by the invariant functions $T_i(\nu, Q^2)$.

The values of $\sigma(0°)$ are shown in Fig. 5, where we give for comparison the results of Cini and Stroffolini[3] for $\sigma_{C\text{-}S}(0°)$ in the barycentric frame. A significant difference can be seen in the near-threshold region.

7. For an estimate of $R_1 - R_2$ and $R_5 - R_6$ the

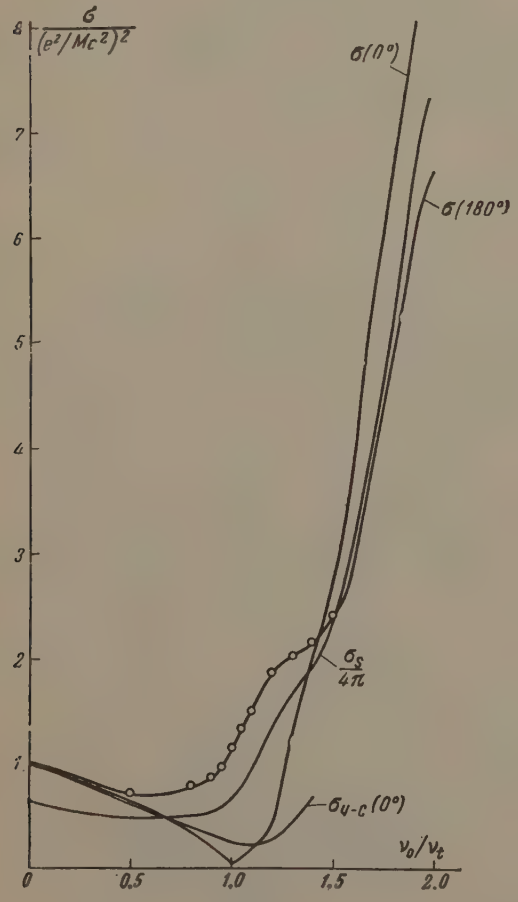

FIG. 5

dispersion relations (6) are not sufficient. Let us consider the function

$$F(\nu) = w^{-2}\varphi(\nu) = (M^2\nu^2/2w^2)\,[(T_1 + T_3)' - \nu(T_2 + T_4)']. \tag{19}$$

As can be seen from B, Eq. (4), we have

$$F(\nu) = \frac{w}{M}\left\{R_1 - R_2 - \frac{2M\nu}{w(w+M)}(R_3 - R_4)\right\}. \tag{20}$$

A study of the dispersion relation for $F(\nu)$ makes it possible to estimate $R_1 - R_2$ if $R_3 - R_4$ is known. In the energy region under consideration the coefficient of $(R_3 - R_4)$ in Eq. (20) is of the order of ν/M, however since the value of $R_3 - R_4$ is large (in comparison with $R_1 - R_2$), the second term in Eq. (20) cannot be ignored. The function $\varphi(\nu)$ introduced in Eq. (19) is an analytic function of ν with a cut along $\nu_t < \nu < \infty$, satisfying the crossing symmetry condition:

$$\varphi(\nu) = \varphi^*(-\nu). \tag{21}$$

Thus, for $\nu \ll \nu_t$ the function $\varphi(\nu)$ is a real function and

$$\varphi(\nu) \cong a + b\nu^2, \tag{22}$$

$$F(\nu) = \frac{\varphi(\nu)}{M^2 + 2M\nu} \cong \frac{a}{M^2}\left(1 - \frac{2\nu}{M}\right) + b\nu^2 + \ldots \tag{23}$$

We see that the linear term in $F(\nu)$ is fully determined by the first term in Eq. (22). It therefore follows from Eq. (20) that for small ν

$$R_1 - R_2 = -(e^2/M)(1 - 3\nu/M) + O(\nu^2)$$

and the linear term in $R_1 - R_2$ and in $F(\nu)$ are fully determined by the requirement of crossing symmetry, as is discussed in detail in B.

The function $F(\nu)$ introduced in Eq. (19) is an analytic function of ν with cuts along $\nu_t < \nu < \infty$ and $-\infty < \nu < -\nu_t$ and a (kinematic) pole at

$$w^2 = M^2 + 2M\nu = 0.$$

The requirements of crossing symmetry lead to the relation

$$F(-\nu) = \frac{M^2 + 2M\nu}{M^2 - 2M\nu} F^*(\nu),$$

and for small ν

$$F(\nu) \cong -(e^2/M)(1 - 2\nu/M) + O(\nu^2).$$

Applying the Cauchy formula to $F(\nu_0)$, for $\rho \to \infty$, along the contour shown in Fig. 6 and writing a dispersion relation with a subtraction we obtain

$$F(\nu_0) = -\frac{e^2}{M}\left(1 - \frac{2\nu_0}{M}\right) + \frac{\nu_0^2}{2\pi i}\int_C \frac{F(\nu)\,d\nu}{\nu^2(\nu - \nu_0)} = -\frac{e^2}{M}\left(1 - \frac{2\nu_0}{M}\right)$$

$$+ \frac{\nu_0^2}{\pi} P\int_{\nu_t}^{\infty} \operatorname{Im} F\left[\frac{1}{\nu - \nu_0} + \frac{M^2 + 2M\nu}{M^2 - 2M\nu}\frac{1}{\nu + \nu_0}\right]\frac{d\nu}{\nu^2}$$

$$+ \frac{\nu_0^2}{2\pi i}\int_{C_+} \frac{F(\nu + i\varepsilon)}{\nu^2(\nu - \nu_0)}\,d\nu + \frac{\nu_0^2}{2\pi i}\int_{C_-} \frac{F(\nu - i\varepsilon)}{\nu^2(\nu - \nu_0)}\,d\nu$$

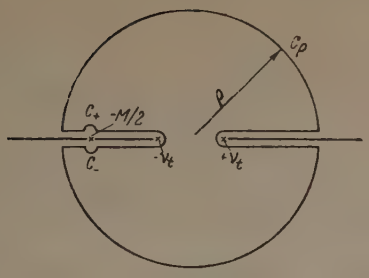

FIG. 6

and

$$\mathrm{Re}\,F(\nu_0) = -\frac{e^2}{M}\left(1-\frac{2\nu_0}{M}\right) + K(\nu_0) + \frac{4\nu_0^2\,\mathrm{Re}\,F(M/2)}{M(\nu_0+M/2)}\,; \quad (24)$$

$$K(\nu_0) = \frac{\nu_0^2}{\pi}\int_{\nu_t}^{\infty} \mathrm{Im}\,F(\nu)\left[\frac{1}{\nu-\nu_0} + \frac{M^2+2M\nu}{M^2-2M\nu}\frac{1}{\nu+\nu_0}\right]\frac{d\nu}{\nu^2}\,. \quad (25)$$

Since

$$K(M/2) = 0,$$

Re F(M/2) cannot be determined from Eq. (24), and this quantity enters as a free parameter, which must be determined starting from the experimental data. Under the restriction to photoproduction in the states with $J \leq 3/2$ only we get

$$\mathrm{Im}\,F(\nu) = \nu\left\{\frac{M}{w}(|E_1|^2 - |M_1|^2) + 2(|E_3|^2 - |M_3|^2)\left(1+\frac{1}{2}\frac{w-M}{w}\right) + \frac{1}{2}\frac{M}{w}(|E_2|^2 - |M_2|^2)\left(1+\frac{1}{6}\frac{w-M}{w}\right)\right\}. \quad (25')$$

In Fig. 7 are shown the results of estimating Re ($R_1 - R_2$) with the help of Eq. (24) when the contribution proportional to Re F(M/2) is ignored.

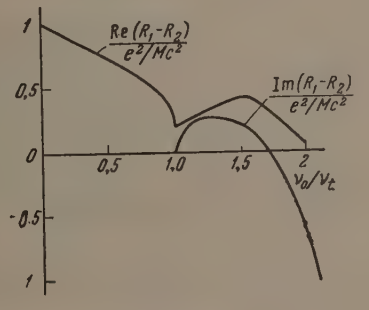

FIG. 7

For an estimate of $R_5 - R_6$ at $Q^2 = 0$, as can be seen from B, Eq. (4), it is sufficient to consider the function

$$\psi(\nu_0) = \tfrac{1}{2}\nu_0^2[T_5' + \tfrac{1}{2}(T_1+T_3)]' = \left(\frac{w_0}{M}\right)^3 \times\left\{\frac{w_0}{\nu_0}(R_5-R_6) + \frac{M}{w_0+M}[R_1 - R_2 - (R_3 - R_4)]\right\}, \quad (26)$$

for which the dispersion relation has the form

$$\mathrm{Re}\,\psi(\nu_0) - \psi(0) = \frac{2\nu_0^2}{\pi}\,\mathrm{P}\int_{\nu_t}^{\infty}\frac{\mathrm{Im}\,\psi(\nu)\,d\nu}{\nu(\nu^2-\nu_0^2)}\,, \quad (27)$$

where, according to B, Eq. (2),

$$\psi(0) = -e^2(2+\lambda)/2M, \quad (28)$$

$$\mathrm{Im}\,\psi(\nu) = (w/M)^2\left\{w\left[\tfrac{1}{6}(|E_2|^2 - |M_2|^2) + \mathrm{Re}\,(E_2^*M_3 - M_2^*E_3)\right] + M\nu(M+w_0)^{-1}[3(|E_3|^2 - |M_3|^2) + \tfrac{1}{4}(|E_2|^2 - |M_2|^2) + \mathrm{Re}\,(E_2^*M_3 - M_2^*E_3)]\right\}. \quad (29)$$

The results of estimating Re ($R_5 - R_6$) at $Q^2 = 0$ for Re F(M/2) = 0 are shown in Fig. 4. Estimates of the quantities $R_3 \pm R_4$ and $R_5 - R_6$, which play a dominant role in the differential cross section for $\nu_0 \gtrsim 1$, do not differ appreciably from those obtained previously.[6]

The results here obtained are of interest from the point of view of the study of the energy dependence of amplitudes near the threshold of a new reaction.[6] In that case all estimates can be carried out to the end. Let us call attention to the dependence of the amplitude Re ($R_1 + R_2$), whose value continues to fall off also above threshold. This result indicates that a sharp energy dependence of the imaginary parts of the amplitudes above threshold may also for other processes lead to a displacement of the near-threshold minimum (or maximum) of the cross section relative to the reaction threshold.

In Figs. 5 and 8—11 are shown the results of the calculations, with the help of $R_i(\nu, 0)$, of angular distributions

$$\sigma(\theta) = \sum_{l=0}^{3} B_l \cos^l\theta$$

for the angles $\theta = 90$, 135, 139 and 180°, and also of the total elastic scattering cross section

$$\sigma_s/4\pi = B_0 + B_2/2$$

and of the polarization of recoil nucleons for $\theta = 90°$. The experimental data are summarized in[10] and[17].

The coefficient

$$B_3(\nu_0) = 2[|R_5 + R_6|^2 - |R_5 - R_6|^2]$$

is near to zero in the entire energy region $\nu_0 \lesssim 2$.

The experimental data, apparently, indicate that the quantity Re ($R_5 - R_6$) is positive. We were not able to achieve this by introducing Re F(M/2) ≠ 0. The requirement that Re ($R_5 - R_6$) be positive leads to large (negative) values for Re F(M/2), which at the same time significantly

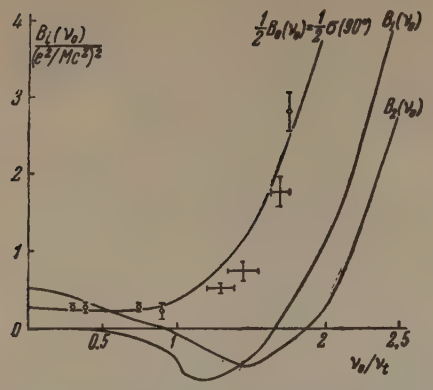

FIG. 8. Energy dependence of the coefficients in the angular distribution. The experimental points are from [9,10,17].

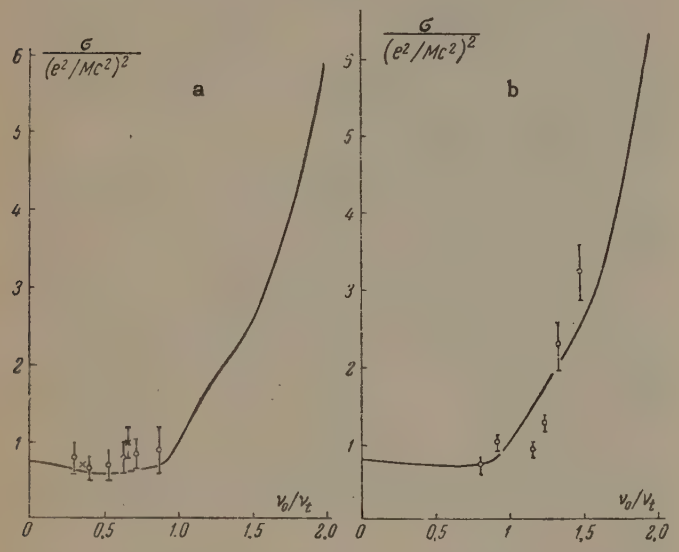

FIG. 9. Energy dependence of the scattering cross section: a – for $\theta = 135°$, b – for $\theta = 139°$. The experimental data are from [9,10,17].

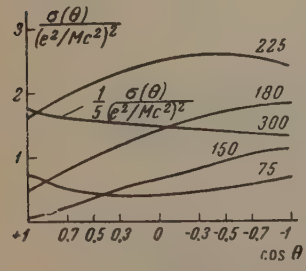

FIG. 10. Differential cross sections at different photon energies (indicated on the curves).

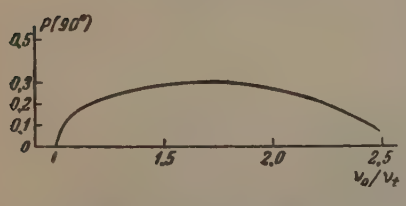

FIG. 11. Polarization of recoil protons.

increases the contribution of $|R_1 - R_2|^2$ to the cross section and does not lead to an improvement in the agreement with the experimental data.

It is necessary to remark that outside the region $1 < \nu_0 < 1.3$ a satisfactory agreement between the dispersional analysis and experimental data is obtained. In the region $1 < \nu_0 < 1.3$, which is particularly sensitive to dispersion effects, it is apparently necessary to take into account contributions from higher states, for which it is necessary to have information on pion photoproduction in a larger energy region.

[1] Gell-Mann, Goldberger, and Thirring, Phys. Rev. **95**, 1612 (1954). M. L. Goldberger, Phys. Rev. **99**, 979 (1955).

[2] A. A. Logunov, Dissertation, Joint Inst. for Nucl. Research (1959).

[3] M. Cini and R. Stroffolini, Nucl. Phys. **5**, 684 (1958).

[4] R. H. Capps, Phys. Rev. **106**, 1031 (1957); **108**, 1032 (1957).

[5] T. Akiba and I. Sato, Progr. Theor. Phys. **19**, 93 (1958).

[6] L. I. Lapidus and Chou Kuang-chao, JETP **37**, 1714 (1959) and **38**, 201 (1960), Soviet Phys. JETP **10**, 1213 (1960) and **11**, 147 (1960).

[7] M. Jacob and J. Mathews, Phys. Rev. **117**, 854 (1960).

[8] M. Gell-Mann and M. L. Goldberger, Proc. 1954 Glasgow Conf. on Nucl. and Meson Physics, Pergamon Press, London-N.Y. (1954).

[9] Hyman, Ely, Frisch, and Wahlig, Phys. Rev. Lett. **3**, 93 (1959).

[10] Bernardini, Hanson, Odian, Yamagata, Auerbach, and Filosofo, Nuovo cimento **18**, 1203 (1960).

[11] F. E. Low, Proc. 1958 Ann. Intern. Conf. on High Energy Physics at CERN, p. 98.

[12] Glasser, Seeman, and Stiller, Bull. Amer. Phys. Soc. **6**, 1 (1961).

[13] L. I. Lapidus and Chou Kuang-chao, JETP **41**, 294 (1961), Soviet Phys. JETP **14**, 210 (1962).

[14] L. I. Lapidus and Chou Kuang-chao, JETP **41**, 491 (1961), Soviet Phys. JETP **14**, 352 (1962)

[15] Y. Yamaguchi, Progr. Theor, Phys. **12**, 111 (1954). S. Minami and Y. Yamaguchi, Progr. Theor. Phys. **17**, 651 (1957).

[16] S. Minami, Photon-Proton Collision at 250-800 Mev (preprint).

[17] Govorkov, Gol'danskii, Karpukhin, Kutsenko, Pavlovskaya, DAN SSSR **111**, 988 (1956), Soviet Phys. "Doklady" **1**, 735 (1957). Gol'danskii, Karpukhin, Kutsenko, and Pavlovskaya, JETP **38**, 1695 (1960), Soviet Phys. JETP **11**, 1223 (1960). V. V. Pavlovskaya, Dissertation, Phys. Inst. Acad. Sci. (1961).

Translated by A. M. Bincer
261

SOME CHARACTERISTICS OF EXTENSIVE AIR SHOWERS

A. A. POMANSKII

P. N. Lebedev Physics Institute, Academy of Sciences, U.S.S.R.

Submitted to JETP editor May 19, 1961

J. Exptl. Theoret. Phys. (U.S.S.R.) 41, 1556-1561

The hypothesis that a decreasing fraction of energy is transferred to pions as the primary-particle energy increases is shown to be inconsistent with experimental data on the altitude dependence of extensive air showers. It is also shown that the number of nuclear-active particles depends strongly on the relative number of baryons among all secondary particles produced in an elementary nuclear interaction.

EARLIER calculations by Nikol'skii and the present author[1,2] on the development of extensive air showers are here continued. The results obtained in[2] agreed with experimental findings regarding the altitude dependence of showers and the energy flux carried by the electron-photon component. The ratio of the mean energy of primary particles inducing showers with a given number of particles at the observation altitude, to the total number of shower particles, was consistent with the values usually assumed for the conversion coefficient from the number of particles to the primary-particle energy. However, some of the calculated quantities did not agree with experiment. Thus, too large a number of nuclear-active particles was computed in extensive showers of $N \geq 10^5$ particles at the given mountain altitude, compared with the experimental result.[3] There was also a discrepancy regarding the energy flux carried by nuclear-active particles (Table I). It was pointed out in[2] that the principal causes of disagreement are first, the hypothesis of a decreased elasticity coefficient of nucleon interaction as the nucleon energy diminishes to the 10^{11}—10^9 ev range, and, secondly, the large number of secondary particles, other than pions, identified as nucleons.

The foregoing conclusions were taken into account in the present calculation. Certain experimental results obtained in recent studies of elementary interactions at high energies,[4-7] were also considered. The nuclear emulsion results collected in the review by Koba and Takagi[8] were taken into consideration while selecting a model for the elementary nuclear interaction event. It was also considered that nucleons, antinucleons, and pions are produced in interactions between nuclear-active particles and the nuclei of air atoms. The principal assumptions on which the calculation is based can be summarized in the following manner.

A. Interaction of a Nucleon with the Nucleus of an Air Atom

1) All incoming nucleons retain 0.6 of the primary energy E_0.

2) The number of secondary pions as a function of E_0 is determined from the dashed line in Fig. 1. For $E_0 \leq 10^{10}$ ev the dependence of multiplicity on E_0 agrees with experiment[5,6] within error limits. For $E_0 > 10^{10}$ ev, $N \sim E_0^{1/4}$ was assumed, in agreement with experiment[4] and with contemporary theory.[9]

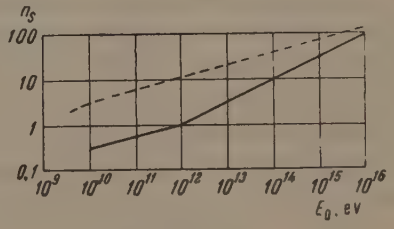

FIG. 1

3) The fraction of secondary nucleons and antinucleons in the incoming-particle energy range 10^{10} ev $\leq E_0 \leq 10^{12}$ ev was taken as ~10% of all secondary particles.* For $E_0 > 10^{12}$ ev the conclusions in[7] were taken into account, regarding the decreased fraction of energy transferred to the pion component with increasing primary-particle energy E_0. We assumed that for $E_0 > 10^{12}$ ev the fraction of nucleons and antinucleons increases monotonically, reaching 27% of the total number of

*We neglected the formation of secondary nucleons and antinucleons for $E_0 < 10^{10}$ ev.

secondary particles at $E_0 = 10^{15}$ ev (the continuous line in Fig. 1).

4) The fraction Δ of energy transferred to pions when $E_0 \leq 10^{10}$ ev was taken to be 0.4.* At high energies we assumed, following the Bristol group,[7] that the energy fraction transferred to the pion component diminishes monotonically as E_0 increases; but we assumed a slower rate of decrease compared with that in[7] (Fig. 2). It was assumed that 30% of Δ is carried away by a single pion (a π^0 meson, with probability $\frac{1}{3}$), and that 70% is divided equally among the remaining pions. When $E_0 < 10$ Bev the energy is divided equally among all pions.

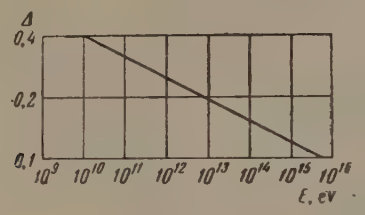

FIG. 2

5) Secondary nucleons and antinucleons carry away the energy $E_{n,\bar{n}} = (0.4-\Delta)E_0$, which is distributed equally among all particles of this type.

B. Interaction of $\pi^{\pm}$ Mesons with the Nuclei of Air Atoms

1) The inelasticity coefficient was taken to be unity, but energy spectra of the secondary particles were assumed harder than in nucleon-induced events. It was assumed that a $\pi^{\pm}$ meson, (in $\frac{2}{3}$ of the events) or a π^0 meson (in $\frac{1}{3}$ of the events) with energy $0.6\,E_0$ is produced.

2) The number and energy distribution of other secondary particles is the same as in nucleon-induced events.

C. Antinucleon Collision Events assumed Similar to Events Induced by $\pi^{\pm}$ Mesons

The calculation was performed by the method of successive generations. The different parameters of extensive air showers were derived in exactly the same manner as in[2]. The mean free interaction path of nuclear-active particles was taken as $\lambda_0 = 75$ g/cm^2; we considered nuclear interactions with $E_{na} \geq 3.7 \times 10^9$ ev. The results are given in Tables I and II, where all quantities pertain to showers with the given numbers of particles at the altitude of the Pamir (3860 m). We

*This is close to the value $\Delta = 0.44$ given in[6] for E = 9 Bev.

Table I

No. of particles	10^4				10^5			10^6	
Shower parameters	Present work	Data of[2]	Checking calculation	Experimental	Present work	Data of[2]	Experimental	Present work	Data of[2]	Experimental
Conversion coefficient from N to E_0	$3.3 \cdot 10^9$	$2.6 \cdot 10^9$	—	—	$2.9 \cdot 10^9$	$2 \cdot 10^9$	—	$2.4 \cdot 10^9$	$1.6 \cdot 10^9$	—
I_m/I_s	7	16	—	14 ± 3	4,7	16	14 ± 3	3,7	16	14 ± 3
Energy flux carried by nuclear-active particles, ev	$6.4 \cdot 10^{12}$	$6 \cdot 10^{12}$	$(4.4 \pm 1.3) \cdot 10^{12}$		$6.3 \cdot 10^{13}$	$4.6 \cdot 10^{13}$	$\leqslant 1.1 \cdot 10^{14}$	$5.6 \cdot 10^{14}$	$4 \cdot 10^{14}$	$(2.3 \pm 0.8) \cdot 10^{14}$

Table II

No. of particles	10^4				10^5				10^6			
Kind of nuclear-active particles	Present work	Data of[2]	Checking calculation	Experimental	Present work	Data of[2]	Checking calculation	Experimental	Present work	Data of[2]	Checking calculation	Experimental
Nucleons	46	228	—	—	357	1480	—	—	2780	11300	—	—
Antinucleons	22	—	—	—	183	—	—	—	1830	—	—	—
$\pi^{\pm}$ mesons	27	36	—	—	230	210	—	—	1960	1000	—	—
All nuclear-active particles	95	264	32	250 ± 50	770	1690	237	400 ± 100	6570	12300	1740	1650 ± 400

took into account the fluctuations in the depth of the first nuclear interaction participated in by the primary particles.

Table I gives the intensity ratio I_m/I_s of showers of a given number of particles at the mountain altitude (3860 m) and at sea level. The ratios obtained in the present calculation differ from experimental results regarding the altitude dependence of showers (as between the Pamir and Moscow),[10] whereas in[2] there was approximate agreement. The discrepancy is especially marked for showers having large numbers of particles. The anomalously small difference noted in the present work between shower intensity in the Pamir and Moscow, especially for showers with large numbers of particles, is associated with the weak absorption of cascades formed by high-energy particles.

Electron-photon cascades calculated according to the nuclear-cascade scheme are shown in Fig. 3, compared with those in[2]. With increasing primary-particle energy cascade absorption is slower in the present work than in[2]. This results from the hypothesis, adopted in agreement with the Bristol group,[7] that the energy fraction transferred to the pion component decreases as the incident-nucleon energy increases while the energy fraction retained by the nucleon remains constant at 0.6 E_0.

It was assumed in our calculations that an incoming nucleon always retains the fraction 0.6 of its initial energy E_0, while the remaining fraction 0.4 E_0 is distributed among secondary nucleons, antinucleons, and pions. We also accepted the conclusion arrived at in[7] that the energy fraction transferred to pions (and therefore to π^0 mesons) decreases as E_0 increases. This leads to a slower

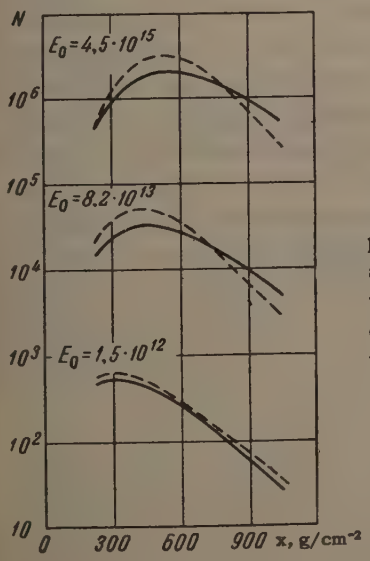

FIG. 3. No. of shower particles as a function of atmospheric depth for three values of E_0. Continuous curves – present calculation; dashed curves – from[2].

absorption of nuclear-active cascades and of the accompanying electron-photon component. In[2] it was calculated that the fraction of incident-nucleon energy transferred to pions remains practically unchanged beginning with $E_0 \geq 10^{13}$ ev. The energy expended by the nuclear-active cascade to produce γ rays therefore depended only slightly on primary-particle energy.

Thus, if we assume a decreasing transfer of energy to pions as the primary-nucleon energy increases while a constant fraction (> 0.5) of the energy is retained by the nucleon, without admitting any other important channels for energy transfer to the electron-photon component, our results disagree with the experimental altitude dependence of showers. The same conclusion was reached in[11].

Reference[1] presents one possible version of variation in the elementary event, which, while admitting a decrease of energy transfer to pions, brings the calculation into closer agreement with the experimental altitude dependence. It was there postulated that at primary energies $\geq 10^{14}$ ev an electron-photon component is produced, to which the fraction 0.63 of the primary-particle energy is transferred, without involving pions. For the sake of simplicity[1] direct energy transfer to the electron-photon component was considered, although the same result can obviously be achieved by introducing any rapidly decaying particles (see[12], for example).

The large energy fraction retained by the primary nucleon up to the very highest energies results in an increased number of high-energy nuclear-active particles in showers (compare the present work with[2]). This can be seen from the integral spectra of nuclear-active particles in Fig. 4. It must be noted that the increasing fraction of high-energy nuclear-active particles is accompanied by an increased flux of energy carried by the nuclear-active particles. This augments the discrepancy between the calculated and experimental energy flux given in Table I (as compared with[2]).

The last line of Table II gives the numbers of nuclear-active particles in showers having different total numbers of particles. Our calculated number of nuclear-active particles is considerably smaller than that given in[2]. In order to account for this reduction we checked the composition of the nuclear-active component at mountain altitude, i.e., we calculated separately the number of nucleons and the number of $\pi^{\pm}$ mesons included among all nuclear-active particles in extensive air showers (Table II).

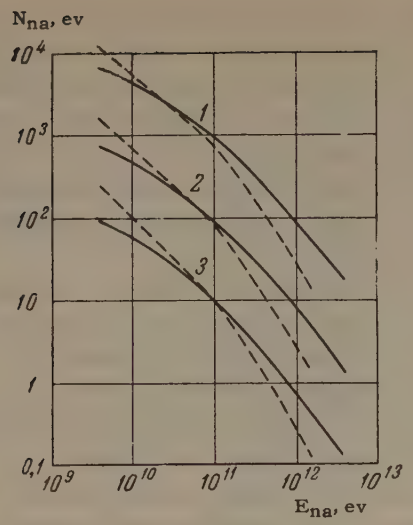

FIG. 4. Integral spectra of nuclear-active particles in extensive air showers with different total numbers of particles: $1-10^6$, $2-10^5$, $3-10^4$ particles. Continuous curves – present calculation; dashed curves – from [2].

Table II shows that nuclear-active particles at the mountain altitude are mainly nucleons,* and their number at the given altitude is apparently determined by the relative number of nucleons among all secondary particles created in an elementary event. This is evident from a comparison with[2], where the relative number of nucleons was taken to be constant at 0.27. The relative combined number of nucleons and antinucleons in the important energy range was 0.1 in the present work.

Two additional calculations were performed as a check. In the first of these the model differed from that in[2] only by taking 0.08 instead of 0.27 as the constant relative number of nucleons among all secondary particles produced in an elementary event. Table II gives the results of this check.

The second checking calculation was based on postulates differing from those formulated at the beginning of the present article. All secondary nucleons and antinucleons were replaced with charged pions having the multiplicity and energy distribution that had been taken for the secondary nucleons and antinucleons. Thus in nucleon-induced events the secondary particles will include only one ("primary") nucleon, while in events induced by $\pi^{\pm}$ mesons no nucleons will be formed. Recoil nucleons have energy $E \ll 3.7$ Bev and were disregarded in our calculations. For a shower observed at the mountain altitude and induced by a primary particle having energy 8×10^{13} ev, the relative number of nuclear-active particles ($\pi^{\pm}$ mesons) was found to be 0.002 instead of 0.0095 according to Table I.

The total number of nuclear-active particles at the given altitude therefore depends strongly on the relative number of nucleons (and hyperons) among the secondary particles produced in elementary events of nuclear interaction between nucleons, or $\pi^{\pm}$ mesons, and the nuclei of air atoms. We conclude from the foregoing that when reliable data are available for the number of nuclear-active particles in an extensive air shower, it becomes possible to derive a mean value for the relative number of baryons among the secondary particles produced in elementary events when the energy of the colliding particles is 10^{10}—10^{12} ev.

The author is indebted to S. I. Nikol'skii for valuable comments and a discussion of the results, and also to G. T. Zatsepin and E. I. Tukish for discussions of the results.

*These results are also valid at sea level.

[1] S. I. Nikol'skii and A. A. Pomanskii, Trans. Internat. Conf. on Cosmic Rays IUPAP, Vol. 2, 1960, p. 235.

[2] S. I. Nikol'skii and A. A. Pomanskii, JETP **39**, 1339 (1960), Soviet Phys. JETP **12**, 934 (1961).

[3] Nikol'skii, Vavilov, and Batov, DAN SSSR **111**, 71 (1956), Soviet Phys.-Doklady **1**, 625 (1957).

[4] Grigorov, Guseva, Dobrotin et al., op. cit.[1], Vol. 1, 1960, p. 140.

[5] Belyakov, Wang, Glagolev, et al. JETP **39**, 937 (1960), Soviet Phys. JETP **12**, 650 (1961).

[6] Wang, Visky, Gramenitskii, et al., JETP **39**, 957 (1960), Soviet Phys. JETP **12**, 663 (1961).

[7] Duthie, Fisher, and Fowler, op. cit.[1], Vol. 1, 1960, p. 28.

[8] Z. Koba and S. Takagi, Fortschr. Physik **7**, 1 (1959).

[9] E. L. Feĭnberg, UFN 70, 333 (1960), Soviet Phys.-Uspekhi 3, 147 (1960).

[10] Kulikov, Nesterova, Nikol'skii et al., op cit,[1], Vol. 2, 1960, p. 87.

[11] E. V. Gedalin, JETP **40**, 178 (1961), Soviet Phys. JETP **13**, 123 (1961).

[12] A. Ueda and C. B. A. McCasker, Nuclear Phys. **26**, 35 (1961).

Translated by I. Emin
262

CYCLOTRON RESONANCE IN A VARIABLE MAGNETIC FIELD

V. N. LUGOVOĬ

P. N. Lebedev Physics Institute, Academy of Sciences, U.S.S.R.

Submitted to JETP editor May 19, 1961

J. Exptl. Theoret. Phys. (U.S.S.R.) 41, 1562-1565 (November, 1961)

The electrical conductivity tensor is calculated for an electron gas (plasma or semiconductor in the conduction band) situated in a magnetic field with a variable (harmonic) component parallel to the constant component. If the electric field induced by the variable magnetic field is comparable to the characteristic "plasma field" (1), the analysis will be valid only under the condition $p\tau \gtrsim 1$ (p is the cyclic frequency of the variation of the variable component of the magnetic field, τ is the effective mean time between electron collisions). It is shown that under these conditions the absorbing properties of the medium depend appreciably on the variable component of the magnetic field. Contrary to the opinion previously expressed[4,5] negative absorption is impossible.

RECENTLY discussions have taken place of the problem of the utilization of cyclotron resonance in semiconductors in order to obtain systems with negative absorption when the magnetic field has a variable component parallel to the constant component. It was supposed that negative absorption at the cyclotron resonance frequency $\omega_c = eH/mc$ can occur as a result of a parametric variation of the magnetic field at a frequency p close to the frequency $2\omega_c/n$ ($n = 1, 2, \ldots$).

In this paper we consider cyclotron (diamagnetic) resonance in a plasma or in a semiconductor in the case when the magnetic field $\mathbf{H}$ has a variable (harmonic) component parallel to the constant component. In this discussion we also take into account the electric field $\mathbf{E}_1$ induced by the variable magnetic field. If the field $\mathbf{E}_1$ is strong (cf., below), then the discussion is carried out subject to the condition (2) which is the condition under which separate maxima can be distinguished on the curve showing the absorption of energy in a weak external monochromatic field ($\mathbf{E}_2$). From subsequent discussion it follows that under these conditions the intensity of absorption (for $\mathbf{E}_2$) depends in an essential manner on the properties of the variable magnetic field (dependence on the properties of the field $\mathbf{E}_1$ is not significant). In particular, at the cyclotron resonance frequency ω_c this absorption can be reduced to zero. However, negative absorption is impossible.

We consider a certain volume of plasma or of a semiconductor situated in a homogeneous magnetic field $\mathbf{H}$ directed along the z axis ($H_z = H_0 - H_1 \cos pt$). Generally speaking, this volume will be simultaneously situated in a variable electric field $\mathbf{E}_1$ of frequency p. The plasma (or the semiconductor) under consideration situated in the field $\mathbf{H}$ (and also in the field $\mathbf{E}_1$ induced by it) represents a certain medium. We shall be interested in the electrical conductivity of this medium, and in the absorption in this medium of energy from a weak homogeneous electric field $\mathbf{E}_2 = \mathbf{E}_{20} \cos \omega t$ (external with respect to the medium under consideration, and having a general orientation with respect to the field $\mathbf{H}$). The small contribution to the electrical conductivity (absorption) due to the heavy particles (molecules, ions) will not be taken into account, so that the given medium, in effect, represents an electron gas in the magnetic field $\mathbf{H}$ (and in the electric field $\mathbf{E}_1$).

The properties of this gas (in particular, the electrical conductivity and the absorptive power) depend on the fields $\mathbf{H}$ and $\mathbf{E}_1$. The field $\mathbf{E}_1$ must be regarded weak if its amplitude $\mathbf{E}_{10}$ satisfies the inequality

$$E_{10} \ll E_p = \sqrt{3kTme^{-2}\delta(p^2 + 1/\tau_0^2)}, \qquad (1)$$

where E_p is the characteristic "plasma field", e and m are the charge and the mass of the electron, k is the Boltzmann constant, T is the absolute temperature in the absence of $\mathbf{E}_1$, δ is the average relative fraction of the energy transferred in the collision of an electron with a heavy particle, and τ_0 is the effective time between collisions in the absence of $\mathbf{E}_1$. In this discussion the kinetic parameters of the electron gas under consideration (in particular τ) do not differ from their values in the absence of $\mathbf{E}_1$. However, if $E_{10} \gtrsim E_p$,

then the field $\mathbf{E}_1$ is strong, and this, in the general case, determines the dependence of τ on $\mathbf{E}_1$ (and consequently, on the time). However, if the frequency p satisfies the condition

$$p\tau \gtrsim 1, \tag{2}$$

then the effective time between collisions τ "does not have time" to follow the variations of $\mathbf{E}_1$. In this case the quantity τ is a function only of the amplitude E_{10} [$\tau = \tau(E_{10})$] and is independent of the time.*

In order to determine the properties of interest to us for the medium under consideration we shall assume that it is situated in a weak external monochromatic field $\mathbf{E}_2 = \mathbf{E}_{20}\cos\omega t$ (we note right away that, in general, these properties can depend on the initial phase φ_0 if the field $\mathbf{E}_2$ is written in the form $\mathbf{E}_2 = \mathbf{E}_{20}\cos(\omega t + \varphi_0)$; however, in the present case this dependence is absent, as can be verified by a direct solution of the problem), and we shall utilize the equation for the average electron velocity[1-3]

$$m(d\mathbf{v}/dt + \mathbf{v}/\tau) = e(\mathbf{E} + c^{-1}[\mathbf{vH}]), \tag{3}$$†

where $\mathbf{E} = \mathbf{E}_1 + \mathbf{E}_2$. In future we shall consider only those cases when the quantity τ does not depend on the time. This is possible under the condition (2) if the field $\mathbf{E}_1$ is strong, and for any arbitrary frequency p if the field $\mathbf{E}_1$ is weak.

Since Eq. (3) is linear the total current density $\mathbf{J}$ ($\mathbf{J} = Ne\mathbf{v}$, N is the electron density) is the sum $\mathbf{J}_1 + \mathbf{J}_2$ of the currents corresponding to $\mathbf{E}_1$ and $\mathbf{E}_2$ [in both cases we have $\tau = \tau(E_{10})$]. It can be easily seen that in the steady state the time average of the energy of the total electric field $\mathbf{E}$ absorbed per unit time per unit volume of the medium can be decomposed into components which determine the absorption respectively for $\mathbf{E}_1$ and $\mathbf{E}_2$. In particular, for $\mathbf{E}_2$ this absorption is given by the expression

$$I_\omega = \lim_{T\to\infty}\frac{1}{T}\int_0^T \mathbf{J}_2\mathbf{E}_2\,dt. \tag{4}$$

The electrical conductivity tensor $\sigma_{ik}(\omega)$ for the medium under consideration determines in the usual manner the relation between the components of the harmonic component $\mathbf{J}_{2\omega}$ (of frequency ω) of the current $\mathbf{J}_2$ and the components of the field $\mathbf{E}_2$. At the same time

$$I_\omega = \tfrac{1}{2}(\mathrm{Re}\,\sigma_{xx}(\omega)E_{2x0}^2 + \mathrm{Re}\,\sigma_{yy}(\omega)E_{2y0}^2 + \mathrm{Re}\,\sigma_{zz}(\omega)E_{2z0}^2). \tag{5}$$

Thus, the problem reduces to finding the periodic solution of the equation for $\mathbf{J}_2$:

$$m(d\mathbf{J}_2/dt + \mathbf{J}_2/\tau(E_{10})) = e(Ne\,\mathbf{E}_2 + c^{-1}[\mathbf{J}_2\mathbf{H}]). \tag{6}$$

From this equation it follows immediately that in the coordinate system which we have selected $\sigma_{zx} \equiv \sigma_{xz} \equiv \sigma_{zy} \equiv \sigma_{yz} \equiv 0$, and that the usual expression holds for σ_{zz} in the absence of a magnetic field.[1,2] In order to determine the remaining components of the electrical conductivity tensor, we shall assume that the field $\mathbf{E}_2$ is directed perpendicular to the z axis. We obtain

$$\frac{dJ_{2x}}{dt} + \frac{J_{2x}}{\tau} = \frac{e}{mc}(H_0 - H_1\cos pt)J_{2y} + \frac{Ne^2}{m}E_{2x0}\cos\omega t,$$

$$\frac{dJ_{2y}}{dt} + \frac{J_{2y}}{\tau} = -\frac{e}{mc}(H_0 - H_1\cos pt)J_{2x} + \frac{Ne^2}{m}E_{2y0}\cos\omega t. \tag{7}$$

It can be easily shown that the fundamental system of solutions of (7) (for $E_{2x0} = E_{2y0} = 0$) has the form

$$Y_1 = e^{-t/\tau}\begin{pmatrix}\sin(\omega_c t - \Delta\sin pt)\\ \cos(\omega_c t - \Delta\sin pt)\end{pmatrix},$$

$$Y_2 = e^{-t/\tau}\begin{pmatrix}-\cos(\omega_c t - \Delta\sin pt)\\ \sin(\omega_c t - \Delta\sin pt)\end{pmatrix}. \tag{8}$$

Here $\omega_c = eH_0/mc$, $\Delta = eH_1/pmc$. On the basis of (8) we can easily find the desired solution of (7) in the presence of the field $\mathbf{E}_2$. As a final result we obtain

$$\mathrm{Re}\,\sigma_{xx}(\omega) = \frac{Ne^2}{2m}\sum_{n=-\infty}^{\infty}J_n^2(\Delta)\left\{\frac{1/\tau}{(\omega+\omega_c-np)^2+1/\tau^2} + \frac{1/\tau}{(\omega-\omega_c+np)^2+1/\tau^2}\right\},$$

$$\mathrm{Im}\,\sigma_{xx}(\omega) = \frac{Ne^2}{2m}\sum_{n=-\infty}^{\infty}J_n^2(\Delta)\left\{\frac{\omega+\omega_c-np}{(\omega+\omega_c-np)^2+1/\tau^2} + \frac{\omega-\omega_c+np}{(\omega-\omega_c+np)^2+1/\tau^2}\right\},$$

$$\mathrm{Re}\,\sigma_{yx}(\omega) = \frac{Ne^2}{2m}\sum_{n=-\infty}^{\infty}J_n^2(\Delta)\left\{\frac{\omega-\omega_c+np}{(\omega-\omega_c+np)^2+1/\tau^2} - \frac{\omega+\omega_c-np}{(\omega+\omega_c-np)^2+1/\tau^2}\right\},$$

$$\mathrm{Im}\,\sigma_{yx}(\omega) = \frac{Ne^2}{2m}\sum_{n=-\infty}^{\infty}J_n^2(\Delta)\left\{\frac{1/\tau}{(\omega+\omega_c-np)^2+1/\tau^2} - \frac{1/\tau}{(\omega-\omega_c+np)^2+1/\tau^2}\right\},$$

$$\sigma_{xy} = -\sigma_{yx}, \qquad \sigma_{yy} = \sigma_{xx}. \tag{9}$$

Here $J_n(\Delta)$ is a Bessel function of the n-th order.

From the equations obtained above it can be seen that the components of the electrical conductivity tensor depend both on the variable magnetic

*Strictly speaking, the condition for τ to be constant has the form[1,2] $p \gg \delta/\tau$, where δ – the mean relative fraction of the energy lost by an electron in a collision with a heavy particle – is always much smaller than unity.

†$[\mathbf{vH}] = \mathbf{v}\times\mathbf{H}$.

field (or Δ), and also on the electric field $\mathbf{E}_1$. The dependence on $\mathbf{E}_1$ consists of the fact that the effective time between collisions τ is a function of the amplitude E_{10}. If the field $\mathbf{E}_1$ is strong, then expressions (9) are valid under the condition (2) (in a weak field $\mathbf{E}_1$ they hold for any arbitrary value of p). In this case the intensity of absorption I_ω is determined by (5), from which it can be seen that only the absorption of energy of the component of the electric field $\mathbf{E}_2$ perpendicular to $\mathbf{H}$ depends on the variable magnetic field H_1, and that this absorption, in turn, is determined by the quantity $\mathrm{Re}\,\sigma_{xx}(\omega)$.

Equation (2) for the applicability of expressions (9) in a strong field $\mathbf{E}_1$ means in the case of $\mathrm{Re}\,\sigma_{xx}(\omega)$ that this function has separate maxima in the neighborhood of the frequencies $\pm\omega_c \pm kp$ ($k = 0, 1, 2, \ldots$).

The dependence of the absorption curve on $\mathbf{E}_1$ is unimportant in the sense that it leads only to a change in the shape of these maxima, but does not qualitatively alter the absorption picture. However, the dependence of $\mathrm{Re}\,\sigma_{xx}(\omega)$ on the variable component of the magnetic field (or on Δ) is essential, and for all Δ the quantity $\mathrm{Re}\,\sigma_{xx}(\omega) > 0$.

For $H_1 = 0$ only $J_0(0) = 1$ is different from zero, and this gives the well-known expression for cyclotron resonance.[1-3] As H_1 increases the number of noticeable maxima increases. Moreover, from the properties of Bessel functions it follows that the height of each fixed maximum periodically falls to zero and increases again. In particular, the principal maximum (at the frequency ω_c) disappears after the field H_1 is introduced when Δ coincides with the first zero of $J_0(\Delta)$.

The author is deeply grateful to F. V. Bunkin for useful comments and discussion.

[1] V. L. Ginzburg and A. V. Gurevich, UFN 70, 201 (1960), Soviet Phys. Uspekhi 3, 115 (1960).

[2] V. L. Ginzburg, Rasprostranenie elektromagnitnykh voln v plazme (Propagation of Electromagnetic Waves in a Plasma), Gostekhizdat, 1960.

[3] Dresselhaus, Kip, and Kittel, Phys. Rev. 98, 368 (1955).

[4] A. S. Tager and A. D. Gladun, JETP 35, 808 (1958), Soviet Phys. JETP 8, 560 (1959).

[5] B. Lax, Quantum Electronics (Symposium), New York, 1960.

Translated by G. Volkoff
263

THEORY OF NUCLEAR RESONANCE IN PARAMAGNETIC MEDIA

R. Kh. TIMEROV and K. A. VALIEV

Physico-technical Institute, Kazan' Branch, Academy of Sciences, U.S.S.R.;
Kazan' Pedagogic Institute

Submitted to JETP editor May 22, 1961; resubmitted October 15, 1961

J. Exptl. Theoret. Phys. (U.S.S.R.) **41**, 1566-1575 (November, 1961)

A general theory is presented of the shape and width of nuclear magnetic resonance lines in paramagnetic media. The interaction between nuclear and electron spins in the system is due to dipole-dipole and contact forces. Precession, relaxation and exchange motions in the electron spin system and thermal motion of the particles of the medium were taken into account. Formulas have been obtained for the half-width $\Delta\omega_{1/2}$ and for the shift δ of the nuclear resonance line in the limiting cases of fast and slow thermal motion in the medium.

1. INTRODUCTION

THE influence of paramagnetic atoms of a substance on nuclear resonance manifests itself in the decrease in the relaxation times $T_{\parallel}$ and $T_{\perp}$ of the longitudinal and the transverse components (with respect to the external field) of the nuclear magnetization **M**, and also in the shift δ of the nuclear resonance frequency ω_I. These effects are due to the action of the magnetic field of the paramagnetic atoms on the nuclear moments, an action that varies in time (as a result of free precession, electron-spin relaxation processes, and exchange and thermal motions). In a number of theoretical papers[1-3] these effects were studied in the case of substances with a low concentration of paramagnetic ions and without taking the interaction between them into account; a consequence of this was the derivation of the theory of additivity of effects of paramagnetic atoms on the relaxation times $T_{\parallel}$ and $T_{\perp}$: $T_{\parallel}^{-1}$, $T_{\perp}^{-1} \sim N_S$ (N_S is the concentration of the paramagnetic atoms). Experiments carried out at low concentrations of the paramagnetic substance have confirmed this conclusion.[4,5]

At a high concentration of paramagnetic atoms exchange interactions between them can arise which result in exchange of electron spin orientations; this process will give rise to changes in the internal fields simultaneous with changes due to precession, electron spin relaxation and thermal motion. As a result of this, the internal fields must average out to a greater degree than in the absence of exchange, and this must manifest itself in a decrease in the effectiveness of the influence on the relaxation times $T_{\parallel}$ and $T_{\perp}$ of additional paramagnetic atoms newly added to the substance. Under these conditions the relation $T_{\parallel}^{-1}$, $T_{\perp}^{-1} \sim N_S$ must break down.

The present paper contains a theory of the shape and of the width (of the relaxation time $T_{\perp}^{-1}$) of the resonance line due to nuclei in paramagnetic media, with account of the exchange interactions between the paramagnetic atoms, which are in turn modulated by the thermal motion in the system. The last circumstance is particularly important in the discussion of this phenomenon in liquids. The results of this paper show that changes in the line width and in the shift δ of the resonance frequency of nuclei in paramagnetic media can turn out to be a direct method for studying exchange interactions which are important in the physics of magnetic phenomena. The calculations are carried out utilizing the method of Kubo and Tomita.[6]

We note here in addition to [1-5] some theoretical papers preceding the present paper and close to it in content. Moriya has considered the effect of exchange on nuclear relaxation both of diamagnetic[7] and of paramagnetic[8] atoms in antiferromagnetic crystals. The relaxation studied by Moriya consists of the transfer of energy from nuclear spins to spin waves (at low temperatures) and to the exchange system (at high temperatures). On the other hand, one of the present authors[9] has made a study of the relaxation of nuclei of paramagnetic atoms in magnetically dilute crystals due to the hyperfine interaction between nuclear and electron spins; in this case the dominant process is the lattice relaxation of electron spin. The object of these papers was to investigate the possibility of observing nuclear resonance for nuclei of paramagnetic atoms. Some of the conclusions reached in [7-9] and also in [1-5] are contained in the present paper as special cases.

In Sec. 2 we evaluate the autocorrelation function for the component M_X of the nuclear magnetization; in Secs. 3 and 4 we have calculated the half-width and the shift of the resonance line due to nuclei in a liquid and a solid paramagnetic medium respectively.

2. THE AUTOCORRELATION FUNCTION FOR THE NUCLEAR MAGNETIZATION

We consider a substance which contains per unit volume N_I identical magnetic nuclei whose resonance is being studied, and N_S paramagnetic atoms. The shape of the absorption line $I(\omega)$ is given by the Fourier transform of the autocorrelation function $G(t)$ of the component of the magnetic moment parallel to the direction (x) of the variable magnetic field[6]:

$$I(\omega) = \frac{1}{2\pi}\int_{-\infty}^{\infty} G(t)\, e^{-i\omega t}dt, \tag{1}$$

$$G(t) = \langle\{\hat{M}_x(t)\,\hat{M}_x(0)\}\rangle. \tag{2}$$

The angle brackets in (2) denote averaging of the symmetrized product $\{\dot{M}_X(t)\,\dot{M}_X(0)\}$ utilizing the density matrix $\hat{\rho}$; since the gaps between the magnetic sublevels are small ($\hbar\omega \ll kT$), we can assume

$$\rho = 1/(2I+1)^{N_I}(2S+1)^{N_S}; \tag{2a}$$

and finally obtain

$$\hat{M}_x(t) = \exp(it\hat{\mathcal{H}}/\hbar)\,\hat{M}_x \exp(-it\hat{\mathcal{H}}/\hbar), \tag{3}$$

where $\hat{\mathcal{H}}$ is the Hamiltonian for the system without the variable field which includes in our case the Zeeman energies

$$\hat{\mathcal{H}}_z^I = \gamma_I H_0 \sum_k \hat{I}_k^z, \qquad \hat{\mathcal{H}}_z^S = \gamma_S H_0 \sum_l \hat{S}_l^z$$

of the nuclear and the electronic moments in a constant magnetic field H_0 ($H_0 \parallel z$, $\gamma_I = g_I\beta_N$, $\gamma_S = g\beta$), the energy of interaction of nuclear and electronic moments

$$\hat{\mathcal{H}}_{IS} = \gamma_I\gamma_S\sum_{k>l} r_{kl}^{-3}[\hat{\mathbf{I}}_k\hat{\mathbf{S}}_l - 3r_{kl}^{-2}(\hat{\mathbf{I}}_k\mathbf{r}_{kl})(\hat{\mathbf{S}}_l\mathbf{r}_{kl})] + \hbar\sum_{k>l} A_{kl}\hat{\mathbf{I}}_k\hat{\mathbf{S}}_l,$$

the energy of the exchange interaction of electron spins among themselves

$$\hat{\mathcal{H}}_e = \hbar\sum_{i>j} J_{ij}(r_{ij})\,\hat{\mathbf{S}}_i\hat{\mathbf{S}}_j,$$

the kinetic energy of the system $\hat{\mathcal{H}}_K$ and the energy $\hat{\mathcal{H}}_{SK}$ of interaction of the electron spin system with $\hat{\mathcal{H}}_K$.

We separate the Hamiltonian $\hat{\mathcal{H}}$ into three parts:

$$\hat{\mathcal{H}}_1 = \hat{\mathcal{H}}_z^I, \qquad \hat{\mathcal{H}}_2 = \hat{\mathcal{H}}_z^S + \hat{\mathcal{H}}_{SK} + \hat{\mathcal{H}}_K + \hat{\mathcal{H}}_e, \qquad \hat{\mathcal{H}}' = \hat{\mathcal{H}}_{IS} \tag{4}$$

($\hat{\mathcal{H}}'$ is the perturbation), which satisfy the commutation relations

$$[\hat{\mathcal{H}}_1, \hat{\mathcal{H}}_2] = [\hat{\mathcal{H}}_2, \hat{M}_x] = 0. \tag{5}$$

On substituting into (2) the solution of the Heisenberg equation

$$i\hbar\dot{\hat{M}}_x = [\hat{M}_x(t), \quad \hat{\mathcal{H}}_1 + \hat{\mathcal{H}}_2 + \hat{\mathcal{H}}']\,, \tag{6}$$

we obtain the first terms of the series $G(t) = \Sigma G_n(t)$ ($G_1(t) = 0$):

$$G_0(t) = \tfrac{1}{6}N_I\gamma_I^2 I(I+1)\,[e^{i\omega_I t} + \text{c.c.}], \tag{7}$$

$$G_2(t) = -\tfrac{1}{6}N_I\gamma_I^2 I(I+1)\Big[e^{i\omega_I t} \times \sum_\gamma \sigma_\gamma^2 \int_0^t d\tau\,(t-\tau)\,e^{i\omega_\gamma\tau} f_\gamma(\tau) + \text{c.c.}\Big], \tag{8}$$

where

$$\sigma_\gamma^2 = \hbar^{-2}\langle|[\hat{M}_+^{(0)}, \hat{\mathcal{H}}'_\gamma(0)]|^2\rangle / \langle|\hat{M}_+^{(0)}|^2\rangle, \tag{9}$$

$$\hat{M}_\pm^{(0)} = \gamma_I\sum_k(\hat{I}_k^x \pm i\hat{I}_k^y),$$

$$f_\gamma(\tau) = \hat{N}\langle[\hat{M}_+^{(0)}, \hat{\mathcal{H}}'_\gamma(\tau)]\,[\hat{\mathcal{H}}'_{-\gamma}(0), \hat{M}_-^{(0)}]\rangle, \tag{10}$$

$$\hat{\mathcal{H}}'(\tau) = \sum_\gamma e^{i\omega_\gamma\tau}\hat{\mathcal{H}}'_\gamma(\tau) = \sum_\gamma e^{i\omega_\gamma\tau}\exp(i\tau\hat{\mathcal{H}}_2/\hbar)\,\hat{\mathcal{H}}'_\gamma\exp(-i\tau\hat{\mathcal{H}}_2/\hbar). \tag{11}$$

Here σ_γ^2 is the contribution to the second moment of the resonance line (in frequency units) due to $\hat{\mathcal{H}}'_\gamma$ (the contributions of the individual terms in the perturbation $\hat{\mathcal{H}}_{IS}$ to the second moment are additive); $f_\gamma(\tau)$ is the correlation function for the quantities $\hat{\mathcal{H}}'_\gamma(\tau)$ which vary in time under the influence of $\hat{\mathcal{H}}_2$ [modulation of the perturbation by "motion" (in the broad sense of this word)]; $\hat{N}$ is a formal operator defined by the relation

$$\hat{N}A(t) = A(t)/A(0).$$

We note that $G_0(t)$ describes the unperturbed motion of the nuclear magnetization—the free precession.

In order to obtain $f_\gamma(\tau)$ of the form (10) we have to evaluate

$$\hat{\mathcal{H}}'_\gamma(\tau) = \exp[i\hbar^{-1}\tau(\hat{\mathcal{H}}_z^S + \hat{\mathcal{H}}_{SK} + \hat{\mathcal{H}}_K + \hat{\mathcal{H}}_e)] \times \hat{\mathcal{H}}'_\gamma\exp[-i\hbar^{-1}\tau(\hat{\mathcal{H}}_z^S + \hat{\mathcal{H}}_{SK} + \hat{\mathcal{H}}_K + \hat{\mathcal{H}}_e)]. \tag{12}$$

The presence of $\hat{\mathcal{H}}_Z^S$ gives in (12) time factors of the form $\exp(i\beta\omega_S\tau)$, $\beta = 0, \pm1$. $\hat{\mathcal{H}}_{SK}$ describes relaxation processes for the components of the electron spin, so that in them we can take[1)] for $f_\gamma(\tau)$

[1)] A review of papers on the relaxation of electron spins in liquids is available in the book by S. A. Al'tshuler and B. M. Kozyrev[10]; c.f., also[11].

$$\hat{N}\langle \hat{S}_\beta(\tau)\hat{S}_{-\beta}(0)\rangle = \exp(-|\tau|/T_\beta), \qquad T_\beta = \begin{cases} T_1, & \beta = 0 \\ T_2, & \beta = \pm 1 \end{cases} \tag{13}$$

Further, we assume that the time variations of the exchange energy

$$\hat{\mathcal{H}}_e(\tau) = \exp(i\tau\hat{\mathcal{H}}_K/\hbar)\,\hat{\mathcal{H}}_e \exp(-i\tau\hat{\mathcal{H}}_K/\hbar)$$

under the influence of thermal motion in the system $\hat{\mathcal{H}}_K$ are characterized by the correlation time τ_e:

$$\hat{N}\langle \hat{\mathcal{H}}_e(\tau)\hat{\mathcal{H}}_e(0)\rangle = \exp(-|\tau|/\tau_e). \tag{14}$$

On taking into account the fact that usually $\langle|\hat{\mathcal{H}}_e|^2\rangle \ll \langle|\hat{\mathcal{H}}_K|^2\rangle$, we expand (12) into a series in powers of $\hat{\mathcal{H}}_e$; in this case it turns out that the effect of $\hat{\mathcal{H}}_e$ on the correlation function for the perturbation $f_\gamma(\tau)$ will manifest itself in the term in the expansion quadratic in $\hat{\mathcal{H}}_e$ (the term linear in $\hat{\mathcal{H}}_e$ gives zero on averaging).

Taking into account what we have just said with respect to $\hat{\mathcal{H}}'_\gamma(\tau)$ and $f_\gamma(\tau)$, and after simple but fairly lengthy calculations we can obtain

$$\langle|[\hat{M}_+^{(0)}, \hat{\mathcal{H}}'_\gamma(0)]|^2\rangle f_\gamma(\tau)$$
$$= \sum_\beta \sum_{\alpha=1,2} e^{i\beta\omega_S\tau}\langle|[\hat{M}_+^{(0)}, \hat{\mathcal{H}}^{IS}_{\gamma\beta,\alpha}(0)]|^2\rangle f_{\gamma\beta,\alpha}(\tau)$$
$$\times (1 - \omega^2_{e\gamma\beta,\alpha}F(\tau))\exp(-|\tau|/T_\beta); \tag{15}$$

$$f_{\gamma\beta,1}(\tau) = \hat{N}\sum_{k>l}\langle \exp(i\hbar^{-1}\tau\hat{\mathcal{H}}_K)\Phi_{kl}^{\gamma\beta}$$
$$\times \exp(-i\hbar^{-1}\tau\hat{\mathcal{H}}_K)\Phi_{kl}^{-\gamma,-\beta}\rangle$$
$$= \hat{N}\sum_{k>l}\langle \Phi_{kl}^{\gamma\beta}(\tau)\Phi_{kl}^{-\gamma,-\beta}(0)\rangle, \tag{16}$$

$$f_{\gamma\beta,2}(\tau) = \hat{N}\sum_{k,l}\langle \exp(i\hbar^{-1}\tau\hat{\mathcal{H}}_K)A_{kl}^{\gamma\beta}(r_{kl})$$
$$\times \exp(-i\hbar^{-1}\tau\hat{\mathcal{H}}_K)A_{kl}^{-\gamma,-\beta}(r_{kl})\rangle$$
$$= \hat{N}\sum_{k,l}\langle A_{kl}^{\gamma\beta}(\tau)A_{kl}^{-\gamma,-\beta}(0)\rangle;$$

$$F(\tau) = \int_0^\tau (\tau - \tau')\,d\tau' \exp(-|\tau|/\tau_e), \tag{17}$$

$$\omega^2_{e\gamma\beta,\alpha} = \langle|[\hat{\mathcal{H}}_e, [\hat{M}_+^{(0)}, \hat{\mathcal{H}}^{IS}_{\gamma\beta,\alpha}]]|^2\rangle / \hbar^2\langle|[\hat{M}_+^{(0)}, \hat{\mathcal{H}}^{IS}_{\gamma\beta,\alpha}]|^2\rangle. \tag{18}$$

Here $\hat{\mathcal{H}}^{IS}_{\gamma\beta,\alpha}$ are the terms in the expansion of the energy of interaction between nuclear and electron spins in terms of the Zeeman frequencies of nuclear and electron spins (cf. the table):

$$\hat{\mathcal{H}}' = \hat{\mathcal{H}}_{IS} = \sum_{\gamma,\beta}(\hat{\mathcal{H}}^{IS}_{\gamma\beta,1} + \hat{\mathcal{H}}^{IS}_{\gamma\beta,2})$$
$$= \sum_{\gamma,\beta}\Big[\sum_{k>l}\{kl\}_{\gamma\beta,1}\Phi_{kl}^{\gamma\beta} + \sum_{k,l}\{kl\}_{\gamma\beta,2}A_{kl}^{\gamma\beta}\Big].$$

The subscript α distinguishes quantities which refer to the dipole ($\alpha = 1$) and the hyperfine ($\alpha = 2$) interactions.

We shall be interested in the shape of the resonance line out to distances from the center of the line of the order of its width. Information with respect to this part of the line will be obtained if we carry out the integration in (8) up to $t \sim T_\perp^0$, where $T_\perp^0$ is the transverse relaxation time of the nuclei in the absence of motion.[6] It can be easily shown that $F(\tau) = \tau^2/2$ for $T_\perp^0 \ll \tau_e$ and $F(\tau) = |\tau|\tau_e$ for $T_\perp^0 \gg \tau_e$. Then, following [6] and denoting $\omega^2_{e\gamma\beta,\alpha} = \omega_e^2$ (cf. the table), we can write

$$1 - \omega^2_{e\gamma\beta,\alpha}F(\tau) \approx \exp[-\omega_e^2 F(\tau)]$$
$$= \begin{cases} \exp(-\tau^2\omega_e^2/2), & T_\perp^0 \ll \tau_e \qquad (19.1) \\ \exp(-|\tau|\tau_e\omega_e^2), & T_\perp^0 \gg \tau_e \qquad (19.2) \end{cases}$$

The quantity $\omega^2_{e\gamma\beta}$ (18) has the meaning and the dimensions of the square of the exchange frequency.

For the correlation function (16) for the coordinate part of the perturbation $\mathcal{H}^{IS}_{\gamma\beta,1}$ which varies under the influence of the thermal classical motion of $\hat{\mathcal{H}}_K$ we can take as usual[1]

$$f_{\gamma\beta,1}(\tau) = \exp(-|\tau|/\tau_1). \tag{20.1}$$

With respect to the hyperfine interaction energy two cases must be distinguished. If we have in mind the interaction of the electron and nuclear spins belonging to different particles moving independently then we can set

$$f_{\gamma\beta,2}(\tau) = \exp(-|\tau|/\tau_2), \tag{20.2}$$

where τ_2 stands for the lifetime of the diamagnetic particle in the solvate shell of the paramagnetic ion. Obviously in a solid we shall have $\tau_2^{-1} = 0$. But if we consider the isotropic interaction of the nuclear moment of the ion with its own electron moment (the anisotropic part is usually not very great and its effect is negligible), then we have $\tau_2^{-1} = 0$, and

$$f_{\gamma\beta,2} = 1, \tag{20.3}$$

since this interaction is not modulated by thermal motion.

Now on substituting (15) into (8) and taking into account (19) and (20) we obtain for $G_0(t) + G_2(t)$ the expression (omitting a constant factor)

$$e^{i\omega_I t}\Big\{1 - \sum_{\alpha=1,2}\sum_{\gamma,\beta}\sigma^2_{\gamma\beta,\alpha}\int_0^t d\tau\,(t-\tau)\,e^{i(\gamma\omega_I+\beta\omega_S)\tau}$$
$$\times \exp[-|\tau|\tau_\alpha^{-1} - |\tau|T_\beta^{-1} - \omega_e^2F(\tau)]\Big\} + \text{c.c.}, \tag{21}$$

which can be approximately represented in the form

$$\exp\Big\{i\omega_I t - \sum_{\alpha=1,2}\sum_{\gamma,\beta}\sigma^2_{\gamma\beta,\alpha}\int_0^t d\tau\,(t-\tau)e^{i(\gamma\omega_I+\beta\omega_S)\tau}$$
$$\times \exp[-|\tau|\tau_\alpha^{-1} - |\tau|T_\beta^{-1} - \omega_e^2F(\tau)]\Big\} + \text{c.c.} \tag{22}$$

$\gamma\beta$	$\{kl\}_{\gamma\beta,1}$	$\Phi_{kl}^{\gamma\beta}/\gamma_I\gamma_S r_{kl}^{-3}$	$\{kl\}_{\gamma\beta,2}$	$A_{kl}^{\gamma\beta}$	$\sigma^2_{\gamma\beta,1}$	$\sigma^2_{\gamma\beta,2}$
00	$\hat{I}_k^z\hat{S}_l^z$	$1-3\cos^2\vartheta_{kl}$	$\hat{I}_k^z\hat{S}_l^z$	A_{kl}	$\frac{1}{3}S(S+1)\sigma_{IS}^2$	$\frac{1}{3}S(S+1)\langle A^2\rangle$
01	$\hat{I}_k^z\hat{S}_l^-$	$-\frac{3}{2}\sin\vartheta_{kl}\cos\vartheta_{kl}\exp(i\varphi_{kl})$	0	0	$\frac{1}{4}S(S+1)\sigma_{IS}^2$	0
0—1	$\hat{I}_k^z\hat{S}_l^+$	$-\frac{3}{2}\sin\vartheta_{kl}\cos\vartheta_{kl}\exp(-i\varphi_{kl})$	0	0	$\frac{1}{4}S(S+1)\sigma_{IS}^2$	0
10	$\hat{I}_k^-\hat{S}_l^z$	$-\frac{3}{2}\sin\vartheta_{kl}\cos\vartheta_{kl}\exp(i\varphi_{kl})$	0	0	$\frac{1}{4}S(S+1)\sigma_{IS}^2$	0
11	$\hat{I}_k^-\hat{S}_l^-$	$-\frac{3}{4}\sin^2\vartheta_{kl}\exp(2i\varphi_{kl})$	0	0	$\frac{1}{2}S(S+1)\sigma_{IS}^2$	0
1—1	$-\frac{1}{4}\hat{I}_k^-\hat{S}_l^+$	$1-3\cos^2\vartheta_{kl}$	$\frac{1}{2}\hat{I}_k^-\hat{S}_l^+$	A_{kl}	$\frac{1}{12}S(S+1)\sigma_{IS}^2$	$\frac{1}{3}S(S+1)\langle A^2\rangle$
—10	$\hat{I}_k^+\hat{S}_l^z$	$-\frac{3}{2}\sin\vartheta_{kl}\cos\vartheta_{kl}\exp(-i\varphi_{kl})$	0	0	0	0
—11	$-\frac{1}{4}\hat{I}_k^+\hat{S}_l^-$	$1-3\cos^2\vartheta_{kl}$	$\frac{1}{2}\hat{I}_k^+\hat{S}_l^-$	A_{kl}	0	0
—1—1	$\hat{I}_k^+\hat{S}_l^+$	$-\frac{3}{4}\sin^2\vartheta_{kl}\exp(-2i\varphi_{kl})$			0	0

Here

$$\hbar^2\sigma_{IS}^2 = N_I^{-1}\sum_{k>l}\left|\Phi_{kl}^{00}\right|^2 = \frac{8}{3}N_I^{-1}\sum_{k>l}\left|\Phi_{kl}^{01}\right|^2 = \frac{8}{3}N_I^{-1}\sum_{k>l}\left|\Phi_{kl}^{11}\right|^2 = \frac{4}{5}\gamma_I^2\gamma_S^2\sum_l\langle r_{kl}^{-6}\rangle$$

for an isotropic distribution (powders, glasses and liquids);

$$\langle A^2\rangle = N_I^{-1}\sum_{k,\,l}\left|A_{kl}^{\gamma\beta}\right|^2;$$

with $A_{k,\,l}^{\gamma\beta} = A_{k,\,l}$ $\quad \omega^2_{e\gamma\beta,\,\alpha} = \omega_e^2 = \frac{2}{3}\langle J^2\rangle S(S+1) = \frac{2}{3}N_S^{-1}\sum_{i\neq j}J_{ij}^2 S(S+1)$.

We now carry out calculations of the line shape for two limiting cases—fast motion (liquids) and slow motion (viscous liquids, solids) of the molecules of the system.

3. FAST THERMAL MOTION: $T_\perp^0 \gg \tau_e$

In order to find the line shape $I(\omega)$ near its maximum one should in the case $T_\perp^0 \gg \tau_e$ evaluate the Fourier transform (1) of the autocorrelation function (22) making use of (19.2); in this case we obtain a Lorentz line of half-width $\Delta\omega_{1/2}$ and with its center at the frequency[2] $\omega_I + \delta$:

$$\Delta\omega_{1/2} = S(S+1)\sigma_{IS}^2\left\{\frac{1}{3}K_{01} + \frac{1}{2}\frac{K_{11}^{-1}}{K_{11}^{-2}+\omega_S^2} + \frac{1}{4}\frac{K_{01}^{-1}}{K_{01}^{-2}+\omega_I^2} + \frac{1}{2}\frac{K_{11}^{-1}}{K_{11}^{-2}+(\omega_S+\omega_I)^2} + \frac{1}{12}\frac{K_{11}^{-1}}{K_{11}^{-2}+(\omega_I-\omega_S)^2}\right\} + \frac{1}{3}S(S+1)\langle A^2\rangle\left\{K_{02} + \frac{K_{12}^{-1}}{K_{12}^{-2}+(\omega_I-\omega_S)^2}\right\}, \quad (23)$$

$$-\delta = S(S+1)\sigma_{IS}^2\left\{\frac{1}{2}\frac{\omega_I}{K_{01}^{-2}+\omega_I^2} + \frac{1}{2}\frac{\omega_I+\omega_S}{K_{11}^{-2}+(\omega_I+\omega_S)^2} + \frac{1}{12}\frac{\omega_I-\omega_S}{K_{11}^{-2}+(\omega_I-\omega_S)^2}\right\} + \frac{1}{3}S(S+1)\langle A^2\rangle\frac{\omega_I-\omega_S}{K_{12}^{-2}+(\omega_I-\omega_S)^2}; \quad (24)$$

$$K_{0,\alpha}^{-1} = \tau_\alpha^{-1} + T_1^{-1} + \tau_e\omega_e^2, \qquad K_{1,\alpha}^{-1} = \tau_\alpha^{-1} + T_2^{-1} + \tau_e\omega_e^2. \quad (25)$$

We discuss formulas (23) — (25) briefly. First, it follows from the definition of $K_{0,\alpha}^{-1}$, $K_{1,\alpha}^{-1}$ in (25) that the half-width and the shift of the resonance line due to nuclear spins are determined by the velocities of thermal motion, by the electron relaxation or by the electron exchange motion depending on which process proceeds at the greatest rate: τ_α^{-1}, T_β^{-1} or $\tau_e\omega_e^2$. For paramagnetic ions of the type Cu^{2+}, VO^{2+} etc. T_1^{-1}, $T_2^{-1} \sim 10^8$ sec^{-1}; for other paramagnetic ions (Ti^{3+}, Fe^{2+}, Co^{2+} from the iron group, the rare earth ions) the relaxation times are very short, and, apparently, one can take[10] $T_1^{-1} > 10^{10}$ sec^{-1}.

In nonviscous liquids $\tau_1^{-1} \sim 10^{11}$ sec^{-1}. One can suppose that the values of τ_e^{-1} will be somewhat greater than the values of τ_1^{-1} in view of the greater sensitivity of the exchange energy to the

[2] The shift δ must be measured from the frequency $\omega_I + \Delta$, where Δ is a line shift of the Knight type (cf.[5]) which is proportional to the magnetization of the system in the field H_0. In the approximation for the density matrix ρ utilized by us [Eq. (2a)] the constant magnetization of the system, and consequently also Δ, are both equal to zero ($\rho = (2I+1)^{-N_I} \times (2S+1)^{-N_S}$ presupposes all the magnetic energy sublevels to be equally populated).

variations in the distances between the paramagnetic atoms. For rough calculations one can assume that $\tau_e^{-1} \sim \tau_1^{-1}$. The lifetime of a particle in the solvate shell of the ion τ_2, as a rule, will be greater than the relaxation times T_1 and T_2; in these cases the effect of thermal motion on the hyperfine interaction will become unobservable. Moreover, in concentrated solutions, $\sigma_{IS}^2 \gg \langle A^2 \rangle$, since the internal field amounts to $\sim 10^3$ oe, while $|A| \sim 10-10^2$ oe. In concentrated solutions ω_e can attain values of $10^{10}-10^{11}$ sec^{-1}.

These estimates show that very different situations can be realized in practice. The case appears to be of interest when the dominant terms in $K_{\beta,\alpha}^{-1}$ are the terms $\omega_e^2\tau_e + \tau_\alpha^{-1}$. It is realized in solutions of relatively high concentrations of paramagnetic particles with not too short relaxation times T_1, T_2. Then

$$K_{\beta,\alpha} = \tau_\alpha/(1 + \tau_\alpha\tau_e\omega_e^2)$$

and for $K_{\beta,\alpha}^{-1} \gg \omega_I, \omega_S$ we obtain from (23) the following expression for the half-width

$$\Delta\omega_{1/2} = \tfrac{20}{12} S(S+1)\sigma_{IS}^2\tau_1/(1 + \tau_1\tau_e\omega_e^2) + \tfrac{2}{3} S(S+1)\langle A^2\rangle \tau_2/(1 + \tau_2\tau_e\omega_e^2). \quad (26)$$

For large values of ω_e^2 we obtain on neglecting in the denominators of (26) unity in comparison with $\tau_\alpha\tau_e\omega_e^2$

$$\Delta\omega_{1/2} = S(S+1)\left[\tfrac{20}{12}\sigma_{IS}^2 + \tfrac{2}{3}\langle A^2\rangle\right]/\tau_e\omega_e^2. \quad (26.1)$$

Since σ_{IS}^2, ω_e^2, $\langle A^2\rangle \sim N_S$ (we are considering the hyperfine interaction with an electron spin belonging to a different ion), then it follows from (26.1) that in this range the dependence of $\Delta\omega_{1/2}$ on concentration will be due to the variations in τ_e which increases as the concentration is increased; therefore, $\Delta\omega_{1/2}$ will decrease. Further, in accordance with (23), the line width will gradually diminish as the external field increases. In weak fields ($K_{\beta,\alpha}^2\omega_S^2 \ll 1$) the observed width is given by (26). In strong fields $K_{\beta,\alpha}^2\omega_S^2 \gg 1$ (but $K_{\beta,\alpha}^2\omega_I^2 \ll 1$) we have

$$(\Delta\omega_{1/2}) = \tfrac{7}{12} S(S+1)\sigma_{IS}^2 K_{\beta,1} + \tfrac{1}{3} S(S+1)\langle A^2\rangle K_{\beta,2}.$$

In the absence of exchange (low concentration of paramagnetic ions), (23) together with (25) become similar to the well known formulas from [3,12].

Of some interest are the investigations of the line shift $-\delta$ [formula (24) gives the shift in units of rad/sec]. In order of magnitude the value of $-\delta$ is close to the line width. As can be seen from (24), $-\delta$ passes through a maximum (as the external field is varied) at $\omega_I = K_{01}^{-1}$ and $\omega_S + \omega_I = K_{11}^{-1}$. At the same time the shift diminishes as the velocity of the motion $K_{\beta,\alpha}^{-1}$ increases.

4. SLOW THERMAL MOTION: $T_\perp^0 \ll \tau_e$

The condition $T_\perp^0 \ll \tau_e, \tau_1, \tau_2$ corresponds to a slow modulation of the exchange, hyperfine and dipole interactions with the thermal motion. The nature of the phenomenon is in this case determined by the exchange and the relaxation motions in the electron spin system. The nuclear absorption line near its maximum has a Lorentz shape, since the approximate autocorrelation function assumes the following form for $T_\perp^0 \ll \tau_e$ [cf. (19.1)]:

$$\exp\left\{i\omega_I t - t\sum_{\gamma,\beta}\sigma_{\gamma\beta}^2\int_0^\infty \exp\left[-\tau\left[T_\beta^{-1} - i(\gamma\omega_I + \beta\omega_S)\right] - \tau^2\omega_e^2/2\right]d\tau\right\} + \text{c.c.},$$

$$\sigma_{\gamma\beta}^2 = \sigma_{\gamma\beta,1}^2 + \sigma_{\gamma\beta,2}^2. \quad (27)$$

The factor multiplying it in the exponent of the exponential determines the position of maximum intensity $\omega_I + \delta$ (cf. footnote [2]), while the factor multiplying $-t$ determines the half width $\Delta\omega_{1/2}$:

$$\Delta\omega_{1/2} = \sqrt{\frac{\pi}{2}}\frac{1}{\omega_e}\sum_{\gamma=0}^{1}\sum_{\beta=-1}^{1}\sigma_{\gamma\beta}^2 \operatorname{Re} L(z_{\gamma\beta}), \quad (28)$$

$$\omega_I + \delta = \omega_I - \sqrt{\frac{\pi}{2}}\frac{1}{\omega_e}\sum_{\substack{\gamma=0\\ |\gamma|+|\beta|\neq 0}}^{1}\sum_{\beta=-1}^{1}\sigma_{\gamma\beta}^2 \operatorname{Im} L(z_{\gamma\beta}); \quad (29)$$

$$z_{\gamma\beta} = (\gamma\omega_I + \beta\omega_S - iT_\beta^{-1})/\omega_e\sqrt{2}, \quad (30)$$

$$L(z) = e^{-z^2} - i2W(z)/\sqrt{\pi}, \qquad W(z) = e^{-z^2}\int_0^z e^{x^2}dx. \quad (31)$$

We present a brief analysis of formulas (28)–(31). In a number of cases (Mn^{2+}, Cr^{3+}, VO^{2+}) the electron relaxation times $T_\beta = T_1, T_2$ are comparatively long, $\sim 10^{-7}-10^{-8}$ sec (cf., the discussion in Sec. 3), so that $T_\beta^{-1} \ll \omega_S \neq 0$; therefore in $z_{\gamma\beta}$ the imaginary part can be neglected if $\beta \neq 0$. Moreover, let $T_\beta\omega_e \gg 1$. Then the formula for the half width of the line (28) assumes the following form:

$$\Delta\omega_{1/2} = \sqrt{\frac{\pi}{2}}\omega_e^{-1}\left[\sigma_{00}^2 + \sigma_{10}^2 + \sum_{\gamma=0,1}\sum_{\beta=\pm 1}\sigma_{\gamma\beta}^2\exp\left[-\frac{(\gamma\omega_I + \beta\omega_S)^2}{2\omega_e^2}\right]\right], \quad (32)$$

analogous to the well known formulas for the half-width of the electron resonance line.[6] For the line shift δ we obtain in the present case ($T_\beta^{-1} \ll |\beta\omega_S|$, $\beta \neq 0$)

$$-\delta = \sqrt{2}\omega_e\sum_{\gamma=0,1}\sum_{\beta=\pm 1}\sigma_{\gamma\beta}^2 W\left(\frac{\gamma\omega_I + \beta\omega_S}{\sqrt{2}\omega_e}\right). \quad (33)$$

On taking into account the fact that $\gamma\omega_I + \beta\omega_S \approx \beta\omega_S$, we obtain from (33) the expression

$$-\delta = \sqrt{2}\omega_e^{-1} S(S+1)\left[\tfrac{5}{12}\sigma_{IS}^2 - \tfrac{1}{3}\langle A^2\rangle\right] e^{-y^2}\int_0^y e^{x^2}dx, \quad (34)$$

which reaches a maximum[13] at $y \equiv \omega_S/\sqrt{2}\omega_e = 0.925$.

Thus, by measuring the width (32) and the shift of the resonance frequency (34) one can find the exchange frequency ω_e.

In the opposite case $T_\beta^{-1} \gg |\gamma\omega_I + \beta\omega_S|$ (weak fields) one can set $z_{\gamma\beta}$ equal to $-i/\sqrt{2}\omega_e T_\beta$. Then the shift $\delta = 0$, since in such an approximation $L(z_{\gamma\beta})$ is real, while the half width of the line $\Delta\omega_{1/2}$ does not depend on the constant magnetic field, but will vary strongly as the concentration of the paramagnetic atoms is varied:

$$\Delta\omega_{1/2} = \sqrt{\frac{\pi}{2}}\frac{1}{\omega_e} S(S+1)\left\{\left(\tfrac{7}{12}\sigma_{IS}^2 + \tfrac{1}{3}\langle A^2\rangle\right)e^{u^2}\right.$$
$$\times\left(1 - \frac{2}{\sqrt{\pi}}\int_0^u e^{-x^2}dx\right) + \left(\tfrac{13}{12}\sigma_{IS}^2 + \tfrac{1}{3}\langle A^2\rangle\right)e^{v^2}$$
$$\left.\times\left[1 - \frac{2}{\sqrt{\pi}}\int_0^v e^{-x^2}dx\right]\right\},$$
$$u = 1/\sqrt{2}\,T_1\omega_e, \qquad v = 1/\sqrt{2}\,T_2\omega_e. \quad (35)$$

In the case of very strong exchange T_1^{-1}, $T_2^{-1} \ll \omega_e$ expression (35) reduces to

$$\Delta\omega_{1/2} = \sqrt{\frac{\pi}{2}}\frac{1}{\omega_e} S(S+1)\left[\tfrac{5}{3}\sigma_{IS}^2 + \tfrac{2}{3}\langle A^2\rangle\right]. \quad (J)$$

In the case of weak exchange, when the exchange motion in the electron spin system is slower than the relaxation motions (T_1^{-1}, $T_2^{-1} \gg \omega_e$), formula (35) is inapplicable and we must repeat the calculation, neglecting in (27) the quantity $\omega_e^2\tau^2/2$ in comparison with τ/T_β; we do not reproduce here the formulas obtained in this case, since they coincide exactly with (23) and (24) with $K_{\beta,\alpha}^{-1} = T_\beta^{-1}$. In the case $\omega_e \approx T_\beta^{-1}$ one should utilize formula (35) and tables of functions[13] for estimating the line width.

In conclusion we wish to make some remarks. As can be seen from a detailed discussion of the formulas obtained, systematic measurements of the width and the shift of nuclear magnetic resonance lines in paramagnetic media can serve as an important means of studying exchange and relaxation motions in an electron spin system and thermal motion of the molecules of the medium. Preliminary measurements carried out in the laboratory of the Kazan' Pedagogic Institute have demonstrated agreement between the conclusions of the present theory and experiment.

Note added in proof (October 15, 1961). In solids with a low concentration of paramagnetic particles (in the absence of exchange) the phenomenon of spin diffusion can exert an essential influence on the nonsecular part $(\Delta\omega_{1/2})_{nS}$ of the line width (the terms in the formulas for $\Delta\omega_{1/2}$ containing the frequency ω_I). In these cases $(\Delta\omega_{1/2})_{nS}$ should be replaced by the expression $(1/2T_1)$, where T_1 has been evaluated taking spin diffusion[14] into account.

[1] Bloembergen, Purcell, and Pound, Phys. Rev. 73, 678 (1948).

[2] N. Bloembergen and W. C. Dieckinson, Phys. Rev. 79, 179 (1950).

[3] N. Bloembergen, J. Chem. Phys. 27, 572 (1957).

[4] A. I. Rivkind, DAN SSSR 102, 1197 (1955).

[5] A. Lösche, Kerninduktion, Deutscher Verlag der Wissenschaften, Berlin, 1957.

[6] R. Kubo and K. Tomita, J. Phys. Soc. Japan 9, 888 (1954).

[7] T. Moriya, Progr. Theoret. Phys. (Kyoto) 16, 23 (1956).

[8] T. Moriya, Progr. Theoret. Phys. (Kyoto) 16, 641 (1956).

[9] K. A. Valiev, FMM (Phys. of Metal and Metallography) 6, 193, 776 (1958); Uchenye zapiski kazanskogo universiteta (Sci. Papers of Kazan' University) 117, Sec. 5, 149 (1957); JETP 36, 1743 (1959), Soviet Phys. JETP 9, 1242 (1959).

[10] S. A. Al'tshuler and B. M. Kozyrev, Elektronnyi paramagnitnyi rezonans (Electron Paramagnetic Resonance), Fizmatgiz, 1961.

[11] K. A. Valiev and M. M. Zaripov, JETP 41, 756 (1961), Soviet Phys. JETP 14, 545 (1962).

[12] R. L. Conger and P. W. Selwood, J. Chem. Phys. 20, 383 (1952).

[13] K. A. Karpov, Tablitsy funktsii $w(z) = \exp(-z^2)\int_0^z \exp(x^2)\,dx$ v kompleksnoi oblasti (Tables of the function $w(z) = \exp(-z^2)\int_0^z \exp(x^2)\,dx$ in the complex domain), AN SSSR, 1957.

[14] N. Bloembergen, Physica 25, 386 (1949); G. R. Khutsishvili, Trudy Instituta fiziki AN Gruz. SSR (Proc. Inst. Phys., Acad. Sci. Georgian S.S.R.) 4, 3 (1956); P. G. de Gennes, J. Phys. Chem. Solids 7, 345 (1958); W. E. Blumberg, Phys. Rev. 119, 79 (1960).

Translated by G. Volkoff
264

BIMUONIUM PRODUCTION IN ELECTRON-POSITRON SCATTERING

V. N. BAĬER and V. S. SYNAKH

Nuclear Physics Institute, Siberian Division, Academy of Sciences U.S.S.R.

Submitted to JETP editor May 26, 1961

J. Exptl. Theoret. Phys. (U.S.S.R.) 41, 1576-1581 (November, 1961)

We investigate the formation and the properties of the bound state of a positive and negative muon (bimuonium). We discuss the probability of its observation.

1. INTRODUCTION

WHEN electron and positron beams moving in opposite directions collide, electromagnetic pair production may occur. In particular, these pairs may be produced in the bound state, or in the form of atomic systems such as $(\pi^+\pi^-)$, $(\mu^+\mu^-)$, (K^+K^-), etc. The electromagnetic decay time of such systems (i.e., the lifetime for decay into electron-positron pairs or into photons) is much shorter than the weak-interaction decay time for the same particles. The resulting decay of these systems will therefore lead to additional contributions to the electron-positron scattering and annihilation cross sections. It will be shown below that these effects can be observed under certain conditions.

The study of these bound states is not without importance, since it may lead to information on the interaction between the particles of which they are composed, especially for low energies. In particular, data on the $(\pi^+\pi^-)$ and (K^+K^-) systems may give the S-phase shifts for $\pi\pi$ (KK)-scattering.

These bound states may be thought of as unstable particles which one may treat by the apparatus of quantum field theory.[1,2] It is easily shown that the density of final states can in this case be written in the form

$$\rho(p^2)\,d^4p = \operatorname{Im} G(p^2)\,d^4p, \tag{1.1}$$

where $G(p^2)$ is the Green's function for the unstable particle (which for us is the bound state).

In this article we will investigate the $(\mu^+\mu^-)$ system in detail; we shall call it bimuonium. This system has the lowest production threshold (103.5 Mev) and can be calculated exactly, since one may with good accuracy consider the muon-muon interaction to be purely electromagnetic.[3]

FIG. 1

2. BIMUONIUM DECAY

Bimuonium decay is more complicated than the analogous positronium decay, since positron-electron pairs can be produced as well as photons.*

Let us find the probability for bimuonium decay into an electron-positron pair in the lowest order of perturbation theory. Figure 1 gives the Feynman diagram for this process. Here and henceforth we shall use a cross-hatched rectangle to denote the bimuonium bound state, and double lines to denote free muons. In the ladder approximation the diagram of Fig. 1 is the sum of those in Fig. 2. We sum the contributions from these diagrams by the method described by Alekseev[4] and obtain the following expression for the matrix element of the $(\mu^+\mu^-) \to e^+ + e^-$ process:

$$M = e^2 \int \varphi^*(x_1, x_2)\,\gamma_\nu C^+ D(x_1 - x_2)\,[C\gamma_\nu]_{\rho_1\rho_2}\,\psi_{\rho_2\rho_1}(x_3, x_4) \times \delta(x_1 - x_2)\,\delta(x_3 - x_4)\,d^4x_1 d^4x_2 d^4x_3 d^4x_4. \tag{2.1}$$

Here ψ is the bimuonium wave function, a solution of the Bethe-Salpeter equation[5] in the ladder approximation, φ is the wave function of the free electron and the free positron, and C is the charge conjugation operator (we choose the representation in which $C = \alpha_2$).†

The Bethe-Salpeter equation does not include the virtual annihilation diagrams of bimuonium, since they form part of the radiative corrections, and we shall not include these in what follows.

*Conversion of a free $\mu^+\mu^-$ pair into an electron-positron pair has been studied also by Zel'dovich.[12]

†We choose the system of units in which $\hbar = c = 1$, $e^2 = 1/137$; the metric is defined by $ab = \mathbf{a}\cdot\mathbf{b} - a_0 b_0$.

FIG. 2

Transforming (2.1) to the momentum representation and going to the rest system of the bimuonium, we obtain

$$M = -i\pi \frac{e^2}{\mu^2}\left[\bar{u}(p_-)\gamma_\mu v(p_+)\right] \mathrm{Sp}\int C\gamma_\nu \psi(p)\, d^4p\, \delta(P - p_- - p_+)$$
$$= M_1 \delta(P - p_- - p_+). \qquad (2.2)$$

Here P is the total momentum of the bimuonium, p is the relative momentum of the particles making up the bimuonium, and p_- and p_+ are the electron and positron momenta. In the photon Green's function in (2.2) we have set $P_0 = 2\mu - \delta \approx 2\mu$ ($\delta = 1.41$ kev is the bimuonium binding energy, and μ is the muon mass).

The integration over p_0 can be carried out in (2.2), if one makes use of the identity

$$\int \psi(p)\, dp_0 = 2\pi\psi(\mathbf{p}, t = 0). \qquad (2.3)$$

We proceed, carrying all calculations through to linear terms in the relative velocity v. To this accuracy the bimuonium wave function at time t = 0 is of the form [6]

$$\begin{pmatrix} \psi_{00} & \psi_{01} \\ \psi_{10} & \psi_{11} \end{pmatrix} = \begin{pmatrix} f & -f\sigma^T \mathbf{p}/2\mu \\ \sigma \mathbf{p} f/2\mu & 0 \end{pmatrix} \Phi(\mathbf{p}), \qquad (2.4)$$

where $\Phi(\mathbf{p})$ is a solution of the nonrelativistic Schrödinger equation for bimuonium, and f is the two-component spin wave function of bimuonium. To the accuracy we are working with we have

$$\int F(\mathbf{p})\,\Phi(\mathbf{p})\, d^3\mathbf{p} = (2\pi)^3 F(\mathbf{p}=0)\,\Phi(\mathbf{x}=0)$$
$$+ \frac{(2\pi)^3}{i}\frac{\partial F(\mathbf{p}=0)}{\partial p_n}\frac{\partial \Phi(\mathbf{x}=0)}{\partial x_n}, \qquad (2.5)$$

so that

$$M_1 = -i\pi (2\pi)^4 e^2 \mu^{-2} (\bar{u}\hat{B}v), \qquad (2.6)$$

where

$$B_0 = (i/2\mu)\,\mathrm{Sp}\,[\sigma_2 (f\sigma_k^T + \sigma_k f)\nabla_k \Phi(\mathbf{x}=0)],$$
$$\mathbf{B} = -\mathrm{Sp}\,(\sigma_2 \sigma f)\,\Phi(\mathbf{x}=0). \qquad (2.7)$$

It follows from (2.7) that only the S state of bimuonium with a symmetric spin function (orthobimuonium) can decay into an electron-positron pair, as one may have expected from considerations of charge parity conservation. With our approximations such decay cannot take place from states with higher orbital angular momenta.

Summing over the spins of the final particles and averaging over the initial spin states, we obtain the expression

$$\Gamma_n = e^{10}\mu/6n^3; \qquad (2.8)$$

for the probability per unit time of bimuonium decay into an electron-positron pair from the nS state; for n = 1 this gives 5.6×10^{11} sec^{-1}.

The two-photon and three-photon bimuonium decay rates can be obtained from the analogous expressions for positronium.[7] For the nS state we have

$$\Gamma_{2\gamma} = e^{10}\mu/2n^3 = 1.66\cdot 10^{12} n^{-3} \text{ sec}^{-1} \text{ (parabimuonium)}, \qquad (2.9)$$

$$\Gamma_{3\gamma} = \frac{4e^2}{9\pi}(\pi^2 - 9)\,\Gamma_{2\gamma} = 1.5\cdot 10^9 n^{-3} \text{ sec}^{-1} \text{ (orthobimuonium)}. \qquad (2.10)$$

It is thus seen that orthobimuonium decays essentially only into an electron-positron pair. We shall henceforth neglect three-photon annihilation.

3. NONRADIATIVE BIMUONIUM PRODUCTION IN ELECTRON-POSITRON COLLISIONS

This process is the inverse of the decay process treated in Sec. 2. We can therefore use the matrix element of (2.6). Recalling (1.1), we see that the cross section may be written

$$\sigma_{\text{non}} = \tfrac{1}{2}(2\pi)^{-4}\int |M_1|^2\, \mathrm{Im}\, G(P^2)\, d^4P. \qquad (3.1)$$

In the c.m.s., we have

$$G(P^2)\, d^4P = (2\pi)^{-3}\, d^3P \rho(P_0)\, dP_0; \qquad (3.2)$$

where

$$\rho(P_0)\, dP_0 = \frac{\Gamma}{2\pi}\frac{dP_0}{[P_0 - (2\mu - \delta)]^2 + \Gamma^2/4}. \qquad (3.3)$$

After summing over final spins and averaging over the spins of the initial particles, we obtain*

$$\sigma_{\text{non}}^{(n)} = \frac{\pi e^{10}}{8n^3\mu}\frac{\Gamma_n}{[P_0 - (2\mu - \delta)]^2 + \Gamma_n^2/4}, \qquad (3.4)$$

where E is the initial energy of the electron (or positron). At resonance (i.e., when $E = \mu - \delta/2$), we find the cross section given by

$$\sigma_{\text{non}}^{(n)} = 3\pi/n^3\mu^2 = 0{,}33\cdot 10^{-24} n^{-3}\,\text{cm}^2. \qquad (3.5)$$

As is well known, when high-energy electrons and positrons interact, the radiative corrections become important, and the most important contribution comes from the so-called doubly logarithmic terms.[8,9] The radiative corrections to bimuonium production can be calculated in the way it was done by Kheĭfets with one of the present authors.[9] Assuming that the maximum energy the photons can carry off is of the order of the level width, we obtain

*The transformation of an electron-positron pair into a $\mu^+\mu^-$ pair was first discussed by Berestetskii and Pomeranchuk.[13]

$$\sigma_R^{(1)} = \sigma_{non}^{(1)} \exp\left(-\frac{4e^2}{\pi} \ln\frac{\mu}{m} \ln\frac{\mu}{\Gamma}\right) = 0.27\ \sigma_{non}^{(1)}. \quad (3.6)$$

where m is the electron mass.

4. RADIATIVE BIMUONIUM PRODUCTION IN ELECTRON-POSITRON COLLISIONS

Also of interest is bimuonium production accompanied by emission photons. It is clear that this process can be of interest only in the neighborhood of the threshold, and we therefore need consider only soft gamma radiation for which

$$\omega/\mu \ll 1. \quad (4.1)$$

The photon emission process may take place in such a way that one of the photons carries more energy than all the others. This process can be treated by perturbation theory, the criterion for the validity of which is of the form [10]

$$e^2 \ln\frac{\mu}{m} \ll 1, \qquad \frac{e^2}{\pi} \ln\frac{\mu}{m} \ln\frac{\mu}{\omega_{min}} \ll 1. \quad (4.2)$$

This equation shows that we may set ω_{min} roughly equal to the width of the 1S state of bimuonium, [8,2] namely

$$\omega_{min} = \Gamma_1 \approx 4 \cdot 10^{-4}\ \text{ev} \quad (4.3)$$

and thus that we may use perturbation theory to treat the region of maximum interest, in which

$$\Gamma < \omega \ll \mu. \quad (4.4)$$

The case of softer gamma emission was treated in Sec. 3.

Diagrams for this process are shown in Figs. 3 and 4. For nonrelativistic bimuonium energies, the diagrams of Fig. 3 correspond to orthobimuonium production, while the diagrams of Fig. 4 correspond to parabimuonium. There is thus no interference between the corresponding matrix elements. Simple calculations show that parabimuonium production is less likely by a factor of $(\omega/\mu)^2$ than orthobimuonium production. Therefore we shall henceforth restrict our considerations to the diagrams of Fig. 3. In the c.m.s. the matrix element for these diagrams can be written

$$M = -ie^3 (2\pi)^4 \sqrt{\frac{2\pi}{\omega}} \frac{4\pi}{P^2} \bar{v}\left[\hat{B}^{(1)} \frac{i(\hat{p}_- - \hat{k}) - m}{(p_- - k)^2 + m^2} \hat{e} + \hat{e} \frac{i(\hat{p}_- - \hat{P}) - m}{(p_- - P)^2 + m^2} \hat{B}^{(1)}\right] u\delta(P + k - p_- - p_+), \quad (4.5)$$

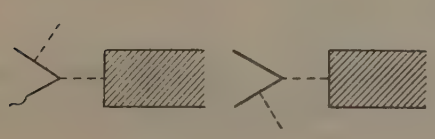

FIG. 3

FIG. 4.

where

$$B_\mu^{(1)} = \mathrm{Sp} \int C\gamma_\mu \psi(p)\, d^4p. \quad (4.6)$$

In order to calculate $B^{(1)}$, one must know the bimuonium wave function in the electron-positron c.m.s. Following Alekseev [6] and making use of (4.1), one easily arrives at the conclusion that up to factors linear in $|\mathbf{P}|/\mu = \omega/\mu$ and v, and at time t = 0

$$\begin{pmatrix} \psi_{00} & \psi_{01} \\ \psi_{10} & \psi_{11} \end{pmatrix} = \begin{pmatrix} f & f\sigma^T(\mathbf{P} - \mathbf{p})/2\mu \\ \sigma(\mathbf{P} + \mathbf{p})\, f/2\mu & 0 \end{pmatrix} \Phi(\mathbf{p}). \quad (4.7)$$

Recalling (2.3) and (2.5), averaging over the spins of the initial particles and summing over final spins, one finds that the differential cross section for radiative production of orthobimuonium in the nS state may be written*

$$d\sigma_{rad}^{(n)} = \frac{1}{4n^3} \frac{e^{12}(\mathbf{ep}_-)^2}{\mu^2 (E\omega - \mathbf{p}_-\mathbf{k})^2}, \quad (4.8)$$

where

$$\omega \approx 2E - (2\mu - \delta).$$

After summing over the photon polarizations and integrating over the angle of emission, one finds the total cross section to be†

$$\sigma_{rad}^{(n)} = \frac{\pi}{2n^3} \frac{e^{12}}{\mu^2} \left(2 \ln\frac{\mu}{m} - 1\right) \frac{\mu}{\omega}, \quad (4.9)$$

$$\sigma_{rad} = \sum_n \sigma_{rad}^{(n)} = 3.6\pi \cdot 10^{-38} \frac{\mu}{\omega} \text{cm}^2. \quad (4.10)$$

As for bimuonium states with higher angular momenta, to the accuracy with which we are working they do not occur.

5. PROBABILITY OF OBSERVING BIMUONIUM

Since electrons and positrons in accelerator beams have some spread in energy, all the expressions obtained must be averaged over their energy spectra. If the energy distribution function of the electrons is $\rho_1(E_1)$, while that of the positrons is $\rho_2(E_2)$ and the cross section for the process is $\sigma(E_1, E_2)$, the averaged cross section becomes

*This same equation can be obtained by an elementary calculation in which the final muons are described by plane waves and the production of the bound state is accounted for by including the factor $|\Phi(0)|^2$. [11]

†One need not take into account the instability of the final state due to (1.1).

$$\langle\sigma\rangle = \int \sigma(E_1, E_2)\rho_1(E_1)\rho_2(E_2)dE_1 dE_2. \quad (5.1)$$

Assuming for simplicity that the electrons and positrons are uniformly distributed in energy over some interval ΔE close to threshold, we obtain

$$\langle\sigma_{rad}\rangle = 3.6\pi\cdot 10^{-38}\frac{\mu}{\Delta E}\left(\ln\frac{\Delta E}{\omega_{min}} - 1\right)\text{cm}^2, \quad (5.2)$$

$$\langle\sigma_R\rangle = 0.16\,\pi^2\frac{e^{10}}{\mu^2}\frac{\mu}{\Delta E}. \quad (5.3)$$

It is seen from this that measurable cross sections (of the order of 10^{-31} cm^2) can be obtained only with narrow energy distributions in the beam ($\Delta E \sim 1$ kev), which is quite difficult to do with modern equipment.

As orthobimuonium decays into an electron-positron pair, its existence will manifest itself as an essentially isotropic supplementary contribution to the cross section for ordinary elastic electron-positron scattering, namely

$$\frac{d\sigma_{sup}}{d\Omega} = \frac{\langle\sigma_R\rangle + \langle\sigma_{rad}\rangle}{4\pi}. \quad (5.4)$$

setting $\Delta E = 1$ kev, we obtain

$$d\sigma_{sup}/d\Omega = 1.6\cdot 10^{-32}\ \text{cm}^2/\text{sr}; \quad (5.5)$$

for comparison we mention that for $\theta = 90°$, the elastic scattering cross section in the neighborhood of the threshold for bimuonium production is 1.1×10^{-30} cm^2/sr.

We note that the energy gap corresponding to $\Delta\nu = 4.2\times 10^{13}$ cycles between the orthobimuonium and parabimuonium ground states makes it possible to induce transitions between them by means of electromagnetic radiation of this frequency, and thus to attenuate decay from the orthobimuonium state (parabimuonium decays into two photons). Calculations show that the decay rate of the order of 10^{11} sec^{-1} requires a radiation density of about 1 erg/cm^3-cycle.

[1] P. T. Matthews and A. Salam, Phys. Rev. **115**, 1079 (1959).

[2] J. Schwinger, Ann. Phys. **9**, 169 (1960).

[3] Garwin, Hutchinson, Penman, and Shapiro, Phys. Rev. **118**, 271 (1960).

[4] A. I. Alekseev, JETP **34**, 1195 (1958), Soviet Phys. JETP **7**, 826 (1958).

[5] E. E. Salpeter and H. A. Bethe, Phys. Rev. **84**, 1232 (1951).

[6] A. I. Alekseev, JETP **36**, 1435 (1959), Soviet Phys. JETP **9**, 1020 (1959).

[7] A. I. Akhiezer and V. B. Berestetskii, Kvantovaya elektrodinamika (Quantum Electrodynamics), 2d Ed., Fizmatgiz (1959).

[8] V. N. Baĭer and S. A. Kheĭfets, JETP **40**, 613 (1961), Soviet Phys. JETP **13**, 428 (1961).

[9] V. N. Baĭer and S. A. Kheĭfets, JETP **40**, 715 (1961), Soviet Phys. JETP **13**, 500 (1961).

[10] A. A. Abrikosov, JETP **30**, 96 (1956), Soviet Phys. JETP **3**, 71 (1956).

[11] A. D. Sakharov, JETP **18**, 631 (1948).

[12] Ya. B. Zel'dovich, JETP **36**, 646 (1959), Soviet Phys. JETP **9**, 450 (1959).

[13] V. B. Berestetskii and I. Ya. Pomeranchuk, JETP **29**, 864 (1955), Soviet Phys. JETP **2**, 580 (1956).

Translated by E. J. Saletan
265

MAGNETIC RESONANCE SATURATION IN CRYSTALS

B. N. PROVOTOROV

Institute of Chemical Physics, Academy of Sciences, U.S.S.R.

Submitted to JETP editor May 28, 1961

J. Exptl. Theoret. Phys. (U.S.S.R.) 41, 1582-1591 (November, 1961)

A kinetic equation for magnetic resonance in solids is deduced from the quantum equation for the density matrix. With the aid of this equation, equations describing the variation of the absorption and dispersion signals with increasing high-frequency field amplitude H_1 are derived. According to these equations, the absorption and dispersion lines become narrower, and $\chi''(\omega, H_1)$ decreases at a faster rate than $\chi'(\omega, H_1)$ with increasing H_1, in agreement with previous experimental observations.[2]

THE fundamental equation of the theory of magnetic resonance in solids is given by Bloembergen, Purcell, and Pound[1]:

$$dn(t)/dt = -\gamma^2 H_1^2 \pi g(\Delta)\, n(t) + (n_0 - n(t))/T_1. \quad (1)$$

Here $n(t)$ is the difference in the populations of the two levels between which the high-frequency field induces transitions, n_0 is the equilibrium population difference of the two levels, $\Delta = \omega - \omega_0$, $\gamma = \mu/\hbar$, ω and H_1 are the frequency and amplitude of the high-frequency field, $\omega_0 = \mu H_0/\hbar$, $s\mu$ is is the magnetic moment of the particle, H_0 is the dc magnetic field, and T_1 is the spin-lattice relaxation time.

This equation was deduced from qualitative considerations. While in principle it provides a correct description of the phenomena observed in the region of weak saturation, this equation disagrees strongly with experiment in the region of strong saturation.[2,3] For example, as H_1 is increased the absorption line first broadens but with further increase in H_1, it becomes narrow again and acquires a Lorentz shape. Such narrowing cannot be deduced from Eq. (1). According to Eq. (1) the absorption line shape has the form

$$P(\Delta, H_1) = \frac{\hbar\omega}{2} \frac{\varepsilon(\Delta) n_0}{1 + \varepsilon(\Delta) T_1}, \qquad \varepsilon(\Delta) = \gamma^2 H_1^2 \pi g(\Delta). \quad (2)$$

It can be immediately seen from this expression that the absorption line should widen with increasing H_1 for all values of H_1.

Our problem is to obtain a kinetic equation from the rigorous equation for the density matrix and to derive the magnetic resonance equations from this kinetic equation. The equation for the density matrix has in our case the form

$$\frac{\partial \rho(t)}{\partial t} = -\frac{i}{\hbar}\Big[-\hbar\omega_0 \hat{I}_z + \frac{\mu H_1}{2}(\hat{I}^1 e^{i\omega t} + \hat{I}^{-1} e^{-i\omega t}) + \hat{H}_{dip}, \rho(t)\Big],$$

$$\hat{H}_{dip} = g^2\hbar^2 \sum_{i>k} \left(\frac{\hat{s}_i \hat{s}_k}{r_{ik}^3} - 3\frac{(\hat{s}_i r_{ik})(\hat{s}_k r_{ik})}{r_{ik}^5} \right). \quad (3)$$

Here $\hat{I}_X$, $\hat{I}_Y$, $\hat{I}_Z$ are the projection operators of the total spin on the coordinates axes, $\hat{I}^{\pm 1} = \hat{I}_X \pm i\hat{I}_Y$, s_i is the spin operator situated on the i-th crystal lattice site, and r_{ik} is a vector connecting the i-th and k-th crystal lattice sites. For simplicity we have neglected here all interactions other than the magnetic dipole-dipole interaction.

To make clear the nature of the physical processes occurring in the spin system under the action of the high-frequency field, it is convenient to transform to a rotating coordinate system. As is well known, this is done with the aid of the transformation[2,4]

$$\rho(t) = \exp(i\omega \hat{I}_z t)\ \rho'(t) \exp(-i\omega \hat{I}_z t), \quad (4)$$

where $\rho'(t)$ is the density matrix in the rotating coordinate system. Substituting (4) into (3), we obtain

$$\frac{\partial \rho'(t)}{\partial t} = -\frac{i}{\hbar}\Big[\hbar\Delta \hat{I}_z + \frac{\mu H_1}{2}(\hat{I}^1 + \hat{I}^{-1}) + \sum_{m=-2}^{+2} \hat{H}^m e^{im\omega t}, \rho'(t)\Big]. \quad (5)$$

Here $\hat{H}^0$ is the secular part of the dipole-dipole interaction, which commutes with $\hat{I}_Z$. Rapidly oscillating terms of the type $\hat{H}^m e^{im\omega t}$ can be neglected, since they can give a significant contribution only in the satellites.[2,4]

The initial conditions in the rotating coordinate system will have the form

$$\rho_0' = \frac{\exp\{(\hbar\omega_0\hat{I}_z - \hat{H}^0)/kT_0\}}{\mathrm{Sp}\exp\{(\hbar\omega_0\hat{I}_z - \hat{H}^0)/kT_0\}}. \quad (6)$$

(In the usual system of coordinates we assume statistical equilibrium at the initial moment of time.)

From Eq. (5) it is easy to see that

$$\mathrm{Sp}\,\rho'(t)\,(\hat{H} + \tfrac{1}{2}\mu H_1(\hat{I}^1 + \hat{I}^{-1})) = \mathrm{const};$$
$$\hat{H} = \hbar\Delta\hat{I}_z + \hat{H}^0. \quad (7)$$

Below, we shall find this relation necessary for the selection of the correct solution of Eq. (5).

Going over in Eq. (5) to the interaction representation

$$\rho'(t) = e^{-i\hat{H}t/\hbar}\rho''(t)\,e^{i\hat{H}t/\hbar}, \quad (8)$$

we obtain for $\rho''(t)$

$$\partial\rho''(t)/\partial t = -i\hbar^{-1}[V(t), \rho''(t)], \quad (9)$$

$$V(t) = \tfrac{1}{2}\mu H_1\, e^{i\hat{H}t/\hbar}(\hat{I}^1 + \hat{I}^{-1})\, e^{-i\hat{H}t/\hbar}. \quad (10)$$

To derive the kinetic equation we use Zwanzig's method,[5] the gist of which is the application of the projection operator $\hat{P}$. Let us divide the density matrix $\rho''(t)$ into two parts:

$$\rho''(t) = \rho_1(t) + \rho_2(t), \quad \rho_1(t) = \hat{P}\rho''(t),$$
$$\rho_2(t) = (1 - \hat{P})\,\rho''(t).$$

where $\hat{P}$ is the projection operator which extracts from the density matrix $\rho''(t)$ the part that is diagonal in the representation in which $\hat{I}_Z$ and $\hat{H}^0$ are simultaneously diagonal. (In what follows we shall always be using this representation.) Multiplying Eq. (9) from the left by $\hat{P}$ and $1 - \hat{P}$, we obtain respectively

$$\partial\rho_1(t)/\partial t = -i\hbar^{-1}\hat{P}L(t)\,\rho_2(t), \quad (11)$$

$$\partial\rho_2(t)/\partial t = -i\hbar^{-1}\hat{L}(t)\,\rho_1(t) - i\hbar^{-1}(1 - \hat{P})\,\hat{L}(t)\,\rho_2(t), \quad (12)$$

where the operator $\hat{L}(t)$ is defined by the relation

$$\hat{L}(t) = [V(t), \rho(t)].$$

In Eq. (11) we have omitted the term $\hat{P}\hat{L}(t)\rho_1(t)$, which is equal to zero because the diagonal matrix elements of the operator $[V(t), \rho_1(t)]$ are equal to zero [see the definition (10)]. For the same reason the factor $1-\hat{P}$ is omitted from the first term of the right member of Eq. (12).

Multiplying Eq. (12) on the left by an operator $\hat{A}(t)$ satisfying the operator equation

$$\partial\hat{A}(t)/\partial t = i\hbar^{-1}\hat{A}(t)(1 - \hat{P})\hat{L}(t), \quad (13)$$

we obtain

$$\rho_2(t) = \hat{A}^{-1}(t)\left(\rho_2(0) - i\hbar^{-1}\int_0^t dt'\,\hat{A}(t')\hat{L}(t')\rho_1(t')\right). \quad (14)$$

Here the operator $\hat{A}^{-1}(t)$ is defined by the relation $\hat{A}^{-1}(t)\hat{A}(t) = 1$. In virtue of the relations (6) and (8), we can write $\rho_2(0) = 0$. Substituting Eq. (14) in Eq. (11), we find

$$\rho_1(t) = -\frac{1}{\hbar^2}\int_0^t dt''\int_0^{t''} dt'\,\hat{P}\hat{L}(t'')\,\hat{A}^{-1}(t'')\,\hat{A}(t')\,\hat{L}(t')\,\rho_1(t') + \rho_1(0). \quad (15)$$

If we now expand the operators $\hat{A}^{-1}(t)$ and $\hat{A}(t)$ in this equation in a series in the small quantity $\hat{L}(t)$ and discard all terms except those quadratic in $\hat{L}(t)$, then we arrive at the equation for the diagonal part of the density matrix

$$\rho_1(t) = -\frac{1}{\hbar^2}\int_0^t dt''\int_0^{t''} dt'\,\hat{P}\hat{L}(t'')\,\hat{L}(t')\,\rho_1(t') + \rho_1(0). \quad (16)$$

With the aid of this equation we shall now calculate the difference $\rho_1(t+\tau) - \rho_1(t)$ for $\hbar/H_{\mathrm{loc}} \ll \tau \ll \hbar/\mu H_1$, where $H_{\mathrm{loc}} = \mu/d^3$, and d is the separation between neighboring magnetic moments in the crystal lattice:

$$\rho_1(t+\tau) - \rho_1(t) = -\frac{1}{\hbar^2}\int_t^{t+\tau} dt''\int_0^{t''} dt'\,\hat{P}\,[V(t'')\,[V(t'), \rho_1(t')]]. \quad (17)$$

Expressing the operators occurring in V(t) as Fourier integrals,[6]

$$\hat{I}^{\pm1}(t) = \exp\left(\frac{i}{\hbar}\hat{H}^0 t\right)\hat{I}^{\pm1}\exp\left(-\frac{i}{\hbar}\hat{H}^0 t\right) = \int_{-\infty}^{+\infty} d\omega\,\hat{I}_\omega^{\pm1} e^{i\omega t},$$

$$\hat{I}_\omega^{\pm1} = \frac{1}{2\pi}\int_{-\infty}^{+\infty} dt\,e^{-i\omega t}\exp\left(\frac{i}{\hbar}\hat{H}^0 t\right)\hat{I}^{\pm1}\exp\left(-\frac{i}{\hbar}\hat{H}^0 t\right), \quad (18)$$

we obtain, upon taking

$$\exp(i\Delta\hat{I}_z t)\,\hat{I}^{\pm1}\exp(-i\Delta\hat{I}_z t) = \hat{I}^{\pm1}\exp(\pm i\Delta t),$$

into account

$$\rho_1(t+\tau) - \rho_1(t) = -\left(\frac{\mu H_1}{2\hbar}\right)^2\int_t^{t+\tau} dt''\int_0^{t''} dt'\int_{-\infty}^{+\infty} d\omega''\int_{-\infty}^{+\infty} d\omega'\exp(i\omega''t'' + i\omega' t')$$
$$\times\{\hat{P}\,[\hat{I}_{\omega''}^1\,[\hat{I}_{\omega'}^{-1}, \rho_1(t')]]\exp(i\Delta(t'' - t'))$$
$$+ \hat{P}\,[\hat{I}_{\omega''}^{-1}\,[\hat{I}_{\omega'}^1, \rho_1(t')]]\exp(-i\Delta(t'' - t'))\}.$$

In the right member of this equality we have omitted the vanishing terms

$$\hat{P}\,[\hat{I}^1(t'')\,[\hat{I}^1(t'), \rho_1(t')]].$$

If it is now recalled that $\rho_1(t')$ is a diagonal operator, and the operator $\hat{I}_\omega^{\pm1}$ has, by virtue of Eq. (18), nonvanishing matrix elements only for transitions with an energy change $\hbar\omega$, then it is easy to see that

$$\hat{P}\,[\hat{I}_{-\omega''}^1[\hat{I}_{\omega'}^{-1}, \rho_1(t')]] = \delta(\omega'' + \omega')\,\hat{P}'\,[\hat{I}_{-\omega''}^1\,[\hat{I}_{\omega'}^{-1}, \rho_1(t')]]. \quad (19)$$

[The operator $\hat{P}'$, besides separating out the diagonal parts of the operators that follow, also eliminates the singular functions $\delta(0)$ contained in the diagonal matrix elements of the operators $\hat{I}^1_\omega \hat{I}^{-1}_{-\omega}$ and $\hat{I}^{-1}_\omega \hat{I}^1_{-\omega}$ by definition (18).] Consequently,

$$\rho_1(t+\tau) - \rho_1(t) = -\left(\frac{\mu H_1}{2\hbar}\right)^2 \int_t^{t+\tau} dt'' \int_0^{t''} dt' \int_{-\infty}^{+\infty} d\omega'' \{\hat{P}' [\hat{I}^1_{-\omega''} [\hat{I}^{-1}_{\omega''}, \rho_1(t')]] \times \exp[i(\omega''+\Delta)(t''-t')] + \hat{P}' [\hat{I}^{-1}_{\omega''} [\hat{I}^1_{-\omega''}, \rho_1(t')]] \times \exp[-i(-\omega''+\Delta)(t''-t')]\}.$$

Changing now the variable of integration in the second component in the curly brackets of this equation from ω'' to $-\omega''$ and using the easily verified relation

$$\hat{P}' [\hat{I}^1_{\omega''} [\hat{I}^{-1}_{-\omega''}, \rho_1(t')]] = \hat{P}' [\hat{I}^{-1}_{-\omega''} [\hat{I}^1_{\omega''}, \rho_1(t')]],$$

we obtain, after integrating over t',

$$\rho_1(t+\tau) - \rho_1(t) = -\frac{1}{2}\left(\frac{\mu H_1}{\hbar}\right)^2 \int_t^{t+\tau} dt'' \int_{-\infty}^{+\infty} d\omega'' \frac{\sin[(\omega''+\Delta)t'']}{\omega''+\Delta} \hat{P}' \times [\hat{I}^1_{\omega''} [\hat{I}^{-1}_{-\omega''}, \rho_1(t)]].$$

We have replaced here $\rho_1(t')$ by $\rho_1(t)$ in the integration over t'. This change is completely justified in our case, for when $H_1 \ll H_{loc}$, $\rho_1(t)$ changes markedly in the time interval $\hbar/\mu H_1$, whereas

$$\int_{-\infty}^{+\infty} d\omega'' \cos[(\omega''+\Delta)(t''-t')] \hat{P}' [\hat{I}^1_{\omega''} [\hat{I}^{-1}_{-\omega''}, \rho_1(t')]]$$

is a rapidly changing function of $t''-t'$, which differs from zero only in the region $|t''-t'| \lesssim \hbar/\mu H_{loc}$, since the spectral width of the operators $\hat{I}^{\pm 1}_\omega$ is $\sim \mu H_{loc}/\hbar$. For the same reason we can replace $\rho_1(t+\tau) - \rho_1(t)$ by $\tau d\rho_1(t)/dt$ when $\tau \ll \hbar/\mu H_1$.

The integration over ω'' in Eq. (21) is easily accomplished, for when $\hbar/\mu H_{loc} \ll t''$ the function $\sin[(\omega''+\Delta)t'']/(\omega''+\Delta)$ can be replaced by $\pi\delta(\omega''+\Delta)$. This comes about because the function $\hat{P}'[\hat{I}^1_{\omega''}[\hat{I}^{-1}_{\omega''}, \rho_1(t')]]$ changes with frequency much more slowly than $\sin[(\omega''+\Delta)t'']/(\omega''+\Delta)$ when $t'' \gg \hbar/\mu H_{loc}$. With this in mind, we find

$$\frac{d\rho_1(t)}{dt} = -\frac{\pi}{2}\left(\frac{\mu H_1}{\hbar}\right)^2 \hat{P}' [\hat{I}^1_{-\Delta} [\hat{I}^{-1}_{\Delta}, \rho_1(t)]]. \quad (22)$$

We shall now show that this equation corresponds to the conservation law

$$\frac{d}{dt} \mathrm{Sp}\{\rho_1(t)\hat{H}\} = 0. \quad (23)$$

(This relation derives from Eq. (7) under the condition $H_1 \ll H_{loc}$.) In fact, after making use of Eq. (22), we obtain

$$\frac{d}{dt} \mathrm{Sp}\{\rho_1(t)\hat{H}\} = -\frac{\pi}{2}\left(\frac{\mu H_1}{\hbar}\right)^2 \mathrm{Sp}\{\hat{P}' [\hat{H}, \hat{I}^1_{-\Delta}] [\hat{I}^{-1}_{\Delta}, \rho_1(t)]\}.$$

We note further that the commutator $[\hat{H}, \hat{I}^1_{-\Delta}]$ vanishes, since it is easy to obtain from definition (18) the relations

$$[\hat{H}^0, \hat{I}^1_{-\Delta}] = -\hbar\Delta \hat{I}^1_{-\Delta}, \qquad [\hat{I}_z, \hat{I}^1_{-\Delta}] = \hat{I}^1_{-\Delta}. \quad (24)$$

From this we obtain the desired Eq. (23).

Because of Eq. (24), any function of the operator $\hat{H}$ will commute with the operator $\hat{I}^1_{-\Delta}$. Hence the stationary solution of Eq. (22) will be an arbitrary function $\rho_{st} = f(\hat{H})$. In order to find the actual solution it is necessary to require that the solution $\rho_{st} = f(\hat{H})$ possess, by virtue of the homogeneity of our macroscopic system, the property of quasi-independence of the separate parts of the system $f(\hat{H}) = f(\hat{H}_1) f(\hat{H}_2)$. Here $\hat{H}_1$ and $\hat{H}_2$ refer to any two arbitrarily chosen parts of the system for which $\hat{H}_1 + \hat{H}_2 \approx \hat{H}$. The only normalized solution of this type would be

$$\rho_{st} = \exp(-\hat{H}/kT^*)/\mathrm{Sp}\exp(-\hat{H}/kT^*). \quad (25)$$

The quantity T^* can be defined by making use of Eq. (23):

$$T^* = T_0 \frac{\Delta^2 + \mathrm{Sp}(\hat{H}^0)^2/\mathrm{Sp}\hat{I}_z^2}{\omega_0\Delta + \mathrm{Sp}(\hat{H}^0)^2/\mathrm{Sp}\hat{I}_z^2}. \quad (26)$$

(In deriving this relation it has been assumed that $\hbar\omega_0/kT_0$ and $\hbar\Delta/kT^*$ are small in magnitude.)

As a consequence of the definitions (4) and (8) it is possible to substitute $\rho''(t)$ in place of $\rho(t)$ in the calculation of the mean values of $\hat{H}^0(t) = \mathrm{Sp}[\hat{H}^0\rho(t)]$ and $\hat{I}_Z(t) = \mathrm{Sp}[\hat{I}_Z\rho(t)]$. Taking ρ_{st} from Eq. (27) and ρ_0 from Eq. (6), we obtain when $\Delta = 0$

$$\mathrm{Sp}(\hat{H}^0\rho_0) = \mathrm{Sp}(\hat{H}^0\rho_{st}), \qquad \mathrm{Sp}(\hat{I}_z\rho_{st}) = 0,$$

because $\hbar\omega_0/kT_0$ and $\hbar\Delta/kT^*$ are small and because $\mathrm{Sp}(\hat{I}_Z\hat{H}_0) = 0$, as can be verified by direct calculation. This means that the average value of the energy of the dipole-dipole interaction in the case $\Delta = 0$ is not changed after the high-frequency field is turned on, and the average value of the projection of the total spin $I_Z(t)$ tends to zero in accordance with Eq. (1).

A completely different situation arises in the case $\Delta \neq 0$. In this case the absorption of each quantum of the high frequency field is accompanied by a change of $\hbar\Delta$ in the dipole-dipole energy. This process leads to a limitation of the absorbing capability of the spin system. As a consequence $I_Z(t)$ no longer approaches zero, but

$$I_{z\,st} = \frac{\hbar\omega_0}{kT_0} \frac{\Delta^2}{\Delta^2 + \mathrm{Sp}(\hat{H}^0)^2/\mathrm{Sp}\hat{I}_z^2}. \quad (27)$$

Here $\mathrm{Sp}\,(\hat{H}^0)^2/\mathrm{Sp}\,\hat{I}_z^2 \sim \langle\omega^2\rangle$, where $\langle\omega^2\rangle$ is the second moment of the absorption line. Hence, for resonant frequencies within the absorption line, $I_{z\,st}$ can attain values $\sim I_{z0}/2$, whereas Eq. (1) gives zero for $I_{z\,st}$ under these conditions. This contradiction is not accidental, because Eq. (1) does not take into account changes in the energy of the dipole-dipole interaction in the saturation process, which leads to a cessation of absorption of high-frequency quanta at values of I_z that are different from zero.

A comparison of the stationary solution, Eq. (25), with the initial value of the density matrix, Eq. (6), shows that the application of a sufficiently weak high-frequency field leads only to a change in the exponents of the coefficients for the operators $\hat{I}_z$ and $\hat{H}^0$. This change in $\rho_1(t)$ is due to the strong disordering influence of the dipole-dipole interaction. Before the application of the high-frequency field the magnetic dipoles of the spin system precess incoherently about the constant magnetic field. Consequently the components of transverse magnetization equal zero.

The influence of the high-frequency field is manifest in the emergence of coherent precession of the magnetic moments, i.e., in the appearance of transverse components of magnetization M_x and M_y. The dipole-dipole interaction, on the other hand, tends to bring the spin system to a state of equilibrium with $M_x = M_y = 0$. Lowe and Norberg [7] measured directly the decay time of the transverse magnetization. It turned out to be equal to $\sim\hbar/\mu H_{loc}$. Therefore in the case of sufficiently weak high frequency fields we can consider, with an accuracy of $\sim H_1/H_{loc}$, that the spin system will be characterized at every instant of time by an equilibrium partition function. The most general form of the equilibrium partition function is [8]

$$\rho_1(t) = \exp(\alpha(t)\hat{I}_z + \beta(t)\hat{H}^0)/\mathrm{Sp}\exp(\alpha(t)\hat{I}_z + \beta(t)\hat{H}^0). \quad (28)$$

All of the foregoing has pertained to the case in which there is no contact between the spin system and the lattice. However it is obvious that all the above reasoning is appropriate also for the case $\hbar/\mu H_{loc} \ll T_1$ (T_1 is the spin-lattice relaxation time). Since this condition is fulfilled almost always in solids, we shall consider Eq. (28) as valid in solids even when spin-lattice interaction is present.

It is easily seen that the form of the solution (28) incorporates solutions corresponding to the BPP equation as a special case. In fact, in the two-level BPP model it is assumed that the levels corresponding to the same projections I_z have the same populations in the saturation process. Such a population distribution is obtained if $\beta(t)$ is set equal to zero in Eq. (28). Then, from the equations introduced below [see (36) and (37)], it is seen that for a value of $I_z(t)$ proportional to the population difference of the levels, an equation of the BPP type is obtained.

It is interesting to note that a density matrix of the form

$$\rho_1(t) = C\exp(\alpha(t)\hat{I}_z) \quad (29)$$

cannot, generally speaking, be a solution of Eq. (22) because the exact conservation law (23) is not obeyed when $\rho_1(t)$ is in the form (29). In fact, noting that the normalization condition $\mathrm{Sp}\,\rho_1(t) = 1$ gives $C = (2s+1)^{-N}$, where s is the spin of an individual particle and N is the total number of particles in the sample [$\alpha(t)$ and $\beta(t)$ can be considered small if the initial temperatures are not too low], we obtain

$$\frac{\partial}{\partial t}\mathrm{Sp}(\rho_1(t)\hat{H}) = \alpha'(t)\hbar\Delta(2s+1)^{-N}\mathrm{Sp}\,\hat{I}_z^2. \quad (30)$$

From the equality obtained it is obvious that the rigorous conservation law (23) is compatible with the form of the solution (29) and with the BPP equation corresponding to it only if $\Delta = 0$. Consequently the BPP equation can be considered correct only when $\Delta = 0$. This explains why the spin-lattice relaxation times measured by Redfield in the course of using the BPP equation for the analysis of his experiment were found to be correct, in spite of the fact that the absorption line observed under strong saturation failed to coincide with the theoretical curve. The point is that the saturation curve was taken by Redfield precisely at $\Delta = 0$, where the BPP equation can be considered correct. But measuring the shape of the absorption line, associated with a transition in the region $\Delta \neq 0$ in the strong saturation case, led Redfield perfectly naturally to results that were incompatible with the BPP equation.

In order to determine $\alpha(t)$ and $\beta(t)$ we shall calculate with the aid of Eq. (22) the derivative

$$\frac{d}{dt}\mathrm{Sp}\,\rho_1(t)\hat{I}_z = -\frac{\pi}{2}\left(\frac{\mu H_1}{\hbar}\right)^2(2s+1)^{-N}$$
$$\times\mathrm{Sp}\{\hat{P}'\hat{I}_z[\hat{I}^1_{-\Delta}[\hat{I}_\Delta^{-1}, \exp(\alpha(t)\hat{I}_z + \beta(t)\hat{H}^0)]]\}. \quad (31)$$

Using the equalities

$$[\hat{H}^0, \hat{I}_\Delta^{-1}] = \hbar\Delta\hat{I}_\Delta^{-1}, \qquad [\hat{I}_z, \hat{I}_\Delta^{-1}] = -\hat{I}_\Delta^{-1},$$

it is easy to verify the relation

$$[\exp(\alpha(t)\hat{I}_z + \beta(t)\hat{H}^0), \hat{I}_\Delta^{-1}]$$
$$= \exp(\alpha(t)\hat{I}_z + \beta(t)\hat{H}^0)\hat{I}_\Delta^{-1}(1 - \exp(-\alpha(t) + \hbar\Delta\beta(t))).$$

Considering the easily verified equality

$$\mathrm{Sp}\,(\hat{P}'\hat{I}_z\,[\hat{I}^1_{-\Delta},\hat{A}\,]) = -\,\mathrm{Sp}\,(\hat{P}'\,[\hat{I}^1_{-\Delta},\hat{I}_z]\,\hat{A}), \qquad (32)$$

we further find

$$\frac{dI_z(t)}{dt} = -\frac{\pi}{2}\left(\frac{\mu H_1}{\hbar}\right)^2 (2s+1)^{-N}\,(\alpha(t) - \hbar\Delta\beta(t)) \times \mathrm{Sp}\,\{\hat{P}'\hat{I}^1_{-\Delta}\hat{I}_\Delta^{-1}\exp(\alpha(t)\,\hat{I}_z + \beta(t)\,\hat{H}^0)\}. \qquad (33)$$

We note that in the right-hand member of this equation it is now possible to replace the exponential by unity, because of the smallness of $\alpha(t)$ and $\beta(t)H^0$. For the same reason we obtain for the average values of $I_Z(t)$ and $H^0(t)$

$$I_z(t) = \alpha(t)\,(2s+1)^{-N}\mathrm{Sp}\,\hat{I}_z^2 = \tfrac{1}{3}\alpha(t)\,Ns\,(s+1),$$
$$H_0(t) = \beta(t)\,(2s+1)^{-N}\,\mathrm{Sp}\,(\hat{H}^0)^2. \qquad (34)$$

Substitution of $\alpha(t)$ and $\beta(t)$ from these expressions into Eq. (33) yields

$$dI_z(t)/dt = -\,(\mu H_1/\hbar)^2\,\pi g(\Delta)\,(I_z(t) - y(t)),$$
$$y(t) = \hbar\Delta\frac{H_0(t)}{\overline{H}_0^2}, \qquad \overline{H}_0^2 = \frac{\mathrm{Sp}\,(\hat{H}^0)^2}{\mathrm{Sp}\,\hat{I}_z^2},$$
$$g(\Delta) = \frac{\mathrm{Sp}\,(\hat{P}'\hat{I}^1_{-\Delta}\hat{I}_\Delta^{-1})}{2Ns(s+1)\,(2s+1)^N/3}. \qquad (35)$$

The expression for dy/dt is easily obtained, using the conservation law, Eq. (23):

$$dH_0(t)/dt = -\,\hbar\Delta dI_z(t)/dt,$$
$$dy(t)/dt = (\hbar^2\Delta^2/\overline{H}_0^2)\,\pi g(\Delta)\,(I_z(t) - y(t)).$$

If we now take into account the spin-lattice relaxation in the manner of Bloembergen, Purcell, and Pound,[1] we arrive at the following system of equations:

$$dI_z(t)/dt = -\,(\mu H_1/\hbar)^2\,\pi g(\Delta)\,(I_z(t) - y(t)) + (I_{0z} - I_z(t))/T_1, \qquad (36)$$

$$dy(t)/dt = (\hbar^2\Delta^2/\overline{H}_0^2)\,(\mu H_1/\hbar)^2\,\pi g(\Delta)\,(I_z(t) - y(t)) + (y_0 - y(t))/T_1'. \qquad (37)$$

Here I_{0Z} and y_0 are the initial values of $I_Z(t)$ and $y(t)$, while T_1 and T_1' are the times for the spin-lattice relaxation of $I_Z(t)$ and $H_0(t)$.

For the energy absorbed per unit time in steady state we find, with the aid of these equations (in our case $y_0 \ll I_{0Z}$),

$$P(\Delta, H_1) = \varepsilon(\Delta)\,\hbar\omega\,(I_{z\,\mathrm{st}} - y_{\mathrm{st}}) = \frac{\hbar\omega\varepsilon(\Delta)\,I_{0z}}{1 + \varepsilon(\Delta)\,T_1\,(1 + \hbar^2\Delta^2 T_1'/\overline{H}_0^2 T_1)}. \qquad (38)$$

In the case of strong saturation, when $\varepsilon(\Delta)T_1 \gg 1$, we can neglect the ones in the denominator of Eq. (38), after which we obtain a relatively narrow Lorentz absorption line

$$P(\Delta, H_1) = \frac{\hbar\omega}{T_1'}\,\frac{\overline{H}_0^2}{\hbar^2\Delta^2 + \overline{H}_0^2 T_1/T_1'}. \qquad (39)$$

In order of magnitude $\overline{H}_0^2$ equals $(\mu H_{\mathrm{loc}})^2$.

Redfield[2] has investigated nuclear magnetic resonance absorption in metals. Even with $H_1 = 0.4$ oe he was able to observe the appearance of the narrow Lorentz absorption line. If, following[2], we take for aluminum $T_1 = 4 \times 10^{-3}$ sec and $2\pi g(0) = 10^{-4}$ sec, then we find for the saturation parameter $\varepsilon(\Delta)T_1 \sim 10$. In other words, the field value $H_1 = 0.4$ oe corresponds to the region of strong saturation and consequently the absorption line shape in correspondence to our Eq. (39) should be Lorentzian, just as Redfield observed.

In order to investigate the behavior of the dispersion signal it is necessary to determine the non-diagonal part of the density matrix $\rho_2(t)$. In order to determine $\rho_2(t)$ we make use of Eq. (14). Although this equation was obtained for the case in which there is no contact between the spin system and the lattice, it can be used also for the case $\hbar/\mu H_{\mathrm{loc}} \ll T_1$. The point is that the inclusion of such a weak spin-lattice interaction cannot have a significant influence on the rate of change of the off-diagonal matrix elements $(\rho_2(t))_{nm}$, equal to $\sim \mu H_{\mathrm{loc}}/\hbar$. [The rate of change with time of the diagonal matrix elements $(\rho_1(t))_{nn}$ for $H_1 \ll H_{\mathrm{loc}}$ is very small, $\sim \mu H_1^2/\hbar H_{\mathrm{loc}}$, as can be seen from Eq. (22), hence it is impossible to neglect the spin-lattice interaction in the determination of the change with time of the function $\rho_1(t)$.]

If we carry out in Eq. (14) a power series expansion in the small quantity $\hat{L}(t)$, as has already been done in the derivation of Eq. (22), and keep only the terms of lowest order in $\hat{L}_1(t)$, then we arrive at the equation

$$\rho_2(t) = -\frac{i}{\hbar}\int_0^t dt'\,[V(t'), \rho_1(t')]. \qquad (40)$$

The function $\rho_1(t)$ is determined by Eqs. (36), (37), (34), and (28). Hence Eq. (40) gives the desired non-diagonal part of the density matrix. To calculate the average values of $I_{X,Y}(t)$ in the rotating coordinate system it is now necessary to determine the non-diagonal part of the density matrix $\rho_2'(t)$ in the same system of coordinates. Using the rule for transforming to rotating coordinates, Eq. (8), and the fact that $\rho_1(t)$ is diagonal, we obtain

$$\rho_2'(t) = -\frac{i}{\hbar}\int_0^t dt'\,[V(t-t'), \rho_1(t')]. \qquad (41)$$

Using further the expansions (18), we find

$$I_{x,y}(t) = \frac{\mu H_1}{4\hbar}\,i^{1/2\pm 1/2}\int_{-\infty}^{+\infty} d\omega \int_0^t dt'\,\mathrm{Sp}\,\{\hat{P}'\hat{I}^1_{-\omega}\,[\hat{I}_\omega^{-1}, \rho_1(t')]\} \times \{\exp[i(\omega - \Delta)(t-t')] \mp \exp[i - (\omega - \Delta)(t-t')]\}. \qquad (42)$$

In the derivation of this relation use was made of the easily verified relations

$$\mathrm{Sp}\,\{\hat{P}'\hat{I}^{1}_{-\omega}[\hat{I}^{-1}_{\omega}, \rho_1(t')]\} = -\mathrm{Sp}\,\{\hat{P}'\hat{I}^{-1}_{\omega}[\hat{I}^{1}_{-\omega}, \rho_1(t')]\}.$$

Note that the function $\rho_1(t)$ changes significantly only in the time interval $\hbar H_{loc}/\mu H_1^2$, and the function

$$\int_{-\infty}^{+\infty} d\omega\ \mathrm{Sp}\,\{\hat{P}'\hat{I}^{1}_{-\omega}[\hat{I}^{-1}_{\omega}, \rho_1(t')]\}\exp[i(\omega-\Delta)(t-t')]$$

differs from zero only in the region $|t-t'| \lesssim \hbar/\mu H_{loc}$ [cf. derivation of Eq. (21)]. Hence in the integration over the time in the right member of Eq. (42) $\rho_1(t')$ can be considered a constant, equal to $\rho_1(t)$, and the integration over t' extended to $+\infty$. Changing further the variable of integration t' to $t-t'$ and using the well known relation[9]

$$\int_0^{\infty} d\tau e^{i\omega\tau} = \pi\delta(\omega) + P\frac{i}{\omega} \qquad (43)$$

(the symbol P means that the integrals over ω are to be taken in the sense of the principal value), we obtain

$$I_{x,y}(t) = \frac{\mu H_1}{4\hbar}\int_{-\infty}^{+\infty} d\omega\ \mathrm{Sp}\,\{\hat{P}'\hat{I}^{1}_{-\omega}[\hat{I}^{-1}_{\omega}, \rho_1(t)]\}$$

$$\times\, i^{1/2\pm 1/2}\left\{\left(\pi\delta(\omega-\Delta) + P\frac{i}{\omega-\Delta}\right)\right.$$

$$\left.\mp\left(\pi\delta(\omega-\Delta) - P\frac{i}{\omega-\Delta}\right)\right\}. \qquad (44)$$

Substitution of $\rho_1(t)$ from Eqs. (36), (37), (34), and (28) leads to

$$I_x(t) = -(\mu H_1/\hbar)\, I_z(t)\, J_1(\Delta) + \left(\frac{\mu H_1 y(t)}{\hbar\Delta}\right) J_2(\Delta), \qquad (45)$$

$$I_y(t) = (\mu H_1/\hbar)\,\pi g(\Delta)\,(I_z(t) - y(t));$$

$$J_1(\Delta) = P\int_{-\infty}^{+\infty}\frac{d\omega g(\omega)}{\omega-\Delta}, \qquad J_2(\Delta) = 1 + \Delta J_1(\Delta) \qquad (46)$$

[the derivation of these equations is completely analogous to the derivation of Eq. (35).]

Determining $I_{z\,st}$ and y_{st} from (36) and (37) we obtain for χ'_{st} and χ''_{st} the expressions

$$\chi'_{st} = \frac{\mu I_{x\,st}}{2H_1} = -\frac{\mu^2 I_{0z}}{2\hbar}\left\{\frac{(1+\varepsilon(\Delta)T_1'\hbar^2\Delta^2/\overline{H}_0^2)\,J_1(\Delta)}{1+\varepsilon(\Delta)T_1(1+\hbar^2\Delta^2 T_1'/\overline{H}_0^2T_1)}\right.$$

$$\left.-\frac{\varepsilon(\Delta)T_1'(\hbar^2\Delta/\overline{H}_0^2)\,J_2(\Delta)}{1+\varepsilon(\Delta)T_1(1+\hbar^2\Delta^2T_1'/\overline{H}_0^2T_1)}\right\}, \qquad (47)$$

$$\chi''_{st} = \frac{\mu I_{y\,st}}{2H_1} = \frac{\mu^2 I_{0z}}{2\hbar}\,\frac{\pi g(\Delta)}{1+T_1\varepsilon(\Delta)(1+\hbar^2\Delta^2T_1'/\overline{H}_0^2T_1)}. \qquad (48)$$

As expected, Eq. (48) agrees with the expression for energy absorbed per unit time calculated earlier [see (38)]. In strong saturation at small values of Δ the greatest term in the right member of Eq. (47) is the second. Because of the presence of the additional factor $(1+\hbar^2\Delta^2T_1'/\overline{H}_0^2T_1)^{-1}$ this term will lead to a more narrow dispersion line relative to the dispersion line in the absence of saturation. Such a narrowing of the dispersion line was actually observed by Redfield.[2]

It is to be noted that for $\varepsilon(\Delta)T_1 \ll 1$ Eq. (47) goes over into the well known formula

$$\chi'_{st}(\Delta) = -\mu^2 I_{0z} J_1(\Delta)/2\hbar. \qquad (49)$$

For a comparison with the experimental data and theory of Redfield[2] we calculate $(d\chi'_{st}/d)_{=0}$. Differentiating Eq. (47), we obtain for $\varepsilon(\Delta)T_1 \gg 1$

$$\left.\frac{d\chi'_{st}}{d\Delta}\right|_{\Delta=0} = \frac{\mu^2 I_{0z}}{4}\,\frac{\hbar}{\overline{H}_0^2}, \qquad (50)$$

in view of the equality $dJ_2(\Delta)/d\Delta = 0$. Comparison of this formula with Eq. (41) of Redfield's paper[2] shows that our Eq. (50) transforms into Redfield's formula, which agrees well with experiment, when $H_1^2 \ll \overline{H}_0^2 = \delta H^2$, if, in correspondence with Redfield, it is assumed that the quantity $y(t)$, quadratic in spin, relaxes under the influence of the lattice twice as fast as $I_z(t)$. (Redfield's theory is valid only in cases of very strong saturation.)

In conclusion, the author thanks N. D. Sokolov for his interest in the work, and also V. L. Ginzburg, S. V. Tyablikov, and D. N. Zubarev for discussions of the results.

[1] Bloembergen, Purcell, and Pound, Phys. Rev. 73, 679 (1948).

[2] A. Redfield, Phys. Rev. 98, 1787 (1955).

[3] D. Abell and W. Knight, Phys. Rev. 93, 940 (1954).

[4] F. Bloch, Phys. Rev. 105, 1206 (1957).

[5] R. Zwanzig, J. Chem. Phys. 33, 1338 (1960).

[6] R. Kubo and E. Tomita, J. Phys. Soc. Japan 9, 888 (1954).

[7] I. Lowe and R. Norberg, Phys. Rev. 107, 47 (1957).

[8] L. D. Landau and E. M. Lifshitz, Statistical Physics, Addison-Wesley, Reading, Mass. 1958. Sec. 4.

[9] A. I. Akhiezer and V. B. Berestetskii, Kvantovaya elektrodinamika (Quantum Electrodynamics), Gostekhizdat, 1951, p. 126. [AEC tr. 2876].

Translated by L. M. Matarrese
266

QUANTUM OSCILLATIONS OF THE THERMODYNAMIC QUANTITIES OF A METAL IN A MAGNETIC FIELD ACCORDING TO THE FERMI-LIQUID MODEL

Yu. A. BYCHKOV and L. P. GOR'KOV

Institute of Physics Problems, Academy of Sciences, U.S.S.R.

Submitted to JETP editor May 31, 1961

J. Exptl. Theoret. Phys. (U.S.S.R.) 41, 1592-1605 (November, 1961)

Quantum field theory methods are used to study the influence of Fermi-liquid effects on the oscillations of the thermodynamic quantities of a metal in a magnetic field. It is shown that the periods of the oscillations can be calculated by the usual scheme of I. Lifshitz and Kosevich. Deviations from the usual results appear in the amplitudes of the oscillations and are due to the change of the effective magneton of an excitation owing to the interaction between the electrons.

1. INTRODUCTION

THE theory of the oscillations of the magnetic susceptibility in metals, which was first constructed in a paper by I. Lifshitz and Kosevich,[1] is based on definite ideas about the structure of the energy levels of a metal in a magnetic field. It is assumed that these levels can be constructed on the basis of a quantization of the levels of individual excitations treated as an ideal Fermi gas. However, the electrons in a metal are a sort of Fermi liquid. The theory of the Fermi liquid, constructed by Landau[2,3] in its application to liquid He^3, shows that in such a system effects of the interaction between the excitations play a large role. The correlations that thus arise are of the order of interatomic distances. The question arises as to how the presence of these interactions between the excitations affects the various quantum phenomena in the theory of metals in magnetic fields.

We shall here treat the de Haas-van Alphen effect for the electrons in a metal on the model of the isotropic Fermi liquid. Generally speaking, the situation in the case of electrons is complicated by specific features of the Coulomb interaction. We shall assume that the long-range part of the Coulomb interaction is already screened off. The final formulas obtained below contain only the characteristics of the free-electron spectra (without a field), and therefore, in our opinion, cannot depend on this assumption. The same arguments also apply to the question of the effects of anisotropy.

The results obtained in this paper show that when the spin susceptibility is not taken into account the expression for the oscillating part of the magnetic moment can be obtained on the basis of the usual concept of a system of electrons as a gas of quasiparticles. This same result has been obtained in a paper by Luttinger[4] which has recently appeared. In that paper, however, the analysis of the Green's functions of the electrons in the magnetic field was made only in perturbation theory to terms of first order in the interaction, i.e., terms that give only a trivial renormalization of the chemical potential. Also Luttinger did not investigate the question of the effect of the paramagnetic susceptibility. The whole difference from previously known formulas arises in including the paramagnetic susceptibility, which, as is well known,[2] depends strongly on the Fermi-liquid properties of the system.

Our further study will be made by the methods of quantum theory. We shall be interested only in the quantum oscillations of all quantities. The value of the susceptibility in a weak magnetic field cannot be expressed in terms of the characteristics of the spectrum, since its diamagnetic part depends also on electrons that are located "deep" below the Fermi surface. For simplicity we shall confine ourselves to the temperature absolute zero.

2. THE ENERGY SPECTRUM

We shall begin with a study of the properties of the Green's functions of electrons in a magnetic field. As usual,[3] the Green's function $G(x, x')$ is defined as an average over the ground state of the system:

$$G(\mathbf{r}, \mathbf{r}'; t - t')\,\delta_{\alpha\beta} = -i\langle T(\psi_\alpha(\mathbf{r}, t)\,\psi_\beta^+(\mathbf{r}', t'))\rangle. \quad (1)$$

The particle field operators $\psi_\alpha(x)$, $\psi^+_\beta(x')$ include the dependence on the magnetic field H; we choose the vector potential $\mathbf{A}(\mathbf{r})$ of the field in the form

$$\mathbf{A}(\mathbf{r}) = \{-Hy, 0, 0\}. \quad (2)$$

The dependence of the Green's function (1) on the coordinates can be represented in the following way:

$$G(x, x') = \exp\{-i(eH/2c)(y+y')(x-x')\} \times G(\mathbf{r}-\mathbf{r}'; t-t'). \quad (3)$$

This follows from gauge invariance, since when we make a displacement of the origin of coordinates, $y \to y + b$, the operators $\psi(x)$ and $\psi^+(x)$ transform according to the law

$$\psi \to \psi e^{-ieHbx/c}, \qquad \psi^+ \to \psi^+ e^{ieHbx/c}. \quad (4)$$

We shall be dealing with $G(\mathbf{r}, \mathbf{r}'; \epsilon)$, the Fourier component of (1) with respect to the time difference $t-t'$. In the absence of a magnetic field

$$G^0(\mathbf{r}-\mathbf{r}'; \varepsilon) = \frac{1}{(2\pi)^3}\int G^0(\mathbf{p}, \varepsilon)\, e^{i\mathbf{p}(\mathbf{r}-\mathbf{r}')}\, d\mathbf{p}.$$

For small ϵ the function $G^0(\mathbf{p}, \epsilon)$ has a pole near the Fermi surface of the form[3]

$$G^0(\mathbf{p}, \varepsilon) = a/(\varepsilon - v(p-p_0) + i\delta(\varepsilon)). \quad (5)$$

The value of $\epsilon = v(p-p_0)$ determines the spectrum of the Fermi liquid.

In a magnetic field the form of the Green's function near the Fermi surface is decidedly altered owing to the quantization of the levels. We shall show, however, that the energy spectrum of the electrons in the magnetic field can be obtained from the expression (5) by the usual rules of quasiclassical quantization, as was also suggested in the paper by I. Lifshitz and Kosevich.[1]

To prove this assertion we write the Dyson equation satisfied by the Green's function $G(\mathbf{r}, \mathbf{r}'; \epsilon)$ in coordinate space:

$$\left[\varepsilon + \mu - \frac{1}{2m}\left(\hat{\mathbf{p}} - \frac{e}{c}\mathbf{A}\right)^2\right] G(\mathbf{r}, \mathbf{r}'; \varepsilon) - \int \Sigma(\mathbf{r}, \mathbf{r}''; \varepsilon)\, G(\mathbf{r}'', \mathbf{r}'; \varepsilon)\, d^3\mathbf{r}'' = \delta(\mathbf{r}-\mathbf{r}'). \quad (6)$$

Here $\hat{\mathbf{p}} = -i\partial/\partial\mathbf{r}$, μ is the chemical potential of the electrons in the magnetic field, and $\Sigma(\mathbf{r}, \mathbf{r}''; \epsilon)$ is the so-called self-energy part arising from the interactions between the particles in the Fermi liquid. We shall not specify concrete forms for these interactions. The spectrum of the system is determined by the eigenvalues of the operator which appears in square brackets in Eq. (6).

In the notation of second quantization the Hamiltonian for the interaction of the electrons with the magnetic field (2) takes the form

$$H_{int} = \int \psi^+(\mathbf{r}')\left[\frac{e}{2mc}(\hat{\mathbf{p}} - \hat{\mathbf{p}}')_x + \frac{e^2Hy}{2mc^2}\right] Hy\psi(\mathbf{r})\, d^3\mathbf{r}, \quad (7)$$

where $\hat{p}_x$ and $\hat{p}_{x'}$ denote differentiation ($\hat{p}_x = -i\partial/\partial x$) with respect to the corresponding arguments in the limit $\mathbf{r} \to \mathbf{r}'$. We shall now investigate the dependence of the self-energy part $\Sigma(\mathbf{r}, \mathbf{r}'; \epsilon)$ on the magnitude of the magnetic field. According to Eq. (7) an increment of the magnetic field, $H \to H + \delta H$, is equivalent to an additional interaction Hamiltonian:

$$\delta H_{int} = \delta H \int \psi^+(\mathbf{r}')\left[\frac{e}{2mc}(\hat{\mathbf{p}} - \hat{\mathbf{p}}')_x + \frac{e^2Hy}{mc^2}\right] y\psi(\mathbf{r})\, d^3\mathbf{r}. \quad (7')$$

Using the usual diagram technique to calculate from Eq. (7') the change $\delta\Sigma(\mathbf{r}, \mathbf{r}'; \epsilon) = (\partial\Sigma/\partial H)\delta H$, we can assign to this quantity the diagram shown in Fig. 1. The cross denotes the operator in square brackets in the integrand in Eq. (7'); the circle denotes the complete vertex part in the magnetic field, $\Gamma_{\alpha\beta,\gamma\delta}(\xi_1, \xi_2; \xi_3, \xi_4)$.

FIG. 1

The vertex part is defined as usual by the relation

$$\langle T(\psi_\alpha(\xi_1)\psi_\beta(\xi_2)\psi^+_\gamma(\xi_3)\psi^+_\delta(\xi_4))\rangle = G_{\alpha\gamma}(\xi_1, \xi_3)\, G_{\beta\delta}(\xi_2, \xi_4) - G_{\alpha\delta}(\xi_1, \xi_4)\, G_{\beta\gamma}(\xi_2, \xi_3) + i\int G_{\alpha\alpha'}(\xi_1, \xi_1')\, G_{\beta\beta'}(\xi_2, \xi_2') \times \Gamma_{\alpha'\beta',\gamma'\delta'}(\xi_1', \xi_2'; \xi_3', \xi_4')\, G_{\gamma'\gamma}(\xi_3', \xi_3)\, G_{\delta'\delta}(\xi_4', \xi_4) \times d^4\xi_1' d^4\xi_2' d^4\xi_3' d^4\xi_4'.$$

In the absence of the magnetic field $\Gamma_{\alpha\beta,\gamma\delta}(\xi_1, \xi_2; \xi_3, \xi_4)$ has Fourier components of the form $(2\pi)^4\Gamma_{\alpha\beta,\gamma\delta}(p_1, p_2; p_3, p_4) \times \delta(p_1 + p_2 - p_3 - p_4)$. As is well known,[3] the vertex part plays an important role in the theory of the Fermi liquid.

The diagram of Fig. 1 gives the following result for the derivative $\partial\Sigma/\partial H$:

$$\delta_{\alpha\beta}\frac{\partial\Sigma(\mathbf{r}, \mathbf{r}'; \varepsilon)}{\partial H} = \frac{i}{2\pi}\int d\omega' \int d^3\mathbf{r}_1 d^3\mathbf{r}_2 d^3\mathbf{l}\left[\frac{e}{2mc}(\hat{\mathbf{p}} - \hat{\mathbf{p}}')_{l_x} + \frac{e^2H}{mc^2} l_y\right] l_y \Gamma_{\alpha\gamma,\gamma\beta}(\mathbf{r}, \varepsilon; \mathbf{r}_1, \omega'; \mathbf{r}_2, \omega'; \mathbf{r}', \varepsilon)\, G(\mathbf{l}, \mathbf{r}_1; \omega') \times G(\mathbf{r}_2, \mathbf{l}'; \omega'); \qquad \hat{\mathbf{l}}_x = -i\frac{\partial}{\partial l_x}. \quad (8)$$

It is convenient to make a transformation of this expression. To do so we note that under the

infinitesimal transformation (4) $\Sigma(\mathbf{r}, \mathbf{r}'; \epsilon)$ changes by the quantity

$$-i(eH/c)\,\delta b\,(x-x')\,\Sigma(\mathbf{r}, \mathbf{r}'; \varepsilon).$$

At the same time, under the displacement of the origin, $y \to y + \delta b$, the Hamiltonian (7) receives the increment

$$\delta H_{int} = \delta b \int \psi^+(\mathbf{r}') \left[\frac{e}{2mc}(\hat{\mathbf{p}} - \hat{\mathbf{p}}')_x + \frac{e^2 H y}{mc^2}\right]_{\mathbf{r}'\to\mathbf{r}} \psi(\mathbf{r})\, d^3\mathbf{r}.$$

Then, in analogy with Eq. (8), we get

$$-\frac{ie(x-x')}{c}\delta_{\alpha\beta}\,\Sigma(\mathbf{r}, \mathbf{r}'; \varepsilon)$$
$$= \frac{i}{2\pi}\int d\omega' \int d^3\mathbf{r}_1 d^3\mathbf{r}_2 d^3\mathbf{1}\left[\frac{e}{2mc}(\hat{\mathbf{p}} - \hat{\mathbf{p}}')_{l_x} + \frac{e^2 H}{mc^2} l_y\right]$$
$$\times \Gamma_{\alpha\gamma,\gamma\beta}(\mathbf{r}, \varepsilon; \mathbf{r}_1, \omega'; \mathbf{r}_2, \omega'; \mathbf{r}', \varepsilon)$$
$$\times G(\mathbf{1}, \mathbf{r}_1; \omega')\, G(\mathbf{r}_2, \mathbf{1}'; \omega').$$

Combining this last relation with Eq. (8), we find

$$\frac{\partial \Sigma_{\alpha\beta}(\mathbf{r}, \mathbf{r}'; \varepsilon)}{\partial H} = -i\frac{e(x-x')(y+y')}{2c}\Sigma_{\alpha\beta}(\mathbf{r}, \mathbf{r}'; \varepsilon)$$
$$+ M_{\alpha\beta}(\mathbf{r}, \mathbf{r}', \varepsilon), \qquad (9)$$

$$M_{\alpha\beta}(\mathbf{r}, \mathbf{r}'; \varepsilon) = \frac{i}{2\pi}\int d\omega' \int d^3\mathbf{r}_1 d^3\mathbf{r}_2 d^3\mathbf{1}\left[\frac{e}{2mc}(\hat{\mathbf{p}} - \hat{\mathbf{p}}')_{l_x}\right.$$
$$\left. + \frac{e^2 H l_y}{mc^2}\right][l_y - (y+y')/2]\, G(\mathbf{1}, \mathbf{r}_1; \omega')\, G(\mathbf{r}_2, \mathbf{1}'; \omega')$$
$$\times \Gamma_{\alpha\gamma,\gamma\beta}(\mathbf{r}, \varepsilon; \mathbf{r}_1, \omega'; \mathbf{r}_2, \omega'; \mathbf{r}', \varepsilon). \qquad (10)$$

We shall show below that the terms in $\Sigma_{\alpha\beta}(\mathbf{r}, \mathbf{r}'; \epsilon)$ that come from $M_{\alpha\beta}(\mathbf{r}, \mathbf{r}'; \epsilon)$ are of the order $H^{3/2}$ in the magnetic field, whereas for our purposes it is enough to know the spectrum of the system correct to terms of the order H. Neglecting the last term in Eq. (9), we get

$$\Sigma_{\alpha\beta}(\mathbf{r}, \mathbf{r}'; \varepsilon) = \exp\left\{-\tfrac{1}{2} ieHc^{-1}(x-x')(y+y')\right\}$$
$$\delta_{\alpha\beta}\,\Sigma^0(\mathbf{r} - \mathbf{r}'; \varepsilon), \qquad (11)$$

where $\Sigma^0(\mathbf{r} - \mathbf{r}'; \epsilon)$ is the self-energy part in the absence of the magnetic field.

The expression (11) for $\Sigma(\mathbf{r}, \mathbf{r}')$ can be written symbolically in the form

$$\Sigma(\mathbf{r}, \mathbf{r}') = \hat{\Sigma}^0(\hat{\mathbf{p}} - e\mathbf{A}/c).$$

In fact, let us apply the "Hamiltonian"

$$\hat{h} = \frac{1}{2m}\left(\hat{\mathbf{p}} - \frac{e}{c}\mathbf{A}\right)^2 + \hat{\Sigma}^0\left(\hat{\mathbf{p}} - \frac{e}{c}\mathbf{A}\right)$$

to an arbitrary function $\psi(\mathbf{r})$ and go over to the p representation. As Zil'berman[5] has shown, in the momentum representation the operator $\hat{h}$ can be written in the following form:

$$\hat{h}\psi_{\mathbf{p}} = \left\{\frac{1}{2m}\left(p_x + i\frac{eH}{c}\frac{d}{dp_y}\right)^2 + \frac{1}{2m}(p_y^2 + p_z^2)\right.$$
$$+ \int \Sigma^0(\mathbf{s}; \varepsilon) \exp\left[-i\left(p_x + \frac{ieH}{c}\frac{d}{dp_y}\right)s_x - ip_y s_y\right.$$
$$\left.\left. - ip_z s_z\right] d^3\mathbf{s}\right\}\psi_{\mathbf{p}}. \qquad (12)$$

The expression (12) contains definite prescriptions as to the order of the operators p_y and d/dp_y (the requirement of complete symmetry of the Hamiltonian[5]). In the isotropic model of the Fermi liquid, which we are using in this paper, the self-energy part $\Sigma^0(\mathbf{p}, \epsilon)$ is a function of $|\mathbf{p}|^2$ only. At the same time it is obvious that under the condition that $\Sigma^0(\hat{\mathbf{p}} - e\mathbf{A}/c)$ is to remain Hermitian different requirements as to the order of the operators p_y and d/dp_y in $\Sigma^0(\hat{\mathbf{p}} - e\mathbf{A}/c)$ lead to Hamiltonians (12) which differ by terms of order in the energy eigenvalues not lower than H^2. For this reason it is more convenient to choose $\Sigma^0(\hat{\mathbf{p}} - e\mathbf{A}/c)$ in the form $\Sigma^0(\hat{\mathbf{p}} - e\mathbf{A}/c) \equiv \Sigma^0(|\hat{\mathbf{p}} - e\mathbf{A}/c|^2)$.

The exact eigenvalues and eigenfunctions of the operator

$$\left(\hat{\mathbf{p}} - \frac{e\mathbf{A}}{c}\right)^2 = \left(\hat{p}_x + \frac{ieH}{c}\frac{d}{dp_y}\right)^2 + \hat{p}_y^2 + \hat{p}_z^2$$

are well known:[6]

$$\left(\hat{\mathbf{p}} - \frac{e\mathbf{A}}{c}\right)^2 \psi_{\mathbf{p},n} = [p_z^2 + (2n+1)eH/c]\,\psi_{\mathbf{p},n},$$
$$\psi_{\mathbf{p},n} = \exp\{-icp_x p_y/eH - cp_y^2/2eH\} H_n(p_y\sqrt{c/eH}),$$

where $H_n(x)$ are the Hermite polynomials. Therefore the Green's function of a particle in a magnetic field can be written near the Fermi surface (in the p representation) in the following way:

$$G(\mathbf{p}, \mathbf{p}'; \varepsilon)$$
$$= \sum_n \frac{\psi_n(\mathbf{p})\,\psi_n^*(\mathbf{p}')\,\delta(p_x - p_x')\,\delta(p_z - p_z')}{\varepsilon + \mu - (n+1/2)eH/mc - p_z^2/2m - \Sigma^0(p_z^2 + 2(n+1/2)eH/c) + i\delta(\varepsilon)}. \qquad (13)$$

According to Eq. (5), when the magnetic field H = 0,

$$G^0(\mathbf{p}, \mathbf{p}'; \varepsilon) = \frac{\delta(\mathbf{p} - \mathbf{p}')}{\varepsilon + \mu - p^2/2m - \Sigma^0(p^2, \varepsilon) + i\delta(\varepsilon)}$$
$$= \frac{a\delta(\mathbf{p} - \mathbf{p}')}{\varepsilon - v(p - p_0) + i\delta(\varepsilon)}. \qquad (14)$$

Here a is a renormalization constant, and p_0 is the Fermi limiting momentum, which is determined from the equation

$$p_0^2/2m + \Sigma^0(p_0, 0) = \mu.$$

As is well known,[11] the electrons important for the de Haas-van Alphen effect are those near the Fermi surface i.e., the electrons in the region in which $(2n+1)eH/c + p_Z^2 \approx p_0^2$. Therefore if we introduce the notation m* for the "effective" mass ($v = p_0/m^*$), there follows directly from Eqs. (13) and (14) the following expression for the Green's function of electrons in a magnetic field near the Fermi surface:

$$G(\mathbf{p}, \mathbf{p}'; \varepsilon) = \sum_n \psi_n(\mathbf{p})\psi_n^*(\mathbf{p}')\,\delta(p_x - p_x')\;\delta(p_z - p_z')G_n(p_z, \varepsilon),$$

$$G_n(p_z, \varepsilon) = a/(\varepsilon + p_0^2/2m^* - (n + 1/2)\,\omega^* - p_z^2/2m^* + i\delta(\varepsilon)), \quad (15)$$

where $\omega^* = eH/m^*c$. As is shown below, the constants a, m^*, and p_0 depend on the field H only through terms of order $H^{3/2}$.

The Greens' function far from the Fermi surface [$|(2n+1)eH/c + p_z^2 - p_0^2| \sim p_0^2$] contains no sharp poles; this is due to the strong damping of the excitations in this region (for small ϵ the damping $\delta(\epsilon)$ of the excitations in Eq. (15) increases like $|\epsilon|\epsilon/\mu$). Therefore the contributions to the various quantities from these distant regions give no oscillating singularities and can be expanded in powers of the field strength.

Let us discuss the behavior of the Green's function $G(\mathbf{r}, \mathbf{r}'; \epsilon)$ in the coordinate representation. In the absence of a magnetic field

$$G^0(\mathbf{r} - \mathbf{r}'; \varepsilon) = \frac{1}{(2\pi)^3}\int G^0(\mathbf{p})\, e^{i\mathbf{p}(\mathbf{r}-\mathbf{r}')}d^3\mathbf{p}.$$

The Green's function $G(\mathbf{R}, \epsilon)$ expresses the correlation of the electrons at different points of space. At distances large in comparison with atomic distances the only electrons that contribute are those moving like "free" electrons, i.e., those from the region near the Fermi surface. Electronic excitations far from the Fermi surface are strongly damped because of collisions with each other and contribute to the Green's function $G(\mathbf{r} - \mathbf{r}'; \epsilon)$ only at atomic distances. If in the function $G(\mathbf{r} - \mathbf{r}'; \epsilon)$ we separate out the term (5) that has a singularity near the Fermi surface,

$$G^0(\mathbf{p}, \varepsilon) = \frac{a}{\varepsilon - v(p - p_0) + i\delta(\varepsilon)} + g(\mathbf{p}, \varepsilon)$$

[so that $g(\mathbf{p}, \epsilon)$ has no singularities], it is easy to see that for small ϵ the behavior of the function $G^0(\mathbf{R}, \epsilon)$ at distances $Rp_0 \gg 1$ is given by

$$G^0(\mathbf{R}, \varepsilon) = \frac{am^*}{2\pi R}\begin{cases}\exp(ip_0R + i\varepsilon R/v), & \varepsilon > 0\\ \exp(-ip_0R - i\varepsilon R/v), & \varepsilon < 0.\end{cases} \quad (16)$$

In the case of large ϵ the function $G^0(\mathbf{R}, \epsilon)$ is rapidly damped at distances $Rp_0 \sim \epsilon^2/\mu^2$.

Returning to the Green's function in a magnetic field, we conclude that its behavior at large distances is also determined by the singular part of the expression (15). It is easy to verify that in the coordinate representation $G(\mathbf{r}, \mathbf{r}'; \epsilon)$ (for $|\mathbf{r} - \mathbf{r}'| \gg 1/p_0$) can be written in the following form:

$$G(\mathbf{r}, \mathbf{r}'; \varepsilon) = \exp[-i(eH/2c)(x - x')(y + y')]$$
$$\times \frac{eH}{c(2\pi)^2}\sum_n e^{-eHc^2/4c}L_n\left(\frac{eH}{2c}\rho^2\right)$$
$$\times \int \frac{ae^{ip_z(z-z')}dp_z}{\varepsilon + p_0^2/2m^* - (n+1/2)\,\omega^* - p_z^2/2m^* + i\delta(\varepsilon)}$$
$$= \exp\{-i(eH/2c)(x - x')(y + y')\}\,\overline{G}(\mathbf{R}, \varepsilon), \quad (17)$$

$L_n(x)$ are the Laguerre polynomials. [Here and in what follows we use the notation $\rho^2 = (x - x')^2 + (y - y')^2$]. As can be seen from Eq. (17), generally speaking the magnetic field causes a decided change in the character of the dependence of $G(\mathbf{r}, \mathbf{r}'; \epsilon)$ on $\mathbf{R}$. In the limit of weak magnetic field, $\omega^* \ll p_0^2/2m^*$, for large n and $\rho \ll cp_0/eH$,

$$e^{-eH\rho^2/4c}L_n(eH\rho^2/2c) \approx J_0(\sqrt{2eHn/c}\,\rho).$$

By replacing the summation over n by an integration, we would again arrive at the result (16).

A special role is played in Eq. (17) by terms with values of $(n + 1/2)\omega^*$ close to $p_0^2/2m^*$ (small p_z). Let $\Delta < \omega^*$ and $p_0^2/2m^* = \Delta + \omega^*(N_0 + 1/2)$; then each such term in Eq. (17) contributes to $G(\mathbf{R}, \epsilon)$ a small quantity of the order

$$\sim \frac{eH}{c}e^{-eH\rho^2/4c}L_{N_0}\left(\frac{eH}{2c}\rho^2\right)e^{i\Delta|z-z'|}\Delta^{-1/2}.$$

This expression is exponentially damped for $\rho \gg cp_0/eH$ and is a plane wave in its dependence on $|z - z'|$. This part of the G-function determines the oscillations of all the quantities in which we are interested.

Coming now to an estimate of the term $M(\mathbf{r}, \mathbf{r}'; \epsilon)$ dropped from Eq. (9), let us rewrite this term in a somewhat different form, by substituting Green's functions in the formula (3):

$$M_{\alpha\beta}(\mathbf{r}, \mathbf{r}'; \varepsilon) = \frac{i}{2\pi}\int d\omega \int d^3\mathbf{r}_1 d^3\mathbf{r}_2 d^3\mathbf{l}\left(l_y - \frac{y + y'}{2}\right)$$
$$\times \exp\{-i(eH/2c)[(r_{1y} + l_y)(r_{1x} - l_x)$$
$$+ (r_{2y} + l_y)(l_x - r_{2x})]\}\,\Gamma_{\alpha\gamma,\gamma\beta}(\mathbf{r}, \varepsilon; \mathbf{r}_1, \omega; \mathbf{r}_2, \omega; \mathbf{r}', \varepsilon)$$
$$\times\Big\{(e^2H/2mc^2)\,G(\mathbf{l} - \mathbf{r}_1, \omega)\,G(\mathbf{r}_2 - \mathbf{l}, \omega)$$
$$\times\left(l_y - \frac{r_{1y} + r_{2y}}{2}\right) + \frac{ie}{2mc}\left[\frac{\partial G(\mathbf{l} - \mathbf{r}_1, \omega)}{\partial r_{1x}}G(\mathbf{r}_2 - \mathbf{l}, \omega)\right.$$
$$\left. - G(\mathbf{l} - \mathbf{r}_1, \omega)\frac{\partial G(\mathbf{r}_2 - \mathbf{l}, \omega)}{\partial r_{2x}}\right]\Big\}. \quad (18)$$

This expression involves integrals containing G-functions of the differences of coordinates between the various points of the diagram of Fig. 1. The region of integration in which these differences are of the order of interatomic distances are of no interest, since their contribution to Eq. (18) is of the order H (and of order H^2 in Σ).

Let the distances $|\mathbf{l} - \mathbf{r}_i|$ be large in comparison with atomic distances. In this region we can use for the Green's functions the asymptotic expression (17). In estimating the quantity (18) we shall assume that the magnetic field is weak, and set it equal to zero wherever possible. In particular, for the vertex part we use the expression for zero field. Let us rewrite this expression in the following way:

$$\Gamma_{\alpha\gamma,\gamma\beta}(\mathbf{r}, \varepsilon; \mathbf{r}_1\omega; \mathbf{r}_2, \omega; \mathbf{r}', \varepsilon) = \frac{1}{(2\pi)^9}\int \Gamma^0_{\alpha\gamma,\gamma\beta}(\mathbf{p}_1, \varepsilon; \mathbf{p}_2, \omega; \mathbf{p}_2 + \mathbf{k}, \omega; \mathbf{p}_1 - \mathbf{k}, \varepsilon) \exp[i\mathbf{p}_1(\mathbf{r} - \mathbf{r}') + i\mathbf{p}_2(\mathbf{r}_1 - \mathbf{r}_2) + i\mathbf{k}(\mathbf{r}' - \mathbf{r}_2)]\, d^3\mathbf{p}_1 d^3\mathbf{p}_2 d^3\mathbf{k}. \quad (19)$$

The Fourier component $\Gamma^0_{\alpha\gamma,\gamma\beta}(\mathbf{p}_1, \mathbf{p}_2; \mathbf{p}_3, \mathbf{p}_4)$ in Eq. (19) involves momenta p of the order of the Fermi momentum and has important variations in this region only for changes $\Delta p \sim p_0$. Besides this, in the region of integration over 1 in Eq. (18) where $|1-r|$ is large the important values of k in Eq. (19) are small, and therefore we can neglect the dependence of the vertex part on k.

Thus as a function of $|\mathbf{r}_2 - \mathbf{r}_1|$ and $|\mathbf{r} - \mathbf{r}'|$ the expression (19) is rapidly oscillating at atomic distances. [Close to the Fermi surface $|\mathbf{p}_1|$, $|\mathbf{p}_2| \sim p_0$ the Fourier components $\Gamma_{\alpha\gamma,\gamma\beta}(\mathbf{p}_1, \mathbf{p}_2; \mathbf{p}_2, \mathbf{p}_1)$ in Eq. (19) depend only on the angle between the vectors $\mathbf{p}_1$ and $\mathbf{p}_2$]. Consequently, for purposes of the integration over $\mathbf{r}_1$ and $\mathbf{r}_2$ in Eq. (18) for $|1-r_1| \gg 1/p_0$, for which values only the Fourier components with momenta close to the Fermi surface are important in the functions $G(1-r_1, \omega)$, the vertex part (19) is essentially a δ function of $\mathbf{r}_1 - \mathbf{r}_2$ and $\mathbf{r} - \mathbf{r}'$. This fact is the expression of a fundamental physical assumption of the theory of the Fermi liquid,[2] according to which the interaction between the particles is a short-range one, and all of the correlations that arise between them fall off rapidly at atomic distances. (For the electrons in a metal the Coulomb interaction is also screened off at distances of the order of atomic distances.) Nevertheless this assertion is not completely rigorous.

As has been shown by Landau,[3] in a number of cases the vertex part can have a "long-range" part. Such singularities are due to the diagrams in the vertex part which are shown in Fig. 2, a. In this diagram the squares denote irreducible vertex parts which have no singularities in the direction 1 — 2. In fact, substituting in these diagrams the expressions (16) for the Green's functions and integrating over the frequencies of the internal lines, we get ($R_{12} \gg 1/p_0$)

$$\int G^0(\mathbf{R}_{12}, \omega)\, G^0(\mathbf{R}_{12}, \omega - \varepsilon)\, d\omega \sim \frac{a^2 m^{*2}\varepsilon}{(2\pi R_{12})^2} e^{i\varepsilon R_{12}/v},$$

where ϵ is the small frequency transfer. Figure 2, b shows this same diagram in the momentum representation, and from it we can see that the slowly decreasing dependence in the vertex part is due to small frequency and momentum transfers in the Fourier component $\Gamma^0(p_1, p_2; p_3, p_4)$. In Eq. (19) such a small transfer can correspond

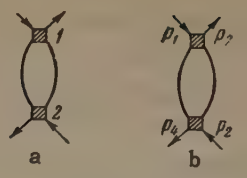

FIG. 2

either to a small value of k or to a small transfer $|\mathbf{p}_3 - \mathbf{p}_1| \approx |\mathbf{p}_2 - \mathbf{p}_1| \ll p_0$. Obviously in the latter case the contribution from these singularities in Eq. (19) is small, because of the smallness of the region of integration over p_1 and p_2. As for the small values of k, the question of these singularities arises owing to the fact that in Eq. (18) there is a factor $l_y - r_y = l_y - r_{1y} + r_{1y} - r_y$, and the quantity $|r_{1y} - r_y|$ may not be small. It is easy to see, however, that in zeroth order in the field we have by considerations of symmetry

$$\int (s_y - r_y)\, G^0(\mathbf{s} - \mathbf{r})\, G^0(\mathbf{s} - \mathbf{r})\, d^3\mathbf{s} \equiv 0$$

and therefore in Eq. (18) the factor $l_y - (y + y')/2$ can be replaced by $l_y - r_{1y}$. We shall not present the detailed proof that all of these assumptions correspond to dropping in $\mathbf{M}(\mathbf{r}, \mathbf{r}')$ terms that are of higher order in the field strength H as compared with the estimate that we get on the assumption that the vertex part is equal to the expression for this part in the absence of a magnetic field and is of short-range character.

Accordingly, in Eq. (18) we now take $|\mathbf{r}_2 - \mathbf{r}_1| \sim |\mathbf{r}_1 - \mathbf{r}| \sim 1/p_0$. We can drop the exponential factors in Eq. (18). By considerations of symmetry the term in the square brackets that contains derivatives of the Green's functions is identically zero. Therefore instead of Eq. (18) we get

$$M_{\alpha\beta}(\mathbf{r}, \mathbf{r}') \approx \frac{ie^2H}{4\pi mc^2}\int d\omega \int d^3\mathbf{r}_1 d^3\mathbf{r}_2 d^3\mathbf{l} \left(l_y - \frac{r_{1y} + r_{2y}}{2}\right)^2 \times G(\mathbf{l} - \mathbf{r}_1, \omega)\, G(\mathbf{r}_2 - \mathbf{l}, \omega)\, \Gamma^0_{\alpha\gamma,\gamma\beta} \times (\mathbf{r}, \ ; \mathbf{r}_1, \omega; \mathbf{r}_2, \omega; \mathbf{r}', \varepsilon). \quad (20)$$

According to the foregoing the quantity $\mathbf{M}(\mathbf{r}, \mathbf{r}')$ of Eq. (20) is determined by the region of integration $|\mathbf{l} - \mathbf{r}_1| \gg 1/p_0$ and $\omega \ll \mu$. For small ϵ and ω we can neglect the frequency dependence of Γ^0 in Eq. (19). We shall denote the corresponding Fourier component by $\Gamma^0_{\alpha\gamma,\gamma\beta}(\mathbf{p}_1, \mathbf{p}_2)$. Thus it follows from Eq. (20) that

$$M_{\alpha\beta}(\mathbf{r}, \mathbf{r}') \approx \frac{ie^2H}{4\pi mc^2}\left[\int \frac{d^3\mathbf{p}}{(2\pi)^6} e^{i\mathbf{p}_1(\mathbf{r} - \mathbf{r}')} \int \frac{d\Omega}{4\pi} \Gamma_{\alpha\gamma,\gamma\beta}(\mathbf{p}_1, \mathbf{p}_2)\right] \frac{1}{2} \times \int G^2(\mathbf{R}, \omega)\, \rho^2 d^3\mathbf{R}. \quad (21)$$

Proceeding to the calculation of this last integral, we substitute in it the Green's function (17):

$$\int G^2(\mathbf{R},\omega)\,\rho^2 d^3\mathbf{R} = \frac{a^2}{(2\pi)^2}\left(\frac{eH}{c}\right)^2 \iint \sum_{n,m} \frac{dp_z d\omega}{(\omega - E_n + i\delta(\omega))(\omega - E_m + i\delta(\omega))} \times \int_0^\infty \rho^2 d\rho\, e^{-eH\rho^2/4c} L_n\left(\frac{eH}{2c}\rho^2\right) L_m\left(\frac{eH}{2c}\rho^2\right),$$

$$E_n = (n + 1/2)\,\omega^* + p_z^2/2m^* - p_0^2/2m^*,$$

$$E_m = (m + 1/2)\,\omega^* + (p_z - q)^2/2m^* - p_0^2/2m^*. \qquad (21')$$

In the expression for E_m we have introduced a small quantity q. The point is that the integral in question is not uniquely defined: the expression

$$\int d\omega \int G(\mathbf{R},\omega)\,G(\mathbf{R},\omega-\omega_0)\,\rho^2 e^{iqz} d^3\mathbf{R}$$

has different limits for ω_0, $q \to 0$, depending on whether $\omega_0/q \to 0$ or $q/\omega_0 \to 0$. For the case of no magnetic field the singularities of such integrals have been studied by Landau.[3] To give a meaning to the integral (21') we must take the limit $\omega_0/q \to 0$, which corresponds to the fact that $M(\mathbf{r}, \mathbf{r}'; \epsilon)$ is being calculated in a field that is constant in time but weakly nonuniform along the z axis. Therefore, strictly speaking, the quantity given by Eq. (21) is a definite one of the two vertex parts Γ^k and Γ^ω introduced by Landau,[3] namely Γ^k. For our estimates this is of course unimportant.

In calculating the integral of Laguerre polynomials in Eq. (21') it is helpful to use the exact relation

$$xL_n(x) = (2n+1)L_n(x) - (n+1)L_{n+1}(x) - nL_{n-1}(x). \qquad (22)$$

Therefore $m = n \pm 1$. Integrating Eq. (21') over the frequencies ω, we get

$$Y = \frac{i}{2\pi}\int d\omega G^2(\mathbf{R},\omega)\,\rho^2 d^3\mathbf{R} = \frac{a^2}{2\pi^2}\sum_{n,m}\int \frac{dp_z}{E_n - E_m}\int_0^\infty xL_n(x)L_m(x)e^{-x}dx$$

($E_n > 0$, $E_m < 0$). Using Eq. (22) and performing the integration over p_z, we find after simple manipulations

$$Y = (2m^*)^{1/2}\frac{a^2}{\pi^2}\sum_n \left\{\frac{1}{2}\frac{n+1/2}{[p_0^2/2m^* - \omega^*(n+1/2)]^{1/2}} - \frac{1}{\omega^*}\sqrt{\frac{p_0^2}{2m^*} - \omega^*(n+1/2)}\right\}.$$

The summation is taken over all values of n for which the radicand is positive.

It is not hard to verify that this quantity can be represented in the following way:

$$\frac{eH}{c}Y = -\frac{\sqrt{2m^*}}{\omega^*}\frac{a^2}{\pi^2}\frac{\partial}{\partial H}\left\{\frac{eH}{c}\sum_n \sqrt{\frac{p_0^2}{2m^*} - \omega^*(n+1/2)}\right\}. \qquad (23)$$

The sum in the curly brackets has been repeatedly

FIG. 3

investigated in the literature.[7,8] Using the expression obtained by Sondheimer and Wilson,[8] which is accurate to terms of order H^2,

$$\frac{1}{2\pi^2}\frac{eH}{c}\sum_n \sqrt{\mu - \omega^*(n+1/2)} = \frac{p_0^3}{3\pi^2}\left\{1 + \frac{3}{2\pi}\left(\frac{\omega^*}{\mu}\right)^{3/2}\sum_{r=1}^\infty \frac{(-1)^r}{r^{3/2}}\sin\left(2\pi r\frac{\mu}{\omega^*} - \frac{\pi}{4}\right)\right\}$$

and substituting it in Eq. (23), we get finally

$$\frac{eH}{c}Y = -\frac{\sqrt{2m^*}}{\omega^*\pi^3}a^2\frac{\partial}{\partial H}\left\{\left(\frac{\omega^*}{\mu}\right)^{3/2}\varphi\left(\frac{\mu}{\omega^*}\right)\right\},$$

where $\varphi(x)$ is a rapidly oscillating function. Thus in actual fact the terms that correspond to $M(\mathbf{r}, \mathbf{r}'; \epsilon)$ give in Eq. (14) a correction to the energy levels of the excitations of the order $H^{3/2}$.

3. THE OSCILLATING SINGULARITIES OF THE THERMODYNAMIC FUNCTIONS

Let us now proceed to the derivation of the formula for the thermodynamic potential. In order to separate out the small terms that have an oscillating character, it is more convenient to start from the expression for the derivative $\partial N/\partial\mu$ of the particle-number density with respect to the chemical potential of the system. The particle-number density is connected in a simple way with the Green's function (1) of the system:

$$N = -iG_{\alpha\alpha}(x, x')_{x'\to x,\, t'\to t+0}.$$

The expression for the derivative $\partial N/\partial\mu$ can be obtained by the following arguments (cf. [9]). Let us place the system in a weak and slowly varying potential field $\delta U(\mathbf{r})$. Then the quantity $\mu + \delta U = \mu_0$ is conserved throughout the system. On the other hand, the interaction of the system with the field $\delta U(\mathbf{r})$ is described by the Hamiltonian

$$H_{int} = \int \psi^+(x)\,\delta U\psi(x)\,d^3\mathbf{r}.$$

According to the usual rules of the diagram technique the change of the Green's function in first order in δU can be represented by the first diagram of Fig. 3. In the limit of a δU independent of the coordinates, $\delta U = -\delta\mu$, we get

$$\frac{\partial N}{\partial\mu} = i\int G_{\alpha\gamma}(x, l)\,G_{\gamma\alpha}(l, x)\,d^4l - \int d^4\xi_1 d^4\xi_2 d^4\xi_3 d^4\xi_4 d^4l\, G_{\alpha\alpha_1}(x,\xi_1)\,G_{\beta\alpha_2}(l,\xi_2)\,G_{\alpha_3\beta}(\xi_3, l)\,G_{\alpha_4\alpha}(\xi_4, x') \times \Gamma_{\alpha_1\alpha_2,\,\alpha_3\alpha_4}(\xi_1,\xi_2;\xi_3,\xi_4)$$

or, when we go over to Fourier components with respect to the difference of the time coordinates,

$$\frac{\partial N}{\partial \mu} = \frac{i}{2\pi}\int d\omega \int G_{\alpha\gamma}(\mathbf{r}, \mathbf{1}; \omega)\, G_{\gamma\alpha}(\mathbf{1}, \mathbf{r}; \omega)\, d^3\mathbf{1}$$
$$- \frac{1}{(2\pi)^2}\iint d\omega d\omega' \int d^3\mathbf{s}_1 d^3\mathbf{s}_2 d^3\mathbf{s}_3 d^3\mathbf{s}_4 d^3\mathbf{1} G_{\alpha\alpha_1}(\mathbf{r}, \mathbf{s}_1; \omega)\, G_{\alpha_4\alpha}$$
$$\times (\mathbf{s}_4, \mathbf{r}; \omega)\, \Gamma_{\alpha_1\alpha_2, \alpha_3\alpha_4}(\mathbf{s}_1, \omega; \mathbf{s}_2, \omega'; \mathbf{s}_3, \omega'; \mathbf{s}_4, \omega)\, G_{\beta\alpha_2}$$
$$\times (\mathbf{1}, \mathbf{s}_2; \omega')\, G_{\alpha_3\beta}(\mathbf{s}_3, \mathbf{1}; \omega').$$

For simplicity let us first investigate the singularities of the first term in the right member of Eq. (24). These singularities are due to electrons near the Fermi surface, and therefore in this case it is sufficient to use the asymptotic expression (17) for the Green's functions. Substituting this expression in the integral and carrying out the integration, we get

$$\frac{i}{2\pi}\int d\omega \int G_{\alpha\gamma}(\mathbf{r}, \mathbf{1}; \omega)\, G_{\gamma\alpha}(\mathbf{1}, \mathbf{r}; \omega)\, d^3\mathbf{1}$$
$$= \frac{2i}{(2\pi)^3}\left(\frac{eH}{c}\right)^2 a^2 \sum_n \int d\omega \int \frac{dp_z}{(\omega - E_n + i\delta(\omega))(\omega - E_n' + i\delta(\omega))}$$

(here in $E_n' = \omega^*(n + \frac{1}{2}) + (p_z - q)^2/2m^* - p_0^2/2m^*$ we have introduced a small momentum; this corresponds to the fact that in deriving Eq. (24) we started from the condition for equilibrium of the system in a field $\delta U(\mathbf{r})$ constant in time but slowly varying in space). Integrating the resulting expression first over ω, and then over p_z, we arrive at the expression

$$\frac{\sqrt{2m^*}}{2\pi^2}\left(\frac{eH}{c}\right)a^2 \sum_n \left(\frac{p_0^2}{2m^*} - \omega^*(n + {}^1/_2)\right)^{-1/2}. \qquad (25)$$

In the sum (25) a special role is played by the values of n for which the radicand is small. These terms give the nonanalytic part of the integral under consideration. At the same time the main contribution as regards magnitude comes from values of n for which $n\omega^* \sim p_0^2/2m^*$. For a weak field the summation over the main region can be replaced by an integration, and from this we find

$$a^2 m^* p_0/\pi^2. \qquad (26)$$

(A contribution to $\partial N/\partial\mu$ of this same order of magnitude is given by the distant regions.) Let us again introduce the number N_0, the integer part of $p_0^2/2m^*$ in units ω^*: $p_0^2/2m^* = (N_0 + \frac{1}{2})\omega^* + \Delta$ ($\Delta > 0$). The terms in the sum (25) for which $(N_0 - n) \ll N_0$ are of the order of

$$(\sqrt{2m^*}/2\pi^2)(eH/c)(a^2/\sqrt{\Delta})$$

and remain small in comparison with (26) provided that

$$\Delta \gg \omega^*\left(\omega^* \Big/ \frac{p_0^2}{2m^*}\right). \qquad (27)$$

The condition (27) imposes a restriction on the study of the detailed structure of the oscillations in the immediate neighborhood of the Fermi surface. It must be remembered, however, that the actual region of interest for the de Haas-van Alphen effect just coincides with the condition (27), since in the magnetic fields that are obtainable up to the present time one begins to get a violation of the condition (27) only at the very lowest temperatures. Therefore in our later discussion of the quantum case we shall assume that the condition (27) is always satisfied.

In order to separate out the irregular part of the expression (25) we substitute $n \to N_0 - k$. Subtracting from the new sum the terms that diverge at the upper limit, we get

$$\frac{\sqrt{2m^*}}{2\pi^2}\left(\frac{eH}{c}\right)a^2\left[\sum_0^{N_0}(\sqrt{\Delta + \omega^* k})^{-1/2} - 2\sqrt{N_0}/\sqrt{\omega^*}\right]_{N_0\to\infty}$$
$$= \frac{\sqrt{2m^*}}{2\pi^2} m^* a^2 \sqrt{\omega^*}\,\zeta\left(\frac{1}{2}, \frac{\Delta}{\omega^*}\right), \qquad (28)$$

where $\zeta(s, x)$ is the generalized Riemann zeta function[10]:

$$\zeta(s, x) = -\frac{\Gamma(1-s)}{2\pi i}\int_{\infty}^{(0+)} \frac{(-z)^{s-1}e^{-xz}}{1 - e^{-z}}\, dz.$$

Thus apart from regular terms of higher orders in eH/cp_0^2 the integration of the two G-functions in the loop of Fig. 4 a leads to the appearance of small terms which are rapidly oscillating functions of the ratio cp_0^2/eH.

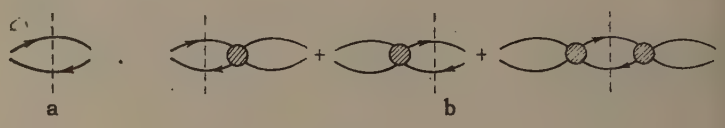

FIG. 4

Returning to Eq. (24), we see that singularities (28) in $\partial N/\partial\mu$ arise in every loop (cf. Fig. 3) in which there are two horizontal lines (with their arrows in opposite directions). Since these terms are small, we have to separate each such loop only once. In particular, the loop can belong to the diagram for a vertex part. As the result of the separation of the singular terms the situation arises which is shown graphically in Fig. 4 b. The loop from which the singularity is separated out is marked with a vertical dashed line. Since these terms are small, we can set the magnetic field strength equal to zero in all the other parts of the diagram.

In this connection we recall once again that the singularity (28) is due to the behavior at large distances $r - 1$ of the Green's function in the loop of Fig. 4 a. Therefore, using the same procedure

with the vertex part as in the derivation of Eq. (21), we get instead of Eq. (24) the following result:

$$\frac{\partial N}{\partial \mu} = \frac{\sqrt{2m^*}m^*}{2\pi^2}\sqrt{\omega^*}\zeta\left(\frac{1}{2}, \frac{\Delta}{\omega^*}\right)\Phi^2,$$

$$\Phi = a\left\{1 + \frac{i}{2(2\pi)^4}\int \Gamma^{0k}_{\alpha\gamma,\,\gamma\alpha}(p_1, p_2)\, G^0(p_1, \omega)\, G^0(p_2, \omega)\, d^4p\right\} \quad (29)$$

(the vector p_1 is taken on the Fermi surface). In accordance with what was said earlier, our choice between the two limits Γ^{0k} and $\Gamma^{0\omega}$ introduced by Landau[3] must be to take the limit Γ^{0k}, which means that the potential field used in the derivation of Eq. (24) is strictly independent of the time.

The connection of the renormalization factor Φ with physical quantities has been established by Pitaevskii.[9] It turns out that in the absence of a magnetic field

$$\Phi = a\left(\frac{\partial G^{-1}}{\partial \mu}\right)_{p=p_0,\ \omega=0} = \frac{p_0}{m^*}\frac{dp_0}{d\mu}. \quad (29')$$

Substituting this result in the expression obtained earlier, we get

$$\frac{\partial N}{\partial \mu} = \frac{1}{\sqrt{2m^*}\,4\pi^2}\sqrt{\omega^*}\left(\frac{dp_0^2}{d\mu}\right)^2\zeta\left(\frac{1}{2}, \frac{\Delta}{\omega^*}\right). \quad (30)$$

We must calculate the thermodynamic quantities N and Ω (the potential) in terms of the variables μ and V. According to Eqs. (14) and (23), apart from terms of the order $H^{3/2}$ the quantity $p_0(\mu)$ which appears in Eq. (29) and also in Eq. (25) is a function of the chemical potential as defined on the Fermi surface in the absence of a magnetic field. Taking for the oscillating part of Ω only the double integral of the rapidly oscillating terms $\zeta(1/2, \Delta/\omega^*) = \varphi(cp_0^2/eH)$, we get

$$\delta\Omega_{osc} = -\frac{i4m^{*2}\omega^{*5/2}}{3\sqrt{2m^*}\,\pi^2}\zeta\left(-\frac{3}{2}, \frac{\Delta}{\omega^*}\right)$$

$$= \frac{m^{*3/2}\omega^{*5/2}}{4\pi^4}\sum_1^\infty r^{-5/2}\cos\left(2\pi r\frac{\Delta}{\omega^*} - \frac{\pi}{4}\right),$$

that is, an expression which agrees with the results of I. Lifshitz and Kosevich[1] (in the isotropic model).

4. THE EFFECT OF THE SPIN ON THE OSCILLATIONS

In the scheme that has been expounded it is easy to include also the interaction of the magnetic field with the spin magnetic moment of the electron. The paramagnetic susceptibility of a Fermi liquid has been calculated by Landau.[2] In a metal, however, one cannot separate the paramagnetic part of the susceptibility from the diamagnetic part. At the same time the latter, as we have already said, is due to all of the electrons, and not just to those near the Fermi surface, and therefore cannot be expressed in terms of the characteristics of the spectrum. Owing to this we shall concern ourselves here only with the effect of the spin susceptibility on the quantum oscillations of the thermodynamic quantities.

Let us find how the Green's function (15) changes its form when we include in the Hamiltonian (7) the additional term

$$-\beta\int \psi^+(\mathbf{r})(\sigma\mathbf{H})\psi(\mathbf{r})\, d^3\mathbf{r}.$$

To do this we again consider the derivative $\partial\Sigma_{\alpha\beta}(\mathbf{r}, \mathbf{r}'; \epsilon)/\partial H$. Using the results obtained earlier, we get instead of Eq. (9)

$$\partial\Sigma_{\alpha\beta}(\mathbf{r}, \mathbf{r}'; \varepsilon)/\partial H = -(ie/2c)(x - x')(y + y')\,\Sigma_{\alpha\beta}(\mathbf{r}, \mathbf{r}'; \varepsilon)$$
$$+ \frac{i}{2\pi}\beta\int d\omega\int d^3\mathbf{r}_1 d^3\mathbf{r}_2 d^3\mathbf{l}\,\Gamma_{\alpha\rho,\,\tau\beta}(\mathbf{r}, \varepsilon; \mathbf{r}_1, \omega; \mathbf{r}_2, \omega; \mathbf{r}', \varepsilon)$$
$$\times G_{\lambda\rho}(\mathbf{l}, \mathbf{r}_1; \omega)\, G_{\tau\chi}(\mathbf{r}_2, \mathbf{l}; \omega)\,(\sigma\mathbf{n})_{\chi\lambda} \quad (31)$$

(n is a vector in the direction of the field). It is not hard to verify that in the last term we can set H = 0 from the very beginning. Substituting here the expression (19), we get

$$\frac{1}{(2\pi)^6}\int e^{i\mathbf{p}_1(\mathbf{r}-\mathbf{r}')}d^3\mathbf{p}_1\frac{i}{2\pi}\int d\omega d^3\mathbf{p}_2\Gamma^k_{\alpha\rho,\tau\beta}(\mathbf{p}_1, \varepsilon; \mathbf{p}_2, \omega; \mathbf{p}_2, \omega; \mathbf{p}_1, \varepsilon)$$
$$\times G^2(\mathbf{p}_2, \omega)\,(\sigma\mathbf{n})_{\rho\tau}.$$

Because the free functions are isotropic and because for momenta $\mathbf{p}_1$ close to the Fermi surface the integral in brackets (sic) is a slowly varying function of $|\mathbf{p}_1|$, we can write the second term in the right member of Eq. (31) in the form

$$A\,(\sigma\mathbf{n})_{\alpha\beta}\delta(\mathbf{r} - \mathbf{r}'), \quad (32)$$

where A is a constant. It follows from Eqs. (31) and (32) that as before the Green's function is of the form (15), but the energy of the excitations is compounded of the orbital part $\omega^*(n + 1/2) + p_Z^2/2m^*$ and the spin part $-\xi\sigma\cdot\mathbf{H}$, where ξ is the "effective" magnetic moment of the electron spin: $\xi = a(\beta + A)$. The connection between ξ and the magnitude of the paramagnetic susceptibility is given by relations obtained by Landau.[2]

We can now proceed to the calculation of $\partial N/\partial\mu$. Here the calculations are of a nature quite analogous to that of those done in the preceding section. We first concern ourselves with the calculation of the first term in the formula (24):

$$\frac{i}{2\pi}\int d\omega d^3\mathbf{l}\ \mathrm{Sp}\,\hat{G}(\mathbf{r}, \mathbf{l}; \omega)\,\hat{G}(\mathbf{l}, \mathbf{r}; \omega)$$
$$= \frac{i}{(2\pi)^3}\left(\frac{eH}{c}\right)^2 a^2\sum_n\iint d\omega dp_z\left[(\omega - E_n)^2 + \frac{1}{4}\xi^2H^2\right]$$
$$\times [(\omega - E_n + \xi H/2 + i\delta)(\omega - E_n - \xi H/2 + i\delta)$$
$$\times (\omega - E_n' - \xi H/2 + i\delta)(\omega - E_n' + \xi H/2 + i\delta)]^{-1}.$$

As before, we first integrate this expression over

$d\omega$. Here we note that the integral vanishes both in the case in which all of the poles of the integrand are on one side of the axis of ω, and also in the case in which there are two poles above the axis and two below. The integral is different from zero only in the region of $E_n = \pm\xi H/2$. Defining the integral in a suitable way as a k-limit, we finally get for the first term

$$\frac{1}{4\pi^2}\sqrt{2m^*}\left(\frac{eH}{c}\right)a^2\sum_n\left\{[p_0^2/2m^* - \omega^*(n+1/2) - \xi H/2]^{-1/2} + \left[\frac{p_0^2}{2m^*} - \omega^*\left(n+\frac{1}{2}\right) + \xi H/2\right]^{-1/2}\right\}, \quad (33)$$

that is, the only difference from the formulas written before is that the single sum over n is replaced by the average of two terms with $p_0^2/2m^* \to p_0^2/2m^* \pm \xi H/2$.

Let us now recall that in the second term of Eq. (24) the singularity (33) can be separated out in three ways, as shown in Fig. 4 b. Since the terms involving the magnetic field are small, we can set the field equal to zero in all quantities except the two Green's functions marked with the dashed line in the diagram. In the isotropic model the integral is

$$\int \Gamma_{\alpha\rho,\,\rho\beta}(p_1,p_2;\,p_2,\,p_1)G(p_2)\,G(p_2)d^4p_2 = \frac{1}{2}\delta_{\alpha\beta}\int \Gamma_{\gamma\rho,\,\rho\gamma}(p_1,\,p_2;\,p_2,p_1)\,G^2(p_2)\,d^4p_2.$$

When this fact is used it is not hard to show that the sum of all of the loops of Fig. 4 b gives a singularity of the form (33) multiplied by the renormalization factors (29). Thus instead of Eq. (30) we get as the final result for $\partial N/\partial\mu$

$$\frac{\partial N}{\partial\mu} = \frac{\sqrt{\omega^*}}{8\pi^2\sqrt{2m^*}}\left(\frac{dp_0^2}{d\mu}\right)^2\left\{\zeta\left(\frac{1}{2},\,\frac{\Delta}{\omega^*}+\frac{\xi H}{2\omega^*}\right)+\zeta\left(\frac{1}{2},\,\frac{\Delta}{\omega^*}-\frac{\xi H}{2\omega^*}\right)\right\},$$

and for the oscillating part of the thermodynamic potential

$$\sigma\Omega_{osc} = -\frac{2m^{*2}\omega^{*5/2}}{3\pi^2\sqrt{2m^*}}\left\{\zeta\left(-\frac{3}{2},\,\frac{\Delta+\xi H/2}{\omega^*}\right) + \zeta\left(-\frac{3}{2},\,\frac{\Delta-\xi H/2}{\omega^*}\right)\right\}. \quad (34)$$

The oscillating parts of all the thermodynamic quantities are usually stated in the form of series of harmonics.[1] For example, by going from Eq. (34) to the oscillating part of the free energy, we get for the magnetic moment the expression

$$M_{osc} = -\frac{m^{*3/2}(\beta^* H)^{3/2}\mu}{2\pi^3\hbar^3 H}\sum_1^\infty\frac{(-1)^r}{r^{3/2}}\cos\left(\frac{\xi}{\beta^*}\pi r\right) \times \sin\left(\pi r\frac{cp_0^2}{e\hbar H}-\frac{\pi}{4}\right),$$

where $\beta^* = e\hbar/m^*c$, and ξ can be connected with the paramagnetic susceptibility χ and with the coefficient γ in the linear term in the heat capacity per unit volume $c = \gamma T$, if we use the results obtained in Landau's paper[2]:

$$\xi/\beta^* = 4\pi^2\chi/3\beta\beta^*\gamma. \quad (36)$$

In this last formula $\beta = e\hbar/mc$ is the magnetic moment of the free electron. Although the factor with the cosine has indeed been written previously, it was then assumed that the spin energy of the electron was equal to $-\beta\sigma\cdot\mathbf{H}$; that is, the Fermi-liquid properties were not taken into account, and the result of this was that the argument of the cosine was written $\pi rm^*/m$.

We also mention that according to Landau's results[2]

$$\frac{1}{\chi} = \beta^{-2}\left(\bar{\zeta}+\frac{4\pi^2}{3\gamma}\right), \quad \bar{\zeta} = \frac{1}{4\pi}\int\zeta(\Omega)\,d\Omega.$$

$\bar{\zeta}$ is the integral of the spin part of the function f[2] of the Fermi liquid:

$$f_{\sigma\sigma'}(\mathbf{p},\,\mathbf{p}') = f(\mathbf{p},\,\mathbf{p}') + \zeta(\mathbf{p},\,\mathbf{p}')\,(\sigma\sigma')$$

(all of the notations are taken from the paper of Abrikosov and Khalatnikov[11]). Therefore from this one could get an estimate of the size of the Fermi-liquid effects in a metal. In particular, the sign of $\bar{\zeta}$ is very interesting, since for $\zeta > 0$ there could exist in a metal spin oscillations of the type of zeroth sound.[2,11]

In conclusion the writers express their gratitude to Academician L. D. Landau for a discussion of the results of this work and for his comments.

[1] I. M. Lifshitz and A. M. Kosevich, JETP **29**, 743 (1955), Soviet Phys. JETP **2**, 646 (1956).

[2] L. D. Landau, JETP **30**, 1058 (1956), Soviet Phys. JETP **3**, 920 (1956).

[3] L. D. Landau, JETP **35**, 97 (1958), Soviet Phys. JETP **8**, 70 (1959).

[4] J. M. Luttinger, Phys. Rev. **121**, 1251 (1961).

[5] G. E. Zil'berman, JETP **32**, 296 (1957), Soviet Phys. JETP **5**, 208 (1957).

[6] L. D. Landau and E. M. Lifshitz, (Quantum Mechanics), Pergamon, 1948.

[7] Yu. B. Rumer, JETP **18**, 1081 (1948).

[8] E. Sondheimer and A. Wilson, Proc. Roy. Soc. **A210**, 173 (1951).

[9] L. P. Pitaevskii, JETP **37**, 1794 (1959), Soviet Phys. JETP **10**, 1267 (1960).

[10] Higher Transcendental Functions, Bateman Ms Project, New York, 1953, Vol. 1, p. 24.

[11] A. A. Abrikosov and I. M. Khalatnikov, UFN **66**, 177 (1958), Soviet Physics Uspekhi **1**, 68 (1959).

Translated by W. H. Furry
267

EFFECT OF THE PION MASS DIFFERENCE ON THE $K_{\pi 3}$ DECAY PROBABILITIES

V. B. MANDEL'TSVEĬG and V. V. SOLOV'EV

Submitted to JETP editor May 31, 1961

J. Exptl. Theoret. Phys. (U.S.S.R.) 41, 1606-1608 (November, 1961)

We calculate the effect of the π-meson mass difference on the relations between the probabilities for the different $K_{\pi 3}$ decays. It is found that when the $\pi^{\pm}$ is replaced by the π^0, the phase volume is increased by about 12%. The ratios of the statistical weights are given for these decays.

IT is known[1-4] that the four τ decays of the K mesons*

$$K^+ \to \pi^+ + \pi^- + \pi^+ \quad (\tau_0),$$
$$K_2^0 \to \pi^0 + \pi^- + \pi^+ \quad (\tau_1),$$
$$K^+ \to \pi^0 + \pi^0 + \pi^+ \quad (\tau_2),$$
$$K_2^0 \to \pi^0 + \pi^0 + \pi^0 \quad (\tau_3)$$

satisfy the isotopic-spin relations

$$W(\tau_2)/W(\tau_0) = \tfrac{1}{4}, \tag{1}$$
$$W(\tau_3)/W(\tau_1) = \tfrac{3}{2}, \tag{2}$$
$$W(K_2^0 \to 3\pi)/W(K^+ \to 3\pi) = 1. \tag{3}$$

Relations (1) and (2) are easily obtained if one assumes that the π mesons produced are in the pure T = 1 state. For this it is sufficient to assume the selection rule $\Delta T \leq {}^3/_2$ (we assume the π-meson state to be completely symmetric, since the energies liberated in the τ decays are small). As for (3), it is a direct consequence of the $\Delta T = {}^1/_2$ rule; therefore an experimental measurement of this ratio is a verification of this rule.

The $\Delta T = {}^1/_2$ rule is not exact, as follows, for instance, from the existence of the $K^+ \to \pi^0 + \pi^+$ decay, which this rule would forbid. Nevertheless, we shall consider the relations obtained with its aid strictly correct, and shall calculate the effect of the mass difference between the $\pi^{\pm}$ and the π^0 only on the volume in phase space. Because of the low energies liberated in the $K_{\pi 3}$ decays, this will have a relatively large effect.

The matrix element for a $K_{\pi 3}$ decay is

$$M_\tau = f_\tau \varphi_K \varphi_1 \varphi_2 \varphi_3,$$

where φ_K is the K-meson wave function, φ_1, φ_2, and φ_3 are the meson wave functions, and f_τ is a function depending on the energies of the π's and including the effect of isotopic spin on the branching ratios for the possible reactions. (Since the energy liberated is small, one may consider f_τ a constant.) For the decay probability we obtain

$$W(\tau) = \frac{f_\tau^2}{(2\pi)^5 2m_K} \int \frac{d\mathbf{k}_1 d\mathbf{k}_2 d\mathbf{k}_3}{2E_1 2E_2 2E_3} \delta^4 (k_1 + k_2 + k_3 - k).$$

By simple algebraic operations, this expression can be transformed to the form

$$W(\tau) = \frac{f_\tau^2}{64\pi^3} \frac{\sqrt{\beta}\, t_m^2}{m_K} \int_0^1 \sqrt{y(1-y)} \left\{\frac{1+\alpha y}{1-\beta\alpha y}\right\}^{1/2};$$

$$\beta = \left(\frac{m_K + \mu}{m_K - \mu}\right)^2 - 1, \quad \alpha = \frac{t_m}{2\mu},$$

$$t_m = (m_K + 2m - \mu)(m_K - 2m - \mu)/2m_K,$$

where t_m is the maximum kinetic energy of a π meson (μ is the mass of the unpaired meson, while m is the mass of the paired mesons). The integral can be calculated by expanding $[(1 + \alpha y)/(1 - \beta\alpha y)]^{1/2}$ as a power series in α (note that $\alpha \approx {}^1/_6$). We have carried this expansion out to terms in α^3. (Carrying it out to terms in α^4 would give a correction in the fourth decimal place.)

The final form for the probability then becomes

$$W(\tau) = \frac{f_\tau^2}{512\pi^2} \frac{\sqrt{4\gamma - 1}}{m_K} t_m^2 \{1 + \gamma\alpha + \tfrac{5}{8}\gamma(3\gamma - 1)\alpha^2 + \tfrac{7}{16}(10\gamma^2 - 6\gamma + 1)\alpha^3\},$$

$$\gamma = \tfrac{1}{4}(\beta + 1).$$

The following values were used for the masses[5] (given in Mev):

$$m_{\pi^\pm} = 139.59 \pm 0.05, \quad m_{K^+} = 493.9 \pm 0.2,$$
$$m_{\pi^0} = 135.00 \pm 0.05, \quad m_{K^0} = 497.8 \pm 0.6.$$

The uncertainties in the masses will lead to errors no greater than 0.002 in the ratios of the volumes in phase space. We give below the results of the calculations for $W(\tau_i)/W(\tau_k)$ (the numbers are the ratio of the statistical weight of the reaction designated in the column to the statistical weight of the reaction designated in the row):

*The τ_0 and τ_2 decays are often denoted by τ and τ'.

	τ_0	τ_1	τ_2	τ_3
τ_0	1	0.822	0.803	0.675
τ_1	1.217	1	0.977	0.822
τ_2	1.245	1.024	1	0.841
τ_3	1.481	1.217	1.189	1

It is easily seen that replacing a $\pi^{\pm}$ by the π^0 meson increases the volume in phase space by about 12%. Thus corrections for the mass differences change the decay ratios for $K_{\pi 3}$ decays in the following way:

$$W(\tau_2)/W(\tau_0) = \tfrac{1}{4} \to 0.311^*,$$

$$W(\tau_1)/W(\tau_3) = \tfrac{2}{3} \to 0.547,$$

$$W(K_2^0 \to 3\pi)/W(K^+ \to 3\pi) = 1 \to 1.311.$$

The relations between the decay probabilities were calculated also for the case in which the energies do not appear in the denominator of the integrand (noninvariant volume in phase space), i.e., for

$$W_\tau = g_\tau \int d\mathbf{k}_1 d\mathbf{k}_2 d\mathbf{k}_3 \delta^4(k_1 + k_2 + k_3 - k).$$

The calculations are carried through similarly as above, and the results obtained are very close to those for the invariant volume in phase space (as might have been expected in view of the low energy liberated). For this case one obtains

$$\rho(\tau_0) : \rho(\tau_1) : \rho(\tau_2) : \rho(\tau_3) = 1 : 1.248 : 1.240 : 1.526,$$

where ρ is the statistical weight.

The authors express their deep gratitude to L. B. Okun' for suggesting the problem and for directing the work, and to I. Yu. Kobzarev for valuable advice.

*Dalitz' calculation of this ratio[2] gave 0.325.

[1] R. H. Dalitz, Proc. Phys. Soc. (London) **A66**, 710 (1953).

[2] R. H. Dalitz, Proc. Phys. Soc. (London) **A69**, 527 (1956).

[3] L. B. Okun', Usp. Fiz. Nauk **61**, 535 (1957).

[4] V. B. Berestetskii, Dokl. Akad. Nauk SSSR **92**, 519 (1953).

[5] Proc. of the 1960 Ann. Int. Conf. on High Energy Phys. of Rochester, Univ. of Rochester, 1960, p. 878.

Translated by E. J. Saletan
268

THE EQUATION OF STATE AT ULTRAHIGH DENSITIES AND ITS RELATIVISTIC LIMITATIONS

Ya. B. ZEL'DOVICH

Submitted to JETP editor May 31, 1961

J. Exptl. Theoret. Phys. (U.S.S.R.) 41, 1609-1615 (November, 1961)

The most rigid equation of state compatible with the requirements of relativity theory is $p = \epsilon \sim n^2$, $D \to c$, where p is the pressure, ϵ the volume density of energy, n the density of baryons, D the speed of sound, and c the speed of light. This differs from the previously proposed asymptotic behavior $3p = \epsilon \sim n^{4/3}$, $D \to 3^{-1/2}c$. The case of interaction of the baryons through a vector field is considered and it is shown (both by considering the interaction of pairs of baryons and by using the stress tensor of the field) how in this case the equation $p = \epsilon \sim n^2$ is realized and how the transition to the equation $3p = \epsilon$ occurs as the mass of the field quanta goes to zero.

1. INTRODUCTION

IN connection with the problem of the last stage of the evolution of heavy stars—gravitational collapse—there is now intensified discussion of the question of the equation of state of matter at ultrahigh densities.[1-4] Attempts are being made to perfect the idea of a neutron condensation, which was first put forward by Landau,[5] on one hand by taking into account the various elementary particles, and on the other by taking into account the nuclear interaction between nucleons (and other baryons). Here use is sometimes made of the approximation of a rigid repulsion of nucleons, which leads to an infinite pressure at a finite density. It is obvious that near such a state the speed of sound D would exceed the speed of light, $D > c$. The rigid repulsion is in obvious contradiction with the theory of relativity, and its use in discussing the asymptotic behavior of the equation of state makes no sense, even in case the rigid-repulsion model does give satisfactory numerical agreement for the usual range of nuclear densities. What are the actual limitations imposed by relativity on the law of repulsion and on the asymptotic behavior of the equation of state?

It is generally assumed[6] that already from the special theory of relativity there follows the inequality $3p \leq \epsilon$, where p is the pressure and ϵ the energy density, and ϵ includes the rest masses of the particles. The grounds advanced for this are that for the electromagnetic field $3p = \epsilon$ and for free noninteracting particles with non-vanishing rest masses $3p < \epsilon$. We shall construct below an example of a relativistically invariant theory in which $3p > \epsilon$ is possible and in the limit $p = \epsilon$. An example of this kind is a classical vector field with a mass, interacting with stationary classical point charges.

In Sec. 2 the field equations are formulated and the interaction energy of the charges is found as a function of the density of the charges and of the pressure; then in the limit of large density $p \to \epsilon$ (Sec. 3). The same result is obtained in a more formal way by considering the stress tensor T_{ik} of the vector field (Sec. 4).

If the energy density ϵ has a power-law dependence on the charge density n (the density of the particles that are sources of the field), $\epsilon = an^\nu$, then the energy and pressure of one particle are

$$\varepsilon_1 = An^{\nu-1}, \qquad p = -d\varepsilon_1/d(1/n) = (\nu-1)an^\nu = (\nu-1)\varepsilon.$$

Thus the asymptotic behavior $3p = \epsilon$ corresponds to $\nu = 4/3$, whereas our asymptotic behavior $p = \epsilon$ corresponds to $\nu = 2$, $p = \epsilon = an^2$.

Finally, the speed of sound is given by the formula (cf. [7])

$$D^2 = c^2 \partial p/\partial \varepsilon,$$

so that for $3p = \epsilon$ we have $D = 3^{-1/2}c$, whereas our asymptotic behavior gives in the limit $D = c$; from this it can be seen that the equation of state obtained from the model of the vector field is the most rigid one possible. A higher ratio $p/\epsilon > 1$ and a higher power $\nu > 2$ are impossible in principle, since a relativistic theory cannot give $D > c$.

When the quantity that plays the role of the mass of the quanta of the vector field goes to zero one gets the well known result which holds for the electromagnetic field, $3p \leq \epsilon$ (Sec. 5).

The main purpose of the present work is to bring out the possibility in principle of a violation of the previously proposed relation $3p \leq \epsilon$.

The choice of the vector field with a mass has been influenced by a paper by Kobzarev and Okun',[8] which develops the theory of the interaction of baryons through a field of heavy neutral vector mesons (vectons). If this theory is confirmed, then at ultrahigh densities (exceeding by a large factor the density of nucleons in nuclei) the pressure will be mainly due to the repulsion of the baryons ($p = an^2$) and not to their Fermi energy ($p_F = Bn^{4/3}$) (Sec. 6). The question of which baryons, and how many kinds of baryons, are to be regarded as elementary particles[9] will then have no effect on the asymptotic behavior of the equation of state.

2. THE FIELD EQUATIONS

Let us take the Lagrangian density in the form

$$L = -\frac{1}{16\pi} F_{ik}^2 - \frac{1}{8\pi}\mu^2 A_k^2, \qquad S_f = i\int L d^4x, \tag{2.1}$$

$$\partial A_k/\partial x_k = 0, \qquad F_{ik} = \partial A_k/\partial x_i - \partial A_i/\partial x_k. \tag{2.2}$$

We everywhere set $c = 1$; the metric used is $A_k^2 = A^2 + A_4^2$, $A_4 = iA_0 = i\varphi$. In the quantum theory the mass m of the field quanta is expressed in terms of the constant μ: $m = \mu\hbar$.

We must add to S_f the terms corresponding to the motion of the charges and their interaction with the field:

$$S_p = -M\int ds, \qquad S_i = g\int A_k\, dx_k, \tag{2.3}$$

where M is the mass of the charges (baryons) and g is their charge.

Varying A, we get the field equations

$$\frac{\partial F_{ik}}{\partial x_k} = -\sum_k \frac{\partial^2 A_i}{\partial x_k^2} = -\mu^2 A_i + 4\pi j_i, \tag{2.4}$$

and varying the trajectories of the particles we get the equations of motion of the particles. These latter do not differ from the equations of motion of particles of charge g in an electromagnetic field F_{ik}.

For a point charge at rest at the origin j_k is

$$j_4 = i\delta(x), \qquad j = 0$$

and Eq. (2.4) has the solution

$$\varphi = ge^{-\mu r}/r, \qquad A = 0. \tag{2.5}$$

3. THE INTERACTION OF THE CHARGES AND THE EQUATION OF STATE

Two charges at rest repel each other with the force

$$|f_{12}| = -g^2 \frac{d}{dr_{12}}(e^{-\mu r_{12}}/r_{12}). \tag{3.1}$$

The interaction energy of the two charges is

$$g\varphi_{r_1}(r_2) = g^2 e^{\mu r_{12}}/r_{12}. \tag{3.2}$$

Here the action of its own potential on a given charge is obviously included in the mass M of the charge.

In classical theory with quadratic L and linear equations there is no limitation on the application of the principle of superposition. Let us consider a system composed of a large number of charges. Its total energy is

$$E = \sum M_r + \frac{g^2}{2}\sum_{s\neq t}\frac{1}{r_{st}} e^{-\mu r_{st}}. \tag{3.3}$$

If the average density of charges is n and we assume that $n^{-1/3} < \mu^{-1}$, we find as the energy of one charge

$$E_1 = M + \frac{g^2 n}{2}\int e^{-\mu r}\frac{dv}{r} = M + \frac{2\pi g^2 n}{\mu^2}. \tag{3.4}$$

From this we find the energy density

$$\varepsilon = nE_1 = Mn + 2\pi g^2 n^2/\mu^2 \tag{3.5}$$

and the pressure

$$p = -\partial E_1/\partial(1/n) = 2\pi g^2 n^2/\mu^2. \tag{3.6}$$

It can be seen from Eqs. (5) and (6) that in the limit of large n we indeed have $p \to \epsilon$.

The pressure could also have been found from the virial theorem

$$\begin{aligned} 3pV &= \sum r_s f_s = \sum_{s\neq t} r_s f_{st} = \frac{1}{2}\sum_{s\neq t} r_{st} f_{st} \\ &= \frac{g^2}{2}\sum_{s\neq t} r_{st} e^{-\mu r_{st}}(1+\mu r_{st}) r_{st}^{-2} \\ &= nV\frac{g^2 n}{2}\int \frac{e^{-\mu r}}{r}(1+\mu r)\, dv = 6\pi g^2 n^2 V/\mu^2; \end{aligned} \tag{3.7}$$

the result naturally agrees with Eq. (3.6).

The increase of E_1 with the density n and the law $p \sim n^2$ are due not to the decrease of the distance to the nearest neighbor, but to the increase of the number of neighbors at a given constant distance $\sim 1/\mu$, which plays the most important part in the integrals (3.4) and (3.7).

Let us assume that the mass of the vector meson is much smaller than that of the baryon,

and that the coupling constant is in a definite range of values:

$$m < M, \quad \hbar c\,(m/M)^2 < g^2 < \hbar c\,(M/m). \tag{3.8}$$

Then it is easy to verify that the state in which we are interested, with $3p > \epsilon$, is attained at a density at which both the characteristic length $1/\mu$ and the distance to the nearest neighbor $n^{-1/3}$ are larger than the classical baryon radius g^2/Mc^2 and larger than the baryon Compton wavelength $\hbar/Mc$.*

Consequently the conclusion that states with $3p > \epsilon$ are possible is not due to the extrapolation of the theory to a region in which there are doubts as to its applicability (concerning the potential in the region in which we are interested see the end of Section 6). The interaction law (3.1), (3.2), which has led to the equation of state (3.5), (3.6), was not chosen arbitrarily, but comes from the relativistically invariant field theory with the Lagrangian (2.1).

We remind the reader that the purpose of this paper is to settle the question of the logical possibility of the inequality $3p > \epsilon$ in a relativistic theory; the question of the actual existence of the neutral vector field remains open.

4. THE STRESS TENSOR

The stress tensor, whose diagonal components are $T_{44} = -\epsilon$, $T_{xx} = T_{yy} = T_{zz} = p$ ([6], p. 108), is obtained from L by the formula

$$T_{ik} = L\delta_{ik} - \frac{\partial A_l}{\partial x_i}\,\frac{\partial L}{\partial\,(\partial A_l/\partial x_k)}\,. \tag{4.1}$$

As in the case of the electromagnetic field, to symmetrize this tensor we subtract from it the quantity

$$\frac{1}{4\pi}\,\frac{\partial}{\partial x_l}\,(A_i F_{kl}).$$

According to the field equations (3.4), in the absence of charges (cf. [6], p. 103)

$$\frac{\partial}{\partial x_l}\,(A_i F_{kl}) = F_{kl}\frac{\partial A_i}{\partial x_l} + A_i\frac{\partial F_{kl}}{\partial x_l} = F_{kl}\frac{\partial A_i}{\partial x_l} - \mu^2 A_i A_k. \tag{4.2}$$

From this we finally get the following expressions:

$$\varepsilon = -T_{44} = [\mathbf{E}^2 + \mathbf{H}^2 + \mu^2\,(\mathbf{A}^2 + \varphi^2)/8\pi]/8\pi, \tag{4.3}$$

$$3p = T_{xx} + T_{yy} + T_{zz} = (\mathbf{E}^2 + \mathbf{H}^2)/8\pi + \mu^2\,(3\varphi^2 - \mathbf{A}^2)/8\pi. \tag{4.4}$$

For a system of stationary charges distributed with uniform density n the field equations give

$$-\Delta\varphi = -\mu^2\varphi + 4\pi g n, \tag{4.5}$$

from which we have for a system of large dimensions ($|\Delta\varphi| \ll \mu^2\varphi$)

$$\varphi = 4\pi g n/\mu^2, \qquad \varepsilon = 2\pi g^2 n^2/\mu^2, \qquad 3p = 6\pi g^2 n^2/\mu^2. \tag{4.6}$$

Adding to the field energy density the energy density coming from the rest mass of the charges, $\epsilon_p = Mn$ (the charges do not contribute to the pressure), we get again the expressions (3.5) and (3.6) and the result

$$p \to \varepsilon, \quad 3p > \varepsilon \quad \text{for} \quad n > \mu^2 M/4\pi g^2, \varphi > M.$$

In (4.5) the system of point charges with the density $\Sigma g\delta(\mathbf{r} - \mathbf{r}_i)$ has been replaced by a continuous and uniform charge density. We have thus lost the singularities $\varphi \sim (\mathbf{r} - \mathbf{r}_i)^{-1}$, $|\mathbf{E}| \sim (\mathbf{r} - \mathbf{r}_i)^{-2}$ near the individual charges. These singularities should indeed not be taken into account, since the corresponding energy density has been included in the experimental rest mass of the particles (charges), and the contribution to the pressure is compensated by internal forces, which in classical theory secure the existence of elementary charges.

Let us consider the field in a region free from charges. From (4.3) and (4.4) we find

$$\varepsilon - 3p = \mu^2\,(\mathbf{A}^2 - \varphi^2)/4\pi. \tag{4.7}$$

We try to find the potentials in the form of a combination of plane waves

$$\mathbf{A}_k\,(x, t) = \Sigma \mathbf{a}_k e^{ikx - i\omega t}, \qquad \varphi_k\,(x, t) = \Sigma\varphi_k e^{ikx - i\omega t}. \tag{4.8}$$

From the field equations we get the relation

$$\omega^2 = k^2 + \mu^2, \tag{4.9}$$

and from the supplementary condition (2.2) the relation

$$\omega_k\varphi_k = \mathbf{a}_k\mathbf{k}, \tag{4.10}$$

from which it follows that $|\varphi_k| < |\mathbf{a}_k|$, and consequently, according to Eq. (4.7), $\epsilon > 3p$ for such a field.

Thus the free vector field with a mass actually gives $\epsilon > 3p$, in accordance with the picture of heavy field quanta with spin 1, nonvanishing rest mass, and speed of motion less than c. But the relation $\epsilon > 3p$ can be violated for a field of charges. What is the cause of this difference?

It must be remembered that the Lagrangian of the vector field involves not three (the number $2s + 1$ of components of the spin $s = 1$), but four components of the potential, so that the content of the theory is not exhausted by the concept of heavy particles with spin 1. The fourth component just describes the static repulsion. Electrodynamics also is not exhaustively described by the trans-

*The inequalities (3.8) at the same time assure the validity of the condition $1/\mu > n^{-1/3}$, which is necessary for the replacement of the sum (3.3) by the integral (3.4).

verse field quanta, but has also the longitudinal Coulomb field. In this connection we may remark that the present theory of the weak interaction can be formulated as the interaction of the fermion current with a vector meson field. Furthermore, the theory includes 0—0 transitions in β decay, which could not be understood from the point of view of the emission by the nucleus of a meson with spin 1 and subsequent decay of this meson into e and ν. Here also the fourth component of the vector meson field comes into action.[10] In electrodynamics $\epsilon \to 3p$ for $\epsilon \to \infty$, both for the free quanta and for the Coulomb interaction. In the theory we are now considering, with the term $\mu^2 A^2$ in L for the free quanta, we naturally have $\epsilon > 3p$, but for the analog of the Coulomb interaction $\epsilon < 3p$; we only have to remember that we cannot confine ourselves to the consideration of the free vector-field quanta alone.

5. THE TRANSITION TO ELECTRODYNAMICS

The transition to the case $\mu = 0$, i. e., to ordinary electrodynamics, is not entirely trivial, since the expressions for ϵ and p, Eqs. (3.4)—(3.6) have the quantity μ^2 in the denominator. The solution of the paradox is that these formulas are valid only for $\mu > 1/R$, where R is the dimensions of the system, and that the equations change their form before μ reaches zero.

The physical peculiarity of the system in question is that the system is not neutral; there is a charge density, which is everywhere of the same sign. With the Coulomb interaction ($\mu = 0$) the energy of such a system cannot be written as $V\epsilon(n)$. In an infinite system with a finite charge density the energy density diverges in the Coulomb case. Let us consider a finite system of charges. In such a system we must prescribe a pressure to retain the charges. According to the virial theorem we get [the notation is as in Eq. (3.7)]

$$3\int p\,dv = 3\bar{p}V = \sum_s \mathbf{r}_s \mathbf{f}_s = \frac{1}{2}\sum \mathbf{r}_{st}\mathbf{f}_{st}. \qquad (5.1)$$

But for the Coulomb potential

$$\mathbf{r}_{st}\mathbf{f}_{st} = e^2/r_{st} = u_{st}, \qquad (5.2)$$

so that

$$3\int p\,dV = 3\bar{p}V = E_{es} = \bar{\varepsilon}_{es}V, \qquad 3\bar{p} = \bar{\varepsilon}_{es}, \qquad (5.3)$$

where the index es denotes the electrostatic part of the energy (the energy density). Recalling also the contribution to ϵ from the rest masses of the charges, we get for the Coulomb field $3\bar{p} < \bar{\epsilon}$, in agreement with[6].

In the argument that led to Eq. (4.6) we cannot let μ go to zero, since Eq. (4.5) for the potential has the solution (4.6) only so long as $|\Delta\varphi| \ll |\mu^2\varphi|$. In order of magnitude, $\Delta\varphi = -\varphi/R^2$, where R is the dimensions of the system. For $\mu < 1/R$, the solution of Eq. (4.5) will be of the form

$$\varphi \sim R^2 gn, \qquad \varepsilon_\varphi \sim \mu^2\varphi^2 \sim \mu^2 R^4 g^2 n^2, \qquad (5.4)$$

where ϵ_φ is the contribution to ϵ from the term $\mu^2\varphi^2$ [cf. Eq. (4.3)]; ϵ_φ goes to zero as it should for $\mu \to 0$, but only after μ has become smaller than 1/R. On the other hand, for $\mu < 1/R$ the contribution to ϵ from $\mathbf{E}^2$ becomes finite, whereas for $\mu \gg 1/R$ this quantity was proportional to the surface, and not to the volume of the system. The term in $\mathbf{E}^2$ occurs with the same coefficient in ϵ and 3p in the forms (4.3) and (4.4), so that again for the field (electrodynamical) part $\epsilon = 3p$.

6. ON THE PRACTICALITY OF THE STATIONARY-CHARGE MODEL

Is the model we have considered, for which we can have $\epsilon < 3p$, a mechanically possible model, a stable one? What could be expected under the actual conditions of an ultradense gas, with quantum phenomena taken into account?

According to Eq. (3.6) the pressure is proportional to n^2, and consequently $\partial p/\partial n > 0$. This sign assures the stability of the system against macroscopic fluctuations of the density n for a prescribed $\bar{n}$ in the volume. On the microscopic scale, according to the field equations (2.4), at the point where the i-th particle is located the potential $\varphi_{(i)}$ produced by all the other particles satisfies the equation

$$\Delta\varphi_{(i)} = \mu^2\varphi_{(i)}, \qquad (6.1)$$

and since $\varphi_{(i)} > 0$ and grad $\varphi_{(i)} = 0$ by considerations of symmetry, $\varphi_{(i)}$ has a minimum, which corresponds to stable equilibrium of the i-th particle, if this particle is at a site of a regular lattice with all the other sites occupied by the other particles.

As we know from Earnshaw's theorem, in the case of the Coulomb interaction a system of charges does not have a stable configuration: the charges enclosed in a given volume will concentrate themselves on the walls of the volume. This property of the system is changed, however, when Coulomb's law is replaced by the potential $e^{-\mu r}/r$.

According to Kobzarev and Okun',[8] we may take for quantum estimates

$$g^2/\hbar = 1, \qquad m = \hbar\mu = M/2, \tag{6.2}$$

with g assumed the same for all three elementary baryons (n, p, Λ in the scheme of Sakata and Okun'). Then the value of the density at which $3p = \epsilon$ is reached is

$$n_c = \mu^2 M/4\pi g^2 = M^3c^3/16\pi\hbar^3, \tag{6.3}$$

which corresponds to the nearest-neighbor distance

$$r_{c(ik)} = 4\hbar/Mc = 2/\mu = 0{,}8 \text{ fermi} \tag{6.4}$$

The value of n_c is twenty times the nuclear density that corresponds to the known expression $R = 1.2A^{1/3}$ f for the radius of a heavy nucleus. At $n \approx n_c$, however, we can still not expect that the formulas will apply, because the density is not large enough for us to regard the nucleons as "crushed" and quit giving separate consideration to other baryons and π and K mesons.

The law

$$\varepsilon = 2aN + aN^2, \qquad p = aN^2;$$

$$N = n/n_c, \qquad a = \tfrac{1}{2} n_c Mc^2 = M^4c^5/100\hbar^3 \tag{6.4}$$

at best applies for $N > 10$, i.e., just in the region which, in Salpeter's opinion,[4] is impossible because of the "incompressibility" of the hard cores of the nucleons.

Let us estimate the quantum corrections. On the assumption of three types of independent particles (cf. [9]) the energy of the free Fermi gas can be approximated by the expression

$$\varepsilon = 2aN\sqrt{1 + 0.2\,N^{2/3}} \to 0.9\,aN^{4/3}, \qquad N \gg 1, \tag{6.5}$$

which replaces the term 2aN in the expression (6.4). The effect of the interaction on the quantum kinetic energy of ultradense matter can be estimated by considering the zero-point energy of the Debye spectrum of the matter with the speed of sound equal to c, the density ϵ/c^2, and 3n independent vibrations per unit volume. We get

$$\varepsilon_d = 1.0\,\hbar c n^{4/3} \approx 0.9\,aN^{4/3}. \tag{6.6}$$

Although in the region in which we are interested, the potential $g\varphi$ exceeds the rest mass of the particles (charges), we may suppose that as usual the vacuum polarization depends on the fields (**E**, **H**), and not on the potentials, since the equations for motion of particles and pair production are not changed by the addition of the term μ^2A^2 to L. In the system considered the fields do not increase with increase of n. Finally, the quantum motion of the baryons, even with speeds $\sim c$, does not change the charge density they produce, which is involved in the equation for φ. Thus on the assumptions of Kobzarev and Okun' about the role of the vector meson field as the basis of the strong interaction we can evidently expect that the asymptotic behavior of the equation of state will be $p = \epsilon \sim n^2$.

The present work was discussed in April 1961 at the School of Physics in Nor-Amberd, organized by the Institute of Physics of the Academy of Sciences of the Armenian S.S.R. I take occasion to express my gratitude to the participants in the discussion, and particularly to G. S. Saakyan, for helpful comments.

[1] D. Landau and E. M. Lifshitz, Statisticheskaya fizika (Statistical Physics), Fizmatgiz, 1959.

[2] V. A. Ambartsurmyan and G. S. Saakyan, Astronom. Zh. **37**, 193 (1960), Soviet Astronomy 4, 187 (1960).

[3] A. G. W. Cameron, Astrophys. J. **130**, 884 (1959).

[4] E. E. Salpeter, Ann. Phys. **11**, 393 (1960).

[5] L. D. Landau, Physik. Z. Sowjetunion 1, 285 (1932).

[6] L. D. Landau and E. M. Lifshitz, Teoriya polya (Field Theory), Fizmatgiz, 1960.

[7] L. D. Landau and E. M. Lifshitz, Mekhanika sploshnykh sred (Mechanics of Continuous Media), Gostekhizdat, 1953.

[8] Yu. I. Kobzarev and L. B. Okun', JETP **41**, 499 (1961), Soviet Phys. JETP **14**, 358 (1962).

[9] Ya. B. Zel'dovich, JETP **37**, 569 (1959), Soviet Phys. JETP **10**, 403 (1960).

[10] N. Byers and R. Peierls, Nuovo cimento **10**, 520 (1958).

Translated by W. H. Furry
269

DISPERSION THEORY OF DIRECT NUCLEAR REACTIONS

I. S. SHAPIRO

Institute for Theoretical and Experimental Physics, Academy of Sciences, U.S.S.R.

Submitted to JETP editor June 3, 1961

J. Exptl. Theoret. Phys. (U.S.S.R.) 41, 1616-1627 (November, 1961)

It is assumed that the main contribution to the amplitude of a direct nuclear process comes from Feynman diagrams whose singularities are closest to the physical region of the variables. Using energy dispersion relations, a singular integral equation is derived which takes account of interaction in the initial and final states. This equation admits of a simple iteration procedure, the first iteration yielding the distorted wave method. It is found that, apart from pole diagrams corresponding to the Butler mechanism and also to exchange stripping and heavy pick-up reactions, more complex diagrams can also give a significant contribution to the direct process mechanism. This result is illustrated by the reactions $Be^9(d, n)B^{10}$, $Be^9(\alpha, t)B^{10}$, and $C^{12}(d, p)C^{13}$. The mechanism of some reactions of the (x, yz) type, and in particular, of reactions in which clusters are knocked out, is considered from the same viewpoint.

1. INTRODUCTION

1. Formulation of the problem. A large amount of experimental data indicates that the direct reactions of the type

$$A + x \to B + y, \tag{1a}$$

$$A + x \to B + y + z \tag{1b}$$

are well described by Feynman diagrams with a small number of internal lines. The simplest pole diagram for deuteron stripping has been considered by Amado,[1] and corresponds to the Butler theory of stripping. The present paper is devoted to a further application of dispersion relations to the theory of direct processes. We shall mainly be concerned with processes of the type (1a). In this section we explain the notation and formulate the basic theorems of our work.

2. Kinematical relations. Reaction (1a) is characterized by two independent kinematic variables. These can be chosen as any two of the following three quantities: a) the kinetic energy E, of the colliding particles, b) the square of the momentum transfer,

$$q^2 = (\mathbf{p}_y - \mathbf{p}_x)^2, \tag{2}$$

where $\mathbf{p}_x$ and $\mathbf{p}_y$ are the momenta of the particles x and y, and c) the square of the sum of the momenta of particles x and y,

$$p^2 = (\mathbf{p}_x + \mathbf{p}_y)^2. \tag{3}$$

In the center-of-mass system of the colliding particles, which will be used throughout the following considerations, these three variables are connected through the simple relation

$$q^2 + p^2 = 4(m_{xA} + m_{yB})E + 4m_{yB}Q. \tag{4}$$

Here m_{xA} and m_{yB} are the reduced masses of particles x and y, and Q is the energy released in the reaction, or its threshold:

$$Q = m_A + m_x - m_B - m_y \tag{5}$$

(we assume throughout $\hbar = c = 1$).

The variables q^2 and E will be chosen most frequently as independent variables. However, in certain cases (exchange stripping, heavy pick-up) it is convenient to use p^2 instead of q^2.

3. Unitarity and analyticity. The unitarity condition

$$SS^+ = 1 \tag{6}$$

for the S matrix written in the form

$$S = 1 + i(2\pi)^4 T; \tag{7}$$

$$T = \mathcal{B} + i\mathcal{A}, \qquad \mathcal{A} = \mathcal{A}^+, \qquad \mathcal{B} = \mathcal{B}^+, \tag{8}$$

leads to the well known formula

$$\mathcal{A}_{if} = \frac{(2\pi)^4}{2}\sum_n T_{in}T^+_{nf}. \tag{9}$$

The summation (integration) in (9) goes over all intermediate states n for which the transitions $i \to n$, $n \to f$ are allowed by the conservation laws. The matrices T and $\mathcal{A}$ are of the form

$$T_{kl}(q^2, E) = M_{kl}(q^2, E)\,\delta_{\lambda_k\lambda_l}\delta^4(l-m), \quad (10)$$

$$\mathcal{A}_{kl}(q^2, E) = A_{kl}(q^2, E)\,\delta_{\lambda_k\lambda_l}\delta^4(l-m). \quad (11)$$

The arguments of the δ functions in (10) and (11) are the momenta and energies of the states k and l; the index λ denotes the set of discrete quantum numbers. The quantity A_{kl} is the absorptive part of the amplitude M_{kl}. The basic postulate of the theory of dispersion relations is the assumption that the amplitudes $M_{kl}(q^2, E)$ are analytic functions of their arguments. The amplitude $M_{kl}(q^2, E)$ has singular points (poles or branch points) and is, therefore, in general a function defined on several sheets. In the theory of dispersion relations one is concerned with only one of these sheets, called the physical sheet. $M_{kl}(z)$ satisfies the relation

$$M_{kl}(Z^*) = M^+_{kl}(Z), \quad (12)$$

where

$$Z = q^2, E.$$

2. THE REACTION A + x → B + y

1. Pole diagrams. The part of the sum (9) which corresponds to transitions f → n in which one particle b of those emitted in the transition i → n is absorbed, can be written in the form

$$A_{if} = 2\pi m_b \delta(p_b^2 - 2m_b E_b) \sum_{s_b} M_{ib} M^+_{bf}. \quad (13)$$

The summation in (13) goes over the spin variable s_b of particle b; m_b, p_b, and E_b are the mass, momentum, and energy of the intermediate particle b. Using (13), it is easy to show that the amplitude M_{if} has a pole at

$$p_b^2 = 2m_b E_b$$

and is near this pole of the form

$$M_{if} = 2m_b \frac{\Sigma s_b M_{ib} M^+_{bf}}{p_b^2 - 2m_b E_b - i\eta}, \qquad \eta \to +0. \quad (14)$$

The pole amplitude (14) is described by a Feynman diagram with a single internal line. Figure 1a shows Amado's diagram corresponding to the Butler theory of stripping. For example, in the reaction (d, p) we have b = n, in the reaction (He^3, p), b = d, etc. The diagram of Fig. 1b corresponds to a pick-up process. For the reaction (p, d) we have b = n, for the reaction (n, α), b = He^3, etc.

Figure 1c shows a diagram corresponding to exchange stripping and heavy pick-up. For example, in the reaction B^{11}(d, n)C^{12} we have

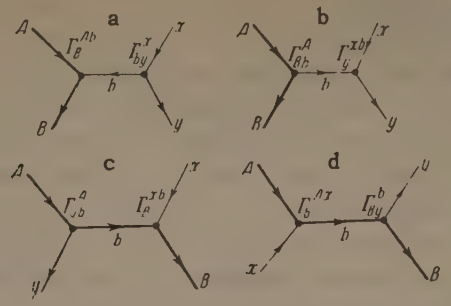

FIG. 1. a – pole diagram for the stripping reaction, b – pole diagram for the pick-up reaction, c – pole diagram for the exchange stripping and heavy pick-up reaction, d – quasi-compound process.

b = B^{10}. The diagram of Fig. 1d is reminiscent of the formation and decay of a compound nucleus, but the actual situation is somewhat more complicated. The point is that the compound nucleus is related to complex poles situated on the nonphysical sheet. The Feynman diagrams corresponding to the compound nucleus on the physical sheet are complicated and their singular points are branch points, not poles. We emphasize in this connection that the poles of the diagrams of Fig. 1 a to d lie on the real axis and correspond to such states of the nuclei b which can not decay under emission of nuclear particles (β decay or radiative transitions are not excluded). In this sense the diagram of Fig. 1d corresponds to a direct reaction which may be called a quasi-compound process. The diagrams of Fig. 1 a to d describe all possible pole terms in the amplitudes of direct reactions of the type (1a). From formula (14), which corresponds to these diagrams, one can immediately derive a number of important features of direct processes of the type (1).

For the ordinary stripping reaction (Fig. 1a) we have according to the energy and momentum conservation laws

$$p_b^2 - 2m_b E_b = q^2 + 2m_b[\mu_{yB}\varepsilon^B_{AB} + (1-\mu_{yB})\varepsilon^x_{yb} + (\mu_{yB} - \mu_{xA})E]. \quad (15)$$

Here

$$\varepsilon^\alpha_{\beta\gamma} = m_\beta + m_\gamma - m_\alpha \quad (16)$$

is the binding energy of particles β and γ in the nucleus α, and

$$\mu_{\alpha\beta} = m_{\alpha\beta}/m_\alpha. \quad (17)$$

If $m_{\alpha\beta} \approx m_\alpha$, formula (15) goes over into the simple relation

$$p_b^2 - 2m_b E_b \approx q^2 + 2m_b \varepsilon^B_{Ab}. \quad (18)$$

It is seen from (15) and (18) that the amplitude

for the stripping reaction has a pole in the variable q^2 for nonphysical values of this variable ($q^2 < 0$). It follows that the amplitude assumes its largest value at the smallest physically admissible value of q^2. This occurs when the particles y are emitted in the same direction as that of the incoming particles x.

In the pick-up reaction (Fig. 1b) the pole also lies in the region of nonphysical values of q^2:

$$q^2 = -2m_b [\mu_{yB}\varepsilon^A_{Bb} + (1-\mu_{yB})\varepsilon^y_{xb} + (\mu_{xA}-\mu_{yB})E]. \quad (19)$$

The best approximation to the pole is given by the smallest physically possible values of q^2. The angular distribution must have a maximum in the forward direction.

In exchange stripping and heavy pick-up reactions (Fig. 1c), the pole occurs at nonphysical values of the variable p^2:

$$p^2 = -2m_b [(1-\mu_{By})\varepsilon^B_{xb} + \mu_{By}\varepsilon^A_{yB} + (\mu_{xA}-\mu_{By})E]. \quad (20)$$

If $m_A, m_B \gg m_x, m_y$, then $\mu_{By} \ll 1$, $\mu_{xA} \approx 1$ and

$$p^2 = -2m_b(E + \varepsilon^B_{xb}). \quad (21)$$

It follows from (20) and (21) that exchange stripping and heavy pick-up should be most important in exothermal reactions, where E can be small. It is also clear that the angular distribution should have a backward minimum.

In the quasi-compound process (Fig. 1d) the pole occurs at negative values of the energy E:

$$E = -\varepsilon^b_{xA}. \quad (22)$$

It follows that the angular distribution will be isotropic for the quasi-compound process. For this reason it is difficult to separate the contribution of the quasi-compound process from that of reactions which go through the compound nucleus stage.

The assertions made above on the angular distributions would be exact if the amplitudes $M_{if}(q^2, E)$ had no other singular points besides the pole corresponding to the particle b [in this case the numerator of formula (14), as the residue of an analytic function, is a constant]. If there are other singular points, we can still write the amplitude in the form (14), but the numerator will not be a constant any more. It will be a slowly varying function of the variables q^2 and E if the other singularities are much farther removed from the boundary of the physical region than the pole under consideration. In the opposite case the variation of the numerator of (14) with q^2 and E in the physical region can be just as or even more important than the variation of the denominator.

It should be emphasized here that we must consider not only the singular points on the physical sheet but also those on the other sheets (for example, if we are near a pole corresponding to a compound nucleus level, the amplitude of the reaction will be a sensitive function of E although the singular points on the physical sheet may lie far away from the considered region of values of E). Since the nucleus has a radius R, the point $|q^2| = 1/R^2$ is of special physical significance. In terms of the theory of dispersion relations, this means that the reaction amplitude has a singularity in this region of values of the variable q^2. On the other hand, it is very difficult to tell immediately which Feynman diagram corresponds to this singularity. This can be done only in the case of the deuteron. The dimensions of heavier nuclei are, apparently, determined by singularities in the variable q^2 which lie on the nonphysical sheet.* We emphasize that this last assertion is to be regarded as a hypothesis. It is important mainly for the derivation of dispersion relations in q^2 on the basis of the diagrams considered in part 3 of this section. In dealing with pole diagrams it is sufficient to have in mind, first, that the singularity which determines the dimensions of the nucleus is not a pole on the physical sheet and, second, that the numerator of (14) must be regarded as a function of qR. This corresponds to the Butler theory, which is therefore described by the pole diagrams of Figs. 1a and 1b.

Formula (14) can be rewritten appropriately by introducing the vertex parts Γ representing averages over the spin variable s_b. Thus we write for the diagram of Fig. 1a, for example,

$$\overline{M_{ib}M^+_{bf}} \equiv \pi m_b^{-1}\Gamma^x_{by}(qR_x, s_x, s_y)\,\Gamma^{Ab}_B(qR_B, s_A, s_B). \quad (23)$$

The upper indices of Γ denote the variables of the particles coming into the vertex and the lower indices correspond to the particles coming out of the vertex. R_x and R_B are the effective radii of the vertices, and s_A, s_B, s_x, and s_y are the spin variables of the particles A, B, x, and y.

*It was noted by V. N. Gribov that the singularity corresponding to the radius of the nucleus may be due to the finite range of the nucleon-nucleon forces. It is, therefore, possible that this singularity corresponds to complicated Feynman diagrams with internal π-meson lines. The main motivation for this point of view comes from the fact that, contrary to the deuteron case, the nuclear three body problem has no solution in the approximation of δ-function forces between the nucleons.

With the new notation, formula (14) for the diagram of Fig. 1a takes the form

$$M_{if} = 2\pi\Gamma_B^{Ab}\,\Gamma_{by}^{x}/(q^2+\varkappa_b^2), \tag{24}$$

where the quantity $\varkappa_b^2$ is defined by formula (15). The differential cross section has the form

$$\frac{d\sigma}{d\Omega_y} = m_{xA}m_{yB}\,\frac{(2J_B+1)(2J_y+1)}{(2J_A+1)(2J_x+1)}\,\frac{p_y\overline{(\Gamma_{Ab}^{B})^2}\;\overline{(\Gamma_{by}^{x})^2}}{p_x(q^2+\varkappa_b^2)^2}. \tag{25}$$

Here*

$$\overline{(\Gamma_{b\beta}^{\alpha})^2} = \overline{(\Gamma_{\alpha}^{b\beta})^2} = \sum_{s_\alpha, s_\beta} |\Gamma_{b\beta}^{\alpha}|^2, \tag{26}$$

and $d\Omega_y$ is the element of solid angle in the momentum space of particle y.

The values of the quantities $\left[\overline{(\Gamma_{b\beta}^{\alpha})^2}\right]^{1/2}$ at the pole (i.e., for $q^2 = -\varkappa_b^2$) are called the reduced vertex parts and are denoted by $\gamma_{b\beta}^{\alpha}$:

$$\gamma_{b\beta}^{\alpha} = \left[\overline{(\Gamma_{b\beta}^{\alpha})^2}\right]^{1/2}_{q^2=-\varkappa_b^2}. \tag{27}$$

The reduced vertex part γ_{Ab}^{B} in deuteron stripping or pick-up reactions (b = p, n) is given in terms of the reduced width of the reaction and the reduced vertex part γ_{pn}^{d} represents the normalization factor of the internal deuteron wave function.

Through the introduction of the reduced vertex parts we have achieved a uniform parametrization of the theory of direct processes. What is important here is that the cross sections of the various processes can involve the same reduced vertex parts (for example, the cross sections for the reactions A(d, n)B and A(α, t)B contain the same reduced vertex part γ_{Ap}^{B}). It is therefore possible to establish a quantitative connection between different types of direct nuclear reactions. It should be emphasized, however, that it is not easy to carry through such a program, since the pole type mechanism of direct processes is not the only and not even always the most important mechanism (see part 3 of this section). In cases where the pole diagram gives the dominating contribution to the reaction amplitude, the reduced vertex parts can be determined from the experimental data by extrapolating formula (25).†

In formula (25) we have summed over the spin variables of the emitted particles y. It is, however, easy to convince oneself that the polarization of the particles y vanishes in the pole approximation if the beam of particles x and the target nucleus A are unpolarized and the polarization of the residual nuclei B is not fixed in the experiment. This result has a simple physical interpretation. It is seen from (25) that the whole process can be regarded as consisting of two independent processes characterized by the two vertices. One of these vertices represents the decay of an unpolarized particle. There will thus be a correlation between the polarizations of the particles into which the decay takes place, and the summation over the spin variable of one of these particles (b) causes the vanishing of the polarization of the other particle (y or B).

We note further that the effect of the interference between different pole diagrams should be small as a rule, since the poles corresponding to interfering diagrams lie in different regions of the variables (an exception is the interference between the diagrams of Figs. 1c and 1d).

2. Interaction in the initial and final states. The interaction in the initial and final states is described by terms in the unitarity condition which correspond to the transitions

$$i \to n = A + x \to A' + x', \qquad n \to f = A' + x' \to B + y;$$
$$i \to n = A + x \to B' + y', \qquad n \to f = B' + y' \to B + y.$$

The diagrams corresponding to these transitions are shown in Figs. 2a and b. In the first case the particle x is scattered by the nucleus A, after which the nuclear reaction takes place. In the second case (Fig. 2b) the first transition is the nuclear reaction, while the last transition is a scattering of particle y by nucleus B. In both cases the intermediate states contain two virtual particles. Integration over momenta and energy of the intermediate particles leads to the formula

$$A_{xy} = \frac{p_x}{4\pi}\int f^*_{x'x}M_{x'y}\,d\Omega_{x'} + \frac{p_y}{4\pi}\int M^*_{y'x}f_{y'y}\,d\Omega_{y'}, \tag{28}$$

where $A_{xy} \equiv A_{if}$, $M_{xy} \equiv M_{if}$; $f_{x'x}$ and $f_{y'y}$ are the scattering amplitudes

* By definition

$$\Gamma_{\beta\gamma}^{\alpha} = (\Gamma_{\alpha}^{\beta\gamma})^*.$$

†To carry out the extrapolation, we must first "weaken" the dependence of the vertex parts on qR. Experience indicates then that one should divide $d\sigma/d\Omega_y$ by $[j_{l_B}(qR_B) \times j_{l_x}(qR_x)]^2$. The order of the spherical Bessel functions l_B and l_x and the radii R_B and R_x are chosen such that the angular distribution is "smoothed out." The extrapolation into the nonphysical region can then be carried out immediately with the help of (25). The guiding consideration in choosing R_B and R_x is the circumstance that these quantities must be close to the radii of the nuclei B and x. The numbers l_B and l_x can be interpreted as the orbital angular momenta of the particle b in the nuclei B and x. We emphasize that this interpretation is essential for finding the angular momenta and parities of the states of the nucleus B, but for the extrapolation procedure itself this identification only serves as a guiding principle in choosing the smoothing factor.

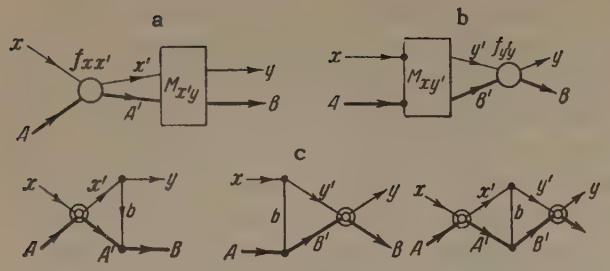

FIG. 2. General diagrams taking account of the interaction in the initial (2a) and final (2b) states, c – inclusion of the initial and final state interactions for the simplest (pole type) reaction mechanism.

$$f_{x'x} = \frac{m_{xA}}{2\pi} M_{x'x}, \qquad f_{y'y} = \frac{m_{yB}}{2\pi} M_{y'y}; \tag{29}$$

$$p_x = \sqrt{2m_{xA}E}, \qquad p_y = \sqrt{2m_{yB}(E+Q)}; \tag{30}$$

$d\Omega_{x'}$ and $d\Omega_{y'}$ are elements of solid angle in the momentum space of the intermediate particles x' and y'. The integration sign in (28) also implies summation over the spins of the intermediate particles.

If the inelastic process $A + B \rightleftarrows B + y$ gives a small contribution to the scattering amplitudes $f_{x'x}$ and $f_{y'y}$, so that the latter can be regarded as independent quantities, the following relation holds:

$$\int f^*_{x'x} M_{x'x}\, d\Omega_{x'} = \int f_{xx'} M^*_{yx'}\, d\Omega_{x'}. \tag{28a}$$

[Under these assumptions this equation is a consequence of the fact that one can interchange the positions of the matrices T and T^+ in formula (9)].

In order to construct the entire amplitude from the absorptive part of (28), we must know the position of the branch points of the amplitude $M_{xy}(E)$ in the variable E. We shall assume that these branch points are determined by the simplest Feynman diagrams shown in Fig. 2c. The first diagram gives the branch point E = 0, the second, E = −Q, and the third gives two branch points, E = 0, and E = −Q. It follows that for Q < 0 the amplitude is analytic in the complex E plane with a cut along the real axis from 0 to ∞. If Q > 0, the cut will start at the point E = −Q. Taking this into account, we have the following dispersion relation in the variable E:

$$M_{xy}(E) = M^0_{xy}(E) + \frac{1}{\pi}\int_{E_0}^{\infty} \frac{A_{xy}(E')}{E' - E - i\eta}\, dE'. \tag{31}$$

Here $M^0_{xy}(E)$ is the sum of the two pole terms and

$$E_0 = \begin{cases} 0, & Q<0 \\ -Q, & Q>0 \end{cases}. \tag{32}$$

Formula (31) represents an integral equation for $M_{xy}(E)$ whose kernel is given in terms of the scattering amplitudes $f_{x'x}$ and $f_{y'y}$. The latter can be taken from experiment or calculated on the basis of the optical model. Equations of the type (31) have been considered by Omnes,[2] who indicated methods for an exact solution. In order to establish the connection between Eq. (31) and the distorted wave method (DWM) usually employed in the theory of direct reactions, we must consider the iterations of this equation. The zeroth iteration,

$$M_{xy} = M^0_{xy} \tag{33}$$

gives the Butler theory. The first iteration leads to terms which correspond to the distorted wave method:

$$M^{(1)}_{xy} = M^0_{xy} + \frac{1}{4\pi^2}\int_{E_0}^{\infty}\int \frac{dE'\, d\Omega_{x'}}{E' - E - i\eta} p_x(E')\, M^0_{x'y}(E')\, f_{xx'}(E') + \frac{1}{4\pi^2}\int_{E_0}^{\infty}\int \frac{dE'\, d\Omega_{y'}}{E' - E - i\eta} p_y(E')\, f^{(E')}_{y'y} M^0_{xy'}(E'). \tag{34}$$

In deriving (34) we have made use of the reality of the pole term M^0_{xy} in (28a). The reaction amplitude in the approximation of the DWM can be written in the form

$$M_{xy}\ (\text{DWM}) = \int \psi^+_y(\mathbf{p}_y, \mathbf{p}'_y)\, M^0_{x'y'}(\mathbf{p}'_x, \mathbf{p}'_y)\, \psi_x(\mathbf{p}_x, \mathbf{p}'_x)\, d^3p'_x\, d^3p'_y, \tag{35}$$

where ψ_x and ψ_y are the wave functions of the particles x and y.

The identity of (34) with the corresponding terms of (35) is easily established by using

$$\psi_x = \delta(\mathbf{p}_x - \mathbf{p}'_x) + \frac{1}{2\pi^2}\frac{f_{xx'}(\mathbf{p}_x, \mathbf{p}'_x)}{p'^2_x - p^2_x - i\eta}, \tag{36}$$

$$\psi_y = \delta(\mathbf{p}_y - \mathbf{p}'_y) + \frac{1}{2\pi^2}\frac{f^*_{yy'}(\mathbf{p}_y, \mathbf{p}'_y)}{p'^2_y - p^2_y + i\eta}. \tag{36a}$$

Besides the terms contained in (34), the amplitude (35) also has a term in which the product of the scattering amplitudes $f_{xx'}$ and $f_{y'y}$ enters. This term is obtained from (31) in the second iteration. However, in this order still more terms appear which contain products of like amplitudes, $f_{xx'}f_{x'x''}$ and $f_{y'y''}f_{y''y}$, and correspond, therefore, to "double scattering" of the particles x and y by the nuclei A and B. Since these terms do not appear in (35), it follows from our analysis that the account of the product $f_{xx'}f_{y'y}$ in the DWM is in excess of the accuracy of the approximation. Reliable information on the accuracy of the DWM can be obtained by comparing the numerical solution of (31) with the amplitude (35).

Let us restrict ourselves to the case where the iteration procedure converges rapidly (this con-

dition is probably too stringent). This means that

$$\bar{k}|\bar{f}|/4\pi^2 \ll 1, \tag{37}$$

where $\bar{k}$ and $\bar{f}$ are certain effective values of the wave number and the scattering amplitude giving the most important contribution to the integrals in (31) and (34). Expressing $|\bar{f}|$ in terms of the scattering cross section $\bar{\sigma}_s$, we obtain the inequality

$$\bar{k}\sqrt{\bar{\sigma}_s}/4\pi^2 \ll 1. \tag{38}$$

For an estimate we set, in the case of neutrons, $\bar{\sigma}_s \approx \pi R^2$, and find from (38)

$$\bar{k}R/4\pi^{3/2} \ll 1, \tag{38a}$$

which is equivalent to the long wavelength approximation.

We can tell by looking at (31) and (28) under what conditions the initial and final state interactions do not appreciably distort the angular distribution of the emitted particles. This will be the case when the scattering amplitudes $f_{xx'}$ and $f_{y'y}$ are nearly δ functions in the scattering angles, i.e., if the scattering goes mainly into small angles. This situation obtains approximately in the case of nucleons with energies higher than 10 Mev.

Of the experimentally observed quantities, the polarization of the emitted particles is the most sensitive to the inclusion of the initial and final state interactions. It should be kept in mind, however, that the interaction in the initial and final states is not the only source of the polarization in direct processes. A significant contribution to the polarization of the outgoing particles may come from more complicated diagrams, which will be considered in part 3 of this section.

3. Triangular singularities. The pole mechanism of direct processes considered in the preceding discussion can predominate if the amplitude $M_{xy}(q^2)$ has, besides the poles, no other singular points lying close to the physical region or in the neighborhood of the poles. This situation, however, is realized only seldom, so that the direct reaction mechanism can be quite different from the pole mechanism and in particular, from the Butler mechanism. Let us consider here some Feynman diagrams which correspond to branch points in q^2.

We restrict our considerations to diagrams with three internal lines. The general type of such diagrams is shown in Fig. 3. The direct mechanism corresponding to the diagram of Fig. 3a, for example, consists in the following. The

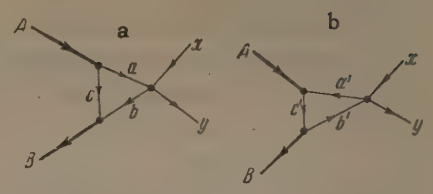

FIG. 3. The simplest triangular diagrams for the reaction A(x, y)B.

nucleus A emits particle a, which collides with particle x. As a result of the reaction

$$a + x \to y + b. \tag{39}$$

the particle b is formed, which is then captured by the nucleus c with formation of the final nucleus B. The three line vertices in this diagram are functions of q'R (as in the case of pole diagrams), where q' are the momenta transferred in the vertex. The four line vertex is the amplitude for the process (39), which also depends in general on q^2.

The singularities of the diagram of Fig. 3 considered below have nothing to do with the dependence of the vertices on q^2 and are determined only by the masses of the particles A, B, x, y, a, b, and c. The branch point closest to the physical region corresponding to the diagram of Fig. 3 is found by the general rules formulated by Landau[3] and developed in the paper of Okun' and Rudik.[4] In our case these rules lead to the formula

$$\tfrac{1}{2}q^2 = -(m_y - m_x)[Q' - \mu_{yB}Q + (\mu_{yB} - \mu_{xA})E] - m_a m_b (\sqrt{\varepsilon^A_{ac}/m_{ac}} + \sqrt{\varepsilon^B_{bc}/m_{bc}})^2. \tag{40}$$

Here

$$Q' = m_a + m_x - m_b - m_y. \tag{41}$$

The analogous formula for the diagrams of the type of Fig. 3b is obtained from (40) by making the interchanges $x \rightleftarrows A$, $y \rightleftarrows B$.

The singularity defined by (40) belongs to the class of the so-called "anomalous thresholds," which were first considered by Karplus, Sommerfield, and Wichmann.[5] As is known, these singularities occur in those cases where the following inequalities are satisfied for the vertices, e.g., the vertex $A \to a + c$:

$$m_A < m_a + m_c, \tag{42}$$

$$m_A^2 > m_a^2 + m_c^2. \tag{42a}$$

This is precisely the situation realized in nuclear reactions. The appearance of the branch points (40) is connected with the fact that for the values q^2 given by (40) the relation between the energy and the momentum of the intermediate particles is the same as for free particles. Since, on the other hand, the real decay $A \to a + c$ is impossi-

Singular points of the diagram of Fig. 3a with various virtual particles a, b for the reaction $Be^9(d, t)B^{10}$

a		n	p	d	t
b	p	d	p+p	He^5	α
$-q^2$, Mev × a.m.u.	2306 (pole)	62.8	299	467	432

ble because of the inequality (42), the singular point (40) lies always in the region of nonphysical (negative) values of q^2.

Let us now consider some examples of nuclear reactions on the basis of the foregoing discussion. In the table we have listed the values of $-q^2$ for the reaction $Be^9(\alpha, t)B^{10}$, computed according to (40) with E = 27.7 Mev. The first number in the table is the value of $-q^2$ at the pole [Fig. 1a, formula (15), b = p]. The other numbers in the table give the branch points of the graph of Fig. 3a for various virtual particles a, b, and c. All data in the table refer to the ground states of the nuclei A, B, and c (the singular points corresponding to excited states of the virtual nucleus c lie in the region of higher values of $-q^2$).

The table shows that the branch point closest to the pole is given by the graph with a = n, b = d, and c = Be^8. The presence of a branch point so close to the pole implies that the mechanism of the reaction $Be^9(\alpha, t)B^{10}$ is certainly not of the pure Butler type. The graph of Fig. 3a will give a contribution to the reaction amplitude which is comparable with that of the pole diagram. Indeed, the boundary of the physical region lies at q^2 = 16.8 Mev × a.m.u.* Thus the ratio of the square of the pole amplitude and the interference term due to the presence of the diagram of Fig. 3a can be of order unity, since the part of the amplitude corresponding to this diagram drops off roughly like $1/(q^2 + q_0^2)$, where q_0^2 is the singular point determined by (40).

The situation is similar in the case of the deuteron stripping reaction $Be^9(d, n)B^{10}$. Here the scattering amplitude has a pole at $q^2 = -13.2$ Mev × a.m.u. and the branch point corresponding to the diagram of Fig. 3a with a = n, b = d, and c = Be^8 lies at $q^2 = -48.4$ Mev × a.m.u. There is hence no reason to expect that the Butler mechanism plays the most important role in the reaction $Be^9(d, n)B^{10}$. In the light of our discussion, the results of Vlasov and co-workers [6] now become perfectly understandable. These results are that the ratios of the reduced widths of the reactions leading to the formation of the nucleus B^{10} in various states are different in the reactions $Be^9(d, t)B^{10}$ and $Be^9(d, n)B^{10}$.

In a number of cases the closest branch points lie much farther away from the pole than in the case of the reactions $Be^9(d, t)B^{10}$ and $Be^9(d, n)B^{10}$. For example, in the reaction $C^{12}(d, p)C^{13}$ the pole lies at $q^2 \approx -12$ Mev × a.m.u. and the nearest branch point (diagram of Fig. 3a, a = b, b = d, c = B^{11}) lies at $q^2 = -200$ Mev × a.m.u. However, even in this case the relative importance of the pole diagram and the diagram of Fig. 3a can be estimated only if there are data on the reduced vertex parts and the amplitudes of the reaction (39). Thus the knowledge of the amplitudes of nuclear reactions with light nuclei is of prime importance for the understanding of the direct interaction mechanism in complex nuclei.

An essential factor in the investigation of the direct interaction mechanism is the measurement of the polarization of the reaction products. Contrary to the situation in the pole type mechanism, we have now in the case of the diagram of the type of Fig. 3 that the polarization of the particle y is determined not only by the interaction in the initial and final states, but also by the polarization due to the reaction (39). It should be emphasized that the angular distribution of the emitted particles provides a less sensitive test of the direct reaction mechanism.

3. ON THE REACTIONS A + x → B + y + z

As in the case of the reactions (1a), the simplest diagrams for the reactions (1b) are the pole type ones. These diagrams for the processes (x, dx), (π^-, 2n), and (K^-, Λ^0n) are shown in Fig. 4 a and b. A number of experimental results now available indicate that the pole type mechanism predominates, but the contributions from other diagrams cannot be excluded just on the basis of these data. Thus, for example, it was observed in the work of Ozaki and co-workers [7] that the neutrons in the reaction (π^-, 2n) are emitted preferably into opposite directions. This result corresponds to the pole

FIG. 4. a – pole diagram for the reaction (x, xd), b – pole diagram for the reactions (π^-, 2n) and (K^-, Λ^0 n).

*a.m.u. ≡ atomic mass units

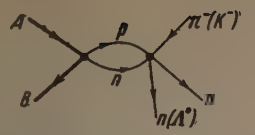

FIG. 5. The simplest non-pole-type diagram for the reactions (π^-, 2n) and (K^-, Λ°n).

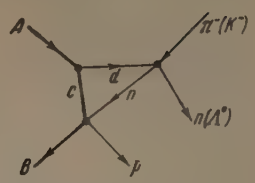

FIG. 6. The simplest diagram for the reactions (π^-, pn) and (K^-, Λ°p).

diagram of Fig. 4b, but cannot be obtained from the diagram of Fig. 5, which involves the emission of a neutron and a proton in a singlet state by the nucleus A. It follows that the interpretation of the reaction mechanism requires the comparison of data on different processes.

If the pole diagrams are the most important, the cross sections for the processes corresponding to the diagrams of Figs. 4 a, b, and 5 should agree numerically (if the reduced vertex parts γ^A_{Bd} are the same). It should be noted in this connection that the "knocking-out" of deuterons from nuclei is not surprising within the framework of dispersion theory, since there is no reason to believe that the reduced vertex parts γ^A_{Bd} are equal to zero. The quantitative description of this process requires, at least, the knowledge of the scattering cross section of the particles x on a free deuteron in a wide region of energies and of the reduced vertex parts γ^A_{Bd}. For this it is necessary to compare with data on other processes (which are rather sparse at the present time).

What has been said above about the knocking out of deuterons applies equally well to other "knock-out" processes, i.e., processes of the type (x, xy). This provides us with a uniform approach to the mechanism of the knocking out of different types of complex particles ("clusters") from the nucleus. We shall not quote here the formulas for the cross sections of the processes of the type (2) in the pole approximation, since they can be found in the well-known paper of Chew and Low.[8]

In the case of reactions (2) the inclusion of diagrams more complicated than the diagrams of Figs. 4 and 5 is beset with a number of difficulties. This has to do with the fact that to each diagram with five external lines there correspond five independent kinematic variables, and the position of the singular points in one variable depends on the values of the other variables. Nevertheless, the interactions in the initial and final states can be included for many processes with nonrelativistic energies in exactly the same manner as was done in Sec. 2. Of particular interest is the study of the reactions (π^-, pn) and (K^-, Λ^0p) with the help of this method. The simplest diagram for these reactions is shown in Fig. 6. The reaction amplitude corresponding to this diagram satisfies the integral equation (31) with $f_{\gamma'\gamma}$ replaced by the amplitude M_{np} of the reaction c(n, p)B [using formula (29)]. However, to carry out this program we must require more complete experimental data than are available at the present time.

4. CONCLUDING REMARKS

The method discussed in this paper has a number of attractive features: it is illustrative, does not make use of perturbation theory, and leads to formulas that are transparent in their physical content and relates amplitudes for various processes to one another. This last circumstance leads to a definite experimental program for the verification of the original assumptions (namely, the possibility of a description of the direct processes in terms of Feynman diagrams). The formalism developed is essentially a phenomenological theory of direct processes which is completely analogous to the Breit-Wigner theory of the compound nucleus. These two theories may be called twins in that they are both dealing with the singularities on different sheets of one and the same analytic function. Like the Breit-Wigner theory of the compound nucleus, our method does not pretend to a calculation of the reduced widths of the nuclear reactions but provides a uniform procedure for extracting such levels from the experimental data and establishes a quantitative relation between nuclear reactions which, at first glance, seem to be completely different.

The author expresses his gratitude to L. D. Landau and K. A. Ter-Martirosyan for several valuable comments.

[1]R. D. Amado, Phys. Rev. Lett. 2, 399 (1959).

[2]R. Omnès, Nuovo cimento 8, 316 (1958).

[3]L. D. Landau, Nucl. Phys. Phys. 13, 181 (1959).

[4]L. B. Okun' and A. P. Rudik, Nucl. Phys. 15, 261 (1960).

[5]Karplus, Sommerfield, and Wichmann, Phys. Rev. 111, 1187 (1958) and 114, 376 (1959).

[6]Vlasov, Kalinin, Oglobin, and Chuev, JETP 39, 1468 (1960), Soviet Phys. JETP

[7]Ozaki, Weinstein, Glass, Loh, Neimala, and Wattenberg, Phys. Rev. Lett. 4, 533 (1960).

[8]G. F. Chew and F. E. Low, Phys. Rev. 113, 1640 (1959).

Translated by R. Lipperheide
270

INCOHERENT SCATTERING OF ELECTRONS BY NUCLEI AND THE MAGNETIC RADIUS OF THE NEUTRON

M. Ya. KOBIASHVILI

Tbilisi State University

Submitted to JETP editor June 3, 1961

J. Exptl. Theoret. Phys. (U.S.S.R.) 41, 1628-1631 (November, 1961)

It is shown that the seemingly apparent smaller size of the neutron, compared with that of the free proton, observed in the experiments of Hofstadter on the Be^9 nucleus can be partially explained by the binding of the neutron in the given nucleus. The mean square radius of the neutron magnetic-moment distribution thus appears to be larger if the neutron motion is taken into account.

1. It has been shown in several recent papers that the curve for the cross section of scattering of fast electrons by a point-like proton does not agree with the experimental data. The situation can be rectified by assuming that the charge and the magnetic moment of the proton are distributed in space. The best agreement with experiment is attained in this case when these distributions are approximated by an exponential or near-exponential model with a mean-square radius $r_p = 0.8$ f. To study the structure of the neutrons, we used H^2 and Be^9 nuclei[1,2], which contain a weakly-bound neutron. We started from the fact that at large momentum transfers and at large scattering angles θ, one observes only incoherent scattering[3] (the momentum transferred k is much greater than the reciprocal of the mean distance between nucleons), which can be represented as the sum of the cross sections of the scattering by individual nucleons of the nucleus. Under these conditions the main contribution to the incoherent spectrum is made by scattering on the magnetic moment of the nucleon, while the scattering on the specific charge of the nucleon can be neglected.

Starting with the foregoing, we used the "area method"[1,2] to determine the magnetic form factor, assuming the nucleons of the nucleus to be free and independent. Measurements made on H^2 and Be^9 yielded values $r_n = 0.8$ f and 0.53 f for the mean-square radius of the distribution of the neutron magnetic moment (in the exponential model). It was suggested that the apparent reduction in the neutron dimensions in measurements on the Be^9 nucleus is due to the greater role of the meson-exchange effects in this nucleus and also to the interaction between the emitted neutron and the nuclear remnant.[2] Since the neutron is assumed free in the interpretation of the experimental data, it is of interest to ascertain whether an account of the neutron binding in the Be^9 nucleus leads to an increase in r_n. The present article is devoted to this question.

2. Since the electric form factor of the neutron is $F_{1n} \sim 0$[3] the energy of interaction between the electron and the neutron is determined by the interaction between the magnetic moment of the neutron with the magnetic field of the electron; therefore

$$H' = -\int \mathbf{M}[\nabla \mathbf{A}]\, d\tau. \qquad (1)$$

where

$$\mathbf{M} = \frac{e\hbar}{2Mc} f_{2n}(|\mathbf{r} - \mathbf{r}'_n|)\chi_n \sigma_n, \qquad (2)$$

f_{2n} is a structural function characterizing the distribution of the magnetic moment, χ_n is the anomalous magnetic moment of the neutron, and $\mathbf{A}$ is the Møller potential.[4]

To take into account the motion of the center of mass we can use the model of two bodies (core + neutron), the interaction between which we describe by a spherical symmetrical potential well of depth V_0 and width $R_0 = r_0 A^{1/3}$ f.

The ground state, in accordance with the shell theory for light nuclei, is described by known spin-angle functions,[5] and the final state can be determined with the aid of the Born approximation, if the energy of the free neutron is sufficiently large. Then, after several mathematical manipulations, we obtain for the cross section of electrodisintegration of a nucleus with mass number A, wherein an electron of energy q_i is scattered within a solid angle $d\Omega$ and has an energy in the interval dq_f, the following expression

$$\sigma_n(\theta, q_f) = d^2\sigma/d\Omega dq_f = \sigma_{n0} F_{2n}^2(kr_n)\,\gamma(x, r_0)\,q_i^{-1}, \qquad (3)$$

where σ_{n0} is the Rosenbluth cross section for the scattering of an electron by a point-like free neutron,[6] and F_{2n} is the form factor of the neutron, the Fourier transform of the structural function; the remaining quantities, which take into account the binding of the neutron, are

$$\gamma(x, r_0) = \frac{A}{A-1}\frac{2\eta}{\pi}(a^2+b^2)\,b^2\,\frac{R_0 Mc}{\hbar}\left(1+\frac{2q_i}{Mc^2}\sin^2\frac{\theta}{2}\right)^2$$

$$\times f(x)\int_{z_1}^{z_2}\varphi(z, r_0)\,dz, \qquad (4)$$

where

$$f(x) = (1 + x^2 - 2x\cos\theta)$$

$$^{-1/2}x\left\{1+\frac{q_i}{Mc^2}\left[1-x\left(1+2\alpha_0\sin^2\frac{\theta}{2}\right)\right]\right\},$$

$$\varphi(z) = \left[\frac{j_l(a)\,zj_{l-1}(z) - aj_{l-1}(a)\,j_l(z)}{(b^2-z^2)(a^2+z^2)}\right]^2 z;$$

$$\alpha_0 = q_i/\mu_0, \qquad \mu = \frac{A-1}{A}M, \qquad x = q_f/q_i,$$

$$\eta = [j_{l-1}(a)\,j_{l+1}(a)]^{-1}, \qquad a = \frac{R_0}{\hbar}\sqrt{2\mu(V_0-\varepsilon_n)},$$

$$b = \frac{R_0}{\hbar}\sqrt{2\mu\varepsilon_n}, \qquad z_{2,1} = \left|\frac{A-1}{A}kR_0 \pm k_n R_0\right|, \qquad (5)$$

M and μ_0 are the masses of the neutron and of the target nucleus, ε_n and k_n are the binding energy and the wave vector of the neutron, while j_l is a spherical Bessel function.

In the derivation of (3), account must be taken of the energy and the momentum conservation laws, the use of which yields

$$q_i - q_f = W + E_c, \qquad W = q_i - q_f\,[1 + \alpha_0(1-\cos\theta)], \qquad (6)$$

where E_c is the kinetic energy of the scattering nucleus and W the excitation energy transferred to the emitted neutron.

Integrating (3) with respect to dq_f we obtain

$$\sigma_n(\theta) = \sigma_{n0}\xi(r_0, r_n), \qquad (7)$$

where the value of ξ, which is equal to

$$\xi(r_0, r_n) = \int_{x_1}^{x_2} F_{2n}^2(kr_n)\,\gamma(x, r_0)\,dx = F_{2n}^2(\zeta)\,C(r_0), \qquad (8)$$

can be connected with the experimentally-measured value of $R = \sigma_n/\sigma_p$[2] by the relation

$$R = A(\theta, q)\,\xi(r_0, r_n)\,F_p^{-2}, \qquad (9)$$

with $A(\theta, q)$—ratio of the Rosenbluth cross sections for the scattering of an electron by a point-like free neutron and proton.

3. Let us apply these formulas to scattering on Be^9, the incoherent electron spectrum of which was observed by Ehrenberg and Hofstadter,[2] who

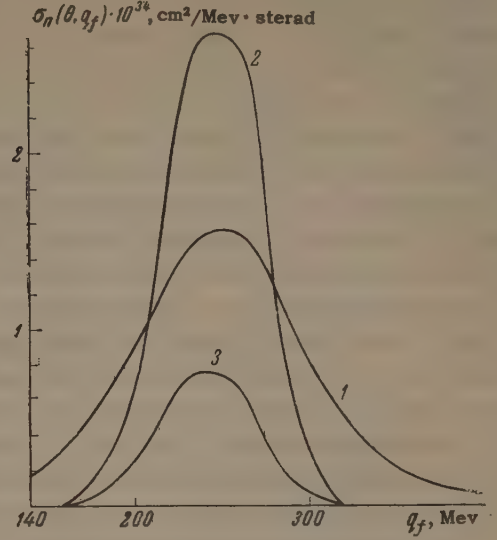

obtained R = 1.17 at q_i = 500 Mev and $\theta = 135°$. Using these data, we obtain for $F_p^2 = 0.15$[2]

$$\xi(r_0, r_n) = \int_{0.4}^{0.65} F_{2n}^2(kr_n)\,\gamma(x, r_0)\,dx = 0{,}39, \qquad (10)$$

where the integration limits were chosen in accordance with the energy region for which R had been determined.

It is known that the neutron in Be^9 is in a $p_{3/2}$ state and its binding energy is ε_n = 1.67 Mev. Obviously, we can use in this case the Born approximation, since the emitted neutron acquires an energy not less 150 Mev. Calculations have shown that $C(r_0) = 1.12$ when $r_0 = 1$ and increases to 1.43 at $r_0 = 2.4$. Thus, an account of the neutron binding can lead to an increase in r_n. We assume $r_0 = 2.4$ because a value $R_0 = 5$ f ($V_0 = 12.17$ Mev) yielded good agreement with experiment at low energies.[7]

The figure shows the cross section $\sigma_n(\theta, q_f)$ for a point-like neutron with r_0 having values 1 and 2.4 (curves 1 and 2), and also for a neutron with exponential distribution of the magnetic moment at $r_0 = 2.4$ and $r_n = 0.6$ f (curve 3). All the curves have a maximum at $q_f \sim 250$ Mev, which agrees with the variation of the experimental cross section.[2] It is possible to integrate in (10)

$f_{2n}(r)$	r_n	r_n (ξ=1)
$r^{-2}e^{-r}$	0.85	0.68
$r^{-1}e^{-r}$	0.65	0.56
e^{-r}	0.6	0.53
re^{-r}	0.58	0.51
r^2e^{-r}	0.57	0.50
e^{-r^2}	0.56	0.49
$r^2e^{-r^2}$	0.54	0.47

from zero to infinity because the function $\sigma_n(\theta, q_f)$ assumes very small values when $x < 0.4$ and $x > 0.65$.

Using formula (10) and also the table from Hofstadter's paper,[3] we can find the mean-square radius for different neutron magnetic-moment distributions. The results of the calculations are listed in the table, which also contains the values of the mean-square radius obtained from (9) under the assumption that $\xi = 1$ (free neutron).

On the other hand, research on H^2 yields values $r_n = r_p = 0.8$ f, which does not agree with the value of r_n listed in the table. The reason for this discrepancy may be, first, the inaccuracy of the experiment and second the fact that in the interpretation of the experimental data we neglected certain effects, an account of which can change r_n. It has been assumed, in particular, that 1) the electrons are scattered by stationary free nucleons, 2) the emitted nucleon does not interact with the remaining nucleons, and 3) the dimensions of the nucleon remain unchanged under the influence of the nuclear forces.

One can think that the equality of the neutron and free-proton radii, obtained in the experiments on H^2 (assuming the charge independence hypothesis to be valid), corroborates the foregoing assumptions made for the deuteron, in which the nucleons stay the greater part of the time outside the range of the nuclear forces. This conclusion may not prove to be completely true for Be^9. Indeed, as can be seen from the table, an account of the neutron bond leads to an increase in the mean-square radius. Regardless of how reliable the experimental data are, we can conclude therefore that in the interpretation of the experimental results obtained by the "area method" for nuclei such as Be^9, C^{13}, or O^{17} the effect of the binding of the nucleons in the nucleus must be taken into account.

In conclusion, the author is grateful to Prof. V. I. Mamasakhlisov for interest and attention to the work.

[1] M. Yearian and R. Hofstadter, Phys. Rev. 110, 552 (1958); Phys. Rev. 111, 934 (1958).

[2] H. F. Ehrenberg and R. Hofstadter, Phys. Rev. 110, 544 (1958).

[3] R. Hofstadter, Revs. Modern Phys. 28, 214 (1956).

[4] R. Hofstadter, Ann. Rev. of Nucl. Science, Stanford, (1957) Vo. 7.

[5] A. S. Davydov, Teoriya atomnogo yadra (Theory of the Atomic Nucleus), Fizmatgiz, 1958.

[6] M. Rosenbluth, Phys. Rev. 79, 615 (1950).

[7] E. Guth, Phys. Rev. 76, 234 (1949).

Translated by J. G. Adashko
271

ACCELERATION OF A CLOUD OF IONIZED GAS WHOSE OWN MAGNETIC FIELD SCATTERS AN ELECTRON BEAM

G. A. AKAR'YAN

P. N. Lebedev Physics Institute, Academy of Sciences, U.S.S.R.

Submitted to JETP editor June 4, 1961

J. Exptl. Theoret. Phys. (U.S.S.R.) 41, 1632-1633 (November, 1961)

We consider acceleration of a plasma with its own magnetic field in the scattering of an incident electron beam. Two ways of increasing the amount of energy extracted from the electrons are indicated: multiple scattering of the electron beam by the magnetized plasma, and application of induction inertia ("increasing the weight") of electrons in a powerful current. It is noted that the effect can be employed in plasma accelerators and that it may occur in astronomical processes.

WE consider the mechanism whereby a cloud of ionized gas with its own magnetic field is accelerated when an electron beam is incident on the cloud. Its own magnetic field makes the plasma opaque to the electrons, and the strong scattering of the electrons is accompanied by an effective transfer of momentum to the plasma, in view of its connection between the plasma and the force lines of the frozen-in field which produces the scattering. This acceleration mechanism is the opposite of the Fermi mechanism for the acceleration of particles (by reflection from moving cosmic plasma clouds with 'frozen-in' magnetic fields), since it uses the reaction of the cloud.

An incident nonrelativistic electron current J acts on a magneto-plasma cloud from which the electrons are strongly scattered or reflected, with an effective force $F \approx m_0 v_e J/e$. For example, if $J = 10$ amp and the electron velocity is $v \approx 0.3c$ we obtain $F \approx 10^3$ dynes, which accelerate a plasma with mass $M \approx m_i N \approx 10^{-12}$ g (the total number of particles is $N \approx 10^{12}$) to a velocity $u \approx Ft/M \approx 10^6$ cm/sec within $t \approx 10$ μsec.

To increase the acceleration force and to improve the utilization of the beam energy, the electrons can be multiply reflected from two magnetized clouds or from a cloud and a magnetic mirror (concentration of force lines of an external magnetic field), with the electron beam injected along the mirror axis. In scattering and reflection from a magnetized plasma, the electron velocity direction changes or a shift from the axis takes place, and the electrons remain locked for a long time between the mirror and the magnetized cloud.

Another possible method of intensifying the action of the electrons on the plasma is based on an inductive increase of the electron mass. If the incoming beam has a noticeable inductance (i.e., $N_1 r_0 L_1 \gg 1$, where N_1 is the running number of charges, r_0 their classical radius, and L_1 the running induct), then the momentum transferred by the beam can exceed the mechanical momentum of the beam particles in view of the inductive increase in the particle mass $m' = m_0 (1 + N_1 r_0 L_1) \gg m_0$. In this case the effective force is

$$F = m_0 \{1 + N_1 r_0 L_1\} v_e J/e \approx L_1 J^2/c^2.$$

For example, even when $J \approx 10$ kiloamp and $L_1 \approx 10$ we obtain $F \approx 10^6$ dynes, i.e., high acceleration of the cloud is expected when a plasma cloud with frozen-in magnetic field is injected in a gas-discharge current.

The limiting velocity u_{max} which a magnetized cloud opaque to electrons and ions can acquire in a gas discharge can be readily determined by equating the pressures of the electron and ion beams in the coordinate system of the moving cloud:

$$(v_i + u_{max})^2 \approx (v_e - u_{max})^2 m'/m_i,$$

where v_e and v_i are the ordered velocities of the electrons and ions. When $v_i \ll u_{max} \ll v_e$ we obtain $u_{max}^2 \approx m' v_e^2/m_i \approx c^{-2} J^2 L_1/m_i N_1$.

We note that the process need not necessarily be nonstationary for an inductive mass increase to occur. Even in stationary scattering of the current by an obstacle or in stationary flow of current over the obstacle, the obstacle will be acted upon by a force determined by the value of the current and by the running inductance, in accordance with the formula given above (this can be readily verified by calculating directly the forces

of interaction between the unperturbed and perturbed portions of the current).

It is not difficult to produce special plasma-magnetic inhomogeneities: when a plasma is produced in a magnetic field, partial capture of the field by the produced plasma takes place spontaneously. If the plasma is produced in a gas discharge, the residual currents and fields are also retained in the plasma.

The momentum can be transferred to the plasma not only by scattering of the electron beam on the plasma's own field, but by scattering of the beam on the inhomogeneities that the plasma produces in the external magnetic field (on the bends of the force line and on the strengthened edge field crowded out by the plasma).

In cosmic space this process can occur near stars, in the regions where currents circulate and plasma-magnetic inhomogeneities—turbulences—exist. The large scales of the processes (large N_1 and long acceleration paths, the long times of confinement of the self-magnetic fields and of equalization of the inhomogeneities) may cause these processes to produce bursts of accelerated cosmic particles.

The reduction in the penetrating ability of a plasma with internal magnetic field can manifest itself also in the transfer of momentum of a magnetized plasma stream incident on a layer of another plasma. Such a process is the apparent cause of the pressure that the solar plasma stream, which carries an internal magnetic field, exerts on the plasma of the tails of comets.

Translated by J. G. Adashko
272

OPTICAL MODEL OF THE NUCLEUS WITH A POLYNOMIAL POTENTIAL

A. V. LUK'YANOV, Yu. V. ORLOV, and V. V. TUROVTSEV

Nuclear Physics Institute, Moscow State University

Submitted to JETP editor June 6, 1961

J. Exptl. Theoret. Phys. (U.S.S.R.) 41, 1634-1643 (November, 1961)

A study is made of the shape of the potential for the nuclear optical model with surface absorption. For a polynomial potential, we choose a set of parameters which gives a good description of the experimental data on scattering of 14 Mev neutrons. A comparison is made of various potentials.

1. INTRODUCTION

EXTENSIVE use is made at present of the optical model with a potential whose real part has the form proposed by Woods and Saxon.[1] However, as we have shown previously,[2] from an investigation of a polynomial potential with volume absorption and not including spin-orbit interaction, the polynomial potential leads to similar results, other things being equal. Although the optical model with volume absorption and omitting spin-orbit interaction gives the correct dependence of the integral cross sections (total cross section σ_t, elastic scattering σ_s and absorption σ_r) on mass number A for medium and heavy nuclei and describes the qualitative features of the differential elastic scattering cross section for $\theta < 90°$, it nevertheless has various deficiencies. In the region of light nuclei, the cross section ratio σ_s/σ_r is too high compared with experiment, the computed differential cross sections have deep minima which are not seen experimentally and the backward scattering is too large. The work of Bjorklund and Fernbach[3] (which we abbreviate as BF) shows that this defect can be eliminated by using a potential which includes spin-orbit interaction and which has a maximum of its imaginary part at the nuclear boundary (surface absorption). In the present work we have investigated the optical model with surface absorption and including effects of spin-orbit interaction, but in contrast to the work of BF, in which the real part was the Woods-Saxon potential and the imaginary part was Gaussian, we describe the potential by means of polynomials.

2. THE POLYNOMIAL POTENTIAL

We have found the parameter values which give agreement with the experimental data on scattering of 14-Mev neutrons for a nuclear potential of the following form* (cf. Fig. 1):

$$V = V_{CR}\rho(r) + iV_{CI}q(r) - V_{SR}\left(\frac{\hbar}{\mu c}\right)^2 \frac{1}{r}\frac{d\rho}{dr}\sigma\mathbf{l};$$

$$\rho(r) = \begin{cases} 1, & 0 \leqslant r \leqslant R - d_r \\ \frac{1}{2} - \frac{15}{16}\left(\frac{r-R}{d_r}\right)\left[\frac{1}{5}\left(\frac{r-R}{d_r}\right)^4 - \frac{2}{3}\left(\frac{r-R}{d_r}\right)^2 + 1\right], & R - d_r \leqslant r \leqslant R + d_r, \\ 0, & r \geqslant R + d_r \end{cases} \quad (1)$$

$$q(r) = \begin{cases} 0, & 0 \leqslant r \leqslant R - d_i, \\ \left[1 - \left(\frac{r-R}{d_i}\right)^2\right]^2, & R - d_i \leqslant r \leqslant R + d_i, \\ 0, & r \geqslant R + d_i, \end{cases}$$

where $R = (r_0 A^{1/3} + \delta)$ and μ is the π-meson rest mass.

The determination of the phases and cross sections was done by standard methods, by a numerical solution of the Schrödinger equation with the potential (1) in the region $R - d \leq r \leq R + d$, where $d = \max\{d_r, d_i\}$. The method was essentially the same as that described previously.[2] The pair of second-order differential equations corresponding to the two directions of the neutron spin was reduced to a system of first-order equations, which was solved by the Runge-Kutta method. As initial conditions we chose the function and its first derivative at the point $r = R - d$, where their analytic expressions are known.

It is a very difficult problem to vary simultaneously all the parameters of the potential (V_{CR}, V_{CI}, V_{SR}, d_r, d_i, r_0 and δ). However the solution is simplified by the fact that the range of parameter

*After this work was completed, there appeared the paper of Green et al.[5] on a nonlocal optical model, in which the real part of the potential is also described by a fifth-degree polynomial.

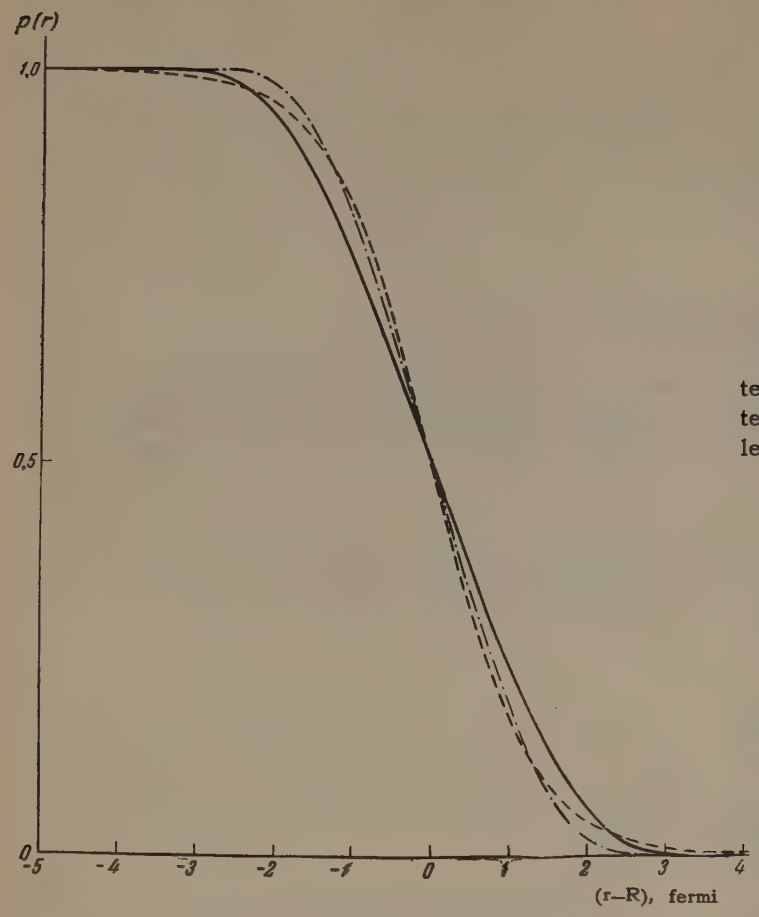

FIG. 1. Real parts of the potentials. Solid curve-potential (1) with the parameters of (3); dashed curve – potential (4); dot-dashed curve – for potential (1) giving least squares fit to potential (4).

values and the behavior of the cross section as a function of certain of them has been studied fairly well. In particular this enables us beforehand to make a reasonable choice of the parameters V_{CR} and V_{SR}. Fixing V_{CR} subject to the condition that the parameters r_0 and δ, which determine the nuclear radius, remain free, is entirely permissible because of the well known ambiguity of the type $V_{CR} - R$. Thus the value $V_{CR} = 44$ Mev is definitely acceptable, since it surely lies in the right range (it coincides with the value used in [3]). The value $V_{SR} = 7.7$ Mev was taken from the work of Levintov.[6] Changing this parameter within reasonable limits has an insignificant effect on the cross sections (in particular on the integral cross sections). It might be improved by using data on the polarization of scattered neutrons, but unfortunately there are as yet no such data for 14 Mev neutrons.

In choosing the other parameters, we used computations showing the variation of the cross section when each of the parameters d_r, d_i and V_{CI} was changed individually. Over a wide range of values, the dependence of the cross sections σ_t and σ_r on the parameters d_r and d_i is close to linear, which greatly simplifies the problem of choosing these parameters. To good accuracy, the cross sections σ_t and σ_r, as functions of d_r with all other parameters fixed, can be represented as

$$\sigma = \sigma^{(0)} + \alpha d_r. \qquad (2)$$

The value of $\sigma^{(0)}$ is independent of d_r; the coefficient α is almost constant for medium and heavy nuclei ($\alpha \sim 33$ fermi for σ_r, $\alpha \sim 40$ fermi for σ_t), and is somewhat lower for the light nuclei ($\alpha \sim 15$ fermi for σ_r, $\alpha \sim 30$ fermi for σ_t). The closeness of the values of α for σ_t and σ_r in the first case indicates a weaker dependence of the integral elastic scattering on the parameter d_r. But the shape of the angular distribution of the elastically scattered neutrons is extremely sensitive to changes of the parameter d_r. With increasing d_r, the oscillations in the diffraction pattern become less sharp, and the minima in the cross sections at angles $\theta > 90°$ are shifted somewhat toward smaller angles (the shift being different for different nuclei). The choice of the parameters d_r, d_i, V_{CI}, r_0 and δ could be made by the method described previously, in which one considers a series of fixed values of one of the parameters, for example V_{CI}. It turned out, however, that the value $V_{CI} = 11$ Mev, used by BF, enables us to find the range of values of the parameters d_r, d_i, r_0 and δ for which the cross sections σ_t and σ_r are in good agreement with experiment. We chose the following parameter values:

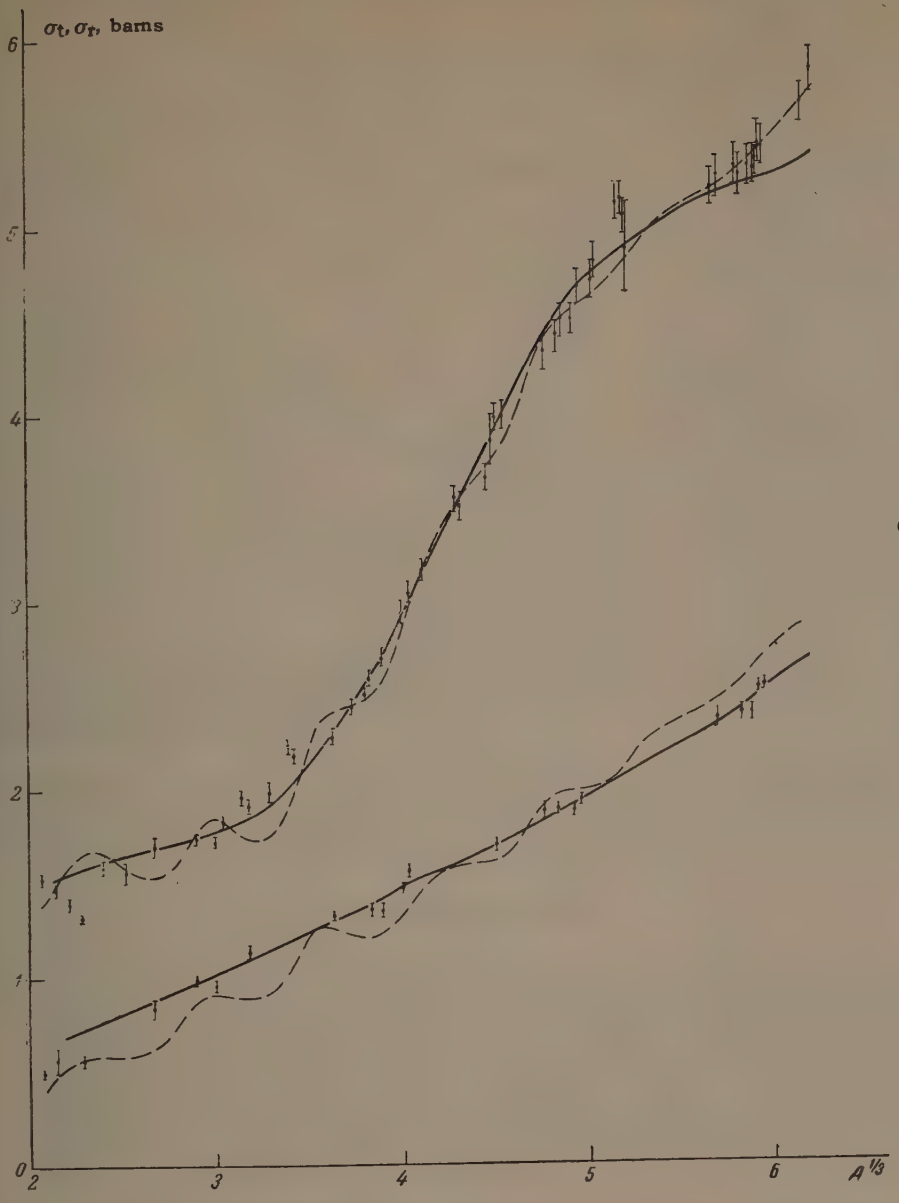

FIG. 2. Comparison of theoretical and experimental dependence of σ_t (upper curves) and σ_r (lower curves) on mass number A. The solid lines are the theoretical cross sections calculated for the potential (1) with the parameter values (3); the dashed lines are theoretical cross sections from [2]. The experimental data, indicated by the vertical dashes, are taken from [7, 8].

$$V_{CR} = 44\,\text{Mev}, \quad V_{CI} = 11\ \text{Mev}, \quad V_{SR} = 7.7\,\text{Mev},$$
$$d_r = 3.36\ \text{f}, \quad d_i = 1.62\ \text{f}, \quad r_0 = 1.25\ \text{f},$$
$$\delta = 0. \qquad (3)$$

The cross sections σ_t and σ_r calculated with these parameter values are shown together with the experimental data in Fig. 2. For comparison we also give the analogous curves from [2]. The results demonstrate the considerable improvement in the agreement with experiment, especially for the light nuclei.

Although the choice of parameters was made on the basis of the integral cross sections, the agreement of the differential elastic cross section with experiment is good on the whole (Fig. 3). This is an additional confirmation of the correct choice of the parameters. The absence of deep minima and strong backward scattering in the computed angular distributions shows that the defects cited in the introduction are eliminated by using the potential (1). The reduction of the cross section for elastic scattering at angles $\sim \pi$ is associated with the spin-orbit interaction (Fig. 4).* The introduction of surface absorption reduces considerably the oscillations in the diffraction pattern and makes possible a good description of the experimental integral cross sections for nuclei over almost the whole periodic table, with parameters which are independent of mass number A.

The agreement of the computed angular distributions with the experiments is not exact. But the optical model in its present form cannot pretend to give exact agreement, since it describes only the

*A qualitative explanation of this effect is given by I. S. Shapiro. [11]

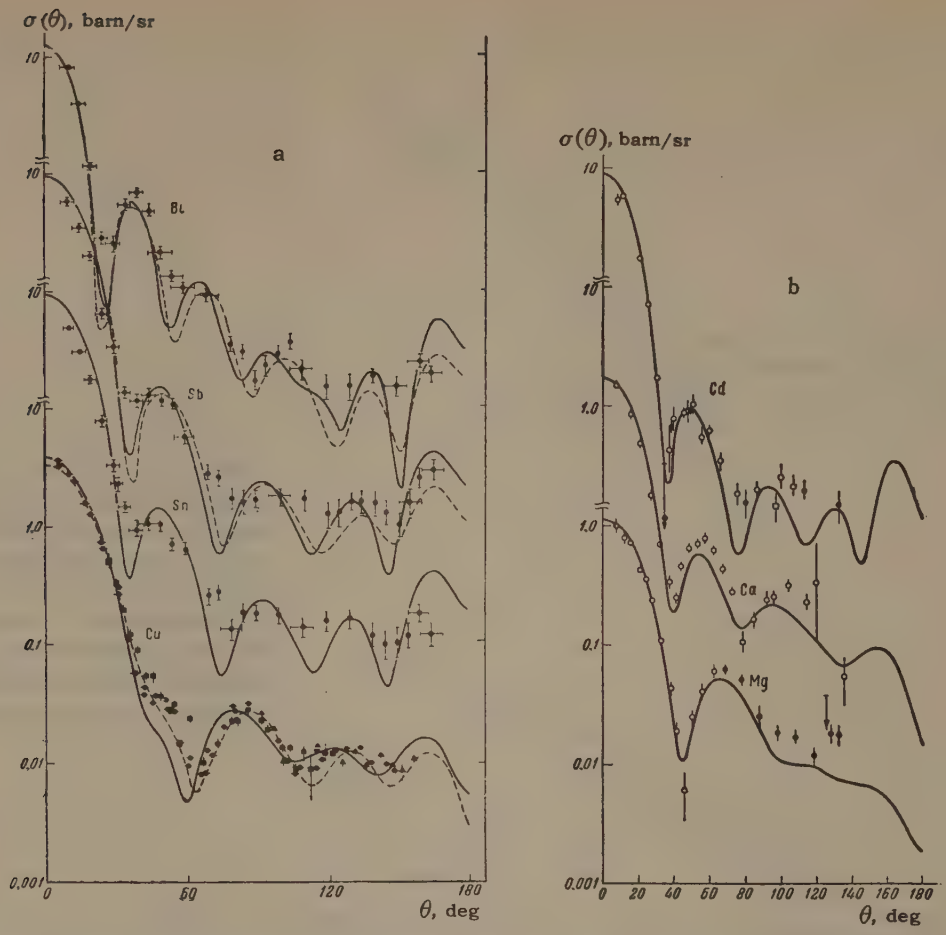

FIG. 3. Comparison of theoretical and experimental angular distributions of elastically scattered neutrons. The solid curves are the differential cross sections calculated with the potential (1) for the parameter values (3), for all nuclei except Mg, for which the computations were made with the potential (4) and the parameter a = 0.74 fermi, instead of a = 0.65 fermi (the value a = 0.74 fermi gives agreement with the experimental integral cross sections). The dashed curves are similar results from BF. The experimental data for Mg, Ca, Cd (E_n = 14.6 Mev) are taken from [9], those for Sn, Sb, Bi (E_n = 14 Mev) from [10], and those for Cu (E_n = 14 Mev) from BF. The computed values are for a neutron energy E_n = 14 Mev for all nuclei except Ca and Cd, for which E_n = 14.6 Mev (the difference in the results for E_n = 14.6 and 14 Mev being negligible). The ordinate scales for the various curves are shifted vertically.

averaged properties of nuclei. For example, it is known [12] that the differential cross section can change considerably from one isotope to another, i.e., for a change of A by one unit. At the same time, the optical model, in which the only dependence on A is via the nuclear radius ($R = 1.25\ A^{1/3}$ fermi), can give only a smooth dependence on A and is incapable of explaining such variations.

Increasing V_{SR} from the Levintov value of 7.7 Mev to 10.35 Mev practically does not change the agreement with experiment (BF used the value V_{SR} = 8.3 Mev). This causes an essential reduction only in the backward elastic scattering, for which there are unfortunately no data. This dependence of the angular distributions on the spin-orbit coupling strength is demonstrated in Fig. 5, which shows the differential cross sections for different values of V_{SR}. Thus our preliminary choice of the parameter V_{SR} is entirely reasonable, and could be improved only by using polarization data. It is interesting to note that the computed cross sections, including the differential cross sections, are practically unchanged when we reverse the sign of this parameter.

The insensitivity to the sign of the spin-orbit interaction is not difficult to understand. The spin-orbit terms which appear in the equations corresponding to the two values of the total angular momentum of the neutron ($j = l \pm \frac{1}{2}$) differ only in having the factors l and $-(l + 1)$, respectively. For large l, we can neglect 1 compared to l. Consequently the amplitudes of scattered waves calculated from the solution of the equations with $j = l \pm \frac{1}{2}$ will be close to those calculated for the equations with $j = l \mp \frac{1}{2}$ in which we have changed the

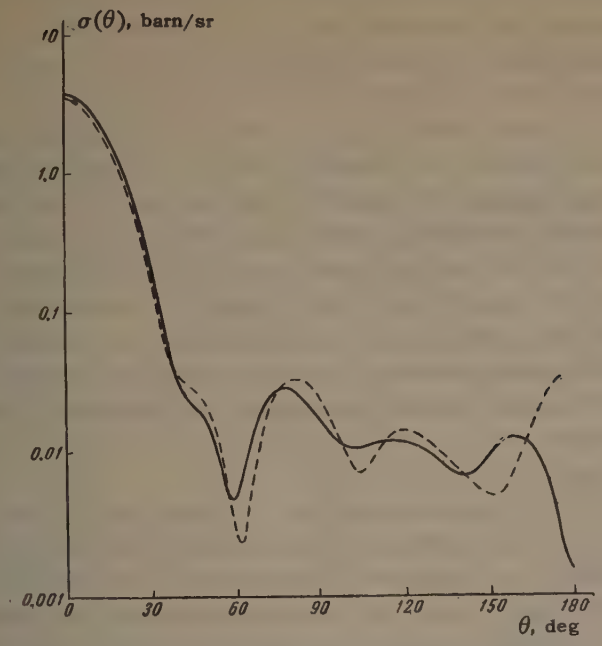

FIG. 4. Influence of spin-orbit interaction on differential elastic scattering cross section: solid curve for V_{SR} = 8.28 Mev, dashed curve for V_{SR} = 0.

sign of V_{SR}. For large l, the cross sections are symmetric under interchange of the amplitudes obtained from the equations corresponding to the two different values of the total angular momentum of the neutron. Therefore the corresponding partial waves are insensitive to a change in sign of V_{SR}. For small l the change in sign of V_{SR} is unimportant because the spin-orbit potential is small compared to the other terms in the equation. Thus the insensitivity of the cross sections to the change in sign of V_{SR} is caused, on the one hand, by the smallness of the spin-orbit coupling, which in particular cases permits us to treat the spin-orbit term as a perturbation, and on the other hand by the smallness of the neutron spin compared to the orbital angular momentum when l is sufficiently large. For the same reasons, changing the polarization of the elastically scattered neutrons practically reduces to just a change in sign.

The picture is different when we consider bound states on the shell model, where the sign of the spin-orbit coupling constant is extremely important, since it determines the ordering of the levels with different values of j. As shown by experiment, the levels with $j = l + \frac{1}{2}$ always lie below those for $j = l - \frac{1}{2}$, i.e., the potential should be deeper for the first case. This determines the sign of the spin-orbit interaction in the shell model. The

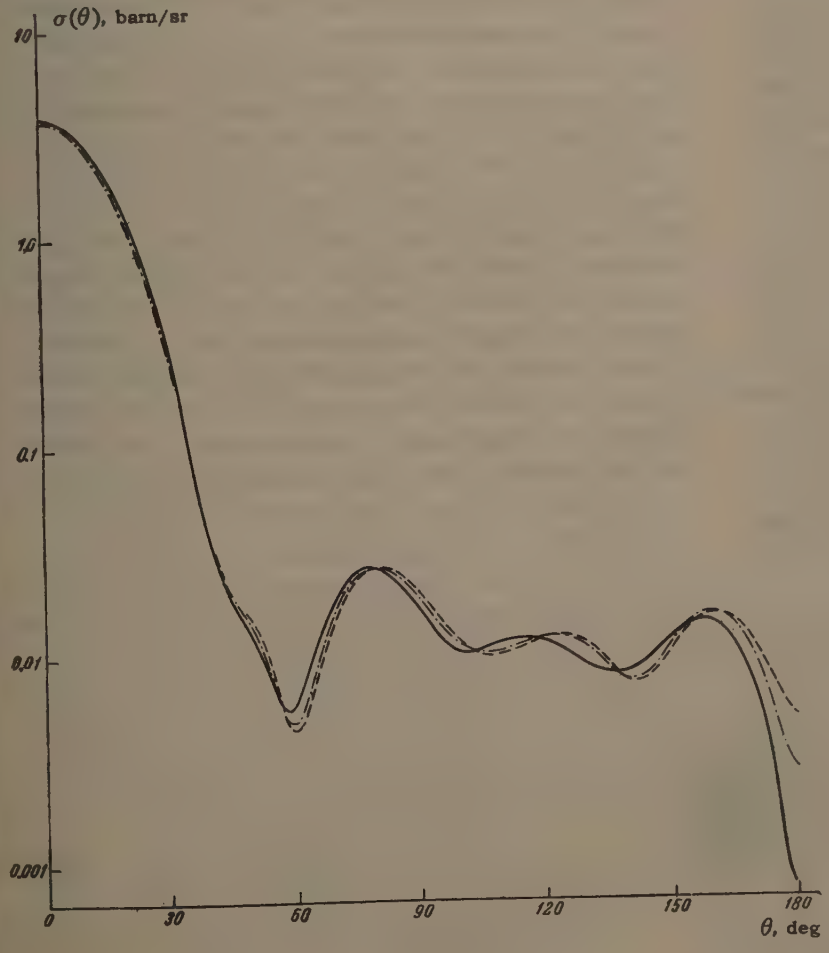

FIG. 5. Dependence of angular distribution on strength of spin-orbit coupling: solid curve for V_{SR} = 10.35 Mev, dot-dash curve for V_{SR} = 8.3 Mev, dashed curve for V_{SR} = 7.7 Mev.

computations in the present work were made with the sign which gives the correct ordering of levels.

3. THE WOODS-SAXON POTENTIAL AND ITS COMPARISON WITH THE POLYNOMIAL POTENTIAL

Except for the parameters d_r and V_{SR}, all the parameters of the potential (1), for which one can get a good description of the experimental cross sections, agree with those of BF. As was shown above, the difference in the values of the parameter V_{SR} (7.7 and 8.3 Mev) cannot be significant. But our value of d_r (3.36 fermi) gives a value of the diffuseness $\Delta \approx 3.44$ fermi which is considerably different from the value $\Delta \approx 2.84$ which follows from BF. (Δ is the size of the region over which the absolute value of the real part of the potential drops from 0.9 to 0.1 of its maximum value.) In order to find the reason for this disagreement, calculations were made with a potential having the same parameters as BF:

$$\rho(r) = \left[1 + \exp\left(\frac{r-R}{a}\right)\right]^{-1}, \qquad q(r) = \exp\left[-\left(\frac{r-R}{b}\right)^2\right];$$
$$a = 0.65 \text{ f}, \quad b = 0.98 \text{ f}, \quad R = 1.25\, A^{1/3} \text{ f},$$
$$V_{CR} = 44 \text{ Mev}, \quad V_{CI} = 11 \text{ Mev}, \quad V_{SR} = 8.3 \text{ Mev}. \tag{4}$$

Computations were done with the potential (4) for Al and Cu. In both cases the computed integral cross sections were lower than the experimental values and, consequently also lower than the theoretical cross sections of BF. The difference in the total cross sections reaches around $\sim 6-8\%$. The results are given together with the experimental data in Table I. In the same table we give the results of computations for Cu using a potential of the form (1), giving a least squares fit to potential (4) (so that the diffuseness is almost the same for both). The cross sections found for these two potentials differ relatively little; in particular the total cross sections differ by less than 2%. There is a somewhat larger difference between corresponding cross sections σ_r, apparently resulting from the fact that the approximation of the Gaussian by a fourth-degree polynomial is not sufficiently accurate.

A comparison of the corresponding differential cross sections is shown in Fig. 6. In the region of large angles, the angular distribution for the polynomial potential is shifted somewhat to the left relative to the analogous curve for the potential (4). A comparison of the results for potentials (1) and (4), giving a least-squares fit to one another, shows that potentials with the same diffuseness give almost equivalent results, irrespective of the analytic form of the functions describing the potential.

In the computations with the potential (4), we again used the Runge-Kutta method for solving the Schrödinger equation. However in this case the solution at the initial point is not known analytically. We therefore found it by two different methods: either by representing the solution as a power series and determining the coefficients in the expansion from the condition that the solution be finite at the origin, or by choosing the starting point r_1 at some distance from the center of the nucleus, where the change in the potential can still be neglected and where, consequently, we can obtain a solution in analytic form. The computations of the starting data must be carried to the required accuracy. In particular, when the solution near the origin is represented in terms of spherical Bessel functions one should use the exact tables,[13] since the use of the usual recursion relations leads to a great loss of accuracy. The exactness of the solution of the equation also is determined by the choice of step in the Runge-Kutta method and by the joining radius, beyond which the nuclear potential is set equal to zero. Our values for these quantities are in good agreement with those of Buck et al.[14] Table II illustrates the dependence of the computational results on the position of the initial and final points, $x_1 = k_0 r_1$ and $x_2 = k_0 r_2$, for the case of Cu with a

Table I

	σ_t, b		σ_r, b	
	Al	Cu	Al	Cu
Experiment [7,8]	1.73±0.03	2.96±0.06	0.97±0.02	1.49±0.02
Theory, with potential and parameters (3)	1.77	2.96	1.01	1.49
Theory with potential (4)	1.63	2.73	0.97	1.40
Theory with potential (1) approximating potential (4)	—	2.69	—	1.33
According to BF [8]	—	—	1.02	1.50

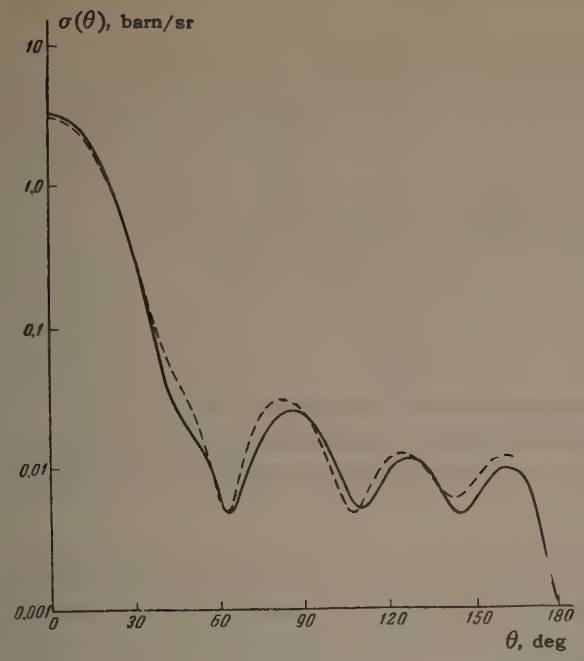

FIG. 6. Comparison of differential cross sections for Cu, calculated using potential (4) (solid curve), and with a potential (1) giving a least-squares fit to potential (4) (dashed curve).

particular choice of parameters ($k_0 = \sqrt{2MV_{CR}/\hbar^2}$). The results of the computation, using the two different methods for determining the starting values, agree to sufficient accuracy. We give them, in barns:

	σ_t	σ_s	σ_r
Expansion in power series:	2.732	1.329	1.403
Using solution for constant potential:	2.733	1.329	1.404

The correctness of the calculations with potential (1) was checked by a hand computation. The program for potential (4) was entirely analogous to that for potential (1). The only difference between the programs arose from the difference between the right hand sides of the equations, and the calculation of these was also checked by hand computation. Thus we may assume that our results are reliable.

4. CONCLUSIONS

1. Using a potential with surface absorption and including spin-orbit coupling, one can get a satisfactory description of the experimental cross sections (total, absorption and elastic) for a wide range of nuclei, with a set of parameters which is independent of mass number A.

2. One can equally well use a potential described by polynomials or a potential of the Woods-Saxon type, since to sufficiently good approximation they give equivalent results.

3. Our computations using the potential and parameter values given by Bjorklund and Fernbach[3] give integral cross sections which are somewhat different from the results in their paper. In particular, the total cross sections calculated by us are less than the experimental values (with a difference which reaches $\sim 6-8\%$).

Table II

x_1	x_2	σ_t, b	σ_s, b	σ_r, b
0.871	11.871	2.736	1.332	1.404
0.871	13.871	2.745	1.337	1.408
0.871	15.871	2.746	1.338	1.408
0.871	17.871	2.746	1.338	1.408
0.871	25,871	2.746	1.338	1.408
0.4355	20.4355	2.746	1.338	1.408
2.2451	20.2451	2.747	1.339	1.408
3.2451	20.2451	2.751	1.344	1.408
2.2451	11.2451	2.731	1.335	1.396

The authors express their sincere thanks to Prof. I. S. Shapiro for his interest in the work and discussion of the results; to Prof. A. N. Tikhonov, under whose direction the computational part of the work was done, and to V. M. Martynova, who did most of the programming and the computations on the "Strela" digital computer of Moscow State University.

[1] R. D. Woods and D. S. Saxon, Phys. Rev. 95, 577 (1954).

[2] Luk'yanov, Orlov, and Turovtsev, JETP 35, 750 (1958), Soviet Phys. JETP 8, 521 (1959); Nuclear Phys. 8, 325 (1958).

[3] F. Bjorklund and S. Fernbach, Phys. Rev. 109, 1295 (1958).

[4] Culler, Fernbach, and Sherman, Phys. Rev. 101, 1047 (1956).

[5] Wyatt, Wills, and Green, Phys. Rev. 119, 1031 (1960).

[6] I. I. Levintov, JETP 30, 987 (1956), Soviet Phys. JETP 3, 796 (1956).

[7] Coon, Graves, and Barschall, Phys. Rev. 88, 562 (1952).

[8] MacGregor, Ball, and Booth, Phys. Rev. 108, 726 (1957).

[9] W. G. Gross and R. G. Jarvis, Nuclear Phys. 15, 155 (1960).

[10] L. A. Rayburn, Phys. Rev. 116, 1571 (1959).

[11] I. S. Shapiro, UFN 75, 61 (1961), Soviet Phys.-Uspekhi 4, 674 (1962).

[12] Vanetsyan, Klyucharev, and Fedchenko, Atomnaya énergiya 6, 661 (1959).

[13] Tables of Spherical Bessel Functions, New York, 1947.

[14] Buck, Maddison, and Hodgson, Phil. Mag. 5, 1181 (1960).

Translated by M. Hamermesh
273

SCATTERING OF POLARIZED NEUTRONS BY FERROMAGNETS AND ANTIFERROMAGNETS

Yu. A. IZYUMOV and S. V. MALEEV

Leningrad Physico-technical Institute, Academy of Sciences, U.S.S.R.; Institute for Metal Physics, Academy of Sciences, U.S.S.R.

Submitted to JETP editor June 9, 1961

J. Exptl. Theoret. Phys. (U.S.S.R.) 41, 1644-1648 (November, 1961)

We consider the change in polarization resulting from scattering of polarized neutrons by ferromagnets and antiferromagnets. We show how one can determine the magnetic scattering cross section from measurements of the scattering cross section in a given direction and the polarization of the scattered neutrons.

RECENTLY one of the present authors showed[1] that by studying the polarization resulting from the scattering of unpolarized neutrons by ferromagnets one can, in certain cases, separate out from the scattering in a given direction a part which is due to inelastic magnetic scattering and a part which is due to magneto-vibrational scattering. It is obvious that polarization cannot result from the scattering of unpolarized neutrons by antiferromagnets. This is related to the fact that the system as a whole (neutron + scatterer) is not characterized by any pseudovector along which the polarization of the scattered neutron might be directed. (The direction of magnetization of the sublattices does provide an axis for the system, but not a direction, since the sublattices are equivalent.) Nevertheless it is obvious that the polarization vector can be rotated upon scattering of polarized neutrons in an antiferromagnet. Similarly, in the scattering of polarized neutrons by a ferromagnet, in addition to a change in the magnitude of the polarization vector there may also be a rotation of its direction.

In this paper we show how, by studying the polarization after scattering, one can separate from the cross section for scattering in a given direction parts which are associated with inelastic magnetic scattering and with magneto-vibrational scattering. We start with the scattering by ferromagnets. It is well known that the neutron polarization vector after scattering is given by the formula

$$\mathbf{P} = \mathrm{Sp}\, f^{+}\sigma f\rho / \mathrm{Sp}\, f^{+}f\rho, \qquad (1)$$

where $\frac{1}{2}\sigma$ is the neutron spin and

$$\rho = \tfrac{1}{2}(1 + \sigma \mathbf{P}_0) \qquad (2)$$

is the spin density matrix of the incident neutrons, $\mathbf{P}_0$ is the polarization of the beam before the scattering, and f is the scattering amplitude which, according to Halpern and Johnson,[2] is given by the formula

$$f = \frac{1}{N}\sum_l e^{i\mathbf{q}\mathbf{R}_l}\left[A_l + \frac{1}{2}B_l(\mathbf{I}_l\sigma)\right] - \frac{N_m}{N}\frac{1}{N_m}\sum_j e^{i\mathbf{q}\mathbf{R}_j} \times \gamma r_0 F(q)\,(\sigma - (\mathbf{e}\sigma)\,\mathbf{e},\ \mathbf{S}_j). \qquad (3)$$

Here N is the total number of atoms in the system, $\mathbf{R}_l$ and $A_l + \frac{1}{2}B_l(\mathbf{I}_l\sigma)$ are the coordinate and the nuclear scattering amplitude of the l'th atom (where $\mathbf{I}_l$ is the spin of the nucleus of the l'th atom). The sum on l is extended over all atoms in the system (where N_m is the number of magnetic atoms), $\mathbf{R}_j$ and $\mathbf{S}_j$ are the coordinate and spin of the j'th magnetic atom (where the sum over j goes over all the magnetic atoms in the system)*, $\mathbf{q} = \mathbf{p} - \mathbf{p}'$ is the momentum transferred by the neutron to the scatterer, $\mathbf{e} = \mathbf{q}/q$, $F(q)$ is the magnetic form factor of the atom, γ is the absolute value of the neutron magnetic moment in nuclear magnetons, and $r_0 = e^2(mc^2)^{-1}$ is the classical radius of the electron.

For simplicity, we shall assume that the ferromagnet consists of atoms of one sort, i.e., $N_m = N$ and the sum over l coincides with the sum over j. Using (1) — (3), it is easy to calculate the polarization vector resulting from the nuclear scattering and the interference between nuclear and magnetic scattering (such interference being possible both for elastic scattering and for scattering with emission or absorption of phonons), and also the polarization vector resulting from magnetic inelastic scattering; in doing this we shall assume that the nuclei are unpolarized.

The polarization vector from incoherent nuclear scattering of neutrons has the form

*For simplicity, we assume that all the magnetic atoms in the system are identical.

$$\mathbf{P}_{\text{inc}} = \mathbf{P}_0 \frac{\overline{|A_l|^2} - |\overline{A}_l|^2 - \frac{1}{12}\overline{|B_l|^2 I_l(I_l+1)}}{\overline{|A_l|^2} - |\overline{A}_l|^2 + \frac{1}{4}\overline{|B_l|^2 I_l(I_l+1)}}. \quad (4)$$

The bar denotes an average over the distribution of isotopes in the lattice.

The polarization vector for neutrons which are scattered without a change in the magnetic state of the scatterer (i.e. without emission or absorption of spin waves) is given by the formula

$$\mathbf{P}_{nm} = \{\mathbf{P}_0|\overline{A}_l|^2 - 2\gamma r_0 F(q)\langle S_z\rangle(\operatorname{Re}\overline{A}_l\mathbf{M} + \operatorname{Im}\overline{A}_l[\mathbf{M}\mathbf{P}_0]) + \gamma^2 r_0^2 F^2(q)\langle S_z^2\rangle[2\mathbf{M}(\mathbf{M}\mathbf{P}_0) - \mathbf{P}_0 M^2]\}\{|\overline{A}_l|^2 - 2\gamma r_0 F(q)\langle S_z\rangle \operatorname{Re}\overline{A}_l(\mathbf{M}\mathbf{P}_0) + \gamma^2 r_0^2 F^2(q)\langle S_z^2\rangle M^2\}^{-1}, \quad (5)^*$$

where the vector $\mathbf{M}$ is

$$\mathbf{M} = \mathbf{m} - (\mathbf{em})\,\mathbf{e} \quad (6)$$

($\mathbf{m}$ is a unit vector along the direction of magnetization of the scatterer), and $\langle S_z\rangle$ and $\langle S_z^2\rangle$ are the average values of the spin projection along the direction of magnetization and of its square; it is usually assumed that $\langle S_z\rangle^2 = \langle S_z^2\rangle$. In particular, expression (5) gives the polarization of neutrons which are scattered in the directions of the Bragg peaks, since along these directions we can neglect the contribution to the total intensity from incoherent nuclear scattering and from inelastic scattering.

The polarization vector $\mathbf{P}_{\vec{m}}^{+}$ (or $\mathbf{P}_{\vec{m}}^{-}$) which results from scattering with emission (or absorption) of one spin wave, or more precisely from a scattering process in which the total number of spin waves increases (or decreases) by unity, and in which phonons may be emitted or absorbed, has the form

$$\mathbf{P}_{\vec{m}}^{\pm} = \frac{\mp 2\mathbf{e}(\mathbf{em}) + 2\mathbf{M}_x(\mathbf{M}_x\mathbf{P}_0) + 2\mathbf{M}_y(\mathbf{M}_y\mathbf{P}_0) - \mathbf{P}_0(M_x^2 + M_y^2)}{1 + (\mathbf{em})^2 \pm 2(\mathbf{P}_0\mathbf{e})(\mathbf{em})}. \quad (7)$$

The x and y coordinate axes are perpendicular to the direction of $\mathbf{m}$. The vectors $\mathbf{M}_{x,y} = \mathbf{n}_{x,y} - (\mathbf{e}\cdot\mathbf{n}_{x,y})\mathbf{e}$, while $\mathbf{n}_x$ and $\mathbf{n}_y$ are unit vectors in the directions of the x and y axes. It is easily seen that the expression (7) is independent of rotation around the direction of the vector $\mathbf{m}$. We shall show this when we discuss polarization from antiferromagnets (see below).

The average value of the polarization vector of the neutrons scattered in a given direction has the form†

$$\mathbf{P} = \frac{\mathbf{P}_{\text{inc}}\sigma_{\text{inc}}(\mathbf{n}) + \mathbf{P}_{nm}\sigma_{nm}(\mathbf{n},\mathbf{P}_0) + \mathbf{P}_{\vec{m}}^{+}\sigma^{+}(\mathbf{n},\mathbf{P}_0) + \mathbf{P}_{\vec{m}}^{-}\sigma^{-}(\mathbf{n},\mathbf{P}_0)}{\sigma_{\text{inc}}(\mathbf{n}) + \sigma_{nm}(\mathbf{n},\mathbf{P}_0) + \sigma_{\vec{m}}^{+}(\mathbf{n},\mathbf{P}_0) + \sigma_{\vec{m}}^{-}(\mathbf{n},\mathbf{P}_0)}. \quad (8)$$

Here $\mathbf{n}$ is the scattering direction, σ_{inc} is the cross section for incoherent scattering, and

$$\frac{\sigma_{nm}(\mathbf{n},\mathbf{P}_0)}{\sigma_n(\mathbf{n})} = 1 + \frac{-2\gamma r_0 F(q)\langle S_z\rangle \operatorname{Re}\overline{A}_l\mathbf{M}\mathbf{P}_0 + \gamma^2 r_0^2 F^2(q)\langle S_z^2\rangle M^2}{|\overline{A}_l|^2}, \quad (9)$$

$$\frac{\sigma_{\vec{m}}^{\pm}(\mathbf{n},\mathbf{P}_0)}{\sigma_{\vec{m}}^{\pm}(\mathbf{n})} = \frac{1 + (\mathbf{em})^2 \pm 2(\mathbf{P}_0\mathbf{e})(\mathbf{em})}{1 + (\mathbf{em})^2}, \quad (10)$$

where $\sigma_n(\mathbf{n})$ is the cross section for nuclear scattering of unpolarized neutrons, and $\sigma_{\vec{m}}^{\pm}(\mathbf{n})$ is the cross section for magnetic scattering of unpolarized neutrons in which the number of spin waves increases or decreases by unity.

The quantity $\sigma_{nm}(\mathbf{n},\mathbf{P}_0)$ is the cross section for coherent scattering of polarized neutrons (with no change in the magnetic state of the scatterer). It consists of the coherent nuclear scattering cross section, the cross section for magneto-vibrational scattering, and an interference term. The expression on the right of formula (9) includes all three of these terms; $\sigma_{\vec{m}}^{\pm}(\mathbf{n},\mathbf{P}_0)$ is the cross section for magnetic scattering of polarized neutrons with increase or decrease of the number of spin waves by unity. Since neutrons which undergo scatterings of different types do not interfere, formula (8) is obtained by adding the vectors (4), (5), and (7) with weights corresponding to the relative intensities of the different scattering processes.

Formula (8) describes the polarization of neutrons scattered in a given direction. In writing it we have neglected the fact that the vector $\mathbf{e}$ depends on the energy of the scattered neutrons. We can do this because usually the intensity of neutrons from magnetic scattering is significantly different from zero only when $\mathbf{q}$ is approximately equal to τ (where τ is any vector of the reciprocal lattice), but then $\mathbf{e} = \mathbf{q}q^{-1} \approx \tau/\tau$, so that it is independent of the energy. It is interesting to note the following. When $\sigma_{\text{inc}}(\mathbf{n}) = 0$ (which is the case for a lattice consisting of atoms of a single spinless isotope), the polarization vector of the neutrons scattered into a given direction is given by a linear combination of the three vectors $\mathbf{P}_{mn}$, $\mathbf{P}_{\vec{m}}^{+}$ and $\mathbf{P}_{\vec{m}}^{-}$, which in general are not coplanar. These vectors are defined by (5) and (7). From these equations, we see that we can calculate them beforehand if we know the nuclear scattering amplitude, the vector $\mathbf{e}$, $F(q)$, $\mathbf{P}_0$ and $\langle S_z\rangle$. Thus, having measured $\mathbf{P}$, we can determine the coefficients appearing in these three vectors. By measuring, in addition, the total cross section in the same direction,

*$[\mathbf{MP}_0] = \mathbf{M}\times\mathbf{P}_0$; $(\mathbf{MP}_0) = \mathbf{M}\cdot\mathbf{P}_0$.

†In general there is also a polarization whose vector has the form $\mathbf{P}' = 2(\mathbf{P}\mathbf{M}_0)\mathbf{M}/M^2 - \mathbf{P}_0$, which is associated with the absorption or emission of an even number of spin waves. We shall neglect this polarization, since it can be shown that such processes are improbable; in any case it is easy to include it if necessary.

$$\sigma(\mathbf{n}, \mathbf{P}_0) = \sigma_{mn}(\mathbf{n}, \mathbf{P}_0) + \sigma_m^+(\mathbf{n}, \mathbf{P}_0) + \sigma_m^-(\mathbf{n}, \mathbf{P}_0),$$

we can obviously determine $\sigma_{mn}(\mathbf{n}, \mathbf{P}_0)$, $\sigma_m^+(\mathbf{n}, \mathbf{P}_0)$ and $\sigma_m^-(\mathbf{n}, \mathbf{P}_0)$ individually, and consequently find $\sigma_n(\mathbf{n})$ and $\sigma_m^{\pm}(\mathbf{n})$.

Now let us go on to the scattering from antiferromagnets. Since the chemical elementary cell of an antiferromagnet consists, as a rule, of atoms of different sorts, we cannot represent the incoherent nuclear scattering in the form (4). However, the essential point for us is that this polarization is proportional to the polarization vector of the incident beam, and can therefore be written in the form

$$\mathbf{P}_{inc} = \alpha \mathbf{P}_0, \tag{11}$$

where the coefficient α has a quite complicated form which does not matter for our purposes. We give the expression only for the case of purely elastic scattering:

$$\alpha = \frac{\sum \left\{ (|A_i|^2 - |\bar{A}_i|^2) - \frac{1}{12} |\overline{B_i}|^2 I_i (I_i+1) \right\} e^{-2W_i}}{\sum \left\{ (|A_i|^2 - |\bar{A}_i|^2) + \frac{1}{4} |\overline{B_i}|^2 I_i (I_i+1) \right\} e^{-2W_i}}, \tag{12}$$

where the summation over i extends over all atoms in the chemical unit cell, and W_i is the Debye-Waller factor for the i'th atom of the cell.

The polarization does not change in coherent nuclear scattering. The interference term between nuclear and magnetic scattering does not appear in the expression for the polarization. This is easily understood if we note that in the ferromagnetic case the interference term contained the spontaneous magnetization vector linearly. Since the spontaneous magnetization in an antiferromagnet is equal to zero and the sublattices are completely equivalent, it is obvious that the interference must go to zero.

The polarization vector resulting from scattering with no change in the magnetic state of the scatterer (or with a change in state for which the total number of spin waves changes by an even number) is easily calculated if we assume that the antiferromagnet consists of two sublattices. It has the form

$$\mathbf{P}_{m0} = 2(\mathbf{M}\mathbf{P}_0)\mathbf{M}/M^2 - \mathbf{P}_0, \tag{13}$$

where $\mathbf{M} = \mathbf{m} - (\mathbf{e}\cdot\mathbf{m})\mathbf{e}$, and $\mathbf{m}$ is the direction of the magnetization vector of either sublattice.

In particular, this formula describes the polarization of neutrons scattered into those Bragg peaks of the magnetic scattering which do not coincide with nuclear Bragg peaks, since in these directions we can neglect all scattering processes other than magnetic elastic scattering. It is not hard to show that the vector $\mathbf{P}_{m0}$ is equal to $\mathbf{P}_0$ in absolute value. Resolving the vector $\mathbf{P}_0$ into two components, parallel and perpendicular to $\mathbf{M}$, and substituting in (13), we can easily show that $\mathbf{P}$ is obtained from $\mathbf{P}_0$ by a rotation about $\mathbf{M}$ through 180°.

Thus if $\mathbf{P}_0$ is parallel to $\mathbf{M}$, then the polarization is not changed by the magnetic reflection, and this result is obviously valid for any Bragg peak. But if $\mathbf{P}_0$ is perpendicular to $\mathbf{M}$, then for magnetic Bragg peaks which do not coincide with nuclear peaks the polarization changes sign, while for magnetic Bragg peaks which coincide with nuclear peaks the polarization is equal to

$$\mathbf{P} = \mathbf{P}_0 (\sigma_{nuc} - \sigma_{mag}) / (\sigma_{nuc} + \sigma_{mag}), \tag{14}$$

where σ_{nuc} and σ_{mag} are the cross sections for nuclear and magnetic scattering in the direction of the Bragg peak. From here on the cross sections for nuclear and magnetic scattering are taken for the total number of atoms in the scatterer.

We still must find the formula for the polarization vector from scattering in which the number of spin waves changes by one. Noting that such scattering is associated with the components of the atomic spin vectors which are perpendicular to the magnetization of the sublattices, we can get the formula

$$\mathbf{P}_{m1} = 2\frac{\mathbf{M}_x(\mathbf{M}_x\mathbf{P}_0) + \mathbf{M}_y(\mathbf{M}_y\mathbf{P}_0)}{M_x^2 + M_y^2} - \mathbf{P}_0 \tag{15}$$

(for more detail concerning inelastic scattering from antiferromagnets, cf. [4]). This expression can be written in invariant form:

$$\mathbf{P}_{m1} = 2\frac{\mathbf{P}_{0\perp} - \mathbf{e}_\perp(\mathbf{P}_0\mathbf{e}) + \mathbf{e}(\mathbf{em})(\mathbf{MP}_0)}{1 + (\mathbf{em})^2} - \mathbf{P}_0, \tag{16}$$

where $\mathbf{P}_{0\perp}$ and $\mathbf{e}_\perp$ are the components of the vectors $\mathbf{P}_0$ and $\mathbf{e}$, perpendicular to the vector $\mathbf{m}$. Thus, for example, $\mathbf{P}_{0\perp} = \mathbf{P}_0 - (\mathbf{Pm})\mathbf{m}$. It is natural that the scattering in an antiferromagnet with absorption or with emission of spin waves is the same, since the operators for creation and annihilation of spin waves enter symmetrically in the scattering amplitude if we disregard factors which are unimportant in calculating the polarization (cf. [4]). Now using (11), (13) and (15), we can represent the average polarization of the neutrons scattered in a given direction in the form

$$\mathbf{P} = \frac{\alpha\sigma_{inc}(\mathbf{n})\mathbf{P}_0 + \sigma_{m0}(\mathbf{n})\mathbf{P}_{m0} + \sigma_{m1}(\mathbf{n})\mathbf{P}_{m1}}{\sigma_n(\mathbf{n}) + \sigma_{m0}(\mathbf{n}) + \sigma_{m1}(\mathbf{n})}. \tag{17}$$

Here $\sigma_n(\mathbf{n})$ is the cross section for nuclear scattering in the direction of $\mathbf{n}$, $\sigma_{m0}(\mathbf{n})$ is the cross section for magnetic scattering in which the number of spin waves does not change or changes by

an even number, and finally $\sigma_{m1}(\mathbf{n})$ is the cross section for scattering in which the number of spin waves changes by unity. With respect to the applicability of this formula, the same remark applies as was made concerning formula (8). Formula (17) obviously allows us to determine α, $\sigma_{m0}(\mathbf{n})$ and $\sigma_{m1}(\mathbf{n})$ if we know the polarization P_0 and the total cross section for scattering in the given direction:

$$\sigma(\mathbf{n}) = \sigma_n(\mathbf{n}) + \sigma_{m0}(\mathbf{n}) + \sigma_{m1}(\mathbf{n}). \qquad (18)$$

It should be mentioned that (17), like formula (8), is valid only close to Bragg peaks, so that $e \approx \tau/\tau$.

[1] S. V. Maleev, JETP 40, 1224 (1961), Soviet Phys. JETP 13, 860 (1961).

[2] O. Halpern and M. H. Johnson, Phys. Rev. 55, 898 (1939).

[3] S. V. Maleev, JETP 34, 1518 (1958), Soviet Phys. JETP 7, 1048 (1958).

[4] V. G. Bar'yakhtar and S. V. Maleev, JETP 39, 1430 (1960), Soviet Phys. JETP 12, 995 (1961).

Translated by M. Hamermesh
274

THE HEATING OF A GAS BY RADIATION

A. S. KOMPANEETS and E. Ya. LANTSBURG

Institute of Chemical Physics, Academy of Science, U.S.S.R.

Submitted to JETP editor June 12, 1961

J. Exptl. Theoret. Phys. (U.S.S.R.) 41, 1649-1654 (November, 1961)

The problem considered is that of the radiative propagation in a cold gas of heat originally confined in some finite region of the gas itself. It is assumed that the temperature of the hot gas is so high that the gas inside the region is transparent for the radiation. The expansion of the heated region occurs on account of radiative heat exchange with the outer, nontransparent, layer adjacent to the cold gas, and the transfer of the energy of the radiation in this layer is assumed to be diffusive. The process of expansion is regarded as a quasi-stationary propagation of the boundary of the heated region in the form of a plane wave moving through the cold gas. A method is indicated for calculating the speed of propagation of the boundary, which takes into account the nonequilibrium state of the radiation in the internal, transparent part of the heated region in the gas.

1. INTRODUCTION. STATEMENT OF THE PROBLEM

AT high temperatures, of the order of 10^5 °K and above, energy transfer in a gas occurs mainly by radiation, although the fractional part of the energy that is in the form of radiation may be small (in comparison with the energy of the matter).

The problem of the propagation of heat from a point source can be solved simply in the case in which the range of the radiation and the internal energy of the matter depend on the temperature according to a power law.[1-3] A characteristic feature of the solution is a broad "plateau" of the temperature in the middle of the heated region and a steep drop at its edge. It is easy to understand this behavior of the solution, since in the middle, where the thermal conductivity is larger, the temperature is more easily equalized; it is obvious that a strict power-law dependence of the thermal conductivity on the temperature is not necessary for this result.

If the temperature dependence of the range of the radiation in the gas is strong enough, the solution obtained in this way can lead to the following internal contradiction: the range of the radiation inside the hot region is comparable with, or even larger than, the size of the region itself. It is obvious that the mechanism of energy transfer can then not be described in terms of thermal conductivity, whereas the basis of the solution in [1-3] was the thermal-conduction mechanism, i.e., the assumption of local thermodynamic equilibrium between the radiation and the matter.

In the present paper we consider the case in which this assumption does not hold, as can happen at temperatures $\sim 10^6$ °K and higher. In this case (even after a number of simplifying assumptions) a rigorous statement of the problem for the entire heated region is possible only by the use of the integral equation of radiative transfer. If, however, the range varies strongly enough with the temperature, the problem can be solved to good approximation by a simpler method.

Let the size of the hot region be R. Then the temperature T_0 at which the range is equal to R is given by the equation

$$l(T_0) = R. \tag{1}$$

The definition of $l(T)$ will be given later. When l depends strongly on T, the dependence of the temperature T_0 on R is weak.

According to the definition (1) the whole heated region divides into two parts: an inner part which is transparent, and an outer part of small transparency bordering on the cold gas. Actually, on the low-temperature side the gas becomes transparent again at temperatures below $\sim 10^4$ °K.[4] Therefore there is a leakage of energy from the hot region "to infinity." If, however, the temperature in the inside region is sufficiently high, we can neglect the effect of this leakage in the overall energy balance of the entire heated region. Accordingly we assume that the temperature of the outer cold gas and the range of the radiation in it are equal to zero.

2. THE TRANSPARENT INNER REGION

Let us now consider the state of the radiation in the transparent region. Since the range of the radiation in this region is large in comparison with its size, we must suppose that the energy density U_1 of the radiation inside the hot region is constant over its cross section (but varies with time). Furthermore U_1 is much smaller than the equilibrium energy density aT^4 of radiation at the temperature T of the matter inside the region ($a = 7.55 \times 10^{-15}$ erg cm^{-3} deg^{-4}). It is obvious that everywhere inside the transparent region $T > T_0$. The drop of the temperature to T_0 near the boundary of the transparent region is not due to the radiation, but occurs in some other way (for example, by electronic thermal conductivity). Since the temperature drop takes place in a distance shorter than the range of the radiation, the energy density U of the radiation at the boundary of the transparent region is the same as inside the region, that is, it is equal to U_1.

It is not hard to estimate the order of magnitude of U_1. Namely

$$U_1(T) \approx RaT^4/l(T). \tag{2}$$

Thus here the range $l(T)$ characterizes the emissive power per unit volume of the hot gas, which is equal to $caT^4/l(T)$ (c is the speed of light). The quantity $[l(T)]^{-1}$ is equal to the spectral absorption coefficient averaged over the Planck distribution with induced emission taken into account.[5] For our further work it is convenient to introduce the effective temperature T_1 of the radiation by the formula $U_1 \equiv aT_1^4$, or

$$T_1 = T\,[R/l(T)]^{1/4}. \tag{3}$$

In order for the heated region to expand by radiative energy transfer, it is necessary that each point of the nontransparent region receive radiation of a temperature T_1 somewhat higher than the local temperature of the matter. In our present problem the energy density of the radiation can considerably exceed the local equilibrium density aT^4 (in the approximation of radiative thermal conductivity this excess is regarded as infinitely small). In particular, at the boundary of the nontransparent region at $T = T_0$ we must also have the inequality

$$U_1 > aT_0^4. \tag{4}$$

Let us find the condition for this inequality to hold. By means of Eqs. (1) and (2) ratio U_1/aT_0^4 can be written in the form $l(T_0)aT^4/l(T)aT_0^4 = (T/T_0)^{4-n}$. For a completely ionized gas the power-law index n is $7/2$.[5,6] In an incompletely ionized gas it is smaller than $7/2$; that is, the inequality (4) is satisfied for $T > T_0$.

3. THE NONTRANSPARENT OUTER LAYER AND ITS SPEED OF PROPAGATION

The nontransparent region is that in which the temperature falls from T_0 to zero. The thickness of this region is much smaller than R, and therefore as an approximation it can be treated as a plane layer. In other words, at each instant we can assume that the transparent region occupies a half-space, and the state of the radiation in it is characterized by the temperature T_1. The boundary of the transparent region will then shift toward the colder gas at a constant speed $v(T_1, T_0)$. Any point of the nontransparent layer will shift at the same speed, in accordance with the fact that its thickness is much smaller than R.

Thus we have reduced the problem of the heating of a gas by radiation to that of finding the quasi-stationary mode of propagation of a plane thermal wave into the cold gas (cf.[7]). The radial distributions of the temperatures T of the matter and T_1 of the radiation are shown qualitatively in Fig. 1. The dashed area corresponds to the nontransparent layer.

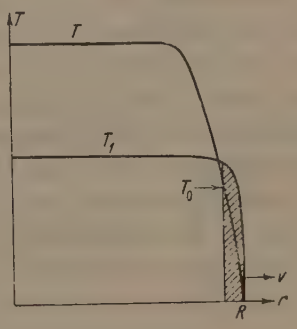

FIG. 1

Let us now write down the equation of radiative transfer of heat in the nontransparent region. For the energy density ϵ of the matter and the energy flux S we obviously have the relation

$$\partial(\varepsilon + U)/\partial t + \partial S/\partial x = 0. \tag{5}$$

We shall neglect all types of energy transfer other than the radiative transfer. At the high temperatures we are dealing with here the energy transfer by radiation occurs so rapidly that the gas does not have time to react to the change of pressure and is not set in motion; in other words, we can neglect the hydrodynamic energy transfer. We assume that $\epsilon = \rho c_V T$, where ρ is the density

of the gas and c_V is the specific heat at constant volume, which we shall assume is independent of the temperature. Let us now write the energy-balance equation for the radiation alone:

$$\partial U/\partial t + \partial S/\partial x = c\,(aT^4 - U)/l\,(T). \qquad (6)$$

The right member of Eq. (6) expresses the balance between the emission and absorption of radiative energy.

Since the range of the radiation decreases rapidly as the temperature falls, we can take it to be much smaller than the thickness of the region. Then we can treat the radiative transfer of energy in the diffusive approximation, [4] so that

$$S = -\tfrac{1}{3}\, l' c \partial U/\partial x. \qquad (7)$$

In the approximation of radiative thermal conductivity one puts aT^4 instead of U in this equation. In the present problem this approximation is inadequate, since it leads to a zero speed of propagation. The range l' is not the same average over frequencies as the range $l\,(T)$ used earlier, which characterizes the emissive power of the transparent region of the hot gas. We shall, however, suppose for simplicity that in the nontransparent region the l of Eq. (6) and the l' of Eq. (7) are equal (cf. [4,8]).

The boundary conditions for the system (5)—(7) are as follows: at the boundary of the transparent region $T = T_0$, $U = U_1$; at the forward boundary of the heated gas $T = 0$, $S = 0$, $U = 0$.

Since we are looking for a stationary mode of propagation, we must assume that all quantities depend on the coordinates and the time only through the argument $x - vt$.* In addition, it is convenient to introduce the optical thickness τ, whose differential is

$$d\tau = dx/l\,(T)$$

(the coordinate x is measured in the direction of decreasing temperature), and go over to dimensionless quantities

$$\gamma = \frac{aT_0^4}{\varepsilon\,(T_0)}, \quad \beta = \frac{v}{c}, \quad u = \frac{U}{aT_0^4}\left(\frac{\gamma}{\sqrt{3}\beta}\right)^{4/3}, \quad s = \frac{\sqrt{3}S}{caT_0^4}\left(\frac{\gamma}{\sqrt{3}\beta}\right)^{4/3},$$

$$u_1 = \frac{U_1}{aT_0^4}\left(\frac{\gamma}{\sqrt{3}\beta}\right)^{4/3}, \quad u_p = \left(\frac{T}{T_0}\right)^4\left(\frac{\gamma}{\sqrt{3}\beta}\right)^{4/3}, \quad u_{p_0} = \left(\frac{\gamma}{\sqrt{3}\beta}\right)^{4/3}. \qquad (8)$$

Integration of Eq. (5) under the condition $T = S = U = 0$ (or $u_p = s = u = 0$) at the forward boundary of the heated gas at once leads to the equation

$$s = u_p^{1/4} + \sqrt{3}\beta u. \qquad (9)$$

By eliminating $d\tau$ we can get instead of the two equations (6) and (7) one ordinary differential equation

$$\frac{ds}{du} = \sqrt{3}\beta + \frac{u - u_p}{s} = \sqrt{3}\beta + \frac{u}{s} - \frac{(s - \sqrt{3}\beta u)^4}{s}, \qquad (10)$$

which, along with Eq. (9), connects the quantities s, u, and β (or the dimensional quantities S, U, and v). For a given value of the parameter β the last equation can be integrated in a unique way with the boundary condition $s = 0$, $u = 0$. At the boundary of the transparent region (with $T = T_0$, $U = U_1$, or $u_p = u_{p_0}$, $u = u_1$) this gives a quantity $s\,(u_1; \beta)$, which, according to Eq. (9), is to be equated to $u_{p_0}^{1/4} + 3^{1/2}\beta u_1$. From this one can determine the required value of the speed $\beta\,(u_1, u_{p_0})$ or $v\,(T_1, T_0)$.

Of course only those solutions for which $\beta = v/c \leq 1$ have physical meaning. In a number of cases a necessary condition for this is the inequality $U \ll \epsilon$, which we shall take as a basis for our further calculations.

The omission of U in Eq. (5) corresponds to the neglect of the second term in the right member of Eq. (9). Equation (10) can then be rewritten in the form

$$\frac{ds}{du} = \sqrt{3}\beta + \frac{u}{s} - s^3, \qquad (11)$$

with the initial condition $s = 0$ for $u = 0$.

The speed β of the wave is determined from the condition $U = U_1$ for $T = T_0$ (or $u = u_1$ for $u_p = u_{p_0}$), and the equation for the determination of β takes the form

$$s\,(u_1;\ \beta) = u_{p_0}^{1/4}. \qquad (12)$$

Through the singular (saddle) point $u = 0$, $s = 0$ only one integral curve (the separatrix) goes into the region of positive values of the quantities (Fig. 2, curve 1). We have shown in this same diagram the curve $s = u^{1/4}$, which corresponds to Eq. (9) without the second term in the right member; this is curve 2 of Fig. 2 (i.e., curve 2 corresponds to equilibrium values of the energy density of the radiation, $u = u_p$). To the prescribed values u_1 and u_p (i.e., T_1 and T_0) there correspond the points I and II on curves 1 and 2. It is obvious that Eq. (12) will be satisfied if the points I and II have the same ordinate, and from this it is clear that the speed β can be found in a unique way.

It can be seen from Fig. 2 that the actual energy density of the radiation is always larger than the equilibrium value u_p; as has been remarked,

*We note that the solution of the form $f(x - vt)$ for the equations of radiative heat transfer has also been considered earlier by a number of authors. [4,9,10]

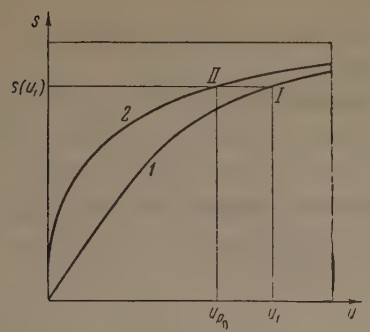

FIG. 2

this is necessary for the propagation of the thermal wave.

4. SOME SPECIAL CASES

In the general case Eq. (11) cannot be integrated in terms of known functions. Therefore we shall consider limiting cases.

1) $(T_1 - T_0)/T_1 \ll 1$. This case corresponds to the part of the curve 1 of Fig. 2 that belongs to large values of u, where the curves 1 and 2 are close to each other. For values of the argument the solution of Eq. (11) is of the form

$$s(u, \beta) \approx u^{1/4}(1 - 1/16u^{3/2}). \tag{13}$$

Here we have already dropped a term proportional to β, since β turns out to be a small quantity. Substituting the value of $s(u, \beta)$ for $u = u_1$ from Eq. (13) in Eq. (12), we get

$$\beta = \frac{v}{c} = \frac{4}{\sqrt{3}}\gamma\left(\frac{T_1 - T_0}{T_1}\right)^{1/2}. \tag{14}$$

It can be seen from Eq. (14) that if the original inequality $(T_1 - T_0) \ll T_1$ is satisfied, then even for $\gamma \sim 1$ we have $\beta \ll 1$. Therefore it is legitimate to use the more exact equation (10). This gives a more accurate value of the speed:

$$\beta = \frac{v}{c} = \frac{4}{\sqrt{3}}\frac{\gamma}{\sqrt{1+\gamma}}\left(\frac{T - T_0}{T_1}\right)^{1/2}. \tag{14a}$$

2) $T_1 \gg T_0$, but $U_1 \ll \epsilon(T_0)$. Small values of u are then important, and this corresponds to the approximate solution of Eq. (11)

$$s(u, \beta) \approx u\left(1 + \frac{\beta\sqrt{3}}{2}\right). \tag{15}$$

For $\beta \ll 1$ we get the expression

$$\beta = U_1/\sqrt{3}\,\varepsilon(T_0). \tag{16}$$

3) $\gamma \ll 1$, and T_1/T_0 is of the order of several units. We then get $\beta \ll 1$. Neglecting β in Eq. (11), we reduce this equation to a Riccati equation, which can be integrated in terms of Bessel functions of pure imaginary argument.[11] Equation (12) for the determination of the speed is then written in the form

$$I_{3/4}\left(\tfrac{4}{3}u_1^{3/2}\right) / I_{-1/4}\left(\tfrac{4}{3}u_1^{3/2}\right) = (T_1/T_0)^2. \tag{17}$$

Since $T_1 > T_0$, this equation always has a solution. Here we have assumed that $T_1 - T_0$ is not small in comparison with T_1. Then u_1 is obviously of the order of several units, and the speed is found from the equation

$$\beta = \frac{v}{c} = \frac{1}{\sqrt{3}}\frac{\gamma}{u_1^{3/4}}\left(\frac{T_1}{T_0}\right)^3. \tag{18}$$

After the speed v of the boundary of the heated gas has been determined as a function of T_1 and T_0, the problem of the propagation of the thermal wave is solved from considerations of balance. Neglecting the energy contained in the region where the temperature falls, we have the energy equation

$$\tfrac{4}{3}\pi R^3 [U_1(T) + \varepsilon(T)] = E, \tag{19}$$

which, together with the equation

$$dR/dt = v(T_1, T_0) \tag{20}$$

and the relations (1) and (2), determines R and T as functions of the time t (here T is the actual temperature of the matter in the transparent region, and E is the total energy in the wave).

The problem we have considered has meaning only as long as $T_1 > T_0$. If it turns out in the course of the solution of a given system that T_1 and T_0 are comparable, the further work of solution can be conducted in the approximation of radiative thermal conduction, since when this is true the radiation has come into equilibrium with the matter (cf. [1-3]). If the time at which this occurs is sufficiently large, there may have been time for a rather large hydrodynamical expansion of the hot region.

In conclusion we express our gratitude to Yu. P. Raĭzer for helpful discussions.

[1] Ya. B. Zel'dovich and A. S. Kompaneets, Sb. posvyashch. 70-letiyu akad. A. F. Ioffe (Collection of papers honoring the 70th birthday of Academician A. F. Ioffe), AN SSSR, 1950, page 61.

[2] G. I. Barenblatt, PMM (Appl. Math. and Mech.) **16**, 67 (1952).

[3] É. I. Andriankin, JETP **35**, 428 (1958), Soviet Phys. JETP **8**, 295 (1959).

[4] Zel'dovich, Kompaneets, and Raĭzer, JETP **34**, 1278, 1447 (1958), Soviet Phys. JETP **7**, 882, 1001 (1958).

[5] Yu. P. Raĭzer, JETP **37**, 1079 (1959), Soviet Phys. JETP **10**, 769 (1960).

[6] V. V. Bibikov and V. I. Kogan, in Collection: Fizika plazmy i problema upravlyaemykh termoyadernykh reaktsii (Plasma Physics and the Problem of Controlled Thermonuclear Reactions) AN SSSR, 1958, Vol. 3, page 86.

[7] Ya. B. Zel'dovich, Teoriya goreniya i detonatsii (The Theory of Combustion and Detonation), AN SSSR, 1944.

[8] Unsöld, Physik der Sternatmosphären, Springer Verlag, Berlin, 1938.

[9] G. I. Barenblatt, PMM (Appl. Math. and Mech.) 17, 739 (1953).

[10] I. V. Nemchinov, PMTF 1, 36 (1960).

[11] G. N. Watson, Theory of Bessel Functions, Cambridge Univ. Press, 1944, pages 85, 95.
E. Jahnke and F. Emde, Tables of Functions with Formulas and Curves, Dover Publications, New York, 1943, p. 235.

Translated by W. H. Furry
275

COLLECTIVE EXCITATIONS IN A SUPERCONDUCTOR

V. G. VAKS, V. M. GALITSKII, and A. I. LARKIN

Submitted to JETP editor June 15, 1961

J. Exptl. Theoret. Phys. (U.S.S.R.) 41, 1655-1668 (November, 1961)

We apply quantum field theory methods to find the collective excitation spectrum of a superconductor. We use the possibility to formulate superconductivity theory as a one-dimensional relativistic problem. We construct the Bethe-Salpeter equation for two-particle Green's functions, whose poles determine the excitation spectrum, in the weak coupling approximation. We obtain for a system of neutral particles a sound wave branch which does not terminate at momenta k of the order Δ, but continues into the large momentum region, and the excitation energy approaches 2Δ exponentially. In the case of charged particles the plasma oscillation dispersion is changed very little by superconductivity. We find a set of excitations with non-vanishing momenta; for small k their energy is close to 2Δ, differing by an amount quadratic in the coupling constant. For each non-vanishing component of the angular momentum along k there is one branch of the excitation spectrum which does not terminate for small k. In the large-momentum region, the energy of these excitations approaches 2Δ exponentially.

1. INTRODUCTION

THE recently developed theory of superconductivity is based upon the existence of a bound state of particles near the Fermi surface. The presence of this bound state leads to a gap in the single-particle excitation spectrum, since such excitations indicate the break-up of a bound pair. Apart from the single-particle excitations excited states corresponding to the motion of a pair can occur in the spectrum of superconductors. The interaction between the moving pair and the other pairs leads to the propagation of a collective excitation in the medium of the bound pairs. It is essential here that in excitations of this nature the particle pairs act as units in contradistinction to the situation in single-particle excitations. A study of the collective excitations is important to ascertain the stability of a state and the existence of superconductivity in it, for this requires that the appropriate criterion be satisfied by all branches of the spectrum. The collective excitations may also be important for the electrodynamics and the thermodynamics of superconductors.

The collective excitations of this kind may be considered to be bound states of two particles or quasi-particles with a non-vanishing total momentum. If the interaction between particles is non-vanishing only in the S-state, then only one kind of collective excitations with vanishing angular momentum is possible. This excitation is a sound wave in the electron system and changes into a plasma oscillation with a larger frequency when the Coulomb interaction is taken into account. Turning on an interaction with higher harmonics leads to the appearance of a number of branches of the spectrum with different angular momenta. Long-wavelength excitations of this kind were considered by Bogolyubov[1] and by Bardasis and Schrieffer.[2]

In the present paper we use Green's functions to study collective excitations. We consider the case of zero temperature. Treating the excitations as bound quasi-particle states enables us to determine their spectrum from the poles of the two-particle Green's function. We use for the evaluation of this function a method based upon the formal resemblance of our problem to a one-dimensional relativistic problem; the role of the mass is played by the magnitude of the gap, Δ, and that of the only spatial momentum is played by the nearness of the particle energy to the energy at the Fermi surface. We find the limiting frequencies and the dispersion of the oscillations with arbitrary angular momentum l in the long-wavelength region of the excitations; the results are the same as those obtained earlier by other methods for particular cases. We use the example of excitations with $l = 1$, $m = 0$ to study the spectrum $\omega(k)$ near its endpoint $\omega = 2\Delta$. We show that there are a number of branches of oscillations in the region of relatively large wave vectors. These branches may make an appreciable contribution to the electrodynamic and thermodynamic properties of superconductors.

2. THE RELATIVISTIC FORMULATION OF SUPERCONDUCTIVITY THEORY

We write the Lagrangian $\mathcal{L}(x)$ in the form

$$\int \mathcal{L}(x)\,dx = \int dx u^+(x)\left(i\frac{\partial}{\partial t} + \frac{1}{2m}\frac{\partial^2}{\partial \mathbf{x}^2} + \mu\right)u(x) + \frac{1}{2}\int dx\,dy\,u^+(x)\,u(x)\,D(x-y)\,u^+(y)\,u(y). \quad (1)$$

The spinor $u(x)$ is here the electron field operator, $x = (\mathbf{x}, t) \equiv (\mathbf{x}, x_0)$, $dx = d\mathbf{x}\,dx_0$, and μ is the chemical potential. In the case of an interaction through a potential, the function D is of the form $D(\mathbf{x}-\mathbf{y}) = V(\mathbf{x}-\mathbf{y})\,\delta(x_0 - y_0)$. For an electron interaction retarded by the exchange of phonons, D is the phonon Green's function,[3] which in the zeroth approximation is equal to

$$D^0_{ph}(x) = (2\pi)^{-4}\int dk\,d\omega e^{ikx}\frac{2\pi^2\lambda_0}{mp_F}\frac{\omega_k^2}{\omega_k^2 - \omega^2}, \quad (2)$$

where ω_k is the phonon frequency, p_F the momentum at the Fermi surface, and $\lambda_0 > 0$ Fröhlich's parameter.[4]

If we write the interaction in this form we can at the same time take into account both the direct Coulomb interaction between the electrons and the interaction through the phonons, so that for the complete problem we have

$$D(x-y) = D_{ph}(x-y) - \frac{e^2}{|\mathbf{x}-\mathbf{y}|}\delta(x_0 - y_0). \quad (3)$$

It is well known[5] that when there is superconductivity we must use three kinds of Green's functions:

$$\mathcal{G}_{\alpha\beta}(x-y) = \langle T u_\alpha(x)\,u^+_\beta(y)\rangle,$$

$$F_{\alpha\beta}(x-y) = \langle T u_\alpha(x)\,u_\beta(y)\rangle,$$

$$F^+_{\alpha\beta}(x-y) = \langle T u^+_\alpha(x)\,u^+_\beta(y)\rangle; \quad F^+_{\alpha\beta}(0^+) = -F_{\alpha\beta}{}^*(0^+). \quad (4)$$

Here α and β are spinor indices; the average is taken over the ground state of the Lagrangian (1).* It is convenient to write the functions $\mathcal{G}$, F, and F^+ in the unified form $\langle T u^{1,2}(x) u^{1,2}(y)\rangle$, where $u^1(x) = u(x)$ and $u^2(x) = u^+(x)$. To do this it is natural to combine the operators u and u^+ into one operator $\psi(x)$ with components $\psi_1 = u_{1/2}$, $\psi_2 = u_{-1/2}$, $\psi_3 = -iu^+_{-1/2}$, and $\psi_4 = iu^+_{1/2}$, or, in "split" form

$$\psi(x) = \begin{pmatrix} u(x) \\ \sigma_y u^+(x) \end{pmatrix}, \quad (5)$$

where σ_y is a Pauli matrix. This enables us to give the theory a relativistic form. We introduce four-by-four matrices γ_i:

$$\gamma_3 = \begin{pmatrix} 0 & i \\ -i & 0 \end{pmatrix}, \quad \gamma_4 = \begin{pmatrix} 0 & 1 \\ 1 & 0 \end{pmatrix}, \quad \gamma_5 = \begin{pmatrix} 1 & 0 \\ 0 & -1 \end{pmatrix},$$

$$\gamma_1 = \begin{pmatrix} 1 & 0 \\ 0 & 1 \end{pmatrix}, \quad C = \begin{pmatrix} \sigma_y & 0 \\ 0 & -\sigma_y \end{pmatrix} \quad (6)$$

and the operator $\bar\psi(x) = \psi^+(x)\gamma_4$. The matrices γ_i satisfy the usual anticommutation relations

$$\{\gamma_3, \gamma_4\} = \{\gamma_3, \gamma_5\} = \{\gamma_4, \gamma_5\} = 0, \quad \gamma_3^2 = \gamma_4^2 = \gamma_5^2 = 1. \quad (7)$$

We define the Green's function, as usually, by

$$G(x-y) = i\langle T\psi(x\ \bar\psi(y)\rangle. \quad (8)$$

We can write the matrix G in expanded form:

$$G(x-y) = i\begin{vmatrix} F(x-y)\,\sigma_y & \mathcal{G}(x-y) \\ -\mathcal{G}(y-x) & \sigma_y F^+(x-y) \end{vmatrix}. \quad (9)$$

In the notation of (5) and (6), the Lagrangian (1) becomes

$$\int \mathcal{L}(x)\,dx = -\frac{i}{2}\int \bar\psi(x)\hat p\psi(x)\,dx - \frac{1}{8}\int dx\,dy\,\bar\psi(x)\,\gamma_3\psi(x)\,D(x-y)\,\bar\psi(y)\,\gamma_3\psi(y). \quad (10)$$

Here

$$\hat p = \gamma_3 p_3 + \gamma_4 p_4, \quad p_4 \equiv ip_0 = -\frac{\partial}{\partial t}, \quad p_3 = -\frac{1}{2m}\frac{\partial^2}{\partial \mathbf{x}^2} - \mu.$$

In the momentum representation the Green's function for non-interacting particles can be written as

$$G_0(p) = 1/i\hat p = -i\hat p/p^2, \quad (11)$$

where

$$p^2 = p_3^2 + p_4^2 = p_3^2 - p_0^2.$$

In the following we shall be interested in the values of all quantities only near the Fermi surface. In that region we can divide the integration over $d^4p \equiv (2\pi)^{-4}d\mathbf{p}\,dp_0$ into integrals over the angles of the vector $\mathbf{p}$ and a double integral over p_3 and p_0:

$$d^4p = \frac{p^2 dp\,d\Omega\,dp_0}{(2\pi)^4} \approx \frac{p_F m}{2\pi^2}\frac{d\Omega}{4\pi}\frac{dp_3\,dp_0}{2\pi} \equiv \rho\frac{d\Omega}{4\pi}d^2p \quad (12)$$

(where $\rho = (2\pi^2)^{-1}mp_F$ is the level density near the Fermi surface), and the integration over the angles can be left to the last. This is the form of a one-dimensional relativistic problem, so that we can use the well-developed technique of relativistic calculations.

We write Dyson's equation for the Green's funtion in the usual form

*Because we have introduced the term μu^+u into the Lagrangian (1), the functions F and F^+ depend only on the difference x–y, in contradistinction to[5].

$$G(p) = G_0(p) - G_0(p)\,\Sigma(p)\,G(p), \qquad (13)$$

where Σ is the self-energy part. From (13) we have

$$G(p) = 1/(i\hat{p} + \Sigma). \qquad (14)$$

In first approximation Σ is determined by the diagram of Fig. 1 and is expressed by the equation

$$\Sigma(p) = -i\int \gamma_3 G(p')\,\gamma_3 D(p-p')\,d^4p'. \qquad (15)$$

The non-diagonal elements of Σ are in this approximation reduced to a renormalization of the chemical potential and the particle mass. We shall assume that this renormalization has taken place so that $p_3 = \mathbf{p}^2/2m_* - u_*$, where m_* and μ_* are the effective mass and chemical potential. For what follows, the diagonal elements of the matrix Σ are important since they determine the gap in the energy spectrum. If we denote this diagonal part by $\hat{\Delta}$ we have from the definitions (9) and (4)

$$\hat{\Delta} = \begin{pmatrix} \Delta & 0 \\ 0 & \Delta^* \end{pmatrix}. \qquad (16)$$

FIG. 1

The phase constant in Δ can be chosen arbitrarily and below we shall assume Δ to be real. $G(p)$ is then of the form

$$G(p) = \frac{1}{i\hat{p} + \Delta} = \frac{\Delta - i\hat{p}}{p^2 + \Delta^2}. \qquad (17)$$

The single-particle excitation spectrum is determined by the pole $p_0 = (p_1^2 + \Delta^2)^{1/2}$ of $G(p)$. From (15) we have for Δ the equation

$$\Delta = -i\int D(p-p')\frac{\Delta}{p'^2 + \Delta^2}d^4p'. \qquad (18)$$

With logarithmic accuracy, the region near the Fermi surface is the important one in Eq. (18). In that region D depends only on the angle between p and p': $D(p-p') = D(\mathbf{n}\cdot\mathbf{n}')$, $\mathbf{n} = \mathbf{p}/p$, $\mathbf{n}' = \mathbf{p}'/p'$. Assuming that the attraction in an S-state predominates in the interaction in D we find that Δ is independent of the angles and satisfies the relation

$$1 = -ig_0\int \frac{d^3p}{p^2 + \Delta^2} \qquad \left(g_0 = p\int D(\mathbf{nn}')\,d\mathbf{n}'/4\pi\right). \qquad (19)$$

If we cut off, as is usually done,[6,1,5] the logarithmically diverging integral at the limiting phonon frequency ω_D, we get for Δ the well-known equation

$$1 = g_0 \ln(\omega_D/\Delta) \equiv g_0 L. \qquad (20)$$

More complicated diagrams entering into Σ give terms of order $\omega_D/\mu \ll 1$ or terms in which the degree of the logarithm is less than the degree of the interaction constant, for instance, $g_0^2 L$,[7] so that if $g_0 \ll 1$ it is sufficient to limit oneself to the simplest diagram of Fig. 1. When the interaction is not too weak we must replace the dotted line in Fig. 1 by an irreducible four-pole (see, for instance, [8]).

3. TWO-PARTICLE GREEN'S FUNCTIONS

The collective excitation spectrum is determined by the poles of the two-particle Green's function which in our case can be written as a matrix

$$K(1, 2; 3, 4) = i\langle T\psi(1)\bar{\psi}(2)\psi(3)\bar{\psi}(4)\rangle. \qquad (21)$$

Dyson's equation for K is of the form

$$K = -iGG - iGG\int \Gamma K\,d\tau, \qquad (22)$$

where Γ is an irreducible four-pole.[9,10] Instead of looking for a pole in the solution of the inhomogeneous integral Eq. (22) we can find the condition that the corresponding homogeneous equation be soluble.[10,11] The kernel of this equation is independent of the variables 3 and 4, and we shall therefore not write these variables out explicitly in K:

$$K(1, 2) = -iG(1)\,G(2)\int \Gamma(1, 2; 1', 2')\,K(1', 2')\,d\tau_{1'}d\tau_{2'}. \qquad (23)$$

In the weak-interaction approximation it is sufficient to limit oneself for the four-pole Γ to the lowest order diagrams:

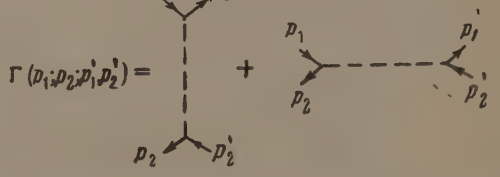

(24)

If we change in the equation for $K_{\mu\nu}(p_1p_2) = \langle\psi_\mu(p_1)\bar{\psi}_\nu(p_2)\rangle$ to the variables $k = p_1 - p_2$ and $p = (p_1 + p_2)/2$ we can write (23) and (24) in the form

$$K_{\mu\nu} = \frac{i}{2}\Big[\Big(G\Big(p + \frac{k}{2}\Big)\gamma_3\Big)_{\mu\rho}\Big(\gamma_3 G\Big(p - \frac{k}{2}\Big)\Big)_{\sigma\nu} + \Big(CG\Big(-p + \frac{k}{2}\Big)\gamma_3\Big)_{\nu\rho}\Big(\gamma_3 G\Big(-p - \frac{k}{2}\Big)\Big)_{\sigma\mu}\Big] \times \int d^4p'\,[D(p-p')\,K_{\rho\sigma}(p', k) - \tfrac{1}{2}D(k)\,\gamma^3_{\rho\sigma}\,\mathrm{Sp}\,\gamma^3 K(p', k)], \qquad (25)$$

where C is given by (6). The integral equation (25) has a solution only if there are well-defined relations between the energy $k_0 = \omega$ and the momentum k of the excitation, and these determine the energy spectrum $\omega(k)$. The variable p characterizes the relative motion of the particles in the excitation.

One can expand the matrix $K_{\mu\nu}$ in terms of any arbitrary set of 16 linearly independent matrices. We write this expansion in the form

$$K_{\mu\nu} = K_i\gamma^i_{\mu\nu} + K_i\gamma^i_{\mu\nu}. \qquad (26)$$

The γ^i are given here by Eqs. (6) and the γ^i are obtained from the γ^i by replacing the two-by-two unit matrices by the Pauli matrices σ:

$$\gamma_1 = \begin{pmatrix} \sigma & 0 \\ 0 & \sigma \end{pmatrix}, \qquad \gamma_3 = \begin{pmatrix} 0 & i\sigma \\ -i\sigma & 0 \end{pmatrix},$$

$$\gamma_4 = \begin{pmatrix} 0 & \sigma \\ \sigma & 0 \end{pmatrix}, \qquad \gamma_5 = \begin{pmatrix} \sigma & 0 \\ 0 & -\sigma \end{pmatrix}. \qquad (6')$$

The K^i describe the excitations with spin zero and the K^i those with spin unity.

The presence of two G's in Eq. (25) leads to the fact that only values of the variables p and p′ near the Fermi surface are important in (25). We noted earlier that in that region

$$D(p - p') = D(\mathbf{nn}') \qquad (\mathbf{n} = \mathbf{p}/p,\ \mathbf{n}' = \mathbf{p}'/p'),$$
$$d^4p = \rho\,(d\Omega/4\pi)\,d^2p.$$

Integrating (25) over d^2p we get for the functions

$$K^i(\mathbf{n}, k) = \int d^2pK^i(p, k), \qquad K^{i\alpha}(\mathbf{n}, k) = \int d^2pK^{i\alpha}(p, k)$$

the equations

$$K^i(\mathbf{n}, k) = P^{i,r}(\omega, \mathbf{nk})\,\rho\int D(\mathbf{nn}')\,K^r(\mathbf{n}', k)\frac{d\mathbf{n}'}{4\pi}$$
$$- 2P^{i,3}\rho D(\mathbf{k})\int K^3(\mathbf{n}', k)\frac{d\mathbf{n}'}{4\pi},$$
$$K^{i\alpha}(\mathbf{n}, k) = P^{i\alpha,r\beta}(\omega, \mathbf{nk})\,\rho\int D(\mathbf{nn}')\,K^{r\beta}(\mathbf{n}', k)\frac{d\mathbf{n}'}{4\pi} \qquad (27)$$

$(\alpha, \beta = x, y, z)$. Here $P(\omega, \mathbf{n}\cdot\mathbf{k})$ is of the form

$$P^{i,r} = \frac{i}{8}\mathrm{Sp}\int d^2p\left[\gamma_iG\left(p + \frac{k}{2}\right)\gamma_3\gamma_r\gamma_3G\left(p - \frac{k}{2}\right)\right.$$
$$\left. + C\tilde{\gamma}_iCG\left(-p + \frac{k}{2}\right)\gamma_3\gamma_r\gamma_3G\left(-p - \frac{k}{2}\right)\right],$$
$$P^{i\alpha,r\beta} = \frac{i}{8}\mathrm{Sp}\int d^2p\left[\gamma^{i\alpha}G\left(p + \frac{k}{2}\right)\gamma_3\gamma^{r\beta}\gamma_3G\left(p - \frac{k}{2}\right)\right.$$
$$\left. + C\tilde{\gamma}^{i\alpha}CG\left(-p + \frac{k}{2}\right)\gamma_3\gamma^{r\beta}\gamma_3G\left(-p - \frac{k}{2}\right)\right]. \qquad (27')$$

Using the equations (i = 1, 3, 5)

$$C\tilde{\gamma}_iC = \gamma_i, \qquad C\tilde{\gamma}_{i\alpha}C = -\gamma_{i\alpha},$$
$$C\tilde{\gamma}_4C = -\gamma_4, \qquad C\tilde{\gamma}_{4\alpha}C = \gamma_{4\alpha}$$

and noting that the trace in $P^{i\alpha,r\beta}$ is proportional to $\delta_{\alpha\beta}$ so that we can replace the matrices γ_i under the trace sign by γ_i, we find

$$P^{i,r} = \tfrac{1}{2}(\Pi^{ir}(\mathbf{n}) + \Pi^{ir}(-\mathbf{n})),$$
$$P^{i\alpha,r\beta} = \delta_{\alpha\beta}\tfrac{1}{2}(\Pi^{ir}(\mathbf{n}) - \Pi^{ir}(-\mathbf{n})) \qquad (i = 1, 3, 5);$$
$$P^{4,r} = \tfrac{1}{2}(\Pi^{4r}(\mathbf{n}) - \Pi^{4r}(-\mathbf{n})),$$
$$P^{4\alpha,r\beta} = \delta_{\alpha\beta}\tfrac{1}{2}(\Pi^{4r}(\mathbf{n}) + \Pi^{4r}(-\mathbf{n})), \qquad (28)$$

where

$$\Pi^{ir}(\omega, \mathbf{nk}) = \frac{i}{4}\mathrm{Sp}\int\gamma^iG\left(p + \frac{k}{2}\right)\gamma^3\gamma^r\gamma^3G\left(p - \frac{k}{2}\right)d^2p. \qquad (28')$$

The parity of the function $P(\mathbf{n})$ determines the parity of the angular momentum of the corresponding excitation. In the following we shall for the sake of simplicity drop the index α of the functions $K^{i,\alpha}$ and denote all functions simply by K^i. The spinor structure of the excitation for the functions K^i with i = 1, 3, 5 is then given by the first term in (26) (spin 0) for even angular momentum, and by the second term (spin 1) for odd angular momentum. For the function K^4, on the other hand, even angular momenta correspond to spin 1 and odd angular momenta to spin 0.

The quantities Π^{ir} are evaluated in the appendix and given by Eqs. (A.9). In order to change from the integral Eq. (28) to an algebraic equation we expand $K^i(\mathbf{n})$ and $D(\mathbf{n}\cdot\mathbf{n}')$ in powers of spherical harmonics:*

$$K^i(\mathbf{n}) = \sum_{lm}K^i_{lm}Y_{lm}(\mathbf{n});$$
$$\frac{1}{4\pi}\rho D(\mathbf{nn}') = \sum_l g_l\left(\frac{2l+1}{8\pi^2}\right)^{1/2}P_l(\mathbf{nn}') = \sum_{lm}g_lY_{lm}(\mathbf{n})\,Y^*_{lm}(\mathbf{n}'). \qquad (29)$$

If we choose the z axis along k, the z component m of the angular momentum will be an integral of motion. If we substitute into the set of Eqs. (28) the explicit form of the quantities

$$\Pi^{ik}_{ll_1m} = \int Y^*_{lm}(\mathbf{n})\,\Pi^{ik}Y_{l_1m}(\mathbf{n})\,d\mathbf{n},$$

we get

$$K^5_{lm} = \sum_{l_1}g_{l_1}\left[(L + \beta^2f)_{ll_1m}K^5_{l_1m}\right.$$
$$\left. + \frac{q_4}{2\Delta}f_{ll_1m}K^3_{l_1m} + \frac{1}{2\Delta}(q_3f)_{ll_1m}K^4_{l_1m}\right]$$
$$- 2\delta_{m0}\rho D(k)\frac{q_4}{2\Delta}f_{l00}K^3_{00},$$

*We use the normalization $\int_{-1}^{1}P^2_{lm}(x)\,dx = 1$.

$$K^3_{lm} = \sum_{l_1} g_{l_1} \Big[\frac{q_4}{2\Delta} f_{ll_1m} K^5_{l_1m} - \Big(f + \frac{q_3^2 - q_3^2 f}{q^2} \Big)_{ll_1m} K^3_{l_1m} + q_4 \Big(\frac{q_3 - q_3 f}{q^2} \Big)_{ll_1m} K^4_{l_1m} \Big] + 2\delta_{m0} \rho D(k) \Big(f + \frac{q_3^2 - q_3^2 f}{q^2} \Big)_{l00} K^3_{00},$$

$$K^4_{lm} = \sum_{l_1} g_{l_1} \Big[-\frac{1}{2\Delta} (q_3 f)_{ll_1m} K^5_{l_1m} - q_4 \Big(\frac{q_3 - q_3 f}{q^2} \Big)_{ll_1m} K^3_{l_1m} - \Big(\frac{q_3^2 - q_3^2 f}{q^2} \Big)_{ll_1m} K^4_{l_1m} \Big] + 2\delta_{m0} \rho D(k)\, q_4 \Big(\frac{q_3 - q_3 f}{q^2} \Big)_{l00} K^3_{00}.$$

$$K^1_{lm} = \sum_{l_1} g_{l_1} (L - f + \beta^2 f)_{ll_1m} K^1_{l_1m}. \qquad (30)$$

Here we have (see appendix)

$$q_3 = \mathrm{k}nv, \quad q_4 = i\omega, \quad q^2 = q_3^2 + q_4^2,$$

$$\beta^2 = -q^2/4\Delta^2, \quad f(\beta) = \frac{\arcsin \beta}{\beta \sqrt{1 - \beta^2}}. \qquad (31)$$

Since Π^{55}, Π^{53}, Π^{33}, and Π^{44} are even functions of $(\mathbf{k}\cdot\mathbf{n})$, and Π^{45} and Π^{43} are odd, Eq. (30) connects the even harmonics K^5_l and K^3_l with the odd harmonic K^4_l and vice versa, so that we can separate the equations for even and odd l. It is also clear from (30) that one can separate the equation for K^1 from those for K^3, K^4, and K^5. One verifies easily that when $k \neq 0$ the equation for K^1 has no non-vanishing solutions so that we shall not consider K^1 in what follows.

4. THE CASE k = 0

When k = 0 the coefficients Π^{ik} are independent of $\mathbf{n}$ so that

$$\Pi^{ik}_{ll_1m} = \delta_{ll_1} \Pi^{ik}_{llm}$$

and the equations for different l become separate ones. We consider first S excitations. In the case of neutral particles D(k) is finite when k = 0. The quantities Π^{45}, Π^{43}, Π^{44}, and hence also K^4, vanish so that (30) becomes

$$g_0 \frac{\omega^2}{4\Delta^2} f K^5_{00} + \frac{i\omega}{2\Delta} f (g_0 - 2\rho D(\omega, 0)) K^3_{00} = 0,$$

$$g_0 \frac{i\omega}{2\Delta} f K^5_{00} - (1 + g_0 f - 2 f \rho D(\omega, 0)) K^3_{00} = 0. \qquad (32)$$

Equations (32) have a solution $K^3_{00} = 0$, $K^5_{00} \neq 0$ when $\omega = 0$. This solution corresponds to the usual sound wave excitations [1,12,13] which are discussed in the next section.

We find now the limiting frequencies of the oscillations with $l \neq 0$. We can put Eq. (30) in the form

$$K^5_{lm} = g_l \Big(L + \frac{\omega^2}{4\Delta^2} f \Big) K^5_{lm} + g_l \frac{i\omega}{2\Delta} f K^3_{lm},$$

$$K^3_{lm} = g_l \frac{i\omega}{2\Delta} f K^5_{lm} - g_l f K^3_{lm}. \qquad (33)$$

If we put the determinant of (33) equal to zero, we find [1]

$$(1 - g_l L)(1 + g_l f) - g_l \omega^2 f / 4\Delta^2 = 0. \qquad (34)$$

If $g_l^2 (g_0 - g_l)^{-1} \ll 1$ the value of ω is close to 2Δ and $f(\omega/2\Delta) \approx \frac{1}{2}\pi (1 - \omega^2/4\Delta^2)^{-1/2}$, and thus

$$\omega_l^2 (0) = 4\Delta^2 (1 - \alpha_l^2), \qquad (35)$$

where

$$\alpha_l = \tfrac{1}{2} \pi g_l^2 (g_0 - g_l)^{-1}. \qquad (35')$$

Equation (35) shows that for any small g_l, regardless of its sign, a bound state of two quasiparticles exists with a binding energy $\sim \Delta \alpha_l^2$. One can understand the existence of this level as follows. For the α_l considered, which are very small compared to unity, the energy of the system is close to 2Δ so that the problem becomes a one-dimensional non-relativistic one. It is well known, however, that in that case there is always a bound state for the particles, however weak the interaction [14]; to be sure, it does not follow from this simple picture that the result is independent of the sign of g_l.

If one of the g_l is very close to g_0 so that $g_l^2 (g_0 - g_l)^{-1} \gg 1$, then ω is close to zero, f = 1, and

$$\omega^2 (0) = 4\Delta^2 (g_0 - g_l)(1 + g_l)/g_0 g_l. \qquad (36)$$

If $g_l > g_0$ the value of $\omega^2(0)$ given by (36) becomes negative. The presence of excitation with an imaginary frequency in the system means that the original state is unstable with respect to these excitations. In the present case this indicates the instability of a state with S-pairing. The stable state will be the one in which pairing occurs with angular momentum l. [2,15]

We note that the instability of the normal, non-superconducting state ($\Delta = 0$) can also be ascertained from the form of K. [16] Putting $\Delta = 0$ in (30) we find that the equations for K^1_{00} and K^5_{00} are the same and have a solution when

$$1 = \frac{g_0}{2} \ln \frac{\omega_D^2}{(-\omega^2)}. \qquad (37)$$

The change in the state caused by this instability leads to the appearance of the gap Δ in the single-particle excitation spectrum, while the frequency of the collective excitations becomes equal to zero [see (32)].

5. SOUND WAVE OSCILLATIONS ($l = 0$)

We consider excitations with $l = 0$. In that case we find that in the first of Eqs. (30) the quantity K_{00}^5 occurring on the left-hand side cancels the logarithmic term $g_0 L K_{00}^5$ on the right-hand side. The subsequent considerations are different for systems of neutral or of charged particles. For neutral particles $D(k)$ is finite for small k and in the first of Eqs. (30) we can drop all terms apart from those involving K_{00}^5, if our accuracy is to terms of the order g_0 or g_1.* The dispersion equation becomes of the form

$$\int_{-1}^{1} (\omega^2 - k^2 v^2 x^2) f(\beta)\, dx = 0. \tag{38}$$

Using (A.10a) and (38) we get for $kv/2\Delta \ll 1$ [1,12,13]

$$\omega^2 = \tfrac{1}{3} v^2 k^2. \tag{39}$$

It turns out unexpectedly that Eq. (38) has also a solution when $kv/2\Delta \gg 1$. This is connected with the fact that if ω is near to 2Δ the integral of the first term in (38) is logarithmically large when we take the region of small x into account. Using the limiting expressions (A.10b) and (A.10c) for f we find

$$\frac{\pi\Delta}{2vk} \ln \frac{4\Delta^2}{4\Delta^2 - \omega^2} - \left(\ln \frac{kv}{\Delta} - 1\right) = 0, \tag{40}$$

and hence

$$2\Delta - \omega = \Delta \exp\left(-\frac{2kv}{\pi\Delta} \ln \frac{kv}{\Delta e}\right). \tag{41}$$

It is not difficult to find the corrections of the order of magnitude of the interparticle interaction g. For instance, in the region of small k we can rewrite Eq. (39) as follows, if we take these corrections into account,

$$\omega^2 = \tfrac{1}{3} k^2 v^2 (1 + g_0 - 2\rho D(0) + g_1). \tag{39'}$$

If the interaction is non-vanishing only in the S state, then $g_1 = 0$, $\rho D(0) = g_0$, and (39′) is the same as Anderson's result. [12]

The branch found here is the sound wave branch in the system of electrons. This branch goes therefore over into plasma waves in a system of charged particles. In that case the function $D(k) \to -4\pi e^2/k^2 \to -\infty$ as $k \to 0$. One must therefore also take into account terms in K_{00}^3 in the set (30). Dropping terms of order g_l we get

$$K_{00}^5 = (1 + g_0\beta^2 f)_{00} K_{00}^5 + \frac{i\omega}{2\Delta} f_{00} (g_0 - 2\rho D(k)) K_{00}^3,$$

$$K_{00}^3 = g_0 \frac{i\omega}{2\Delta} f_{00} K_{00}^5 + (2\rho D(k) - g_0)\left(f - \frac{(knv)^2 (1-f)}{\omega^2 - (knv)^2}\right)_{00} K_{00}^3. \tag{42}$$

Solving (42) for $kv/\omega \ll 1$ and taking into account that then also $\Delta/\omega \ll 1$ we get the following expression for the frequency

$$\omega^2(k) = \tfrac{8}{3} \pi e^2 \rho v^2 + \tfrac{3}{5} k^2 v^2. \tag{43}$$

If we take g_l into account the equation for $\omega^2(0)$ will be of the form

$$\omega^2(0) = \frac{8}{3} \pi e^2 \rho v^2 (1 + g_1) = \frac{4}{3\pi} e^2 p_F m_* \cdot p_F^2 m_*^{-2} (1 + g_1)$$

or, if we use the expression for the effective mass $m_* = m(1 + g_1)$, [17]

$$\omega^2(0) = 4\pi n e^2/m = \omega_{pl}^2. \tag{44}$$

The plasma oscillation frequency (44) has thus the same value as for a free electron gas. [12,1] This result is physically clear since the frequency of the long-wavelength oscillations which occur because of the long-range Coulomb forces cannot be changed by the presence of finite-range forces in the system. We neglect the influence of these forces on the dispersion (43), for when $\Delta/\omega \ll 1$ the corresponding corrections will be the same in superconducting and in non-superconducting systems.

6. EXCITATIONS WITH NON-VANISHING ANGULAR MOMENTUM AT SMALL k ($l \neq 0$, $kv \ll \alpha_1\Delta$)

When $k \neq 0$ the degeneracy with respect to the component m of the angular momentum along the direction of motion is lifted. When $kv \ll \alpha_1\Delta$ the splitting is small and the distance between the levels having different m but the same l is small compared with the distance between levels with different l. In that case l is a good quantum number and the set (30) can be solved, as before, as a set of independent equations for different l. One verifies easily that the influence of neighboring harmonics leads to corrections in the dispersion which are small either in the interaction constant or in the parameter $(kv/\alpha_1\Delta)^2 \ll 1$. When there is Coulomb interaction we must consider more carefully the case $l = 2$, $m = 0$, but one can verify that also in that case the correction is proportional to g. Taking into account the fact that ω is close to 2Δ and neglecting terms k^2v^2 compared to terms k^2v^2/α^2 we get

*For large $kv \gg \Delta$ the corrections to Eq. (38) are of the magnitude $\sim g \ln(kv/\Delta)$. In accordance with the basic approximations in the theory we restrict ourselves to the region $kv \ll \omega_D$ when $g \ln(kv/\Delta) \ll 1$; one can find the correction terms using perturbation theory.

$$K^5_{lm} = g_l (L + f_{llm}) K^5_{lm} + i g_l f_{llm} K^3_{lm},$$

$$K^3_{lm} = i g_l f_{llm} K^5_{lm} - g_l f_{llm} K^3_{lm}. \quad (45)$$

If we use (A.10b) we get from the condition that (45) be soluble for $\omega^2(k)$ the following expression

$$\omega^2_{lm}(k) = 4\Delta^2 (1 - \alpha_l^2) + \tfrac{1}{3} k^2 v^2 (1 + 2C^{l0}_{20}, {}_{l0}C^{lm}_{20,lm}), \quad (46)$$

where C are Clebsch-Gordan coefficients. In particular, we get from (46) when $l = 1$

$$\omega^2_{10}(k) = \omega^2_1(0) + \tfrac{3}{5} k^2 v^2, \quad \omega^2_{1,\pm 1}(k) = \omega^2_1(0) + \tfrac{1}{5} k^2 v^2, \quad (47)$$

which is the same as Bardasis and Schrieffer's result.[2]

For large l Eq. (46) gives

$$\omega^2_{lm}(k) = \omega^2_l(0) + \frac{k^2 v^2}{2} (1 - m^2 l^2) \quad (l \gg 1). \quad (48)$$

7. EXCITATIONS WITH NON-VANISHING ANGULAR MOMENTUM AT LARGE k

When the wave vector k increases the magnitude of the angular momentum l of the excitation ceases to be a good quantum number, and each excitation is a superposition of harmonics with different values of l (but one value of m). For a certain value of k which is about equal to $\Delta a/v$ the excitation energy becomes, generally speaking, equal to 2Δ, and after that the excitation ceases to exist since as $\omega > 2\Delta$ it is unstable with respect to a break-up into two single-particle excitations. We determine now the shape of the spectrum near its endpoint. Let us, for example, consider the case $l = 1$, $m = 0$, and for the sake of simplicity assume that all g_l with $l > 1$ vanish. Up to terms of order g_0 we can neglect in Eqs. (30) the quantity K^4 so that this set becomes

$$K^5_{10} = g_1 (L + f_{110}) K^5_{10} + i f_{110} K^3_{10}, \quad K^3_{10} = i g_1 f_{110} K^5_{10} - f_{110} K^3_{10}. \quad (49)$$

Using Eq. (A.10b) from the appendix we get from (49)

$$1 = 3\alpha_1 \int_0^1 x^2 dx \left(1 - \frac{\omega^2}{4\Delta^2} + \frac{k^2 v^2 x^2}{4\Delta^2}\right)^{-1/2}, \quad (50)$$

where α_1 is given by (35). The end of the spectrum k_{max} is then determined by the value $\omega(k_{max}) = 2\Delta$, and thus

$$k_{max} = 3\alpha_1 \Delta / v. \quad (51)$$

Expanding Eq. (50) near k_{max} we get

$$(4\Delta^2 - \omega^2) \ln \frac{4\Delta^2}{4\Delta^2 - \omega^2} - \frac{v^2}{2} (k^2_{max} - k^2) = 0. \quad (52)$$

It is clear from Eq. (52) that the curve $\omega(k)$ is

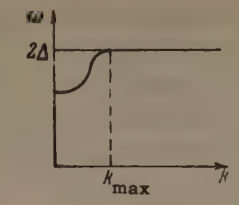

FIG. 2

tangent to the horizontal line $\omega = 2\Delta$ near k_{max} so that the complete $\omega(k)$ curve is of the form given in Fig. 2.

It turns out, however, that for each $m \neq 0$ there is one excitation branch which does not end, even at large k. Indeed, if l and m have the same parity, the matrix elements of f for ω near to 2Δ are logarithmically large because of the small x. This logarithm compensates for the fact that the coupling constant in the right-hand sides of Eqs. (30) is small. Using Eq. (A.13) we can write the set (30) in the form

$$K^5_{lm} = g L K^5_{lm} + \frac{2\pi\Delta}{kv} P_{lm}(0) \ln \frac{\tilde{kv}}{\sqrt{4\Delta^2 - \omega^2}} \sum_{l_1} g_{l_1} P_{l_1 m}(0) (K^5_{l_1 m} + i K^3_{l_1 m}),$$

$$K^3_{lm} = i \frac{2\pi\Delta}{kv} P_{lm}(0) \ln \frac{\tilde{kv}}{\sqrt{4\Delta^2 - \omega^2}} \sum_{l_1} g_{l_1} P_{l_1 m}(0) (K^5_{l_1 m} + i K^3_{l_1 m}). \quad (53)$$

Introducing the notation

$$\chi_m = \frac{2\pi\Delta}{kv} P_{lm}(0) \ln \frac{\tilde{kv}}{\sqrt{4\Delta^2 - \omega^2}} \sum_{l_1} g_{l_1} P_{l_1 m}(0) (K^5_{l_1 m} + i K^3_{l_1 m}), \quad (54)$$

we get for the excitation considered here

$$K^5_{lm} = \frac{1}{1 - g_l L} P_{lm}(0) \chi_m, \qquad K^3_{lm} = i P_{lm}(0) \chi_m. \quad (55)$$

Substituting (55) into (54) we find

$$1 = \frac{4\Delta}{kv} \ln \frac{\tilde{kv}}{\sqrt{4\Delta^2 - \omega^2}} \sum_l \alpha_l P^2_{lm}(0), \quad (56)$$

and hence

$$4\Delta^2 - \omega^2 = \min\{k^2 v^2, 4\Delta^2\} \cdot \exp\left[-\frac{kv}{2\Delta} \left(\sum_l \alpha_l P^2_{lm}(0)\right)^{-1}\right]. \quad (57)$$

Equation (57) is valid apart from a possible numerical factor in front of the exponential, and is applicable in the region

$$kv \gg \Delta \sum_l \alpha_l P^2_{lm}(0). \quad (58)$$

The difficulty of considering the region $k \sim \alpha\Delta/v$ makes it impossible for us to follow in detail the behavior of these branches, starting from $k = 0$. It is, however, clear from the theorem on the non-intersection of terms of the same symmetry[14] that the branch extending into the large k region

is the one with the smallest energy for a given m, that is, the branch with maximum g_l.

When m = 0 an annihilation term with $2\rho D(k)$ is added to the right-hand side of (53). Restricting ourselves to the region $\alpha_l\Delta \ll kv \ll \Delta$ we get

$$K^5_{l0} = g_l L K^5_{l0} + \frac{2\pi\Delta}{kv} P_{l0}(0) \ln \frac{kv}{\sqrt{4\Delta^2-\omega^2}} \times \left[\sum_{l_1} g_{l_1} P_{l_1 0}(0)(K^5_{l_1 0} + iK^3_{l_1 0}) - 2i\rho D(k) K^3_{00} \right],$$

$$K^3_{l0} = \frac{2\pi\Delta}{kv} P_{l0}(0) \ln \frac{kv}{\sqrt{4\Delta^2-\omega^2}} \times \left[\sum_{l_1} g_{l_1} P_{l_1 0}(0)(K^5_{l_1 0} + iK^3_{l_1 0}) - 2i\rho D(k) K^3_{00} \right]. \quad (59)$$

Putting $l = 0$ in the first of Eqs. (55) we see that the expression in square brackets vanishes and that thus $K^3_{10} = K^5_{10} = 0$. The equations do therefore not have a solution with ω close to 2Δ in the region $\alpha\Delta \ll kv \ll \Delta$. All excitation branches with m = 0, $l \neq 0$ which are close to 2Δ for small k stop thus for $kv \sim \alpha_l\Delta$.

We note in conclusion that the results of this paper have been obtained assuming an isotropic model of a metal. Deviations from isotropy [18] may turn out to be important when ω is close to 2Δ. The results are, apparently, little changed at small k, if the relative anisotropy of Δ is less than or of the order of g^2. The case of large k needs separate consideration.

The authors are grateful to A. B. Migdal, S. T. Belyaev, and L. P. Gor'kov for interesting discussions.

APPENDIX

EVALUATION OF THE COEFFICIENTS Π^{ir}

It is convenient to introduce for the evaluation of the quantities Π^{ir} which are defined by Eqs. (28) instead of the 4-vector $k = k_1 - k_2$ the two-dimensional vector q with components

$$q_4 = k_4 = i\omega; \qquad q_3 = (k_1 - k_2)_3 = kp/m_* = knv, \quad (A.1)$$

where v is the particle velocity on the Fermi surface. Using Eq. (17) and writing

$$t_{ir} = -\tfrac{1}{4} \mathrm{Sp}\, \gamma_i (\Delta - \hat{i}p_1) \gamma_3 \gamma_r \gamma_3 (\Delta - i\hat{p}_2),$$
$$p_1 = p + \tfrac{1}{2}q, \quad p_2 = p - \tfrac{1}{2}q, \quad (A.2)$$

we rewrite (28′) in the form

$$\Pi^{ir} = -i \int \frac{d^2p\, t_{ir}}{(p_1^2+\Delta^2)(p_2^2+\Delta^2)}. \quad (A.3)$$

Dropping the odd terms in p in t_{ir} which vanish when we integrate over p, we get for the t_{ir} the following expressions:

$$t_{11} = p_1p_2 - \Delta^2, \quad t_{15} = t_{13} = t_{14} = 0,$$
$$t_{55} = p_1p_2 + \Delta^2, \quad t_{53} = t_{35} = q_4\Delta, \quad t_{54} = -t_{45} = q_3\Delta,$$
$$t_{33} = (p_1)_3(p_2)_3 + (p_1)_4(p_2)_4 - \Delta^2, \quad t_{44} = t_{33} + 2\Delta^2,$$
$$t_{34} = -t_{43} = 2(p_1)_3(p_2)_4. \quad (A.4)$$

The relativistic integrals which we obtained,

$$I(q) = -i \int \frac{\Delta^2 d^2p}{(p_1^2+\Delta^2)(p_2^2+\Delta^2)},$$
$$I_{\alpha\beta}(q) = -i \int \frac{(p_1)_\alpha (p_2)_\beta d^2p}{(p_1^2+\Delta^2)(p_2^2+\Delta^2)} \quad (A.5)$$

$(\alpha, \beta = 3, 4)$ can be evaluated simply using Feynman's method. [19] Applying this method to evaluate I(q) we find

$$I = -i \int_0^1 dx \int \frac{\Delta^2 d^2p}{[p_1^2(1-x) + p_2^2 x + \Delta^2]^2}$$
$$= -i \int_0^1 dx \int \frac{\Delta^2 d^2 f}{[f^2 + \Delta^2 + q^2(x-x^2)]^2}$$
$$= \frac{1}{2} \int_0^1 \frac{\Delta^2 dx}{\Delta^2 + q^2(x-x^2)} \quad (f = p + (q - qx)/2). \quad (A.6)$$

Introducing $\beta^2 = -q^2/4\Delta^2 = [\omega^2 - (\mathbf{k}\cdot\mathbf{nv})^2]/4\Delta^2$, we find

$$I(q) = \frac{1}{2} \frac{\arcsin \beta}{\beta\sqrt{1-\beta^2}} \equiv \frac{1}{2} f(\beta). \quad (A.7)$$

The integral $I_{\alpha\beta}(q)$ contains a logarithmic divergence for large p. We must therefore evaluate instead of $I_{\alpha\beta}(q)$ the convergent quantity $I_{\alpha\beta}(q) - I_{\alpha\beta}(0)$, and find the constant $I_{\alpha\beta}(0)$ by direct "non-covariant" integration, with cutoff at a frequency ω_D taken into account, as when deriving (20). As a result we find

$$I_{\alpha\beta}(q) = I_{\alpha\beta}(0) + \tfrac{1}{2}\delta_{\alpha\beta}(1 - f + \beta^2 f)$$
$$- \tfrac{1}{2} q_\alpha q_\beta q^{-2}(1-f). \quad (A.8)$$

We must bear in mind that the interaction in the l-th harmonic may be cut off at a frequency ω_1 different from ω_D. The resultant logarithm $L(l) = \ln(\omega_1/\Delta)$ may therefore, strictly speaking, be different from $L = \ln(\omega_D/\Delta) = g_0^{-1}$. To simplify our formulae we put henceforth $\omega_l = \omega_D$; if necessary, we can easily make the appropriate corrections. Substituting Eqs. (A.4) to (A.8) into (A.3) we get the following values for the Π^{ir}:

$$\Pi_{11} = L - f + \beta^2 f, \quad \Pi_{55} = L + \beta^2 f, \quad \Pi_{53} = \Pi_{35} = q_4 f/2\Delta,$$
$$\Pi_{54} = -\Pi_{45} = q_3 f/2\Delta, \quad \Pi_{33} = -f - q_3^2 q^{-2}(1-f),$$
$$\Pi_{44} = q_3^2 q^{-2}(f-1), \quad \Pi_{34} = -\Pi_{43} = q_3 q_4 q^{-2}(1-f). \tag{A.9}$$

We give the expressions for the function $f(\beta)$ given by (A.6) and (A.7) in the limiting cases:

1) $\beta \to 0 \quad f(\beta) \to 1,$ (A.10a)

2) $\beta^2 \to 1 - 0 \quad f(\beta) \to \pi/2\sqrt{1-\beta^2},$ (A.10b)

3) $\beta^2 \to -\infty \quad f(\beta) \to -\frac{1}{2}\beta^{-2}\ln(-4\beta^2).$ (A.10c)

We find also with logarithmic accuracy the form of the matrix element f_{ll_1m} for large k. In the integral

$$f_{ll_1m} = \int_{-1}^{1} P_{lm}(x) P_{l_1m}(x) f(\beta)\, dx \tag{A.11}$$

the small x region is important. With $\omega \to 2\Delta$ and small x, Eq. (A.11) can, according to (A.10b) be written in the form

$$f_{ll_1m} \approx P_{lm}(0) P_{l_1m}(0) \int_0^{x_{max}} \frac{2\pi\Delta dx}{\sqrt{4\Delta^2 - \omega^2 + k^2v^2x^2}}. \tag{A.12}$$

If $kv < 2\Delta$, we have $x_{max} \sim 1$; if, however, $kv > 2\Delta$ the function f increases fast according to Eq. (A.10c) starting at $kvx \sim 2\Delta$ so that the expression for $f(\beta)$ which was used in (A.12) becomes inapplicable. The matrix element f_{ll_1m} is thus with logarithmic accuracy equal to

$$f_{ll_1m} = \frac{2\pi\Delta}{kv} \ln \frac{\widetilde{kv}}{\sqrt{4\Delta^2 - \omega^2}} P_{lm}(0) P_{l_1m}(0), \tag{A.13}$$

where

$$\widetilde{kv} = \min\{kv, 2\Delta\}.$$

[1] N. N. Bogolyubov, V. V. Tolmachev, and D. V. Shirkov, Novyĭ metod v teorii sverkhprovodimosti (A New Method in Superconductivity Theory), AN SSSR, 1958.

[2] A. Bardasis and J. R. Schrieffer, Phys. Rev. **121**, 1050 (1961).

[3] R. P. Feynman, Phys. Rev. **84**, 108 (1951).

[4] A. B. Migdal, JETP **34**, 1438 (1958), Soviet Phys. JETP **7**, 996 (1958).

[5] L. P. Gor'kov, JETP **34**, 735 (1958), Soviet Phys. JETP **7**, 505 (1958).

[6] Bardeen, Cooper, and Schrieffer, Phys. Rev. **108**, 1175 (1957).

[7] V. V. Tolmachev and S. V. Tyablikov, JETP **34**, 66 (1958), Soviet Phys. JETP **7**, 46 (1958).

[8] V. G. Vaks and A. I. Larkin, JETP **40**, 1392 (1961), Soviet Phys. JETP **13**, 979 (1961).

[9] E. E. Salpeter and H. A. Bethe, Phys. Rev. **84**, 1232 (1951).

[10] V. M. Galitskii and A. B. Migdal, JETP **34**, 139 (1958), Soviet Phys. **7**, 96 (1958).

[11] M. Gell-Mann and F. Low, Phys. Rev. **84**, 350 (1951).

[12] P. W. Anderson, Phys. Rev. **112**, 1900 (1958).

[13] V. M. Galitskii, JETP **34**, 1011 (1958), Soviet Phys. JETP **7**, 698 (1958).

[14] L. D. Landau and E. M. Lifshitz, Quantum Mechanics, Pergamon Press, 1958.

[15] P. W. Anderson and P. Morel, Phys. Rev. Letters **5**, 136 (1960); V. M. Galitskii, JETP **39**, 1157 (1960), Soviet Phys. JETP **12**, 806 (1961).

[16] A. A. Abrikosov and I. M. Khalatnikov, UFN **65**, 551 (1958), Advances in Phys. **8**, 45 (1959).

[17] L. D. Landau, JETP **30**, 1058 (1956), Soviet Phys. JETP **3**, 920 (1956).

[18] B. T. Geĭlikman and V. Z. Kresin, JETP **40**, 970 (1961), Soviet Phys. JETP **13**, 677 (1961); V. L. Pokrovskii, JETP **40**, 641, 898 (1961), Soviet Phys. JETP **13**, 447, 628 (1961).

[19] R. P. Feynman, Phys. Rev. **76**, 769 (1949).

Translated by D. ter Haar
276

MATRIX ELEMENTS FOR BETA TRANSITIONS

B. N. ZAKHAR'EV, N. I. PYATOV, and V. I. FURMAN

Joint Institute for Nuclear Research

Submitted to JETP editor June 20, 1961

J. Exptl. Theoret. Phys. (U.S.S.R.) 41, 1669-1672 (November, 1961)

Nuclear matrix elements for allowed β transitions of a number of strongly-deformed nuclei are calculated. The matrix elements were computed according to the independent-particle model, and residual interactions between the nucleons were then taken into account. In the independent-particle model the reduced β-decay probabilities ft differ from the experimental values by two or more orders of magnitude. Better agreement between the theoretical values of ft and those observed experimentally can be obtained by taking pair correlations into account.

ONE of the main problems in nuclear theory is the calculation of the nuclear matrix elements. The difficulty of this problem is that a many-body problem must be solved. The first step in this direction was the development of the independent-particle models (i.p.m.). These models, however, provide only a qualitative description of the different properties such as the level sequence, the spins and parities, and certain selection rules for the nuclear processes. The calculation of the matrix elements is thus far quite unreliable.

The interactions not included in the self-consistent field can be taken into account with the aid of the recently developed "configuration mixing" procedure. The corresponding calculations, however, are very cumbersome if the interaction of a large number of particles is to be taken into account. A method that is quite fruitful when applied to nuclear theory is the method of accounting for pair correlations between particles, developed by Bogolyubov.

The purpose of the present work was to calculate the matrix elements of β transitions on the basis of the i.p.m. with account of the residual pair interactions between nucleons (nn and pp interactions of nucleons with equal and opposite momentum projections on the nuclear symmetry axis). For simplicity we confine ourselves to allowed β transitions in strongly-deformed nuclei within the framework of the Nilsson model.[1]

A characteristic of β transitions is the product $f(Z, E)t$, which in our case has the form[2]

$$f(Z, E)\,t = \frac{D}{|\langle 1\rangle|^2 + R\,|\langle \mathbf{s}\rangle|^2}, \qquad (1)$$

where $f(Z, E)$ is the Fermi integral function, t the half-life of the nucleus, and D a constant that depends on the coupling constant g:

$$D = 2\pi^3\hbar^7 \ln 2/m^5c^4g^2 = 6550 \text{ sec};$$

R = 1.7 is the ratio of axial to vector interaction constants

$$|\langle 1\rangle|^2 = \sum_{\mu_f}\left|\left\langle f\left|\sum_p \tau_\pm^p\right|i\right\rangle\right|^2,$$

$$|\langle \mathbf{s}\rangle|^2 = 4\sum_{\mu_f}\left|\left\langle f\left|\sum_p \mathbf{s}_p\tau_\pm^p\right|i\right\rangle\right|^2. \qquad (2)$$

The last expressions represent the squares of the nuclear matrix elements of the β transitions, satisfying the Fermi and Gamow-Teller[3] selection rules, respectively. Here $\tau_\pm$ — isotopic spin operator with integral eigenvalues, $\mathbf{s}$ — usual nucleon spin operator, $|i\rangle$ and $\langle f|$ — the initial and final states of the nuclei, respectively. The summation is over all the nucleons that participate in the transition. Final summation is over the projections μ_f of the momentum of the nucleus in the final state.

In the β transitions considered by us the elements $\langle 1\rangle$ vanish because of the orthogonality of the initial and final states (there are no mirror transitions). Substituting the Nilsson wave functions[1] in the matrix element $\langle \mathbf{s}\rangle$ and going over to a system of coordinates connected with the nucleus, in analogy with [4], we obtain

$$|\langle \mathbf{s}\rangle|^2 = 4\,|\langle I_i 1 K_i\, K_f - K_i\,|\,I_f K_f\rangle \sum a^f_{l\Lambda}\, a^i_{l\Lambda} \times (\chi_{s,\Sigma_f},\ s_{K_f-K_i}\chi_{s,\Sigma_i}) + \langle I_i 1 K_i - K_f - K_i\,|\,I_f - K_f\rangle \times (-1)^{I_f-I_f}\sum a^f_{l\Lambda}\, a^i_{l\Lambda}\,(\chi_{s,-\Sigma_f},\ s_{-K_f-K_i}\chi_{s,\Sigma_i})|^2\,\delta_{N_iN_f}, \qquad (3)$$

where I and K — total momentum of the nucleus and its projection on the symmetry axis, $a_{l\Lambda}$ — coefficients tabulated by Nilsson,[1] $\chi_{s,\Sigma}$ — spin nucleon functions, $\Sigma = \pm 1/2$ — projection of the spin

Allowed β transitions in nuclei with odd A

Parent nucleus	$I\pi\,[Nn_Z\Lambda]$	Daughter nucleus	$I'\pi'[N'n'_Z\Lambda']$	Type of transition	Energy of state of daughter nucleus, kev	$\log_{10}$ ft (i.p.m.)	R_β	$\log_{10}[R_\beta^{-1}$ ft], theory	$\log_{10}$ ft, experiment	Reference
				Type au						
$_{67}Ho^{159}$	$^7/_2-$ [523]	$_{66}Dy^{159}$	$^5/_2-$ [523]	*ec*	?	3.55	0.38	3.97	$\lesssim 5$	[5]
$_{64}Gd^{161}$	$^5/_2-$ [523]	$_{65}Tb^{161}$	$^7/_2-$ [523]	β^-	418	3.42	0.26	4.00	~ 4.8	[5]
$_{67}Ho^{161}$	$^7/_2-$ [523]	$_{66}Dy^{161}$	$^5/_2-$ [523]	*ec*	26	3.55	0.31	4.06	$\lesssim 4.5$	[5]
$_{68}Er^{163}$	$^5/_2-$ [523]	$_{67}Ho^{163}$	$^7/_2-$ [523]	*ec*	0	3.55	0.36	3.99	$\lesssim 5$	[5]
$_{68}Er^{165}$	$^5/_2-$ [523]	$_{67}Ho^{165}$	$^7/_2-$ [523]	*ec*	0	3.55	0.41	3.94	$\lesssim 5$	[5]
$_{67}Ho^{167}$	$^7/_2-$ [523]	$_{68}Er^{167}$	$^5/_2-$ [523]	β^-	700	∞	0.52	3.70	~ 4.8	[5]
$_{70}Yb^{167}$	$^5/_2-$ [523]	$_{69}Tm^{167}$	$^7/_2-$ [523]	*ec*	293	∞	0.39	3.96	$\lesssim 5$	[5]
$_{71}Lu^{173}$	$^9/_2-$ [514]	$_{70}Yb^{173}$	$^7/_2-$ [514]	*ec*	637	3.46	0.45	3.81	5	[7]
$_{70}Yb^{175}$	$^7/_2-$ [514]	$_{71}Lu^{175}$	$^9/_2-$ [514]	β^-	396	3.36	0.35	3.82	4.5	[5]
$_{74}W^{179}$	$^7/_2-$ [514]	$_{73}Ta^{179}$	$^9/_2-$ [514]	*ec*	30	3.46	0.12	4.38	~ 4.6	[8]
$_{94}Pu^{235}$	$^5/_2+$ [633]	$_{93}Np^{235}$	$^7/_2+$ [633]	*ec*	?	3.56	~ 0.03	~ 5.00	$\lesssim 5$	[9]
				Type ah						
$_{62}Sm^{155}$	$^3/_2-$ [521]	$_{63}Eu^{155}$	$^5/_2-$ [523]	β^-	105	∞	0.10	5.38	5.7	[10]
$_{66}Dy^{157}$	$^3/_2-$ [521]	$_{65}Tb^{157}$	$^5/_2-$ [532]	*ec*	327	∞	0.42	4.92	?	[11]
$_{64}Gd^{159}$	$^3/_2-$ [521]	$_{65}Tb^{159}$	$^5/_2-$ [532]	β^-	364	∞	0.08	5.48	6.4—6.7	[5,12]
$_{68}Er^{161}$	$^3/_2-$ [521]	$_{67}Ho^{161}$	$^5/_2-$ [532]	*ec*	826	∞	0.46	4.90	5.4—5.7	[13,14]
$_{68}Er^{171}$	$^5/_2-$ [512]	$_{69}Tm^{171}$	$^7/_2-$ [523]	β^-	425	∞	0.15	5.20	6.3	[5,15]
$_{89}Ac^{231}$	$^3/_2+$ [651]	$_{90}Th^{231}$	$^5/_2+$ [633]	β^-	0	4.78	~ 0.40	~ 5.20	6.6	[9]
$_{90}Th^{231}$	$^5/_2+$ [633]	$_{91}Pa^{231}$	$^3/_2+$ [651]	β^-	166	∞	~ 0.15	~ 5.60	5.8	[9]
$_{93}Np^{239}$	$^5/_2+$ [642]	$_{94}Pu^{239}$	$^7/_2+$ [624]	β^-	512	5.00	0.07	6.15	6.8	[9]
$_{94}Pu^{243}$	$^7/_2+$ [624]	$_{95}Am^{243}$	$^5/_2+$ [642]	β^-	84	∞	0.24	5.62	5.9—6.2	[5,9,12]
$_{90}Th^{231}$	$^5/_2+$ [633]	$_{91}Pa^{231}$	$^5/_2+$ [642]	β^-	84	4.00	~ 0.30	~ 4.50	5.7	[9]
$_{94}Pu^{243}$	$^7/_2+$ [624]	$_{95}Am^{243}$	$^7/_2+$ [633]	β^-	465	4.10	0.62	4.31	5.5—6.0	[5,9]
$_{93}Np^{239}$	$^5/_2+$ [642]	$_{94}Pu^{239}$	$^5/_2+$ [622]	β^-	286	4.71	0.12	5.63	6.9—7.0	[5,9]

on the symmetry axis of the nucleus, N —principal quantum number; the summation in (3) is over l, Λ, Σ_i, and Σ_f.

The calculations performed have shown that the matrix elements depend rather weakly on the deformation. The calculated values of $\log_{10}$ ft are listed in the seventh column of the table.

According to the classification of Mottelson and Nilsson [5] all the transitions are divided into type au transitions (allowed unhindered) and type ah (allowed hindered). The latter are forbidden in the asymptotic quantum numbers N, n_Z, Λ. We note also that in the Nilsson model the β transitions with $\Delta N = 2$ are forbidden.

The effect of pair correlations on the β decay was considered in many papers, for example, those by Solov'ev. [6] In terms of the i.p.m. the residual interactions lead to "smearing" of the Fermi energy surface (E_F). The levels (n) with energy $E_n > E_F$ are partially filled (upon inclusion of the pair correlations) with probability $v_n^2 \leq 1$; the levels with energies $E_n < E_F$ are free, with probability $u_n^2 \geq 0$. It is obvious that the residual pair interactions will hinder the transitions that are allowed in the i.p.m. (the statistical weights of the states participating in the transitions will decrease). On the other hand, the β transitions to the filled levels with $E_n < E_F$, which are forbidden in the i.p.m. (by the Pauli principle) turn out to be allowed in the presence of pair correlations.

The correction factors R_β to the β-transition probabilities, necessitated by the smearing of the Fermi surface, have the following form [6]:

1) β decay of the type

$$R_\beta = [u_{n_i}^{(2n_N)} u_{n_f}^{(2n_Z)}]^2 \prod_{n \neq n_i} (u_n^{(2n_N)} u_n^{(2n_N+1)} + v_n^{(2n_N)} v_n^{(2n_N+1)})^2 \times \prod_{n' \neq n_f} (u_{n'}^{(2n_Z)} u_{n'}^{(2n_Z+1)} + v_{n'}^{(2n_Z)} v_{n'}^{(2n_Z+1)})^2, \quad (4)$$

where n_i and n_f are respectively the initial and final states of the odd neutron and odd proton. Here and throughout $2n_N + 1$, $2n_N$ and $2n_N - 1$ denote the number of the neutrons, and $2n_Z + 1$ etc denote the number of the protons.

2) β decay of the type

$$R_\beta = [v_{n_i}^{(2n_Z)} v_{n_f}^{(2n_N)}]^2 \prod_{n \neq n_i} (u_n^{(2n_Z-1)} u_n^{(2n_Z)} + v_n^{(2n_Z-1)} v_n^{(2n_Z)})^2 \times \prod_{n' \neq n_f} (u_{n'}^{(2n_N-1)} u_{n'}^{(2n_N)} + v_{n'}^{(2n_N-1)} v_{n'}^{(2n_N)})^2. \quad (5)$$

In the case of e-capture the corrections have a similar form. The calculated corrections R_β are listed in the eighth column of the table.

All the foregoing β transition can be divided into transitions with change in the number of paired neutrons (protons) in the shell, and transitions with decay of the odd nucleon. In the i.p.m. there

is no difference between these groups of transitions, but the observed values of ft are somewhat greater for the first group than for the second. This difference is understandable from the point of view of pair correlations, and the calculated corrections R_β reflect this fact.

As can be seen from the table, the theoretical values of ft systematically approach the experimental ones. On the one hand, it is surprising that such an improvement is obtained (the difference $\log_{10}(ft)_{exp} - \log_{10}(ft)_{theor}$ has an average value 0.8), since the calculations are based on very crude premises: the Nilsson model and the inclusion, from among all the residual interactions, of only the pair correlations of nucleons with equal and opposite momentum projections. It must be noted that the characteristics of the "smearing" of the Fermi surface u_n and v_n have been obtained from spectrum calculations,[6] i.e., no additional parameters were involved in the calculation of $(ft)_{theor}$. On the other hand, the calculations did not fulfill the hopes of the greatest optimists, since the calculated values of ft are on the average seven times smaller than the experimentally observed ones. This should serve as a stimulus for further research in this direction.

In conclusion, the authors are grateful to Ya. A. Smorodinskii and V. G. Solov'ev who called their attention to this problem.

[1] S. G. Nilsson, Mat-Fys. Medd. Dan. Vid. Selsk. 29, No. 16, 1955.

[2] A. S. Davydov, Teoriya atomnogo yadra (Theory of Atomic Nucleus), Fizmatgiz, 1958, ch. VI.

[3] O. Bohr and B. Mottelson, Probl. sovr. fiz. 9, 34 (1955). Probably: Mat-Fys. Medd. Dan. Vid. Selsk. 27, No. 16 (1953).

[4] Alaga, Alder, Bohr, and Mottelson, Mat-Fys. Medd. Dan. Vid. Selsk. 29, No. 9, 1955.

[5] B. R. Mottelson and S. G. Nilsson, ibid. 31, 8 (1959).

[6] V. G. Solov'ev, DAN SSSR 133, 325 (1960), Soviet Phys.-Doklady 5, 778 (1961); Izv. AN SSSR ser. fiz. 25, No. 12 (1961), Columbia Tech. Transl. in press; JETP 40, 654 (1961), Soviet Phys. JETP 13, 456 (1961). Liu, Pyatov, Solov'ev, Silin, and Furman, JETP 40, 1503 (1961), Soviet Phys. JETP 13, 1052 (1961).

[7] Bichard, Mihelich, and Harmatz, Phys. Rev. 116, 720 (1959),

[8] Nuclear Data Sheets, 1960.

[9] Stephens, Asaro, and Perlman, Phys. Rev. 113, 313 (1959).

[10] L. C. Schmid and S. B. Burson, Phys. Rev. 115, 447 (1959).

[11] Dzhelepov, Zvol'skii, Nikitin, and Serpienko, Abstracts of Eleventh Annual Conference on Nuclear Spectroscopy, Riga, 1961.

[12] B. S. Dzhelepov and L. K. Peker, Skhemy raspada radioaktivnykh yader (Decay Schemes of Radioactive Nuclei), AN SSSR, 1958.

[13] Dneprovskii, Német, and Peker, JETP 39, 13 (1960), Soviet Phys. JETP 12, 8 (1961).

[14] H. A. Grench and S. B. Burson, Phys. Rev. 121, 831 (1961).

[15] Cranston, Bunker, and Starner, Phys. Rev. 110, 1427 (1958).

Translated by J. G. Adashko
277

ON THE THEORY OF NUCLEON COLLISIONS WITH HEAVY NUCLEI

A. A. EMEL'YANOV

P. N. Lebedev Physics Institute, Academy of Sciences, U.S.S.R.

Submitted to JETP editor June 21, 1961

J. Exptl. Theoret. Phys. (U.S.S.R.) 41, 1673-1674 (November, 1961)

Collisions between nucleons and heavy nuclei are considered within the framework of the hydrodynamic theory. It is shown that the reference system in which the secondary particle angular distribution possesses forward-backward symmetry is not the c system.

BELEN'KII and Milekhin[3,4] have considered the interaction of nucleons with nuclei using the hydrodynamic theory of Landau.[2] If $n < 3.7$ (where n is the number of nucleons in the tube), the problem is solved completely, but if $n > 3.7$, only the dependence of the multiplicity of the process on the dimensions of the nuclei has been obtained. In the present paper we present the results of investigating the symmetry properties of the distribution of shower particles with the help of the hydrodynamic theory for the case $n > 3.7$.[1]

If $n > 3.7$, a region of motion forms in the expanding meson cluster, called the second wave of rarefaction (s.w.r.), which is bounded by the vacuum on one side and on the other by the region of hydrodynamic motion which arises as a result of the reflection of the simple wave on the front of the shock wave[3] (called the first reflected wave). According to Milekhin,[5] the angular distribution of the secondary particles in the one-dimensional approximation[6] is given by the relation

$$\frac{dN}{d\eta} = -\frac{N_0}{3} e^{2y_k} \frac{\partial \Psi(\eta, y_k)}{\partial y_k}, \qquad (1)$$

where $\Psi = \partial\chi/\partial y - \chi$, and $\chi(\eta, y)$ is the hydrodynamic potential determined by the equation of Khalatnikov:[7]

$$3\frac{\partial^2 \chi}{\partial \eta^2} - \frac{\partial^2 \chi}{\partial y^2} - 2\frac{\partial \chi}{\partial y} = 0. \qquad (2)$$

Here $y = \ln(T/T_0)$, $\eta = \tanh^{-1} v$, T is the temperature of the medium, T_0 is the initial temperature, v is the velocity (velocity of light $c = 1$), N_0 is the total number of particles, $y_k = \ln(T_k/T_0)$, and T_k is the decay temperature.

For $|y_k| \gg 1$ the decay of the system is determined by the s.w.r. Solving Eq. (2) for the region of the s.w.r. by the method proposed by Milekhin,[4] we can determine the function $\partial\Psi/\partial y$. With an accuracy up to terms of order $1/|y|$ we have

$$\frac{\partial \Psi}{\partial y} = \frac{\sqrt{3}}{2} e^{-y} \Big[l\left(\frac{\partial I_0(z)}{\partial y} - I_0(z)\right) - t_1 \frac{\partial I_0(z)}{\partial \eta} + \lambda\beta_k (I_0(z) + I_1(z)) \Big],$$

$$\lambda = 3 + \sqrt{3}, \quad \beta_k = (n - 2 - \sqrt{3})(2 + \sqrt{3})/(7 + 4\sqrt{3}),$$

$$z = \sqrt{y^2 - \eta^2/3}, \qquad t_1 = \sqrt{3}\lambda + \frac{(5\sqrt{3} + 9)\lambda\beta_k}{2(2 - \sqrt{3})},$$

$$l = \lambda + \frac{(5 + 3\sqrt{3})\lambda\beta_k}{2\sqrt{3}(2 - \sqrt{3})}. \qquad (3)$$

Using relations (1) and (3), it is easy to show that the angular distribution of the secondary particles has forward-backward symmetry in the reference system moving with respect to the system of the center of gravity with a velocity V, where

$$V = \text{th}\left[\frac{4(n+1) + 3\sqrt{3}}{2(7 + 4\sqrt{3})} - \text{Arth}\left(\frac{n-1}{n+1}\right)\right]. \qquad (4)^*$$

For example, for a tube with $n = 6$ we have $V = 0.4$.

We note in this connection that the experimental determination of the energy of the system by the "half-angle" method leads to a lowering of the value of the energy by a factor $\exp(-2 \tanh V)$ [for $n = 6$ we have $\exp(2 \tanh V) = 2.2$]. The lowering of the energy leads again to a certain rise in the degree of anisotropy of the angular distribution of the shower particles.

For the system as a whole the violation of the symmetry will be due to particles in the simple wave (about one particle) and in the first reflected wave (about four particles). However, the contribution of these particles is small and decreases with increasing energy of the incoming nucleon. This last assertion may become invalid if account is taken of the viscosity, which leads to the formation of an additional number of particles in the region of the simple wave.[8]

*th = tanh, Arth = $\tanh^{-1}$.

[1] P. H. Malhotra and Y. Tsuzuki, Nuovo cimento **18**, 982 (1960). Bartke, Ciok, et al., Nuovo cimento **15**, 18 (1960).

[2] L. D. Landau, Izv. AN SSSR Ser. Fiz. **17**, 51 (1953).

[3] S. Z. Belen'kii and G. A. Milekhin, JETP **29**, 20 (1955), Soviet Phys. JETP **2**, 14 (1956).

[4] G. A. Milekhin, JETP **35**, 1185 (1958), Soviet Phys. JETP **8**, 829 (1959).

[5] G. A. Milekhin, JETP **35**, 978 (1958), Soviet Phys. JETP **8**, 682 (1959).

[6] I. L. Rozental', JETP **31**, 278 (1956), Soviet Phys. JETP **4**, 217 (1957).

[7] I. M. Khalatnikov, JETP **26**, 529 (1954).

[8] A. A. Emel'yanov and D. S. Chernavskii, JETP **37**, 1058 (1959), Soviet Phys. JETP **10**, 753 (1960).

Translated by R. Lipperheide
278

ON THE ANALYTIC PROPERTIES OF THE ONE-FERMION GREEN'S FUNCTION IN THE QUANTUM THEORY OF MANY BODIES

S. V. MALEEV

Leningrad Physico-Technical Institute, Academy of Sciences, U.S.S.R.

Submitted to JETP editor June 22, 1961

J. Exptl. Theoret. Phys. (U.S.S.R.) **41**, 1675-1680 (November, 1961)

The analytic properties of the one-fermion Green's function and of the mass operator in the quantum theory of many bodies are investigated. In particular, the problem of the poles of the mass operator is examined.

We shall investigate the analytic properties of the one-fermion Green's function of a system of interacting Fermi particles in the ground state. This problem has been treated recently in a paper by Luttinger.[1] Luttinger confines himself, however, to the consideration of "normal" Fermi systems, i.e., systems that do not have an energy gap in the spectrum of one-fermion excitations. The present paper deals with the analytic properties of the Green's function for systems of both types (both with and without a gap). In particular, a study is made of the problem of the connection of a gap in the spectrum of the one-fermion excitations with a pole of the mass operator of the fermion. Also it is shown that one subtraction may be necessary for the presentation of the mass operator in the form of a dispersion integral.

For simplicity we shall confine ourselves to spatially homogeneous systems, although the results we obtain can be extended to the case of inhomogeneous systems. Also we shall assume that the number of particles N in the system is very large, and accordingly shall neglect all correction terms of order N^{-1} in the quantities considered.

Let us define the one-fermion Green's function by the equation*

$$G(x, x') = i\langle T(\psi(x)\psi^+(x'))\rangle. \quad (1)$$

Using the fact that $G(x-x')$ depends only on the difference $x-x'$, we represent this function as a Fourier integral:

$$G(x) = \frac{1}{(2\pi)^4}\int dp d\omega e^{ipx-i\omega t} G(p, \omega). \quad (2)$$

As Galitskii and Migdal[2] have shown, $G(p, \omega)$ has the integral representation

$$G(p, \omega) = \int_{-\infty}^{0} d\omega' \frac{A(p, \omega')}{\omega' - \omega + i\delta} + \int_{0}^{\infty} d\omega' \frac{A(p, \omega')}{\omega' - \omega - i\delta}, \quad (3)$$

where ω is the energy measured from the chemical potential μ of the system, and the function $A(p, \omega)$ is nonnegative, i.e., $A(p, \omega) \geq 0$, and satisfies the condition

$$\int_{-\infty}^{\infty} d\omega A(p, \omega) = 1, \quad (4)$$

which is a consequence of the canonical commutation relation

$$\{\psi_\alpha(x, t), \psi_\beta^+(x', t)\} = \delta_{\alpha\beta}\delta(x - x'). \quad (5)$$

We write down Dyson's equation for $G(p, \omega)$:

$$-G^{-1}(p, \omega) = -G_0^{-1}(p, \omega) + M(p, \omega). \quad (6)$$

Here $G_0(p, \omega)$ is the Green's function of the system of noninteracting particles, and $M(p, \omega)$ is what is usually called the mass operator for the fermion.

Equation (6) is essentially a definition of $M(p, \omega)$. As is shown in the paper of Galitskii and Migdal,[2]

$$G_0(p, \omega) = -[\omega + \delta\mu - \zeta_p + i\delta\varepsilon(\zeta_p)]^{-1}$$
$$= -[\omega_0 - \zeta_p + i\delta\varepsilon(\zeta_p)]^{-1},$$
$$\delta\mu = \mu - E_F, \quad \zeta_p = p^2/2m - E_F, \quad (7)$$

where E_F is the Fermi energy, ω_0 is the energy measured from the Fermi energy, and $\epsilon(x) = x|x|^{-1}$.

It follows from Eqs. (3) and (4) that

$$\lim_{|\omega|\to\infty} \omega G(p, \omega) = -1, \quad (8)$$

from which, when we use Eq. (6) and (7), we get

$$\lim_{|\omega|\to\infty} \omega^{-1} M(p, \omega) = 0, \quad (9)$$

i.e., when the absolute value of ω is large $M(p, \omega)$ can increase, but more slowly than ω. It must be noted that Eq. (9) restricts the possible character

*In the literature one often encounters a definition of the Green's function which differs from ours in sign.

of the increase of $M(p, \omega)$ at infinity. Indeed, in general the function $M(p, \omega)$ does not necessarily have to increase for large ω. It can approach a constant or even decrease.

From Eq. (3) there follows an important property of $G(p, \omega)$, regarded as a function of the complex variable ω. First, $G^*(p, \omega) = G(p, \omega^*)$, from which it follows that also $M^*(p, \omega) = M(p, \omega^*)$. Furthermore, as is easily verified, the sign of the imaginary part of $G(p, \omega)$ agrees with that of the imaginary part of the argument. Following Castillejo, Dalitz, and Dyson,[3] we shall call functions that have this property R-functions (see also a paper by Ansel'm and others[4]). It is easy to see that R-functions have the following property: if $H(\omega)$ is an R-function, then $-H^{-1}(\omega)$ is also an R-function. Thus $-G^{-1}(p, \omega)$ and $-G_0^{-1}(p, \omega)$ are also R-functions. When we now use Eqs. (6), (7), and (9), we can verify that $M(p, \omega)$ is also an R-function.

This fact enables us to write a general expression for $M(p, \omega)$ analogous to the representation (3) for the Green's function. To do so we first note that to the zeroes of the Green's function (if there are any) there correspond poles of the function $M(p, \omega)$. On the other hand, an R-function can have poles only of the first order, and these poles must lie on the real axis and have real and negative residues. We readily convince ourselves of this if we note that near a pole any function may be replaced by its principal part (pole term) at that pole. If our function is an R-function, then this principal part is obviously also an R-function. It is not hard to verify that an expression of the type $a(\omega - \Omega)^{-n}$ can be an R-function only for $n = 1$, $a > 0$, and real Ω, and from this there follows the assertion made above about the poles of $M(p, \omega)$.

As has already been noted, the poles of $M(p, \omega)$ correspond to the zeroes of the Green's function. It follows from Eq. (3) that $G(p, \omega)$ can be zero only at points at which $A(p, \omega) = 0$, since $\operatorname{Im} G(p, \omega) \sim A(p, \omega)$ for real ω. On the other hand, as Galitskii and Migdal[2] have shown, $A(p, \omega)$ can be defined in the following way:

$$A(p, \omega) = \begin{cases} \sum_n |\langle n | \psi^+(0) | C_1 \rangle|^2, & \omega > 0 \\ \sum_n |\langle n | \psi(0) | 0 \rangle|^2 & \omega < 0, \end{cases} \tag{10}$$

where the sum is taken over all states of the system which have the momentum p and the energy ω.

From physical considerations it is improbable that this expression would be zero at any isolated value $\omega = \omega(p)$; it is still more improbable that the function $\operatorname{Re} G(p, \omega)$ would simultaneously vanish at $\omega = \omega(p)$. In any case, we cannot indicate any reasonable physical ideas corresponding to such a situation. Therefore in what follows we shall assume that the zeroes of the Green's function can lie only in regions of values of ω where $A(p, \omega) \equiv 0$.

It also follows from Eq. (3) that in these regions $G(p, \omega)$ is continuous and has a continuous positive derivative. Therefore in each region of values of ω where $A(p, \omega) \equiv 0$ there can be not more than one zero of the function $G(p, \omega)$. We shall assume that $A(p, \omega)$ can be zero only in a region near zero, i.e., for values of ω in the range

$$-\Delta_-(p) < \omega < \Delta_+(p); \quad \Delta_\pm(p) > 0, \tag{11}$$

and it follows from Eq. (10) that to this there corresponds a gap in the spectrum of the one-fermion excitations [the connection between the pole of $M(p, \omega)$ and the gap in the one-fermion spectrum has also been investigated by Migdal[5]].

Thus we must consider two cases: 1) there is no gap in the spectrum of the one-fermion excitations, and 2) there is a gap in this spectrum.

To begin with, let us consider the first case (the only one treated by Luttinger[1]). Assuming that $M(p, \omega)$ increases with increasing ω, we have

$$M(p, \omega) = M(p) + \omega \int_{-\infty}^{0} d\omega' \frac{\alpha(p, \omega')}{\omega'(\omega' - \omega + i\delta)} + \omega \int_{0}^{\infty} d\omega' \frac{\alpha(p, \omega')}{\omega'(\omega' - \omega - i\delta)}, \tag{12}$$

where $M(p) = M(p, 0)$ is a real quantity, and

$$\alpha(p, \omega) = \varepsilon(\omega) \operatorname{Im} M(p, \omega) > 0. \tag{13}$$

It is easy to obtain this expression if we make use of the following fact. The Green's function $G(p, \omega)$ is the limiting value of the function defined by Eq. (3) (if we regard it as a function of the complex variable ω) as ω approaches the real axis from above, if $\omega > 0$, and from below, if $\omega < 0$. It is obvious that $M(p, \omega)$ must have this same property. Applying Cauchy's theorem to $\omega^{-1} M(p, \omega)$ and taking C_1 as the path of integration, we get a function whose limiting value as ω approaches the real axis from above coincides with $M(p, \omega)$ for

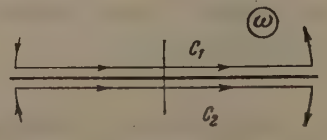

FIG. 1

$\omega > 0$ (Fig. 1). Then taking as the path of integration the contour C_2 of Fig. 1, we get in a similar way an expression for $M(p, \omega)$ for $\omega < 0$. These two expressions are combined in Eq. (12), if we use the fact that $M^*(p, \omega) = M(p, \omega^*)$; it is easy to see that $\alpha(p, \omega)$ must be positive in order for $M(p, \omega)$ to be an R-function.[3,4] If, on the other hand, $M(p, \omega)$ remains bounded (or decreases) as ω increases, then in just the same way, applying Cauchy's theorem to the difference $M(p, \omega) - M(p, \infty)$, we get

$$M(p, \omega) = M(p) + \int_{-\infty}^{0} d\omega' \frac{\alpha(p, \omega')}{\omega' - \omega + i\delta} + \int_{0}^{\infty} d\omega' \frac{\alpha(p, \omega')}{\omega' - \omega - i\delta}, \quad (14)$$

where $M(p) = M(p, \infty)$ is real and $\alpha(p, \omega) > 0$.

Let us go on to the second case. The expression (3), regarded as a function of the complex variable ω, now defines a single analytic function in the plane with cuts from $-\infty$ to $-\Delta_-(p)$ and from $\Delta_+(p)$ to ∞. Therefore $M(p, \infty)$ must also be an analytic function of ∞ in the plane with the same cuts. Applying Cauchy's theorem to the function $M(p, \omega)(\omega - \omega_1)^{-1}$ and integrating along the path shown in Fig. 2, we get as an expression for $M(p, \omega)$

$$M(p, \omega) = M(p, \omega_1) + \delta_p^2 [(\omega_p - \omega)^{-1} - (\omega_p - \omega_1)^{-1}] + \int_{-\infty}^{-\Delta_-(p)} d\omega' \alpha(p, \omega') \left(\frac{1}{\omega' - \omega + i\delta} - \frac{1}{\omega' - \omega_1} \right) + \int_{\Delta_+(p)}^{\infty} d\omega' \alpha(p, \omega') \left(\frac{1}{\omega' - \omega - i\delta} - \frac{1}{\omega' - \omega_1} \right), \quad (15)$$

where $\delta_p^2 \geq 0$, $-\Delta_-(p) < \omega_p < \Delta_+(p)$, $\alpha(p, \omega) > 0$, and $\delta_p^2 \to 0$ if $\Delta_\pm(p) \to 0$; the function $M(p, \omega_1)$ is real, and ω_1 is an arbitrary quantity lying in the interval from $-\Delta_-(p)$ to $\Delta_+(p)$. In particular, we may set $\omega_1 = 0$.

In this expression we have taken account of the fact that, as was shown earlier, $M(p, \omega)$ can have a pole in the region where $A(p, \omega) \equiv 0$, and that the residue at this pole must be negative. If $M(p, \omega)$ remains bounded for large ω (or decreases), then Eq. (15) can be replaced by the expression

$$M(p, \omega) = M(p) + \frac{\delta_p^2}{\omega_p - \omega} + \int_{-\infty}^{-\Delta_-(p)} \frac{d\omega' \alpha(p, \omega')}{\omega' - \omega + i\delta} + \int_{\Delta_+(p)}^{\infty} \frac{d\omega' \alpha(p, \omega')}{\omega' - \omega - i\delta}, \quad (16)$$

where $M(p)$ is real, and the conditions satisfied by δ_p^2, $\alpha(p, \omega)$, and ω_p are the same as before. We note further that a necessary and sufficient

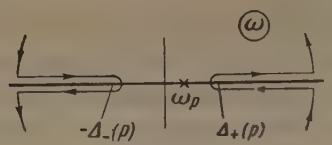

FIG. 2

condition for the existence of a pole of $M(p, \omega)$ are the inequalities

$$G(p, -\Delta_-(p)) < 0, \quad G(p, \Delta_+(p)) > 0. \quad (17)$$

It is interesting to consider as an example the problem of the form of the Green's function and the energies of the elementary excitations in the case in which we can confine ourselves to just the pole term and a constant term in the expression for $M(p, \omega)$. As is well known, the spectrum of the elementary excitations is determined by the zeroes of the expression (6). In our approximation we get from this condition

$$\omega^2 - \omega(\omega_p + \Sigma_p) + \omega_p \Sigma_p - \delta_p^2 = 0,$$
$$\Sigma_p = \zeta_p - \delta\mu - M(p). \quad (18)$$

Solving this equation, we have

$$\varepsilon_p^\pm = \tfrac{1}{2} [\omega_p + \Sigma_p \pm \sqrt{(\omega_p - \Sigma_p)^2 + \delta_p^2}], \quad (19)$$

where ϵ_p^+ is the energy for particles, and ϵ_p^- is the energy for holes. It can be seen from Eq. (19) that $\epsilon_p^+ > \epsilon_p^-$ and equality, $\epsilon_p^+ = \epsilon_p^-$, is impossible, provided only δ_p^2 is not zero. The minimum of the difference $\epsilon_p^+ - \epsilon_p^-$ gives the width of the energy gap in the spectrum of the one-fermion excitations.

The Green's function is obviously of the form

$$G(p, \omega) = -\frac{u_p^+}{\omega - \varepsilon_p^+ + i\delta} - \frac{u_p}{\omega - \varepsilon_p^- - i\delta}, \quad (20)$$

$$u_p^\pm = \left(1 + \frac{\partial M}{\partial \omega}\right)^{-1}\Big|_{\omega = \varepsilon_p^\pm} = \frac{(\omega_p - \varepsilon_p^\pm)^2}{(\omega_p - \varepsilon_p^\pm)^2 + \delta_p^2}. \quad (21)$$

The number density of the particles in the system is given by the equation[2]

$$n = \frac{2}{(2\pi)^3} \int dp \int_{-\infty}^{\infty} d\omega e^{i\omega\delta} G(p, \omega) = \frac{2}{(2\pi)^3} \int dp u^-(p), \quad (22)$$

which can be regarded as an equation for $\delta\mu$.

If the spectrum of the system is symmetrical, i.e., if the energy of a particle, taken as a function of the momentum, differs only in sign from the energy of a hole, then obviously $\omega_p = -\Sigma_p$, and all of the expressions have particularly simple forms:

$$\varepsilon_p^+ = -\varepsilon_p = \sqrt{\Sigma_p^2 + \delta_p^2} = \varepsilon_p,$$
$$u_p^\pm = (\varepsilon_p \pm \Sigma_p)(2\varepsilon_p)^{-1}; \quad u_p^+ + u_p^- = 1. \quad (23)$$

For $\delta\mu = 0$ and $M(p) = 0$ these expressions take the form that they usually have in the theory of superconductivity (cf. the paper by Gor'kov[6]).

In the general case the Green's function has poles in the complex plane, whose positions determine the energies and dampings of the elementary excitations. These poles lie on a sheet of the analytic function $G(p, \omega)$ different from that defined by the expression (3). For particles we have at the pole $\mathrm{Re}\ \omega > 0$ and $\mathrm{Im}\ \omega < 0$, and for holes the opposite signs. Using this fact and separating off the pole terms, we have

$$G(p, \omega) = -\frac{u_+(p)}{\omega - \varepsilon_p^+ + i\Gamma_p^+} - \frac{u_-(p)}{\omega + \varepsilon_p^- - i\Gamma_p^-} - \varphi(p, \omega), \quad (24)$$

where $\varphi(p, \omega)$ has no singularities of the pole type, ϵ_p^+ and Γ_p^+ are the energy and damping for particles, and ϵ_p^- and Γ_p^- are those for holes;

$$u_\pm(p) = \left(1 + \frac{\partial M}{\partial \omega}\right)^{-1}\Big|_{\omega = \pm(\varepsilon_p^\pm - i\Gamma_p^\pm)}. \quad (25)$$

Obviously as the momentum increases the energy of an elementary excitation must approach the energy of a free particle. In this case the imaginary part of the energy of an elementary excitation, i.e., the damping, is of the form

$$\Gamma_p^+ \approx \pi\alpha(p, \zeta_p). \quad (26)$$

In conclusion the author expresses his gratitude to A. A. Ansel'm, V. N. Gribov, G. S. Danilov, and I. T. Dyatlov for helpful discussions.

[1] J. M. Luttinger, Phys. Rev. **121**, 942 (1961).

[2] V. M. Galitskii and A. B. Migdal, JETP **34**, 139 (1958), Soviet Phys. JETP **7**, 96 (1958).

[3] Castillejo, Dalitz, and Dyson, Phys. Rev. **101**, 453 (1956).

[4] Ansel'm, Gribov, Danilov, Dyatlov, and Shekhter, JETP **41**, 619 (1961), Soviet Phys. JETP **14**, 444 (1962).

[5] A. B. Migdal, JETP **40**, 684 (1961), Soviet Phys. JETP **13**, 478 (1961).

[6] L. P. Gor'kov, JETP **34**, 735 (1958), Soviet Phys. JETP **7**, 505 (1958).

Translated by W. H. Furry
279

TRANSFORMATION OF PHOTONS INTO NEUTRINO PAIRS AND ITS SIGNIFICANCE IN STARS

S. G. MATINYAN and N. N. TSILOSANI

Institute of Physics, Academy of Sciences Georgian S.S.R.

Submitted to JETP editor June 24, 1961

J. Exptl. Theoret. Phys. (U.S.S.R.) 41, 1681-1687 (November, 1961)

The cross section for the transformation of a γ quantum into a $\nu\bar{\nu}$ pair is calculated and the cross section for transformation of two photons into $\nu\bar{\nu}$ is estimated. The stellar neutrino luminosities corresponding to these processes are computed. Within a broad range of stellar temperatures and densities, these processes are found to predominate over the bremsstrahlung of $\nu\bar{\nu}$ pairs by electrons.

1. INTRODUCTION

GAMOV and Schoenberg[1] were apparently the first to point out the important role of the energy carried away from stars by neutrinos via K capture and β decay during the process of the stellar evolution.

The great advances in the theory of the universal weak A-V interaction have called attention to the neutrino mechanism of energy loss from stars, connected with the interaction, predicted by the Feynman and Gell-Mann theory,[2] between the electrons and the neutrino $(\bar{e}\nu)(\bar{e}\nu)^+$ in the first order in the weak interaction constant G. Pontecorvo[3] noted that the existence of such an interaction should make possible emission of a neutrino-antineutrino pair in electromagnetic processes instead of emission of a γ quantum (through the virtual pair e^+e^-).

The negligible probability of such processes, compared with that of electromagnetic processes, is obvious. At the high densities and temperatures encountered in stars, however, the energy lost by stars through neutrino-pair formation may turn out to be comparable with or even greater than the energy losses due to γ-quantum emission, owing to tremendous differences between the penetrating abilities of the γ quanta and the neutrinos. In addition, the range of the γ quanta decreases at large Z whereas the cross section for the formation of neutrino pairs increases.

Pontecorvo considered by way of an example the formation of neutrino pairs in collisions between electrons and nuclei.[3] A quantitative investigation of this process as applied to astrophysics was made by Gandel'man and Pinaev.[4]

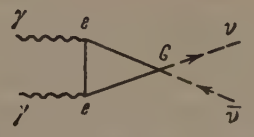

FIG. 1

They obtained the important result that, within a definite region of high temperatures and pressures, the energy carried away by the neutrinos in the aforementioned process exceeds the photon energy loss. This result indicates the need for a detailed study of all the neutrino mechanisms of energy loss from stars. Recently Chiu and Morrison[5] and Chiu and Stabler[6] considered certain possible neutrino mechanisms whereby energy is carried away from stars:*

$$e^- + e^+ \to \nu + \bar{\nu}, \qquad \gamma + e^- \to e^- + \nu + \bar{\nu},$$

$$\gamma + \gamma \to \gamma + \nu + \bar{\nu}.$$

In the present article we investigate quantitatively a new supplementary mechanism by which neutrinos can carry energy away from the stars. In this mechanism the photon breaks up in the Coulomb field of the nucleus into a neutrino-antineutrino pair. In addition, we estimate approximately the effect connected with the process of conversion of two γ quanta into a $\nu\bar{\nu}$ pair. As applied to conditions inside stars, the calculation is carried out in nonrelativistic approximation.

*E. L. Feĭnberg was kind enough to advise us that the second of these processes was considered in detail also by V. I. Ritus, who obtained a much greater value for the neutrino energy loss than indicated in the table of Chiu and Morrison.[5]

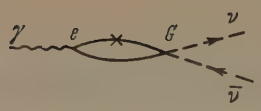

FIG. 2

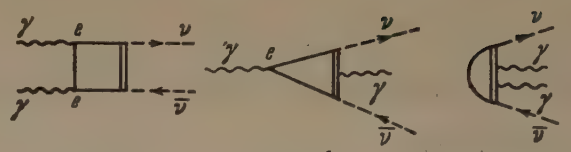

a b c

FIG. 3

2. CROSS SECTION FOR THE PRODUCTION OF A NEUTRINO PAIR BY A PHOTON IN THE FIELD OF THE NUCLEUS

As noted by Gell-Mann,[7] the amplitude of the process wherein two γ quanta are converted into a $\nu\bar{\nu}$ pair, shown in Fig. 1, vanishes in the case of local $(\bar{e}\nu)(\bar{e}\nu)^+$ interaction.

This circumstance is the result of three factors: 1) the invariance under charge conjugation, which forbids any contribution to the amplitude of the matrix element from the vector part of the electron current $e\gamma_\alpha e$, obtained from the original Lagrangian of the local A-V interaction

$$\mathcal{L} = \frac{G}{\sqrt{2}} [\bar{e}\gamma_\alpha (1+\gamma_5)\nu] [\bar{e}\gamma_\alpha (1+\gamma_5)\nu]^+$$

by a Fierz transformation; 2) the impossibility of transitions between system states with spin 1 and two real photons[8,9]; 3) the zero value of the neutrino mass.

Obviously, if one of the photons is replaced by a Coulomb field, argument 2) no longer applies and the process in the corresponding diagram of Fig. 2 should take place if the $(\bar{e}\nu)(\bar{e}\nu)^+$ interaction exists. In addition, if nonlocality (due, for example, to the intermediate charged vector boson) takes place at the vertex G, then the process $\gamma + \gamma \to \nu + \bar{\nu}$ will also occur.[7]

In this section we present an exact calculation of the cross section for Coulomb disintegration of the γ quantum into a $\nu\bar{\nu}$ pair, and obtain in addition a rough estimate of the cross section of the process $\gamma + \gamma \to \nu + \bar{\nu}$ on the assumption that an intermediate boson exists.

We consider the first process $\gamma + A \to A + \nu + \bar{\nu}$ (Fig. 2). Owing to the presence of a pseudo-vector current $e\gamma_\alpha\gamma_5 e$ along with the vector current $e\gamma_\alpha e$ this process, unlike the formally similar process of scattering of a photon in the Coulomb field of a nucleus, is of first order in Z. In addition, owing to invariance under charge conjugation, only the pseudo-scalar current contributes to the amplitude of the process. The gauge invariance of the matrix elements eliminates the divergences (both linear and logarithmic) automatically. Evaluating in standard fashion the integrals and the traces corresponding to the electron loop, we obtain for the matrix element in the non-relativistic approximation (i.e., neglecting the squares of the 4-momenta of all the external lines compared with the square of the electron mass m^2)

$$-\frac{\alpha ZG}{2\pi\sqrt{\omega}} \frac{1}{|q|^2} \varepsilon_{ikl} q_i e_k [\bar{u}(p_\nu)\gamma_l (1+\gamma_5) v(-p_{\bar{\nu}})]. \quad (1)$$

Here ϵ_{ikl} — fully antisymmetrical unit tensor of third rank $(i, k, l = 1, 2, 3)$; ω — frequency of γ quantum; q — momentum transferred to the nucleus, the action of which is usually treated like the action of an external static field; e_k — photon polarization vector; p_ν and $p_{\bar{\nu}}$ — 4-momenta of the neutrino and antineutrino: u and v — the corresponding spinors; $\alpha = 1/137$; $G = 10^{-5}/M_p^2$, M_p — proton mass ($\hbar = c = 1$); Z = nuclear charge.

After averaging over the polarization of the γ quantum and summing over the polarizations of the neutrino and antineutrino, we obtain for the differential cross section

$$d\sigma_1 = \frac{Z^2\alpha^2 G^2}{\pi(2\pi)^6} \frac{\varepsilon_\nu^2(\omega-\varepsilon_\nu)^2}{\omega^2} \frac{d\varepsilon_\nu}{q^2} \left[1 - \frac{(n_\nu q)(n_{\bar{\nu}} q)}{q^2}\right] dn_\nu dn_{\bar{\nu}}, \quad (2)$$

where ϵ_ν — energy of the neutrino, $n_{\nu(\bar{\nu})}$ — unit vector along the direction of emission of ν ($\bar{\nu}$); $q = k - p_\nu - p_{\bar{\nu}}$.

In the integration over the directions of emission of ν and $\bar{\nu}$, the second term in the square brackets drops out, while the first term yields

$$\iint \frac{dn_\nu dn_{\bar{\nu}}}{(k-\varepsilon_\nu n_\nu - \varepsilon_{\bar{\nu}} n_{\bar{\nu}})^2} = \frac{4\pi^2}{\omega(\omega-\varepsilon_\nu)} \left[\ln\frac{\omega(\omega-\varepsilon_\nu)}{\varepsilon_\nu^2} + \frac{2\omega-\varepsilon_\nu}{\varepsilon_\nu}\ln\frac{\omega}{\omega-\varepsilon_\nu}\right]. \quad (3)$$

Integrating, finally, over the neutrino energy we obtain for the total cross section of the production of a neutrino pair by a photon in the field of the nucleus

$$\sigma_1 = (7/576\pi^5) Z^2\alpha^2 G^2 \omega^2. \quad (4)$$

When $\omega = 250$ kev, for example, this section is $0.4\,Z^2 \times 10^{-52}$ cm^2, i.e., negligibly small. However, under conditions prevailing inside stars this cross section causes, as we shall show below, noticeable neutrino emission from very dense "hot" stars.

Let us consider briefly the process $\gamma + \gamma \to \nu + \bar{\nu}$. As mentioned above, it can occur only if a nonlocality exists in the A — V interaction. If this nonlocality is connected with a heavy intermediate

vector boson, (a carrier of weak interactions), then the diagrams contributing to the amplitude of the process will be of the type shown in Fig. 3. The double line in this figure represents the intermediate vector boson of mass M.

To estimate the order of magnitude of the cross section we consider only the contribution corresponding to diagrams of type a, disregarding diagrams such as b and c, in which the γ quanta are absorbed by the heavy particle. Diagram a leads to logarithmically divergent integrals, so that the cross section of the process does not depend strongly on the cut-off momentum L. Taking L to be of the order of the mass of the intermediate meson, which in turn is taken to be of the order of the nucleon mass, we obtain the following approximate estimates for the total cross section for the production of a neutrino pair in a collision between two photons, in the nonrelativistic case (ω^2, $\omega'^2 \ll m^2$):

$$\sigma_2 \approx (\alpha^2 G^2/2\pi^5)\,\omega\omega', \qquad (5)$$

where ω and ω' are the frequencies of the incoming photons in the frame fixed in the star.

3. CONTRIBUTION OF THE CONSIDERED PROCESSES TO THE NEUTRINO EMISSION FROM THE STARS

In this section we explain the role played by the elementary processes considered here in the energy loss from the stars, and compare these processes with bremstrahlung of neutrino pairs by electrons.[3,4] We are essentially interested in the conversion of a photon into a neutron pair in the field of the nucleus.

Let us find the energy $q_\nu^{(1)}$ transferred by the photons to the neutrino pairs in 1 cm^3 per second. Describing the distribution of the photons n_γ by means of Planck's formula with $kT \ll m$, we obtain for $q_\nu^{(1)}$

$$q_\nu^{(1)} = \int \omega \sigma_1 n_n \, dn_\gamma = 3.4 \cdot 10^{-8} \frac{\rho}{\nu} T^6, \qquad (6)$$

where n_n — number of nuclei per cm^3; ρ — density of the matter (in g/cm^3); $1/\nu = \Sigma C_i Z_i^2/A_i$ (C_i is the weight concentration of the element, Z_i its charge, and A_i its atomic weight; the summation is over all the elements contained in interstellar matter); the temperature T is given everywhere in kev.

It must be borne in mind that the rate of energy release obtained here is many times smaller than the rate of energy release in hydrogen reactions, and therefore the neutrino loss can compete with the thermonuclear loss only if the thermonuclear reactions in the star are already practically nonexistent and the star is characterized by a large value of Z.

Gandel'man and Pinaev[4] have shown that although the cross section in the Gamow-Schoenberg process[1] is proportional to G^2 and the neutrino bremsstrahlung cross section[3,4] is proportional to $\alpha^2 G^2$, nonetheless, owing to the lower abundance of the elements with low threshold for the inverse β process and to the anomalously large lifetime of certain nuclei, the process $e^- + A \to e^- + A + \nu + \bar{\nu}$ proposed by Pontecorvo[3] prevails at $T < 100$ kev over the processes considered by Gamow and Schoenberg. We shall therefore compare the effect we are considering with the effect investigated by Gandel'man and Pinaev.[4]

If q_ν is the rate of energy release per cm^3 obtained in [4], we get for a star consisting entirely* of Mg^{24}

$$q_\nu^{(1)}/q_\nu = 2.5 \cdot 10^2 T^{9/2}/\rho. \qquad (7)$$

When $T > 50$ kev and $\rho \approx 10^5$ we obtain $q_\nu^{(1)} > q_\nu$. We see thus that the process $\gamma + A \to A + \nu + \bar{\nu}$ can make an appreciable contribution to the neutrino emission from the stars.

Let us compare now the neutrino luminosity $L_\nu^{(1)}$, corresponding to σ_1, with the values of L_ν obtained in [4]. In addition, we compare $L_\nu^{(1)}$ with the photon luminosity L_γ. We base our calculations, as in [4], on a model of a point source. We have

$$L_\nu^{(1)} = \int q_\nu^{(1)} \, dv = 3.4 \cdot 10^{-8} \frac{1}{\nu} 4\pi \int_0^R \rho T^6 r^2 \, dr, \qquad (8)$$

where R — radius of the star, characterized by a constant central density ρ_c of a convective nucleus with radius $0.169\,R$[11] and temperature T_c. In the remaining part of the star which makes in practice a small contribution to L, we have

$$T = T_c \frac{R/r - 1}{1/\xi - 1}, \qquad \rho = \rho_c \left(\frac{R/r - 1}{1/\xi - 1}\right)^{3.5}$$

($\xi = 0.169$). Integrating (8) and expressing R in terms of ρ_c and T_c using the formulas

$$T_c = 0.7 \cdot 10^{-22} \mu \frac{M}{R},$$

$$\rho = 37M \Big/ \frac{4}{3}\pi R^3 \qquad \left(\frac{1}{\mu} = \sum_i C_i (Z_i + 1)/A_i\right),$$

we determine $L_\nu^{(1)}$ expressed in solar units of luminosity ($L_\odot = 3.78 \times 10^{33}$ erg/sec):

*Present-day data [10] indicate apparently that white dwarfs with mass on the order of the mass of the sun, if formed as the result of evolution of stellar remnants or stars with low initial hydrogen content, consist essentially of Mg^{24}.

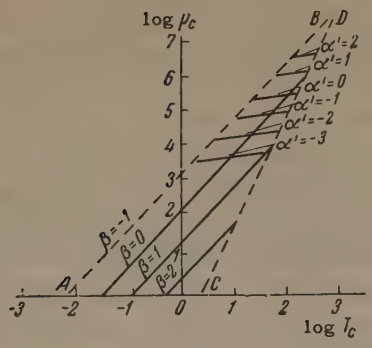

FIG. 4

$$L_\nu^{(1)} = 1.2\cdot 10^{-8}\frac{1}{\nu\mu^{3/2}}\,T_c^{7.5}/\rho_c^{0.5}. \qquad (9)$$

The ratios of $L_\nu^{(1)}$ to the photon luminosity [4] L_γ and to L_ν are

$$L_\nu^{(1)}/L_\gamma = 10^{-11}\rho_c^2/\nu\mu b T_c^{0.5}, \qquad (10)$$

$$L_\nu^{(1)}/L_\nu = 1.3\cdot 10^{2}\mu_e T_c^{1.5}/\rho_c, \qquad (11)$$

where $1/\mu_e = \Sigma C_i Z_i/A_i$, and b is the coefficient in Kramers's formula for the free path of the photon inside the star.

Figure 4 shows on a logarithmic scale the lines $L_\nu^{(1)}/L_\gamma = 10^\alpha$ and $L_\nu^{(1)}/L_\nu = 10^\beta$ for Mg ($\mu = \mu_e = 2$, b = 1, $\nu = 1/6$). In the region bounded by the lines AB and CD we can compare $L_\nu^{(1)}$ with the values of L_ν and L_γ obtained in [4], assuming no degeneracy and low radiation pressure compared with matter pressure. We see that $L_\nu^{(1)} > L_\nu$ over a wide range of temperatures and densities. In addition, when $\rho_c > 10^5$ and 30 kev < T_c < 100 kev, the neutrino luminosity is one order of magnitude or more greater than the photon luminosity.

Let us give, finally, the ultimate formulas corresponding to the process $\gamma + \gamma \to \nu + \bar\nu$, the cross section σ_2, of which was estimated by us approximately in Sec. 2.

To obtain $q_\nu^{(2)}$ we must integrate $(\omega + \omega')\sigma_2$, using a Planck distribution for the frequencies ω and ω':

$$q_\nu^{(2)} = 2\iint (\omega + \omega')\,\sigma_2\, dn_\gamma\, dn_\gamma'. \qquad (12)$$

We obtain

$$q_\nu^{(2)} \approx 1.8\cdot 10^{-8} T^9, \qquad (13)$$

$$q_\nu^{(2)}/q_\nu^{(1)} \approx 3\cdot 10^{-5} T^3. \qquad (14)$$

For the neutron luminosity we obtain, in analogy with (9),

$$L_\nu^{(2)} \approx 5.8\cdot 10^{-9}\mu^{-3/2} T_c^{10.5}/\rho_c^{1.5}. \qquad (15)$$

Furthermore

$$L_\nu^{(2)}/L_\gamma \approx 5.82\cdot 10^{-12} T_c^{2.5}\rho_c/b\mu \qquad (16)$$

and

$$L_\nu^{(2)}/L_\nu^{(1)} \approx 0.48\nu T_c^3/\rho_c. \qquad (17)$$

4. CONCLUSION

The foregoing analysis shows that at high densities and temperatures the neutrino energy loss from stars, and particularly the loss connected with the processes investigated in the present article, assume an important role in the energy release from the stars. At a density $\rho = 10^5$ and a temperature of 42 kev (5×10^8 deg K) (Z = 12), for example, the energy release from one gram of stellar matter per second due to the process $\gamma + A \to A + \nu + \bar\nu$ is 10^3 erg/g-sec, and is much greater than the corresponding energy due to the photons. The investigation shows that in a wide range of densities and stellar temperatures the mechanism considered here prevails over the mechanism of neutrino bremsstrahlung. [3,4]

The neutrino energy loss from stars is apparently particularly important in connection with the problem of white dwarfs and, in general, stars with low photon luminosity. It is known that the lifetime of stars with high luminosity is small compared with the age of the galaxy. On the other hand, in stars with low luminosity the evolutional time scale is very greatly increased (considerably greater than the age obtained for the stars from general cosmological considerations), if evolution due to burning up of hydrogen is taken as the base. [12] In this connection it is interesting to point out that the use of the neutrino luminosity in the analysis of the age of white dwarfs should apparently lead to a considerable reduction in their evolutional time scale.

A related question is that of the initial content of hydrogen in white dwarfs that have not passed through the nova explosion stage, and are the end products of the evolution of an entire star that has exhausted its sources of nuclear energy, so that the energy released is a result of compression.

At small amounts of radiated energy per unit mass and at a finite time scale, the white dwarfs could exhaust their hydrogen only if its initial content was small. The question of the neutrino luminosity of such stars obviously can change our notions concerning the smallness of their hydrogen content. The neutrino energy release apparently plays an important role also in the dynamics of the explosion of supernovae. [1]

No matter how attractive these considerations may be, it must be kept in mind that the question

of the high neutrino luminosity of stars is connected with the still unsolved question whether the $(\bar{e}\nu)(\bar{e}\nu)^+$ interaction of first order in G exists in nature.

[1] G. Gamow and M. Schoenberg, Phys. Rev. **59**, 539 (1941).

[2] R. Feynman and M. Gell-Mann, Phys. Rev. **109**, 193 (1958).

[3] B. M. Pontecorvo, JETP **36**, 1615 (1959), Soviet Phys. JETP **9**, 1148 (1959).

[4] G. M. Gandel'man and V. S. Pinaev, JETP **37**, 1072 (1959), Soviet Phys. JETP **10**, 764 (1960).

[5] H. Y. Chiu and P. Morrison, Phys. Rev. Lett. **5**, 573 (1960).

[6] H. Y. Chiu and R. Stabler, Phys. Rev. **122**, 1317 (1961).

[7] M. Gell-Mann, Phys. Rev. Lett. **6**, 70 (1960).

[8] L. D. Landau, DAN SSSR **60**, 207 (1948).

[9] C. N. Yang, Phys. Rev. **77**, 242 (1950).

[10] E. I. Öpick, in Collection: Nuclear Processes in Stars (Translations), IIL, 1957, p. 108.

[11] S. Chandrasekhar, Introduction to the Study of Stellar Structure, Dover, N. Y.

[12] D. A. Frank-Kamenetskii, Fizicheskie protsessy vnutri zvezd (Physical Processes in Stars), Figmatgiz, 1959.

Translated by J. G. Adashko
280

Letters to the Editor

SINGULARITY IN THE PHOTOPRODUCTION OF π^0 MESONS NEAR THRESHOLD

A. M. BALDIN and A. I. LEBEDEV

P. N. Lebedev Institute, Academy of Sciences, U.S.S.R.

Submitted to JETP editor July 20, 1961

J. Exptl. Theoret. Phys. (U.S.S.R.) **41**, 1688-1689 (November, 1961)

THE analysis of the experimental data on photoproduction of π^0 mesons on protons in the near-threshold energy region [1] has revealed a number of disagreements with conclusions derived on the basis of one-dimensional dispersion relations. [2] The difficulties discussed in [1] in dealing with the photoproduction process on the basis of dispersion relations (a study of this question will be published separately) are, however, to some extent removed by the uncertainties arising from the imprecise estimates of the dispersion integrals. In the analysis of photoproduction in the region of angles $\theta = 0°$, in which the largest discrepancies appeared previously, [1] we have discovered an interesting effect which shows the sensitivity of the differential π^0-photoproduction cross section to slight changes in the dispersion integrals.

Consider the photoproduction cross section at zero degrees:

$$\left.\frac{d\sigma}{d\Omega}\right|_{\theta=0^\circ} = \frac{q}{k}\,|F_1(q^2, \theta = 0^\circ) - F_2(q^2, \theta = 0^\circ)|^2, \quad (1)$$

where q and k are the momenta of the meson and photon in the barycentric frame, and F_1 and F_2 are invariant photoproduction amplitudes. [2] It follows from the analysis of the existing experimental data that ($\omega = \sqrt{1 + q^2}$; we set throughout $\hbar = \mu = c = 1$)

$$(F_1 - F_2)_{\theta=0^\circ} = \left[\sqrt{k\omega}(-0{,}3 + 0.7q) + i \cdot 2.41 \cdot \frac{2}{3}(a_1 - a_3) \times \left(1 - \frac{q^2}{3\omega^2}\right)\sqrt{qq_+}\right] \cdot 10^{-2}, \quad (2)$$

from which it is obvious that at $q_0^2 \approx 0.18$ one has $\mathrm{Re}\,(F_1 - F_2)_{\theta=0^\circ} = 0$ so that the cross section is determined entirely by the small imaginary part of the amplitude, related to the rescattering of charged mesons (a_T is the S-wave scattering length of mesons on nucleons in the state of isotopic spin $\frac{1}{2}$ T, $a_1 - a_3 = 0.245$, [3] and q_+ is the momentum of the π^+ meson). It can be seen from the figure that the cross section for photoproduction at zero degrees, calculated from Eqs. (1) and (2), goes through a sharp minimum in the appropriate energy region of the photons. This characteristic behavior of the cross section is, according to the estimates of Ustinova, [4] not substantially changed by the singularities connected with the threshold of the reaction $\gamma^+ + p \to n + \pi^+$.

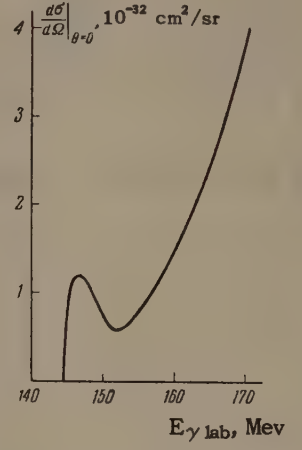

A similar behavior of the cross section follows from rigorous dispersion relations. [2] The calculation of the dispersion integral in this case was performed on the basis of the same assumptions as in [1], with however a careful analysis of the high-energy fall of the p ($\frac{3}{2}$, $\frac{3}{2}$) resonance and without an expansion in powers of cos θ. The calculations gave $q_0^2 = 0.12$ in good agreement with the experimental indications.

From what has been said and from Eq. (2) it follows that a) the location of the minimum in the cross section depends critically on the size of the dispersion integral and, consequently, on possible contributions from the high-energy region and from the $\pi\pi$ interaction; b) the magnitude of the cross section at the minimum determines the difference of the S-wave scattering lengths of pions $a_1 - a_3$, measured in this region of q^2 only indirectly.

To illustrate the first conclusion let us see what would be the effect on the photoproduction of a $\pi\pi$ interaction (see, e.g., [5]). If the parameter characterizing the contribution of the $\pi\pi$ interaction takes on the values $\Lambda/e = 2$ or -2, then $\mathrm{Re}\,(F_1 - F_2)_{\theta=0^\circ}$ vanishes at $q_0^2 \approx 0.05$ and ≈ 0.30 respectively, making the agreement between calculations and experiment worse. A similar effect is obtained if the dispersion integral is changed by 20—30%.

The presence of the indicated effect should make itself strongly felt in the ratio

$[(d\sigma_{dd}/d\Omega)/(d\sigma/d\Omega)]_{\theta=0^\circ}$, where $d\sigma_{dd}/d\Omega$ is the cross section for the process $\gamma + d \rightarrow d + \pi^0$. In the impulse approximation we have for this ratio

$$\left[\frac{d\sigma_{dd}}{d\Omega}\Big/\frac{d\sigma}{d\Omega}\right]_{\theta=0^\circ} = \frac{8}{3}\left|\frac{V}{V+S}\right|^2 I^2, \qquad (3)$$

where V and S stand for the isovector and isoscalar parts of the photoproduction amplitude, and $I^2 \approx 1$ is the deuteron formfactor. In the region $q \approx q_0$, where $|V + S|$ is small, $d\sigma_{dd}/d\Omega$ depends critically on the value of S, and a study of this ratio may provide information on both S-wave photoproduction of π^0 mesons on neutrons and on the $\pi\pi$ interaction, since the latter is connected to the two-pion intermediate state which contributes only to S. In this way the study of the indicated singularity may give rise to valuable information about the parameters of pion physics at low energies.

[1] A. M. Baldin and B. B. Govorkov, DAN SSSR **127**, 993 (1959), Soviet Phys.-Doklady **4**, 851 (1959). A. M. Baldin, JETP **38**, 579 (1960), Soviet Phys. JETP **11**, 416 (1960); Proc. X Intern. Conf. on High Energy Physics at Rochester, 1960, p. 325; JETP **39**, 1151 (1960), Soviet Phys. JETP **12**, 800 (1960).

[2] Logunov, Tavkhelidze, and Solovyov, Nucl. Phys. **4**, 427 (1957); Chew, Goldberger, Low, and Nambu, Phys. Rev. **106**, 1345 (1957).

[3] J. Hamilton and W. S. Woolcock, Phys. Rev. **118**, 291 (1960).

[4] G. K. Ustinova, JETP **41**, 583 (1961), Soviet Phys. JETP **14**, 417 (1962).

[5] J. S. Ball, Phys. Rev. Lett. **5**, 73 (1960).

Translated by A. M. Bincer
281

NEW TYPE OF QUANTUM OSCILLATIONS IN THE ULTRASONIC ABSORPTION COEFFICIENT OF ZINC

A. P. KOROLYUK and T. A. PRUSHCHAK

Institute of Radiophysics and Electronics, Academy of Sciences, Ukrainian S.S.R.

Submitted to JETP editor July 20, 1961

J. Exptl. Theoret. Phys. (U.S.S.R.) **41**, 1689-1691 (November, 1961)

A great deal of attention has recently been directed to the study of the electron structure of metals by ultrasonic means. In the case in which $\kappa l \gg 1$ (κ is the wave vector of the sound, l is the mean free path length of the electrons) oscillations in the absorption coefficient α were observed in a comparatively weak magnetic field perpendicular to the vector κ. These oscillations are due to the coincidence of the cyclotron radius of the electron orbit with an integral number of sound wavelengths.[1,2] The theory of this phenomenon has been considered by V. L. Gurevich[3] and Kaner,[4] who gave the connection between the absorption coefficient and the energy spectrum of the conduction electrons. The quantum oscillations of the absorption coefficient in the perpendicular field were observed experimentally in bismuth and zinc.[5,6] Gurevich, Skobov, and Firsov,[7] predicted the existence of a new quantum effect—gigantic oscillations of the absorption coefficient. The predicted oscillations arise in a non-perpendicular field (in particular, in a longitudinal one) if the following conditions are satisfied:

$$\zeta \gg \hbar\Omega \gg kT, \qquad \varkappa l = \sqrt{\zeta/kT}$$

(ζ is the chemical potential and Ω the cyclotron frequency of the electrons). Both conditions are satisfied at helium temperatures. The frequency of the ultrasound is 100—200 Mc/sec and higher for sufficiently pure metals with only slightly occupied electron bands.

With the aim of observing this phenomenon, we set up experiments in a longitudinal magnetic field ($\mathbf{H} \parallel \kappa$) of intensity up to 35 koe. Single crystals of zinc prepared by zone refining were used. The purity of the samples is characterized by a residual resistance $R_{4.2}/R_{300} = 3 \times 10^{-5}$.

The dependence of $\alpha - \alpha_0$ on the reciprocal of the magnetic field is shown in Fig. 1 (α and α_0 are the absorption coefficients in the field and in the absence of a field, respectively). The wave vector κ and the vector H were directed along the $[10\bar{1}0]$ axis of the crystal; the frequency of the ultrasound was 220 Mc/sec. The absorption coefficient increases markedly with increase in the magnetic field intensity, and in a field $H \sim 10$ koe oscillations appear, the amplitude of which increases rapidly. The period of the oscillations in the inverse field is $\Delta H^{-1} = (0.204 \pm .005) \times 10^{-5}$

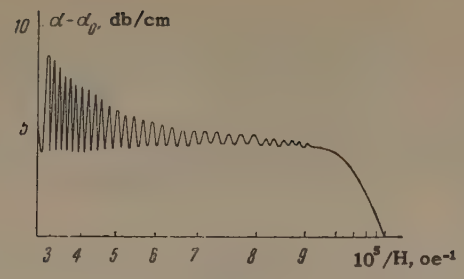

FIG. 1

oe^{-1} and is identical, for this orientation, with the period of the de Haas–van Alphen oscillations of the magnetic susceptibility, measured by Verkin and Dmitrenko[8] (the so-called fine structure of the effect), with accuracy to within the experimental error.

The same dependence for the vectors κ and H directed along $[11\bar{2}0]$ is shown in Fig. 2. The distinctive feature of this curve is the decrease in the coefficient α in comparison with α_0 in the weak field, and its increase in the stronger field, although $\alpha - \alpha_0$ remains negative over the whole range of variation of H. For this orientation, the oscillations of α are beats between two components having neighboring periods $\Delta H^{-1} = (0.16 \pm 0.005) \times 10^{-5}\ oe^{-1}$. These periods differ somewhat more from the period of oscillation of the magnetic susceptibility for the $[11\bar{2}0]$ direction.

The study of the amplitude of the gigantic oscillations was carried out by us at 1.9—4.2° K. The amplitude of the oscillations increases with decrease in temperature.

Evidently, just as in the case of the de Haas–van Alphen oscillations, it is possible to determine the effective mass of the carriers by the temperature dependence of the amplitude; however, a theoretical analysis is still necessary here. The

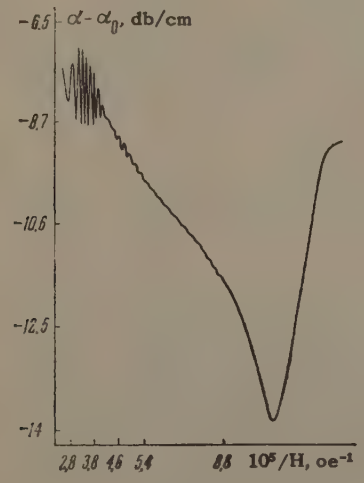

FIG. 2

difference is observed between the periods of oscillation of the magnetic susceptibility and of the gigantic ultrasonic absorption is due to the difference in the cross section areas of the Fermi surface on which the oscillations are realized.

The de Haas–van Alphen effect is determined, as is well known, by the extreme cross sections of the Fermi surface, while gigantic oscillations are realized on that cross section $P_z = P_z^0$, which guarantees the equality $v_z = w$[7] (w is the ultrasonic velocity and v is the Fermi velocity of the electrons).

In conclusion, we thank B. G. Lazarev for interest in the research and also for furnishing the pure zinc.

[1] H. E. Bömmel, Phys. Rev. **100**, 758 (1955).
[2] A. A. Galkin and A. P. Korolyuk, JETP **37**, 310 (1959) and **36**, 1307 (1959), Soviet Phys. JETP **10**, 219 (1960) and **9**, 925 (1959).
[3] V. L. Gurevich, JETP **37**, 71 (1959), Soviet Phys. JETP **10**, 51 (1960).
[4] E. A. Kaner, JETP **38**, 212 (1960), Soviet Phys. JETP **11**, 154 (1960).
[5] D. H. Reneker, Phys. Rev. **115**, 303 (1959).
[6] D. F. Gibbons, Phil. Mag. **6**, 63 (1961).
[7] Gurevich, Skobov, and Firsov, JETP **40**, 786 (1961), Soviet Phys. JETP **13**, 552 (1961).
[8] I. M. Dmitrenko, Dissertation, Khar'kov, 1958.

Translated by R. T. Beyer
282

HEXAGONAL ANISOTROPY IN $MnCO_3$ *AND* $CoCO_3$

JAN KACER and N. M. KREĬNES

Institute for Physics Problems, Academy of Sciences, U.S.S.R.; Physics Institute, Czechoslovak Academy of Sciences

Submitted to JETP editor September 23, 1961

J. Exptl. Theoret. Phys. (U.S.S.R.) **41**, 1691-1692 (November, 1961)

DZYALOSHINSKII has shown[1] that the thermodynamic potential of rhombohedral antiferromagnetic crystals showing weak ferromagnetism contains, among others, a term $K_3 \sin^2 3\varphi$, where φ is an angle taken in the (111) plane. This term is responsible for the hexagonal anisotropy occurring

in the basal plane. In crystals having weak ferromagnetism the spontaneous moment can either be directed along a twofold axis (Dzyaloshinskii's state II), or lie in the plane of symmetry (state III).

We have made measurements of the hexagonal anisotropy in monocrystals of $MnCO_3$ and $CoCO_3$ prepared by a hydrothermal method by N. Yu. Ikornikova in the Crystallography Institute of the U.S.S.R. Academy of Sciences. The crystals of $CoCO_3$ were rather perfect monocrystalline platelets, bound by low-index planes, ~ 0.3 mm thick and 0.8—1 mm in diameter. The $MnCO_3$ crystals were larger, but less perfect. In both cases the trigonal axis [111] was perpendicular to the planes of the platelets.

Circular disks were prepared from these crystals by means of a special tool on an ultrasonic drilling machine. The $CoCO_3$ sample had a diameter of 0.6 mm and a thickness of 0.35 mm. Its measured volume was 1.11×10^{-4} cm^3 and its weight 0.472 ± 0.01 mg, corresponding to a density $\rho = 4.25$ g/cm^3; this is in good agreement with the tabulated value $\rho = 4.13$ g/cm^3. The $MnCO_3$ crystal was found to be much softer, and the shape of the sample after machining was less perfect. Its diameter was 1.3 mm and thickness 0.35 mm.

The anisotropy measurements were carried out on a torsion balance with a quartz suspension 35 μ in diameter. The suspension constant D = 1.86 dyne-cm/rad; the balance constant D' = 1.24×10^{-3} dyne-cm/mm with a precision of reading ~ 0.1 mm.

The measurements were conducted at the temperatures of liquid helium, hydrogen, nitrogen, and at room temperature in a field of 5600 oe; this value is approximately twice as large as the saturating fields of these substances determined by Borovik-Romanov and Ozhogin.[2,3]

The $MnCO_3$ sample showed a weak hexagonal shape anisotropy at all temperatures and practically no crystallographic anisotropy below the Neél point (32.5° K[2]). Our preliminary measurements indicate that the anisotropy, if observed at all, is in every case, less than 1 erg/cm^3. This result is in contradiction to the data of Date,[4] who, using the results of ferromagnetic resonance measurements, obtained for the anisotropy field a value that is at least an order of magnitude greater than that which follows from our data.

Unlike the $MnCO_3$, the $CoCO_3$ sample showed a very strong hexagonal anisotropy. At 4.2° K we obtained a value $K_3 = 634$ erg/cm^3; $K_3 = 0$ at all other temperatures used, which lie above the Neél temperature (18.1° K[3]). Preliminary measurements indicate a very fast drop in K_3 with temperature.

Using the relation $H_c = 18K_3/I_s$ (where H_c is the critical field at which saturation associated with uniform rotation is attained and I_s is the spontaneous ferromagnetic moment per unit volume, equal to 50 cgs esu[3]), we obtain $H_c = 228$ oe.

This value as well as the much smaller one for $MnCO_3$ is an order of magnitude different from the actual saturation field, which in both cases amounts to 2—3 koe. This indicates the presence of some other magnetization processes.

The authors sincerely thank P. L. Kapitza for his interest in the work and A. S. Borovik-Romanov for valuable advice and helpful discussions.

[1] I. E. Dzyaloshinskii, JETP **32**, 1547 (1957), Soviet Physics JETP **5**, 1259 (1957).

[2] A. S. Borovik-Romanov, JETP **36**, 766 (1959), Soviet Phys. JETP **9**, 539 (1959).

[3] A. S. Borovik-Romanov and V. I. Ozhogin, JETP **39**, 27 (1960), Soviet Phys. JETP **12**, 18 (1961).

[4] M. Date, J. Phys. Soc. Japan **15**, 2251 (1960).

Translated by L. M. Matarrese
283

THE PHOTOMAGNETIC EFFECT IN A p-n *JUNCTION*

I. K. KIKOIN and I. N. NIKOLAEV

Submitted to JETP editor September 25, 1961

J. Exptl. Theoret. Phys. (U.S.S.R.) **41**, 1692-1694 (November, 1961)

STUDIES of the photomagnetic effect in semiconductors have shown that illumination of the contacts (electrodes) influences the measured photomagnetic emf, especially at low temperatures. This behavior suggests that the photomagnetic effect may appear in the blocking layer formed at the boundary between a semiconductor and a metal. The present letter describes some experiments designed to check this suggestion.

1. A sample of germanium in the form of a rectangular $10 \times 4 \times 4$ mm parallelepiped was

used. Metallic indium was fused onto one of the 4 × 4 mm ends of the sample, forming a diffused p-n junction. The opposite 4 × 4 end had an ohmic contact (tin). The photomagnetic potential difference between these two contacts was measured with the sample illuminated in a magnetic field normal to the length of the sample. The measured potential difference was the sum of the photomagnetic emf's of the homogeneous part of the sample and of the p-n junction. The two emf's can be separated because the photomagnetic emf in the homogeneous portion is proportional to the illuminated length of the sample, while the junction emf is independent of the illuminated length.

The illuminated length of the sample was varied by moving a rectangular metal screen placed directly in front of the sample. The screen could be moved along the length of the sample from the ohmic contact to the p-n junction. Initially the whole sample was screened. As the screen was moved, the ohmic contact, the homogeneous part of the sample, and the junction were uncovered in the order listed. An emf was recorded without any magnetic field; this was the usual photo-emf across the p-n junction. This emf was balanced out by means of a potentiometer before application of the magnetic field. The potential difference produced by the magnetic field was measured by a null method for two opposite directions of the field. From these two measurements, the odd and even photomagnetic emf's were deduced.

Figure 1 gives the dependence of the measured odd photomagnetic emf at 77° K as a function of the screen displacement x, which represents the length of the illuminated part of the sample. The curve of Fig. 1 shows that initially the photomagnetic emf is proportional to x. Near the position of the junction the emf increases abruptly by an amount U_1, which is obviously the photomagnetic emf of the junction.

2. To check whether the photomagnetic emf is not due to some edge effects, a p-n junction was produced in the middle of an 18 × 4 × 4 sample. Ohmic contacts were deposited on the two 4 × 4 mm ends of the sample and served as potential electrodes. Otherwise the procedure was the same as above.

Figure 2 gives the dependence of the odd photomagnetic emf as a function of the illuminated length of the sample at 300° K. The results of Fig. 2 confirm the existence of the photomagnetic effect across the p-n junction.

3. The same sample was used to measure the photomagnetic emf when direct current was passed through it. When the current was in the "blocking"

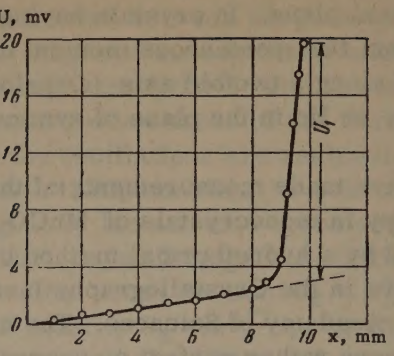

FIG. 1

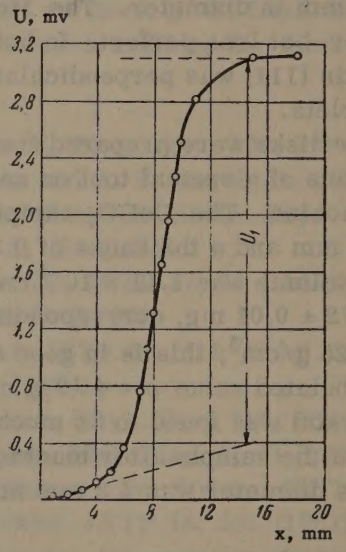

FIG. 2

(reverse) direction the photomagnetic emf was considerably greater than the emf in the absence of the current. In the "passing" (forward) direction the photomagnetic emf was not affected by the direct current (the potential drop across the sample accompanying passage of the current was balanced out).

4. The observed behavior could be considered to represent changes of the photo-emf in a magnetic field,[1] but supplementary experiments showed that the photomagnetic emf is not directly related to the photo-emf appearing across the p-n junction in the absence of a magnetic field.

Suitable treatment of the illuminated surface could alter the sign of the photomagnetic emf (this was observed also in homogeneous samples[2]) without affecting the sign of the primary photo-emf.

The photomagnetic emf was also measured on illumination through a narrow slit moved across the sample. Passage of the slit across the p-n junction produced a sharp maximum of photomagnetic emf.

Apart from the odd photomagnetic emf across the p-n junction, an even emf was also observed, but its nature was not clear.

A detailed description of studies of the photomagnetic effect in p-n junctions will be published later.

[1] G. Blet and J. Vincent, J. phys. radium **19**, 790 (1958).
[2] Brand, Baker, and Mette, Phys. Rev. **119**, 922 (1960).

Translated by A. Tybulewicz
284

SPIN-WAVE HEAT CAPACITY IN ANTIFERROMAGNETIC $MnCO_3$

A. S. BOROVIK-ROMANOV and I. N. KALINKINA

Institute for Physics Problems, Academy of Sciences, U.S.S.R.

Submitted to JETP editor October 11, 1961

J. Exptl. Theoret. Phys. (U.S.S.R.) **41**, 1694-1696 (November, 1961)

INVESTIGATION of the temperature dependence of the heat capacity of antiferromagnetics gives the possibility of verifying the predictions of the theoretical law of dispersion of spin waves. However, up until the present time such investigations have not been carried out. In large part this is connected with the fact that in the usual antiferromagnets, because of the presence of a significant gap in the energy spectrum, the magnetic heat capacity should change exponentially, and in the low temperature region it is found to be small compared with the lattice heat capacity. One of the authors [1] has shown that in the case of the antiferromagnetic carbonates, in which the spins lie in the plane perpendicular to the three-fold axis, the spin-wave spectrum divides into two branches, one of which has practically no gaps. The result is that the magnetic heat capacity, beginning at very low temperatures, should vary according to a cubic law.

In the present work the temperature dependence of the heat capacity of $MnCO_3$ was studied from 1.6 to 80° K. The $MnCO_3$ compound in the form of tiny crystals was obtained by a hydrothermal method by N. Yu. Ikornikova of the Institute of Crystallography of the U.S.S.R. Academy of Sciences. [2] The measurements were carried out in a vacuum calorimeter similar to that used

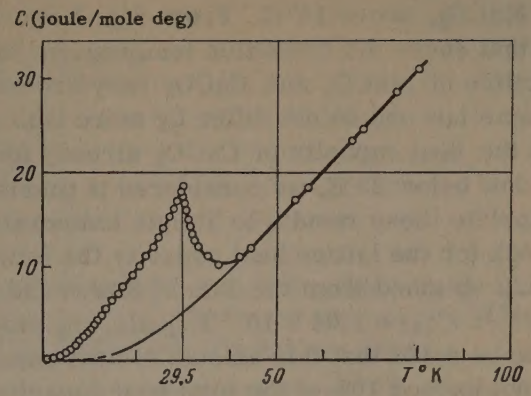

FIG. 1. Temperature dependence of the molar heat capacity of $MnCO_3$ (points and heavy curve) and $CaCO_3$ [7] (light curve) extrapolated to 0° K (dashes).

in [3,4] in the region 1.5—14° K and in an adiabatic calorimeter [5] from 14 to 80° K. The temperature was measured with a bronze thermometer below 4° K, a carbon thermometer between 4° and 14° K [6], and a platinum thermometer above 14° K. Figure 1 shows the general behavior of the heat capacity. The characteristic maximum corresponding to the transition of manganese carbonate from the antiferromagnetic to the paramagnetic state can be seen here. The heat capacity maximum is found at 29.5° K, which is 2.9° lower than T_N = 32.4° K, as determined from magnetic data. [1]

In order to separate out the magnetic heat capacity it was necessary to subtract the lattice and nuclear heat capacities from the data obtained. In order to estimate the specific heat of the lattice we made use of the results of Simon and Swain, [7] who investigated the temperature dependence of the heat capacity of diamagnetic $CaCO_3$, isomorphous

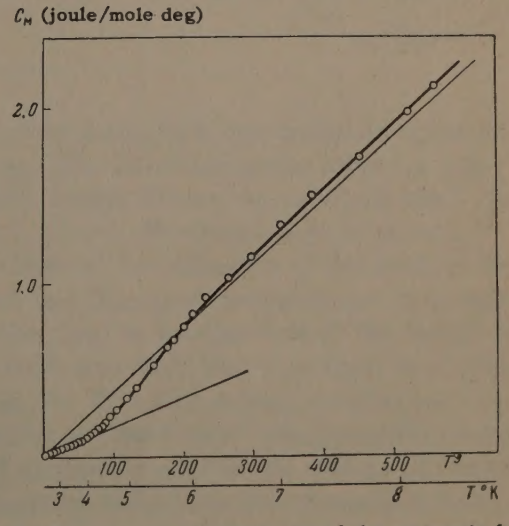

FIG. 2. Temperature dependence of the magnetic heat capacity of $MnCO_3$. (The light lines are according to the spin wave theory from the magnetic data. [1])

with $MnCO_3$, above 14° K. From Fig. 1 it can be seen that above the transition temperature the heat capacities of $MnCO_3$ and $CaCO_3$ vary according to the same law and do not differ by more than 4%. Since the heat capacity of $CaCO_3$ already follows a T^3 law below 25°K, we considered it possible to extrapolate these results to helium temperatures and took for the lattice heat capacity the following formula obtained from the data of Simon and Swain[7]: $C_{lat} = 2.08 \times 10^{-4} T^3$ joule/deg mole. It is to be noted that this amount of heat capacity does not exceed 10% of the total heat capacity of $MnCO_3$ at low temperatures. As is known,[8] ordering of the nuclear moments begins already at helium temperatures in antiferromagnets, leading to an additional contribution to the heat capacity of the form $C_{nuc} = b/T^2$. From our data at low temperatures we find $b = (2.7 \pm 0.5) \times 10^{-2}$ joule/deg mole, which agrees within the limits of error with the value of b for MnF_2.[8]

The magnetic heat capacity C_M obtained from our data after introducing the corrections indicated is plotted in Fig. 2 vs. T^3. We see that up to 3.7° K the heat capacity varies according to the cubic law, agreeing with the formula obtained in [1]:

$$C_M = (4\pi^2 k^2 / 5\mu_B)\, \chi_\perp^0\, \eta T_N (T/T_N)^3 = aT^3.$$

Substituting in this formula the values $\chi_\perp = 43 \times 10^{-3}$, $\eta = 0.24$, $T_N = 32.4°$ K from [1], we obtain $a = 17.5 \times 10^{-4}$ joule/mole deg^4. The experimental value is $a = 18 \pm 0.7 \times 10^{-4}$ joule/mole deg^4. Such good quantitative agreement between the temperature dependences of the spontaneous magnetization and heat capacity of $MnCO_3$ is an important experimental confirmation of the spin wave theory. From 3.7 to 6° K C_M increases sharply and thereafter up to 8.5° K follows the cubic law anew. The coefficient in this new cubic law equals (2.1 ± 0.1) a. This result is also found to be in agreement with the prediction of spin wave theory, according to which the magnetic heat capacity should increase with a doubled coefficient after excitation of the second branch (which has a gap kT_{AE}). An approximate estimate of the size of the gap from a consideration of the transition region gives $T_{AE} = 15°$ K.

The authors sincerely thank Acad. P. L. Kapitza for his constant interest in the work, and also Prof. P. G. Strelkov for valuable advice on the method of measurement and N. Yu. Ikornikova, who prepared the $MnCO_3$.

[1] A. S. Borovik-Romanov, JETP **36**, 766 (1959), Soviet Phys. JETP **9**, 539 (1959).

[2] N. Yu. Ikornikova, Kristallografiya **5**, 761 (1960), Soviet Phys.-Crystallography **5**, 726 (1961).

[3] M. O. Kostryukova and P. G. Strelkov, DAN SSSR **90**, 525 (1953).

[4] E. S. Itskevich and P. G. Strelkov, JETP **32**, 467 (1957), Soviet Phys. JETP **5**, 394 (1957).

[5] Strelkov, Itskevich, Kostryukov, Mirskaya, and Samoĭlov, J. Phys. Chem. (U.S.S.R.) **28**, 459 (1954).

[6] N. N. Mikhaĭlov and A. Ya. Kaganovskii, PTÉ **3**, 194 (1961).

[7] F. Simon and R. C. Swain, Z. physik. Chem. B**28**, 189 (1935).

[8] A. H. Cooke and D. J. Edmonds, Proc. Phys. Soc. (London) **71**, 517 (1958).

Translated by L. M. Matarrese
285